Exploring the Synthesis of Human Milk Oligosaccharides and Their Effects on Immunometabolism

A dissertation submitted to Trinity College Dublin, The University of Dublin in candidature for the degree of Doctor of Philosophy

February 2026

Alanna Slater

B.A. (Mod) Immunology

School of Biochemistry and Immunology

Trinity Biomedical Sciences Institute
Trinity College Dublin

Supervisors:

Prof. Gavin P. Davey

Dr. Rita M. Hickey

Declaration

I declare that this thesis has not been submitted as an exercise for a degree at this or any other university and it is entirely my own work. I confirm that the work has been completed in full compliance with relevant university policies, including the Academic Integrity policy, the Trinity Policy on Good Research Practice, and the guidance on AI and GenAI in Teaching, Learning, Assessment and Research.

I agree to deposit this thesis in the University's open access institutional repository or allow the Library to do so on my behalf, subject to Irish Copyright Legislation and Trinity College Library conditions of use and acknowledgement.

I consent to the examiner retaining a copy of the thesis beyond the examining period, should they so wish (EU GDPR May 2018).

Signature:

Date: 19th October 2025

Acknowledgments

Throughout my PhD and the writing of this thesis I am so so so incredibly lucky and grateful to have received a great deal of support and assistance. My family always jokingly had this saying of “the more you learn, the more you earn” and I always thought that this strictly referred to money, but reflecting on the past four years of this PhD. I’ve realised I’ve earned no money but I’ve earned and gained far more than that, and that’s who I’m here to thank today.

First and foremost, I would like to express my deep gratitude to my supervisors, Prof Gavin Davey and Dr Rita Hickey, for all their support, guidance, and encouragement throughout this journey. I am deeply grateful for all that you have taught me. Your insightful feedback pushed me to sharpen my thinking and brought my work to a higher level. Thank you for taking a chance on me and giving me the opportunity to grow not only as a scientist but as a person. I always knew your doors were open or that you were just a WhatsApp away and that reassurance made this process less lonely than it might otherwise have been. The wisdom you imparted has extended well beyond the lab bench, and for that, I will always be deeply grateful. Supervisors really make or break the PhD and I think I was very lucky with mine. And to Gavin, thank you for never putting a swear jar in the lab - I’d have gone bankrupt before year one.

To the Davey Lab, past and present (and extensions of the Davey Lab). Thank you all for the guidance, encouragement, craic and patience. To Cormac, my brother in the lab, my partner in crime in every disaster and every triumph. For three years we were inseparable, so much so that people stopped saying my name without saying yours as well. We’ve been called the terrible two, and I think that’s fair as we were rarely more than a few feet apart. I couldn’t have asked for a better buddy, even if you did drive me to madness more times than I can count, and together we probably drove Gavin near to early retirement. I still don’t know how either of us managed to do any serious lab work in between the tears of laughter. I think you’re a cracking scientist and an even better friend. I know we will always be great pals even if we don’t have the shackles of the lab chaining us together. A special thanks to Dr Jer Hayes for both the craic over the years and the odd scientific advice when I needed it. I still maintain that Limerick is the greatest hurling county of our nation. To Sahar,

Smaller Gavin, Isabel, Alex and Conor, thank you for explaining the same things to me a million times over, for tolerating my constant interruptions and general noise in the lab, and for giving your time so freely whenever I needed help. I am forever indebted to each of you. To Alexandra and Matthew - you guys were such a great addition to the lab and I am so grateful for the friendship that came from it. Big things are coming for you both and I am so excited to hear about it.

To the Hickey/Glyco Lab, past and present, again I cannot thank you all enough. Coming to Cork nearly three years into my PhD was daunting to say the least after being a self-proclaimed Dub for six years, but all of you made the transition so much easier and I always felt so welcome (even if I will never warm to Cork itself). To Ramesha, you are such a light to this lab. I appreciate everything you do. You never fail to make me smile because yours is so infectious. To Orla, you turned every day into a little lighter one. I never thought a PhD would have me up a best friend along the way. Between the lockouts, the tea breaks, leaving the lab at 2am and the fact that you somehow Pavlov-conditioned me into eating lunch at exactly 12:30pm every day, you made the last year not only easier but genuinely joyful. You are one of the kindest souls, and an amazing friend I hope to never live without. I don't know what I am going to do without the best two-person office in Teagasc, even though we probably talked more than worked (despite our unresolved language barrier).

Of course, no PhD is completed without the help of tech and support staff. I would like to sincerely thank Dr. Barry Moran for his flow cytometry expertise and Dr. Gavin McManus for the help with all things microscopy. Liam Cross for his technical aid and being a general lifesaver over the years. To Audrey, Martha and all the tech staff in the Teaching Lab. To Des and the lads of the delivery bay. Also, a special thanks to Rustam, Laavanya and all the CMU staff. To the lads in academic registry that let me run my ego a few times a year. The biggest thank you to Helen and Ramesha (again) for their help in the HPLC aspect of my project. Thanks also to Dave for never letting a parcel of mine go astray in Moorepark. To all the tech staff in Teagasc and Trinity, as well as countless others I would forever be naming.

I would like to say thanks to my fellow occupants of the 4th and 5th floor in the TBSI and everyone in the Food Biosciences department in Moorepark, who have been my confidants, support system, and inspiration throughout this process. You have all been such a vital part of my journey, my every day, my survival and I am forever grateful for the friendships that I have made. To Cian and Frannie, it is scary to think we walked into Immunology together in 2019 and from that day you've been the backbone of my life. You're basically family at this stage. I love you both to bits. Even with Frannie across the Atlantic now, nothing's changed, I'm still bursting with pride for you both and couldn't imagine having gone through this without ye. Here's to 3/3 doctors. To Fran and Della, having only met you in March 2024 and now I can't imagine life without you. You're two of the most genuinely lovely people I've ever met and I'm very glad ye arrived into my life when you did. My desk neighbours Louisa and Andrea for always listening to me ramble on no matter what time of day or how busy you were. The Italian group I was adopted into in Fermoy for constantly feeding me on every occasion possible, big or small. All of you are scientists which is frankly terrifying, because firstly I witness all of our group chats and secondly once we're finished the doctor-to-normal-person ratio in my friend group is going to be outrageous.

To my friends outside of science - AJ, Andrew, Caitlin, Carol, Dina, Niamh, Rosie and everyone in between. Whether we were friends 10 minutes or 10 years. Thank you all for reminding me that life was bigger than the four walls of the lab. Thank you for dragging me out for one too many drinks (alcoholic or caffeine based), for not letting me wallow in self-doubt, and for shutting me up whenever I started talking about dropping out. For even just texting me asking how I am. You may not have known what I was doing day to day, but you knew exactly how to keep me standing. Friends like you don't come around often, and I am lucky beyond words that you are mine. I would also like to extend my heartfelt thanks to all the other members of my gorgeous family, friends, and loved ones for their constant support and understanding throughout this process.

To my wonderful grandparents, Teresa and Paul, who I more consider to be my best friends - you are one of my greatest gifts in life. I will forever treasure the (many) years of college I spent with you both. Your house was my home away from home. Every drive to the train

station and gourmet meal will always have a place in my heart. I will carry those memories with me forever, and no words can capture how grateful I am for that time.

To my baby brother, Ciarán, thank you for being the person who has quietly inspired me all my life, more than you know. You have this way of surpassing every milestone I reach with ease, and instead of frustrating me, it only makes me prouder every single day. You're just such a gifted young man, and if I make you half as proud as you do me - I'm doing alright. You may not always say much, but when you do, your words carry weight, and I'll always hold onto them. I couldn't have asked for a better brother or a better companion to grow up alongside.

Now finally, to my parents, Saoirse and Paul, who have been my constant source of love, support, and inspiration throughout my life. All I have ever wanted in life is to make you proud of me. I am forever grateful for the foundation you have provided for me. I owe every success, every achievement, every ounce of who I am to you. Thank you for every unseen sacrifice, every quiet reassurance, every loud cheer. This dissertation, this PhD, is not mine alone - it belongs to you as much as it belongs to me (although I know mam knows this already - "Dr Mom"). There is no achievement, no milestone I've reached, that hasn't been touched by the sacrifices you've made and the lessons you've imparted. I hope that in some small way, this accomplishment reflects the love and support you've given me every single day of my life and the appreciation that I have for it all. Thank you, Mam and Dad, for always being there for me and for teaching me the importance of hard work, determination, and never giving up on my dreams.

So, in conclusion, if it takes a village to raise a child, I've learned it takes at least two villages, several pubs, and one or two bad decisions to raise a PhD.

Thank you all for being a part of mine.

Abstract

Human milk oligosaccharides (HMOs) are the third most abundant component of human milk after lactose and lipids, yet were long considered to play only a passive, gut-localised nutritional role. In that context, they were largely characterised as prebiotic substrates, selectively fermented by commensal microbes to generate immunomodulatory short-chain fatty acids. However, HMOs are not simply dietary components confined to the intestinal lumen. Their synthesis is the result of tightly regulated activity by a family of glycosyltransferase enzymes expressed within mammary epithelial cells (MECs), which dictate the structural diversity and functional specificity of these glycans. Importantly, evidence now confirms that a proportion of ingested HMOs can translocate across the intestinal barrier and enter systemic circulation, implying that their biological activity extends beyond the gut-microbiota axis and may involve direct engagement with circulating immune cells.

This thesis explores their role as active immunometabolic signals that directly influence cellular energetics and effector function across innate immune lineages. Through the use of highly purified 2′-fucosyllactose (2′-FL), 3′-sialyllactose (3′-SL), and 6′-sialyllactose (6′-SL), Chapters 3-5 interrogate macrophages, dendritic cells (DCs), and T-cells across basal and inflammatory states. Metabolic flux analysis, transcriptional profiling, complex assays, ROS and cytokine measurements, phagocytosis assays, and receptor signalling readouts collectively demonstrate that HMOs do not act as uniform anti- or pro-inflammatory agents. Instead, they function in a structure and context dependent manner; sialylated HMOs suppress mitochondrial respiration while enhancing glycolysis, priming macrophages for antimicrobial readiness yet preventing hyperinflammation, whereas 2′-FL preserves oxidative balance and restrains activation. In DCs, 6′-SL in particular, enforces metabolic quiescence, while T-cells remain largely unaffected; supporting a model in which adaptive immunity is shaped indirectly through antigen-presenting cells rather than direct glycan interference. These findings establish HMOs as context-sensitive immunomodulators that reprogramme immune cell metabolism to shape downstream function, aligning them with the broader paradigm of immunometabolism.

Structural variation may correlate with immunological potency, but most HMOs, remain prohibitively expensive or unavailable due to limitations in microbial, enzymatic and chemical synthesis platforms. Chapter 6 confronts this bottleneck by attempting to reconstruct HMO biosynthesis within mammalian cells. HEK293 cells were engineered with selected glycosyltransferases in an attempt to determine whether endogenous metabolic machinery could be leveraged to generate sialylated oligosaccharides *in vitro*. Catalytic specificity was retained across constructs, enabling low but detectable production of terminally sialylated HMOs, supported by intracellular nucleotide sugar pools. Crude glycosyltransferase isolation assays further revealed that enzyme activity was pH dependent, with optimal production observed at pH 6.5. Collectively, these findings establish a foundation for scalable cell-based synthesis not only of simple structures such as 3′-SL and 6′-SL, but potentially of more complex branched glycans including lacto-*N*-neotetraose (LNnT).

Together, this data delivers two key messages. First, HMOs are not inert sugars but rather immunometabolic regulators with structure specific signalling capacity**.** Second, their therapeutic potential remains under explored not because of biological uncertainty, but because of manufacturing constraints. HMOs will require the development of further re-engineered biosynthetic platforms before they can be used clinically. This thesis therefore advances both immunological understanding and translational feasibility, highlighting HMOs as a class of maternally derived immune regulators and identifying the cellular and engineering strategies required to understand their full therapeutic value.

Table of Contents

DECLARATION I

ACKNOWLEDGMENTS II

ABSTRACT VI

TABLE OF CONTENTS VIII

LIST OF FIGURES XI

LIST OF TABLES XXII

LIST OF ABBREVIATIONS XXIV

RESEARCH OUTPUT XXVI

CHAPTER 1: INTRODUCTION 1

1.1. HMO Composition 3

1.2. Indirect Implications of HMOs on Immune System Function 8

1.3. Receptors For HMOs and Immune System Interaction 12

1.4. Immunological Impacts HMOs 15

1.5. Immune Cell Metabolism 26

1.6. Clinical Relevance of HMOs in Immunity 27

1.7. Biosynthesis Pathways of HMOs 28

1.8. Current Industrial Methods of HMO Synthesis, Separation and Detection 32

1.9. In Silico Advances in Glycosyltransferases and HMO Synthesis 36

1.10. Analytical Techniques in HMO Structure Elucidation 38

1.11. Aims of Thesis 39

CHAPTER 2: MATERIALS AND METHODS 41

2.1. Materials and Reagents 42

2.2. Buffers 45

2.3. Methods 47

2.4. Analysis Software and Programs 72

2.5. Experimental Animals and Ethics 73

CHAPTER 3: EFFECT OF HUMAN MILK OLIGOSACCHARIDES ON METABOLIC PATHWAYS IN MACROPHAGES 74

3.1. Introduction 75
3.2. Methods 78
3.3. Effect of HMOs at Given Concentrations on Macrophage Viability ..80
3.4. Effects of HMOs on Macrophages Vary With Concentration 82
3.5. Metabolic Profiles of Macrophages Vary With Activation State 85
3.6. Effects of HMOs on Unactivated M0 Macrophages 90
3.7. Effects of HMOs on Classically Activated M1 Macrophages 99
3.8. Effect of HMOs on Macrophages Over 6 Hour LPS Stimulation 110
5.1. Effects of HMOs on Alternatively Activated M2 Macrophages 116
3.9. Discussion 124

CHAPTER 4: IMMUNOMODULATORY EDDECTS OF HUMAN MILK OLIGOSACCHARIDES IN MACROPHAGES 132

4.1. Introduction 133
4.2. Methods 136
4.3. The Effect of HMOs on TLR2 and TLR4 Activation 139
4.4. Effect of HMOs on Mitochondrial ROS Production And Phagocytic Bacterial Clearance in Macrophages 144
4.5. The Effect of HMOs on Pro and Anti-Inflammatory Cytokine Release in Macrophages 152
4.6. Discussion 157

CHAPTER 5: METABOLIC AND FUNCTIONAL EFFECTS OF HUMAN MILK OLIGOSACCHARIDES ON DENDRITIC CELLS AND T-CELLS 167

5.1. Introduction 168
5.2. Methods 171
5.3. HMOs Cytotoxic Effect in DCs and T-Cells 174
5.4. Metabolic Profiling of DC Subsets by OCR and ECAR 177
5.5. HMOs Effect on Metabolic Phenotype in DCs 181

5.6. HMOs Effect on Metabolic Phenotype in LPS Activated DCs 187
5.7. HMOs Temporal Effect on DCs 196
5.8. Metabolic Profiling of Effector and Memory T-Cells 201
5.9. HMOs Effect on Effector T-Cell Metabolism 205
5.10. HMOs Effect on Memory T-Cell Metabolism 211
5.11. HMOs Temporal Effects on T-Cells 219
5.12. Immunomodulatory Effects of HMOs on DCs and T-Cells 224
5.13. Discussion 230

CHAPTER 6: HETEROLOGOUS EXPRESSION AND FUNCTIONAL EVALUATION OF GLYCOSYLTRANSFERASES FOR HUMAN MILK OLIGOSACCHARIDES SYNTHESIS 239

6.1. Introduction 240
6.2. Methods 243
6.3. Validation of Glycosyltransferase Constructs for Heterologous Expression 246
6.4. Evaluation of Glycosyltransferase Expression in Heterologous Mammalian Systems 257
6.5. Preparation of Glycosyltransferase Gene Fragments for Construct Assembly 268
6.6. In Silico Modelling of HMO Biosynthesis 272
6.7. Assembly of Multigene Glycosyltransferase Constructs 275
6.8. Assessment of Heterologous Glycosyltransferase Expression for HMO Production 291
6.9. In Vitro Characterisation of Glycosyltransferase Activity Across pH Conditions for HMO Production 297
6.10. Discussion 309

CHAPTER 7 319

BIBLIOGRAPHY 328

List of Figures

Chapter 1

Figure 1. 1**: Human Milk Composition**.....2

Figure 1. 2: **Mechanistic Representation of HMOs Interaction with the Gut-Immune Axis.** 9

Figure 1. 3**: Interaction of HMOs with Immune Cells and Receptors.**.....13

Figure 1. 4**: Known Effects of HMOs on the Immune Response**.....16

Figure 1. 5: **Networks of HMO biosynthesis simulated using Glycologue.**.....37

Chapter 2

Figure 2. 1: **Chemical Structure of HMOs Used From Carbosynth** 43

Figure 2. 2**: PGEN2-DEST Vector Plasmid from DNASU Plasmid Repository**..45

Figure 2. 3: **Timeline of Murine Cell Culture Protocols for BMDMs, BMDCs, and Spleen-Derived T-cells.** 49

Figure 2. 4: **Standard Curve for IL-1β.**.....52

Figure 2. 5: **Standard Curve for IL-10.**.....52

Figure 2. 6: **Standard Curve for TNF-α.**.....53

Figure 2. 7: **Measurement of Oxidative Phosphorylation via OCR using The Seahorse XF Metabolic Flux Analyser** 56

Figure 2. 8: **U Measurement of Glycolysis via ECAR using The Seahorse XF Metabolic Flux Analyser** 57

Figure 2. 9: **Summary of Analytes Detected During Seahorse XF Metabolic Flux Assay for Glycolysis and Oxidative Phosphorylation**.....58

Figure 2. 10: **Analysis of BMDM Integrity via Flow Cytometry:**.....60

Figure 2. 11: **Analysis of BMDC Integrity via Flow Cytometry:**.....61

Figure 2. 12: **Analysis of T-Cell Integrity via Flow Cytometry:** 62

Figure 2. 13: **MitoSOX gating panel** 63

Chapter 3

Figure 3. 1: **Cell Viability of Macrophages Following HMO Treatment**.....81

Figure 3. 2: **Basal OCR Analysis of BMDMs Treated with Increasing Concentrations of HMOs** 83

Figure 3. 3: **Basal ECAR Analysis of BMDMs Treated with Increasing Concentrations of HMOs** 84

Figure 3. 4: **Metabolic Profiling of Macrophage Subsets by OCR Measurements**87

Figure 3. 5: **Metabolic Profiling of Macrophage Subsets by ECAR Measurements** 88

Figure 3. 6: **Gene Expression Analysis of Oxidative Phosphorylation and Glycolysis in Macrophage Subsets** 89

Figure 3. 7: **OCR Measurements in BMDMs Treated with Individual HMOs**....93

Figure 3. 8: **Expression of Oxidative Phosphorylation Genes in BMDMs Treated with HMOs** 94

Figure 3. 9: **Complex I Enzymatic Activity in BMDMs Following Treatment with 5-HMO Mix** 95

Figure 3. 10: **ECAR Measurements in BMDMs Treated with Individual HMOs**96

Figure 3. 11: **Expression of Glycolytic Genes in BMDMs Treated with HMOs** ..97

Figure 3. 12: **Lactate Production in BMDMs Following HMO Treatment**.....98

Figure 3. 13: **OCR Measurements in LPS-Activated BMDMs Treated with HMOs**.....102

Figure 3. 14: **Expression of Oxidative Phosphorylation Genes in LPS-Activated BMDMs Treated with HMOs** 103

Figure 3. 15: **Complex I Enzymatic Activity in LPS-Activated BMDMs Following Treatment with 5-HMO Mix** 104

Figure 3. 16: **ECAR Measurements in LPS-Activated BMDMs Treated with HMOs**.....105

Figure 3. 17: **Expression of Glycolytic Genes in LPS-Activated BMDMs Treated with HMOs** 106

Figure 3. 18: **Lactate Production in LPS-Activated BMDMs Following HMO Treatment** 107

Figure 3. 19: **OCR Measurements in BMDMs with Prolonged LPS-Activation Treated with HMOs** 108

Figure 3. 20: **ECAR Measurements in BMDMs with Prolonged LPS-Activation Treated with HMOs** 109

Figure 3. 21: **6 hour Time-Course Analysis of OCR in BMDMs Following HMO Treatment** 112

Figure 3. 22: **6 hour Time-Course Analysis of ECAR in BMDMs Following HMO Treatment** 113

Figure 3. 23: **6 hour Time-Course OCR Analysis in LPS-Activated BMDMs Following HMO Treatment** 114

Figure 3. 24: **6 hour Time-Course ECAR Analysis in LPS-Activated BMDMs Following HMO Treatment** 115

Figure 3. 25: **OCR Measurements in IL-4-Activated BMDMs Treated with HMOs** 118

Figure 3. 26: **ECAR Measurements in IL-4-Activated BMDMs Treated with HMOs** 119

Figure 3. 27: **OCR Measurements in Prolonged IL-4-Activated BMDMs Treated with HMOs** 120

Figure 3. 28: **ECAR Measurements in Prolonged IL-4-Activated BMDMs Treated with HMOs** 121

Figure 3. 29: **Differential Impact on Glycolytic Reserve in M0, M1, and M2 Macrophages Treated with HMOs** 122

Figure 3. 30: **Differential Impact on Spare Respiratory Capacity in M0, M1, and M2 Macrophages Treated with HMOs** 123

Figure 3. 31: **Schematic Representation of Metabolic Readouts in Immune Cells Treated with HMOs** 124

Chapter 4

Figure 4. 1: **NF-κB Reporter Activity in HEK-Blue™ hTLR4 Cells Following HMO Treatment** 140

Figure 4. 2: **NF-κB Reporter Activity in HEK-Blue™ hTLR2 Cells Following HMO Treatment** 141

Figure 4. 3:**IκBα Expression in Macrophages Following HMO Treatment** 142

Figure 4. 4: **Endotoxin Assessment of HMOs** 143

Figure 4. 5: **Reactive Oxygen Species Production in M0, M1, and M2 Macrophages** 145

Figure 4. 6: **Basal ROS Levels in Macrophages Following HMO Treatment** 146

Figure 4. 7: **ROS Production in Macrophages Under Inflammatory Conditions with HMO Treatment** 147

Figure 4. 8: **ROS Production in Macrophages Under Prolonged LPS-Induced Inflammatory Stress** 148

Figure 4. 9: **Phagocytic Activity of Macrophages Following HMO Treatment** 150

Figure 4. 10: **Bacterial Uptake in Immortalised Macrophages Following HMO Treatment** 151

Figure 4. 11**: TNF-α Production in M1 Macrophages Following HMO Treatment** 153

Figure 4. 12**: IL-10 Production in M1 Macrophages Following HMO Treatment** 154

Figure 4. 13 **: IL-10 Production in M2 Macrophages Following HMO Treatment** 155

Figure 4. 14: **IL-1β Production in M1 Macrophages Following HMO Treatment** 156

Figure 4. 15: **Schematic Overview of HMOs Effect on Macrophage in Resting and Inflammatory States** 166

Chapter 5

Figure 5. 1: **Viability Assessment of DCs Following HMO Treatment**.....175

Figure 5. 2: **Viability Assessment of T-Cells Following HMO Treatment**.....176

Figure 5. 3: **Metabolic Profiling of DC Subsets using OCR Measurements**.....178

Figure 5. 4: **Metabolic Profiling of DC Subsets using ECAR Measurements** 179

Figure 5. 5: **Gene Expression Analysis of Oxidative Phosphorylation and Glycolysis in DC Subsets**.....180

Figure 5. 6: **Mito Stress Test OCR Measurement in Immature DCs Treated with HMOs**.....182

Figure 5. 7: **Mito Stress Test ECAR Measurement in Immature DCs Treated with HMOs** 183

Figure 5. 8: **Extracellular Lactate Production in Immature DCs Following HMO Treatment**.....184

Figure 5. 9: **Expression of Oxidative Phosphorylation Genes in Immature DCs Treated with HMOs**.....185

Figure 5. 10*:* **Expression of Glycolysis Genes in immature DCs Treated with HMOs**.....186

Figure 5. 11: **Mito Stress Test OCR Measurement in Activated DCs Treated with HMOs**.....189

Figure 5. 12: **Mito Stress Test ECAR Measurement in Activated DCs Treated with HMOs** 190

Figure 5. 13: **Extracellular Lactate Production in Activated DCs Following HMO Treatment**.....191

Figure 5. 14: **Expression of Oxidative Phosphorylation Genes in Activated DCs Treated with HMOs**.....192

Figure 5. 15: **Expression of Glycolysis Genes in Activated DCs Treated with HMOs**.....193

Figure 5. 16: **Spare Respiratory Capacity in Immature and Activated DCs Following HMO Treatment** 194

Figure 5. 17: **Glycolytic Reserve in Immature and Activated DCs Following HMO Treatment** 195

Figure 5. 18: **Time-Course of OCR in Immature DCs Over 6 Hours Following HMO Pre-Treatment** 197

Figure 5. 19: **Time-Course of ECAR in Immature DCs Over 6 Hours Following HMO Pre-Treatment** 198

Figure 5. 20: **Time-Course of OCR in DCs Over 6 Hours After 6 hour LPS Stimulation Following Overnight HMO Pre-Treatment** 199

Figure 5. 21: **Time-Course of ECAR in DCs Over 6 Hours After 6 hour LPS Stimulation Following Overnight HMO Pre-Treatment** 200

Figure 5. 22: **Metabolic Profiling of Effector and Memory T-cells Using OCR and ECAR Measurements** 202

Figure 5. 23: **Metabolic Profiling of Effector and Memory T-cells Using OCR and ECAR Measurements** 203

Figure 5. 24: **Gene Expression Analysis of Oxidative Phosphorylation and Glycolysis in T-Cell Subsets** 204

Figure 5. 25: **Mito Stress Test OCR Measurement in Effector T-Cells Treated with HMOs** 206

Figure 5. 26: **Mito Stress Test ECAR Measurement in Effector T-Cells Treated with HMOs** 207

Figure 5. 27: **Extracellular Lactate Production in Effector T-Cells Following HMO Treatment** 208

Figure 5. 28: **Expression of Oxidative Phosphorylation Genes in Effector T-Cells Treated with HMOs** 209

Figure 5. 29: **Expression of Glycolysis Genes in Effector T-Cells Treated with HMOs** 210

Figure 5. 30: **Mito Stress Test OCR Measurement in Memory T-Cells Treated with HMOs** 212

Figure 5. 31: **Mito Stress Test ECAR Measurement in Memory T-Cells Treated with HMOs** 213

Figure 5. 32: **Extracellular Lactate Production in Memory T-Cells Following HMO Treatment** 214

Figure 5. 33: **Expression of Oxidative Phosphorylation Genes in Memory T-Cells Treated with HMOs** 215

Figure 5. 34: **Expression of Glycolysis Genes in Memory T-Cells Treated with HMOs** 216

Figure 5. 35: **Spare Respiratory Capacity in Effector and Memory T-Cells Treated with HMOs** 217

Figure 5. 36: **Glycolytic Reserve in Effector and Memory T-Cells Treated with HMOs** 218

Figure 5. 37: **Time-Course of OCR in Effector T-Cells Over 6 Hours Following Overnight HMO Pre-Treatment** 220

Figure 5. 38: **Time-Course of ECAR in Effector T-Cells Over 6 Hours Following Overnight HMO Pre-Treatment** 221

Figure 5. 39: **Time-Course of OCR in Memory T-Cells Over 6 Hours Following Overnight HMO Pre-Treatment** 222

Figure 5. 40: **Time-Course of ECAR in Memory T-Cells Over 6 Hours Following Overnight HMO Pre-Treatment** 223

Figure 5. 41**: ROS Levels in Immature and Mature DCs Following HMO Production** 225

Figure 5. 42: **TNFα Production in DCs Treated with HMOs** 226

Figure 5. 43: **IL-1β Production in DCs Treated with HMOs** 227

Figure 5. 44: **IL-10 Production in DCs Treated with HMOs** 228

Figure 5. 45 **TNF-α Production in T-Cells Treated with HMOs** 229

Figure 5. 46: **Overview of HMO-Mediated Metabolic Regulation in DCs and T-Cells** 238

Chapter 6

Figure 6. 1: **Plasmid Map Containing B3GALT4 gene** 248

Figure 6. 2: **Plasmid Map Containing B3GNT2 gene**.....249

Figure 6. 3: **Plasmid Map Containing B4GALT4 gene** 250

Figure 6. 4: **Plasmid Map Containing FUT2 gene** 251

Figure 6. 5: **Plasmid Map Containing GCNT3 gene**.....252

Figure 6. 6: **Plasmid Map Containing ST3GAL1 gene**.....253

Figure 6. 7: **Plasmid Map Containing ST6GAL1 gene**.....254

Figure 6. 8: **Plasmid Map Containing ST6GALNAC3 gene** 255

Figure 6. 9: **GFP-Based Transfection Optimisation in HeLa Cells using FUT2 Plasmid**.....259

Figure 6. 10**: Timecourse and GFP-Based Transfection Optimisation in HEK293 Cells using FUT2 Plasmid** 260

Figure 6. 11: **HEK293 cells imaged at 0 hours post-transfection with glycosyltransferase expressing plasmid** 261

Figure 6. 12: **HEK293 cells imaged at 12 hours post-transfection with glycosyltransferase expressing plasmid** 262

Figure 6. 13: **HEK293 cells imaged at 24 hours post-transfection with glycosyltransferase expressing plasmid** 263

Figure 6. 14: **HEK293 cells imaged at 36 hours post-transfection with glycosyltransferase expressing plasmid** 264

Figure 6. 15: **HEK293 cells imaged at 48 hours post-transfection with glycosyltransferase expressing plasmid** 265

Figure 6. 16: **Quantification of GFP-Positive HEK293 Cells Across Constructs**266

Figure 6. 17: **Flow Cytometry Analysis Confirming GFP Expression in Transfected HEK293 Cells**.....267

Figure 6. 18: **In Silico and Actual Agarose Gel of Double-Digested Plasmids Showing Insert and Backbone Separation** 270

Figure 6. 19: **In Silico prediction and Confirmation of Extracted Glycosyltransferase Inserts via Agarose Gel Electrophoresis** 271

Figure 6. 20: **O-Glycologue predictions of HMO structures generated by B4GALT4, B3GNT2, and ST3GAL1 or ST6GAL1 using lactose as a starter molecule**.....273

Figure 6. 21: **HMO structures produced by B4GALT4, B3GNT2 and ST6GAL1 using Lactose as starting molecule** 274

Figure 6. 22: **ST6GAL1 Plasmid Map visualisation and Linearisation by EcoRI Digestion** 277

Figure 6. 23: **B4GALT4 Plasmid Map visualisation and Gene Fragment Isolation by EcoRI and BamHI** 278

Figure 6. 24: **B3GNT2 Plasmid Map visualisation and Gene Fragment Isolation by EcoRI and BamHI** 279

Figure 6. 25: **In Silico gel prediction vs Confirmation Gel of Final Gene Inserts for Gibson Assembly**.....280

Figure 6. 26: **In Silico visualisation of overlapping sequences compatible for GAC** 281

Figure 6. 27: **Temperature Gradient PCR Optimisation for B4GALT4 Amplification with Overhangs**.....283

Figure 6. 28: **Temperature Gradient PCR Optimisation for B3GNT2 Amplification with Overhangs**.....284

Figure 6. 29: **Overview of Gibson Assembly Protocol for Triple-Gene Construct with B3GNT2, B4GALT4 and ST6GAL1** 285

Figure 6. 30: **Transformation of DH5α E. coli with Plasmid** 286

Figure 6. 31: **Predicted Final Plasmid Product Containing All Three Glycosyltransferase Genes** 287

Figure 6. 32: **Restriction Digest screening of Gibson Assembly Cloning products** 288

Figure 6. 33: **Plasmid Map of Two Glycosyltransferases Successfully Transformed into pGeN2-DEST Vector**.....289

Figure 6. 34: **Transfection Efficiency of Plasmid Transformed with Two Glycosyltransferases**.....290

Figure 6. 35: **HPLC chromatograms of a 15-component HMO standard mix for reference peak identification in DMEM**.....293

Figure 6. 36: **HPLC chromatograms of secreted oligosaccharides from ST6GAL1 glycosyltransferase-transfected HEK293 cells**.....294

Figure 6. 37: **HPLC chromatograms of secreted oligosaccharides from ST6GAL1-B3GNT2 glycosyltransferase-transfected HEK293 cells**....295

Figure 6. 38: **HPLC chromatograms of a 15-component HMO standard mix for reference peak identification in MES/HEPES**.....299

Figure 6. 39: **HPLC chromatograms of the LNnT standard for reference peak against Lactose**.....300

Figure 6. 40: **HPLC chromatograms of secreted oligosaccharides from extracted ST6GAL1 treated with lactose and UDP sugars, reaction pH 6.5**.....301

Figure 6. 41: **HPLC chromatograms of secreted oligosaccharides from extracted ST6GAL1 and ST3GAL1 treated with lactose and UDP sugars, reaction pH 6.5**.....302

Figure 6. 42: **HPLC chromatograms of secreted oligosaccharides from extracted B3GNT2, B4GALT4, ST6GAL1 and ST3GAL1 treated with lactose and UDP sugars, reaction pH 7.5**.....303

Figure 6. 43: **HPLC chromatograms of secreted oligosaccharides from extracted B3GNT2, B4GALT4, ST6GAL1 and ST3GAL1 treated with lactose and UDP sugars, reaction pH 6.5**.....304

Figure 6. 44: **HPLC chromatograms of secreted oligosaccharides from extracted B3GNT2, B4GALT4, ST6GAL1 and ST3GAL1 treated with lactose and UDP sugars, reaction pH 5.5**.....305

Figure 6. 45: **HPLC chromatograms of secreted oligosaccharides from extracted B3GNT2-ST6GAL1, B4GALT4 and ST3GAL1 treated with lactose and UDP sugars, reaction pH 7.5** 306

Figure 6. 46: **HPLC chromatograms of secreted oligosaccharides from extracted B3GNT2-ST6GAL1, B4GALT4 and ST3GAL1 treated with lactose and UDP sugars, reaction pH 6.5** 307

List of Tables

Chapter 1

Table 1. 1: **Composition of HMOs**.....3

Table 1. 2 **: Classification of Lewis and Secretor Phenotypes and Their Associated HMOs**.....4

Table 1. 3 **: Names, Abbreviations and Structures of a sample of Neutral HMOs** 5

Table 1. 4**: Names, Abbreviations and Structures of a sample of Fucosylated HMOs**.....5

Table 1. 5: **Names, Abbreviations and Structures of a sample of Sialylated HMOs** 7

Table 1. 6**: Key Enzymes Involved in HMO Synthesis - Substrates, Products, and Functional Insights** 28

Chapter 2

Table 2. 1: **Western Blot Antibodies** 43

Table 2. 2: **Functional Antibodies** 43

Table 2. 3: **Flow Cytometry Antibodies**.....44

Table 2. 4: **Primers used for PCR** 54

Table 2. 5: **Enzymes used in Restriction Digest** 68

Table 2. 6: **Primers used for PCR addition of overhangs for Gibson Assembly Cloning**.....69

Table 2. 7: **Setting of PCR for addition of overhangs for Gibson Assembly Cloning**.....70

Chapter 6

Table 6. 1: **Summary of WPS Data From Plasmids Expressing Human Glycosyltransferases**.....256

Table 6. 2: **Restriction Enzyme Pairs Used for Insert and Backbone Isolation**.269

Table 6. 3: **Forward and Reverse Primer Sequence for Extension of Inserts for Gibson Assembly Cloning compatible overhangs**.....282

Table 6. 4: **Transfection Conditions, Substrate Supplementation, and HPLC Detection of 6′-SL in Glycosyltransferase-Transfected Cells** 296

Table 6. 5: **Summary of HPAEC-PAD results from Eznymatic Reaction** 308

List of Abbreviations

2’-FL	2’-Fucosyllactose
3-FL	3-Fucosyllactose
3’-SL	3’-Sialyllactose
3'-SLNT	3'-Sialyl-lacto-*N*-tetraose
6’-SL	6’-Sialyllactose
6'-SLN	6'-Sialyllactosamine
6'-SLNT	6'-Sialyl-lacto-*N*-tetraose
A2FucT	galactoside 2-α-l-fucosyltransferase
A3FucT	4-galactosyl-*N*-acetylglucosaminide 3-α-l- fucosyltransferase
A4FucT	3-galactosyl-*N*-acetylglucosaminide 4-α-l-fucosyltransferase
aa	Amino Acid
AA	Antimycin A
ATP	Adenosine Triphosphate
ANOVA	Analysis of Variance
APC	Antigen Presenting Cell
B3GalT	*N*-acetyl-β-d-glucosaminide β-1,3-galactosyltransferase
B3GnT	*N*-acetyllactosaminide β-1,3-*N*- acetylglucosaminyltransferase
B4GalT	β-*N*-acetylglucosaminylglycopeptide β-1,4- 22,932 galactosyltransferase
B6GnT	β -1,3-galactosyl-O-glycosyl-glycoprotein- β -1,6-*N*-acetylglucosaminyltransferase
BMDM	Bone Marrow Derived Macrophage
BMDC	Bone Marrow Derived Dendritic Cell
BSA	Bovine Serum Albumin
cIGnT	*N*-acetyllactosaminide β-1,6-*N*- acetylglucosaminyltransferase
CMP	Cytidine 5′-Phosphate
CMP-S	CMP-*N*-acetyl-β-neuraminate
DC	Dendritic Cell
dIGnT	GlcNAcβ1,3Gal β-1,6-*N*-acetylglucosaminyltransferase - (distally acting)
DNA	Deoxyribonucleic Acid
ECAR	Extracellular Acidification Rate
ER	Endoplasmic Reticulum
ETC	Electron Transport Chain
FCCP	Carbonyl cyanide-p-trifluoromethoxy phenylhydrazone
Fuc	Fucose
GALT	Gut Associated Lymphoid Tissue
Gal	Galactose
Glc	Glucose
GlcNAc	N-acetylglucosamine
GDP	Guanosine. 5′-Diphosphate
GDP-f	GDP-α-l-fucose
GM-CSF	Granulocyte-Macrophage Colony Stimulating Factor

GPCR	G-Protein Coupled Receptor
HDAC	Histone Deacetylases
HMO	Human Milk Oligosaccharide
IFN	Interferon
Ig	Immunoglobulin
IL	Interleukin
LNDFH I	Lacto-*N*-difucohexaose I
LNDFH II	Lacto-*N*-difucohexaose II
LNDFH III	Lacto-*N*-difucohexaose III
LNFP I	Lacto-*N*-fucopentaose I
LNFP II	Lacto-*N*-fucopentaose II
LNFP III	Lacto-*N*-fucopentaose III
LNFP V	Lacto-*N*-fucopentaose V
LNH	Lacto-*N*-hexaose
LNnH	Lacto-*N*-neohexaose
LNnT	Lacto-*N*-neotetraose
LNT	Lacto-*N*-tetraose
LNFT	Lacto-*N*-fucotetraose
LPS	Lipopolysaccharide
M-CSF	Macrophage-Colony Stimulating Factor
MHC	Major Histocompatibility Complex
mtROS	Mitochondrial ROS
NADH	Nicotinamide Adenine Dinucleotide
NeuAc	*N*-acetyl-neuraminic acid
OCR	Oxygen Consumption Rate
OPME	One Pot Multi Enzyme
OxPhos	Oxidative Phosphorylation
PAMP	Pathogen Associated Molecular Pattern
PBS	Phosphate Buffered Saline
ROS	Reactive Oxygen Species
Rot	Rotenone
SCFA	Short Chain Fatty Acid
ST3Gal	*N*-acetyllactosaminide α-2,3-sialyltransferase
ST6Gal	β-galactoside α-2,6-sialyltransferase
ST6GlcNac	*N*-acetylglucosamine α-2,6-sialyltransferase
TCR	T-Cell Receptor
TLR	Toll-Like Receptor
TNF- α	Tumor Necrosis Factor-α
UDP	Uridine 5′-Diphosphate
UDP-L	UDP-α-d-galactose
UDP-Y	UDP-*N*-acetyl-β-d-glucosamine

Research Output

Publications

- **Interactions of Human Milk Oligosaccharides with the Immune System**
  Alanna S. Slater[1,2], Rita M. Hickey[1], Gavin P. Davey[2]
  Frontiers in Immunology 2025

- **Glycosyltransferases: Pioneers in Human Milk Oligosaccharide Synthesis and Commercial Production**
  Alanna S. Slater[1,2], Andrew G. McDonald[2], Rita M. Hickey[1], Gavin P. Davey[2]
  Frontiers in Molecular Biosciences 2025

Presentations

- **Poster Presenter at 21st International Milk Genomics Consortium (IMGC) 2024 - UC Davis, California**

Poster Title: "Metabolic Insights and Immunomodulatory Effects of Human Milk Oligosaccharides on Immune Cells"

- **Oral Presenter at 22nd International Society for Research in Human Milk and Lactation (IRSHML) Conference 2024 - Charleston, South Carolina***
  ***(Awarded Gates Foundation Travel Grant)**

Presentation Title: "Metabolic Insights and Immunomodulatory Effects of Human Milk Oligosaccharides on Immune Cells"

Chapter 1

Introduction

Breast milk is often described as the gold standard when it comes to infant nutrition, containing a high content of protein, fat, carbohydrates, vitamins, and minerals. It is regarded as the most beneficial source of nutrients for infant growth and development. As well as transferring maternal antibodies in the form of secretory Immunoglobulin A (IgA) to the infant[1], providing passive immunity to the infant, it is also a source of other immune compounds that help regulate the naïve and developing immune system in the infant. One of the most important of these components is the Human Milk Oligosaccharide (HMO) fraction found in human milk, which is a diverse group of complex sugars. HMOs are the third most abundant component of breast milk, behind only lactose and fat[2] (**Figure 1.1**). The consumption of HMOs by infants has been shown to have a number of beneficial effects on the developing gut microbiome and immune system, as well as influencing neurodevelopment and impacting the overall health of the infant[3,4]. HMOs were originally described when discovered in the 1900s as 'bifidus factor' due to the understanding that HMOs promoted the growth of beneficial bacteria and dampened the growth of pathogenic bacteria[5]. However, it is now understood that HMOs play an even deeper role in the development of the infant immune system.

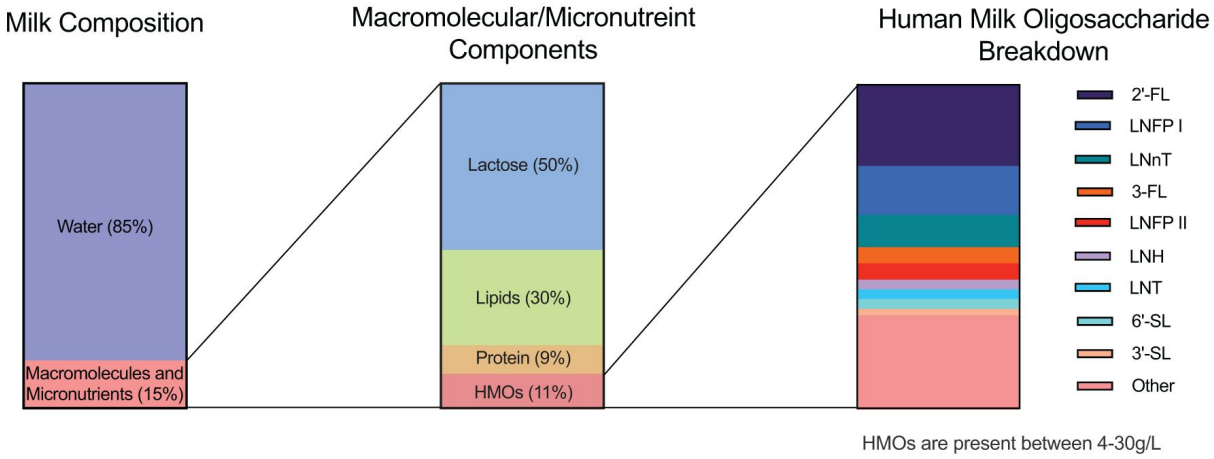

Figure 1. 1**: Human Milk Composition**

Breast milk is composed of approximately 85% water, which provides hydration to the infant. The remaining 15% comprises an assortment of macromolecules and essential micronutrients that play crucial roles in infant development. Within the macromolecule fraction, lactose accounts for approximately 50%, serving as the primary carbohydrate source in breast milk. Lipids, encompassing essential fatty acids and other vital compounds, constitute ~30% of the macromolecules, providing energy and aiding in the absorption of fat-soluble vitamins. Proteins contribute ~9%, delivering essential amino acids necessary

for growth and development. HMOs make up the remaining ~11% of the macromolecules, representing a diverse array of complex carbohydrates exclusive to human milk. Of the HMOs present, three dominant oligosaccharides are highlighted. The first is 2'-fucosyllactose (2'-FL), followed by Lacto-*N*-fucopentaose I (LNFP I) and Lacto-*N*-neotetraose (LNnT). These three HMOs collectively constitute approximately 50% of the total HMOs secreted in breast milk. The remaining 50% encompasses other HMOs, including 3-fucosyllactose (3-FL), Lacto-*N*-fucopentaose II (LNFP II), Lacto-*N*-hexaose (LNH), Lacto-*N*-tetraose (LNT), 3'-sialyllactose (3'-SL), 6'-sialyllactose (6'-SL), and over 200 additional structures.

1.1. HMO Composition

HMOs are generally composed of five different sugar units, glucose (Glc), galactose (Gal), *N*-acetylglucosamine (GlcNAc), fucose (Fuc) and sialic acid (Sia) primarily in the form of NeuAc (**Table 1.1**). More than 200 different HMO structures have been identified in human milk to date and the composition of HMOs can vary greatly between individual lactating mothers[6].

Table 1. 1: **Composition of HMOs**

Name	**Shorthand**	**Letter Symbol**	**Symbol**
Galactose	Gal	A	
Glucose	Glc	G	
N-acetylglucosamine	GlcNAc	GN	
Fucose	Fuc	F	
N-acetylneuraminic acid	NeuAc	NN	

HMOs can generally be further divided into subclasses based on their chemical structure. The composition of HMOs in breast milk is highly variable, influenced by factors such as genetics (particularly the mother's secretor status), stage of lactation and environmental factors. "Secretor Positive"[7] and "Lewis Positive"[8] individuals express specific enzymes involved in HMO synthesis, impacting the types and quantities of HMOs produced (**Table 1.2**). HMOs are broadly categorised into several groups based on their structural components, including neutral (core) HMOs[9], sialylated HMOs[10] and fucosylated HMOs[11]. Neutral HMOs, lacking a charge and neither acidic or basic, include examples such as LNT, LNnT and Lacto-*N*-fucopentaose IV (LNFP IV) (**Table 1.3**). Fucosylated HMOs characterised by a fucosyl group, include structures such as 2'-FL and 3-FL (**Table 1.4**). Sialylated HMOs which are characterised by the presence of a sialic acid residue, typically feature configurations such as 3'-SL and 6'-SL (**Table 1.5**).

Table 1. 2 **: Classification of Lewis and Secretor Phenotypes and Their Associated HMOs**

Classification	***Se* (FUT2)**	***Le* (FUT3)**	**Fucose linkages**	**HMOs Secreted**
Lewis Positive, Secretor Positive	+	+	**α1-2, α1-3, α1-4**	**All HMOs**
Lewis Positive, Secretor Negative	–	+	**α1-3, α1-4**	**3-FL, LNFP-II, LNFP-III**
Lewis Negative, Secretor Positive	+	–	**α1-2, α1-3**	**2′-FL, 3-FL, LNFP-I, LNFP-III**
Lewis Negative, Secretor Negative	–	–	**α1-3**	**3-FL, LNFP-III, LNFP-V**

Table 1. 3 **: Names, Abbreviations and Structures of a sample of Neutral HMOs**

Name	Abbreviation	Structure	Reference
Lacto-*N*-tetraose	LNT	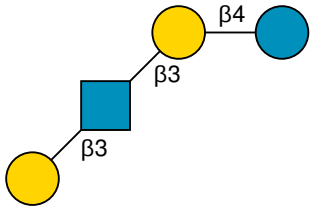	12 13
Lacto-*N*-neotetraose	LNnT	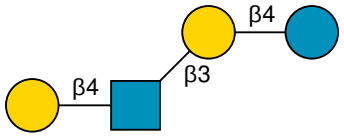	12 13
Lacto-*N*-hexaose	LNH	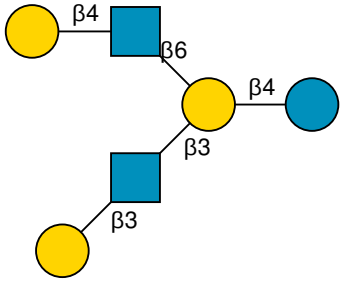	12 13
Lacto-*N*-neohexaose	LNnH	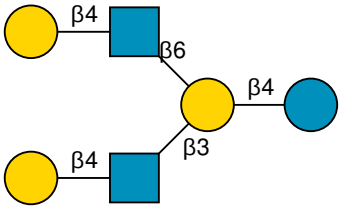	12 13

Table 1. 4**: Names, Abbreviations and Structures of a sample of Fucosylated HMOs**

Name	Abbreviation	Structure	Reference
2'-Fucosyllactose	2'-FL	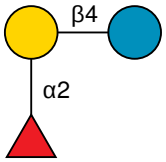	12 13
3-Fucosyllactose	3-FL	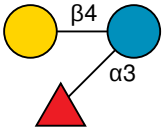	12 13

Difucosyllactose	DFL	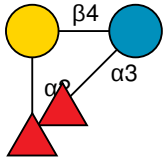	12 13
Lacto-*N*-fucopentaose	LNFP-I	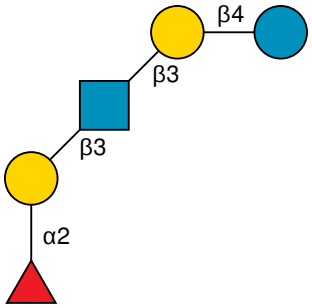	12 13
	LNFP-II	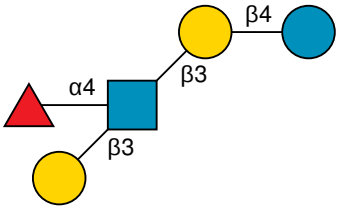	12 13
	LNFP-III	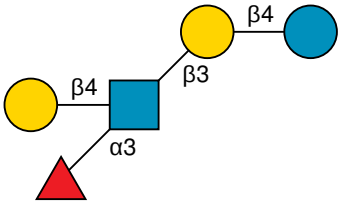	12 13
	LNFP-V	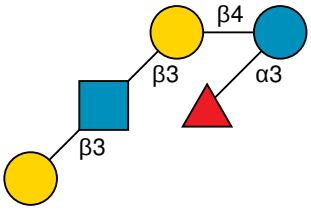	12 13
	LNFP-VI	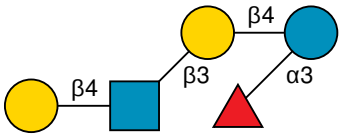	12 13

Difucosylsialyllacto-*N*-hexaose*	DFS-LNH-I	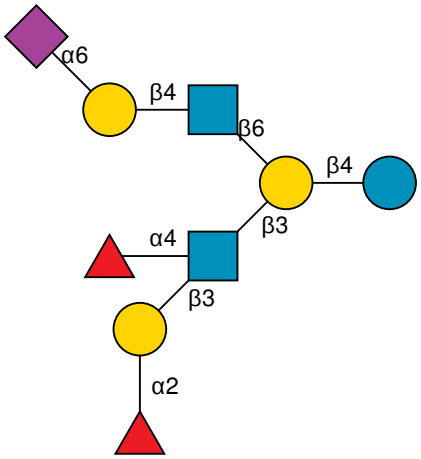	12 13

***Both fucosylated and sialylated**

Table 1. 5: **Names, Abbreviations and Structures of a sample of Sialylated HMOs**

Name	Abbreviation	Structure	Reference
3'-Sialyllactose	3'-SL	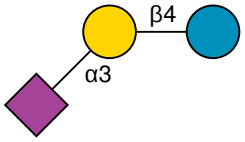	12 13
6'-Sialyllactose	6'-SL	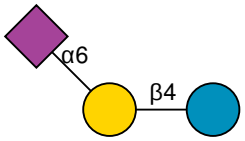	12 13
Sialyllacto-*N*-tetraose	LST a	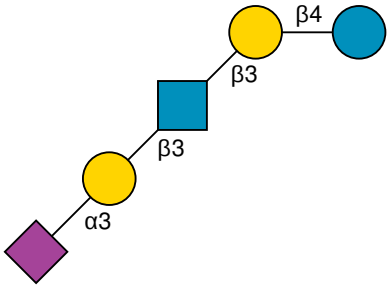	12 13
	LST b	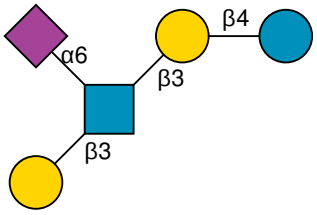	12 13

	LST c	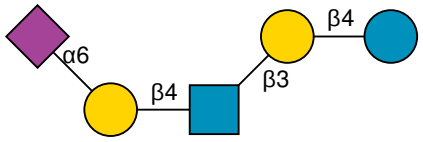	12 13
Disialyllacto-*N*-tetraose	DSLNT	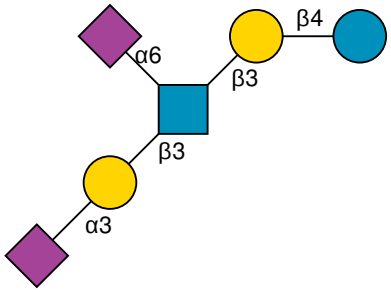	12 13
Fucosylsialyllacto-*N*-neohexaose*	FS-LNnH-I	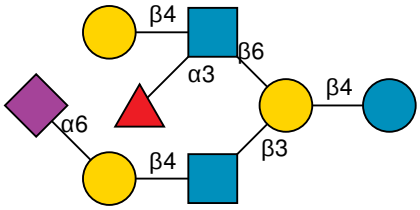	12 13

***Both fucosylated and sialylated**

1.2. Indirect Implications of HMOs on Immune System Function

HMOs can influence broader immune functions both directly and indirectly. A significant mechanism of indirect immune influence is via the gut microbiota whereby HMOs intricately shape the gut microbiota composition, fostering a beneficial bacterial repertoire that in turn alter various immune pathways. Whether by promoting health-associated microbiota or by directly engaging with gut associated immune cells, HMOs influence the overall development and function of the host immune defences (**Figure 1.2**). HMOs elicit expression of inflammatory cytokines and chemokines in gut epithelial cells which allows for the recruitment of innate immune cells. HT-29 colonic epithelial cells were shown to produce a variety of cytokines; such as IL-8, IL-1b, and IL-17C and chemokines; CXCL1, CXCL3, CCL20[14], all of which are key chemoattractants and inflammatory cytokines with the ability to activate a range of immune cells. It is thought that this mechanism occurs to prevent prevalence of pathogenic bacterial colonisation in the gut through priming innate immune cells. HMOs can also enhance mucosal immunity by inducing antimicrobial peptides, secretory IgA antibodies[15] and other immune factors that contribute to mucosal

defence mechanisms. This helps bolster the innate and adaptive immune responses against infections at primary pathogen contact points in the body.

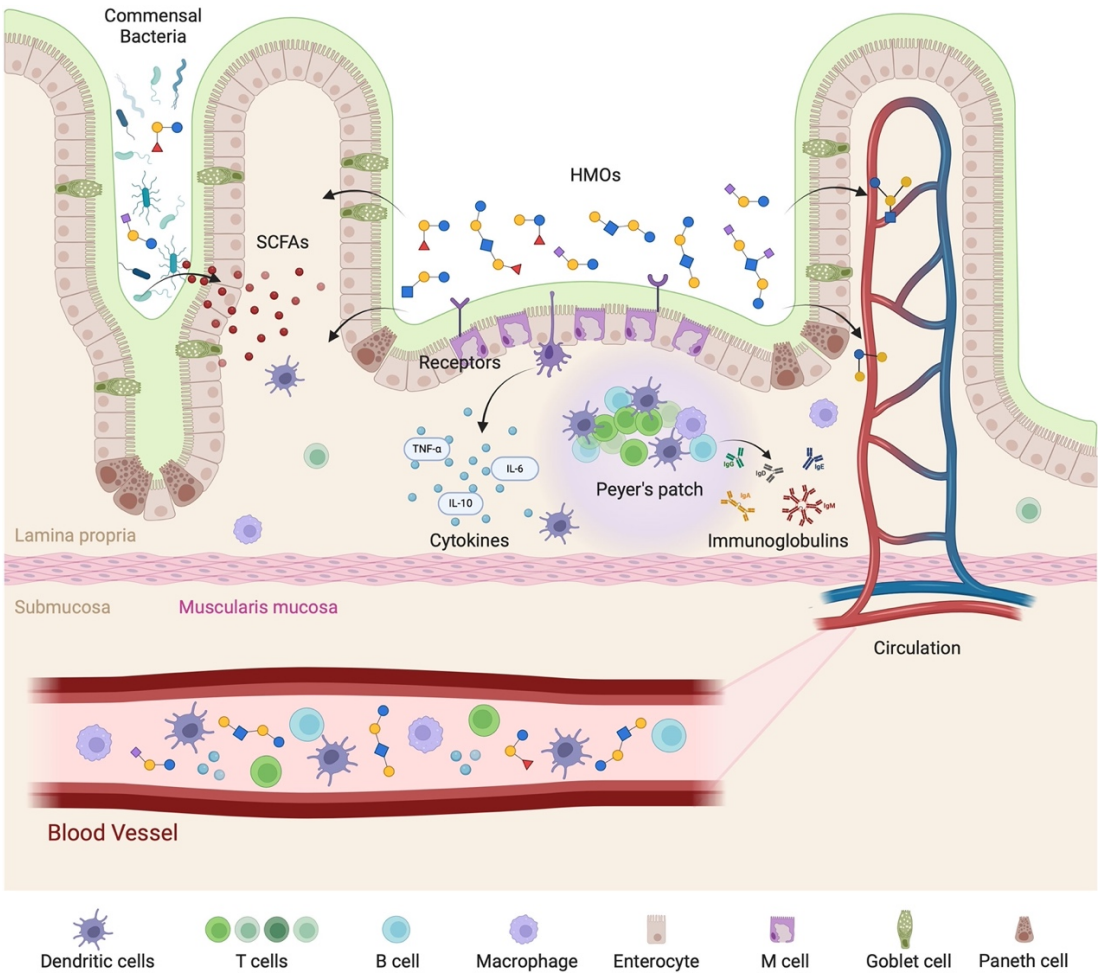

Figure 1. 2: **Mechanistic Representation of HMOs Interaction with the Gut-Immune Axis.**

Effects of HMOs on the Immune System Through Modulation of The Microbiome

These complex sugars facilitate microbial diversity in the infant gut by nurturing various beneficial bacterial species[16]. A diverse gut microbiome correlates with improved overall health outcomes, including better nutrient absorption[17], bolstered immune function, and defence against pathogens[18]. Furthermore, HMOs are recognised for their role in maintaining the integrity of the gut barrier by promoting mucin production[19,20], which is

essential for preventing harmful bacteria and toxins from crossing the gut lumen into the bloodstream. HMOs act as a nutritional source for specific beneficial bacteria, such as *bifidobacteria* and *lactobacilli*, in the infant gut. These bacteria possess glycosidase enzymes capable of breaking down and fermenting HMOs, enabling them to thrive and dominate the gut microbial community[21,22]. Among these, *Bifidobacteria* stand out for their adeptness at utilising HMOs as a fermentation substrate[23]. Consequently, breastfed infants who receive HMOs through breast milk typically harbour a higher abundance of *bifidobacteria* in their gut microbiome compared to their formula-fed counterparts. This selective enrichment of *bifidobacteria* contributes to a more favourable microbial composition overall.

Short-chain fatty acids (SCFAs) also arise from the microbial fermentation of indigestible dietary components within the intestinal tract, serving as an energy source for colonocytes[24]. HMOs are selectively fermented by commensal bacteria, such as *bifidobacteria,* as well as lactobacilli[25], and *Anaerobutyricum hallii*[26], which positively impact the gut microbiome[27], and produce SCFAs[28]. Upon absorption by colonocytes, SCFAs engage with G protein-coupled receptors (GPCRs)[29] and through their interaction with specific receptors and enzymatic pathways, can have a positive impact on the gut barrier, reduce inflammation, and enhance immune function[30]. SCFAs are involved in the metabolism which regulates obesity, type-2-diabetes and insulin resistance[31] therefore their production through HMO fermentation in the gut plays a role in the outcome of these diseases. Additionally, SCFAs modulate histone deacetylases (HDACs)[32], further influencing intestinal mucosal immunity, barrier integrity, and cellular function. Acetate (C2), being convertible to Acetyl-CoA, is a crucial substrate in protein acetylation reactions and can directly influence cellular signalling. Enhanced acetate levels promote the acetylation of glyceraldehyde 3-phosphate dehydrogenase (GAPDH) and augment glycolytic pathways[33], which in turn can give rise to Th1 CD4+ T-cells. Peripherally, SCFAs influence systemic inflammation mainly by inducing Treg differentiation and by regulating the secretion of interleukins[34-36]. These intricate interactions emphasise the pivotal role of HMO-induced SCFAs in orchestrating diverse cellular processes crucial for maintaining intestinal homeostasis and immune function.

Protective Properties of HMOs

Certain HMOs can directly inhibit the growth of pathogens. Various HMOs were found to significantly inhibit the growth of three strains of Group B *Streptococcus* (GBS), indicating antimicrobial activity. This was determined by comparing bacterial biomass in the presence and absence of HMOs, showing significant inhibition across different growth conditions[37].

HMOs can also enhance the effectiveness of antibiotics against MDR bacteria by lowering the minimum inhibitory concentration (MIC) of various antibiotics (gentamicin, erythromycin, clindamycin and minocycline) by a significant amount against GBS[38]. Furthermore, HMOs can boost the potency of trimethoprim, an antifolate antibiotic, resulting in a substantial decrease in MIC against GBS compared to the antibiotic alone[39]. In the case of viral infection; HMOs, 2′FL, LNnT, 6′SL and 3′SL, were studied *in vitro* for their ability to prevent influenza and RSV infections[40]. Results showed that 6′SL and LNnT pre-treatments for 24 hours reduced influenza replication in 16HBE respiratory epithelial cells. RSV protection was shown with 2′FL pre-treatments in both 16HBE and Calu-3 cell lines, but 3′SL pre-treatments only protected in the 16HBE cells. This pre-treatment of respiratory epithelial cells with HMOs may act to strengthen the structural integrity of cell-cell adhesion, similar to what HMOs do in the gut to prevent gastrointestinal bacterial infections[41-43].

Recent research has revealed that HMOs have antimicrobial and antibiofilm effects against gram-positive bacteria, particularly against *Enterococcus faecalis* and *E. faecium* in their planktonic forms and also reduce *S. aureus* biofilm formation[44]. These findings align with previous research indicating the effectiveness of HMOs against primarily Gram-positive bacteria with Ackerman et al. demonstrating biofilm reduction in *Streptococcus agalactiae* and *S. aureus* by 93% and 60% respectively[37] corroborated by other studies[45]. This inhibition of biofilm formation by HMOs may contribute to reducing the virulence and pathogenicity of such bacteria. *In vitro* experiments utilising 3'-SL and 6'-SL resulted in the reduced adhesion of *Clostridium difficile* to human colon cells. Additionally, a downregulation was shown of the *cwp84* gene[46], encoding the Cwp84 protein, a key virulence factor of *C. difficile* which is involved in biofilm formation[47]. As well as preventing biofilm formation, HMOs may also disrupt the structure of biofilm matrices formed by pathogenic bacteria, making them more susceptible to antimicrobial agents or

immune defences. For example, previous studies have demonstrated that HMOs could interfere with the biofilm matrix of GBS[48], a common neonatal pathogen. This disruption of biofilm integrity may enhance the efficacy of antimicrobial treatments against GBS infections.

HMOs possess anti-adhesive properties, in which they inhibit bacterial attachment at mucosal surfaces. A pivotal step in pathogen establishment throughout the body, including the gut and respiratory tract[49]. They do this by acting as decoy receptors, through competitively binding to PAMPs, preventing their adhesion to host cell receptors and subsequent invasion into epithelial cells. This interference disrupts the pathogen's ability to establish infection, thereby conferring protection to the host. HMOs are capable of preventing the attachment of many pathogenic bacteria such as *Escherichia coli*[50], *Vibrio cholerae*, *Salmonella fyris*[51], *Campylobacter jejuni*[52], *Helicobacter pylori*[53,54], and *Streptococcus pneumoniae*[55], or viruses including *Human Rotavirus*[56] and *Parainfluenza Virus (SV5)*[57], among others[58]. The pathogens bind to HMOs which heavily resemble glycan receptors that these pathogens target on the surface of epithelial cells. For example, 2′-FL can mimic the norovirus receptor, blood group antigen (HBGA), serving as a decoy to inhibit the virus attaching to its receptor; HBGA [59]. *In vitro* studies have demonstrated that 2′-FL and 3-FL inhibited the infection of Vero E6 cells by SARS-CoV-2 pseudoviruses. Both HMOs were most effective against the Omicron variant. This suggests that 2′-FL and 3-FL have potential antiviral activity against SARS-CoV-2, by interfering with viral receptor binding [60]. In a similar fashion of preventing pathogenic uptake into epithelial cells via binding glycan receptors by binding to the pathogens, HMOs can bind to the glycan receptors themselves, also preventing pathogenic attachment and establishment within the epithelia.

1.3. Receptors For HMOs and Immune System Interaction

The impact of HMOs on the immune system may be linked to their interaction with specific glycan-binding receptors known as lectins that are expressed on the surface of intestinal epithelial cells. The interaction of HMOs with specific receptors plays a critical role in shaping the development and function of the infant immune system (**Figure 1.3**).

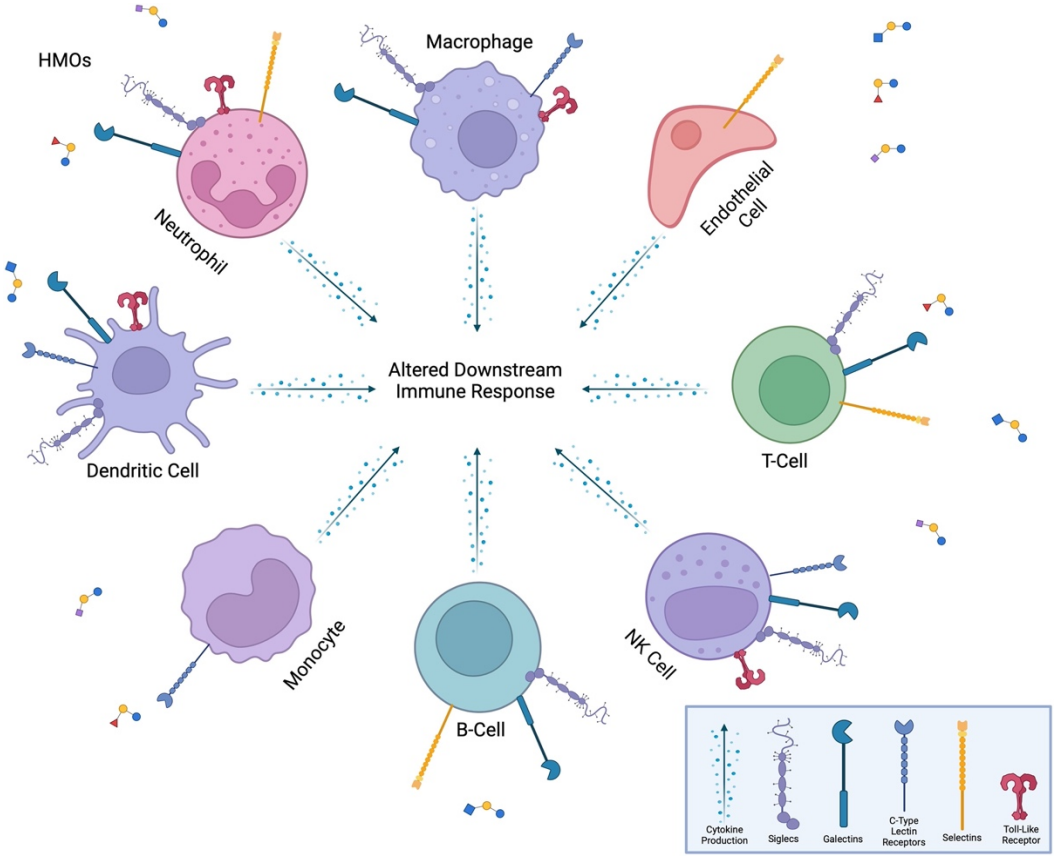

Figure 1. 3**: Interaction of HMOs with Immune Cells and Receptors.**

HMOs influence a diverse range of immune cells, including neutrophils, macrophages, DCs, monocytes, B-cells, T-cells, NK cells, and endothelial cells. HMOs bind to various immune cell surface receptors, modulating immune cell functions. These interactions lead to altered downstream immune responses, such as changes in cytokine production, cell activation, or metabolic activity, thereby shaping the overall immune response.

Galectins, a class of glycan-binding proteins, play crucial roles in intracellular signalling, intercellular communication, cellular proliferation, and survival. These endogenous lectins are expressed and secreted by various cell types, including immune cells, tumor cells, and endothelial cells [61]. Notably, certain HMOs containing β1-3- or β1-4-linked galactose at their non-reducing end can potentially serve as targets for galectin-mediated interactions. A study employing catch-and-release electrospray ionisation mass spectrometry (CaR-ESI-MS) examined the binding affinities of HMOs with three different human galectins Gal-1 (stable mutant of the protein), Gal-3 (C-terminal fragment of the protein), and Gal-7. The

findings revealed that 25 of the 31 HMOs examined exhibit a high binding affinity to these galectins[62,63]. Another study has shown that oligosaccharides can also bind to Gal-2, Gal-8 and Gal-9 as well as the previously mentioned Gal-1, Gal-3 and Gal-7[64].

Several studies have highlighted the potential interactions between HMOs and Sialic-Acid-Binding Immunoglobulin-Like Lectins (siglecs) which are known to bind sialylated glycans[65] and are considered regulators of the immune system[66]. For example, certain HMOs containing sialic acid residues; such as 3'-SL and 6'-SL can serve as ligands for several siglecs expressed on immune cells[67]. HMOs have been found to bind to half of the 14 siglecs currently identified as being expressed on human immune cells, albeit with relatively low affinity[67-71]. By binding to siglecs, HMOs may modulate immune cell function, including activation, migration, and cytokine production

C-type lectin receptors (CLRs) are a diverse group of receptors expressed on various immune cells, including DCs, macrophages, and neutrophils. These receptors recognise specific carbohydrate structures, including those found on pathogens and host cells, and play critical roles in immune surveillance, pathogen recognition, and immune cell activation[72]. Several studies have suggested that HMOs can interact with CLRs expressed on the surface of immune cells such as selectins[73-75] or DC-SIGN[71,76]. HMOs may regulate immune cell activation, cytokine production, and antigen presentation by binding to these CLRs, thereby shaping the developing infant immune system.

Toll-Like Receptors (TLRs) are primarily distinguished as a class of Pathogen Recognition Receptors which recognise very specific Pathogen Associated Molecular Patterns (PAMPs). Multiple studies have shown the interaction between HMOs and TLR4, a receptor known for recognising bacterial lipopolysaccharides (LPS)[77]. HMOs such as 3'-SL[78,79] has been shown to competitively inhibit the activation of TLR4, thereby reducing inflammatory responses and promoting immune homeostasis in the infant gut. Whereas LNFP-III[80,81] induces TLR4 activation leading to the maturation of type-2 DCs which induce a Th2-type T-cell response. This interaction helps prevent excessive immune activation and inflammation, contributing to the development of immune tolerance. HMOs such as 3-FL and LNT2 have been shown to activate TLR2[82], which is involved in

recognising lipid-containing microbial components[83]. HMOs including LNT2[82] and 3'-Galactosyllactose (3'-GL)[78] have also been found to interact with and inhibit TLR3, which recognises viral double-stranded RNA[84]. LNT2, LNnT and 3-FL have been reported to also interact with TLR5[82], which recognises bacterial flagellin[85]. HMOs have been shown to interact with TLR9, which recognises unmethylated CpG motifs present in bacterial DNA[86].

1.4. Immunological Impacts HMOs

There is now evidence that HMOs are present in infant blood, urine and faeces[87-90], which allows us to assume that HMOs interact with cells of the circulating immune system and not just those present at the gut barrier and Gut-Associated Lymphoid Tissue (GALT) (**Figure 1.4**). Many studies have been conducted on how HMOs impact the gut microbiota, and in turn the immune system, but the mechanistic interaction between HMOs and circulating immune cells is still largely unknown. Studies to date that have analysed the effect of HMOs on immune cells have largely focussed on the effect of pooled HMOs isolated from breastmilk, which contains unknown amounts and types of HMOs[14,91-93]. However, an in-depth knowledge on the specific activity of individual HMOs on immune cells is lacking. Due to the variability of types and quantities of HMOs among individual donors, many studies often convey variable results.

HMOs play a vital role in modulating gut immunity and systemic immune responses. HMOs influence GALT by interacting with receptors on enterocytes and immune cells, leading to the release of cytokines such as TNF-α, IL-6, and IL-10. HMOs also promote the growth of beneficial commensal bacteria, which produce SCFAs that support mucosal immunity and gut barrier integrity. Additionally, HMOs are involved in the activation of Peyer's patches, stimulating B cells to produce immunoglobulins that contribute to immune defence. The effects extend beyond the gut, as HMOs and immune-modulating factors enter circulation to influence systemic immune responses.

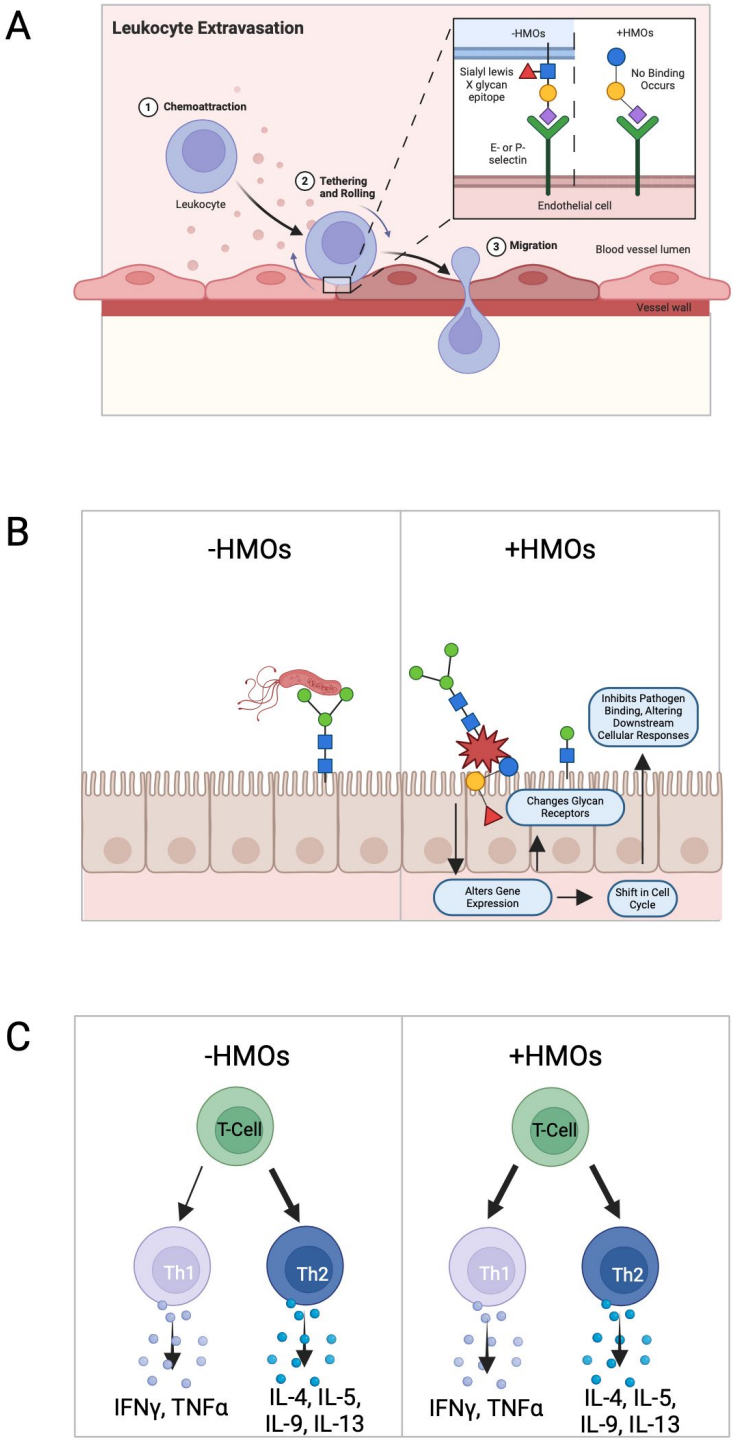

Figure 1. 4**: Known Effects of HMOs on the Immune Response**

(a) HMOs reduce selectin-mediated cell-cell interactions within the immune system. This reduction in leukocyte rolling on activated endothelial cells can potentially minimise mucosal leukocyte infiltration and activation, thereby influencing immune cell dynamics. (b) HMOs directly influence intestinal epithelial cells, modulating the expression of genes involved in various cellular processes leading to alterations in cell surface glycans and other

cellular responses, thereby impacting gut health and functionality. (c) HMOs possess the ability to modulate the production of cytokines by lymphocytes, promoting a balanced Th1/Th2 immune response.

Macrophages

Macrophages are phagocytic cells derived from monocytes that play a crucial role in both innate and adaptive immunity. They engulf and digest pathogens, debris, and dead cells, acting as scavengers and antigen-presenting cells (APCs). Macrophages also secrete cytokines and chemokines to regulate immune responses, promote inflammation, and coordinate tissue repair[94]. HMOs can influence the activation state of macrophages and promote the polarisation of macrophages towards an anti-inflammatory M2 phenotype. Data from a study analysing macrophages in an ischemic stroke mouse model indicated that 2-'FL increases the expression of M2-type genes and decreased M1-type genes[95]. LNFPIII activates macrophages *in vitro* as indicated by upregulation of Gr-1 expression in F4/80+ cells[96]. Additionally, macrophages exposed to LNnT expanded a cell population, phenotypically defined as Gr1+/CD11b+/F4/80+ which typically possess an anti-inflammatory cytokine profile [97]. Using the murine macrophage-like RAW264.7 cell line, a specific fraction of neutral HMOs isolated from breast milk decreased production of nitric oxide (NO) and Prostaglandin-E2 (PGE2)[91] which have been shown to stimulate macrophage polarisation towards a M2 phenotype[98].

In this same study the isolated HMO fraction was observed to stimulate the release of reactive oxygen species (ROS) in RAW264.7 macrophages which aids in bacterial clearance. The study also demonstrated that this fraction activates macrophages through the Nuclear Factor Kappa B (NFκB) and Mitogen Activated Protein Kinase (MAPK) signalling pathways. Further studies analysing *Pseudomonas aeruginosa* K (PAK) infection in THP-1 macrophage-like cells, showed an increase in ROS production but additionally displayed the rapid return of ROS levels to basal amounts post clearance of infection[99]. These results show that HMOs elicit the ROS production to aid in bacterial clearance by macrophages but do not allow for enhanced inflammation due to prolonged ROS production.

HMOs have also been found to enhance the phagocytic activity of macrophages, increasing their ability to engulf and eliminate pathogens. In one study, 2′FL intervention resulted in the higher percentage of macrophage phagocytosis in offspring of supplemented mice as compared to the control group[100]. This enhanced phagocytosis may contribute to the overall antimicrobial activity of macrophages and aid with more effective infection clearance. Another study also showed that sialylated HMOs promoted bacterial clearance through enhanced phagocytic activity [99] thought to be elicited by the presence of sialic acid binding receptors present on macrophages promoting phagocytosis. However, a different study investigating THP-1 cells treated with 6'-SL showed that 6'-SL alone slightly increased phagocytic activity. Cells treated with LPS and 6'-SL, actually decreased phagocytosis compared to cells treated with LPS alone and subsequently a decrease in ROS production was observed with LPS and 6'-SL treated cells[101].

As well as altering physical attributes of macrophage function, HMOs have also been shown to inhibit the infiltration of macrophages to sites of inflammation and also alter population distribution. A study analysing a model of acute lung injury (ALI) demonstrated that mice that were intraperitoneally administered with 3'-SL and 6'-SL prior to LPS challenge had significantly reduced immune cell infiltration caused by LPS[102]. Additionally, a study analysing the ototoxic effect of neomycin demonstrated that 6'-SL prevented the increase in number of macrophages in the cochlear spiral ganglion[101]. This HMO driven mechanism in reducing the infiltration of macrophages to the site of injury or infection, may help limit tissue damage and promote resolution of inflammation. HMOs may also induce changes in population distribution of monocytes and macrophages as these cell populations were observed to be higher in the mesenteric lymph nodes (MLN) with 7 day HMO supplementation of C57BL/6 orally gavaged with 15 mg/day in an *in-vivo* study, while in the spleen, this population was lower in all HMO-supplemented groups compared to their control[103]. 2'-FL and LNFP-I, used in a concentration which could be considered physiological, negatively influenced mononuclear cells (MNC) activation by decreasing their proliferation in a dose-dependent fashion[104].

HMOs can also modulate inflammatory responses in macrophages by influencing the production of inflammatory mediators. Some studies propose that HMOs may modulate

cytokine production in immune cells towards a more balanced and less inflammatory state. For instance, certain HMOs have been shown to promote the production of anti-inflammatory cytokines such as IL-10 and IL-4 while suppressing the secretion of pro-inflammatory cytokines such as IL1b, IL8, TNF-α and pleiotropic IL-6[102]. 2'-FL and LNFP-I have an inhibitory role on interferon gamma (IFN-γ) and IL-12 production *ex vivo* particularly in MS patients, and prime release of the Th2 cytokine IL-10, displaying an immunomodulatory effect *ex vivo* [104]. A LNnT treated Gr1+/F4/80+ population of macrophages produced lower levels of proinflammatory cytokines, but higher levels of IL-10 and TGF-β *ex vivo*, compared to the untreated control[97]. These findings imply that HMOs could contribute to immune homeostasis and mitigate excessive inflammatory responses helping regulate immune responses. However, other studies in contrast, suggest that the effects of HMOs on cytokine production are inconsistent or even pro-inflammatory in certain cases. For example, in a study analysing LPS activated monocyte-derived macrophages, 3-FL and 3′-SL increased IL-6 secretion. High doses of 2′-FL increase the levels of TNF-α and LNT2 increasing levels of IL-12p70. These results demonstrate that sialylated HMOs and 3-FL added to classically-activated M1 macrophages enhance pro- and anti-inflammatory cytokine production[42].

Specific HMO structures may enhance the production of pro-inflammatory cytokines under certain conditions, potentially exacerbating inflammatory responses. It seems generally that fucosylated HMOs influence an anti-inflammatory cytokine profile, whereas sialylated HMOs have more of a pro-inflammatory cytokine output. The effects of HMOs on cytokine production may vary depending on factors such as cell type, concentration, and the presence of other immune-modulating molecules. These contextual factors can influence the direction and magnitude of immune responses to HMOs and therefore may warrant further research to elucidate the specific mechanisms of action.

Dendritic Cells

DCs are professional APCs that play a pivotal role in initiating adaptive immune responses. They capture antigens in peripheral tissues, process them, and migrate to lymphoid organs where they present antigens to T-cells, in turn activating them. DCs bridge the innate and adaptive immune systems by linking recognition of pathogens to the activation of specific

immune responses[94]. HMOs can influence the maturation state of DCs. A mixture of HMOs derived from human milk samples were found to induce a partially mature state in human monocytes-derived DCs (moDCs), resulting in increased levels of anti-inflammatory IL-10, IL-27, and IL-6, but not pro-inflammatory IL-12p70 and TNF-α[92]. These HMO-treated moDCs, in turn, facilitate the generation of regulatory T-cells (Tregs) from naïve CD4+ T-cells. Notably, this study found that HMOs limited the maturation of human moDCs induced by LPS while maintaining secretion of IL-10 and IL-27 and reducing production of IL-12p70, IL-6, and TNF-α triggered by LPS. This also resulted in higher number of Tregs, while showing a decrease in the number of Tbet+ Th1 cells and IFN-γ production compared to LPS-stimulated moDCs [92]. In an *in vivo* study, peripheral blood mononuclear cells (PBMCs) and MLNs of HMO-fed non-infected pigs had three times less plasmacytoid DCs (pDCs) than those of formula-fed non-infected pigs. In the MLNs, the HMO-fed non-infected pigs had less macrophages, pDCs, and mature DCs but more immature DCs than formula-fed non-infected pigs[105] indicating a potential role of HMOs in modulating DC populations and immune responses.

HMOs can also influence the cytokine production profile of DCs. In one such study, 3′-SL and 6′-SL increased the production of key pro-inflammatory cytokines IL-12p70, IL-23 and TNF-α, and anti-inflammatory IL-6 (in this case) and IL-10 from LPS-activated DCs. 2'-FL has also been shown to induce IL-6 production in DCs[106,107]. In LPS-activated moDCs, 3-FL, 3'-SL, and 6'-SL led to a marked increase in the secretion of IL-6, IL-12p70, IL-23, and TNF-α. However, only the sialylated HMOs caused a significant rise in IL-10 secretion[42]. 3-FL showed a modest immunomodulatory effect by significantly boosting IL-6 and IL-23 secretion levels[108]. These findings, along with other studies, highlight that both the sialylated and fucosylated HMOs enhance production of pro- and anti-inflammatory cytokines in activated DCs, in turn influencing T-cell polarisation thus promoting Th1, Th17, and regulatory immune responses[42,79].This differs from the previous study as individual sialylated HMOs are investigated rather than a mixture of unknown HMOs in unknown quantities isolated from breast milk. MoDCs exposed to 2′-FL and CpG-conditioned Intestinal Epithelial Cells (IECs) induced IFNγ and IL-10 secretion by CD4+ T-cells, promoting the development of a Treg response[109]. This modulation of cytokine production by DCs may contribute to the overall regulation of immune responses by HMOs.

HMOs have been reported to promote immune tolerance in DCs. By inducing the production of anti-inflammatory cytokines and inhibiting the release of pro-inflammatory mediators, HMOs may help dampen DC-mediated immune responses and promote the development of immune tolerance[92]. In mice fed with 1% 2′-FL increased activation of DCs was present in the spleen, evident by higher levels of CD86+ and CD40+ markers. There was also a slight increase in the percentage of CD11c+ MHCII+ DCs. In the MLNs, 2′-FL led to an increase in tolerogenic DCs (CD103+ CD11c+ MHC-II+), known for inducing Tregs and gut-homing molecules. Additionally, CD86 expression decreased while CD40 expression increased in MLN DCs, suggesting a shift towards a more tolerogenic phenotype[110]. Another study showed that HMOs altered the expression levels of programmed-death-ligand-1 (PD-L1) and OX40-L both of which are expressed on healthy APCs such as DCs[111,112] and were significantly increased in the presence of LPS and HMOs as compared to untreated immature DCs, pointing to the potential of HMOs inducing Tregs and skewing immune responses[113] towards homeostasis.

HMOs can affect the antigen-presenting function of DCs and modulate the expression of co-stimulatory molecules[114] but not major histocompatibility complex (MHC)[105] molecules on DCs. This was further confirmed by demonstrating in a vaccine model, that 2'-FL induced higher population of antigen specific CD4+ T-cells compared to the untreated control vaccine model[110]. This regulation of antigen presentation of DCs by HMOs may influence the activation and differentiation of T-cells and shape the overall immune response.

T-Cells

T-cells are a type of white blood cell that play a central role in cell-mediated immunity. They can be further divided into several subsets, including CD8+ cytotoxic T-cells (CTLs), CD4+ helper T-cells (Th1, Th2, Th17, Tfh), and Tregs. CTLs destroy infected or abnormal cells, Th cells assist other immune cells by releasing cytokines and activating B-Cells, while Tregs help maintain immune tolerance and prevent autoimmune reactions[94]. The interaction between HMOs and T-cells is an intricate one. With numerous HMO variants potentially engaging with these circulating lymphocytes, HMOs are known to regulate the

balance between promoting pro- and anti-inflammatory T-cell responses. Different HMOs may induce varied alterations in T-cell phenotypes, and these effects can be context-specific, depending on whether the immune system is in a state of homeostasis or facing an infection. Taking this into consideration, studies involving HMOs interaction with T-cells have led to varied results.

HMOs have the ability to modulate the immune system and reduce inflammation, as they may skew T-cells to balance Th1 and Th2 responses[115]. Sialylated HMOs derived from pooled human milk were shown to increase IFNγ producing CD4+ and CD8+ T-cells after long term exposure, as well as promote IL-13 producing CD8+ T-cells derived from human cord blood MNC[93]. This study also revealed that these acidic HMOs increased the amount of CD25+/CD4+ T-cells, which are a regulatory subpopulation of T-cells. This was the first indication that HMOs encouraged the establishment of a Th1/Th2 balance. These findings suggest that HMOs impact cytokine production and activation of cord blood-derived T-cells *in vitro*. Hence, oligosaccharides, particularly acidic structures, may influence lymphocyte maturation in breastfed newborns. An *in-vivo* study demonstrated that 7 and 14 days of HMO supplementation led to a reduction in CD4+ and CD8+ T-cells in the MLN at 28 and 35 days when compared to GF controls. However, by day 50, the CD4+ T-cell population had increased in both the 7- and 14 day HMO-treated groups in the MLN. In the spleen, no significant differences were noted at days 28 or 35, but CD4+ T-cell numbers rose at day 50 in both HMO-treated groups. Additionally, the CD4+ to CD8+ T-cell ratio in the MLN increased at day 35 following 14 days of HMO treatment[103]. This agrees with another *in-vivo* study where HMO-fed pigs were found to have 36% more MLN effector memory T-cells compared to the control feed group[105]. Memory T-cells are antigen-experienced cells that mediate a faster and more potent response upon repeat encounter with antigen [116] and therefore HMOs may increase this population to aid in the rapid clearance of certain recurring infection in infants.

HMOs can influence the differentiation of T-cells into different effector subsets. Neonatal rats given daily doses of 2'-FL showed an elevated proportion of T-cells, in both Th and CTL populations. The 2'-FL treatment resulted in a higher percentage of CD62L+ Th lymphocytes. CD62L also known as L-selectin is a key cell adhesion molecule on

lymphocytes and facilitates their migration to lymph nodes for immune surveillance, playing an essential role in initiating immune responses by allowing T-cells to exit the bloodstream[117]. 2'-FL did not however, affect T-cells expressing the activation marker CD25. Additionally, the CTL increase was seen in both TCRαβ+ and TCRγδ+ subsets[118]. *Ex vivo* HMO co-stimulation affected Th cell populations in PBMCs and decreased Th cell populations in response to LPS stimulation. Co-stimulation with isolated HMOs decreased Th cell populations derived from PBMCs stimulated with LPS. This study found that co-stimulation with a sialyllactose mix, or isolated HMO decreased CD4+CD8+ T-cell populations under conditions that would normally stimulate T-cells[119]. Interestingly, a different study analysing HMOs and bovine milk oligosaccharides (BMOs) found that feeding 2'-FL and LNnT or sialic acid-enriched BMOs to 2 day-old pigs through supplemented diets did not alter the profile of PBMC lymphocyte populations. The study findings indicated a synergistic effect of both BMOs and HMOs on Th cell populations[120] suggesting that a more complex combination of oligosaccharides, similar to what is found in human milk, is needed to produce a Th phenotypic cell distribution in formula-fed animals similar to that of breastfed infants. Treatment of female 6-week-old C57BL/6J mice with 2′-FL reduced the proportion of Th17 cells and suppressed Th17-related cytokine production in a skin-inflammation mouse model. Additionally, 2′-FL inhibited the phosphorylation of STAT3 in skin tissue, reducing recruitment of Th17 cells. *In vitro* work in this same study culturing naïve CD4+ T-cells found that 2′-FL inhibited the differentiation of Th17 cells, STAT3 phosphorylation, and RORγt mRNA levels in T-cells under Th17 polarisation[121].

HMOs have been shown to modulate T-cell activation by directly interacting with T-cells or by affecting the function of APCs such as DCs. Certain HMOs, such as 2'-FL, have been found to enhance T-cell activation by promoting the maturation and antigen-presenting capacity of DCs, which subsequently leads to an increase in T-cell proliferation and cytokine production. HMO-conditioned human moDCs promoted Treg generation from naive CD4+ T-cells. Furthermore, HMOs+LPS stimulated DCs induced a higher frequency of Tregs and increased IL-10 production, while a reduction in Th1 frequency and IFN-γ production was detected when compared to LPS-DCs[92]. Studies have also suggested that acidic HMOs enhanced the secretion of IFN-γ and IL-17A from CD4+ T-cells primed by activated DCs and macrophages while reducing the secretion of IL-13. Thus, these

sialylated HMOs 3′-SL and 6′-SL support Th1 and Th17 responses while reducing Th2 responses[42]. HMOs may induce Th1 and Th17 T-cell phenotypes over Th2 to support host defence, tissue repair, and balanced immune responses in breastfed infants. In the MLNs, 2′-FL led to an increase in tolerogenic DCs, which subsequently induce Tregs and gut-homing molecules[110]. However certain HMOs, such as LNFP-III and LNnT have also been observed to indirectly repress Th1 cell proliferation; doing so by promoting the expansion of Gr1+ cells which suppresses naive CD4+ T-cell proliferation *ex vivo*. Coculture with Gr1+ cells does not induce CD4+ T-cell apoptosis but leads to reduced IFN-γ levels and increased IL-13 production[97]. These findings suggest a ligand-specific mechanism of HMOs, resulting in the generation of anti-inflammatory mediators that suppress Th1-type and inflammatory responses.

HMOs have also been reported to induce T-cell tolerance, which is important for preventing autoimmune reactions and maintaining immune homeostasis. By promoting the differentiation and activation of Tregs, HMOs can help suppress excessive immune responses and prevent autoimmune diseases. Offspring of mothers with gestational diabetes mellitus (GDM) were treated with 3′-SL resulting in a significant increase in the proportion of Treg cells and upregulation of RORγt expression[122]. RORγt is crucial for maintaining mucosal tolerance in the gut, and RORγt+ Tregs play a direct role in protecting against food allergy[123]. This indicates that administering HMOs to GDM offspring promotes the development of immune tolerance in newborns.

HMOs can modulate the production of cytokines by T-cells, influencing the balance between pro- and anti-inflammatory immune responses. Studies have shown that certain HMOs can enhance the production of anti-inflammatory cytokines such as IL-10 while reducing the production of pro-inflammatory cytokines such as IFN-γ and IL-17 by T-cells. Treatment with 2′-FL reduced Th17-related cytokine production in a skin-inflammation mouse model. These findings suggest that 2′-FL alleviates psoriasis by modulating the Th17 immune response and cytokine secretion which the authors suggested to be via the STAT3 signalling pathway[121].

When discussing modulation of T-cell function, it is important to consider implications for vaccine efficacy. T-cells play a crucial role in vaccine-mediated immunity, particularly in generating long-term protection against pathogens. Therefore, the question arises as to whether HMOs may alter or promote vaccine function through T-cells. Female 6-week-old C57BL/6JOlaHsd mice in a murine influenza vaccination model receiving high supplemented 2′-FL diet, had a 13% higher CD4+ and a 7.4% higher CD8+ T-cell population detected in comparison to the control vaccinated group, suggesting dietary intervention with 2′-FL increased vaccine-specific T-cell responses. Administration of acidic oligosaccharides boosted vaccine-specific delayed-type hypersensitivity (DTH) responses in a dose-dependent manner *in vivo* by measuring ear swelling in mice 24 hours post antigen injection. This coincided with a decrease in the production of Th2 cytokines by splenocytes *ex vivo* [124]. The findings suggest that the dietary intervention shifted the systemic immune response to the vaccine towards a Th1-skewed profile. Further to this, another study demonstrated the dietary supplementation of the HMO 3'-GL increased Th1 cell activation and attenuated deoxynivalenol (DON)-induced effects in Th1 cell responses in a preclinical influenza vaccine model[125]. Another dietary study in 6 week-old female C57BL/6JOlaHsd mice, containing 2'-FL with short-chain galactooligosaccharides (scGOS) and long-chain fructooligosaccharides (lcFOS) resulted in increased influenza vaccine specific DTH responses, Tregs, and Th1 cells in their MLNs [126]. Additionally, in a Th2-skewed formalin-inactivated respiratory syncytial virus (FI-RSV) vaccination model in mice, acidic HMOs were shown to reduce RSV-specific Th2 cytokine-producing CD4+ T-cells 4- and 6 days post-infection. This was accompanied by increased IFN-γ-producing CD4+ and CD8+ T-cells at 8 days post-infection. These results indicate that particular dietary oligosaccharides may affect the trafficking and effector functions of CD4+ and CD8+ T-cell subsets in the lungs of mice infected with RSV [127]. This is interesting as we enter into a post antibiotic era where a heightened response is needed to develop vaccines for multi-drug resistant (MDR) bacterial species, especially for ESKAPE pathogens which are a group of bacteria known for their ability to "escape" the effects of antibiotics. ESKAPE pathogens include *Enterococcus faecium, Staphylococcus aureus, Klebsiella pneumoniae, Acinetobacter baumannii, Pseudomonas aeruginosa* and *Enterobacter species*. Enhancing Th1 effector T-cell responses is proposed as a key target for vaccine development, given that this T-cell subset is crucial for effectively clearing infections. Memory Th1 cells provide protection against invasive *S. aureus* infection[128] which a vaccine is desperately needed against. Since HMOs have been shown to boost Th1 cell

responses, incorporating these oligosaccharides into a vaccine could be a viable approach to developing a much-needed vaccine against critical pathogens, including *S. aureus.*

1.5. Immune Cell Metabolism

Although HMOs are primarily discussed in the context of with the gut and associated gut microbiota, their potential to influence immune cells and their metabolism has been largely overlooked. Immune responses are fundamentally shaped by metabolic programming; macrophages, DCs and T-cells rely on defined shifts between glycolysis, oxidative phosphorylation, and lipid metabolism to determine activation state, cytokine output, and effector function. These metabolic phenotypes are not secondary consequences of activation but actively regulate immune behaviour[129-131].

While pathways such as fatty acid oxidation, amino acid metabolism, and the pentose phosphate pathway also contribute to immune regulation, the balance between oxidative phosphorylation and glycolysis remains the central axis of immunometabolic control[132]. In macrophages, this balance diverges depending on activation state: resting or alternatively activated (M2-like) macrophages rely predominantly on oxidative phosphorylation and intact tricarboxylic acid (TCA) cycle function to sustain tissue repair, anti-inflammatory signalling, and phagocytosis of necrotic cells. Whereas classically activated (M1-like) macrophages undergo a metabolic shift towards aerobic glycolysis, similar to the Warburg effect supporting rapid ATP generation and biosynthetic activity for cytokine production and microbicidal responses[133]. DCs similarly reprogram metabolism upon activation; immature DCs primarily utilise mitochondrial respiration to maintain homeostasis and antigen sampling, but TLR stimulation triggers a glycolytic switch that fuels cytokine secretion and co-stimulatory molecule expression necessary for T-cell priming[134]. T-cells exhibit comparable metabolic shift as naïve and memory T-cells favour oxidative phosphorylation and fatty acid oxidation to support longevity and quiescence. While effector T-cells, particularly Th1, Th17, and cytotoxic $CD8^+$ subsets, rapidly induce glycolysis upon activation to sustain proliferation and effector molecule synthesis[135]. Thus, across macrophages, DCs, and T-cells, the variation between oxidative phosphorylation and glycolysis is not a passive readout of cellular activity but a regulatory mechanism that dictates immune phenotype and function.

Other dietary and microbial metabolites, such as short-chain fatty acids, have been shown to rewire immune cell metabolism[136], yet whether HMOs exert similar effects remains unresolved. Introducing metabolism as a regulatory layer is essential alongside considering immune modulation by HMOs and provides a mechanistic rationale for investigating their impact beyond receptor binding and signalling alone.

1.6. Clinical Relevance of HMOs in Immunity

The intricate interactions of HMOs with the immune system highlight their multifaceted roles in modulating immune responses and promoting health. A significant aspect of HMO function lies in their impact on gut-associated immune responses. HMOs indirectly modulate the immune system by shaping the gut microbiome, fostering a beneficial microbial environment that supports immune cell homeostasis. In addition to this, HMOs exhibit protective properties, offering defence against pathogens and reducing the risk of infections. However, HMOs directly show immunomodulatory effects and elucidating how these bioactive compounds influence immune cell behaviour and developmental immunomodulation is warranted. HMOs engage with specific receptors on immune cells, leading to diverse responses that are critical during the early stages of immune system development.

The clinical implications of HMOs are profound, particularly in managing allergic diseases, where they have been shown to reduce the incidence and severity of allergic reactions[137-142 140,143]. Their potential in addressing autoimmune[104,144-146] and inflammatory diseases[147-149] also presents a promising avenue for therapeutic intervention. HMOs have immunomodulatory effects beyond infancy and their therapeutic applications are expanding, with ongoing research exploring their efficacy in various clinical settings. Although further clinical studies are needed to elucidate the mechanisms of action and optimise the therapeutic potential of HMOs in these contexts.

The most commonly found HMOs, namely 2'-FL, 3’-SL, and LNT, have been extensively studied for their health benefits. Despite the significant insights gained from these common HMOs, HMOs such as lacto-*N*-hexaose (LNH), disialyllacto-*N*-tetraose II (DSLNT II) and

others remain underexplored. One major reason for this is the difficulty in isolating and producing HMOs commercially. Their low abundance in human milk and the complexity of their structures make it challenging to obtain sufficient quantities for detailed studies. Given the structural diversity and unique properties of these uncommon HMOs, there is a compelling potential for them to exhibit notable immunological effects. Research into these less commonly available HMOs could uncover new mechanisms by which they influence the immune system, offering insights into additional ways that human milk supports infant health and potentially leading to novel therapeutic applications.

1.7. Biosynthesis Pathways of HMOs

The intricate biosynthesis pathways of HMOs are orchestrated by multiple glycosyltransferase reactions. Numerous types of glycosyltransferases are involved in the stepwise construction of HMOs, each adding specific sugars in a defined sequence[150], which ultimately results in the complex structural variety characteristic of HMOs [151] (**Table 1.6**). This sequence-specific action not only ensures the correct architecture of HMOs but also influences their functionality and bioavailability in infant nutrition. An in-depth appreciation of these biosynthetic routes is indispensable for advancing the technology to synthesise HMOs extrinsically, thereby enriching infant formulae with these crucial biochemical constituents. Consequently, this knowledge paves the way for the industrial replication of HMOs, emulating the nuanced biochemical glycan milieu that is naturally present in human milk.

Table 1. 6**: Key Enzymes Involved in HMO Synthesis - Substrates, Products, and Functional Insights**

Enzyme Name	Substrate (Donor)	Substrate (Acceptor)	Product	HMOs Produced	Additional Notes	Refs
Lactose Synthase	UDP-Galactose	Glucose	Lactose	Base unit for HMOs	First enzyme in HMO synthesis,	[152]

					forming lactose.	
B3GALT1	UDP-Galactose	GlcNAc	Lacto-*N*-Biose (LNB)	Base unit for HMOs	First enzyme in HMO synthesis, forming LNB.	[153]
B4GALT1	UDP-Galactose	GlcNAc-containing acceptors	Galβ1-4 GlcNAc (Lactosamine unit)	LNT, LNnT	Adds galactose to form precursors of linear and branched HMOs.	[154] [155]
FUT2	GDP-Fucose	Terminal Gal residues	α1-2-fucosylated glycans	2'-FL	FUT2 activity determines the secretor status in humans.	[156]
FUT3	GDP-Fucose	Galβ1-4GlcNAc residues	α1-3/α1-4-fucosylated glycans	LNFP I	FUT3 is key for Lewis antigen synthesis in HMOs.	[157]
FUT4	GDP-Fucose	Galβ1-4GlcNAc residues	α1-3-fucosylated glycans	LNFP structures	Redundant with FUT3 in some contexts.	[157]
FUT5	GDP-Fucose	GlcNAc or Gal residues	α1-3/α1-4-fucosylated structures	Extended HMOs with α1-3/	Activity overlaps	[158]

				α1-4 linkages	with FUT3 and FUT4.	
FUT6	GDP-Fucose	GlcNAc or Gal residues	α1-3/α1-4-fucosylated glycans	Similar to FUT3, FUT4, FUT5	Key in forming Lewis X antigens.	[158]
ST6GALNAC1	CMP-Sialic Acid	GalNAc residues of O-glycans	α2-6-sialylated glycans	Sialyllacto-*N*-tetraose (LSTa)	Catalyses sialylation of O-glycan cores.	[159]
ST6GALNAC2	CMP-Sialic Acid	GalNAc-Ser/Thr or Galβ1,3GalNAc	α2-6-sialylated glycans	DSLNT	Adds α2-6-linked sialic acid to extended HMOs.	[159]
ST3GAL1	CMP-Sialic Acid	Galβ1-3 GalNAc residues	α2-3-sialylated glycans	Sialyllacto-*N*-neotetraose (LSTc)	Initiates α2-3 sialylation of precursor HMOs.	[160]
ST3GAL3	CMP-Sialic Acid	Galβ1-3/ β1-4Gal residues	α2-3-sialylated glycans	Sialylated branched and linear HMOs	Plays a major role in branching and extending HMOs.	[160]
ST3GAL4	CMP-Sialic Acid	Galβ1-4 GlcNAc residues	α2-3-sialylated glycans	Branched sialylated HMOs	Works in conjunction with FUT enzymes.	[160]

The biosynthesis of HMOs begins with the synthesis of lactose. Lactose, the predominant sugar in human milk, is synthesised from free glucose and UDP-galactose[161] bound by a β1,4 glycosidic bond[152]. This process occurs in the Golgi apparatus of mammary epithelial

cells (MECs). The enzyme lactose synthase (LS; EC 2.4.1.22) is composed of two subunits A: β1,4-galactosyltransferase (encoded by the *B4GALT1* gene; EC 2.4.1.38) and B: α-lactalbumin (encoded by the *LALBA* gene). Together this enzyme complex catalyses the transfer of galactose from UDP-galactose to glucose, forming lactose in the trans-Golgi of MECs.

Fucosylation involves the addition of fucose residues to precursor molecules, including lactose. Fucose can be added in α1-2, α1-3, or α1-4 linkages[162], resulting in different HMO structures. The enzymes responsible for fucose addition are the fucosyltransferases (FUTs), such as FUT1-FUT13, with FUT2,3 and 4 playing the most important role in this mechanism. These enzymes catalyse the transfer of fucose from GDP-fucose as a nucleotide sugar donor to acceptor molecules[163].

Sialylation involves the addition of sialic acid residues to precursor oligosaccharides. Sialic acid can be added in α2-3, α2-6, or α2-8 linkages to terminal positions of oligosaccharide chains. Various sialyltransferase enzymes catalyse the transfer of sialic acid from CMP-sialic acid, to acceptor molecules[164,165], named ST3Gal, ST6Gal, ST6GalNAc, and ST8Sia [166] leading to the formation of structurally diverse HMOs.

The *N*-acetylglucosaminyltransferase family comprises a group of enzymes responsible for catalysing the transfer of *N*-acetylglucosamine (GlcNAc) residues from an activated donor substrate, typically UDP-*N*-acetylglucosamine (UDP-GlcNAc), to acceptor molecules, in this case to the HMO chain. There are several GlcNAc-transferases involved in HMO biosynthesis, including B3GNT2[167]. These enzymes catalyse the formation of numerous linear HMOs, including lacto-*N*-tetraose (LNT) and lacto-*N*-neotetraose (LNnT).

The galactosyltransferase family comprises a group of enzymes responsible for catalysing the transfer of galactose residues from activated donor substrates, such as UDP-galactose or GDP-galactose, to acceptor molecules[168]. Subfamilies of galactosyltransferases include the inverting glycosyltransferases β1-4 (β4GalT), β1-3 (β3GalT), and β1-6 (β6GalT), and retaining galactosyltransferases, α1-3 (α3GalT) and α1-4 (α4GalT), which generate β1-4, β1-3, β1-6, α1-3, and α1-4 linkages, respectively[155]. There are several galactosyltransferases involved in HMO biosynthesis, including B3GALT2 and

B4GALT1[168] with the B3GALT and B4GALT families being the most recognised as being involved in the HMO formation process. These enzymes catalyse the formation of several galactosylated HMOs, including lacto-*N*-tetraose and lacto-*N*-neotetraose.

The glycosyltransferases involved in the elaboration of oligosaccharides can include β1-4 galactosyltransferase, α1-2 fucosyltransferase, α1-3/4 fucosyltransferase, and sialyltransferases. The sequential addition of monosaccharides results in the generation of a wide range of HMO structures with varying glycosidic linkages and branching patterns, contributing to the complexity and functionality of human milk. Further modification of HMOs increases their structural diversity and may enhance their biological activities.

1.8. Current Industrial Methods of HMO Synthesis, Separation and Detection

The current industrial approaches to HMO synthesis primarily involve microbial fermentation with genetically engineered bacteria or yeast, enzymatic synthesis through glycosyltransferases and glycosidases, chemical synthesis, and chemoenzymatic methods. The current synthesis methods used to create HMOs have been widely reviewed [169-172] focusing on optimising production for use in infant formula and other health-related products. Glycosyltransferases play a critical role in these methods, driving the precision and diversity of HMO biosynthesis. While the repertoire of glycosyltransferases involved in HMO biosynthesis is well characterised, efficient reconstruction of these pathways for synthetic or industrial purposes remains a significant challenge due to enzymatic limitations and bottlenecks. Several studies have highlighted that not all glycosyltransferases involved in HMO biosynthesis are equally productive[173]; some exhibit lower catalytic efficiencies or poor expression profiles in heterologous systems, posing hurdles for scalable production. In the case of lactose biosynthesis, although the enzymatic complex lactose synthase (composed of B4GALT1 and α-lactalbumin) is functionally characterised, the rate-limiting step is not always the enzymatic activity itself but rather the availability of glucose in the Golgi apparatus[174], where UDP-galactose is preferentially utilised. In milk oligosaccharide production, the rate-limiting steps often involve the enzymes responsible for fucosylation and other glycosylation reactions, especially in the final steps of biosynthesis, such as the addition of fucose to galactose or N-

acetylglucosamine. In engineered systems, this has necessitated innovations to increase intracellular glucose trafficking or utilisation efficiency. However, because these are enzymes from higher eukaryotes, it was quite difficult to express glycosyltransferases recombinantly in *Escherichia coli.* In recent years, it has been determined that bacterial cell surface glycans also have oligosaccharide structures similar to those of mammalian glycans, which indicates that bacteria also serve as a source of glycosyltransferases and can be expressed in *E. coli*. Recent attempts to mimic these pathways have employed microbial hosts such as *E. coli* and *Saccharomyces cerevisiae*[175], taking advantage of their ability to express bacterial homologs of glycosyltransferases, which are often more tractable and soluble than their mammalian counterparts. Additionally, directed evolution, rational mutagenesis, and structure-guided engineering have been applied to enhance substrate affinity, broaden donor/acceptor specificity, and improve stability of key GTs involved in HMO synthesis[175]. These approaches have led to significant advances in one-pot multienzyme (OPME) systems and *in vivo* HMO biosynthesis platforms[176], although further optimisation is needed to overcome current limitations in yield and structural diversity.

Understanding and addressing these enzymatic bottlenecks is essential not only for improving HMO production but also for expanding the library of accessible glycan structures for functional studies and therapeutic development. Advancing HMO production involves overcoming challenges in scaling glycosyltransferase activity through improved isolation techniques, enhanced enzyme stability, and efficient expression in microbial or mammalian cell cultures. These efforts aim to replicate the benefits of natural HMOs, making them accessible for commercial and therapeutic applications to support infant health and development.

Chemical synthesis involves assembling complex carbohydrate molecules through a series of carefully orchestrated chemical reactions[177]. In the context of HMOs, the core of this process is the glycosylation reaction, where glycosidic bonds between sugar units are formed by reacting an activated glycosyl donor, modified to be highly reactive, with a glycosyl acceptor that has a free hydroxyl group. This reaction is driven by activating agents or catalysts that facilitate the precise formation of these bonds[178]. Chemical synthesis

provides extensive control over the final HMO product, allowing for manipulation of its structure, bond configuration (α or β), regioselectivity (the position of glycosidic bonds), chain length, and branching patterns.

Enzymatic synthesis of HMOs leverages the precision of specific enzymes, to catalyse the assembly of HMOs from simpler sugar molecules. This approach closely mirrors the natural biosynthetic pathways that occur in the human body, where enzymes guide the formation of complex carbohydrate structures with exacting accuracy. Enzymatic synthesis stands out for HMO synthesis due to its high selectivity and mild reaction conditions, making it a sustainable and efficient method for producing HMOs. Several reviews provide in-depth discussions on the catalytic mechanisms of glycosyltransferases relating to the optimisation of enzyme-based HMO synthesis for industrial applications[179,180].

Microbial fermentation for the synthesis of HMOs utilises genetically engineered microorganisms, such as bacteria or yeast, to produce HMOs in significant quantities[181-183]. Advances in strain engineering, fermentation optimisation, and metabolic pathway modifications to enhance HMO yields are reviewed elsewhere[184,185]. These microorganisms are specifically modified to express the enzymes required for HMO biosynthesis including glycosyltransferases, enabling them to efficiently assemble these complex carbohydrates from precursors provided in the fermentation medium. The engineered microbes are cultivated in large-scale fermentation tanks under carefully controlled conditions, including temperature, pH, and nutrient availability, to optimise growth and productivity. During the fermentation process, the microbes metabolise simple sugars or other carbon sources, using them as substrates to drive the enzymatic assembly of HMO structures[185]. As they grow and metabolise these substrates, the introduced enzymes catalyse the step-by-step formation of specific HMOs, which are then secreted into the surrounding fermentation broth. Following fermentation, the HMOs are extracted from the broth and undergo a purification process to remove microbial cells, proteins, and other impurities, resulting in the production of pure, desired oligosaccharides.

Recent advancements in biotechnology have enabled the production of HMOs through the overexpression of glycosyltransferases and other enzymes in engineered systems. For

example, α1,2-fucosyltransferase FutBc from *Bacillus cereus* was utilised for the production of 2′-FL. The *futBC* genes, along with *LAC12*, were introduced into *Saccharomyces cerevisiae*, which produced 27 g/L of 2′-FL from lactose and sucrose[186]. Companies such as Jennewein Biotechnologie, Inbiose, and Abbott Laboratories have patented innovative approaches for HMO synthesis using genetically modified bacteria, such as *Escherichia coli*, transgenic non-human mammals and engineered cell lines. These patents cover the production of various HMOs, including 2'-FL, 3-FL, LNT, and sialylated oligosaccharides, highlighting their potential applications in infant formula and therapeutic products. Bacteria have been widely utilised as host systems, with companies such as Jennewein Biotechnologie GmbH producing sialylated oligosaccharides, 2'-FL, and 3-FL (patents US20210087599A1, EP2927316A1, and WO2010142305A1). Similarly, Glycosyn LLC has focused on generating fucosylated oligosaccharides in bacteria, with patents US9970018B2 and US10815511B2. Yeast-based systems have also proven effective, as demonstrated by Amyris Inc, which developed yeast strains to produce 2'-FL (US10519475B1). Beyond microbial platforms, transgenic non-human mammals have been employed by Abbott Laboratories for the production of HMOs, including 2'-FL and complex glycoproteins (US5750176A, US6204431B1, and US5700671A). Additionally, neutral, non-fucosylated HMOs have been synthesised using genetically engineered cells, including bacteria, yeast, and animal cells, by Inbiose (US12077788B2).

Several HMOs have been produced at a large scale and received regulatory approval for inclusion in infant formulas. The most common HMOs commercially available are 2'-FL and LNnT, both of which have been approved by the U.S. Food and Drug Administration (FDA), the European Food Safety Authority (EFSA)[187], and other regulatory bodies. These HMOs are synthesised using microbial fermentation or enzymatic processes[180]. In the EU, HMOs are regulated as Novel Foods, whereas in the United States, they are categorised as "Generally Recognised as Safe (GRAS)" substances. Indeed, 2'-FL and LNnT are now commonly added to many commercial infant formulas[188] to more closely mimic the benefits of natural breast milk[189,190], contributing to the overall health and development of formula-fed infants. Infant formula containing 2'-FL and LNnT is safe, well-tolerated, and promotes growth appropriate to infant age[191]. As of December 2023 HMOs approved in both the EU and the United States include: 2'-FL[192], 3-FL[193], LNT[194], LNnT[195], 3'-SL[196] and 6'-SL[197], a 2'-FL/difucosyllactose (DFL) mixture[198], and an LNFP-I/2'-FL mixture[199].

The inclusion of these HMOs in infant formulas is a significant advancement in paediatric nutrition, bridging the gap between formula and breast milk, subsequently improving growth and development in infants.

1.9. *In Silico* Advances in Glycosyltransferases and HMO Synthesis

Recent advances in *in silico* modelling have revolutionised our understanding of glycosyltransferases and their application in HMO synthesis. Computational approaches now enable the prediction, simulation, and optimisation of glycosylation pathways, significantly accelerating research and development in this field. The rapid advancements in glycobiology have been supported by the development of comprehensive databases and analytical tools, which facilitate the study of glycosylation patterns and enzyme functions critical for HMO biosynthesis[200]. Additionally, computational approaches, such as knowledge-based systems, have proven effective in predicting glycosylation network behaviour and modelling the effects of enzyme knockouts on *O*-glycosylation, offering strategic insights for glycoengineering applications[201]. Tools such as Rosetta[202] and AlphaFold[203] have provided high-resolution models of these enzymes, facilitating the identification of active sites and key residues involved in substrate binding and catalysis. These insights are particularly valuable for engineering glycosyltransferases with enhanced activity, specificity, or stability, essential for efficient HMO production. Pathway analysis software, such as O-Glycologue, allows for the *in silico* reconstruction of glycosylation networks[204,205]. This tool generates predictive models of oligosaccharide biosynthesis, enabling researchers to map out and optimise glycosyltransferase-mediated pathways for HMO synthesis (**Figure 1.5**)[13]. By incorporating enzyme kinetics, substrate availability, and reaction conditions, these simulations help identify bottlenecks and propose modifications to improve yield and efficiency. The use of machine learning algorithms further enhances the predictive power of *in silico* studies. By analysing large datasets of glycosyltransferase sequences and activities, machine learning models can predict enzyme behaviour under different conditions and suggest mutations to tailor enzymes for specific HMOs [206,207]. Coupled with molecular docking and molecular dynamics simulations, these models provide a comprehensive toolkit for rational enzyme design.

In the context of HMO synthesis, these *in silico* advancements could enable the design of highly efficient synthetic pathways. For example, computational approaches have been used to identify and engineer glycosyltransferases for increased turnover rates and reduced byproduct formation[208,209], with the potential to facilitate scalable HMO production. For example, Rosetta enzyme design has been applied to engineer UGT76G1, resulting in enhanced thermostability and activity. Additionally, predictive models are being used to identify novel glycosyltransferases with unique capabilities, broadening the repertoire of enzymes available for synthetic biology applications.

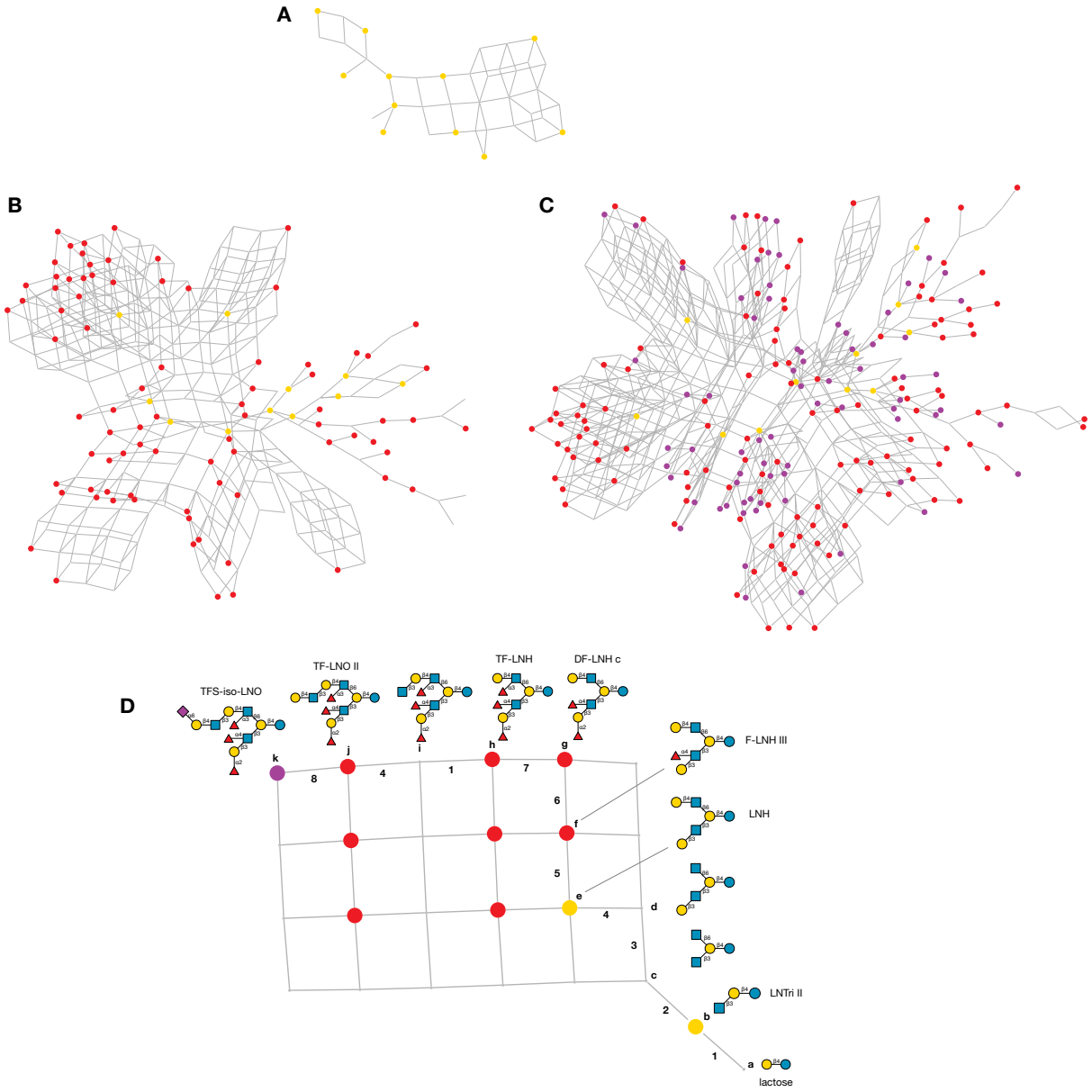

Figure 1. 5: **Networks of HMO biosynthesis simulated using Glycologue.**

Minimal reaction networks generated using the HMO-Glycologue enzyme simulator [201]. Larger nodes represent experimentally characterised structures, coloured according to the type: yellow (core), red (neutral) or purple (acidic), while smaller nodes represent the intermediates predicted by the simulator. **A**. Core structures, afucosylated and asialylated. **B**. Neutral (fucosylated, asialylated) HMOs. **C**. Acidic (sialylated) HMOs. **D**. A proposed biosynthetic network of the acidic HMO, TFS-iso-LNO [210] [151], showing the reactions catalysed by eight of the glycosyltransferase enzymes assumed to be active during lactation: (**1**) β3GnT (iGnT, EC 2.4.1.149) ; (**2**) dIGnT (EC 2.4.1.386); (**3**) β3GalT (EC 2.4.1.86); (**4**) β4GalT (EC 2.4.1.38); (**5**) α4FucT (EC 2.4.1.65); (**6**) α2FucT (type 1) (EC 2.4.1.69); (**7**) α3FucT (EC 2.4.1.152); (**8**) ST6Gal (EC 2.4.3.1). The sequence of enzyme activities (**1**,**2**,**3**,**4**,**5**,**6**,**7**,**1**,**4**,**8**) produces the path through nodes labelled **a**-**k**.

1.10. Analytical Techniques in HMO Structure Elucidation

Quantifying and profiling the diverse range of HMOs is crucial for understanding their role in infant nutrition and for the quality control of HMO production processes. Various analytical techniques are employed to detect different HMOs, determine their quantities, and profile their types. The analysis of HMOs often utilises a separation method paired with a detection system that can deliver linear response curves to determine oligosaccharide concentrations. These methods ensure accurate identification and quantification of HMOs in both natural and industrially synthesised samples. Prior to using analytical technique for HMO quantification and elucidation, HMO samples are processed and isolated, be that from breast milk or alternative synthesis methods. These extractions include; solid phase extraction[211], centrifugal fat separation[212], liquid extraction[213], ultrafiltration[214], organic solvent precipitation[215], and gel filtration chromatography[216].

High-performance liquid chromatography (HPLC) is extensively used for separating and quantifying HMOs[217]. An advantage of HPLC is its ability to accurately quantify industrially synthesised HMOs of known structure, enabling precise monitoring of production yield and purity.

Capillary electrophoresis (CE) separates HMOs based on their charge-to-mass ratio[218] and offers high resolution and efficiency. Techniques such as capillary zone electrophoresis (CZE) and capillary gel electrophoresis (CGE) are employed to analyse HMOs. A big problem with CE is the fact that the migration of the HMOs is determined by this charge-to-mass ratio, which means that structural isomers will elute at the same time, such as 3'-SL and 6'-SL, 2'-FL and 3-FL, etc[219].

Mass spectrometry is a vital tool for the identification and quantification of HMOs due to its sensitivity and specificity[220]. This analytical technique identifies and quantifies substances by measuring the mass-to-charge ratio of ionised particles. Mass spectrometry enables the identification of unknown HMO structures by analysing their molecular weight and fragmentation patterns. Techniques such as Matrix-Assisted Laser Desorption/Ionisation (MALDI-MS) and Electrospray Ionisation (ESI-MS) are widely used[221].

Nuclear Magnetic Resonance (NMR) Spectroscopy is primarily used for structural elucidation[222], it can also quantify HMOs by integrating the signals corresponding to different oligosaccharides[223]. Quantitative NMR (qNMR) provides accurate and non-destructive quantification of HMOs without the need for extensive sample preparation. NMR is particularly useful for analysing complex mixtures and providing absolute quantification of individual components[224].

1.11. Aims of Thesis

Investigating glycosyltransferases and their involvement in HMO biosynthesis opens new opportunities for advancing HMO production methods. By uncovering the intricate mechanisms through which these enzymes assemble complex oligosaccharides, we can identify key targets for optimising synthetic production systems. Such advancements have the potential to improve commercial scalability and also deepen our understanding of the therapeutic applications of HMOs in immune modulation and beyond. By improving our ability to produce HMOs commercially, these insights pave the way for exciting advancements in both research and industry.

Additionally, despite evidence that HMOs play critical roles in shaping early immune development directly and indirectly, the precise mechanisms by which individual HMOs influence immune cell function remain insufficiently defined. Most current literature relies on pooled HMO preparations, *in-vivo* models, indirect readouts such as microbiota-mediated effects, or epithelial and immune co-culture models that do not resolve cell type-specific responses. While several studies suggest that HMOs can directly modulate macrophages, DCs, and T-cells, the reported effects are inconsistent across experimental systems, concentrations, and sources of HMOs. Furthermore, the structural selectivity of immune recognition, whether different sialylated or fucosylated HMOs engage distinct receptors or metabolic pathways remains unclear.

Therefore, this thesis aims:

- To characterise the immunometabolic and immunomodulatory effects of individual HMOs; specifically 2'-FL, 3'-SL, and 6'-SL on primary murine immune cells, with a focus on macrophages, DCs, and T-cells.
- To develop and validate a mammalian cell-based platform for human milk oligosaccharide biosynthesis by engineering HEK293 cells to express key glycosyltransferases involved in lactose elongation and terminal sialylation.

These aims will enable further mechanistic dissection of how HMO structures influence immune function while simultaneously establishing a platform to generate defined HMOs for future functional, therapeutic, and translational studies.

Chapter 2

Materials and Methods

2.1. Materials and Reagents

2.1.1. Reagents

Antimycin A (AA), Adenosine Triphosphate (ATP), Bovine Serum Albumin (BSA), Calcium Chloride, cOmplete™ Mini EDTA-free Protease Inhibitor Cocktail, Cytochrome C, Decylubiquinone (DQ), D-Glucose, Dipotassium Hydrogen Phosphate (Monobasic), DMSO, DTT, EDTA, Ethanol, FCCP, Fetal Bovine Serum (FBS), Ferricyanide, Gentamicin Solution, HEPES, Isopropanol, Itaconate, L-glutamine 100X, Magnesium Chloride, Magnesium Sulphate, MES, Methanol, NADH, NP-40 lysis buffer, Penicillin-Streptomycin Solution, Phosphate Buffered Saline, Poly-D-Lysine, Potassium Cyanide, Potassium EDTA, Potassium Phosphate, Rotenone (Rot), Sodium Acetate Solution, Sodium Chloride, Sodium Hydroxide, Sodium Pyruvate, Succinate, Sucrose, Tetramethyl Ethylenediamine, Trizma Base, Trypsin-EDTA - **Sigma Aldrich, UK.**

AlamarBlue Cell Viability Reagent, Digitonin 5%, Dulbecco's Modified Eagle Medium (DMEM), FastDigest BamHI, FastDigest Bpu10I, FastDigest Bpu1102I, FastDigest EcoRI, FastDigest PfoI, FastDigest Van91I, GeneJET PCR Purification Kit, High glucose (4500 mg/L) RPMI 1640 (1x), Lipofectamine 2000, Trypan Blue solution, L-Glutamine, Manganese(II) chloride tetrahydrate, Mouse Granulocyte Monocyte Colony Stimulating Factose (GM-CSF) Recombinant Protein, Opti-MEM™ I Reduced Serum Medium, pHrodo™ Red S. aureus Bioparticles® conjugate for phagocytosis, Pierce Chromogenic Endotoxin Quant Kit, Pierce Coomassie (Bradford) Protein Assay Kit, SYBR™ Safe DNA Gel Stain, Ultrapure Agarose. - **Thermo Scientific, UK.**

ELISAMAX IL-1β kit, ELISAMAX TNF-α kit, ELISAMAX IL-10 kit, TMB Substrate Reagent Set, Recombinant Mouse IL-10 Protein, Recombinant Mouse IFNγ Protein, Recombinant Mouse IL-4 Protein - **Biolegend.**

Seahorse DMEM media, Seahorse XF assay buffer, Seahorse cell culture plates, utility plates and calibrant solution - **Agilent Technologies, UK.**

Gibson Assembly® Cloning Kit, Q5® High-Fidelity 2X Master Mix - **New England Biolabs UK**

Eagle's Minimum Essential Medium (EMEM) - **American Type Culture Collection (ATCC).**

LPS from E. coli, Serotype EH100 (Ra) (TLRGRADE®) - **Enzo Life Sciences, Inc.**

QIAprep Spin Miniprep Kit, QIAquick Gel Extraction Kit - **Qiagen.**

HP RNA Isolation Kit, Lightcycler 480 Sybr Green I Master - **Roche Diagnostics Ltd.**

SensiFAST cDNA Synthesis Kit **- Meridian Bioscience**

2'-Fucosyllactose (2'-FL), 3'-Sialyllactose (3'-SL), 6'-Sialyllactose (6'-SL), UDP-a-D-galactose, UDP N-acetylglucosamine, GDP-L-fucose, CMP-Neu5Ac - **Biosynth, UK (formerly Carbosynth)**

5-HMO mix was purchased from **Layer Origin** and was comprised of 61.8% 2'-Fucosyllactose (2'-FL), 12.3% Lacto-N-tetraose (LNT), 11.3% Lacto-N-neotetraose (LNnT), 10.5% 6'-Sialyllactose (6'-SL), and 4.1% 3'-Sialyllactose (3'-SL)

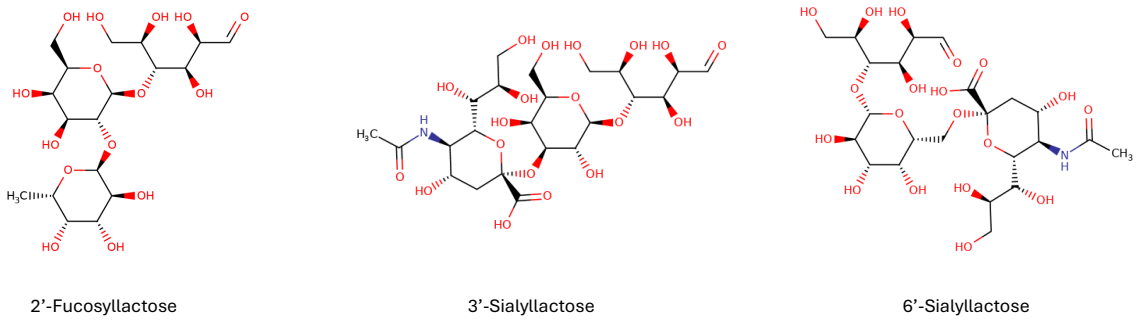

2'-Fucosyllactose 3'-Sialyllactose 6'-Sialyllactose

Figure 2. 1: **Chemical Structure of HMOs Used From Carbosynth**

2.1.2. Antibodies

Table 2. 1: **Western Blot Antibodies**

Antibody	**Supplier**	**Dilution**	**Diluent**
Anti-IkBa	Cell Signalling Technology	1 in 1000	5% Milk/TBST
Anti-B-actin	Cell Signalling Technology	1 in 5000	5% Milk/TBST

Table 2. 2: **Functional Antibodies**

Antibody	**Supplier**	**Dilution**	**Diluent**
Anti-CD3	BD Pharmingen	1 in 1000	Media
Anti-CD28	BD Pharmingen	1 in 4000	Media

Table 2. 3: **Flow Cytometry Antibodies**

Antibody	Supplier	Dilution	Diluent
Live/Dead - BV-510	BD Horizon	1 in 500	PBS
Live/Dead - ZombieAqua	BD Phamingen	1 in 1000	PBS
FC Block	Santa Cruz Biology	1 in 100	PBS
CD11c - PE-Cy7	BD Phamingen	1 in 2000	FACS Buffer
CD11b - PE-Cy7	BD Phamingen	1 in 2000	FACS Buffer
F480 - PerCP5.5	eBioSciences	1 in 2000	FACS Buffer
CD80 - FITC	BD Phamingen	1 in 2000	FACS Buffer
CD86 - PE	Invitrogen	1 in 2000	FACS Buffer
MHC-II - efluor450	Invitrogen	1 in 2000	FACS Buffer
CD3 - FITC	Invitrogen	1 in 2000	FACS Buffer
CD4 - BV421	Invitrogen	1 in 2000	FACS Buffer
CD8a - PerCPCY-5.5	Invitrogen	1 in 2000	FACS Buffer
CD62L - APC	Invitrogen	1 in 2000	FACS Buffer
CD19 - PeCy7	Invitrogen	1 in 2000	FACS Buffer
MitoSOX - PE	BioScience	1 in 1000	PBS

2.1.3. Plasmids

All Plasmids used were obtained from DNASU Plasmid Repository (Arizona State University). Samples are acquired as glycerol stocks in T1/T5 phage resistant DH5-α bacteria. Mammalian expression vector pGEn2-DEST with a CMV promoter and N-terminal 8xHis, AviTag, and Super GFP tags; ampicillin resistance in bacteria was used.

Figure 2. 2**: PGEN2-DEST Vector Plasmid from DNASU Plasmid Repository**

2.2. Buffers

All buffers were pH measured by a corning pH meter model 240, which was calibrated daily using standard buffer solution of pH 4.0, 7.0 and 10.0.

ELISA Buffers

10X PBS: NaCl: 80 g, KCl: 2 g, Na_2HPO_4: 14.4 g, KH_2PO4: 2.4 g and ddH_2O: 800 mL. Dissolve well, then adjust pH to 7.4. Bring up the volume to 1 L with ddH_2O, sterilised by autoclaving.

1X Wash Buffer: 100 mL 10X PBS, 900 mL ddH2O, 50 µL Tween-20

1X Blocking Buffer: 10 mL 10X PBS, 90 mL ddH2O, 1 g BSA. Dissolve well.

Stop Solution: 0.5 M H_2SO_4

Golgi Isolation Buffers

Homogenisation Media (HM): 200 mL dH2O, 0.25 M Sucrose, 10 mM Tris.Cl, pH 7.4

Sucrose Gradient Solutions: 100 mL dH2O, 2 M Sucrose, 10 mM Tris.Cl, pH 7.4. Dilute as needed with 10 mM Tris.Cl pH 7.4 for 1.6 M, 1.2 M and 1 M Sucrose Gradient Solutions

Agarose Gel Buffers

10X TAE Buffer: 1 L dH2O, 48.5 g Tris, 11.4 mL glacial acetic acid, 20 mL 0.5 M EDTA (pH 8.0)

Complex Buffers

STE Buffer: 1 L dH2O, 320 mM Sucrose, 10 mM Tris, 1 mM EDTA, pH 8

Complex I Buffer: 250 mL dH2O, 25 mM KH2PO4, 10 mM $MgCl_2$, pH 7.4

Complex II/III Buffer: 250 mL dH2O, 100 mM KH_2PO_4, 0.3 mM K-EDTA, pH 7.4

Flow Cytometry Buffers

FACS Buffer: 1 mL FBS, 49 ml PBS (2% FBS)

Western Blot Buffers

RIPA Buffer: 50 mM Tris pH 8, 150 mM NaCl, 1% TritonX-100, 0.5% sodium deoxycholate, 0.1% SDS.

Running buffer: 25 mM Tris pH 8.3, 190 mM Glycine, 0.1% SDS

Laemmi Buffer: 8% SDS, 20% 2-mercaptoethanol, 40% glycerol, 0.004% bromophenol blue. 0.25 M Tris, pH 6.8

TBST Buffer: 20 mM Tris pH 7.5, 150 mM NaCl, 0.1% Polysorbate 20 (Tween 20)

Transfer buffer: 25 mM Tris pH 8.3, 190 mM Glycine, 20% methanol

Glycosyltransferase Buffers

Lysis Buffer: 50 mM HEPES, 150 mM NaCl, 10% Glycerol, 0.5% Digitonin, 1 mM DTT, 1X protease inhibitor

HEPES Assay Buffer: 50 mM HEPES, 150 mM NaCl, 10% Glycerol, 5 mM $MnCl_2 \cdot 4H_2O$, 0.1% BSA, 1 mM DTT

MES Assay Buffer: 50 mM MES, 150 mM NaCl, 10% Glycerol, 5 mM $MnCl_2 \cdot 4H_2O$, 0.1% BSA, 1 mM DTT

HPLC Mobile Phase

Buffer A: 100 mM NaOH (ultrapure, freshly prepared and degassed)

Buffer B: 100 mM NaOH, 150 mM Sodium Acetate (ultrapure, freshly prepared and degassed)

2.3. Methods

2.3.1. Cell Culture

All cell culture was performed in Class II HEPA-filtered biosafety cabinets. Cultures were maintained in a humidified atmosphere (5% CO_2) at 37°C. Cells were counted using Trypan Blue dye with a Countess Automated Luna Cell Counter (Life Technology). For volumes of 2 mL or less an eppendorf benchtop centrifuge 5415 was used to spin down samples. For volumes 2-50 mL an eppendorf centrifuge 5810R was used. Gilson pipette set was used to pipette volumes from 0.2 µL to 1 mL.

Bone Marrow Derived Macrophages (BMDMs)

Femur and tibia bones were isolated from a mouse, the bone marrow flushed out from each mouse into falcon tube containing 5 mL of DMEM media by inserting the top of the syringe filled with DMEM into the larger orifice and flushed through. This was spun down at 1400

rpm for 5 minutes. The supernatant was discarded. Red blood cell lysis was performed by adding 3 mL of NH_4Cl (Ammonium-Chloride) Lysing Buffer for 2 minutes to remove all the Erythrocytes. This reaction was stopped by adding 7 mL of DMEM. Cells in solution were strained into a fresh falcon. This was then spun at 1400 rpm for 5 minutes and the supernatant was removed. The pellet was re-suspended in 32 mL of DMEM media and 8 mL of L929 media (20%) and added to T-175 flasks. Cells were fed 10% L929 (4 mL) on day 3. On day 6, the cells were scraped, counted and seeded at 1 x 10^6 cells/ mL in DMEM 10% FBS, 10% L929-conditioned medium for at least 3 hours prior to experiments and treatments.

Bone Marrow Derived Dendritic Cells (BMDCs)

Similarly to BMDMs, femur and tibia bones were isolated from a mouse, the bone marrow flushed out from each mouse into falcon tube containing 5 mL of RPMI media by inserting the top of the syringe filled with RPMI into the larger orifice and flushed through. This was spun down at 1400 rpm for 5 minutes. The supernatant was discarded. Red blood cell lysis was performed by adding 3 mL of NH_4Cl Lysing Buffer for 2 minutes to remove all the Erythrocytes. This reaction was stopped by adding 7 mL of RPMI. Cells in solution were strained into a fresh falcon. This was then spun at 1400 rpm for 5 minutes and the supernatant was removed. The resulting pellet was resuspended in 30 mL of RPMI media with 20 ng/mL GM-CSF and then added to T-175 flasks. Cells were fed 30 mL of media with 20 ng/mL GM-CSF on day 3. On day 6 media was replaced with fresh 30 mL of media with 20 ng/mL GM-CSF. On day 8 cells were fed 30 mL of media with 20 ng/mL GM-CSF. Finally on day 10, cells were removed from the flask, counted, and seeded at 1 x 10^6 cells/ mL with 10 ng/mL GM-CSF for at least 3 hours prior to experiments and treatments.

T-Cell Culture

Spleens were harvested from mice and was mechanically disrupted using the plunger of a 5 mL syringe through a 70 μm cell strainer into a sterile petri dish containing 10 mL of RPMI-1640. This was spun down at 1400 rpm for 5 minutes. The supernatant was discarded. Red blood cell lysis was performed by adding 3 mL of NH_4Cl (Lysing Buffer for 2 minutes to remove all the Erythrocytes. This reaction was stopped by adding 7 mL of RPMI. Cells in solution were strained into a fresh falcon. This was then spun at 1400 rpm

for 5 minutes and the supernatant was removed. The splenocytes were resuspended in complete RPMI-1640 medium supplemented with 10% FBS, 1% penicillin-streptomycin, and 1% L-glutamine at a cell density of $10x10^6$ cells/mL in 24-well plates precoated with anti-CD3 (2 µg/mL) to engage the T-cell receptor (TCR). The cells were also cultured in the presence of recombinant mouse IL-2 (20 U/mL) to support survival and proliferation. After 36 hours post activation, the cells were washed and cultured in IL-2 until day 3 where cultures were maintained with fresh IL-2 or IL-15 every day. After 7 days, cells were analysed for activation and proliferation markers or used for downstream applications.

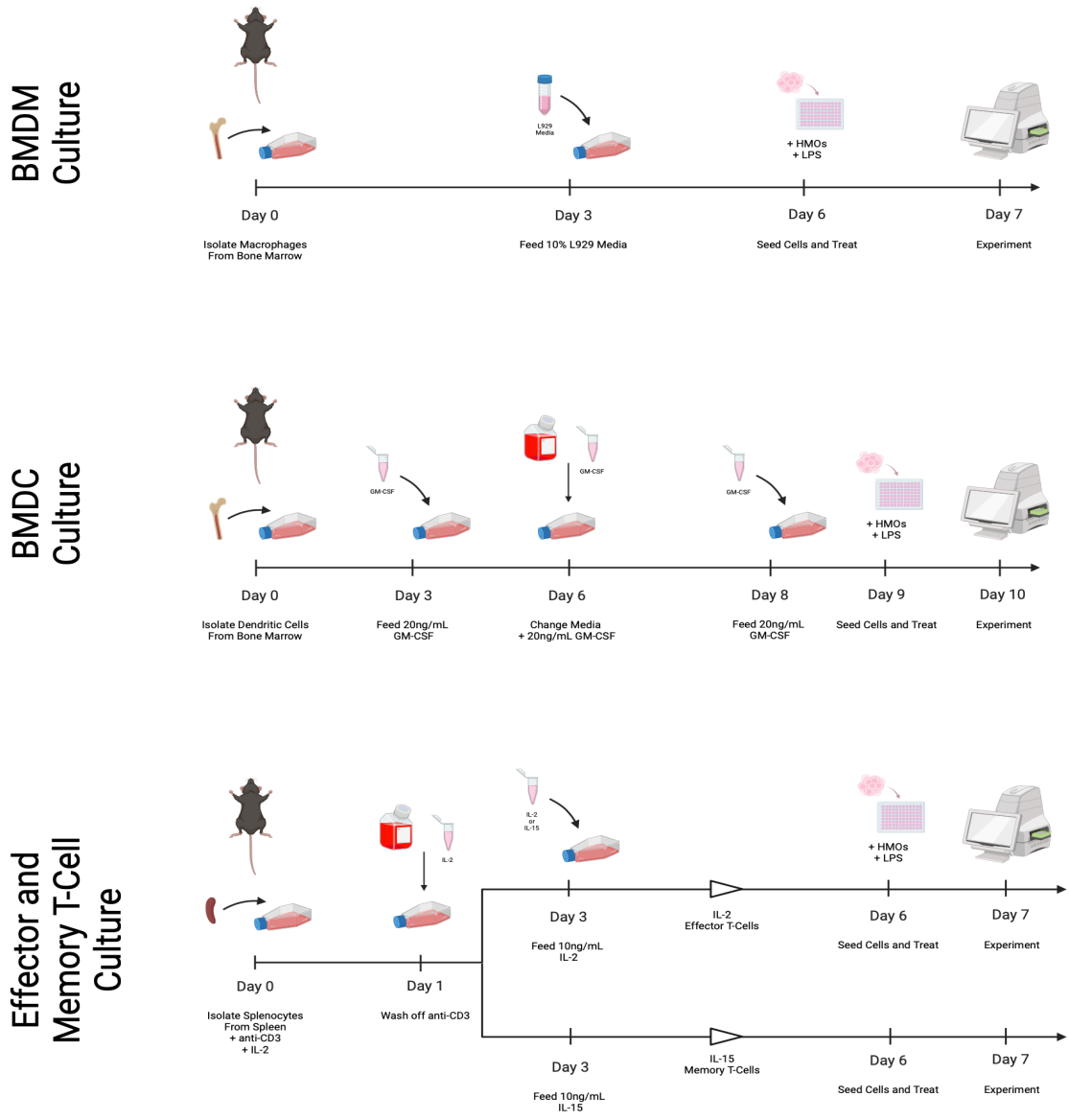

Figure 2. 3: **Timeline of Murine Cell Culture Protocols for BMDMs, BMDCs, and Spleen-Derived T-cells.**

L929 Cell Line

The L929 cell line is a murine fibroblast cell line. L929 cells produce M-CSF required for macrophage differentiation. L929-conditioned medium was generated by seeding $5x10^5$ cells/mL L929 cells in a 175 cm^2 culture flask in 40 mL of medium (RPMI, 10% FBS and 1% penicillin-streptomycin). Cells were left to become confluent for 7 days. The supernatant was then collected and sterile filtered using a 0.45 μm filter. The filtered supernatant was aliquoted and frozen at -80°C.

HEK-293T TLR-2 and TLR-4 Cell Lines

HEK293-TLR2 and HEK293-TLR4 cells are human embryonic kidney 293 (HEK293) cells that have been genetically modified to stably express Toll-like receptor 2 (TLR2) and Toll-like receptor 4 (TLR4). HEK293-TLR2 and HEK293-TLR4 cells were cultured in DMEM supplemented with 10% FBS, 1% penicillin-streptomycin, and 1% L-glutamine. Cells were maintained in a humidified incubator at 37°C with 5% CO_2. Culture media was replaced every 2-3 days, and cells were passaged at approximately 70-80% confluence using 0.25% trypsin-EDTA. For experiments, cells were seeded at the desired density in appropriate culture vessels and allowed to adhere for 24 hours before treatment.

MCF-7 Breast Cancer Cell Line

The MCF-7 is a metastatic breast cancer cell line isolated from a 69-year-old white woman. It is commonly used in breast cancer studies as it possesses the receptors for oestrogen, progesterone, glucocorticoid and retains many characteristics of mammary epithelial cells (MEC). MCF-7 cells were seeded at $5x10^5$ cells/mL in a 75 cm^2 culture flask in 10 mL of complete growth media (EMEM with EBSS, 2 mM L-glutamine, 10% FBS, 0.01 mg/mL Insulin, 1 mM Sodium Pyruvate, 1.5 g/L Sodium Bicarbonate, 1X Non-Essential Amino Acids). Media was replaced every 2 to 3 days. When cells reached a confluency of 70-80% they were detached using 0.5% Trypsin 0.25% EDTA, counted and either subcultured at a 1:5 ratio or used for experimentation.

2.3.2. Cytokine Analysis by Enzyme Linked Immunosorbent Assay (ELISA)

On Day 1, high binding flat-bottom 96 well plates were coated with 100 µL per well of capture antibody diluted in 1X PBS buffer and incubated overnight at 4°C.

On Day 2, plates were washed 3 times in ELISA wash buffer and then dried. 200 µL of assay diluent was added to each well to block any remaining binding sites, and the plate was incubated for minimum 1 hour, maximum 2 hours at room temperature. Standards were made using a serial dilution method in assay diluent. Frozen supernatant samples were thawed and vortexed. The plate was washed 3 times, and the standards and samples were added in triplicate, including assay diluent as a blank. For some cytokines (e.g. TNF-α), samples were diluted to ensure they were within the range of the standard curve. The plates were incubated at 4°C overnight.

On Day 3, plates were washed 3 times, and 50 µL of detection antibody diluted in 1% BSA/PBS was added to each well. Plates were then incubated at room temperature for 1 hour. Plates were washed 3 times. 100 µL of HRP diluted in 1% BSA/PBS was added to each well. Plates were incubated in the dark for 20 minutes at room temperature. Plates were then washed 7 times. 100 µL of TMB substrate reagent was added to each well. The colorimetric reaction was allowed to develop until the lowest standards of the standard curve turned light blue. The reaction was stopped with 25 µL of "stop solution" (0.5 M H_2SO_4). The plates were read using a microplate reader set to a wavelength of 450 nm. Microsoft Excel software was used to generate a standard curve from which the cytokine concentration of the samples was determined.

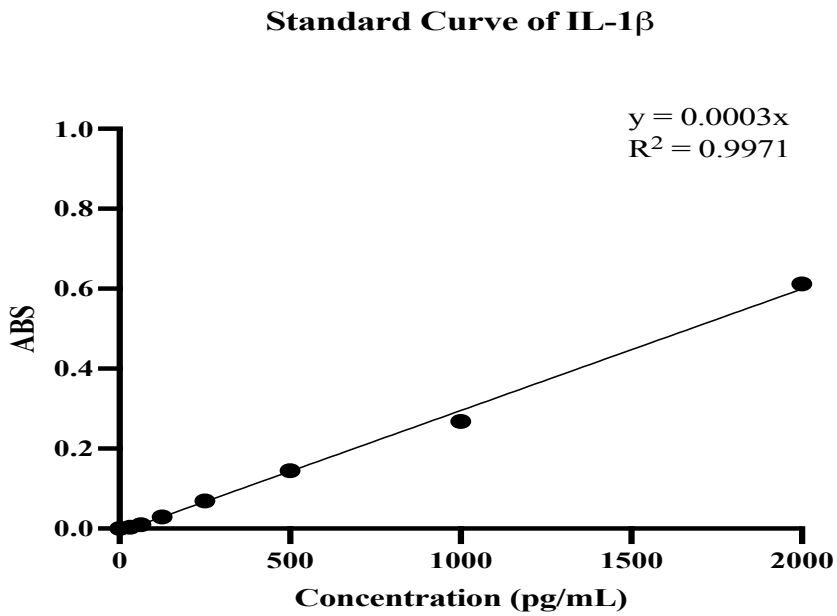

Figure 2. 4: **Standard Curve for IL-1β.**

Standard curve for IL-1β generated for each experiment. Where the slope of the line is defined by y = mx + C and R^2 is the coefficient of determination, measuring goodness-of-fit for linear regression models.

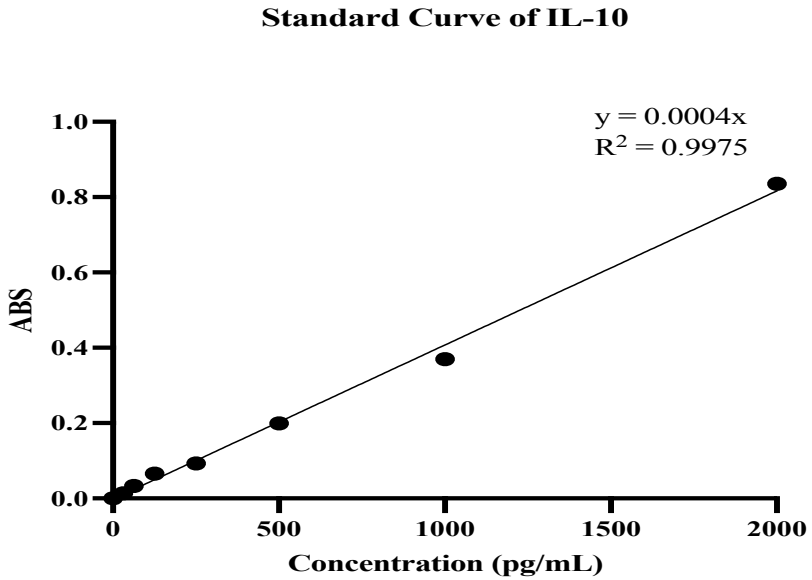

Figure 2. 5: **Standard Curve for IL-10.**

Standard curve for IL-10 generated for each experiment. Where the slope of the line is defined by y = mx + C and R^2 is the coefficient of determination, measuring goodness-of-fit for linear regression models.

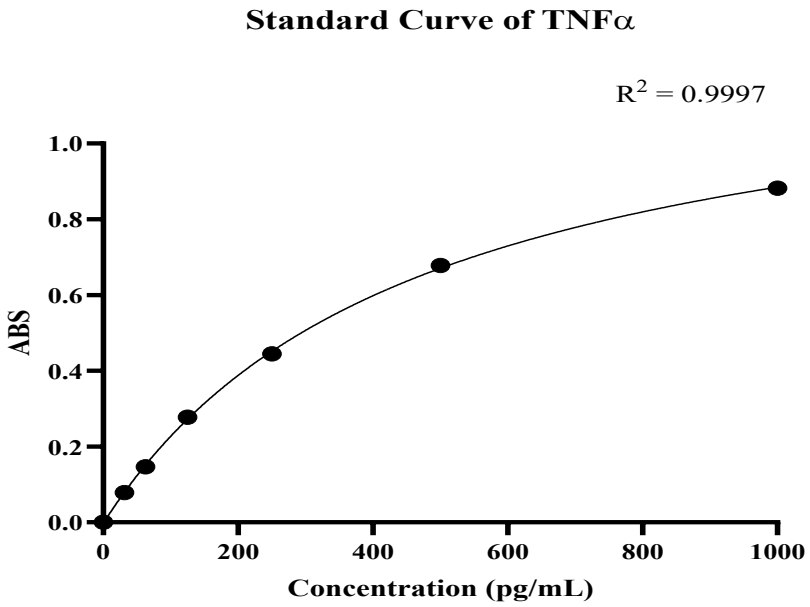

Figure 2. 6: **Standard Curve for TNF-α.**

Standard curve for TNF-α generated for each experiment. Where the slope of the line is defined by y = mx + C and R^2 is the coefficient of determination, measuring goodness-of-fit for quadratic regression models.

2.3.3. **RT-qPCR**

Total RNA was extracted from cells using the RNeasy Mini Kit (Qiagen), following the manufacturer's protocol. Briefly, cells were lysed, and RNA was purified with spin columns after DNase treatment to remove genomic DNA contamination. RNA quantity and purity were assessed by spectrophotometry. For cDNA synthesis, 1 µg of total RNA was reverse transcribed using the High-Capacity cDNA Reverse Transcription Kit (Applied Biosystems), with a reaction volume of 20 µL according to the kit instructions.

RT-qPCR was performed to analyse the expression of key metabolic genes, using SYBR Green Master Mix (Applied Biosystems) in a final reaction volume of 20 µL. Each reaction included 2 µL of cDNA, 0.5 µM of forward and reverse primers specific to each target gene, and nuclease-free water. Amplification was carried out on a real-time PCR system under the following cycling conditions: 95°C for 5 minutes, followed by 40 cycles of 95°C for 15 seconds and 60°C for 1 minute. Expression levels were normalised to a housekeeping gene, and relative gene expression was calculated using the ΔΔCt method.

Table 2. 4: **Primers used for PCR**

Gene	F/R	Primer Sequence
Slc2a1	Forward	GCTTCTCCAACTGGACCTCAAAC
	Reverse	ACGAGGAGCACCGTGAAGATGA
Hk2	Forward	CCCTGTGAAGATGTTGCCCACT
	Reverse	CCTTCGCTTGCCATTACGCACG
Pfkm	Forward	CTGTTCGCTCTACCGTGAGGAT
	Reverse	TTGGAACCACCTTGACCAGTCC
Ldha	Forward	ACGCAGACAAGGAGCAGTGGAA
	Reverse	ATGCTCTCAGCCAAGTCTGCCA
Ndufb6	Forward	CTCCAGTCTCTTCGCTGTTTCTC
	Reverse	CTGGGCTTCGAGCTAACAATGG
Sdha	Forward	GAGATACGCACCTGTTGCCAAG
	Reverse	GGTAGACGTGATCTTTCTCAGGG
Uqcrc1	Forward	AGTGTGGATTGACGCTGGCAGT
	Reverse	CCTCCTTCTCTAAGGCATTGCC
Cox6c	Forward	CGGGTTCATATTGCTGGCGCAT
	Reverse	ACCAGCCTTCCTCATCTCTTCG
Atp5f1	Forward	GGTTCAGAAGCGCCATTACCTC
	Reverse	GTTCTTCCTCCTTGCGACGCAT
Hprt	Forward	GTAACCCGTTGAACCCCATT
	Reverse	CCATCCAATCGGTAGTAGCG

2.3.4. Metabolic Activity Using Seahorse XFe96 Flux Analyser

A Seahorse XFe96 flux analyser was used for the measurement of oxygen consumption rate (OCR) and extracellular acidification rate (ECAR). These measurements were used as an indicator of oxidative phosphorylation rates and glycolysis, respectively.

A day prior to the experiment, a Seahorse cartridge was hydrated using a seahorse calibration buffer incubated in a non-CO_2 incubator at 37°C. Also, day prior to the experiment, cells were seeded in a Seahorse 96 well cell plate. The plates were placed in a CO_2 incubator for 24 hours prior to the initiation of the experiment.

On the day of the experiment, Seahorse media was supplemented with 10 mM glucose, 1 mM pyruvate, and 2 mM glutamine and warmed to 37°C in a non-CO_2 incubator. Cells were washed twice with seahorse media and then media on the cells were changed to seahorse media and this plate was placed in a non-CO_2 incubator for at least 1 hour. The inhibitors used for the assay, Oligomycin, FCCP, Rotenone and Antimycin A were prepared in Seahorse media at 10X concentration. These were then added to designated ports of the Seahorse cartridge plate. The Seahorse cartridge was then calibrated in the analyser, and the cell plate was placed in the Seahorse machine.

To determine the rate of oxidative phosphorylation for Cell Mito Stress (i.e. cellular respiration measured as OCR), we used oligomycin as the ATP synthase inhibitor. Basal rates of oxidative phosphorylation can be determined by the amount of oxygen being consumed over time. This allows you to calculate the actual amount of oxidative phosphorylation. Oligomycin inhibits ATP synthase, but FCCP cleaves it, widening the proton gradient across the inner mitochondrial membrane and maximising oxidative phosphorylation. Antimycin A and rotenone block the electron transport chain, as Antimycin A inhibits complex III and Rotenone inhibits complex I, allowing the calculation of residual oxygen consumption.

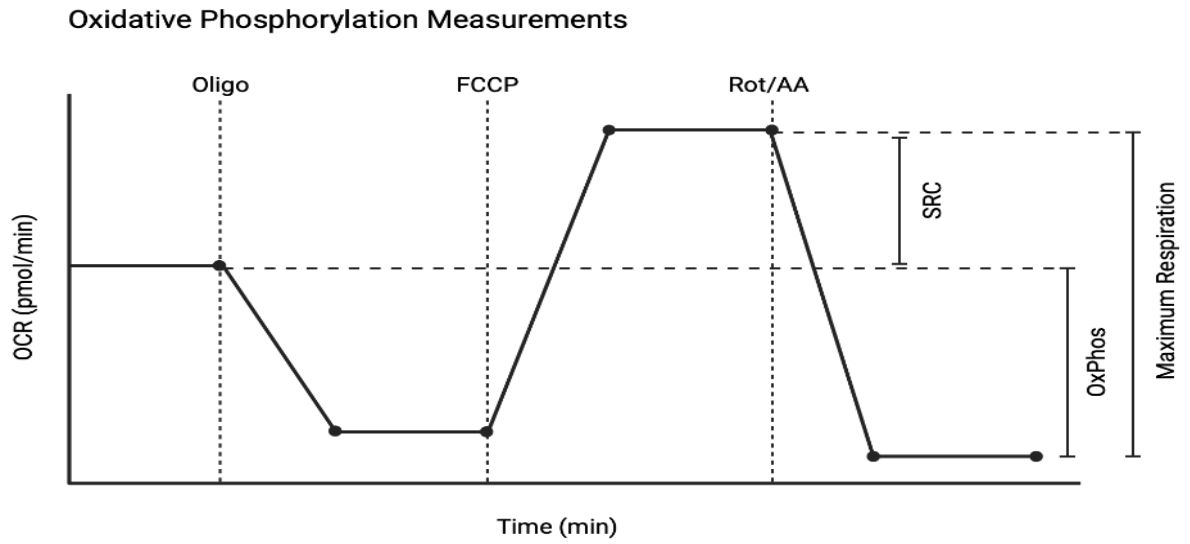

Figure 2. 7: **Measurement of Oxidative Phosphorylation via OCR using The Seahorse XF Metabolic Flux Analyser**

Basal oxygen consumption rates were determined using a 96-well Seahorse flux analyser and were expressed in OCR pmol/minute. After 20 minutes, oligomycin (2 µM) was injected from Port A, which caused OCR to decrease by inhibiting ATP synthase. The next injection, after 20 minutes, was FCCP (0.5 µM), which uncouples proton flow from the ETC, leading to respiration occurring at a maximal rate due to the free flow of electrons. Following 3 readings for 20 minutes at maximal respiration rates, excess concentrations of Rotenone and Antimycin A were injected to completely abolish mitochondrial respiration, giving a measurement of non-mitochondrial respiration. The spare respiratory capacity was calculated by subtracting the basal rate from the maximal rate, which is a measurement of the mitochondrial capacity to increase energy production.

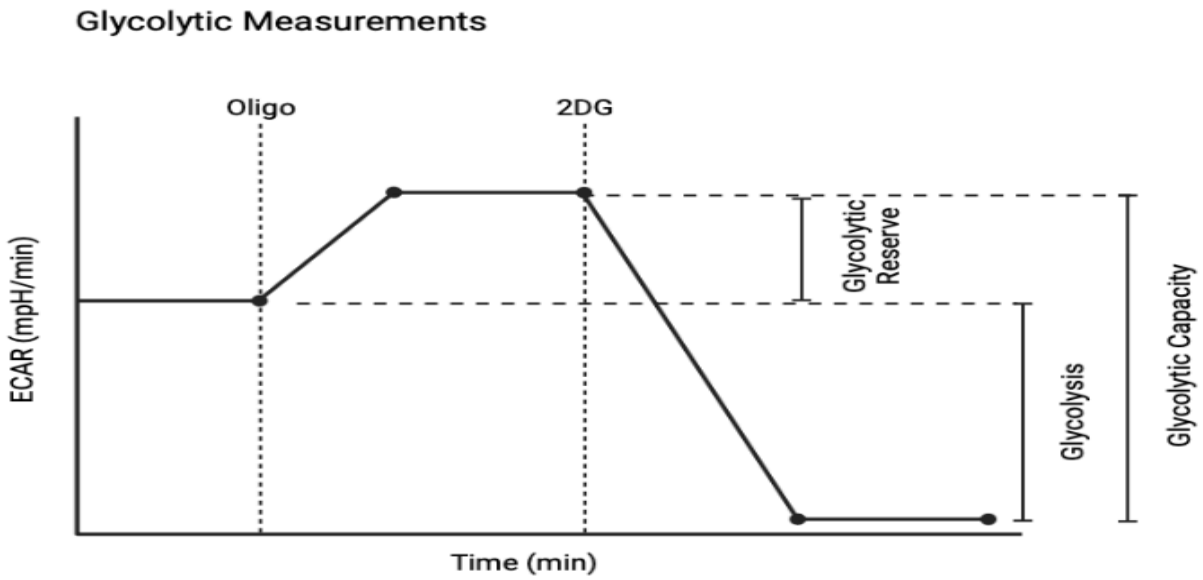

Figure 2. 8: **U Measurement of Glycolysis via ECAR using The Seahorse XF Metabolic Flux Analyser**

Glycolysis was determined by measuring the rate of extracellular acidification resulting from the release of protons during glycolysis. As demonstrated in the representative trace, oligomycin inhibits ATP synthase, and in response, cells increase the rate of glycolysis maximally to compensate for energy production. By comparing the basal rate of glycolysis with the rate after oligomycin treatment, we can determine the extent to which certain cell types can increase glycolysis to compensate for the inhibition of oxphos. To completely inhibit glycolysis, 2-Deoxyglucose is added, which inhibits the rate-limiting first step in glycolysis catalysed by hexokinase, thus preventing glycolysis from occurring.

$$\text{Spare Respiratory Capacity} = \text{Basal OCR Rate} - \text{FCCP OCR Rate}$$

$$\text{Maximal Respiration} = \text{FCCP OCR Rate} - \text{RotAA OCR Rate}$$

$$\text{Glycolytic Capacity} = \text{Oligomycin ECAR Rate} - \text{2DG ECAR Rate}$$

$$\text{Glycolytic Reserve} = \text{Basal ECAR Rate} - \text{Oligomycin ECAR Rate}$$

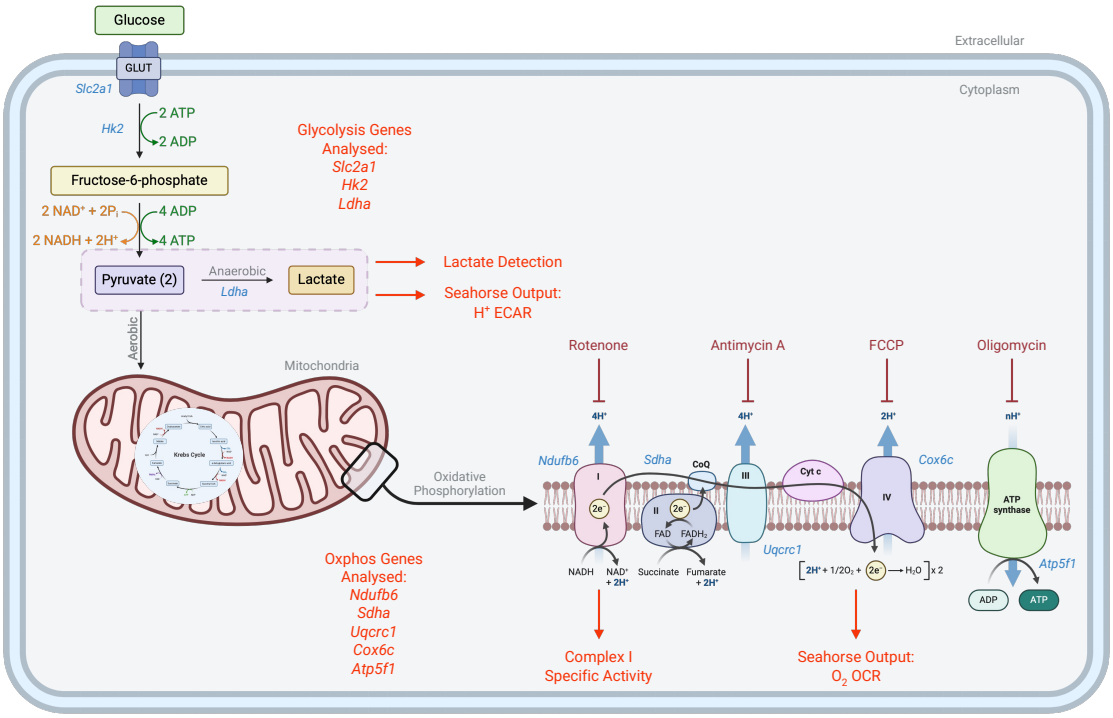

Figure 2. 9: **Summary of Analytes Detected During Seahorse XF Metabolic Flux Assay for Glycolysis and Oxidative Phosphorylation**

2.3.5. Respiratory Chain Complex Activity Assays

Mitochondrial Isolation

To isolate the mitochondria from specific cell types, cultured cells were pelleted and washed once with PBS to remove any residual medium. The cell pellets were resuspended in 1 mL of ice-cold STE buffer and transferred to a 2 mL glass-on-glass Dounce homogeniser. All subsequent steps were performed on ice, using ice-cold STE buffer. Cells were homogenised with 30 strokes using the tight-fitting pestle. The homogenate was transferred to 2 mL Eppendorf tubes and centrifuged at 1000 × g for 10 minutes at 4°C. The supernatant was carefully transferred to a new 2 mL Eppendorf tube and centrifuged again at 1000 × g for 10 minutes to further remove debris. The supernatant was then transferred to a fresh 2 mL Eppendorf tube and centrifuged at 12,000 × g for 15 minutes. The resulting supernatant was either discarded or stored for use as the cytosolic fraction. The remaining pellet, considered the mitochondrial pellet, was washed twice in 0.5 mL of STE buffer. Finally, the pellets were resuspended in STE, snap-frozen using liquid nitrogen, and stored at -80°C for downstream applications.

Complex I Assay

The complex I activity assay was performed following a protocol by Darley and Ursmarr (1987). After isolating mitochondria (described above), followed by 3 freeze-thaw cycles using liquid nitrogen. The assay monitors the oxidation of NADH to NAD+, which results in a decrease in absorbance at 340 nm at 37°C. The reaction mixture consisted of assay buffer, 25 mM phosphate, 0.2 mM NADH, 2.5 mg/mL fatty acid-free BSA, 1 mM KCN, and purified mitochondria (20 µg). The reaction was initiated, and absorbance was monitored for 2-3 minutes to ensure a stable baseline. Subsequently, 50 µM DQ was added to each cuvette to start the reaction, and the reaction rate was monitored for 6-9 minutes using a spectrophotometer. Rotenone (10 µM) was then added to measure rotenone-sensitive rates, with the reaction followed for an additional 5 minutes. Rotenone-sensitive rates were subtracted from the DQ rates, and the Beer-Lambert law (A = εcl) was applied to calculate the enzyme's specific activity. Specific activity was expressed as nmol/min/mg of protein, with an extinction coefficient for NADH in the presence of DQ set at 6.81 mM^{-1} cm^{-1}.

$$\text{Specific Activity (nmol/min/mg)} =$$

$$((\Delta\text{Abs/min})/(6.81 \times 10\text{^}3\ ))(1/1000\varepsilon)\ \ (1/0.02)$$

2.3.6. Flow Cytometry

All flow cytometry analyses were performed using the BD FACS Canto instrument.

Cell Characterisation

Cells were seeded in 6 well plates and treated accordingly. After stimulation, plates were centrifuged, and supernatants were discarded. 10 nM EDTA in PBS was then added to cells to remove them from the dish. The EDTA/PBS solution containing cells was transferred to labelled FACs tubes and washed in 2 mL PBS. FACs tubes were centrifuged, supernatants removed, and cells resuspended in PBS containing fixable viability stain BV510 and Fc block. The cells were left for 15 minutes in the dark at room temperature. After 15 minutes, cells were washed with 2mL PBS, centrifuged and resuspended in 100 µL FACs buffer. The relevant antibody master mix was then added to appropriate tubes. The tubes were left for 30 minutes in the dark at room temperature. After 30 minutes, cells were washed in 1mL PBS, centrifuged, resuspended in 200 µL FACs buffer and acquired immediately.

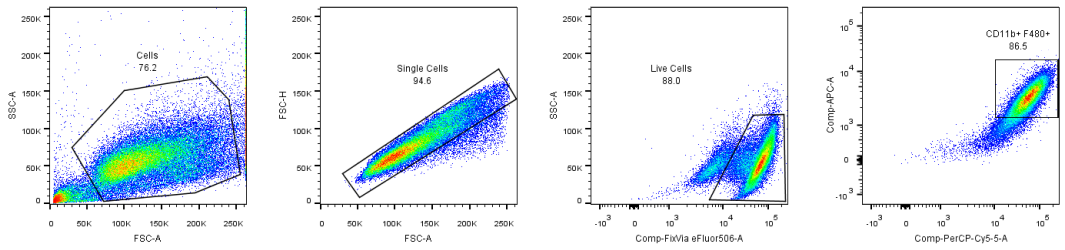

Figure 2. 10: **Analysis of BMDM Integrity via Flow Cytometry:**

The cell population was captured via forward scatter (FSC) and side scatter (SSC) gating as shown in (top). Single live cells were isolated (middle), of which CD11b+/F480+ cells were selected (bottom). High percentage yield of BMDMs, 89.8%.

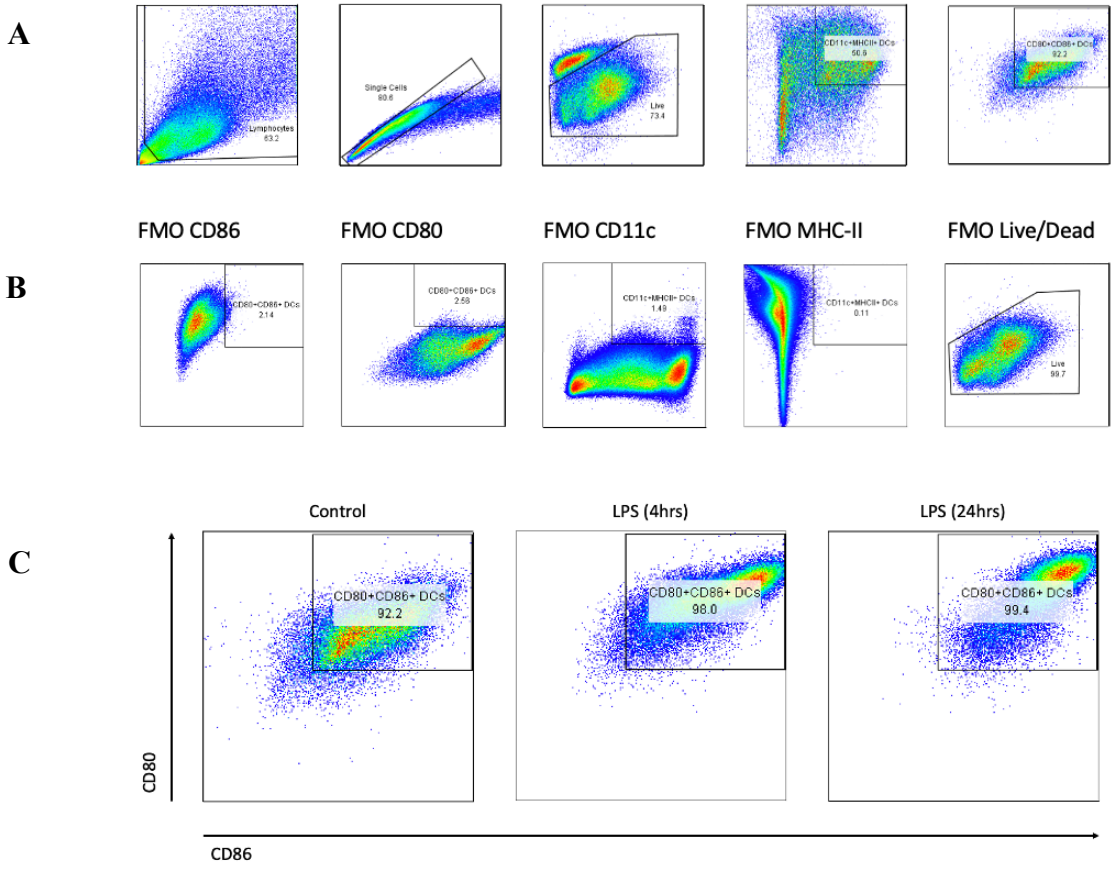

Figure 2. 11: **Analysis of BMDC Integrity via Flow Cytometry:**

The cell population was captured via FSC and SSC gating. Single live cells were isolated, of which CD11c+/MHC-II+ cells were selected, of these cells, expression markers CD80 and CD86 were analysed. Representative plots of Fluorescence Minus One (FMOs) shown in (B) to assist with gating. Representative plots for the change in expression of co-stimulatory markers CD80 and CD86 were analysed across immature (control) and mature (4 hour and 24 hour LPS) DCs (C).

A

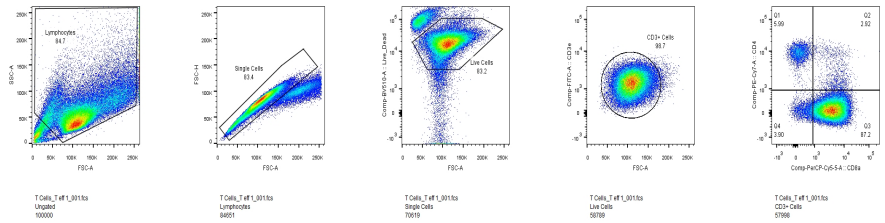

B

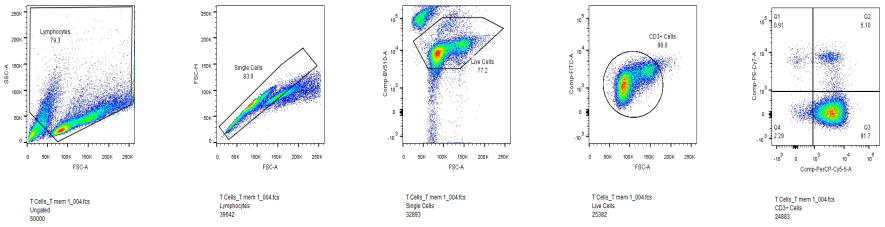

Figure 2. 12: **Analysis of T-Cell Integrity via Flow Cytometry:**

The cell population was captured via FSC and SSC gating. Single live cells were isolated, of which CD3+ cells were selected, of these cells, expression markers CD4, CD8 were analysed. Panel (A) is the gating for the effector T-Cell population. Panel (B) is the gating for the memory T-Cell population

Flow Cytometric Analysis of Reactive Oxygen Species Using MitoSOX

Cells were seeded in 6 well plates and treated accordingly. After cell treatment, cell plates were spun down at 1400 RPM for 5 minutes and supernatants were removed. Cells were removed from wells using ice cold PBS/EDTA and transferred to labelled FACs tubes. Cells were then resuspended in 200 µL of PBS/MitoSOX (5 µM). The tubes were placed in a CO_2 incubator at 37°C for 30 minutes. The cells were then washed twice using PBS and resuspended in 200 µL FACS buffer. Samples were run using PE channel of FACSCanto immediately.

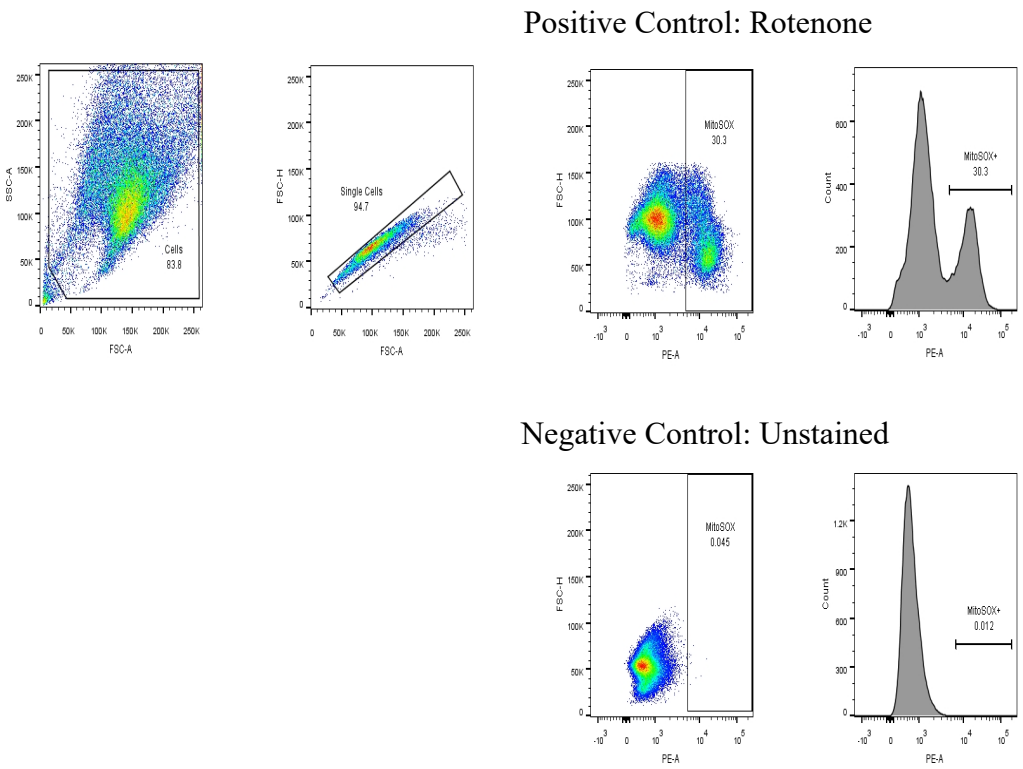

Figure 2. 13: **MitoSOX gating panel**

The cell population was captured via FSC and SSC gating. Single live cells were isolated, of which analysed for MitoSOX fluorescense, FSC-A vs MitoSOX. Rotenone treated cells were used as a positive control and unstained cells were used to aid in the identification of a MitoSOX+ population.

Flow Cytometric Analysis of GFP expressing plasmid

Cells were seeded in 24 well plates at 5×10^5 cells/mL and transfected with GFP-expressing plasmid using Lipofectamine 2000. After 24-48 hours, cells were harvested by spinning plates at 1400 RPM for 5 minutes and removing the supernatant. Cells were detached using ice-cold PBS/EDTA and transferred into labelled FACS tubes. Cells were washed twice with PBS and resuspended in 200 µL FACS buffer. Samples were run using the FITC channel of the FACSCanto immediately.

2.3.7. Protein Analysis

Cell lysis

Radioimmunoprecipitation Assay (RIPA) was the default buffer used for lysing in this project. RIPA efficiently lyses all of the cell's components, leading to the complete release of proteins from all membrane-bound compartments. Preceding lysis, 10 mL of RIPA lysis buffer aliquot was supplemented with cOmplete ULTRA^{TM} Protease Inhibitor Tablets as well as 1 mM sodium orthovanadate, 1 mM β-glycerophosphate, 2.5 mM sodium pyrophosphate. RIPA with protease and phosphatase inhibitors was used for lysis. Immediately before lysis, the cell dish was placed on ice. After washing twice with ice-cold PBS, the dish was dried entirely using an aspirator or a pipette. After removing all PBS, lysis buffer was added. Cells were scraped off the dish using a disposable cell scraper, and the cell lysates were transferred into a 1.5 mL centrifuge tube. These lysates were spun at max speed for 20 minutes at 4°C. After centrifugation, the lysates were transferred to a clean 1.5 mL centrifuge tube, and the cell pellet was discarded. The lysates were stored at -20°C or -80°C long term.

Protein Quantification

Protein concentrations were determined using the Bradford Assay (Bio-Rad Laboratories), following the manufacturer's instructions. BSA standards (0-2 mg/mL) were prepared in the same buffer used for sample preparation. Samples and standards (5 µL) were added to the wells of a 96-well plate, followed by the addition of 250 µL of Bradford reagent. The plate was incubated at room temperature for 15 minutes to allow colour development. After this incubation the plate was read at 595 nm in a spectrophotometer.

Electrophoresis

BioRad Mini-PROTEAN Tetra Cell and SDS-PAGE tris-glycine buffer system were used to analyse protein levels. Gels were made using a 37.5:1 acrylamide mix and were prepared according to Bio-Rad General protocol for Western Blotting and a general gel recipe from Harlow and Lane. Prior to electrophoresis, the lysate samples were diluted to 20 µg/well using X4 Laemmi buffer and RIPA. Lysates were vortexed, centrifuged and denatured at 95°C for 10 minutes. Samples were loaded into lanes in the gel. During electrophoresis, proteins were separated on an SDS- PAGE gel and later transferred from the gel to a polyvinylidene fluoride (PVDF) membrane using a Bio-Rad PowerPac 300. The gel ran for

25 minutes at 80 V to separate the stacking gel and then was changed to 120 V so the resolving gel could fully resolve the proteins.

Immunoblotting

The PVDF membrane was submerged in methanol to activate it, and then it was washed and left covered in dH_2O. Cassette sponges and Whatman filter papers were briefly soaked in transfer buffer. The membrane was carefully applied to the gel surface and arranged between filter papers in the transfer cassette. It was rolled to eliminate air bubbles and secured in the transfer cassette. The transfer was left running at 45 V for 3 hours at 4°C or 15 V overnight at 4°C. Following transfer, the membrane was blocked using 5% milk in TBST for 1hour at room temperature. The membrane was then washed in TBST and then transferred to a plastic container with primary antibody diluted in 5% BSA in TBST with 3% sodium azide and incubated overnight at 4°C on the tube roller. Membranes were washed 3 times in TBST. The membrane was transferred to a falcon tube with 5mL of primary antibody diluted in 5% BSA in TBST with 3% sodium azide. Membranes were incubated for 1 hour on a tube roller and were washed 3 times with TBST for 5 minutes. Pierce™ ECL Western Blotting Substrate was used for the imaging analysis. Reagent A was mixed with Reagent B in an equal ratio at approximately 300-400 µL. The membrane was incubated with ECL for 1-2 minutes and then imaged using a Bio-Rad Image GelDoc machine. ImageLab software was used to capture the chemiluminescence and a colorimetric photograph.

2.3.8. Lactate Measurement

Lactate levels in cell culture supernatants were quantified using the Lactate-Glo™ Assay according to the manufacturer's instructions. Briefly, cells were seeded into 96-well plates at the desired density and allowed to grow under experimental conditions. Supernatants were collected and stored at -80°C until analysis. For the assay, 50 µL of cell culture supernatant or lactate standards (0-100 µM) were added to each well of a white, flat-bottom 96-well plate. Then, 50 µL of the detection reagent was added to each well. Plates were incubated for 1 hour at room temperature, protected from light. Luminescence was measured using a plate reader (RLU).

2.3.9. Alamar Blue Cell Viability Assay

Cells were seeded in 96-well plates and treated with the concentrations of treatments used for other experiments i.e. 100 ng/mL LPS, 5 mM ATP, 2 mM 2'-FL, 1 mM 3'-SL and 6'-SL. Cells with no treatment were used as the 'Live Control'. Cells were treated with a high concentration salt solution (5 M NaCl) or ethanol to be used as the 'Dead Control'. The plates were placed in a CO_2 incubator for 24 hours prior to the initiation of the experiment.

On the day of the experiment, 20 µL from each well was removed and discarded from the 96-well plate and 20 µL of alamarBlue was added to each well. This was allowed to incubate for exactly 4 hours in a CO_2 incubator. The plates were read using a microplate reader set to a wavelength of 570 nm and 600 nm to measure absorbance, using 600 nm as a reference wavelength and normalising relative to these values.

2.3.10. Golgi Isolation From Cultured Cells

Cultured MCF-7 cells were washed twice using 5mL of Homogenisation Media (HM) and resuspended in 3 mL HM. The cells were homogenised by using 10-15 strokes of a tight-fit pestle. The homogenate was then brought to a sucrose concentration of 1.4M by adding 6 mL of 2 M sucrose gradient solution. 6 mL of this sample was transferred to a centrifuge tube. The sample was overlayed with 6 mL of 1.2 M sucrose gradient solution and 3 mL of 0.8 M sucrose gradient solution. The sample was underlayed with 2 mL of a 1.6 M sucrose gradient solution using a syringe and cannula. Cells were centrifuged for 2 hours at 110,000 x g at 4°C. After the 2 hours the Golgi band sits between the 0.8 M/1.2 M sucrose interface due to the Golgi membranes having a much lower density than those of other membrane particles, causing them to float upwards to this band. This band was harvested.

2.3.11. Bacterial Work And Sequencing Of Plasmids

Streak bacterial stocks onto LB agar, Leave plates at 37°C overnight. Inoculate 4 mL LB broth (containing 100 µg/mL ampicillin) with a single colony and incubate in an orbital shaker for 8 hours at 180 rpm, 37°C. Isolate plasmid using Qiagen spin miniprep kit, according to manufacturer's instructions. Once plasmid is isolated, nanodrop is performed to analyse plasmid concentration and purity. Analyse samples at 260/280 nm and 260/230

nm. Samples sent to Eurofins Genomics for analysis of plasmid by Whole Plasmid Sequencing (WPS).

2.3.12. Transfection of HEK-293 Cells

HEK293 cells were seeded in a 24-well plate and incubated overnight at 37°C in a 5% CO_2 incubator to reach 70-90% confluence. For transfection, plasmid DNA (0.5 µg per well) was diluted in 50 µL of Opti-MEM™ reduced serum medium. In a separate tube, 2 µL of Lipofectamine™ 2000 reagent (Invitrogen) was diluted in 50 µL of Opti-MEM™ and incubated at room temperature for 5 minutes. The diluted plasmid DNA and Lipofectamine™ 2000 were mixed gently and incubated for 20 minutes at room temperature to allow DNA-Lipofectamine complex formation. The complexes were then added dropwise to each well containing cells and 500 µL of fresh antibiotic-free growth medium. Cells were incubated at 37°C in a 5% CO_2 incubator for 24-48 hours before downstream analysis. To confirm successful transfection, HEK293 cells were transfected with a plasmid expressing GFP. After transfection, the 24-well plate was transferred to the Incucyte® live-cell imaging system (Sartorius) for real-time monitoring of GFP expression. Imaging began immediately post-transfection, with images taken every 2-4 hours over a 48 hour period.

The Incucyte® system was set to capture both phase-contrast and fluorescence images at 10X magnification. GFP-positive cells were detected by green fluorescence, and the transfection efficiency was assessed by quantifying the percentage of GFP-expressing cells relative to the total cell population using Incucyte® analysis software.

2.3.13. Restriction Digests

Plasmid DNA was digested using selected restriction enzymes (**Table 5**) to verify plasmid integrity and confirm the presence of the desired insert. Each reaction mixture contained 1 µg of plasmid DNA, 1 µL of each restriction enzyme, 2 µL 10X reaction buffer, and nuclease-free water, for a final volume of 20 µL. The reactions were incubated at 37°C for recommended digestion time to allow complete digestion and subsequently denatured (See

Table 2.5). Following incubation, the samples were analysed by gel electrophoresis to confirm successful digestion and the expected fragment sizes.

Table 2. 5: **Enzymes used in Restriction Digest**

Enzyme	Cut Site	Reaction Settings	Inactivation Settings
BamHI - FastDigest	G/GATCC	37°C for 5 minutes	80°C for 5 minutes
Bpu10I - FastDigest	CCTNAGC	37°C for 15 minutes	80°C for 5 minutes
Bpu1102I - FastDigest	GC^TNAGC	37°C for 5 minutes	80°C for 5 minutes
EcoRI - FastDigest	G/AATTC	37°C for 15 minutes	80°C for 5 minutes
PfoI - FastDigest	T^CCNGGA	37°C for 5 minutes	65°C for 10 minutes
Van91I - FastDigest	CCANNNN^NTG	37°C for 5 minutes	65°C for 5 minutes

2.3.14. Agarose Gel Electrophoresis

To assess plasmid DNA, agarose gel electrophoresis was performed following a standardised protocol. A 1% agarose gel was prepared by dissolving 1.25 g of agarose in 125 mL of 1X TAE buffer. The mixture was heated in a microwave until fully dissolved and then cooled to approximately 50°C. To visualise the DNA, SYBR-safe was added to the gel solution at a final concentration of 1:10,000. The agarose solution was poured into a gel casting tray with a comb and allowed to solidify at room temperature for 30-60 minutes.

For sample preparation, plasmid DNA samples were mixed with 6X loading dye (New England Biolabs) in a 1:5 ratio, and a DNA ladder was prepared according to the manufacturer's instructions for size comparison. Once the agarose gel had solidified, it was placed in an electrophoresis chamber filled with 1X TAE buffer, ensuring that the gel was submerged. The mixed samples (12 µL) and DNA ladder (6 µL) were loaded into the wells of the gel. The chamber was then connected to a power supply and run at 75 V for approximately 60-90 minutes, or until the dye front had migrated an appropriate distance through the gel. After electrophoresis, the gel was imaged using a UV transilluminator to visualise the bands.

2.3.15. Gel Extraction

DNA fragments were extracted from agarose gels using the QIAquick Gel Extraction Kit (Qiagen) following the manufacturer's protocol. In brief, excised gel slices were dissolved in Buffer QG at 50°C, and the solution was applied to a QIAquick spin column. After binding, the column was washed with Buffer PE to remove impurities. DNA was then eluted in 30 µL of Buffer EB. The concentration and purity of the recovered DNA were confirmed by nanodrop before use in downstream applications.

2.3.16. PCR for Plasmid DNA Amplification

PCR amplification of plasmid inserts was performed using Q5® High-Fidelity 2X Master Mix (NEB) in 20 µL reactions containing 10 ng of plasmid DNA, 10 µL of master mix, 0.5 µM each of forward and reverse primers (**Table 2.6**), and nuclease-free water to volume. No-template controls were included for each primer set. Amplification was carried out using gene-specific annealing temperatures and extension times (**Table 2.7**). PCR products were analysed by agarose gel electrophoresis, and specific bands were excised and purified using the GeneJET PCR Purification Kit or QIAquick Gel Extraction Kit according to the manufacturer's protocols. DNA concentrations were measured by Nanodrop prior to downstream applications.

Table 2. 6: **Primers used for PCR addition of overhangs for Gibson Assembly Cloning**

Glycosyltransferase	F/R	Primer Sequence
B4GALT4	F	*ggcggcggcggttccggaggaggaggttc*CAAAGCAAAGGAGTTCATG
	R	ggaaccaccaccaccTGCACCAAACCAGAAATC
B3GNT2	F	cccacggcgaattcgCATCAACAAGTTTGTACAAAAAAG
	R	*gaacctcctcctccggaaccgccgccgcc*GCATTTTAAATGAGCACTC
ST6GAL1	F	*ggtggtggtggttc*CCGCCAGACCCTCGGCAG
	R	CGAATTCGCCGTGGGTGATGCCAG

Table 2. 7: **Setting of PCR for addition of overhangs for Gibson Assembly Cloning**

Stage		**Temperature**	**Duration**
Initial		98°C	30 seconds
30 Cycles	Denaturing	98°C	10 seconds
	Annealing	ST6GAL1 - 72°C	30 seconds
		B3GNT2 - 57°C	
		B4GALT4 -56°C	
	Extension	72°C	ST6GAL1 - 6 minutes
			B3GNT2 - 1 minute
			B4GALT4 - 1 minute
Final		72°C	5 minutes

2.3.17. Gibson Assembly Cloning

Inserts were assembled using a commercial Gibson Master Mix in a 20 µL reaction containing vector and inserts at the molar ratios used for this project (ST6GAL1 backbone at 2X molar excess relative to each insert), 0.02-0.1 pmol total DNA per reaction where possible. Reactions were incubated at 50°C for 60 minutes and then placed on ice.

2.3.18. Transformation of DH5α *E. coli*

Chemically competent DH5α cells were thawed on ice. 2 µL of Gibson reaction was mixed with 50 µL competent cells, incubated on ice for 30 minutes, heat-shocked at 42°C for 30 seconds, returned to ice for 2 minutes, then rescued with 950 µL SOC medium at 37°C with shaking for 45-60 minutes. Cells were plated on LB-agar containing 100 µg/mL ampicillin and incubated overnight at 37°C. Colonies were picked into 5 mL LB + ampicillin, grown ~16 hours, and plasmid DNA prepared by miniprep.

2.3.19. Glycosyltransferase Isolation

Cells were harvested by centrifugation. Briefly, cultures were placed on ice and pelleted by centrifugation at 5,000 × g for 5 minutes at 4°C. The supernatant was discarded, and the cell pellet was resuspended in digitonin-based lysis buffer. Samples were incubated on ice for 10 minute to allow selective membrane permeabilisation. The homogenised lysate was then centrifuged at 2,000 × g for 5 minutes at 4°C to remove unlysed cells and large debris. The supernatant was transferred carefully to a fresh pre-chilled tube and subjected to a final clarification step by centrifugation at 20,000 × g for 30 minutes at 4°C. The resulting supernatant, containing the soluble glycosyltransferase fraction, was collected and used directly for enzyme activity assays. Protein concentration was measured using a Bradford assay, and aliquots were kept on ice until use. Heat-inactivated lysate prepared in parallel (95°C, 10 minutes) was used as a negative control.

2.3.20. Glycosyltransferase Enzyme Assay

Reactions were assembled in a final volume of 50 µL. Standard assay buffer consisted of HEPES or MES buffer. CMP-Neu5Ac, UDP-Galactose and UDP-*N*-acetylglucosamine were added at 1 mM, and the acceptor substrate lactose 10 mM. Recombinant enzyme (50 µg final) was added last to initiate the reaction. Control reactions lacking enzyme, donor or acceptor were run in parallel.

2.3.21. High Performance Anion Exchange Chromatography with Pulsed Amperometric Detection (HPAEC-PAD)

Oligosaccharides were quantified by HPAEC-PAD on a Thermo Dionex ICS-6000 system equipped with a CarboPac PA-100 analytical column (2 × 250 mM) and a PA-100G guard column. Detection used pulsed amperometric detection with a gold working electrode and a silver reference electrode. A HMO standard mix (including 3-fucosyllactose (3-FL), 2’-fucosyllactose (2'-FL), lacto-*N*-neotetraose (LNnT), lacto-*N*-neohexaose (LNnH), lacto-*N*-tetraose (LNT), lacto-*N*-hexaose (LNH), sialyllacto-*N*-tetraose a (LSTa), sialyllacto-*N*-tetraose a (LSTc), 6’-siallylactose (6'-SL), 3’-siallylactose (3'-SL), disialyllacto-*N*-tetraose (DSLNT)) was prepared and run as the calibration standard. External standard calibration curves were generated for each quantified HMO. A standard mix was run after every 4 sample injections to monitor retention time stability and detector response.

Cell culture supernatants or conditioned media/buffer were thawed on ice, centrifuged at 8,000 × g for 5minutes to remove particulates, and filtered through 0.22 µM PVDF filters into autosampler vials. Samples were diluted in ultrapure water as required to fall within the calibration range. Samples (5 µL) were injected on to a CarboPac PA100 (2 x 250 mM) column at a flowrate of 0.25 mL/min. Eluent A was 100 mM NaOH and eluent B was 100 mM NaOH+500 mM sodium acetate (NaOAc). Elution was carried out with the following gradient:(t= 0-3 minutes 95% Eluent A; t = 3-13 minutes 88% Eluent A; t = 13-17 minutes 84% Eluent A; t =17- 20 minutes 84% Eluent A; t= 20-22 minutes 82% Eluent A; 22.1-30 min 50% Eluent A; 30.1-50 minutes equilibrated at 95% Eluent A). The column and the detector compartments were maintained at 32°C. Quantification of oligosaccharides was carried out by comparing peak areas to the standard curves carried out for the known standard oligosaccharides above.

2.4. Analysis Software and Programs

Statistical analysis was performed using **GraphPad Prism 9**. All data are presented as mean ± SEM unless otherwise stated. A P-value of 0.05 or less was deemed to be statistically significant. ns for $p > 0.05$, * for $p \leq 0.05$, ** for $p \leq 0.01$, *** for $p \leq 0.001$, **** for $p \leq 0.0001$

Diagrams were created using **Biorender**.

All flow cytometry data was analysed using **Flowjo**.

O-Glycologue is a simulator of the enzymes of O-linked glycosylation, developed and maintained by Andrew McDonald

Western Blot analysed in **Image Lab software**.

Agarose Gels analysed in **ImageStudio software**.

IncuCyte Data analysed in **ImageJ software**.

2.5. Experimental Animals and Ethics

All experimental animals were obtained from the Comparative Medicine Unit, Trinity College Dublin. Unless otherwise stated C57BL/6s were used. Mice were culled using overdose of Carbon Dioxide according to regulations set out by the HPRA and confirmation of death was carried out by cervical dislocation.

Chapter 3

Effect of Human Milk Oligosaccharides on Metabolic Pathways in Macrophages

3.1. Introduction

Macrophages are key effectors of the innate immune system, contributing to host defence, tissue repair, and the resolution of inflammation. These highly plastic cells respond to environmental cues by adopting distinct metabolic and functional states[131]. Classically activated M1 macrophages, which emerge in response to pro-inflammatory stimuli such as LPS and IFN-γ[225], rely heavily on aerobic glycolysis to rapidly generate ATP and biosynthetic precursors for pro-inflammatory functions[226]. This metabolic shift, often compared to the Warburg effect observed in cancer cells, allows for rapid ATP production to support the biosynthetic demands of inflammation[227]. M1 macrophages are characterised by high production of ROS and pro-inflammatory cytokines such as TNF-α and IL-1β[228]. While these cells are essential for antimicrobial defence, persistent activation can contribute to chronic inflammation and tissue damage[229]. Conversely, alternatively activated M2 macrophages, which are induced by IL-4 and IL-13[225], play a crucial role in tissue repair, immune regulation, and the resolution of inflammation. Unlike their M1 counterparts, M2 macrophages primarily depend on oxidative phosphorylation and fatty acid oxidation for energy production[226], which supports their anti-inflammatory and homeostatic functions. These cells express high levels of anti-inflammatory cytokines, enhancing their role in wound healing and immune suppression. The metabolic dichotomy between M1 and M2 macrophages is fundamental to immune balance, and disruptions in this metabolic flexibility are implicated in various pathological conditions, including chronic inflammatory diseases, metabolic syndromes, and autoimmunity[230-232]. Given the central role of metabolism in determining macrophage function, there is growing interest in the potential of nutritional and bioactive molecules to modulate macrophage immunometabolism as a means to therapeutically shape immune responses.

Several functional food components and naturally derived bioactives have been shown to influence macrophage metabolism[233]. For instance, SCFAs, such as butyrate and propionate, produced by microbial fermentation of dietary fibre, have been shown to suppress glycolysis and promote oxidative phosphorylation in macrophages, shifting the balance towards an anti-inflammatory M2 phenotype[234]. β-glucans, complex polysaccharides derived from fungi, have been shown to reprogram macrophage metabolism by enhancing glycolysis and oxidative phosphorylation, contributing to trained immunity which is a form of innate immune memory[235]. Similarly, polyphenols such as

resveratrol and curcumin have demonstrated the capacity to modulate macrophage metabolism by enhancing mitochondrial respiration and reducing ROS production[236,237]. Omega-3 fatty acids such as DHA and EPA have also been reported to influence macrophage polarisation, allowing macrophages to exert an M2 phenotype and suppress pro-inflammatory metabolic pathways[238,239]. These findings highlight the emerging paradigm in which diet-derived molecules can modulate immune cell energetics and function. However, while numerous functional food constituents have been studied in this context, far less is known about the role of HMOs in directly shaping macrophage metabolism, as these are the first foods that infants are exposed to.

HMOs are a structurally diverse class of unconjugated glycans found in high concentrations in human milk, known primarily for their prebiotic effects and their role in establishing the infant gut microbiota[240]. Beyond their interactions with the microbiome, increasing evidence suggests that HMOs can exert direct immunomodulatory effects on epithelial cells, DCs, and macrophages as HMOs can be absorbed into the blood stream[87,241]. Previous studies have shown that specific HMOs can modulate TLR-mediated signaling, suppress inflammatory cytokine production, and influence phagocytosis in macrophages[242]. However, the extent to which HMOs affect the metabolic pathways that underlie macrophage function remains poorly understood. This represents a critical knowledge gap, as the immunological functions of macrophages are intimately linked to their metabolic state. Also, it is not yet known whether HMOs can prevent or attenuate the early metabolic reprogramming that occurs during LPS-induced activation, particularly the rapid induction of aerobic glycolysis between 4- and 6 hours post-stimulation, a transition that often marks the point of irreversible pro-inflammatory commitment.

This chapter focuses on exploring the direct effects of individual predominant HMOs found in breastmilk, 2'-FL, 3'-SL and 6'-SL, on the metabolic pathways of macrophages. By analysing the effects of specific HMOs on glycolysis and oxidative phosphorylation, we aim to uncover how these carbohydrates influence the energy production and metabolic reprogramming of macrophages. Understanding these pathways is crucial, as they are fundamental to the activation, differentiation, and function of macrophages. The rationale for this study arises from the observation that while HMOs are known to interact with

immune cells including macrophages and alter immune responses, the metabolic underpinnings of these effects have not been comprehensively studied. The lack of detailed knowledge on how individual HMOs modulate the metabolic activity of macrophages limits our ability to fully grasp their role in immune system development and function. By addressing this gap, we seek to provide new insights into the metabolic adaptations driven by HMOs, potentially leading to novel therapeutic approaches that harness these interactions to improve immune health.

Aims of This Chapter:

- Determine how individual human milk oligosaccharides (2'-FL, 3'-SL, 6'-SL) alter the basal metabolic profile of BMDMs, focusing on glycolysis and oxidative phosphorylation.
- Link functional metabolic shifts to molecular mechanisms by examining changes in mitochondrial complex I activity and transcriptional regulation of glycolytic and oxidative phosphorylation genes in macrophages treated with HMOs under basal and inflammatory conditions.
- Define the temporal dynamics of HMO-driven metabolic reprogramming by assessing early (0-6 hours) and prolonged exposure effects on oxidative phosphorylation, glycolysis, and metabolite output in resting and activated macrophages.

3.2. Methods

BMDMs were generated from C57BL/6 mice as previously described in Chapter 2. Briefly, bone marrow cells were cultured for 7 days in macrophage differentiation medium supplemented with M-CSF. Unless otherwise stated, cells were seeded at a density of 500,000 cells/mL in the appropriate culture plate format and allowed to adhere and rest for a minimum of 3 hours prior to treatment. Cells were then stimulated HMOs (2 mM 2′-fucosyllactose, 1 mM 3′-sialyllactose, or 1 mM 6′-sialyllactose) in the presence or absence of LPS, 100 ng/mL for either 4 hours, 6 hours or 24 hours, depending on the assay as outlined below. Media treated cells served as controls, or LPS only treated cells served as LPS controls where applicable.

Seahorse Metabolic Flux Assay

Seahorse XF Mito Stress Tests were performed after either 4 hour or 24 hour HMO ± LPS treatment. Cells were washed twice with pre-warmed Seahorse assay medium and incubated in assay medium for 1 hour in a non-CO_2 incubator. Basal OCR was recorded (3 measurements), followed by sequential injections of oligomycin, FCCP, and rotenone/antimycin A, with 3 measurements recorded after each addition.

Seahorse XF Time-Course Metabolic Response Assays were conducted following overnight (16-18 hours) HMO treatment without prior LPS stimulation. Similar to Metabolic Flux assay cells were washed twice with pre-warmed Seahorse assay medium and incubated in assay medium for 1 hour in a non-CO_2 incubator. After baseline OCR measurement, LPS (100 ng/mL) or media (vesicle control) was injected into the wells and OCR or ECAR was recorded every 6 minutes for 6 hours.

Quantitative PCR for Metabolic Gene Expression

After 4 hour HMO ± LPS treatment RNA was extracted, cDNA synthesised, and qPCR performed using SYBR Green Master Mix with 2 µL cDNA and 0.5 µM primers. Cycling conditions were 95 °C for 5 minutes, followed by 40 cycles of 95 °C for 15 seconds and 60 °C for 1 minute. Expression was normalised to housekeeping genes and analysed using the ΔΔCt method.

Complex I Assay

A T-175 flask of BMDMs (containing approximately 40 million cells) was treated with 2 mg/mL 5-HMO mix overnight ± LPS (100 ng/mL) for 4 hours. Cells were then washed twice with PBS, removed from the flask using cell scraper and mitochondria were isolated as per protocol found in chapter 2. Complex Assay was performed as per protocol found in chapter 2.

Extracellular Lactate Production

Following overnight HMO ± 4 hour LPS treatment supernatants were collected by in-plate centrifugation, and 50 µL of each was mixed with 50 µL Lactate-Glo reagent in white-walled 96-well plates. After 1 hour incubation at room temperature, luminescence was measured.

3.3. Effect of HMOs at Given Concentrations on Macrophage Viability

To assess whether HMOs exert a cytotoxic effect on macrophages at the chosen concentrations, an Alamar Blue cell viability assay was performed. BMDMs were treated with increasing concentrations of HMOs; 2'-FL (1 mM, 2 mM, 4 mM), 3'-SL (0.5 mM, 1 mM, 2 mM), and 6'-SL (0.5 mM, 1 mM, 2 mM) in the presence or absence of 100 ng/mL LPS for 24 hours. The results **(Figure 3.1 A-C)** indicate that increasing HMO concentrations resulted in a gradual decline in metabolic activity, suggesting a reduction in viable cells. However, this decrease was not statistically significant for most conditions, with the exception of 4 mM 2'-FL in combination with LPS, which showed a significant reduction in viability. To further confirm cell viability, live BMDMs were stained with ZombieAqua Live/Dead and analysed via flow cytometry **(Figure 3.1 D-G)**. Representative plots show a comparable percentage of live cells across different treatment conditions, further supporting that HMOs do not induce significant cytotoxicity. Quantification of live cell populations **(Figure 3.1 H)** demonstrates that, 2'-FL, 3'-SL, and 6'-SL do not exert toxic effects on macrophages under these conditions.

Based on these findings, the selected HMO concentrations of 2 mM for 2'-FL and 1 mM for both 3'-SL and 6'-SL were deemed appropriate for further experimentation, as these oligosaccharides fall within physiologically relevant ranges found in human milk[243,244].

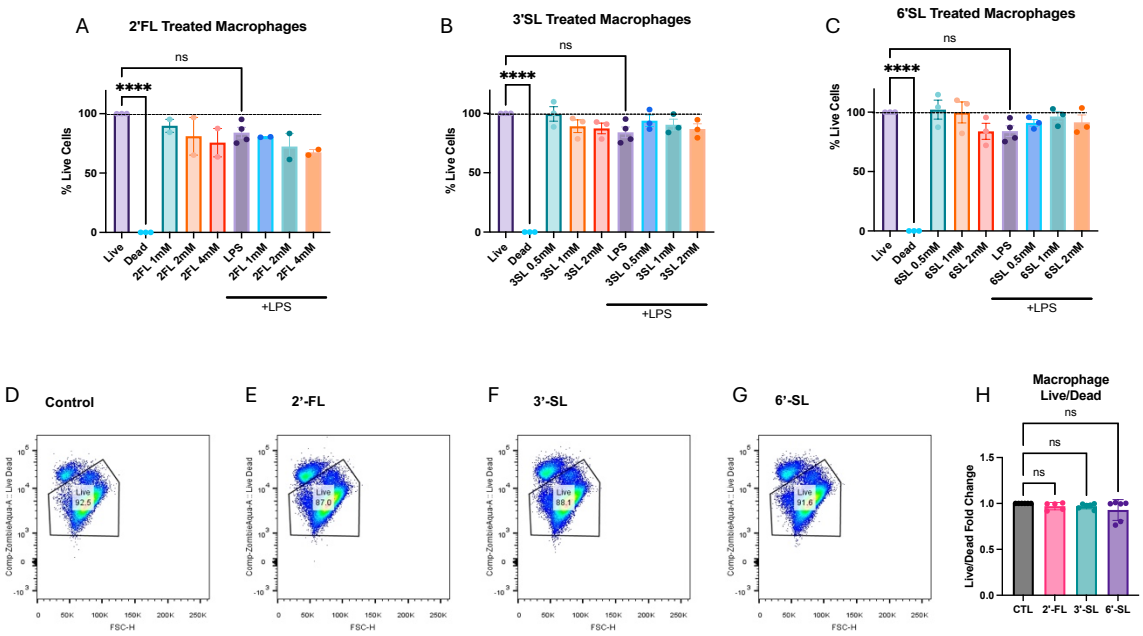

Figure 3. 1: **Cell Viability of Macrophages Following HMO Treatment**

BMDMs treated with increasing concentrations of HMOs ± 100 ng/mL LPS for 24 hours. Alamar blue was added and after 4 hours to cells treated with (A) 2'-FL (B) 3'-SL and (C) 6'-SL, absorbance was measured at 570/600nm. Live cells treated with (D) media control (E) 2'-FL (F) 3'-SL and (G) 6'-SL were stained using ZombieAqua Live/Dead, analysed by flow cytometry. (H) Barchart quantifying live treated cells compared as a fold change of their control. Data shown is from at least 3 independent experiments (n=3). Data is presented as the mean ± SEM. One-way ANOVA was used to calculate statistical significance (A-C) One-way ANOVA was used to calculate statistical significance (H) with a P-value of < 0.05 deemed statistically significant. ns indicates $p>0.05$, **** $p<0.0001$

3.4. Effects of HMOs on Macrophages Vary With Concentration

To determine the concentration at which HMOs; 2'-FL, 3'-SL and 6'-SL affect immune cell metabolism, we selected a concentration range of 1 μM to 1 mM to conduct a dose-response experiment on BMDMs. This range was chosen to reflect the physiologically relevant concentrations observed in the blood of breastfed infants[87], where HMOs are typically detected in micromolar (μM) to low millimolar (mM) levels but could theoretically reach higher concentrations under specific conditions. By encompassing this range, we aimed to capture both the baseline physiological effects and potential impacts of elevated HMO levels on immune cell function. Firstly, the concentration at which HMOs affect the OCR **(Figure 3.2),** and ECAR was determined **(Figure 3.3)** as a measure of oxidative phosphorylation and glycolysis, respectively. A titration of HMO concentrations was used; 2 μM, 20 μM, 200 μM and 2 mM for 2'-FL and 1 μM, 10 μM, 100 μM and 1 mM for 3'-SL and 6'-SL. HMOs caused a decrease in OCR, indicating a decrease in oxidative phosphorylation. For basal OCR the maximum concentration of 2'-FL (2 mM) increased OCR by approximately 20%. For basal OCR, the maximum concentration of both 3'-SL and 6'-SL (1 mM) decreased basal OCR by ~40% **(Figure 3.2)**. HMOs caused an increase in ECAR indicating an increase in glycolysis for all HMOs, with the maximum concentration of 2'-FL, 3'-SL and 6'-SL trending to increasing ECAR, although only 2'-FL was increased significantly **(Figure 3.3)**. The maximum concentrations of all HMOs used in this titration were selected for subsequent experiments, given the statistically significant effects on OCR and ECAR in macrophages.

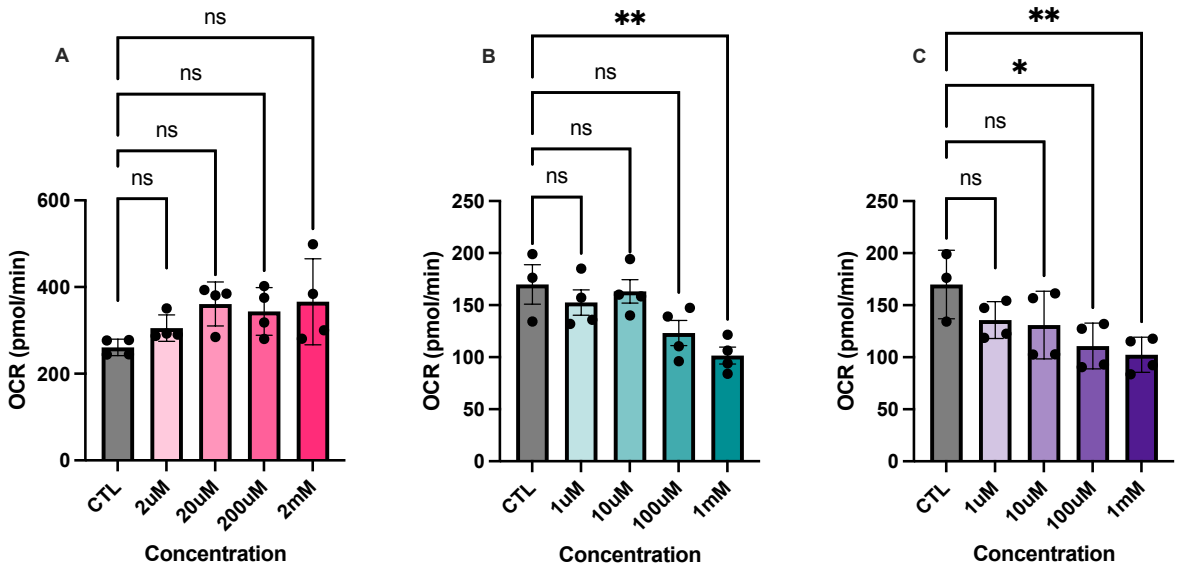

Figure 3. 2: **Basal OCR Analysis of BMDMs Treated with Increasing Concentrations of HMOs**

BMDMs were treated with increasing concentrations of HMOs; (A) 2'-FL (2 µM-2 mM), (B) 3'-SL (1 µM-1 mM), or (C) 6'-SL (1 µM-1 mM). Control used was media with no HMO. Graphs represent normalised OCR data shown n=4 from 2 independent experiments. Data is presented as the mean ± SEM displaying individual data points. One-way ANOVA was used to calculate statistical significance with a P-value of < 0.05 deemed statistically significant. ns indicates $p>0.05$, * $p<0.05$, ** $p<0.01$

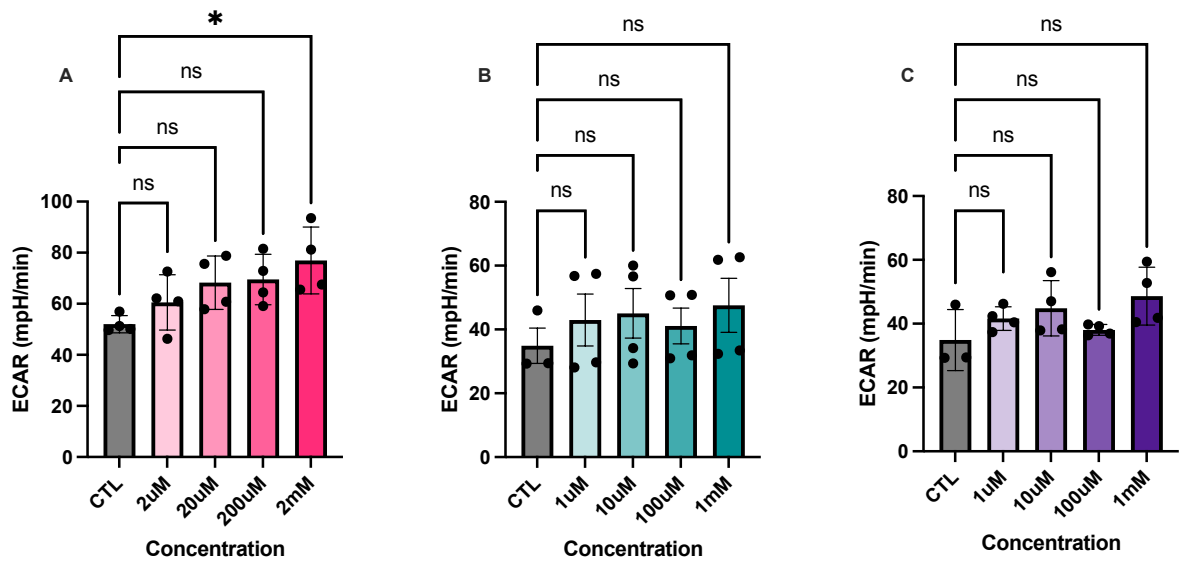

Figure 3. 3: **Basal ECAR Analysis of BMDMs Treated with Increasing Concentrations of HMOs**

BMDMs were treated with increasing concentrations of HMOs; (A) 2'-FL (2 µM-2 mM), (B) 3'-SL (1 µM-1 mM), or (C) 6'-SL (1 µM-1 mM). Graphs represent normalised ECAR data shown n=4 from 2 independent experiments. Data is presented as the mean ± SEM displaying individual data points. One-way ANOVA was used to calculate statistical significance with a P-value of < 0.05 deemed statistically significant. ns indicates $p>0.05$, * $p<0.05$

3.5. Metabolic Profiles of Macrophages Vary With Activation State

The differential effects of HMOs at the optimum concentrations on distinct subsets of macrophages, specifically unactivated (M0), M1 and M2 was determined. Given the distinct roles of these subsets, we hypothesised that HMOs might exert subset-specific effects, potentially enhancing or suppressing their activity depending on the inflammatory context.

The OCR and ECAR profiles were assessed in macrophage subsets to determine metabolic differences under different polarisation conditions. LPS and IL-4 treatments induce distinct metabolic changes in macrophages (**Figure 3.4 and 3.5**) polarising these macrophages into M1 and M2 subsets, respectively. LPS stimulation causes a decrease in OCR and an increase in ECAR, consistent with a shift toward glycolytic metabolism. In contrast, IL-4 treatment results in upregulation of both OCR and ECAR, reflecting enhanced oxidative phosphorylation and glycolytic activity. Following 4 hours of LPS stimulation, OCR decreased by approximately 37% compared to M0 (unstimulated) macrophages. This reduction became more pronounced after 24 hours of LPS treatment, with OCR decreasing by ~54% relative to M0 macrophages. Additionally, FCCP, a mitochondrial uncoupler that reveals the maximal respiratory capacity by collapsing the proton gradient, LPS-treated macrophages at 24 hours exhibited a complete loss of maximal respiratory capacity upon FCCP treatment, indicating diminished mitochondrial flexibility. In contrast, IL-4 treatment for 4 hours increased OCR by ~62% compared to M0 macrophages and doubled their maximal respiratory capacity. After 24 hours of IL-4 stimulation, OCR increased by ~44%, which was slightly lower than the 4 hour treatment but still demonstrated a sustained enhancement in maximal respiratory capacity (**Figure 3.4)**. ECAR in 4 hour LPS treated macrophages increased by 87% compared to M0 (unstimulated) macrophages. This effect was further amplified following 24 hours of LPS treatment, resulting in a 110% increase in ECAR compared to M0 macrophages. Similarly, IL-4 treatment also elevated ECAR in macrophages. A 4 hour IL-4 treatment led to a 125% increase in ECAR relative to M0 macrophages, representing the highest observed enhancement. However, after 24 hours of IL-4 stimulation, ECAR increased by 103%, indicating a slight reduction in the magnitude of the response compared to the 4 hour treatment (**Figure 3.5**).

To investigate the metabolic reprogramming of macrophages upon activation, we performed quantitative PCR analysis on BMDMs stimulated with LPS for 4 hours to induce an M1 phenotype. The expression of genes involved in oxidative phosphorylation and

glycolysis was compared between resting M0 and activated M1 macrophages. As shown in **Figure 3.6 A**, M1 macrophages exhibited a marked downregulation in the expression of key oxidative phosphorylation genes, including *Ndufb6, Sdha, Uqcrc1, Cox6c,* and *Atp5f1* (Complex I-V, respectively) relative to M0 controls. This suggests a suppression of mitochondrial respiratory activity upon LPS stimulation. Conversely, glycolytic gene expression was dramatically upregulated in M1 macrophages, as illustrated in **Figure 3.6 B**. Notably, hexokinase 2 (*Hk2)* expression increased by nearly 300-fold, while glucose transporter 1 (*Slc2a1)* and lactate dehydrogenase a (*Ldha)* were also significantly upregulated compared to M0 macrophages. These findings are consistent with a metabolic switch from oxidative phosphorylation to glycolysis during pro-inflammatory macrophage activation.

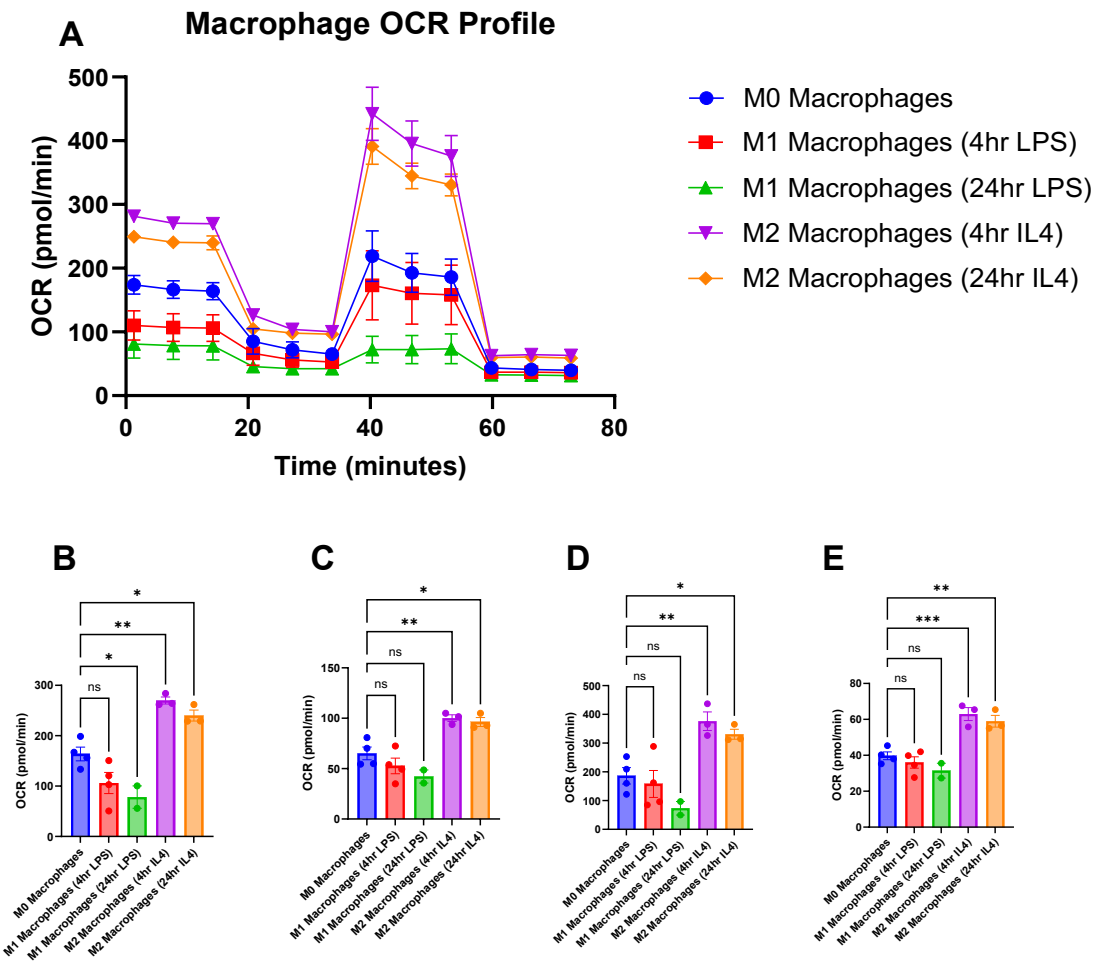

Figure 3. 4: **Metabolic Profiling of Macrophage Subsets by OCR Measurements**

(A) Macrophage OCR Profile: Basal and stress-induced mitochondrial respiration were measured over time in M0 macrophages (blue), M1 macrophages treated with 10*0 ng*/mL LPS for 4 hours (red) or 24 hours (green), and M2 macrophages treated with 4*0 ng*/mL IL-4 for 4 hours (purple) or 24 hours (orange). (B) *B*asal OCR rate (C) *O*ligomycin induced OCR rate (D) FCCP induced OCR rate (E) Rotenone/Antimycin A induced OCR rate. Data shown is from *4* independent experiments (n=*4*). Data is presented as the mean ± SEM. One-way ANOVA was used to calculate statistical significance with a P-value of < 0.05 deemed statistically significant. ns indicates $p>0.05$, * $p<0.05$, ** $p<0.01$, *** $p<0.001$

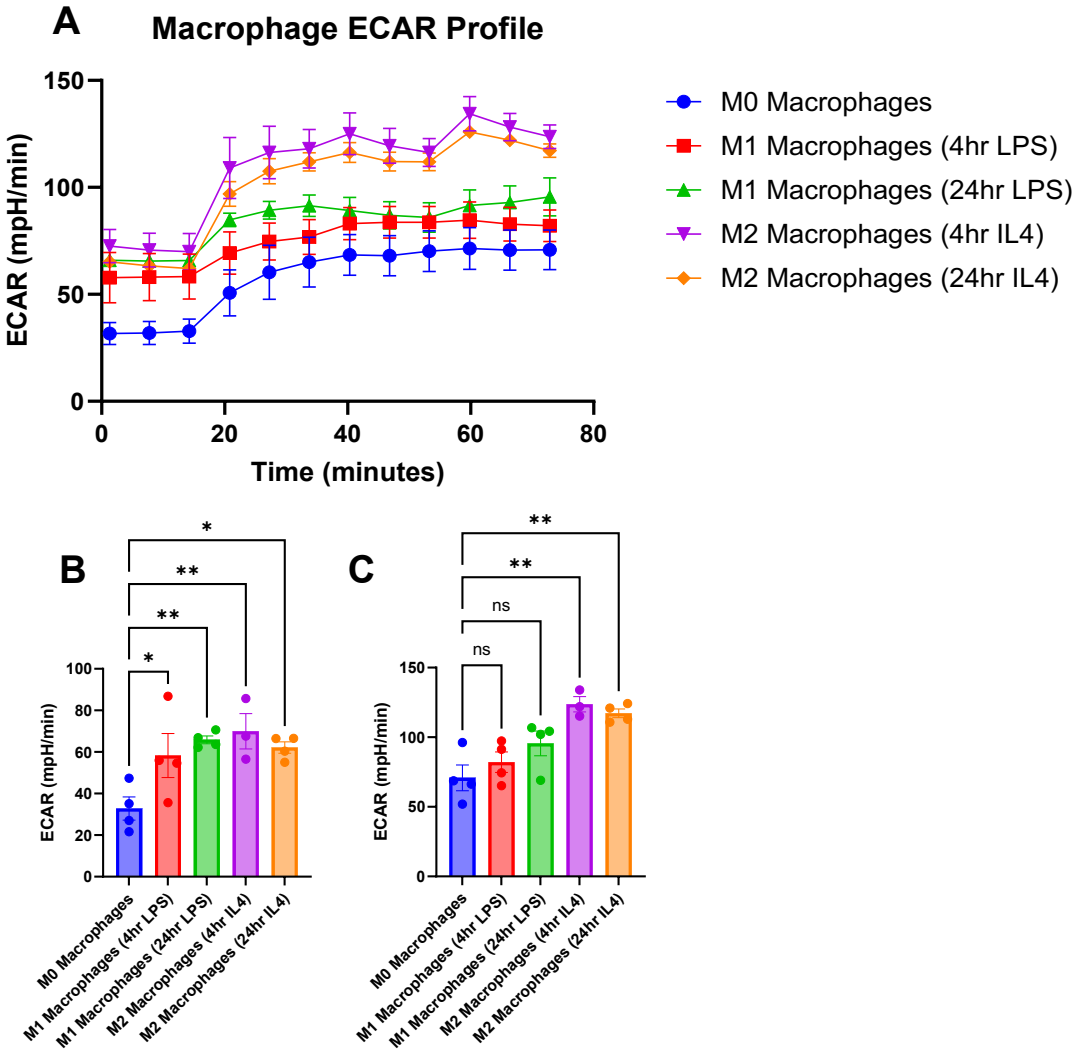

Figure 3. 5: **Metabolic Profiling of Macrophage Subsets by ECAR Measurements**

(A) Macrophage ECAR Profile: Glycolytic activity basal and stress-induced mitochondrial respiration were measured over time in M0 macrophages (blue), M1 macrophages treated with 10*0 ng*/mL LPS for 4 hours (red) or 24 hours (green), and M2 macrophages treated with 4*0 ng*/mL IL-4 for 4 hours (purple) or 24 hours (orange). (B) basal ECAR rate (C) oligomycin induced ECAR rate. Data shown is from *4* independent experiments (n=*4*). Data is presented as the mean ± SEM. One-way ANOVA was used to calculate statistical significance with a P-value of < 0.05 deemed statistically significant. ns indicates $p>0.05$, * $p<0.05$, ** $p<0.01$

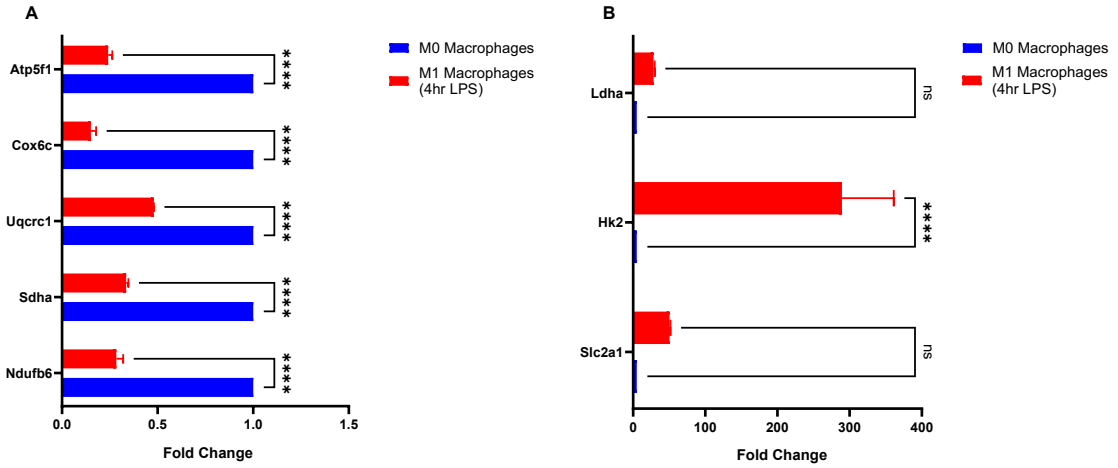

Figure 3. 6: **Gene Expression Analysis of Oxidative Phosphorylation and Glycolysis in Macrophage Subsets**

Quantitative PCR (qPCR) analysis of key metabolic genes involved in oxidative phosphorylation and glycolysis in BMDMs. (A) Expression levels of oxidative phosphorylation-related genes *Ndufb6, Sdha, Uqcrc1, Cox6c,* and *Atp5f1* in untreated M0 macrophages (blue bars) and LPS-stimulated M1 macrophages after 4 hours (red bars). (B) Expression levels of glycolytic genes *Slc2a1, Hk2,* and *Ldha* in M0 (blue bars) and M1 (red bars) macrophages. Data are presented as fold change relative to a control. Data shown is from *4* independent experiments (n=*4*). Data *is* presented as mean ± SEM. ns indicates $p>0.05$, **** $p<0.0001$

3.6. Effects of HMOs on Unactivated M0 Macrophages

To investigate how individual HMOs influence the metabolic activity of unactivated M0 macrophages, we evaluated both mitochondrial respiration and glycolytic flux in BMDMs treated with 2'-FL, 3'-SL, or 6'-SL. Metabolic readouts included OCR, ECAR, gene expression of oxidative phosphorylation and glycolytic enzymes, mitochondrial complex I activity, and lactate production.

A representative time-course trace of OCR following sequential injections of mitochondrial inhibitors in BMDMs treated with 2'-FL, 3'-SL, or 6'-SL is shown (**Figure 3.7 A**). Under basal conditions (prior to the first injection), BMDMs treated with 3'-SL and 6'-SL exhibited lower OCR compared to both untreated and 2'-FL-treated cells, indicating reduced mitochondrial respiration. Upon oligomycin injection, which inhibits ATP synthase and allows measurement of proton leak and non-ATP-linked respiration, OCR dropped across all conditions, with 6'-SL-treated cells having a significantly lower oligomycin rate. This suggests diminished ATP-coupled respiration in this group. The addition of FCCP, caused a marked increase in OCR in untreated, 2'-FL-, and 3'-SL-treated macrophages. In contrast, 6'-SL-treated cells exhibited a blunted response, suggesting limited spare respiratory capacity and reduced mitochondrial plasticity. Finally, rotenone and antimycin A, inhibitors of Complex I and III respectively, reduced OCR to similar minimal levels in all groups, reflecting non-mitochondrial respiration.

Quantitative analysis confirmed these observations (**Figure 3.7 B-E**). Basal OCR was significantly decreased in BMDMs treated with either 3'-SL or 6'-SL (**Figure 3.7 B**), while 2'-FL had no significant effect compared to untreated controls. Oligomycin-induced OCR, reflective of ATP-linked respiration, was markedly lower in only the 6'-SL-treated group (**Figure 3.7 C**), reinforcing the idea that these HMOs impair mitochondrial ATP production. The maximal respiratory capacity, assessed via FCCP-induced OCR, was also reduced but not significantly in 6'-SL-treated cells (**Figure 3.7 D**). Rotenone/antimycin A-induced OCR was comparable across all treatment groups (**Figure 3.7 E**), indicating that non-mitochondrial respiration remained unaffected by HMO treatment.

To determine whether the observed functional mitochondrial suppression was reflected at the transcriptional level, we evaluated the expression of genes involved in the oxidative phosphorylation pathway. A heat map showing the log2-transformed, normalised expression of five key genes; *Ndufb6, Sdha, Uqcrc1, Cox6c,* and *Atp5f1* is presented in

Figure 3.8. BMDMs treated with 3'-SL or 6'-SL showed a consistent downregulation of these genes, indicating a broad suppression of mitochondrial respiratory chain components. Conversely, 2'-FL-treated macrophages exhibited gene expression patterns that were increased compared to untreated controls, further highlighting the specificity of the mitochondrial suppression induced by sialylated HMOs and the variety of effects different HMOs induce in cellular subsets.

To directly assess enzymatic function of the mitochondrial respiratory chain, we quantified Complex I-specific activity using a spectrophotometric assay based on NADH oxidation. A 5-HMO mix significantly reduced Complex I activity in BMDMs (**Figure 3.9**), as indicated by a lower rate of NADH oxidation. This reduction in enzymatic activity corroborates the decreased OCR observed in the Seahorse assay and supports the conclusion that HMOs, particularly those with sialic acid residues, functionally suppress mitochondrial respiration in unactivated macrophages.

We next investigated the effects of HMOs on glycolytic metabolism. A representative ECAR time-course, which serves as a proxy for lactate-associated extracellular acidification and thus glycolytic flux, is shown (**Figure 3.10 A**). Basal ECAR was elevated in macrophages treated with 3'-SL and 6'-SL relative to both control and 2'-FL-treated cells. These findings are quantified (**Figure 3.10 B**), which demonstrates a significant increase in basal ECAR following 3'-SL and 6'-SL treatment, consistent with a metabolic shift toward glycolysis. Following oligomycin injection, ECAR typically increases as cells compensate for the loss of mitochondrial ATP production by upregulating glycolysis. Oligomycin-induced ECAR was unaffected in 3'-SL- and 6'-SL-treated BMDMs compared to controls (**Figure 3.910 C**), suggesting no effect of HMOs on the glycolytic reserve of macrophages.

To determine whether these functional changes were underpinned by transcriptional regulation, we measured expression of key glycolytic genes. A heat map displays the data (**Figure 3.11**), showing a 25-fold increase in expression of *Slc2a1*, 110-fold increase in *Hk2*, and 20-fold increase in *Ldha* in BMDMs treated with 6'-SL. These genes play critical roles in glucose uptake, glycolytic entry, and lactate production, respectively. The upregulation of these transcripts aligns with the elevated ECAR observed, indicating a transcriptionally supported glycolytic shift. 3’-SL treatment resulted in a 6-fold and 5-fold increase in *Hk2* and *Ldha* respectively. In contrast 2’-FL treatment resulted in an observed 20-fold increase in *Ldha* alone.

Finally, we measured lactate production as a terminal readout of glycolytic activity. Elevated extracellular lactate concentrations were observed following treatment with 3'-SL and 6'-SL compared to control and 2'-FL-treated groups (**Figure 3.12**). This result aligns with the elevated ECAR and *Ldha* expression and confirms that increased glycolysis in these cells leads to enhanced metabolic output.

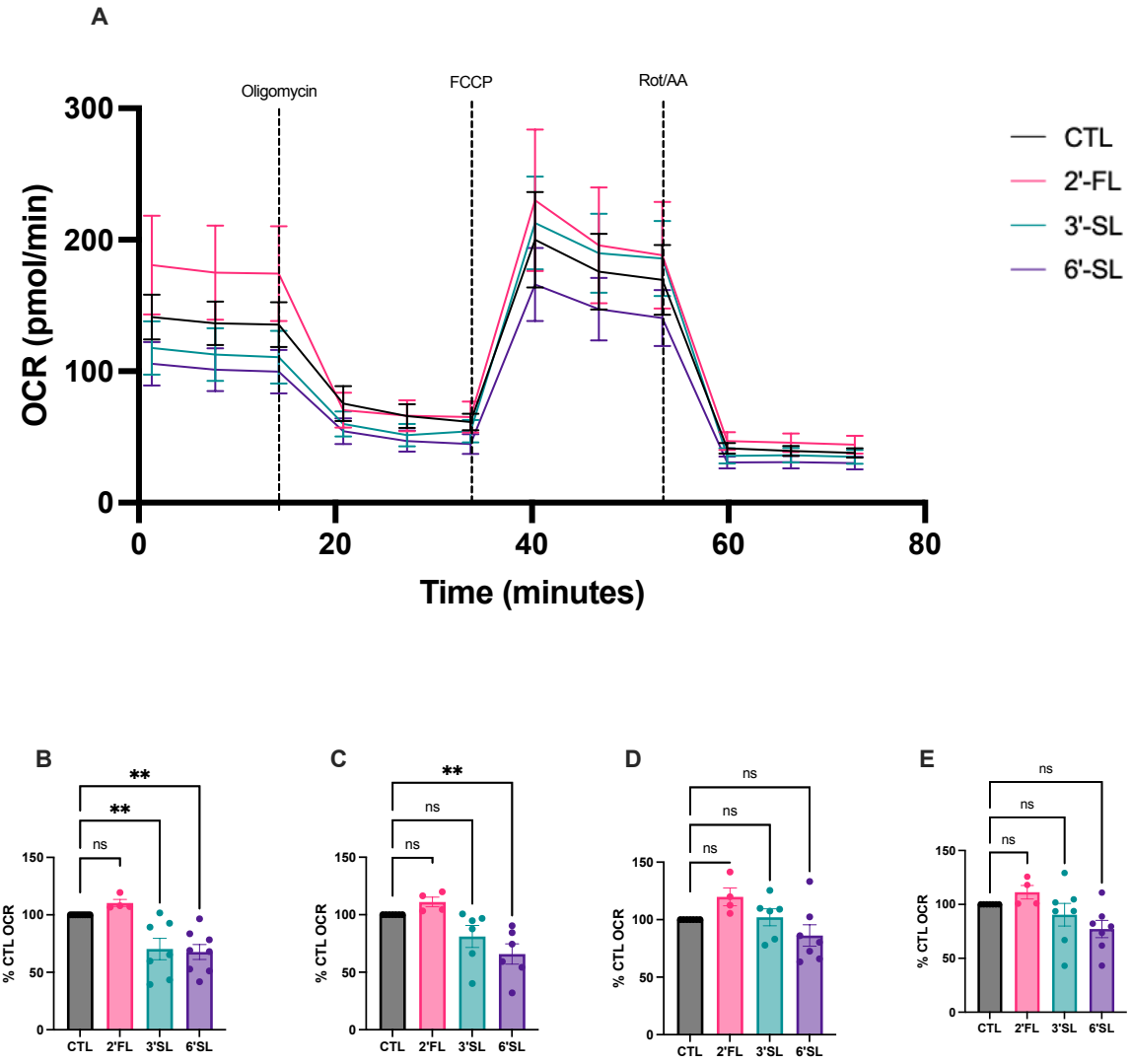

Figure 3. 7: **OCR Measurements in BMDMs Treated with Individual HMOs**

BMDMs were treated with HMOs; 2'-FL (2 mM), 3'-SL (1 mM), or 6'-SL (1 mM). (A) representative time-course graph of OCR. (B) basal OCR rate (C) oligomycin induced OCR rate (D) FCCP induced OCR rate (E) Rotenone/Antimycin A induced OCR rate. Data shown is from 8 independent experiments (n=8). Data is presented as the mean ± SEM. One-way ANOVA was used to calculate statistical significance with a P-value of < 0.05 deemed statistically significant. ns indicates $p>0.05$, ** $p<0.01$

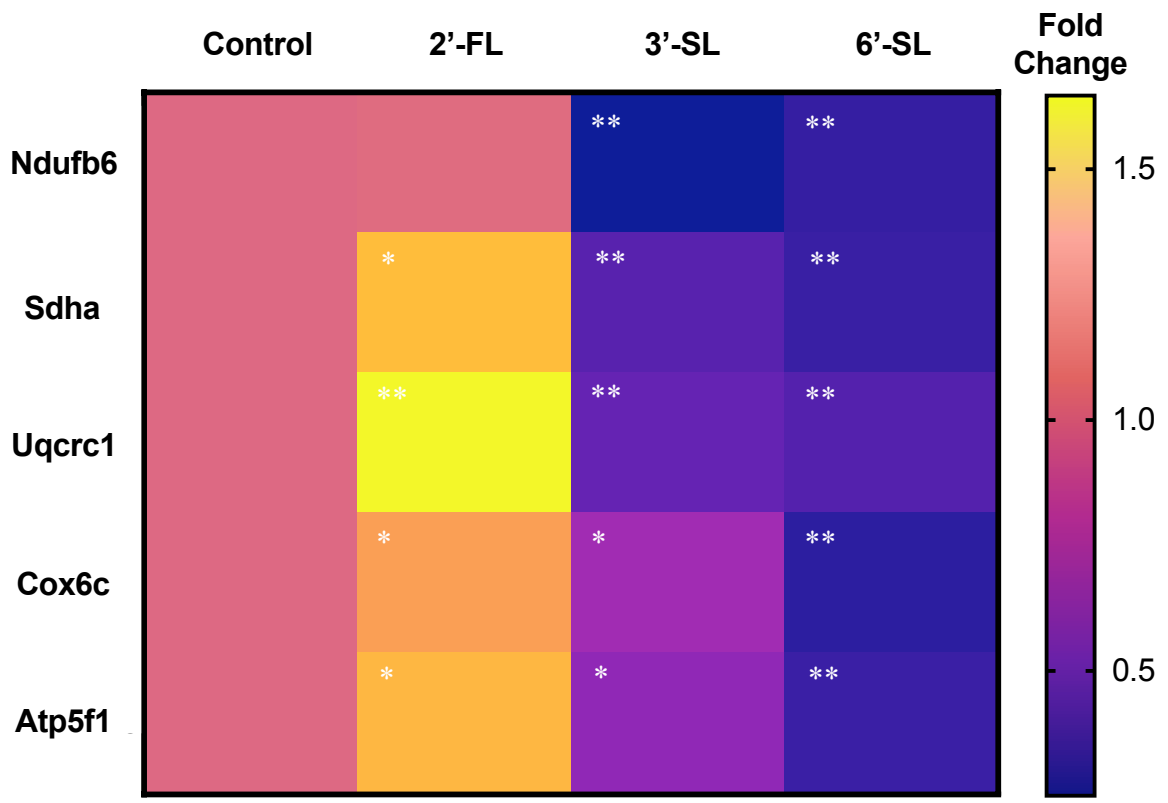

Figure 3. 8: **Expression of Oxidative Phosphorylation Genes in BMDMs Treated with HMOs**

Quantitative PCR analysis was performed to assess the mRNA expression of key genes involved in oxidative phosphorylation (*Ndufb6, Sdha, Uqcrc1, Cox6c, and Atp5f1*) in BMDMs following treatment with HMOs; 2'-FL (2 mM), 3'-SL (1 mM), or 6'-SL (1 mM). The heat map shows relative expression levels, with each column representing a treatment condition and each row representing a specific gene. Expression values are log2-transformed and normalised to housekeeping genes. Data shown is from 3 independent experiments (n=3). * indicates $p<0.05$, ** $p<0.01$

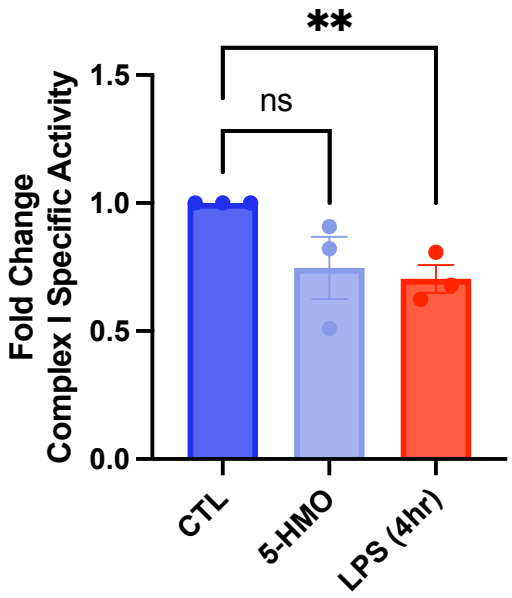

Figure 3. 9: **Complex I Enzymatic Activity in BMDMs Following Treatment with 5-HMO Mix**

The specific activity of complex I in BMDMs ± 5-HMO mix is expressed as pmol/min/mg ± SEM. Data shown is normalised to the control from 3 independent experiments (n=3). A t-test was used to calculate statistical significance with a P-value of < 0.05 deemed statistically significant. ns indicates $p>0.05$, ** $p<0.01$

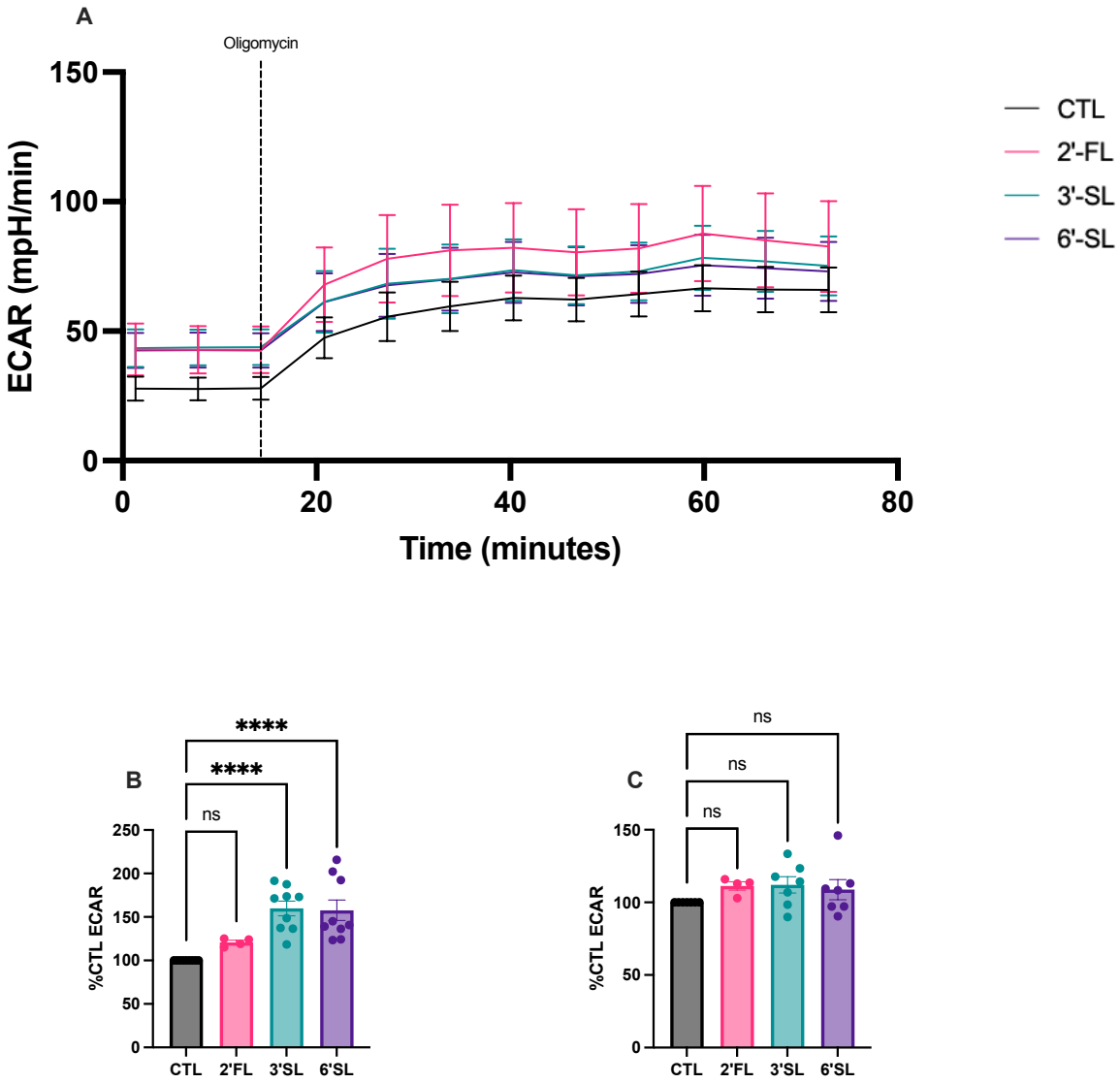

Figure 3. 10: **ECAR Measurements in BMDMs Treated with Individual HMOs**

BMDMs were treated with HMOs; 2'-FL (2 mM), 3'-SL (1 mM), or 6'-SL (1 mM). (A) representative time-course graph of ECAR. (B) basal ECAR rate (C) oligomycin induced ECAR rate Data shown is from 8 independent experiments (n=8). Data is presented as the mean ± SEM. One-way ANOVA was used to calculate statistical significance with a P-value of < 0.05 deemed statistically significant. ns indicates $p>0.05$, **** $p<0.0001$

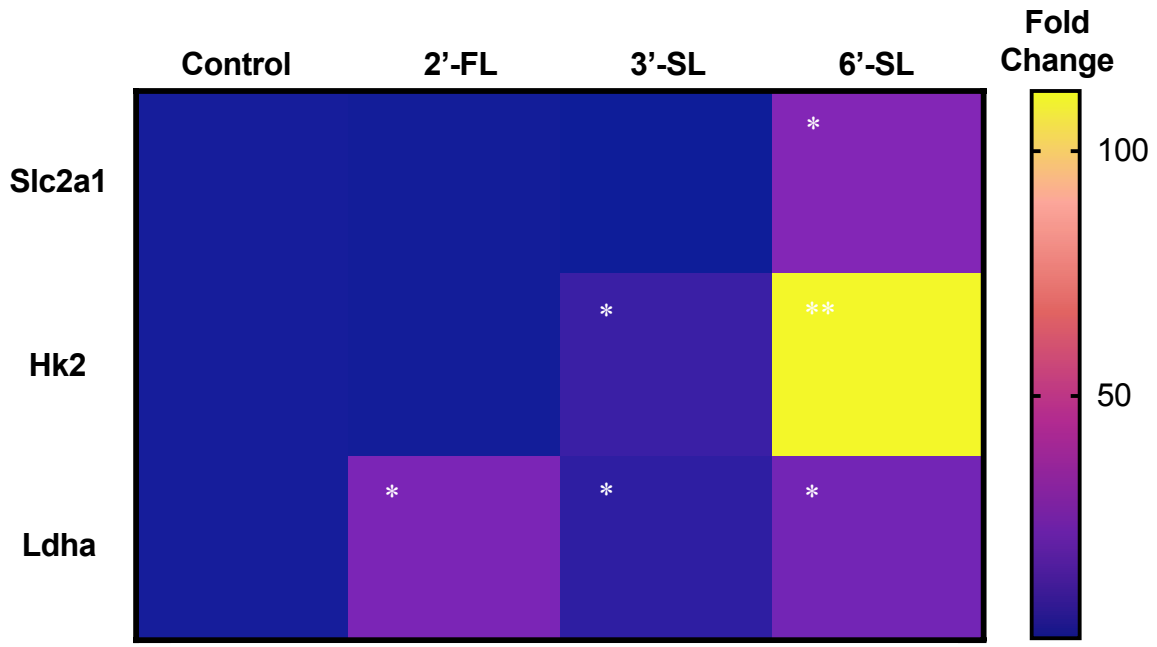

Figure 3. 11: **Expression of Glycolytic Genes in BMDMs Treated with HMOs**

BMDMs were treated with HMOs; 2'-FL (2 mM), 3'-SL (1 mM), or 6'-SL (1 mM) and the expression of key glycolytic genes (*Slc2a1, Hk2, Ldha*) was analysed by quantitative PCR. The heat map presents normalised, log2-transformed expression values, with each row representing an individual gene and each column corresponding to a specific HMOs; 2'-FL (2 mM), 3'-SL (1 mM), or 6'-SL (1 mM). Data shown is from 3 independent experiments (n=3). * indicates $p<0.05$, ** $p<0.01$

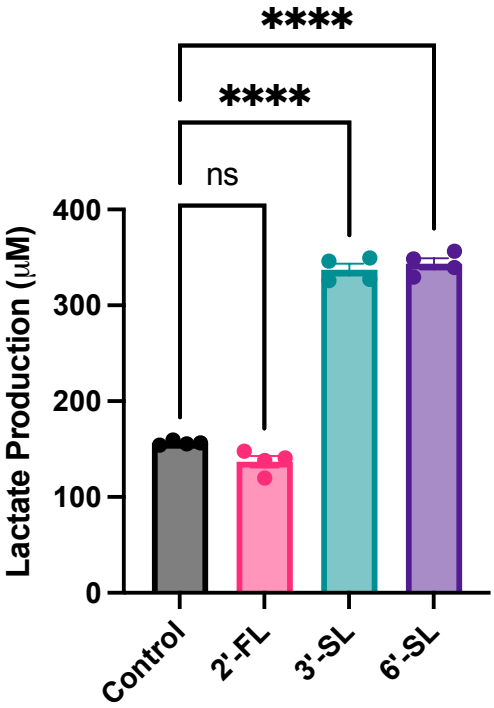

Figure 3. 12: **Lactate Production in BMDMs Following HMO Treatment**

BMDMs were treated with HMOs overnight. Lactate production was measured via lactate quantification assay via luminescence (RLU). Data shown is from 4 independent experiments (n=4). Data is presented as the mean ± SEM. One-way ANOVA was used to calculate statistical significance with a P-value of < 0.05 deemed statistically significant. ns indicates $p>0.05$, **** $p<0.0001$

3.7. Effects of HMOs on Classically Activated M1 Macrophages

To determine how HMOs modulate cellular metabolism in classically activated (M1) macrophages, BMDMs were co-treated with lipopolysaccharide (LPS; 100 ng/mL) and either 2'-FL (2 mM), 3'-SL (1 mM), or 6'-SL (1 mM). A combination of Seahorse extracellular flux analysis, qPCR, enzyme activity assays, and lactate quantification was employed to assess mitochondrial and glycolytic responses.

Mitochondrial respiration was first assessed following 4 hour LPS stimulation using OCR as a proxy for oxidative phosphorylation (**Figure 3.13**). The representative OCR time-course plot (**Figure 3.13 A)** revealed a marked suppression of mitochondrial activity in BMDMs treated with either 3'-SL or 6'-SL in combination with LPS, compared to LPS alone or the 2'-FL condition. Quantification of basal OCR (**Figure 3.13 B**) shows a statistically significant reduction in oxygen consumption in the 3'-SL and 6'-SL groups, indicating an inhibition of mitochondrial respiration. Upon oligomycin injection, which inhibits ATP synthase, ATP-linked respiration (**Figure 3.13 C**) was reduced, however not significantly in the sialylated HMO groups, implying decreased mitochondrial ATP production. FCCP-induced maximal respiration (**Figure 3.13 D**) remained unchanged following HMO treatments, reflecting no change in respiratory reserve capacity. Rotenone/Antimycin A-induced respiration, which reflects non-mitochondrial oxygen consumption (**Figure 3.13 E**), remained largely unchanged in 2'-FL and 3'-SL treated, suggesting that the observed differences were specific to mitochondrial function, 6'-SL treated cells had a significant decrease in this rate.

These functional changes were supported by gene expression analysis of oxidative phosphorylation related genes (**Figure 3.14**). qPCR revealed that treatment with 3'-SL suppressed the transcription of multiple genes encoding components of the mitochondrial electron transport chain, including *Ndufb6* (Complex I), *Sdha* (Complex II), *Uqcrc1* (Complex III), *Cox6c* (Complex IV), and *Atp5f1* (Complex V). The heatmap illustrates a consistent downregulation in the expression of these genes relative to both untreated and 2'-FL conditions, aligning with the functional OCR data and suggesting transcriptional repression of mitochondrial bioenergetics under sialyllactose treatment. Surprisingly, 6'-SL seemed to increase the expression of these oxidative phosphorylation genes at this point.

To further validate mitochondrial dysfunction, enzymatic activity of Complex I was measured via spectrophotometric detection of NADH oxidation at 340 nm (**Figure 3.15**). BMDMs were pre-treated overnight with a mixed HMO solution and stimulated with LPS for 4 hours. Complex I-specific activity was significantly decreased in HMO-treated BMDMs, demonstrating a functional impairment in electron transport at the level of NADH dehydrogenase. This enzymatic reduction corroborates the suppressed mitochondrial respiration observed in OCR assays and suggests that HMOs interfere with early steps of the electron transport chain in M1 macrophages.

In parallel, glycolytic activity was assessed via ECAR (**Figure 3.14**). The ECAR time-course trace (**Figure 3.16 A**) showed enhanced basal acidification in 2'-FL and 3'-SL conditions, suggesting increased glycolytic flux following 4 hour LPS stimulation. Quantitative analysis of basal ECAR (**Figure 3.16 B**) confirmed significantly elevated levels in both 2'-FL and 3'-SL treated BMDMs, while 6'-SL was increased but not significantly. Oligomycin-induced ECAR (**Figure 3.16 C**), which reflects glycolytic capacity in the absence of mitochondrial ATP production, oligomycin-induced ECAR was unaffected in 3'-SL and 6'-SL-treated BMDMs compared to controls, suggesting no effect of HMOs on the glycolytic reserve of macrophages.

These functional changes were further reflected at the transcriptional level. qPCR analysis of glycolytic genes (**Figure 3.17**) revealed decreased expression of *Slc2a1* , *Hk2* , and *Ldha* in response to 3'-SL and 6'-SL treatment. Again, 2'-FL induced an increase in these transcriptional changes, highlighting the unique metabolic reprogramming capacity associated with different HMOs under different inflammatory conditions.

To determine whether the increase in glycolytic gene expression translated into increased metabolic output, lactate production was quantified following 4 hour HMO + LPS co-treatment (**Figure 3.18**). Both 2'-FL and 3'-SL significantly elevated lactate levels, indicating a shift toward aerobic glycolysis in M1-polarised macrophages. 6'-SL treatment did not significantly alter lactate production, further distinguishing its metabolic effects from other HMOs.

To evaluate the persistence of HMO-mediated metabolic effects, BMDMs were treated for 24 hours with LPS and HMOs and metabolic parameters were reassessed. Interestingly, after prolonged stimulation, no significant differences in basal OCR (**Figure 3.19 B**) or ECAR (**Figure 3.20 B**) were observed among treatment groups, as shown in the

representative traces (**Figures 3.19 A and 3.20 A**). Oligomycin, FCCP, and rotenone/antimycin A responses remained similar across conditions (**Figures 3.19 C-E and 3.20 C**), suggesting that the metabolic effects of 3'-SL and 6'-SL are acute and transient, manifesting most strongly within the first few hours of LPS activation.

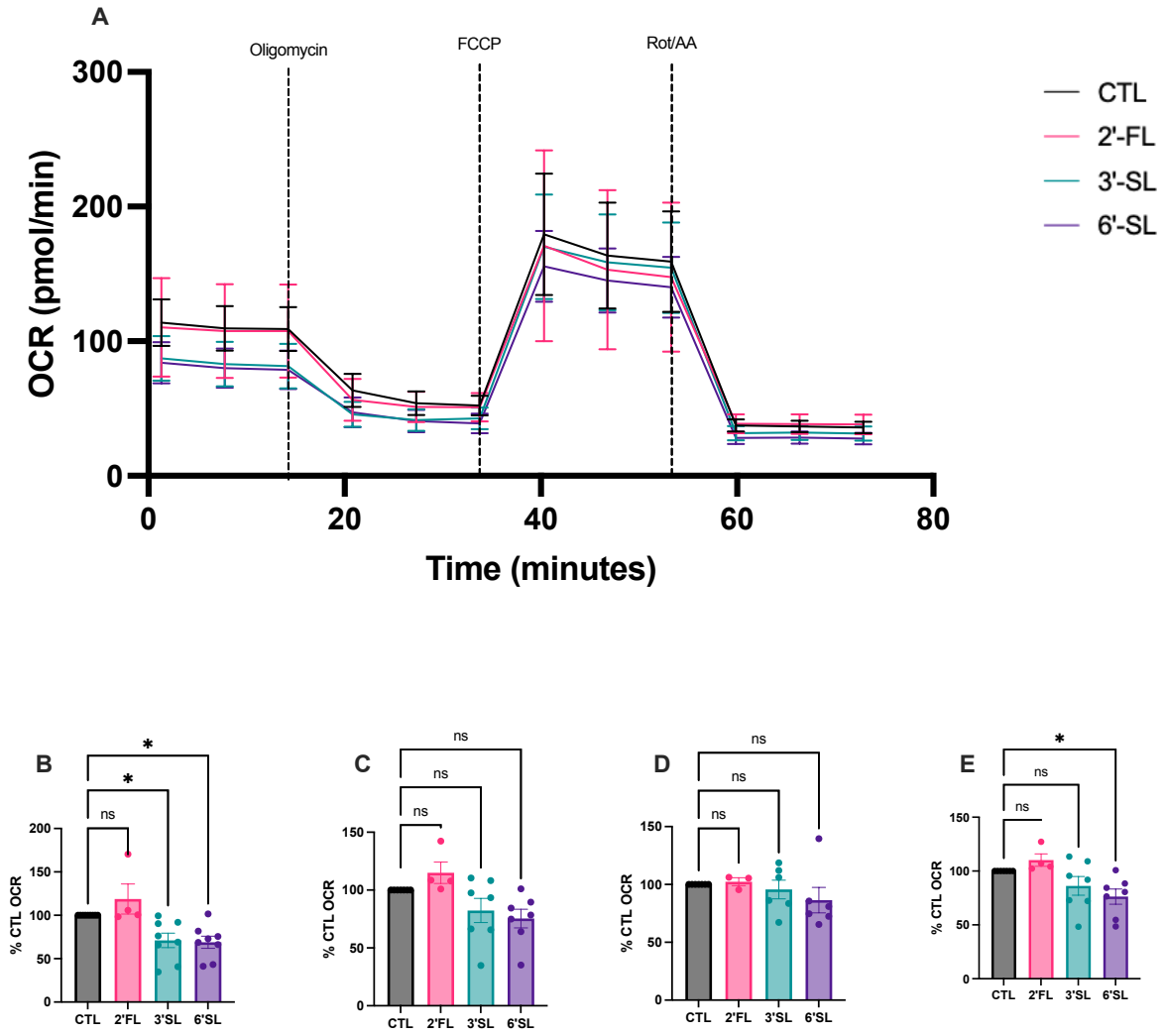

Figure 3. 13: **OCR Measurements in LPS-Activated BMDMs Treated with HMOs**

BMDMs were treated with HMOs; 2'-FL (2 mM), 3'-SL (1 mM), or 6'-SL (1 mM) + LPS (100 ng/mL) for 4 hours. (A) representative time-course graph of OCR. (B) basal OCR rate (C) oligomycin induced OCR rate (D) FCCP induced OCR rate (E) Rotenone/Antimycin A induced OCR rate. Data shown is from 8 independent experiments (n=8). Data is presented as the mean ± SEM. One-way ANOVA was used to calculate statistical significance with a P-value of < 0.05 deemed statistically significant. ns indicates $p>0.05$, * $p<0.05$

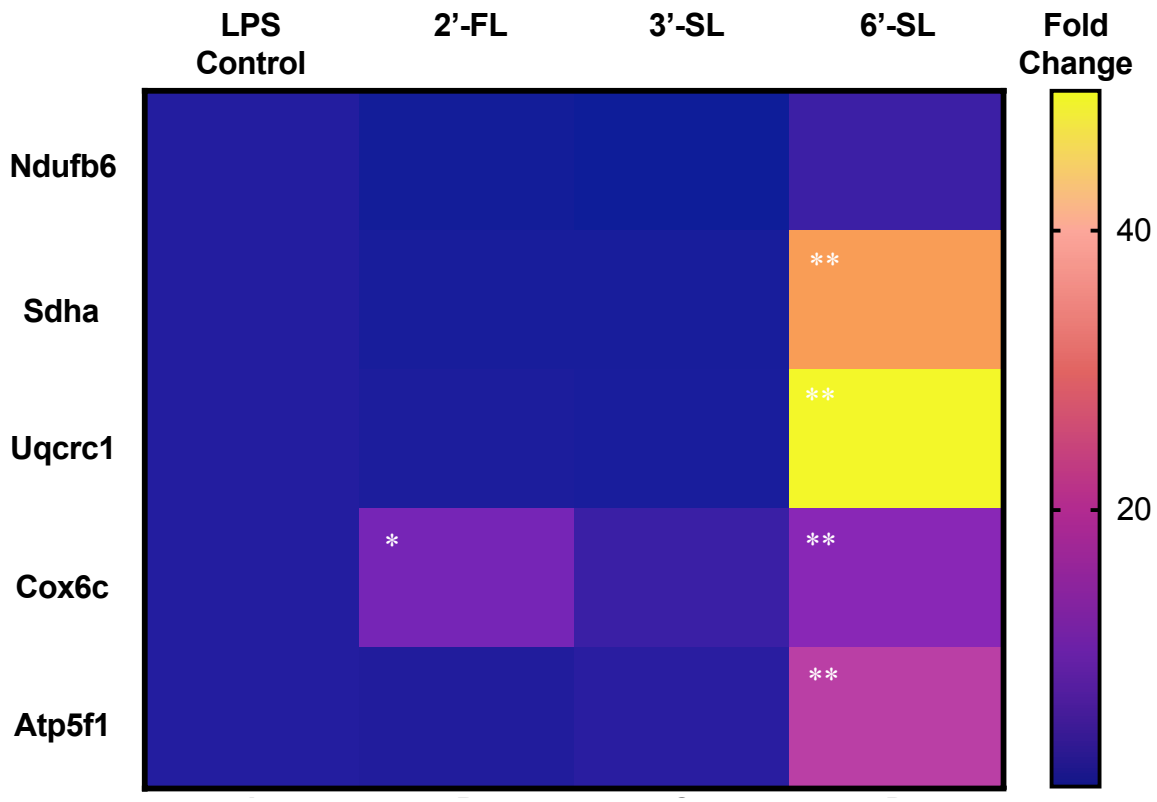

Figure 3. 14: **Expression of Oxidative Phosphorylation Genes in LPS-Activated BMDMs Treated with HMOs**

Quantitative PCR analysis was performed to assess the mRNA expression of key genes involved in oxidative phosphorylation (*Ndufb6, Sdha, Uqcrc1, Cox6c, and Atp5f1*) in BMDMs following treatment with HMOs; 2'-FL (2 mM), 3'-SL (1 mM), or 6'-SL (1 mM) + 100 ng/mL LPS for 4 hours. The heat map shows relative expression levels, with each column representing a treatment condition and each row representing a specific gene. Expression values are log2-transformed and normalised to housekeeping genes. Data shown is from 3 independent experiments (n=3). * indicates $p<0.05$, ** $p<0.01$

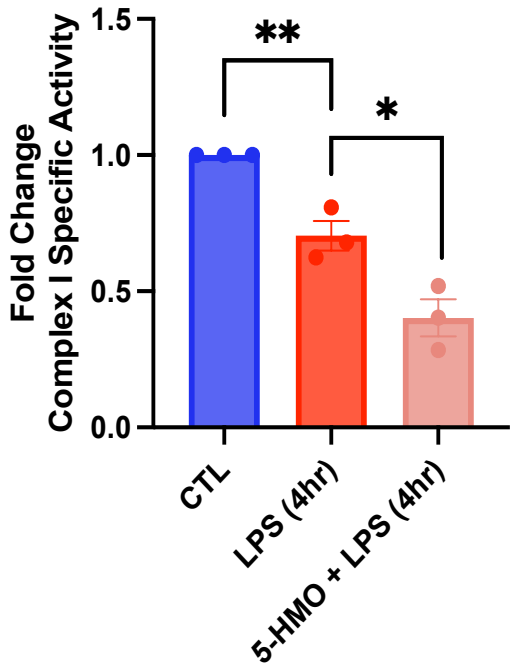

Figure 3. 15: **Complex I Enzymatic Activity in LPS-Activated BMDMs Following Treatment with 5-HMO Mix**

The specific activity of complex I in BMDMs ± 5-HMO mix with LPS 4 hours is expressed as pmol/min/mg ± SEM. Data shown is normalised to control from 3 independent experiments (n=3). A t-test was used to calculate statistical significance with a P-value of < 0.05 deemed statistically significant. * indicates $p<0.05$, ** $p<0.01$

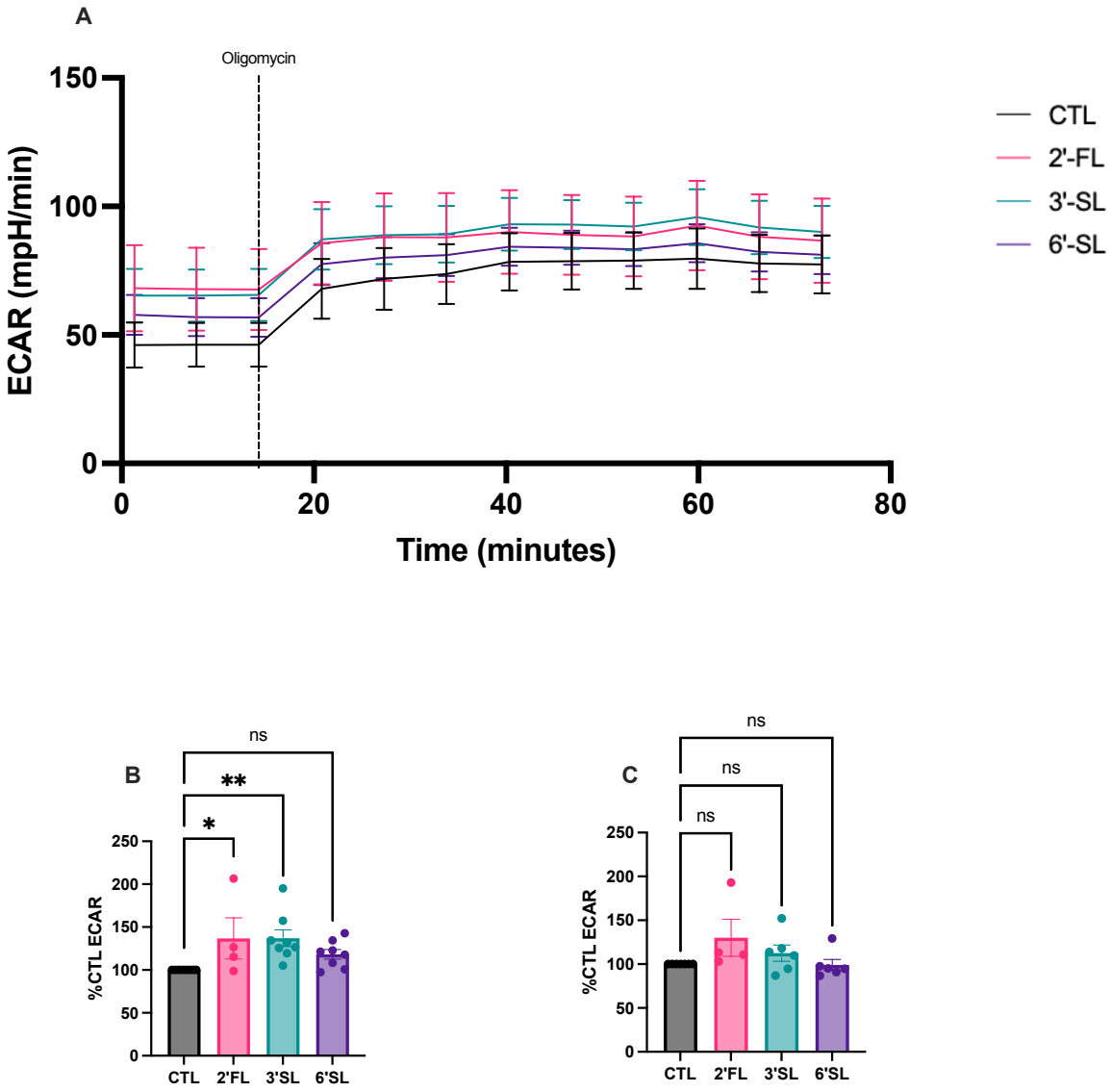

Figure 3. 16: **ECAR Measurements in LPS-Activated BMDMs Treated with HMOs**

BMDMs were treated with HMOs; 2'-FL (2 mM), 3'-SL (1 mM), or 6'-SL (1 mM) + LPS (100 ng/mL) for 4 hours. (A) representative time-course graph of ECAR. (B) basal ECAR rate (C) oligomycin induced ECAR. Data shown is from 8 independent experiments (n=8). Data is presented as the mean ± SEM. One-way ANOVA was used to calculate statistical significance with a P-value of < 0.05 deemed statistically significant. ns indicates $p>0.05$, * $p<0.05$, ** $p<0.01$

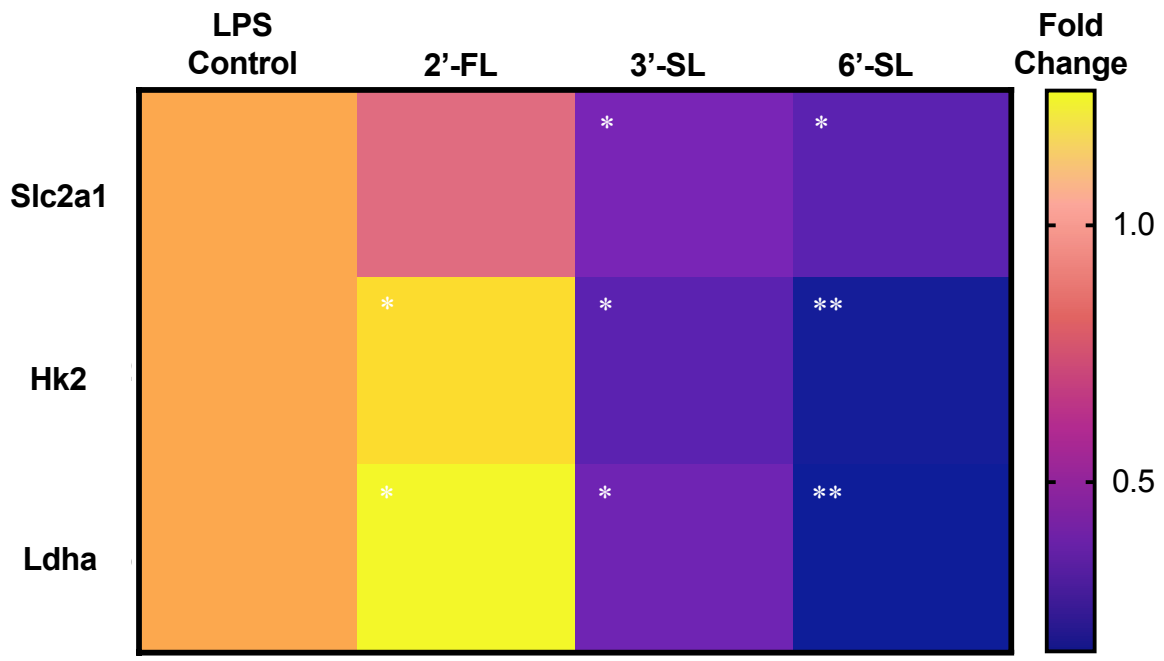

Figure 3. 17: **Expression of Glycolytic Genes in LPS-Activated BMDMs Treated with HMOs**

BMDMs were treated with HMOs; 2'-FL (2 mM), 3'-SL (1 mM), or 6'-SL (1 mM) + 100 ng/mL LPS for 4 hours and the expression of key glycolytic genes (*Slc2a1, Hk2, Ldha*) was analysed by quantitative PCR. The heat map presents normalised, log2-transformed expression values, with each row representing an individual gene and each column corresponding to a specific HMOs; 2'-FL (2 mM), 3'-SL (1 mM), or 6'-SL (1 mM). Data shown is from 3 independent experiments (n=3). * indicates $p<0.05$, ** $p<0.01$

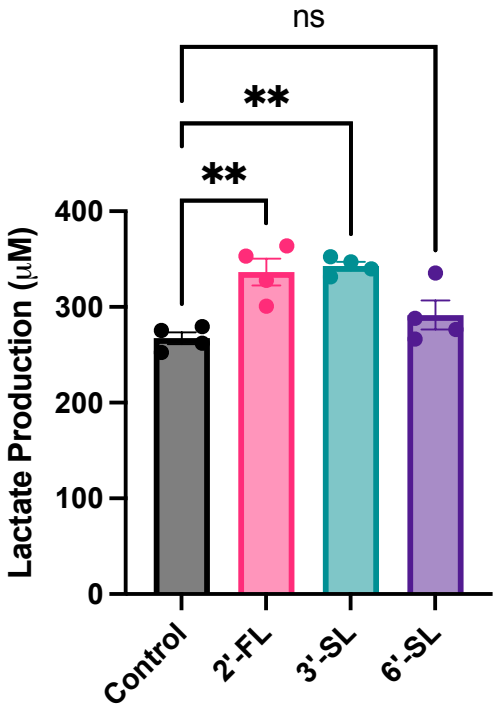

Figure 3. 18: **Lactate Production in LPS-Activated BMDMs Following HMO Treatment**

BMDMs were treated with HMOs overnight and then treated with LPS for 4 hours. Lactate production was measured via lactate quantification assay. Data shown is from 4 independent experiments (n=4). Data is presented as the mean ± SEM. One-way ANOVA was used to calculate statistical significance with a P-value of < 0.05 deemed statistically significant. ns indicates $p>0.05$, ** $p<0.01$

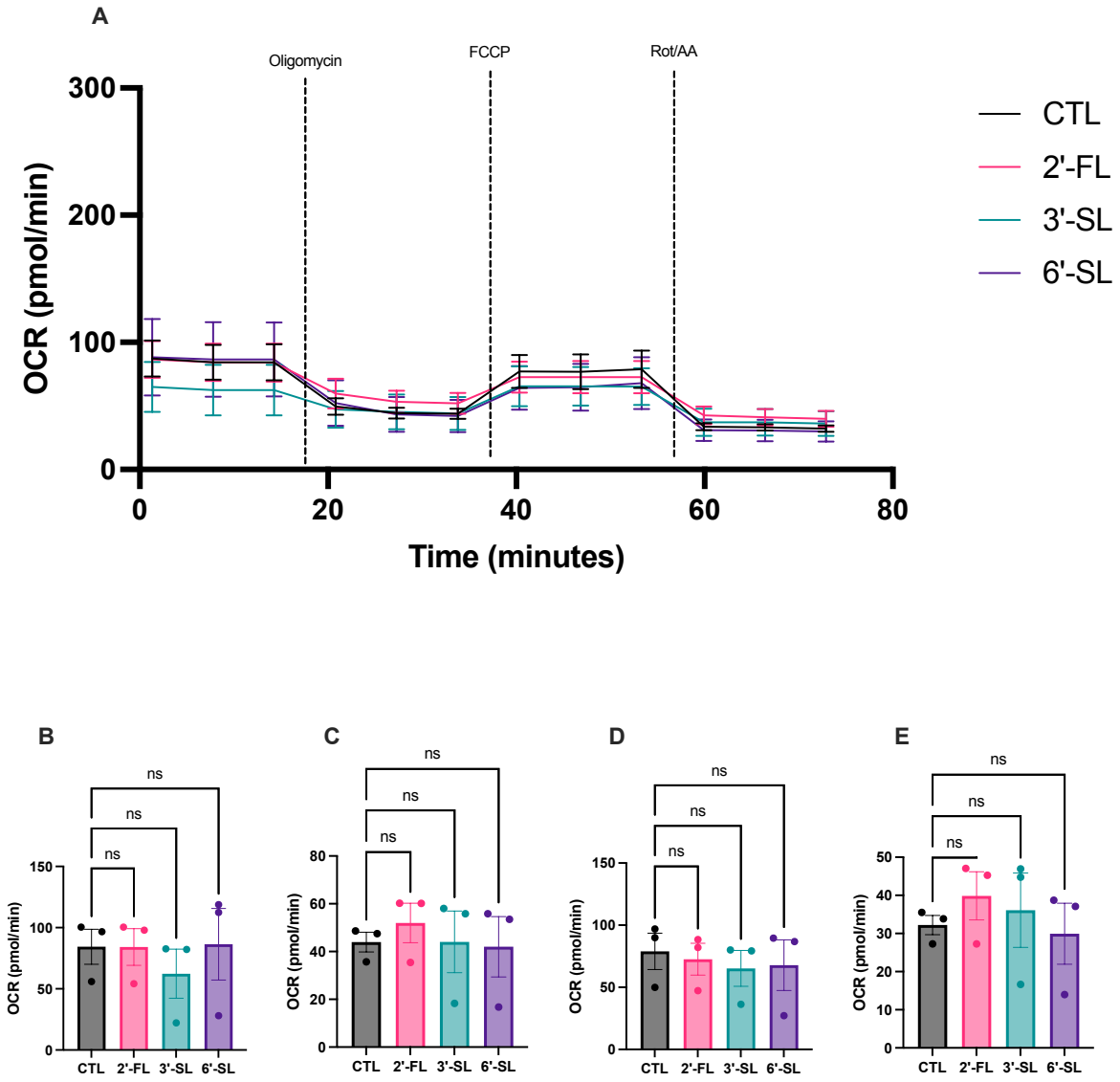

Figure 3. 19: **OCR Measurements in BMDMs with Prolonged LPS-Activation Treated with HMOs**

BMDMs were treated with HMOs; 2'-FL (2 mM), 3'-SL (1 mM), or 6'-SL (1 mM) + LPS (100 ng/mL) for 24 hours. (A) representative time-course graph of OCR. (B) basal OCR rate (C) oligomycin induced OCR rate (D FCCP induced OCR rate (E) Rotenone/Antimycin A induced OCR rate. Data shown is from 3 independent experiments (n=3). Data is presented as the mean ± SEM. One-way ANOVA was used to calculate statistical significance with a P-value of < 0.05 deemed statistically significant. ns indicates $p>0.05$

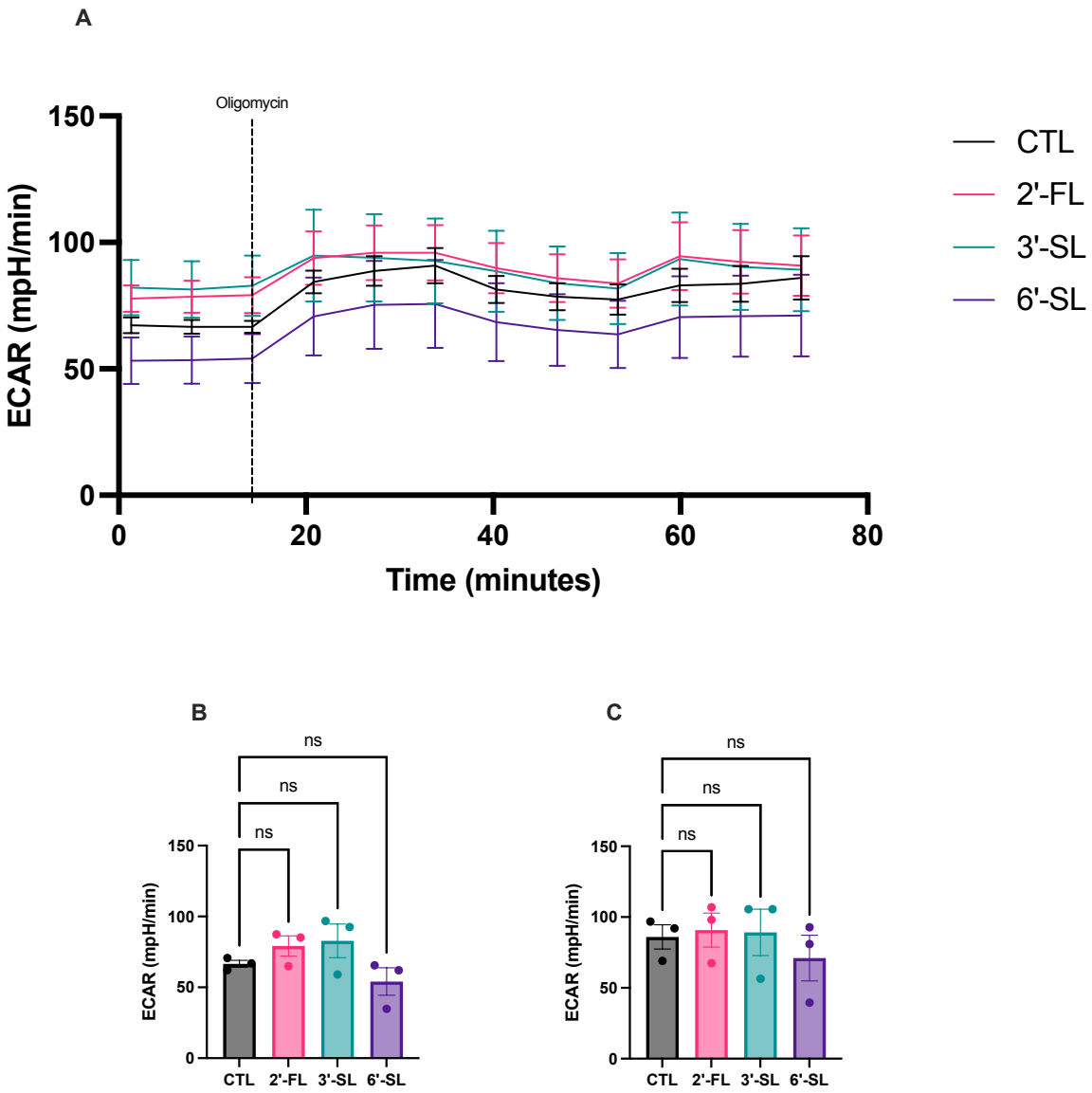

Figure 3. 20: **ECAR Measurements in BMDMs with Prolonged LPS-Activation Treated with HMOs**

BMDMs were treated with HMOs; 2'-FL (2 mM), 3'-SL (1 mM), or 6'-SL (1 mM) + LPS (100 ng/mL) for 24 hours. (A) representative time-course graph of ECAR. (B) basal ECAR rate (C) oligomycin induced ECAR rate. Data shown is from 3 independent experiments (n=3). Data is presented as the mean ± SEM. One-way ANOVA was used to calculate statistical significance with a P-value of < 0.05 deemed statistically significant. ns indicates $p>0.05$

3.8. Effect of HMOs on Macrophages Over 6 Hour LPS Stimulation

To investigate the metabolic effects of HMOs on BMDMs, cells were treated overnight with 2'-FL, 3'-SL, and 6'-SL. During the Seahorse assay, either LPS or media (control) was added, and metabolic activity was tracked over a 6 hour period. OCR and ECAR were measured to assess mitochondrial respiration and glycolytic activity, respectively.

The time-course analysis of OCR demonstrated that HMO-treated BMDMs maintained significantly lower basal OCR levels compared to untreated controls, basal OCR trends were consistent with previous Seahorse metabolic flux assays, where 2'-FL showed a non-significant increase, while 3'-SL and 6'-SL reduced OCR. Throughout the 6 hour assay, OCR remained largely unchanged following media addition, with HMO-treated samples eventually converging with control OCR levels by the final time point (**Figure 3.21 A**). Quantification of OCR at the 6 hour time point confirmed that 3'-SL and 6'-SL treatment led to a return in oxygen consumption to basal levels of the untreated controls (**Figure 3.21 B and C**). Similarly, ECAR analysis revealed that HMO-treated macrophages exhibited increased glycolytic activity at baseline with 2'-FL having no significant effect and both 3'-SL and 6'-SL increasing ECAR. (**Figure 3.22 A**), and this persisted over the 6 hour period. At the 6 hour time point, macrophages treated with 3'-SL and 6'-SL maintained a slightly increased ECAR compared to untreated controls (**Figure 3.22 B and C**), indicating a sustained enhancement of glycolytic metabolism.

To determine whether HMOs influence macrophage metabolism in response to inflammatory stimuli, OCR and ECAR were measured following LPS stimulation. In the presence of LPS, untreated BMDMs exhibited a significant decrease in OCR, while cells pre-treated with HMOs maintained a significantly lower OCR state (**Figure 3.23 A**). By the 6 hour mark, 3'-SL and 6'-SL-treated macrophages displayed a significantly reduced OCR compared to LPS-stimulated controls, indicating a suppression of mitochondrial respiration under inflammatory conditions (**Figure 3.23 C**). Additionally, the impact of HMOs on glycolytic metabolism in LPS-treated macrophages was assessed. While untreated BMDMs exhibited a marked increase in ECAR following LPS stimulation, indicative of a hyper-glycolytic response, HMO-treated cells maintained a significantly lower ECAR over the 6 hour period (**Figure 3.24 A and B**). Quantification at 6 hours

revealed that macrophages treated with 3'-SL and 6'-SL exhibited significantly reduced ECAR compared to LPS-treated controls (**Figure 3.24 C**), suggesting that HMOs prevent macrophages from entering a metabolically overactive glycolytic state in response to inflammatory stimuli.

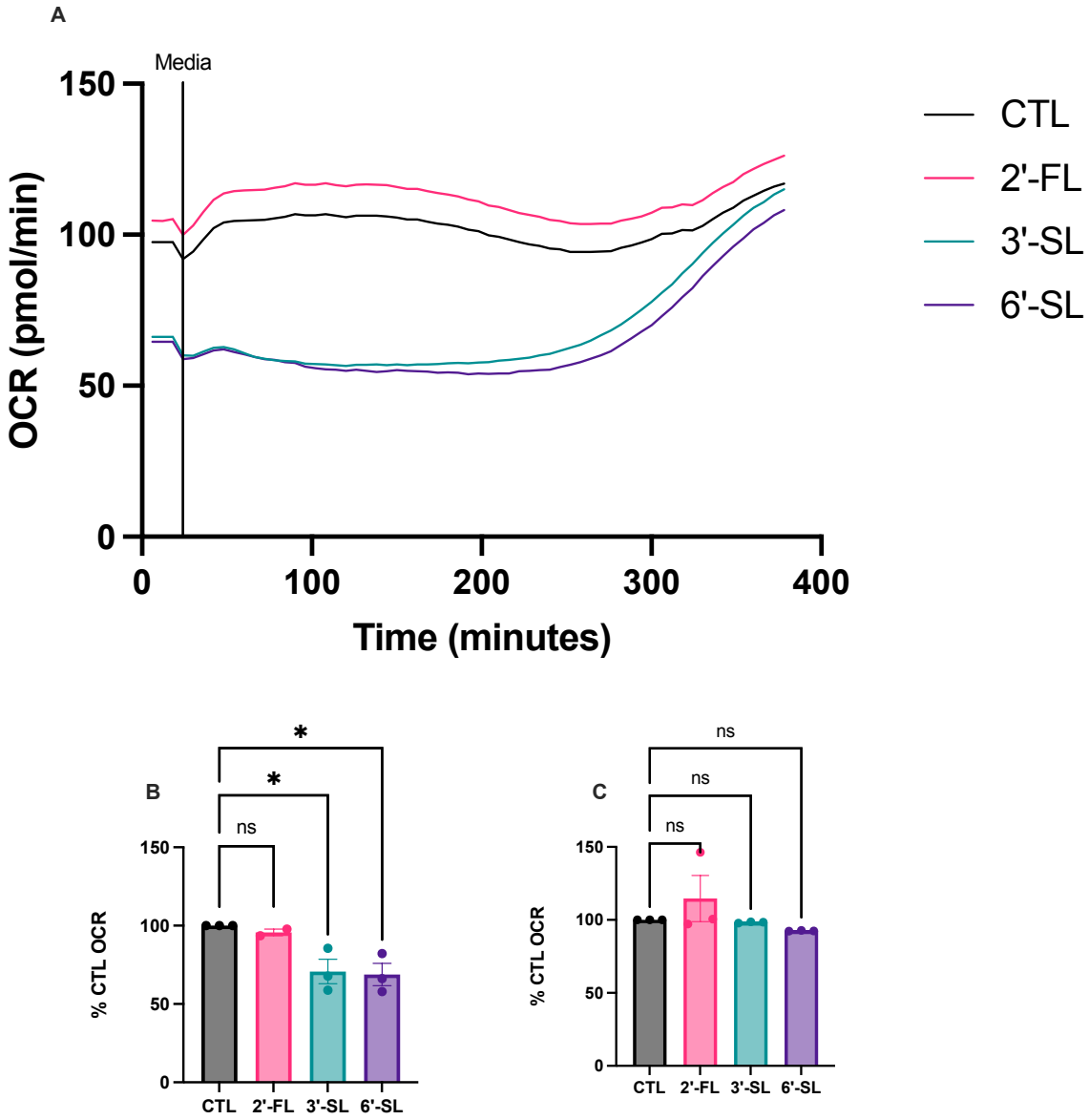

Figure 3. 21: **6 hour Time-Course Analysis of OCR in BMDMs Following HMO Treatment**

BMDMs were treated with HMOs (2 mM 2'-FL and 1 mM 3'-SL and 6'-SL) overnight. Fresh seahorse media replaced the HMOs prior to experiment and OCR was then measured using a SeahorseXFe96 analyser over 6 hours. (A) representative time-course graphs for OCR. (B) basal OCR (C) OCR after 6 hour from 3 independent experiments (n=3). Data is presented as the mean ± SEM. One-way ANOVA was used to calculate statistical significance with a P-value of < 0.05 deemed statistically significant. ns indicates $p>0.05$, * $p<0.05$.

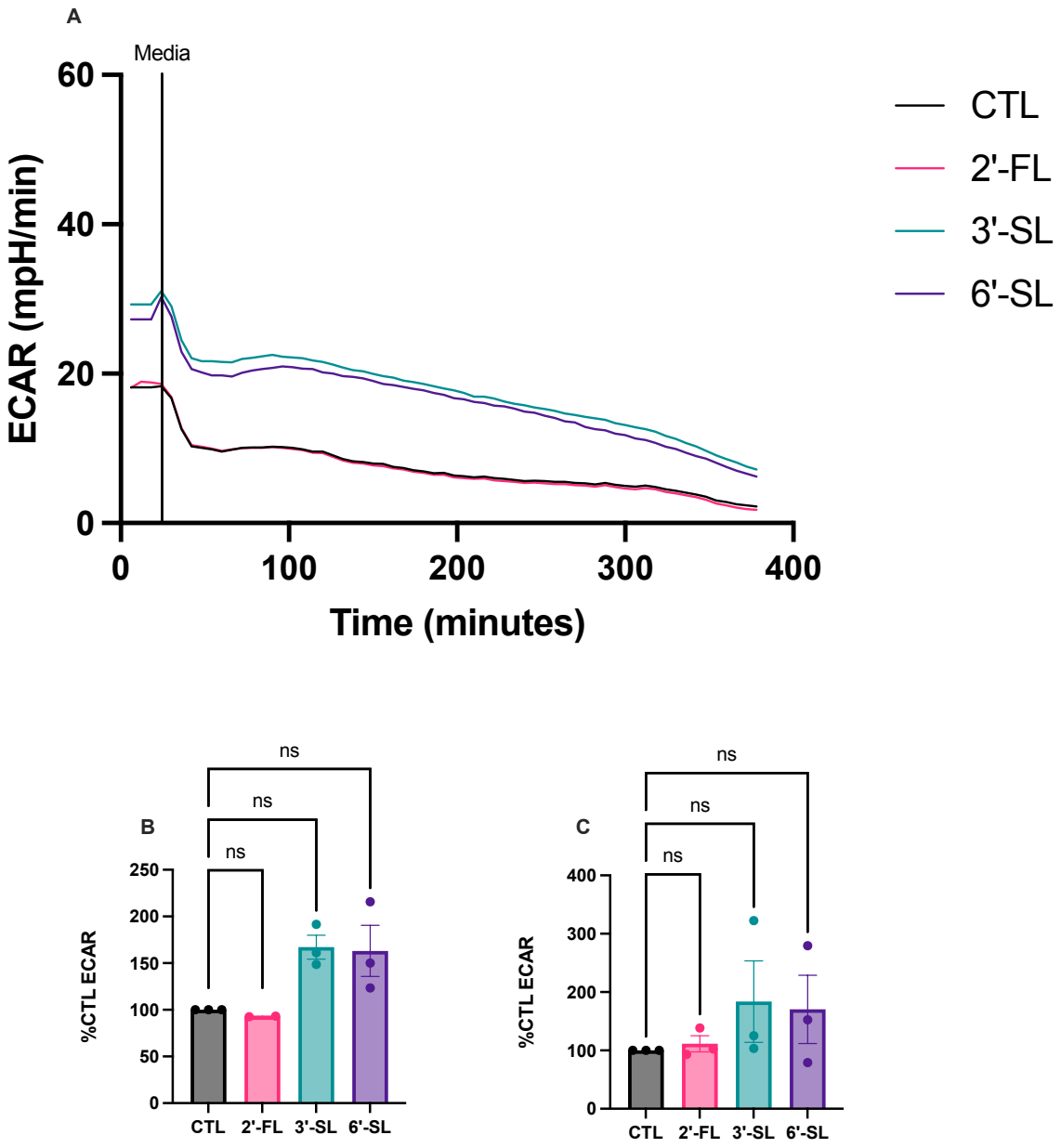

Figure 3. 22: **6 hour Time-Course Analysis of ECAR in BMDMs Following HMO Treatment**

BMDMs were treated with HMOs (2 mM 2'-FL and 1 mM 3'-SL and 6'-SL). Fresh seahorse media replaced the HMOs prior to experiment and ECAR was measured using a SeahorseXFe96 analyser over 6 hours. (A) representative time-course graphs for ECAR. (B) basal ECAR (C) ECAR after 6 hour from 3 independent experiments (n=3). Data is presented as the mean ± SEM. One-way ANOVA was used to calculate statistical significance with a P-value of < 0.05 deemed statistically significant. ns indicates $p>0.05$.

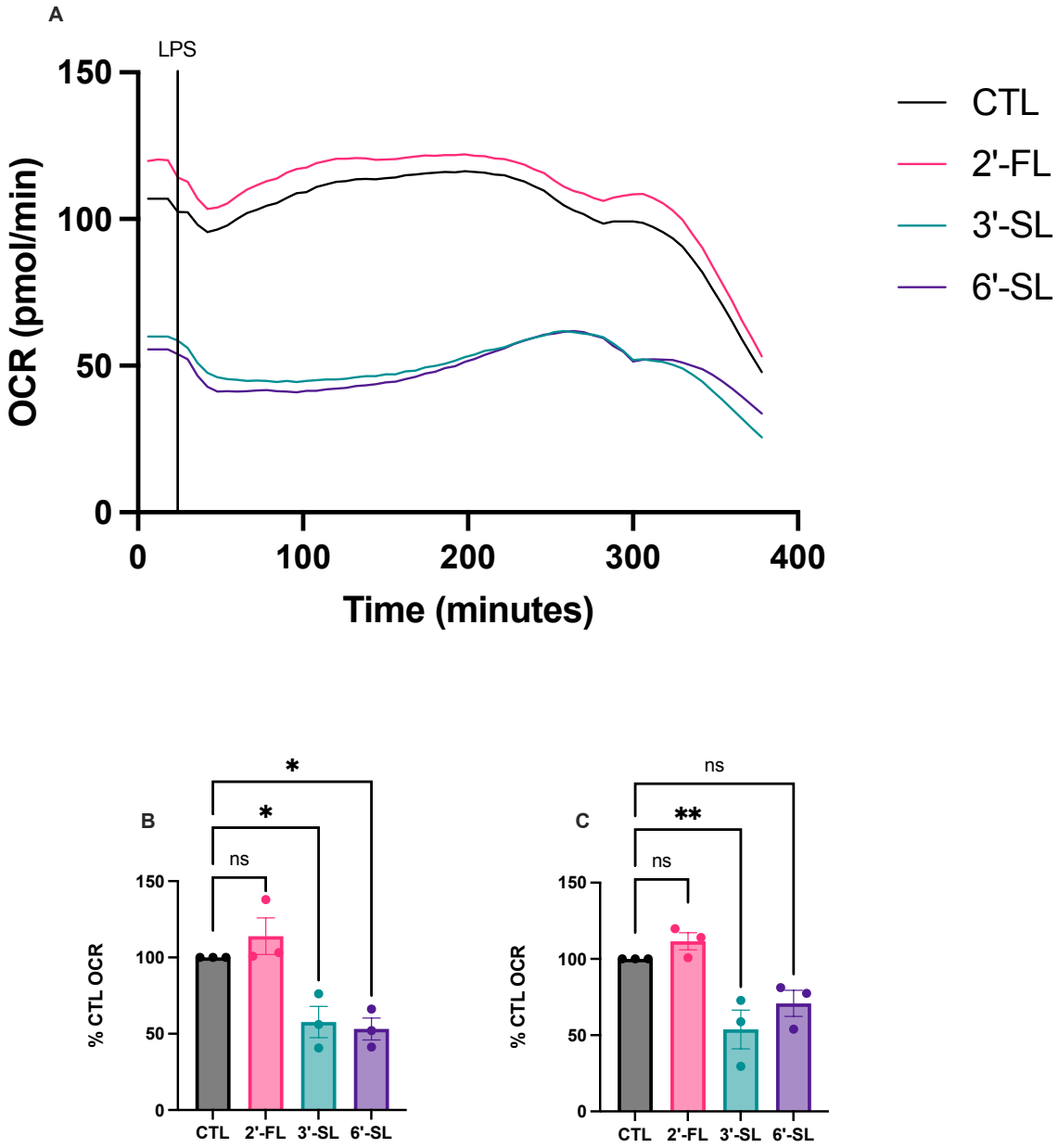

Figure 3. 23: **6 hour Time-Course OCR Analysis in LPS-Activated BMDMs Following HMO Treatment**

BMDMs were treated with HMOs (2 mM 2'-FL and 1 mM 3'-SL and 6'-SL). Fresh seahorse media replaced the HMOs prior to experiment and OCR was measured using a SeahorseXFe96 analyser in the presence of LPS over 6 hours. (A) representative time-course graphs for OCR. (B) basal OCR (C) OCR after 6 hour LPS treatment from 3 independent experiments (n=3). Data is presented as the mean ± SEM. One-way ANOVA was used to calculate statistical significance with a P-value of < 0.05 deemed statistically significant. ns indicates $p>0.05$, * $p<0.05$, ** $p<0.01$

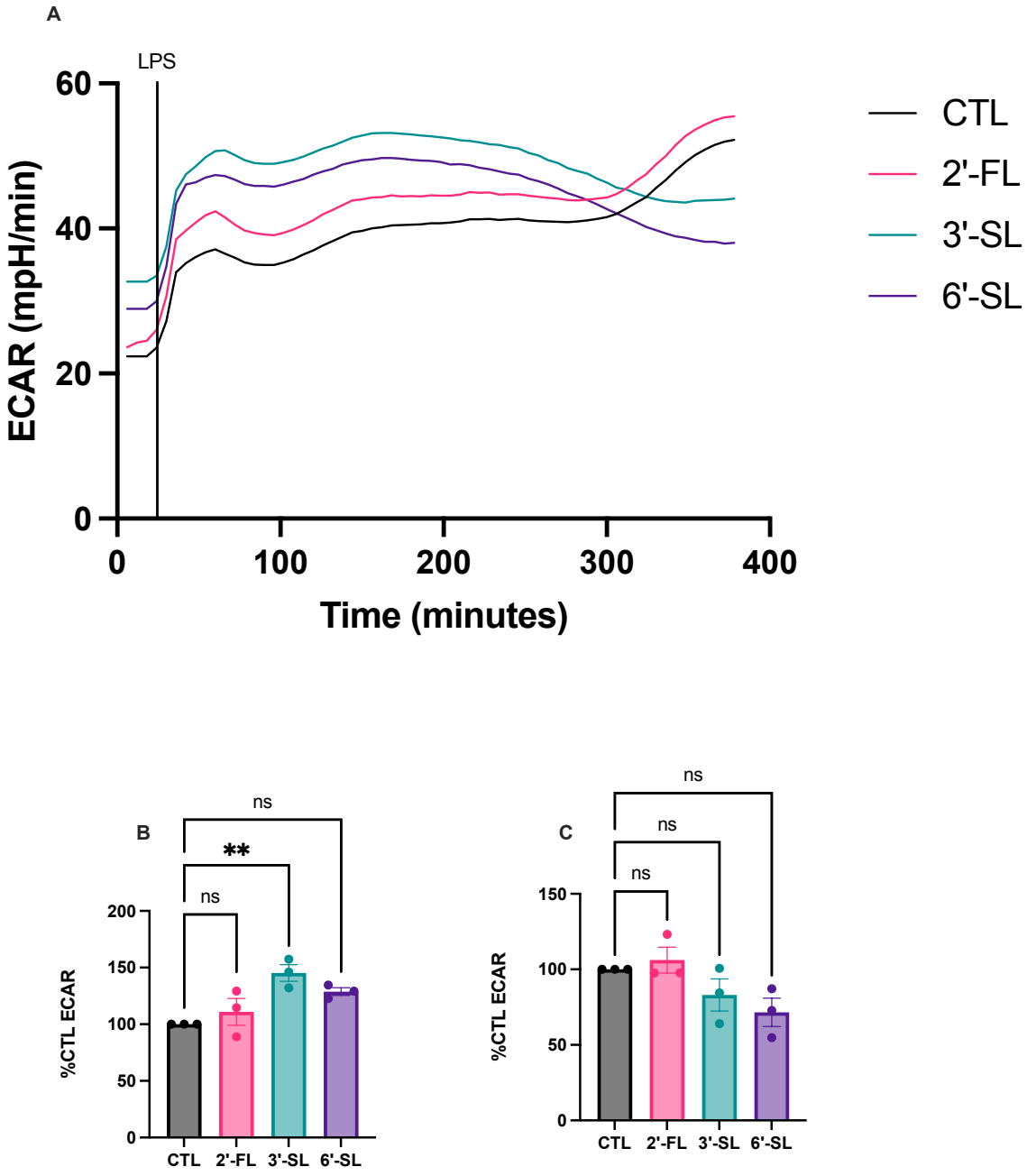

Figure 3. 24: **6 hour Time-Course ECAR Analysis in LPS-Activated BMDMs Following HMO Treatment**

BMDMs were treated with HMOs (2 mM 2'-FL and 1 mM 3'-SL and 6'-SL). Fresh seahorse media replaced the HMOs prior to experiment and ECAR was measured using a SeahorseXFe96 analyser in the presence of LPS over 6 hours. (A) representative time-course graphs for ECAR. (B) basal ECAR (C) ECAR after 6 hour LPS treatment from 3 independent experiments (n=3). Data is presented as the mean ± SEM. One-way ANOVA was used to calculate statistical significance with a P-value of < 0.05 deemed statistically significant. ns indicates $p>0.05$, ** $p<0.01$

5.1. Effects of HMOs on Alternatively Activated M2 Macrophages

To examine the impact of HMOs on the metabolic phenotype of alternatively activated macrophages, BMDMs were polarised into the M2 subtype using IL-4 and subsequently treated with 2'-FL, 3'-SL, or 6'-SL. Metabolic profiling was carried out using a Seahorse XF Analyser to measure OCR and ECAR, capturing both oxidative phosphorylation and glycolytic activity respectively.

As shown in **Figure 3.25**, treatment with 3'-SL and 6'-SL significantly suppressed basal OCR in IL-4-stimulated M2 macrophages, whereas 2'-FL only induced a modest reduction. Specifically, 3'-SL reduced basal OCR by ~25% and 6'-SL by ~30%, compared to a ~10% decrease with 2'-FL. In addition to basal respiration, both 3'-SL and 6'-SL markedly reduced ATP-linked respiration, as measured by oligomycin-sensitive OCR, suggesting a strong inhibition of mitochondrial ATP production. Notably, 6'-SL further impaired maximal respiratory capacity (FCCP-induced OCR) and reduced non-mitochondrial respiration (rotenone/antimycin A-induced OCR), pointing to a broader suppressive effect on mitochondrial function.

Complementary ECAR analysis revealed that 3'-SL significantly elevated basal glycolytic activity (~15% increase), suggesting a compensatory upregulation of glycolysis in response to reduced oxidative phosphorylation (**Figure 3.26**). This was further supported by an increase in oligomycin-induced ECAR, indicating a moderate glycolytic reserve. Interestingly, 6'-SL had the opposite effect, producing a small but statistically significant decrease in ECAR, implying a dual inhibition of both mitochondrial respiration and glycolysis.

To determine whether these metabolic effects persisted under prolonged M2-polarising conditions, BMDMs were exposed to HMOs and IL-4 for extended durations. As illustrated in **Figure 3.27**, both 3'-SL and 6'-SL continued to suppress basal OCR, oligomycin-sensitive OCR, and FCCP-induced OCR under prolonged IL-4 exposure. These results corroborate the sustained impact of sialylated HMOs on mitochondrial activity in M2 macrophages. Similarly, ECAR measurements under these extended conditions (**Figure 3.28**) revealed a consistent pattern; 3'-SL and 6'-SL enhanced basal glycolysis while oligomycin rate was decreased by 6'-SL and 3'-SL slightly increased it, which shows distinct and persistent metabolic responses between the two oligosaccharides.

The functional consequence of these shifts in metabolic parameters was assessed by quantifying glycolytic reserve and spare respiratory capacity across macrophage subtypes. As shown in **Figure 3.29**, neither 2'-FL nor 3'-SL significantly altered glycolytic reserve in M0 or M1 macrophages. However, 6'-SL markedly reduced glycolytic reserve in M0 macrophages, and both 3'-SL and 6'-SL significantly decreased glycolytic reserve in M2 macrophages, indicating limited flexibility in glycolytic adaptation following HMO exposure.

When examining spare respiratory capacity (**Figure 3.30**), no significant differences were observed in M0 or M1 macrophages across any of the HMO treatments. Strikingly, 6'-SL caused a pronounced ~80% reduction in spare respiratory capacity in M2 macrophages. This suggests that 6'-SL profoundly impairs the ability of M2 macrophages to meet energetic demands under stress, potentially rewiring their metabolic plasticity.

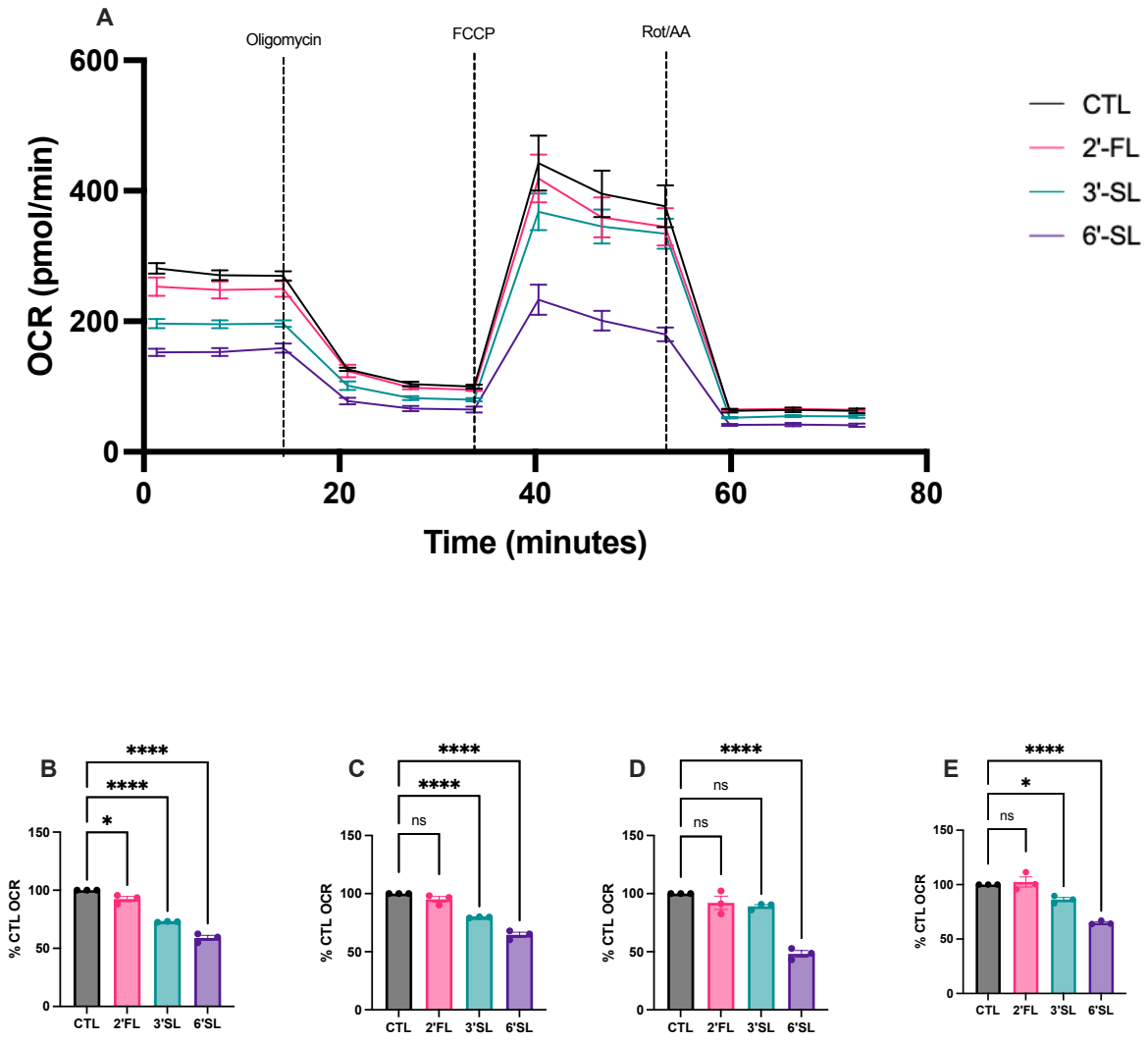

Figure 3. 25: **OCR Measurements in IL-4-Activated BMDMs Treated with HMOs**

BMDMs were treated with HMOs; 2'-FL (2 mM), 3'-SL (1 mM), or 6'-SL (1 mM) + IL-4 for 4 hours. (A) representative time-course graph of OCR. (B) basal OCR rate (C) oligomycin induced OCR rate (D) FCCP induced OCR rate (E) Rotenone/Antimycin A induced OCR rate. Data shown is from 3 independent experiments (n=3). Data is presented as the mean ± SEM. One-way ANOVA was used to calculate statistical significance with a P-value of < 0.05 deemed statistically significant. ns indicates $p>0.05$, * $p<0.05$, **** $p<0.0001$

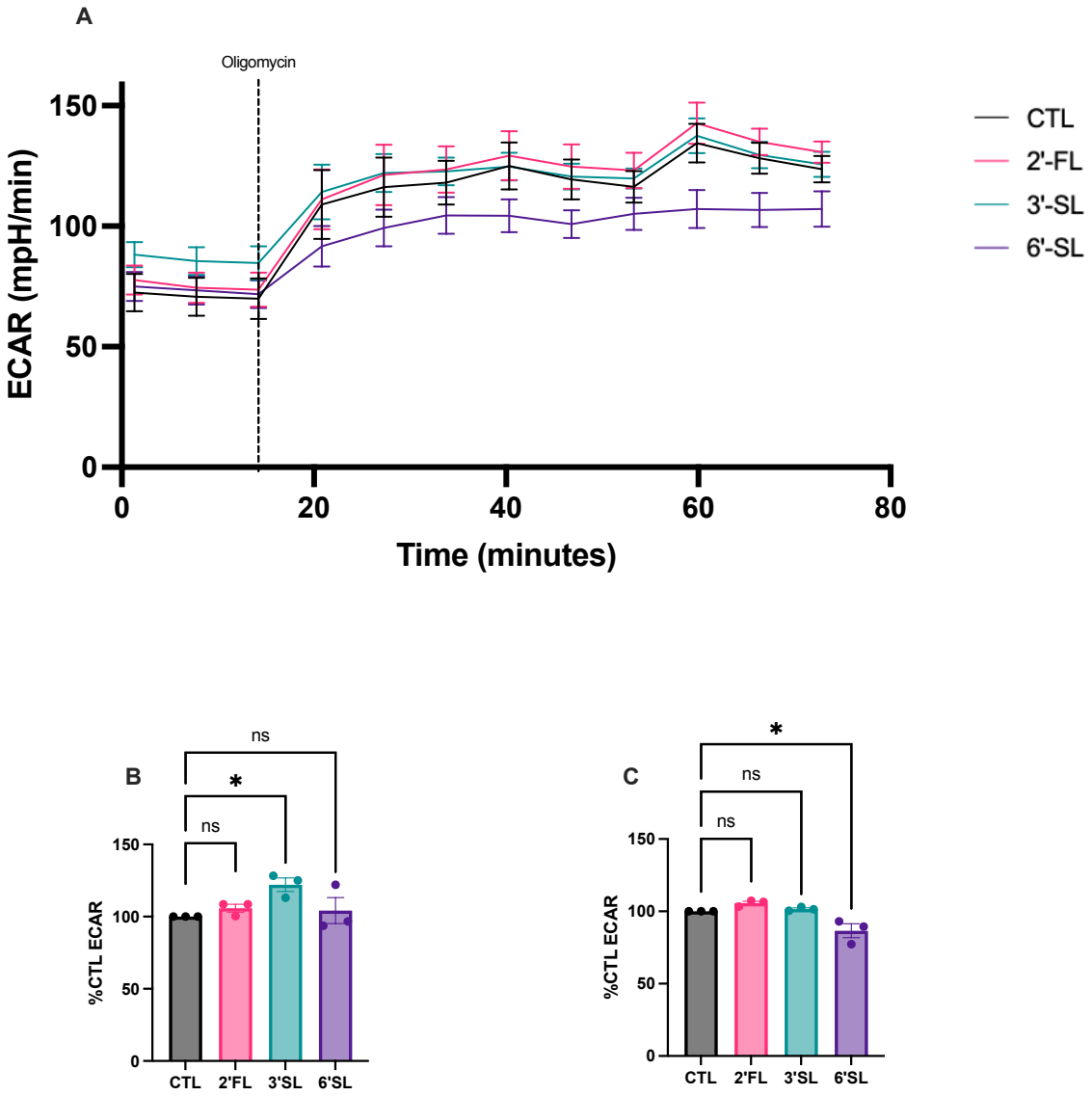

Figure 3. 26: **ECAR Measurements in IL-4-Activated BMDMs Treated with HMOs**

BMDMs were treated with HMOs; 2'-FL (2 mM), 3'-SL (1 mM), or 6'-SL (1 mM) + IL-4 for 4 hours. (A) representative time-course graph of ECAR. (B basal ECAR rate (C) oligomycin induced ECAR rate. Data shown is from 3 independent experiments (n=3). Data is presented as the mean ± SEM. One-way ANOVA was used to calculate statistical significance with a P-value of < 0.05 deemed statistically significant. ns indicates $p>0.05$, * $p<0.05$

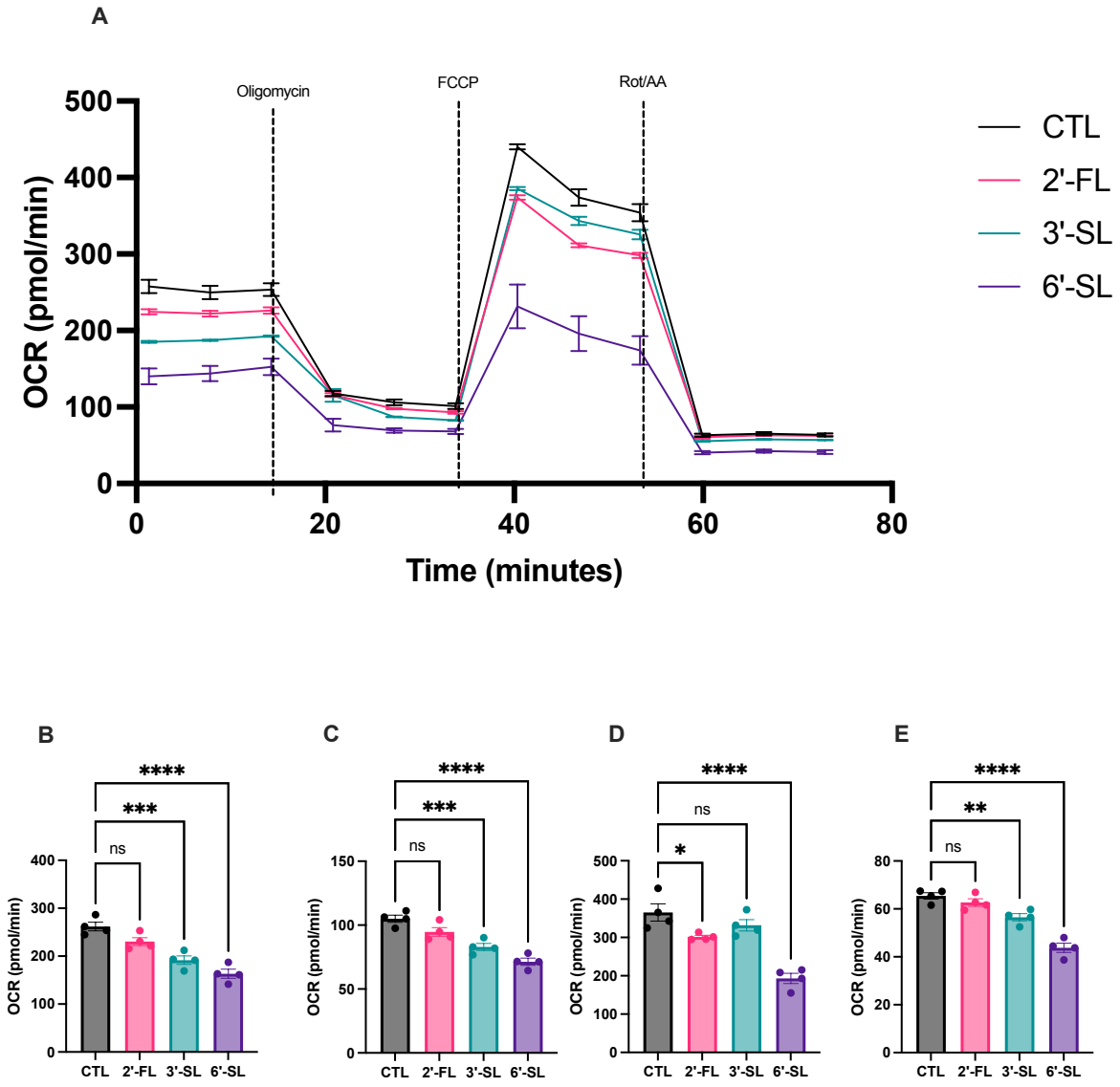

Figure 3. 27: **OCR Measurements in Prolonged IL-4-Activated BMDMs Treated with HMOs**

BMDMs were treated with HMOs; 2'-FL (2 mM), 3'-SL (1 mM), or 6'-SL (1 mM) + IL-4 for 24 hours. (A) representative time-course graph of OCR. (B) basal OCR rate (C) oligomycin induced OCR rate (D) FCCP induced OCR rate (E) Rotenone/Antimycin A induced OCR rate. Data shown is from 3 independent experiments (n=3). Data is presented as the mean ± SEM. One-way ANOVA was used to calculate statistical significance with a P-value of < 0.05 deemed statistically significant. ns indicates $p>0.05$,, ** $p<0.01$, *** $p<0.001$, **** $p<0.0001$

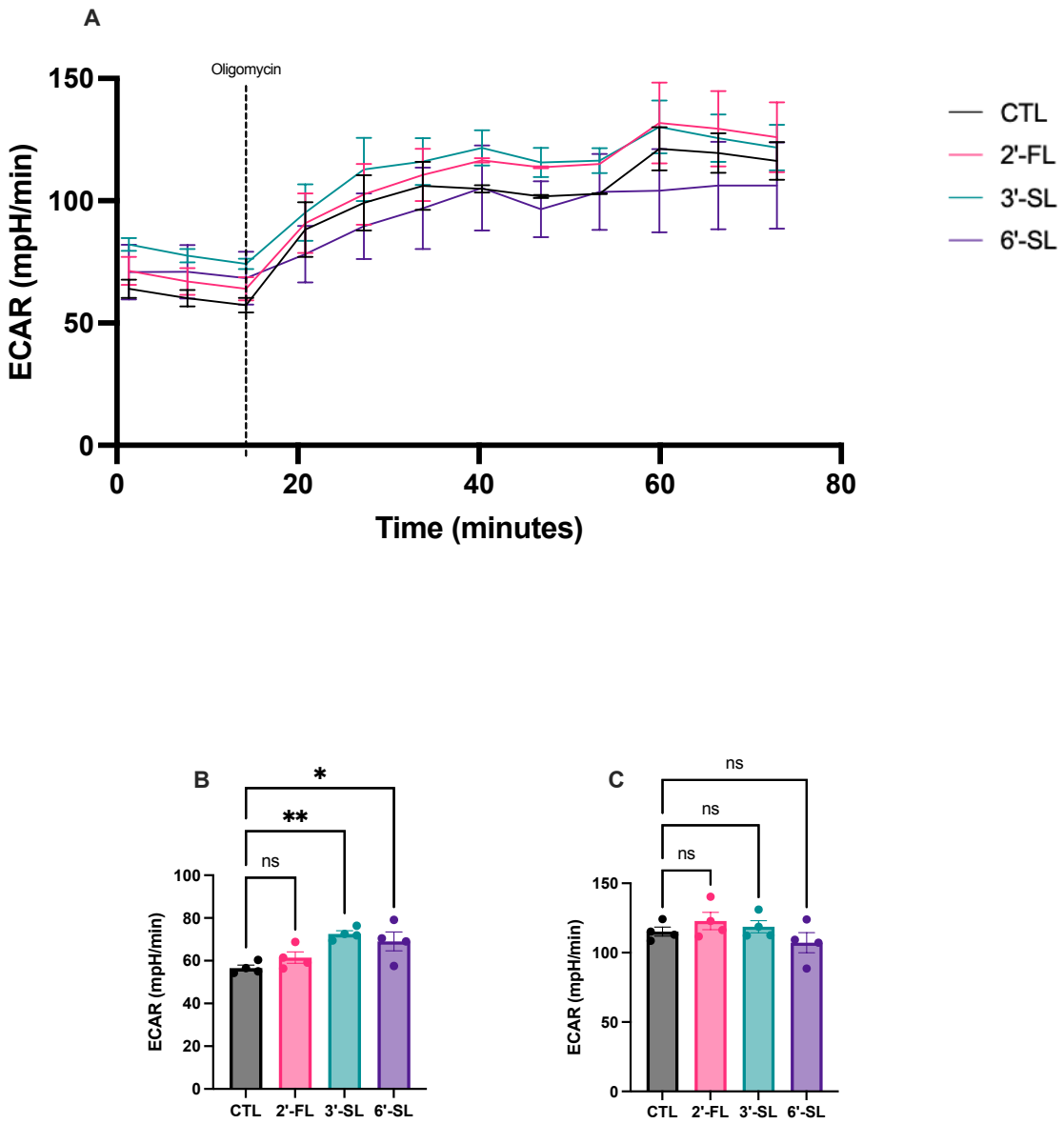

Figure 3. 28: **ECAR Measurements in Prolonged IL-4-Activated BMDMs Treated with HMOs**

BMDMs were treated with HMOs; 2'-FL (2 mM), 3'-SL (1 mM), or 6'-SL (1 mM) + IL-4 for 24 hours. (A) representative time-course graph of ECAR. (B) basal ECAR rate (C) oligomycin induced ECAR rate. Data shown is from at least 3 independent experiments (n=3). Data is presented as the mean ± SEM. One-way ANOVA was used to calculate statistical significance with a P-value of < 0.05 deemed statistically significant. ns indicates $p>0.05$, * $p<0.05$, ** $p<0.01$

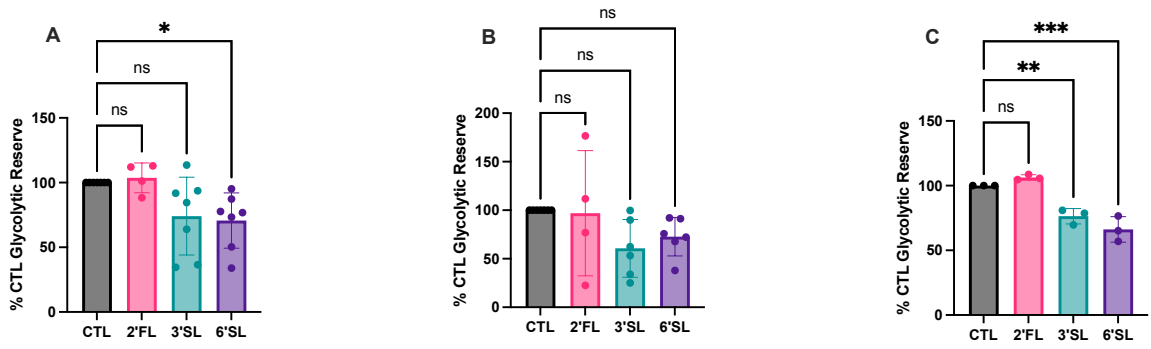

Figure 3. 29: **Differential Impact on Glycolytic Reserve in M0, M1, and M2 Macrophages Treated with HMOs**

BMDMs were polarised into (A) M0 (naïve), (B) M1 (pro-inflammatory, stimulated with 100 ng/mL LPS), or (C) M2 (anti-inflammatory, stimulated with 20 ng/mL IL-4) states and treated with control, 2'-FL (2 mM), 3'-SL (1 mM), or 6'-SL (1 mM). Glycolytic reserve was measured (Oligomycin ECAR Rate - Basal ECAR Rate) and normalised to control values (expressed as % CTL). Data shown is from at least 3 independent experiments (n=3). Data is presented as the mean ± SEM. One-way ANOVA was used to calculate statistical significance with a P-value of < 0.05 deemed statistically significant. ns indicates $p>0.05$, * $p<0.05$, ** $p<0.01$, *** $p<0.001$

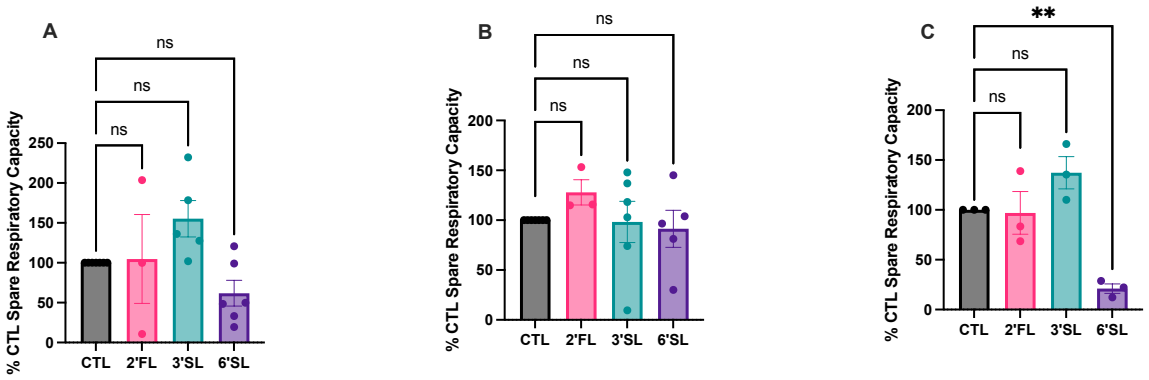

Figure 3. 30: **Differential Impact on Spare Respiratory Capacity in M0, M1, and M2 Macrophages Treated with HMOs**

BMDMs were polarised into (A) M0 (naïve), (B) M1 (pro-inflammatory, stimulated with 100 ng/mL LPS), or (C) M2 (anti-inflammatory, stimulated with 20 ng/mL IL-4) states and treated with control, 2'-FL (2 mM), 3'-SL (1 mM), or 6'-SL (1 mM). Spare Respiratory Capacity was measured (FCCP OCR Rate - Basal OCR Rate) and normalised to control values (expressed as % CTL). Data shown is from at least 3 independent experiments (n=3). Data is presented as the mean ± SEM. One-way ANOVA was used to calculate statistical significance with a P-value of < 0.05 deemed statistically significant. ns indicates $p>0.05$, , ** $p<0.01$,

3.9. Discussion

This chapter provides novel insights into how structurally distinct HMOs; 2'-FL, 3'-SL and 6'-SL modulate the key metabolic pathways of macrophages - oxidative phosphorylation and glycolysis, in their basal (M0), inflammatory (M1) and anti-inflammatory (M2) states. The seahorse metabolic flux assay, to evaluate oxygen consumption and acidification rates to capture real-time shifts in energy production. Gene expression profiles via PCR to understand metabolic regulation at the transcriptional level. Complex I activity and lactate output were measured to identify enzymatic and functional consequences. **Figure 3.31** illustrates the interplay between glycolysis and oxidative phosphorylation in immune cells, highlighting differing HMO structures and activation state of cell is important in deciphering effects.

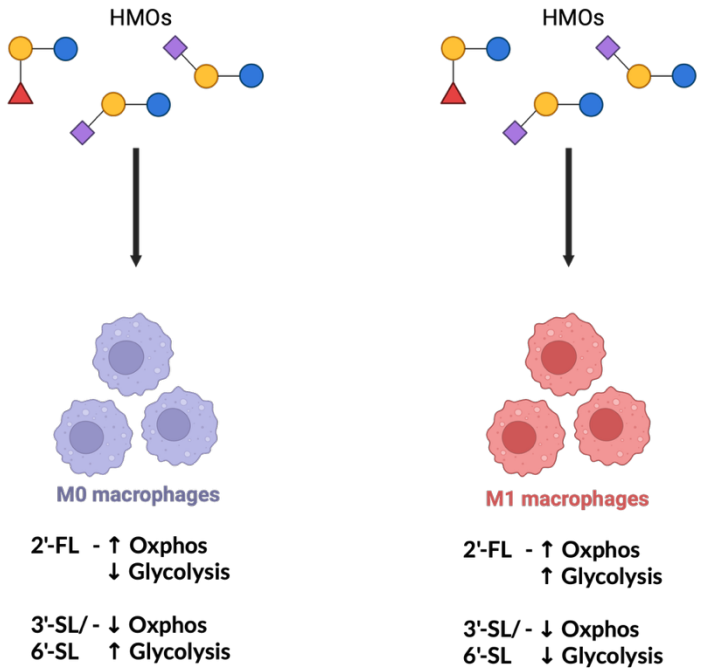

Figure 3. 31: **Schematic Representation of Metabolic Readouts in Immune Cells Treated with HMOs**

The metabolic programming of macrophages is a tightly regulated process that integrates environmental cues to influence immune cell function, phenotype, and fate. The current findings demonstrate that individual HMOs distinctly rewire the bioenergetic profile of unactivated (M0) macrophages, supporting the growing view that HMOs additionally act

as modulators of immune cells beyond their roles in microbiota composition and epithelial barrier support. The pronounced suppression of mitochondrial activity observed with sialylated HMOs suggests a shift away from oxidative phosphorylation, which is typically associated with anti-inflammatory or homeostatic macrophage states. This repression of mitochondrial respiration may reflect a reprogramming toward a more glycolytic phenotype, which is commonly observed in classically activated inflammatory (M1-like) macrophages. However, since these assays were performed under unpolarised, steady-state conditions, the sialylated HMOs may be acting as priming agents that sensitise macrophages to adopt a metabolic configuration more responsive to future activation. This finding is supported by the growing literature describing how pre-conditioning of macrophages can modulate their responsiveness to inflammatory or tolerogenic stimuli[245,246]. The observed metabolic phenotype also shares features with "trained immunity", a recently described phenomenon in which innate immune cells undergo epigenetically imprinted metabolic reprogramming, often characterised by a glycolytic bias and suppression of mitochondrial respiration[247]. In this context, the role of sialylated HMOs may extend beyond transient metabolic influence and could involve long-term effects on macrophage memory or activation thresholds - a hypothesis warranting further mechanistic exploration. The transcriptional repression of mitochondrial genes in response to 3'-SL and 6'-SL implies that the functional changes in bioenergetics are not merely post-translational or acute but are driven by sustained shifts in gene expression, potentially mediated by transcription factors such as NRF1/2 or ERRα. These findings align with earlier studies which show that macrophage metabolic phenotype was coupled to the regulation of mitochondrial gene programs via immunometabolic checkpoints[248].

Interestingly, 2'-FL resulted in a markedly different metabolic profile to the sialylated HMOs, with increasing OCR and ECAR, indicating a metabolic profile more resemblant of M2 macrophages. This highlights that structural differences between HMOs result in divergent immunometabolic outcomes. The apparent lack of mitochondrial suppression and gene expression alteration associated with 2'-FL may suggest a more immunoquiescent, regulatory or even anti-inflammatory role, aligning with previous reports highlighting its anti-inflammatory capacity in the gut and systemic immune contexts[249]. A study on murine models of ischemic stroke found that supplementation with 2′-FL increased the expression of M2-type genes while decreasing M1-type gene expression in microglia[95] . This finding

further suggests that 2'-FL may drive macrophages towards a more M2-macrophage phenotype through altering their metabolic profiles. This observation aligns with findings that certain dietary components can influence macrophage polarisation. The microbial fermentation product butyrate, a key short-chain fatty acid produced by gut commensals, facilitates M2 macrophage polarisation by activating the H3K9/STAT6 signaling pathway, leading to anti-inflammatory effects[250]. 2'-FL may similarly promote an anti-inflammatory state through subtle metabolic reprogramming.

The concurrent elevation in glycolytic flux and expression of key glycolytic enzymes, particularly following treatment with sialylated HMOs, highlights their ability to redirect central carbon metabolism toward lactate-producing pathways. This phenotype may be indicative of macrophages entering a more active metabolic state. Such a state has been proposed to serve roles in tissue remodeling, early pathogen sensing, or sterile inflammation[133]. Similarly, commensal bacteria and their metabolites have also been shown to influence macrophage metabolism in this manner. Certain probiotics can modulate macrophage polarisation; for example, *Bacillus amyloliquefaciens* has been reported to induce M1 macrophage activation, enhancing pro-inflammatory responses[251] with other probiotic strains seemingly having a dual effect on macrophage polarisation[252], simultaneously upregulating selective pro-inflammatory pathways while also enhancing regulatory or repair-associated functions. Interestingly, unlike 3′-SL and 6′-SL, 2′-FL did not exert the same metabolic pressure. Instead, 2′-FL-treated macrophages maintained glycolytic rates closer to baseline, suggesting that fucosylated HMOs may support cellular homeostasis rather than drive metabolic reprogramming via upregulating glycolysis.

Classically activated macrophages when treated with LPS undergo a metabolic shift characterised by reduced mitochondrial respiration and enhanced glycolysis; a hallmark of inflammatory activation to supports rapid ATP generation and biosynthesis[130,253]. In this context, treatment with HMOs appeared to modulate these core metabolic pathways in a structure- and context-dependent manner. Both 3'-SL and 6'-SL accentuated mitochondrial suppression in M1 macrophages, evident from reductions in basal OCR and, in the case of 3'-SL, downregulation of ETC gene expression. Notably, 6'-SL uniquely decreased non-mitochondrial oxygen consumption, suggesting a broader suppression of oxygen-utilising

pathways. However, in contrast to its transcriptional suppression in M0 macrophages, 6'-SL upregulated oxidative phosphorylation-related transcripts in M1 macrophages, indicating a potentially compensatory transcriptional response or a cell-state-specific reprogramming effect[131] or indicative of the decrease in glycolysis that we observed at the 6 hour timepoint in the LPS timecourse assay.

Despite these divergent transcriptional patterns, Complex I activity remained uniformly impaired in both M0 and M1 macrophages following HMO treatment, particularly with the 5-HMO mixture. This consistent inhibition suggests that Complex I may represent a convergent node of metabolic disruption, targeted by multiple oligosaccharide structures. The glycolytic response added further complexity, as although ECAR was elevated in all HMO-treated M1 macrophages, both 3'-SL and 6'-SL paradoxically reduced the expression of key glycolytic genes. The downregulation of glycolytic gene expression observed at the 4 hour timepoint is likely a consequence of the altered metabolic trajectory captured in the time-course data, where both 3'-SL and 6'-SL treatment dampened the expected rise in glycolytic activity between 4- and 6 hours post-stimulation. This temporal uncoupling of LPS-driven glycolytic activation suggests that sialylated HMOs interfere with early metabolic reprogramming signals, thereby attenuating the transcriptional induction of key glycolytic enzymes. In contrast, 2'-FL enhanced both glycolytic gene expression and ECAR, suggesting that it may support rather than disrupt the LPS-induced glycolytic program. These metabolic findings are consistent with recent immunophenotyping studies. For instance, Jepsen et al. (2024) reported that 6'-SL treatment enhanced expression of M1 markers such as CD80, CD137L, and CD18 in human monocyte-derived macrophages challenged with *Staphylococcus aureus*, while suppressing M2-associated markers such as CD163 and *CD200R*[254]. *Such* phenotypic modulation may be metabolically underpinned, as macrophage activation states are tightly coupled to their metabolic programming[255]. Taken together, the data suggest that HMOs, particularly sialylated structures such as 3'-SL and 6'-SL, orchestrate complex and cell-state-specific metabolic rewiring ultimately influencing the inflammatory tone of macrophages.

The temporal metabolic profiles suggest that HMOs, particularly sialylated species, exert temporally distinct effects on macrophage metabolism under both basal and inflammatory

conditions. The observed reduction in basal OCR in 3′-SL- and 6′-SL-treated macrophages may reflect an early shift toward a glycolytic metabolic phenotype, similar to classical M1-like macrophage activation, which favours glycolysis over mitochondrial respiration[256]. In contrast, 2′-FL-treated macrophages displayed a slight, non-significant increase in OCR, indicating a differing metabolic influence. This distinction again aligns with other studies where 2′-FL had modest immunomodulatory effects and pushed macrophages towards a more M2 phenotype[95]. Following control media addition, the gradual return of OCR and ECAR to basal conditions across all HMO treatment groups suggests that in the absence of inflammatory cues, metabolic differences induced by HMOs are not sustained long-term. This implies that HMO-mediated metabolic reprogramming may be transient or require ongoing stimuli (such as microbial products) to maintain distinct bioenergetic profiles.

Under LPS stimulation, all treated macrophages initially experienced a slight reduction in OCR, which is a typical response during early M1 polarisation, where mitochondrial function is suppressed, and glycolysis becomes the primary energy source[255]. Notably, however, only the control and 2′-FL-treated macrophages experienced a dramatic decrease in OCR at later time points (between 4 to 6 hours), while 3′-SL and 6′-SL-treated cells maintained higher mitochondrial function. This suggests that sialylated HMOs may protect against mitochondrial dysfunction during prolonged inflammation; potentially by mitigating LPS-induced mitochondrial stress or preserving respiratory activity. This is consistent with studies showing that excessive inflammatory signaling leads to mitochondrial damage, while anti-inflammatory agents can help maintain mitochondrial homeostasis[257]. The ECAR data further reinforces the theory that sialylated HMOs can modulate inflammatory metabolism. The rapid glycolytic surge following LPS addition is expected as macrophages switch to aerobic glycolysis to support cytokine production and effector functions[258]. Interestingly, while ECAR remained elevated in 3′-SL and 6′-SL-treated cells several hours post LPS treatment, it ultimately declined between 4-6 hours. In contrast, 2′-FL and control cells exhibited a secondary ECAR increase, ultimately to compensate for the sharp decrease in oxidative phosphorylation that we observed at the same time. This pattern suggests that 3′-SL and 6′-SL may potentiate early glycolysis but may also restrain excessive or prolonged glycolytic activation. This is important, as sustained glycolysis is associated with chronic inflammation, while resolution and return

to homeostasis involve restoration of mitochondrial function and reduction of glycolytic flux[129,246].

These findings suggest that 3′-SL and 6′-SL induce a metabolically flexible phenotype in BMDMs, enhancing glycolysis early in inflammation while protecting against mitochondrial dysfunction and preventing excessive metabolic activation. These traits resemble features of macrophages involved in resolution of inflammation or in regulatory phenotypes. While certain commensal bacteria and functional food components exhibit immunomodulatory effects, their mechanisms and outcomes differ from those induced by these specific HMOs. For instance, *Lactobacillus rhamnosus GG (LGG)*, a well-studied probiotic, has been shown to influence macrophage activity, inducing an M1 phenotype[259]. However, upon LPS stimulation, LGG can modulate macrophage polarisation and cytokine production, promoting an anti-inflammatory environment[260]. The effects of LGG is primarily associated with the suppression of pro-inflammatory cytokines such as TNF-α and the enhancement of IL-10 production, rather than the specific metabolic reprogramming observed with 3′-SL and 6′-SL. The ability of specific HMOs to fine-tune macrophage energetics in a context- and time-dependent manner highlights their potential as immunometabolic modulators, with implications for inflammatory disease management and neonatal immune priming.

In alternatively activated M2 macrophages, the observed effects of HMOs highlight the broader role of dietary glycans as modulators of immune metabolism. M2 macrophages are known to rely heavily on mitochondrial oxidative phosphorylation to support their tissue-repairing and anti-inflammatory functions, a profile maintained by signals such as IL-4 and IL-13 through STAT6 activation[130,257]. In this context, subtle interference with mitochondrial flexibility can have consequences for macrophage function, limiting their ability to respond to metabolic or inflammatory stress. This is especially relevant when considering how other environmental cues, such as microbial metabolites or food components, influence M2 macrophage polarisation. For instance, butyrate promotes M2 polarisation and enhances mitochondrial function through epigenetic reprogramming[261]. In an alcoholic liver disease (ALD) model, the prebiotic, inulin reduces inflammation via SCFAs-inducing suppression of M1 and facilitation of M2 macrophages[262]. Our findings,

reveal specific sialylated HMOs may modulate the bioenergetic capacity of M2 macrophages directly and not in a manner observed with established microbial or dietary metabolites. HMO treatment did not significantly alter basal respiration or ATP-linked OCR of M2 macrophages across the board. However, spare respiratory capacity, an important measure of mitochondrial flexibility and resilience, was significantly decreased following 6′-SL treatment. This is particularly notable given that M2 macrophages typically rely on mitochondrial respiration for their anti-inflammatory and tissue repair functions. A decrease in spare capacity suggests that 6′-SL-treated M2 cells may be less equipped to respond to metabolic stress or energetic demands, potentially impairing their functional plasticity. Unlike in M0 and M1 macrophages, glycolytic metabolism was not significantly impacted by HMO treatment in M2 cells, with ECAR remaining largely unchanged. This suggests that the metabolic suppressive effects of 6′-SL are specific to mitochondrial dynamics in the M2 context, rather than triggering a full glycolytic shift.

These findings show the immunometabolic effects of HMOs are both structure- and activation state-dependent. While 2′-FL modestly supported mitochondrial function across macrophage subtypes, 3′-SL and 6′-SL, suppressed mitochondrial respiration, particularly in M0 and M1 states. The shift toward glycolysis in these conditions appears to be a compensatory mechanism, consistent with the inverse relationship between mitochondrial oxidative phosphorylation and glycolytic metabolism observed in many immune contexts. This metabolic phenotype is particularly interesting in light of the functional consequences associated with macrophage energy metabolism: oxidative phosphorylation is typically associated with anti-inflammatory, tissue-repairing phenotypes (e.g., M2 macrophages), while glycolysis is linked to inflammatory and antimicrobial responses (e.g., M1 macrophages). The glycolytic shift in M0 macrophages induced by sialylated HMOs may therefore "prime" them toward a more reactive state. Between the two sialylated HMOs analysed, 6′-SL exerted broader and more potent effects, especially in terms of limiting mitochondrial spare respiratory capacity in M2 macrophages. This suggests a potential for 6′-SL to disrupt metabolic adaptability and mitochondrial resilience in alternatively activated cells. Furthermore, the differences observed between 3'-SL and 6'-SL, despite their shared sialylation, may reflect nuances in receptor engagement or cellular uptake. For instance, studies suggest differential binding affinities of HMOs to lectins, siglecs, and pattern recognition receptors such as TLRs, which may influence downstream signaling

pathways that govern metabolic reprogramming. Fucosylated and sialylated HMOs may engage different sets of receptors[71], which may trigger distinct intracellular signaling cascades leading to this discrepancy. Interestingly, HMOs specifically 6'-SL has been shown to activate GPR35[263], a G-protein coupled receptor (GPCR) which has been shown to regulate macrophage metabolism. It does this by modifying Na^+/K^+-ATPase activity[264], which is one of the cell's largest ATP consumers and a major controller of ion gradients that shape mitochondrial function, membrane potential, secondary transport, and pH[265]. Any GPR35-driven change in pump activity will shift ATP demand and alter electrochemical conditions that govern glycolysis, oxidative phosphorylation, and inflammatory output. This means HMOs could reshape macrophage metabolism indirectly through receptor-mediated regulation of ion handling, rather than acting as metabolic substrates themselves. HMOs may be acting through multiple signaling routes to drive their functional effects. Therefore, future mechanistic studies dissecting these upstream events will be critical in determining how specific structural motifs confer distinct immunometabolic outcomes. These findings are particularly compelling given the emerging interest in immunometabolic regulation as a lever for influencing macrophage phenotype and function in disease states such as infection, inflammation, and cancer.

In conclusion, these findings contribute to a growing body of evidence that HMOs are not merely nutritional substrates but bioactive molecules capable of modulating innate immune cell metabolism. The capacity of 3'-SL and 6'-SL to suppress mitochondrial respiration while enhancing glycolytic activity, even in the absence of inflammatory cues, positions these oligosaccharides as potential regulators of macrophage plasticity. Importantly, the effects were both structure-specific and dependent on macrophage activation state, highlighting the functional diversity of HMOs and the nuanced ways in which they influence immune cell behaviour. While fucosylated HMOs such as 2′-FL exhibited more restrained, potentially anti-inflammatory metabolic effects, similar to microbial metabolites, such as butyrate, which tend to reinforce oxidative metabolism and anti-inflammatory phenotypes. The unique metabolic footprints observed with HMOs suggest engagement of alternative pathways, that remain underexplored in the context of macrophage metabolism. Although the *in vivo* relevance of these findings requires further investigation to fully understand the immunological impact of HMOs, this study provides foundational insight into how specific individual HMOs shape macrophage metabolism.

Chapter 4

Immunomodulatory Effects of Human Milk Oligosaccharides in Macrophages

4.1. Introduction

HMOs have emerged as bioactive molecules with profound immunomodulatory effects. HMOs interaction with the immune system is more commonly attributed to shaping gut microbiota, supporting intestinal barrier function and subsidiary effects to immunity[4]. While substantial research has explored the prebiotic and antimicrobial properties of HMOs[266], their direct immunomodulatory effects on specific circulatory immune cells, particularly on macrophages, remain less understood. While much of the existing literature has focused on the role of HMOs in neonatal immunity, growing evidence suggests that their immunomodulatory properties extend beyond early development, influencing immune cell function in broader contexts, including inflammatory diseases and immune regulation in adulthood. Given that human milk contains over 200 distinct oligosaccharide structures, understanding the immunological effects of individual HMOs is crucial for elucidating their precise biological functions.

Macrophages play a critical role in host defence, inflammation, and tissue repair[267]. These cells can be polarised into distinct phenotypes, with classically activated M1 macrophages displaying a pro-inflammatory profile and alternatively activated M2 macrophages promoting tissue repair and immune resolution[268]. Macrophage effector function is defined by their ability to orchestrate immune responses through cytokine production, which regulates inflammation and tissue repair, ROS generation, which is essential for microbial killing and oxidative signalling, and phagocytosis, which facilitates pathogen clearance and antigen presentation to shape adaptive immunity. Recent research suggests that HMOs can modulate macrophage function by influencing their polarisation[95,254], distribution[103] and cytokine secretion[102]. Studies have shown that 2'-FL, the most predominant HMO in human milk, promotes M2-like gene expression[95], while other HMOs, such as LNnT and LNFP-III, induce distinct macrophage populations with anti-inflammatory potential[96,97]. HMOs also enhance phagocytosis and bacterial clearance, with sialylated HMOs playing a key role in modulating ROS production[99]. Additionally, HMOs influence macrophage infiltration into inflamed tissues, altering immune cell distribution and reducing excessive inflammation in models of lung injury and infection[101,102]. HMOs have been observed to regulate cytokine production, generally promoting an anti-inflammatory profile by increasing IL-10 and IL-4 while suppressing IL-1β, TNF-α, and IL-6[102]. However, the effects are not uniform; certain sialylated HMOs, such as 3'-SL and 3-FL, have been

observed to enhance both pro- and anti-inflammatory cytokine secretion depending on the context[42]. These findings highlight the complexity of HMO-mediated immunomodulation and suggest that specific HMO structures may have differential effects on macrophage activation. Given these diverse and sometimes contradictory results, further research is required to elucidate the precise molecular mechanisms by which HMOs shape macrophage-mediated immune responses.

Despite significant progress, key gaps remain in our understanding of how HMOs influence macrophage function. Many studies investigating HMO bioactivity focus on broad immunomodulatory effects without delineating the molecular mechanisms underlying these interactions. Additionally, while macrophage responses to HMOs have been characterised in some settings, there is a need for more comprehensive analyses incorporating physiological immune stimuli such as LPS or IL-4. Furthermore, studies often focus on cytokine secretion without fully exploring other macrophage effector functions, such as ROS regulation and bacterial clearance, which are crucial for innate immunity. Understanding how HMOs engage with macrophage receptor-mediated signalling pathways, particularly those involved in Nuclear Factor-Kappa B (NF-κB) activation, is another critical area requiring further investigation.

Chapter 3 demonstrates that HMOs can modulate macrophage phenotype by influencing key metabolic pathways, including glycolysis and oxidative phosphorylation. Metabolism is intrinsically linked to macrophage function, with glycolytic metabolism supporting a pro-inflammatory M1 phenotype and enhanced oxidative phosphorylation favouring an M2-like anti-inflammatory state. Notably, 3'-SL and 6'-SL have been shown to shift macrophage metabolism toward glycolysis, suggesting a potential role in promoting an inflammatory or activated state, while other HMOs, including 2'-FL, have been implicated in anti-inflammatory processes. This metabolic reprogramming could have direct implications for the functional outputs of macrophages, including cytokine production, ROS generation and phagocytic uptake. Given the central role of metabolism in macrophage activation, it is likely that the immunomodulatory effects of HMOs are at least partially mediated through metabolic shifts, influencing how macrophages respond to inflammatory stimuli.

This chapter aims to provide a comprehensive analysis of the immunomodulatory effects of HMOs on macrophages, focusing on their impact on effector function, cytokine production, ROS regulation, phagocytosis, and receptor-mediated signalling. The immunomodulatory properties of HMOs were assessed in bone marrow-derived macrophages, using flow cytometry for phenotypic profiling, ELISA for cytokine quantification, and Incucyte® live-cell imaging for phagocytic activity. ROS production was evaluated using MitoSOX™ staining and flow cytometry under both basal and inflammatory conditions. By linking these immune functions to underlying metabolic changes, this work builds upon the findings in Chapter 3 to explore the metabolic basis of HMO-driven immunomodulation. Understanding these mechanisms may offer insights into novel therapeutic strategies for inflammation-driven diseases, including autoimmune conditions, metabolic disorders, and infections. They may also inform the development of functional food components and synthetic HMOs as immunomodulatory agents in both early life and adult health.

Aims of This Chapter:

- Determine how individual HMOs influence key macrophage effector functions, including cytokine production, ROS generation, and phagocytic activity, under both basal and inflammatory conditions.
- Assess the effects of HMOs on receptor-mediated signalling pathways, particularly TLR-induced NF-κB activation, to understand their role in modulating macrophage inflammatory responses.

4.2. Methods

BMDMs were cultured, seeded, treated and rested as per Chapter 3 methods. Other cells used in experiments in this chapter will be otherwise stated.

Cell Viability

Alamar Blue

Alamar Blue Cell Viability was assessed following 24 hour HMO ± LPS treatment. After incubation, 20 µL of Alamar Blue reagent was added per well and cells were incubated for 4 hours. Untreated cells served as live controls, and separate wells were treated with cytotoxic agent to serve as dead controls. Absorbance was measured at 570 nm and 600 nm using a microplate reader.

Flow Cytometry Live/Dead

Flow Cytometry Live/Dead Staining was performed after 24 hour HMO ± LPS treatment. Cells were detached using 10 mM EDTA in PBS, transferred to FACS tubes, washed with 2 mL PBS, centrifuged, and resuspended in fixable viability dye (Zombie Aqua). Samples were incubated 15 minutes at room temperature in the dark, washed, resuspended in FACS buffer, and analysed immediately on a FACSCanto cytometer (PE channel).

IκBα quantification by Western Blot

BMDMs were seeded in 12-well plates at the density previously described and treated with individual HMOs overnight. Cells were then stimulated with LPS (100 ng/mL) for 15, 30, or 60 minutes. At each timepoint, cells were washed twice with ice-cold PBS and lysed. Protein extraction, quantification, SDS-PAGE, transfer, and immunoblotting were performed as per Chapter 2, using IκBα as the target protein and β-actin as the loading control. Band intensities were quantified by densitometry and normalised to β-actin.

HEK-TLR4 and TLR2

HEK293-TLR2 or HEK293-TLR4 cells were seeded at 5×10^4 cells per well in flat-bottom 96-well plates. The following day, cells were treated with HMOs (2′-FL, 3′-SL, 6′-SL) at the indicated concentrations, with ultrapure LPS (100 ng/mL) or Zymosan (100 ng/mL) used as positive controls. Cells were incubated for 24 hours. Supernatants were collected and transferred into fresh 96-well plates for quantification of secreted embryonic alkaline phosphatase (SEAP) using the Quanti-Blue™ detection reagent. SEAP substrate was prepared according to the manufacturer's instructions and 180 µL was added to each well,

followed by 20 µL of culture supernatant. Plates were incubated at 37°C until colour developed (30-120 minutes). Absorbance was measured at 620-655 nm using a microplate reader.

Limulus Amebocyte Lysate (LAL) Assay For Endotoxin Detection

Endotoxin levels in HMO preparations and culture media were assessed using the Pierce Chromogenic Endotoxin Quant Kit (Thermo Scientific) following the manufacturer's instructions. Standards were prepared by serial dilution of the endotoxin control supplied in the kit to generate a standard curve (0.1-1.0 EU/mL). Samples were diluted in endotoxin-free water when required. For each reaction, 50 µL of standards or samples were added to a 96-well plate, followed by 50 µL of LAL reagent. Plates were incubated at 37°C for 10 minutes, after which 100 µL of chromogenic substrate solution was added to each well. After incubation at 37°C for 6 minutes, 100 µL of stop solution (25% acetic acid) was added. Absorbance was read immediately at 405 nm using a microplate reader.

Reactive Oxygen Species (ROS) Production

Following overnight HMO ± 4 hour and 24 hour LPS treatments cells were collected as for Live/Dead assays, washed, and resuspended in PBS containing 5 µM MitoSOX. After 30 minute incubation in the dark at room temperature, cells were washed, resuspended in FACS buffer, and analysed immediately on a FACSCanto cytometer (PE channel).

Phagocytosis Assays

Incucyte Phagocytosis Assay

Phagocytic activity of BMDMs was assessed using the pHrodo™ Red S. aureus BioParticles™ Phagocytosis Kit (Thermo Fisher Scientific) in combination with the Incucyte® live-cell imaging system. BMDMs were seeded in 96-well plates at a density of 60,000 cells per well and were treated overnight with HMOs.

pHrodo™ Red S. aureus BioParticles™ were then added to the wells at a 1:10 (cell-to-particle) ratio. Wells with cells but without BioParticles™ were included as controls. The plate was transferred to the Incucyte® imaging system, and images were captured every 30 minutes over a 12 hour period at 37°C and 5% CO_2. Phagocytosis was quantified based on the fluorescence intensity of internalised BioParticles™, which increase in fluorescence in the acidic environment of the phagosome.

Bacterial Uptake Assay

S. aureus (ATCC 2394) was first streaked on Tryptic Soy Agar (TSA) and incubated overnight at 37°C. The following day, a single colony was inoculated into 10mL of Tryptic Soy Broth (TSB) and incubated overnight at 37°C. The following day the bacteria was centrifuged at 4000rpm for 10 minutes at room temperature. The supernatant was discarded, and the pellet was washed twice with sterile DMEM to remove any residual media. The bacteria were resuspended in DMEM, and the concentration was adjusted to achieve a multiplicity of infection (MOI) of 10, using OD_{600} measurement = 1. iBMDMs were seeded at a density of 1 x 10^6 cells per well in a 12-well plate using DMEM + 10% FBS. The cells were allowed to adhere overnight at 37°C in a 5% CO_2 incubator, the macrophages were treated with HMOs overnight.

To initiate the infection, the prepared *S. aureus* suspension was added to the macrophages to achieve an MOI of 10, followed by incubation at 37°C for 1 hour to allow for bacterial uptake. After incubation, the cells were washed 3 times with DMEM + 40 μg/mL gentamicin to remove non-internalised bacteria. DMEM + 40 μg/mL gentamicin was then added to each well, and the plate was incubated for 1 hour to kill any remaining extracellular bacteria. After this step, the cells were washed 3 more times with PBS to remove any residual gentamicin.

To quantify bacterial uptake, the macrophages were lysed by adding 0.1% Triton X-100 in PBS to each well and incubating for 5 minutes at room temperature. The lysates were collected and serially diluted in MRD. The diluted lysates were plated on TSA and incubated overnight at 37°C. The following day, the resulting colonies were counted to determine the number of internalised bacteria, and results were reported as CFU/mL.

Cytokine Quantification by ELISA

Culture supernatants were collected after overnight HMO ± 4 hour and 24 hour LPS (± 30 minutes 5 μM ATP for IL-1β) treatments. Supernatants were transferred to pre-coated and BSA-blocked ELISA plates. Samples were diluted 1:5 (TNF-α), 1:10 (IL-10), or 1:20 (IL-1β). The remainder of the assay was performed according to the manufacturer's protocol (as detailed in Chapter 2), and absorbance was read at 450 nm.

4.3. The Effect of HMOs on TLR2 and TLR4 Activation

To investigate whether HMOs activate Toll-like receptor (TLR) signalling, human TLR4 and TLR2 reporter HEK293 cells (HEK-Blue™ hTLR4 and HEK-Blue™ hTLR2) were treated with 2'-FL (2 mM), 3'-SL (1 mM), and 6'-SL (1 mM). NF-κB activation was assessed by measuring SEAP levels using the Quanti-Blue™ assay. In HEK-Blue™ hTLR4 cells, 6'-SL treatment resulted in a significant increase in NF-κB activation compared to the untreated control, whereas 2'-FL and 3'-SL had no effect **(Figure 4.1)**. However, when cells were co-treated with LPS, a potent TLR4 agonist, 6'-SL did not further enhance SEAP production beyond that induced by LPS alone **(Figure 4.1)**. A similar pattern was observed in HEK-Blue™ hTLR2 cells, where 6'-SL increased SEAP production, while 2'-FL and 3'-SL had minimal effect **(Figure 4.2)**. However, co-treatment with Zymosan, a TLR2 agonist, did not result in an additive or synergistic increase in NF-κB activity, suggesting that 6'-SL alone is sufficient for TLR2 activation but does not enhance pre-existing TLR2 stimulation **(Figure 4.2)**.

To determine whether these effects were also present in primary immune cells, NF-κB activation was assessed in BMDMs following HMO treatment by measuring IκBα degradation via Western blot analysis. In untreated BMDMs, IκBα levels remained stable over time **(Figure 4.3 B)**. Treatment with 2'-FL and 6'-SL alone showed a very mild increase IκBα expression compared to control cells **(Figure 4.3 C)**, whereas 6'-SL resulted in a reduction in IκBα levels at the 1 hour LPS timepoint, compared to the 1 hour LPS treated control **(Figure 4.3 D)**, consistent with NF-κB activation in macrophages. These data indicate that 6'-SL can modulate NF-κB signalling in both reporter cell lines and primary macrophages, likely through direct engagement with TLR2 and TLR4.

Since bacterial endotoxins such as LPS are potent TLR4 activators, a LAL assay was performed to confirm that the observed activation was not due to endotoxin contamination. The results showed that endotoxin levels for 2'-FL, 3'-SL, and 6'-SL were below the detection threshold **(Figure 4.4)**, confirming that the effects observed were due to HMO-TLR interactions rather than contamination.

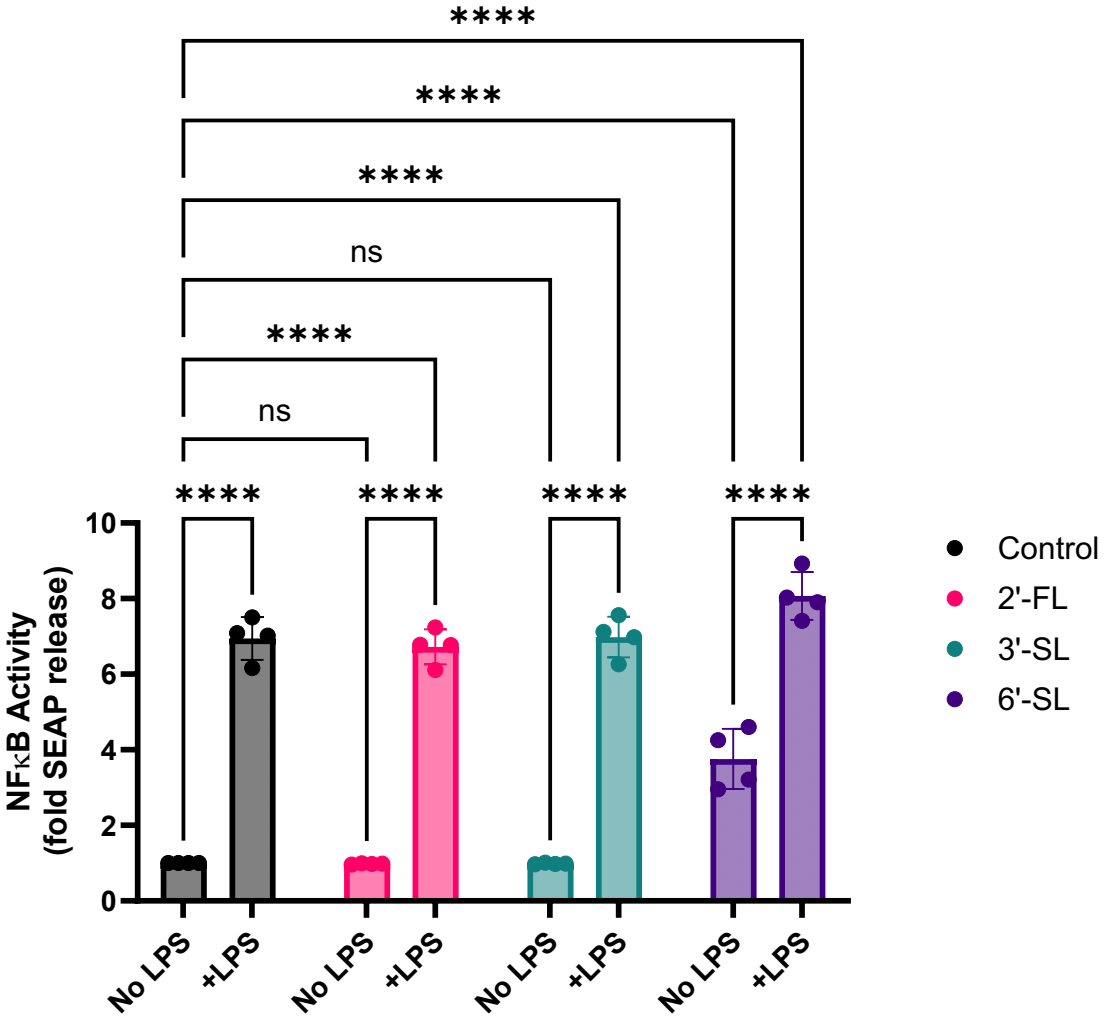

Figure 4. 1: **NF-κB Reporter Activity in HEK-Blue™ hTLR4 Cells Following HMO Treatment**

Human TLR4 reporter HEK293 cells (HEK-Blue™ hTLR4) were treated with HMOs at the indicated concentrations (2 mM 2'-FL, 1 mM 3'-SL and 6'-SL). NF-κB activation was assessed by quantifying secreted embryonic alkaline phosphatase (SEAP) levels using the Quanti-Blue™ assay. Quantified NF-κB activity from HEK-Blue™ hTLR4 treated with HMOs ± LPS (TLR4 agonist). Data shown is from 4 independent experiments (n=4). Data is presented as the mean ± SEM. Two-way ANOVA was used to calculate statistical significance with a P-value of < 0.05 deemed statistically significant. ns indicates $p>0.05$, **** $p<0.0001$

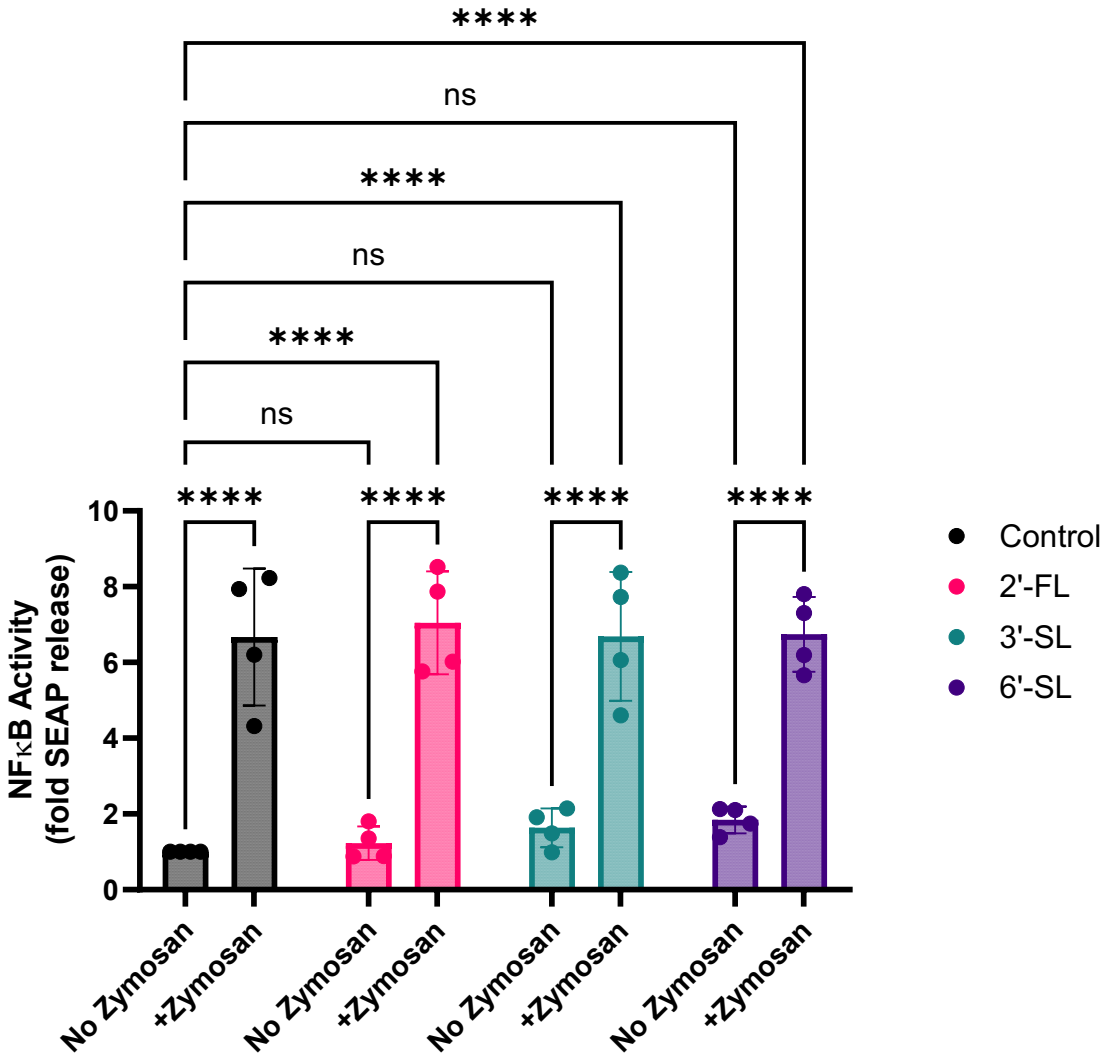

Figure 4. 2: **NF-κB Reporter Activity in HEK-Blue™ hTLR2 Cells Following HMO Treatment**

Human TLR2 reporter HEK293 cells (HEK-Blue™ hTLR2) were treated with HMOs at the indicated concentrations (2 mM 2'-FL, 1 mM 3'-SL and 6'-SL). NF-κB activation was assessed by quantifying secreted embryonic alkaline phosphatase (SEAP) levels using the Quanti-Blue™ assay. Quantified NF-κB activity from HEK-Blue™ hTLR2 treated with HMOs ± Zymosan (TLR2 agonist). Data shown is from 4 independent experiments (n=4). Data is presented as the mean ± SEM. Two-way ANOVA was used to calculate statistical significance with a P-value of < 0.05 deemed statistically significant. ns indicates $p>0.05$, **** $p<0.0001$

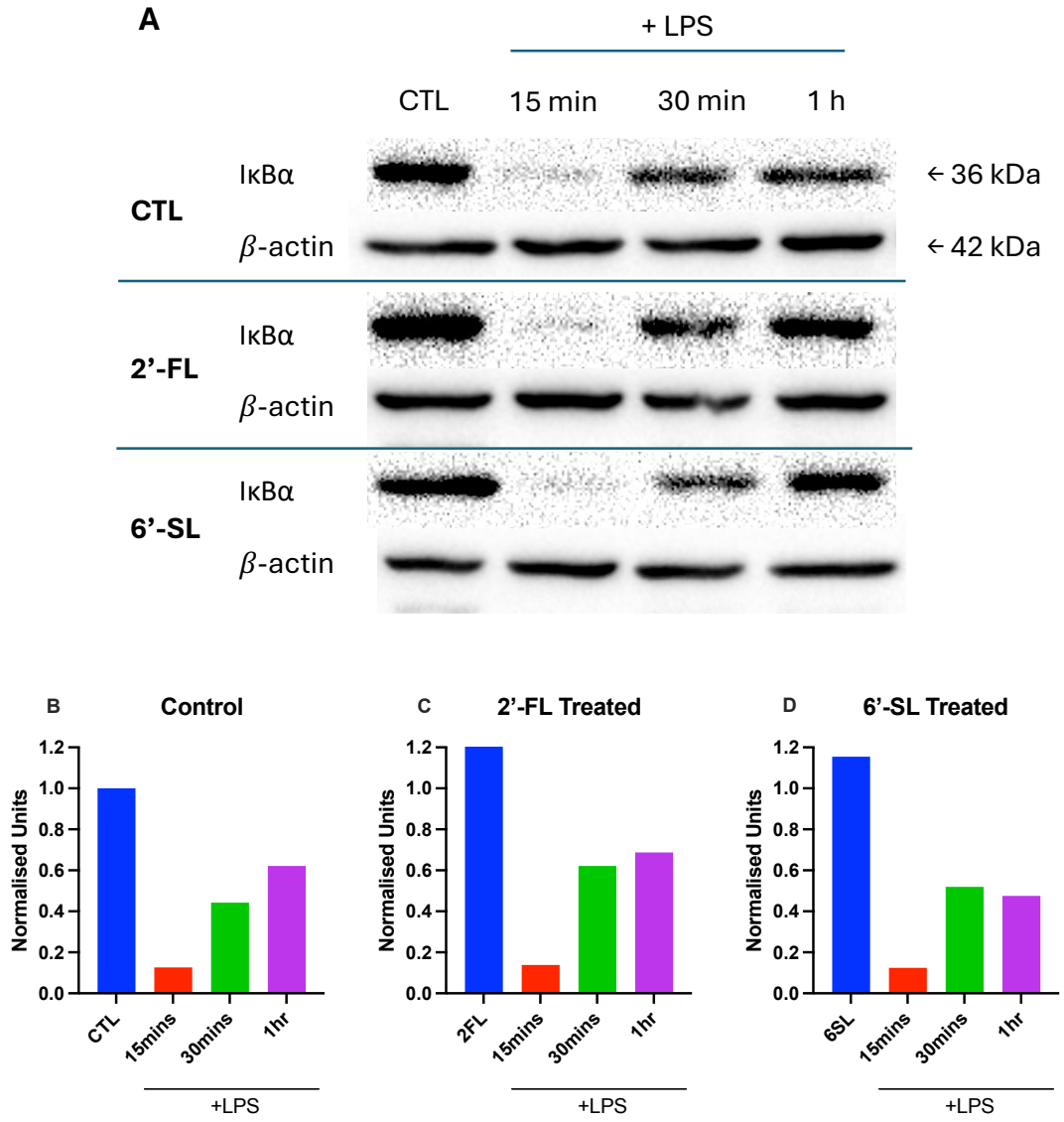

Figure 4. 3:**IκBα Expression in Macrophages Following HMO Treatment**

BMDMs were treated with 2'-FL or 6'-SL (2 mM 2'-FL, 1 mM 6'-SL) ± LPS (100 ng/mL) for the indicated time points. Western blot analysis was performed to assess IκBα degradation as a marker of NF-κB pathway activation. (A) Densitometric analysis shows changes in IκBα levels relative to untreated controls. (B-D) IκBα expression normalised to the untreated control (B) untreated cells (C) 2'-FL treated cells and (D) 6'-SL treated cells. Data shown is from 1 independent experiment (n=1).

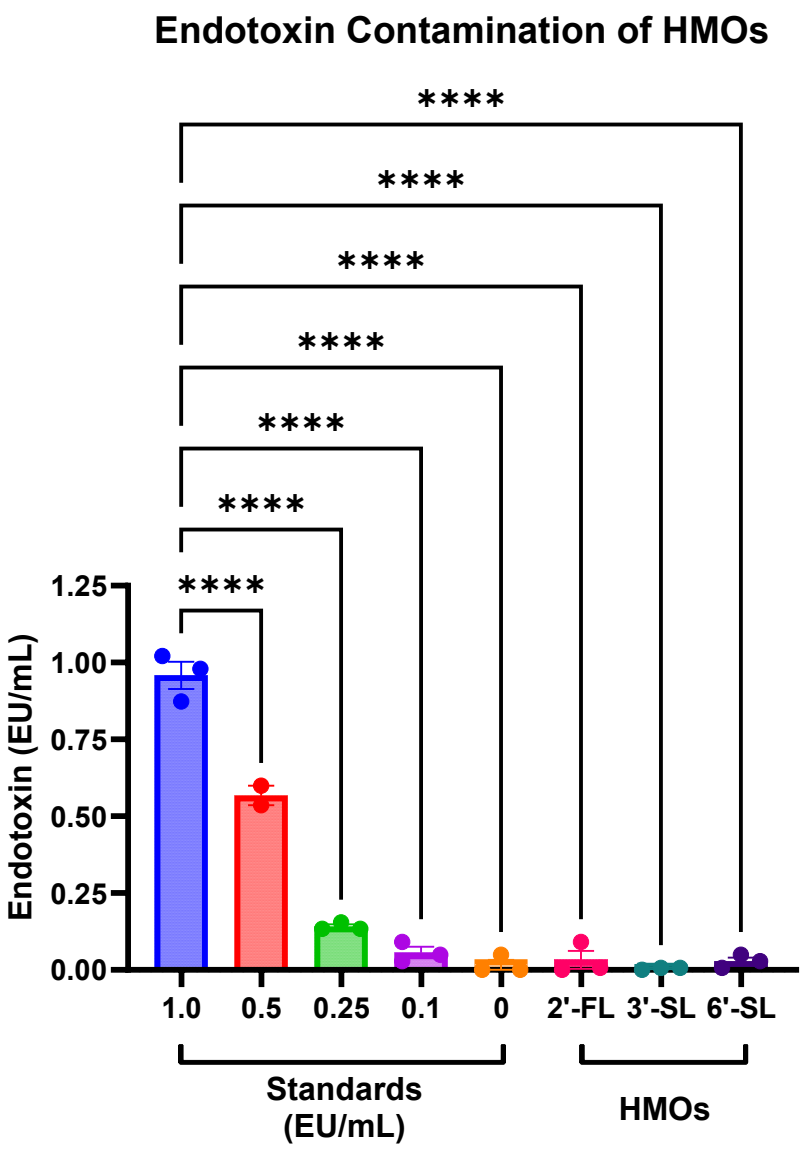

Figure 4. 4: **Endotoxin Assessment of HMOs**

2'-FL, 3'-SL, and 6'-SL were tested using a Limulus Amoebocyte Lysate (LAL) assay at the concentrations used in previous experiments (2 mM, 1 mM and 1 mM, respectively). Data shown is from 1 independent experiment performed in technical triplicate (n=1). Data is presented as the mean ± SEM for technical triplicate. ns indicates $p>0.05$, **** $p<0.0001$

4.4. Effect of HMOs on Mitochondrial ROS Production And Phagocytic Bacterial Clearance in Macrophages

To assess the impact of HMOs on mitochondrial ROS production in BMDMs, flow cytometry analysis using MitoSOX™ staining was performed. Single lives cells, gated CD11b+/F480+ were analysed to confirm high macrophage population. 89.8% of live single cells were observed to be CD11b+/F480+ macrophages **(Figure 2.7)**. ROS production varies across macrophage subtypes, with M1 macrophages exhibiting the highest ROS levels **(Figure 4.5 C, D)** compared to M0 **(Figure 4.5 A)** and M2 macrophages **(Figure 4.5 E, F)**. Treatment with 6'-SL led to a significant increase in basal ROS levels in BMDMs compared to untreated controls and other HMO treated counterparts **(Figure 4.6)**. However, when macrophages were subjected to short-term LPS stimulation (4 hours), no significant differences in ROS production were observed between HMO-treated and untreated groups **(Figure 4.7)**. This suggests that while 6'-SL elevates basal ROS levels, it does not exacerbate oxidative stress under acute inflammatory conditions. To assess the effects of HMOs on macrophages exposed to prolonged inflammatory stress, BMDMs were treated with HMOs followed by 24 hour LPS stimulation. Flow cytometry analysis revealed that all HMOs, significantly reduced ROS production compared to LPS-treated controls **(Figure 4.8)**. These findings suggest that HMOs exert a protective effect by limiting oxidative stress in macrophages under chronic inflammatory conditions.

The role of HMOs in modulating phagocytosis was evaluated using pHrodo™ Red *S. aureus* Bioparticles® and real-time live-cell imaging. BMDMs treated with 6'-SL exhibited significantly increased phagocytic activity, as evidenced by the enhanced fluorescence intensity detected by the Incucyte® system **(Figure 4.9)**. This indicates that 6'-SL promotes bacterial uptake in macrophages. To further validate the impact of 6'-SL on bacterial uptake, immortalised iBMDMs were treated with HMOs prior to bacterial infection. A gentamicin wash was used to eliminate extracellular bacteria, and intracellular bacterial survival was quantified by CFU enumeration. The results demonstrated a significant increase in bacterial uptake in 6'-SL-treated macrophages compared to untreated controls **(Figure 4.10)**. This suggests that 6'-SL enhances macrophage-mediated bacterial clearance.

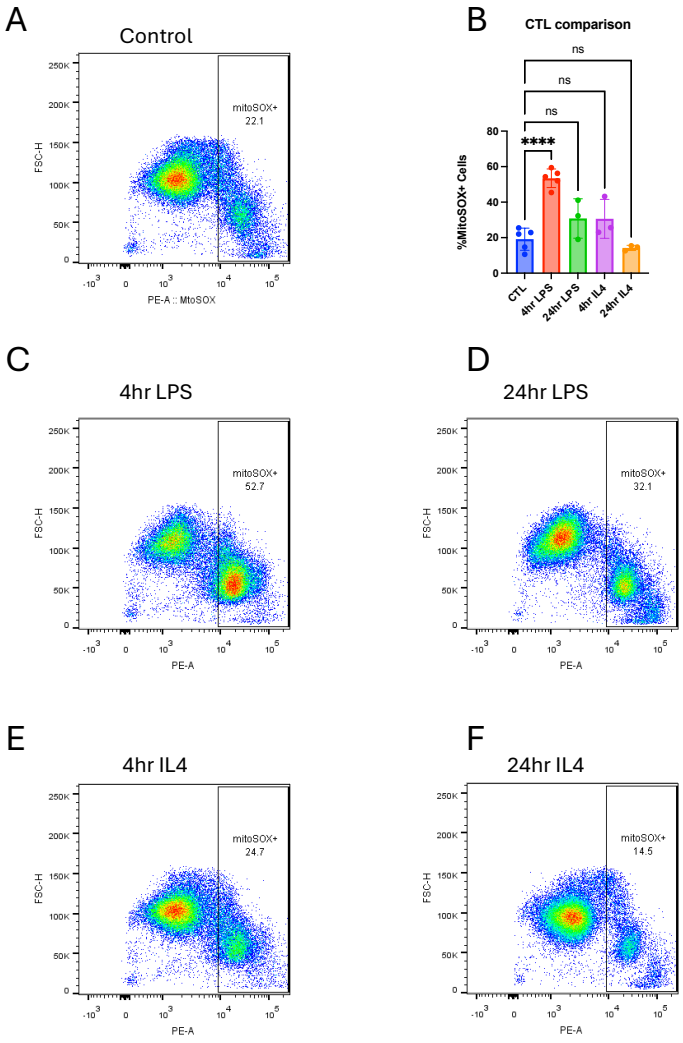

Figure 4. 5: **Reactive Oxygen Species Production in M0, M1, and M2 Macrophages**

Representative flow cytometry histograms and quantification of ROS levels in BMDMs treated with short term (4 hour) or long term (24 hour) LPS or IL-4. BMDMs were stained with MitoSOX™ and analysed by flow cytometry to assess mitochondrial ROS production. (A, C-F) Representative flow plots of MitoSOX™ fluorescence intensity in differentially treated BMDMs (A) Media Control (C) 4 hour LPS treated (D) 24 hour LPS treated (E) 4 hour IL4 treated (F) 24 hour IL4 treated. (B) Quantification of median fluorescence intensity (MFI) normalised and compared to untreated control. Data shown is from at least 3 independent experiments (n=3). Data is presented as the mean ± SEM. One-way ANOVA was used to calculate statistical significance with a P-value of < 0.05 deemed statistically significant. ns indicates $p>0.05$, **** $p<0.0001$

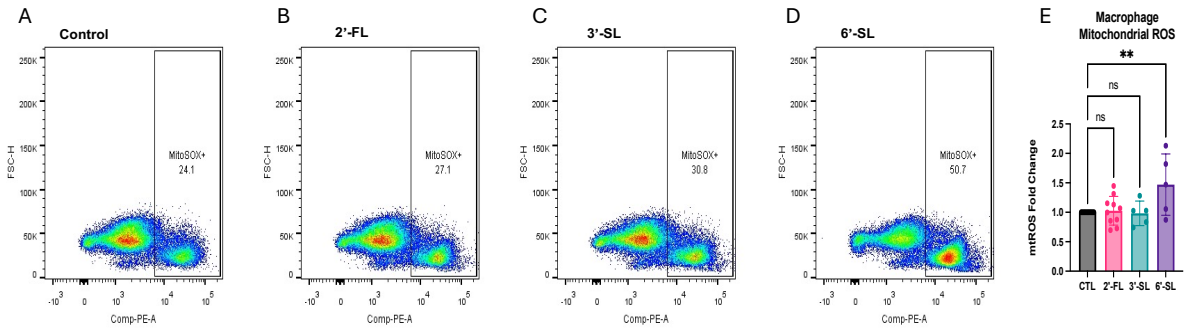

Figure 4. 6: **Basal ROS Levels in Macrophages Following HMO Treatment**

Representative flow cytometry histograms and quantification of ROS levels in BMDMs treated with HMOs. BMDMs were stained with MitoSOX™ and analysed by flow cytometry to assess mitochondrial ROS production. Representative flow plots of MitoSOX™ fluorescence intensity in differentially treated BMDMs (A) Media Control (B) 2'-FL treated (C) 3'-SL treated (D) 6'-SL treated. (E) Quantification of median fluorescence intensity (MFI) normalised and compared to untreated control. Data shown is from at least 4 independent experiments (n=4). Data is presented as the mean ± SEM. One-way ANOVA was used to calculate statistical significance with a P-value of < 0.05 deemed statistically significant. ns indicates $p>0.05$, ** $p<0.01$

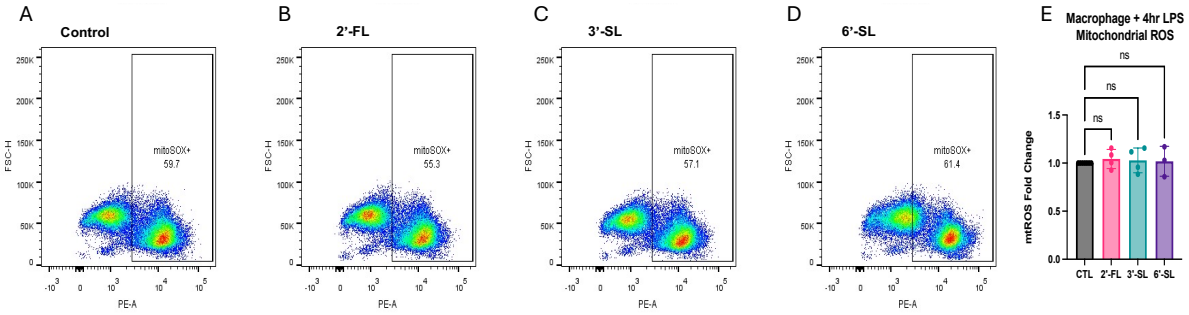

Figure 4. 7: **ROS Production in Macrophages Under Inflammatory Conditions with HMO Treatment**

Representative flow cytometry histograms and quantification of ROS levels in BMDMs treated with HMOs and short term (4 hour) LPS treatment. BMDMs were stained with MitoSOX™ and analysed by flow cytometry to assess mitochondrial ROS production. Representative flow plots of MitoSOX™ fluorescence intensity in differentially treated BMDMs (A) 4 hour LPS treated (B) 2'-FL + 4 hour LPS treated (C) 3'-SL + 4 hour LPS treated (D) 6'-SL + 4 hour LPS treated. (E) Quantification of median fluorescence intensity (MFI) normalised and compared to 4 hour LPS control. Data shown is from at least 3 independent experiments (n=3). Data is presented as the mean ± SEM. One-way ANOVA was used to calculate statistical significance with a P-value of < 0.05 deemed statistically significant. ns indicates $p>0.05$

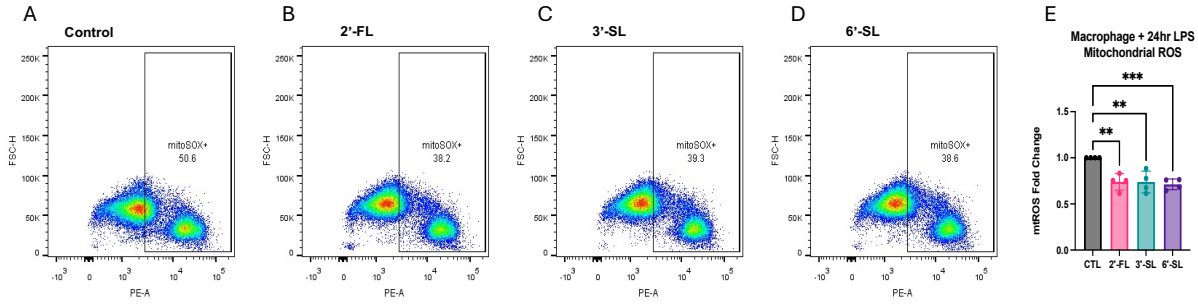

Figure 4. 8: **ROS Production in Macrophages Under Prolonged LPS-Induced Inflammatory Stress**

Representative flow cytometry histograms and quantification of ROS levels in BMDMs treated with HMOs with long term (24 hour) LPS treatment. BMDMs were stained with MitoSOX™ and analysed by flow cytometry to assess mitochondrial ROS production. Representative flow plots of MitoSOX™ fluorescence intensity in differentially treated BMDMs (A) 24 hour LPS treated (B) 2'-FL + 24 hour LPS treated (C) 3'-SL + 24 hour LPS treated (D) 6'-SL + 24 hour LPS treated. (E) Quantification of median fluorescence intensity (MFI) normalised and compared to 4 hour LPS control. Data shown is from at least 3 independent experiments (n=3). Data is presented as the mean ± SEM. One-way ANOVA was used to calculate statistical significance with a P-value of < 0.05 deemed statistically significant. ** Indicates $p<0.01$, *** $p<0.001$

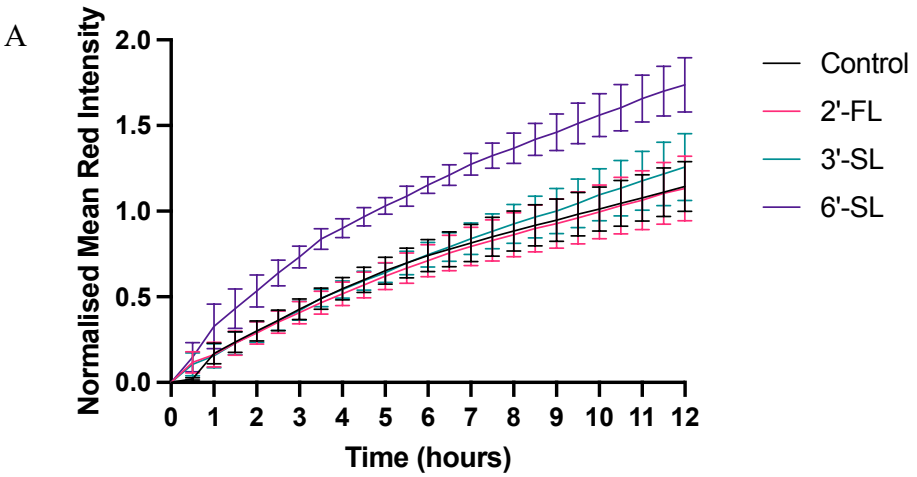
A
Normalised Mean Red Intensity
2.0
1.5
1.0
0.5
0.0
0 1 2 3 4 5 6 7 8 9 10 11 12
Time (hours)
Control
2'-FL
3'-SL
6'-SL

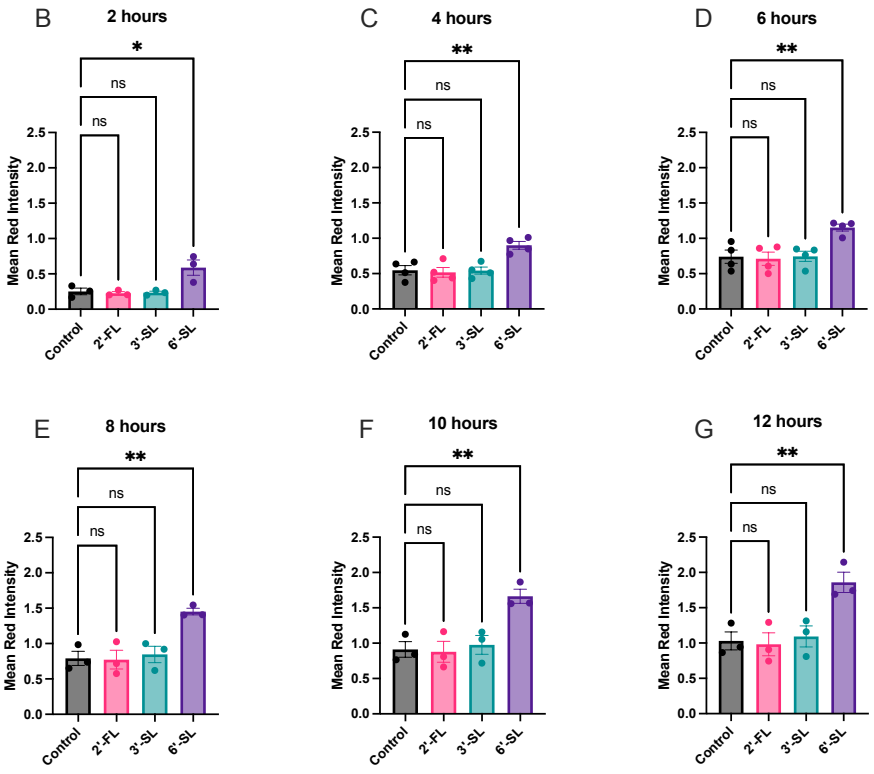
B 2 hours
C 4 hours
D 6 hours
E 8 hours
F 10 hours
G 12 hours
Mean Red Intensity
Control
2'-FL
3'-SL
6'-SL
ns
*
**

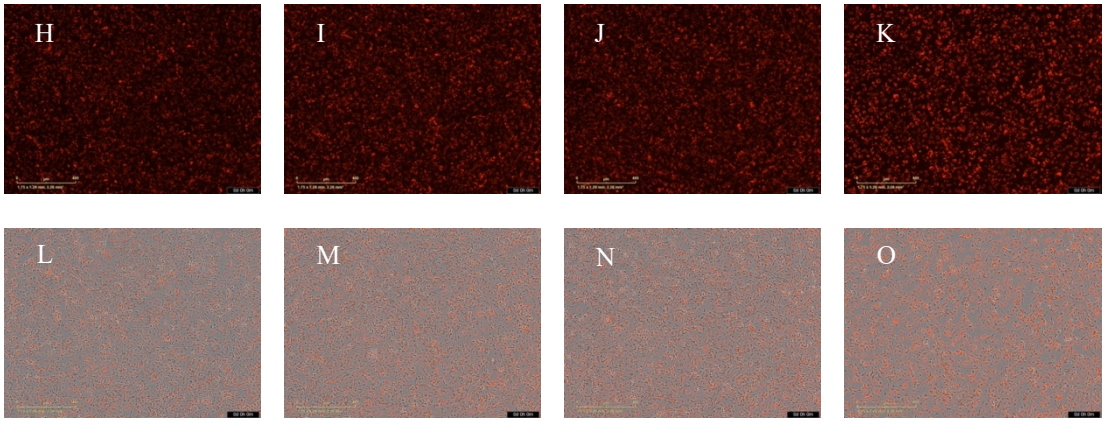
H
I
J
K
L
M
N
O

Figure 4. 9: **Phagocytic Activity of Macrophages Following HMO Treatment**

BMDMs were treated with HMOs prior to assessing phagocytic activity using pHrodo™ Red S. aureus Bioparticles®. Phagocytosis was monitored in real-time using the Incucyte® live-cell imaging system, which quantifies fluorescence intensity as an indicator of bacterial particle uptake. (A) timecourse of phagocytosis quantified as normalised mean red intensity over time (B-G) represent barcharts quantifying mean red intensity at intervals of 2 hours. (H-K) are representative images from the live cells (phase on, red on) at 12 hours treated with (H) untreated control (I) 2'-FL (J) 3'-SL (K) 6'-SL. (L-O) are representative images from the live cells (phase off, red on) at 12 hours treated with (L) untreated control (M) 2'-FL (N) 3'-SL (O) 6'-SL. Data shown is from 3 independent experiments (n=3). Data is presented as the mean ± SEM. One-way ANOVA was used to calculate statistical significance with a P-value of < 0.05 deemed statistically significant. ns indicates $p>0.05$, * $p<0.05$, ** $p<0.01$

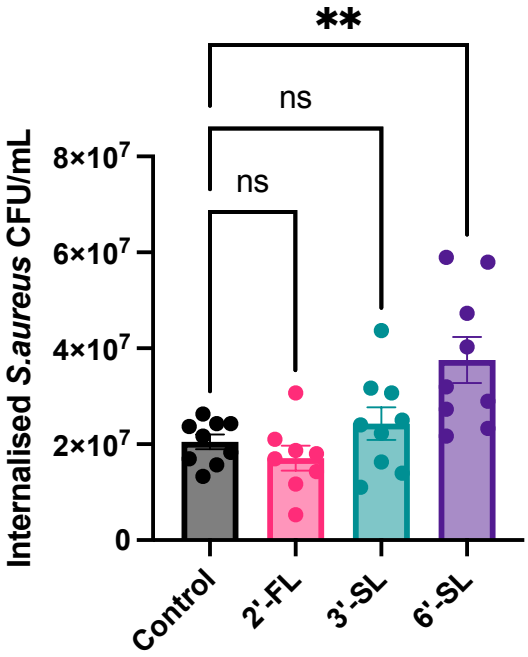

Figure 4. 10: **Bacterial Uptake in Immortalised Macrophages Following HMO Treatment**

Immortalised iBMDMs were pre-treated with HMOs prior to infection with bacteria. quantified CFU. Data shown is from 3 independent experiments (n=3). Data is presented as the mean ± SEM. One-way ANOVA was used to calculate statistical significance with a P-value of < 0.05 deemed statistically significant. ns indicates $p>0.05$, ** $p<0.01$

4.5. The Effect of HMOs on Pro and Anti-Inflammatory Cytokine Release in Macrophages

To examine the impact of HMOs on macrophage cytokine production, TNF-α, IL-10, and IL-1β levels were assessed in BMDMs under different polarised conditions. TNF-α production was measured following short-term (4 hour, 6 hour) and long-term (24 hour) LPS stimulation in the presence or absence of HMOs. HMOs alone did not induce TNF-α secretion in unstimulated macrophages **(Figure 4.11 B)**. Following LPS stimulation, no significant differences in TNF-α production were observed at early time points (4 hour and 6 hour) **(Figure 4.11 C, D**). However, after 24 hours of LPS exposure, HMO treatment significantly reduced TNF-α secretion compared to untreated controls, with 6'-SL exhibiting the strongest suppressive effect **(Figure 4.11 E)**. These results suggest that HMOs exert anti-inflammatory effects in macrophages under prolonged inflammatory conditions.

The effect of HMOs on IL-10 production was examined in both M1 and M2 macrophages. In M1 macrophages, 6'-SL significantly reduced IL-10 secretion following 24 hour LPS stimulation, while 2'-FL and 3'-SL had no significant effect **(Figure 4.12 E)**. No changes were observed at earlier time points (4 hour, 6 hour) **(Figure 4.12 C, D)**, suggesting that 6'-SL specifically influences IL-10 production during sustained inflammation. In contrast, IL-10 secretion in M2 macrophages remained unaffected by HMO treatment at all time points following IL-4 stimulation **(Figure 4.13 B-E)**, indicating that HMOs do not alter IL-10 production in alternatively activated macrophages.

To determine whether HMOs influence inflammasome activation and IL-1β secretion, macrophages were stimulated with LPS for 4 hour, 6 hour, or 24 hour, with ATP added in the final hour. IL-1β levels were increased in macrophages treated with 6'-SL at 4 hours LPS treatment, with no changes to other HMO treatments **(Figure 4.14 C)**. IL-1β secretion was not affected in HMO-treated cells at both 6 hour and 24 hour post-LPS stimulation **(Figure 4.14 D, E)**. When ATP was included, HMO treatment led to a significant decrease in IL-1β levels after 6 hour and 24 hour of LPS stimulation **(Figure 4.14 H, I)**, suggesting that HMOs may attenuate inflammasome activation or IL-1β release under sustained inflammatory conditions.

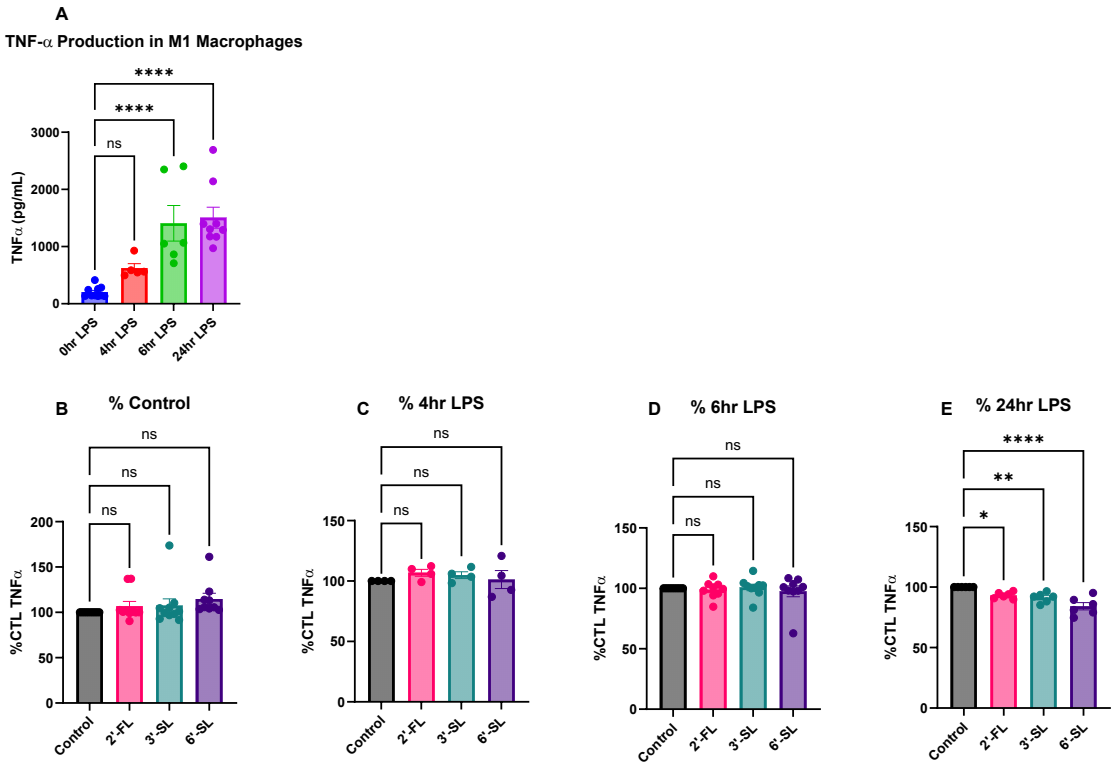

Figure 4. 11**: TNF-α Production in M1 Macrophages Following HMO Treatment**

BMDMs were treated overnight with HMOs (2 mM 2'-FL, 1 mM 3'-SL and 6'-SL) ± LPS (100 ng/mL) for 0hour (CTL), 4 hour, 6 hour and 24 hours. (A) show raw data from ELISA for each control LPS timepoint. (B-E) show data expressed as a percentage of the individual control (B) HMOs treated alone, No LPS (C) HMO treated + 4 hour LPS (D) HMO treated + 6 hour LPS (E) HMO treated + 24 hour LPS. Data shown is from at least 4 independent experiments (n=4). Data is presented as the mean ± SEM. One-way ANOVA was used to calculate statistical significance with a P-value of < 0.05 deemed statistically significant.

ns indicates $p>0.05$, * $p<0.05$, ** $p<0.01$, **** $p<0.0001$

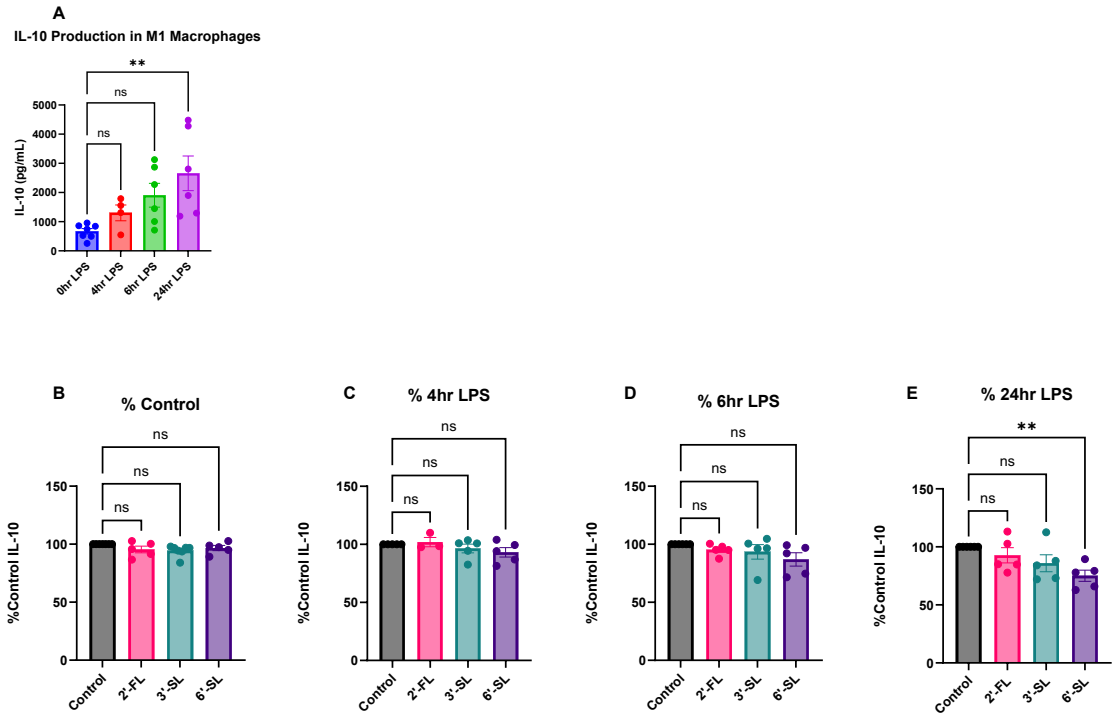

Figure 4. 12**: IL-10 Production in M1 Macrophages Following HMO Treatment**

BMDMs treated overnight with HMOs (2 mM 2'-FL, 1 mM 3'-SL and 6'-SL) ± LPS (100 ng/mL) for 0hours (CTL), 4 hours, 6 hours or 24 hours. (A) show raw data from ELISA for each control LPS timepoint. (B-E) show data expressed as a percentage of the individual control (B) HMOs treated alone, No LPS (C) HMO treated + 4 hour LPS (D) HMO treated + 6 hour LPS (E) HMO treated + 24 hour LPS. Data shown is from at least 4 independent experiments (n=4). Data is presented as the mean ± SEM. One-way ANOVA was used to calculate statistical significance with a P-value of < 0.05 deemed statistically significant.

ns indicates $p>0.05$, ** $p<0.01$,

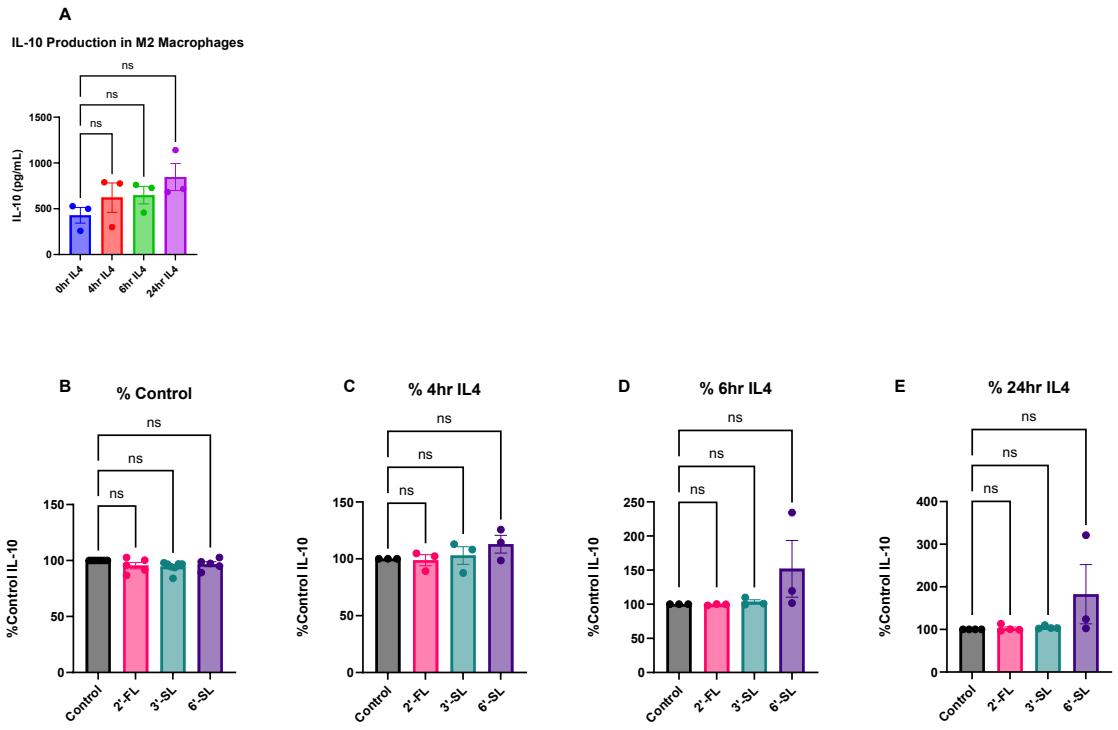

Figure 4. 13 **: IL-10 Production in M2 Macrophages Following HMO Treatment**

BMDMs treated overnight with HMOs (2 mM 2'-FL, 1 mM 3'-SL and 6'-SL) ± IL-4 (20 ng/mL) for 0hours (CTL), 4 hours, 6 hours or 24 hours. (A) show raw data from ELISA for each control IL-4 timepoint. (B-E) show data expressed as a percentage of the individual control (B) HMOs treated alone, No IL4 (C) HMO treated + 4 hour IL4 (D) HMO treated + 6 hour IL4 (E) HMO treated + 24 hour IL4. Data shown is from at least 3 independent experiments (n=3). Data is presented as the mean ± SEM. One-way ANOVA was used to calculate statistical significance with a P-value of < 0.05 deemed statistically significant. ns indicates $p>0.05$

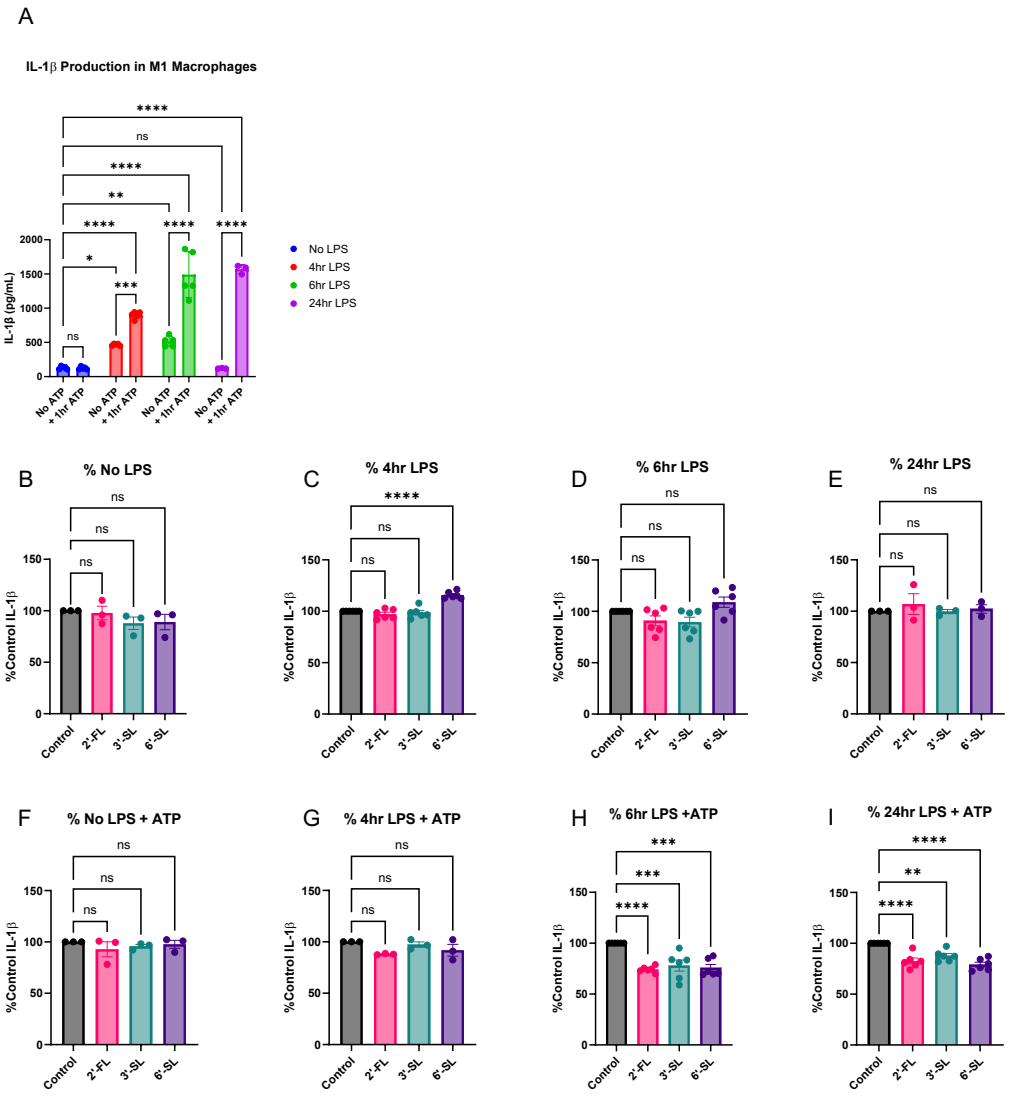

Figure 4. 14: **IL-1β Production in M1 Macrophages Following HMO Treatment**

BMDMS treated overnight with HMOs (2 mM 2'-FL, 1 mM 3'-SL and 6'-SL) ± LPS (100 ng/mL) for 0hours (CTL), 4 hours, 6 hours or 24 hours with the last hour treated ± ATP (5 mM). (A) show raw data from ELISA for each control LPS timepoint. (B-I) show data expressed as a percentage of the individual control (B) HMOs treated alone, No LPS (C) HMO treated + 4 hour LPS (D) HMO treated + 6 hour LPS (E) HMO treated + 24 hour LPS (F) HMOs treated alone, No LPS + 1hour ATP (G) HMO treated + 4 hour LPS and 1 hour ATP (H) HMO treated + 6 hour LPS and 1 hour ATP (I) HMO treated + 24 hour LPS and 1 hour ATP. Data shown is from at least 3 independent experiments (n=3). Data is presented as the mean ± SEM. One-way ANOVA was used to calculate statistical significance with a P-value of < 0.05 deemed statistically significant. ns indicates $p>0.05$, * $p<0.05$, ** $p<0.01$, *** $p<0.001$, **** $p<0.0001$

4.6. Discussion

This chapter examines the impact of HMOs on macrophage effector functions, including cytokine production, ROS generation, phagocytosis, TLR signalling, and cytotoxicity. Through a series of *in vitro* experiments, we assessed how 2'-FL, 3'-SL, and 6'-SL influence macrophage activation and immune responses. We evaluated cytokine secretion profiles to determine the immunomodulatory effects of HMOs, measured ROS production to assess their role in oxidative stress regulation, and analysed phagocytic uptake to investigate their impact on macrophage antimicrobial function. Additionally, we explored HMO interactions with TLR2 and TLR4 to elucidate potential receptor-mediated signalling pathways and performed cytotoxicity assays to confirm their safety in immune cell models. By integrating these findings, this chapter provides a comprehensive analysis of how HMOs shape macrophage function and contribute to immune regulation.

This study firstly confirms that HMOs; 2'-FL, 3'-SL, and 6'-SL are non-cytotoxic to macrophages in this model, as evidenced by maintained cell viability and function upon exposure. This observation aligns with existing literature, which reports the safety, non-toxic effects and lack of apoptotic or necrotic effects of these HMOs in various cellular contexts, including RAW264.7[269], Caco-2[243], HT-29 and HIEC cells[270,271]. Additionally, EFSA assessments have confirmed the safety of 2'-FL, 3'-SL[196] and 6'-SL[272], further supporting the non-cytotoxic nature of these HMOs. Collectively, these findings reinforce the potential of therapeutic applications and validate the use of HMOs in downstream functional assays.

Current data indicates that 6′-SL may modulate TLR-associated signalling in macrophages, whereas 2′-FL and 3′-SL do not exert effects on either TLR2 or TLR4 in the same context. In hTLR4 reporter assays, 6′-SL alone induced measurable NF-κB activity, while co-treatment with LPS did not increase reporter signal, suggesting that 6′-SL interacts with the receptor complex in a manner that may be competitive rather than purely agonistic. Lack of further enhancement in the presence of LPS suggests that 6'-SL and LPS may converge on the same binding site or signalling pathway within TLR4, saturating the receptor's capacity for activation. In contrast, if 6'-SL acted as a co-stimulatory molecule, one might expect potentiation of LPS-induced NF-κB activity. In contrast, 2′-FL and 3′-SL neither

activated nor suppressed TLR2/4 signalling in this model, suggesting differences in structural distinctions of fucosylated versus sialylated HMOs, but also linkage specific differences. The IκBα western blot data in BMDMs, showed decreased IκBα levels in 6′-SL treated, LPS-stimulated macrophages after 1 hour; consistent with transient NF-κB pathway engagement. The data also showed increased IκBα levels in 2'-FL and 6'-SL treated cells, compared to the untreated control macrophages, alongside this 2'-FL allowed for a quicker return of IκBα levels after 30 minutes of LPS treatment compared to the control treatment of LPS alone. IκBα functions as an inhibitor of NF-κB by sequestering it in the cytoplasm, preventing it from translocating to the nucleus to activate pro-inflammatory gene expression. Upon stimulation, IκBα is phosphorylated, ubiquitinated, and subsequently degraded, allowing NF-κB to translocate into the nucleus. Reduced levels of IκBα indicate that this degradation process is occurring, suggesting that NF-κB is more active in 6'-SL-treated macrophages compared to controls and less activated in 2'-FL treated cells.

One interpretation is that 6′-SL could interact directly with the TLR4 complex, but the outcome of this interaction may vary by cell type and receptor density. This interaction could activate both MyD88-dependent or TRIF-dependent pathways, which subsequently lead to the activation of key transcription factors such as NF-κB and MAPKs (p38, JNK). These transcription factors are pivotal in the production of inflammatory cytokines and further downstream anti-microbial processes. Studies in intestinal epithelial systems suggest an inhibitory function, numerous studies found that 6′-SL suppresses TLR4/NLRP3 inflammasome activation, reducing inflammation and tissue injury in NEC models[273-275]. These HMOs were predicted to directly bind to TLR4, preventing activation by NEC causing bacteria and subsequent inflammatory responses. The protective effects were demonstrated in both mouse and piglet models, as well as in human intestinal explants. These studies provide valuable insights for the demonstration that 6'-SL can inhibit TLR4 signalling in intestinal epithelial cells and may suggest a potential mechanism by which HMOs modulate immune responses. Similarly, Yu et al. (2024) reported that 6′-SL attenuates MAPK and NF-κB activation while promoting Nrf2-dependent antioxidant signalling in macrophages treated with LPS, consistent with an anti-inflammatory role[276]. 2′-FL exhibits comparable anti-TLR4 effects in NEC[273] and induces modest transcriptional

changes in TLR4 and its co-receptor MD2 without activating the pathway in intestinal epithelial cells[277].

Current results and those of Jepsen et al. (2024), who observed increased NF-κB reporter activity following 6′-SL treatment in THP1 cells, suggest that 6′-SL can activate NF-κB signalling under certain conditions[254]. This raises the possibility that 6′-SL acts as a partial agonist, capable of weakly engaging the receptor to initiate selective signalling outputs. Differing from these results, Cheng et al. (2019) showed no effect of 2'-FL or 6'-SL on any TLR activation[82], attributing other studies to LPS contamination. However, adding to the complexity, Craft et al. (2019) demonstrated that HMOs, particularly sialylated structures may interact with polymyxin B[278,279], an antibiotic used in some assays to neutralise LPS. Since Cheng et al. (2019) employed polymyxin B in their assays, such interactions could artifactually alter apparent TLR signalling outcomes, further emphasising the need for chemical purity and appropriate assay controls. The fact that 3′-SL consistently does not elicit responses in these results and other TLR assays suggests potential structural and linkage selectivity. Notably, Pessentheiner et al. (2024) observed that 3′-SL administration reduces systemic inflammation and atherosclerosis in mice without evidence of direct TLR4 involvement[280], implying that HMO-mediated immunomodulation may occur through non-TLR pathways such as lectin interactions, or GPCRs. These alternative explanations remain viable for 6′-SL as well, particularly given its effects on macrophage metabolism and ROS production observed elsewhere in this work.

Beyond TLRs, several alternative receptor systems could account for the immunomodulatory effects observed with 3'-SL and 6′-SL. GPR35, a GPCR expressed in macrophages and intestinal epithelial cells, has been reported to bind sialylated glycans[263] and influence cellular metabolism through modulation of the Na^+/K^+ ATPase and downstream MAPK/NF-κB signalling. Engagement of GPR35 could therefore mimic partial TLR4 activation while simultaneously altering redox balance and metabolic tone. Siglec family receptors, which recognise sialylated ligands, present another plausible route, although Perdijk et al. (2018) found no evidence that 3′-SL signals via siglecs, a result corroborated by a study by Pessentheiner et al. (2024)[280]. Receptor affinity could differ substantially between 3′- and 6′-linked sialyllactoses. Siglec engagement typically triggers

immunoreceptor tyrosine-based inhibition motif (ITIM)-mediated inhibitory signalling, potentially explaining the anti-inflammatory effects of HMOs observed in LPS-challenged macrophages. DC-SIGN and related C-type lectins also bind specific glycan motifs and could mediate uptake or signal modulation independent of TLRs. Collectively, these possibilities suggest that HMOs effects may result from multivalent interactions across receptor classes rather than a single canonical pathway, emphasising the need for direct binding studies and receptor-deficient models to resolve their mechanism of action.

This thesis demonstrated that 6'-SL increased basal ROS levels in macrophages, however all tested HMOs significantly reducing ROS production following prolonged stimulation with LPS for 24 hours. This suggests that certain HMOs may initially prime macrophages by increasing basal oxidative stress, potentially enhancing their antimicrobial capacity. However, under prolonged inflammatory stress, HMOs appear to exert a protective effect, reducing excessive ROS production and mitigating inflammation. This dual role is consistent with the concept of "metabolic flexibility", where immune cells adapt their metabolic state based on environmental cues to optimise function while avoiding excessive damage[281]. Yu et al. (2024) investigated the impact of 6′-SL on ROS production in RAW 264.7 macrophages stimulated with LPS. The findings revealed that 6′-SL effectively reduced LPS-induced ROS levels in these macrophages after 24 hour LPS stimulation. This reduction was associated with the activation of the Nrf2 signalling pathway, leading to increased expression of antioxidant enzymes such as heme oxygenase-1 (HO-1)[276]. Additionally, 6′-SL attenuated the phosphorylation of p38 MAPK and Akt pathways, which are known to contribute to oxidative stress and inflammation. These results suggest that 6′-SL exerts a protective effect against LPS-induced oxidative stress in macrophages by modulating key signalling pathways involved in ROS production and antioxidant defence[276]. We observed that 3'-SL also reduced ROS production in prolonged inflammatory conditions. In endothelial cells, Nguyen et al. (2024) demonstrated that 3′-SL reduced LPS-induced superoxide generation and downstream ERK1/2-STAT1 activation via inhibition of the High-Mobility Group Box 1 (HMGB1) and its receptor, the Receptor for Advanced Glycation End-products (RAGE) axis[282], highlighting the capacity to modulate ROS-driven inflammatory signaling in other cell contexts. 2'-FL also significantly reduced ROS production following 24 hour LPS stimulation in this study, suggesting a protective effect against excessive oxidative stress. This finding aligns with

the study by Pak et al. (2023), which demonstrated that 2'-FL attenuates ROS production in microglia following ischemic brain injury[95]. Microglia, the resident macrophages of the brain, play a critical role in neuroinflammation and oxidative stress regulation. The parallels between our findings and those observed in microglia suggest that 2'-FL may exert a broader anti-inflammatory role across different macrophage populations. By limiting excessive ROS generation, 2'-FL could contribute to reducing oxidative damage and inflammation in various pathological conditions, contributing further to its established anti-inflammatory role. Another study analysing *Pseudomonas aeruginosa* K infection in murine macrophage-like THP-1 cells, also reported an increase in ROS production. Interestingly, these cells exhibited a rapid return of ROS levels to baseline post-infection clearance, indicating that while HMOs enhance ROS production to support bacterial clearance, they do not promote prolonged oxidative stress that could exacerbate inflammation. This tightly regulated ROS response highlights the dual role of HMOs in balancing effective pathogen clearance with the prevention of excessive inflammation[99]. These results alongside current findings show that HMOs may elicit the ROS production to aid in bacterial clearance by macrophages but do not allow for prolonged ROS production to cause enhanced inflammation.

Further to this, Zhang et al. (2019) showed that HMOs, specifically a fraction isolated from milk termed HMO-7, increased nitric oxide production and pro-inflammatory cytokine release in murine macrophage-like RAW264.7 cells. In this same study, the isolated HMO fraction was observed to stimulate the release of ROS in RAW264.7 macrophages which aids in bacterial clearance. The study also demonstrated that this HMO fraction activates macrophages through the NF-κB and MAPK signalling pathways, key regulators of the immune response and inflammation[269]. This study further contributes to this understanding by demonstrating that individual HMOs, can alter ROS production in BMDMs under specific inflammatory conditions. This ROS induction appears to be context-dependent, influenced by the oligosaccharide structure, the macrophage activation state, and the nature of the inflammatory stimulus. For example, while HMOs increased basal ROS levels, they suppressed ROS production after prolonged LPS stimulation (24 hour) but not after short-term exposure (4 hour). This suggests that HMOs limit oxidative stress during sustained inflammation while preserving early antimicrobial ROS responses. Low to moderate ROS levels are known to facilitate phagocytosis, antigen processing, and microbicidal activity

and this functional modulation of oxidative stress ties directly into their influence on phagocytic efficiency, as macrophages rely on both ROS generation and engulfment capacity for microbial killing. This aligns with existing literature that defines ROS as modulators rather than mere byproducts of immune activation[283]. HMOs may support macrophage phagocytic function through receptor-mediated signalling but may also do so by modulating redox balance. Excessive ROS have been shown to induce cytoplasmic stiffening, thereby impairing the actin dynamics required for efficient engulfment[284]. By attenuating ROS production under inflammatory stress, HMOs may help preserve the cytoskeletal flexibility needed for continued phagocytosis. While this suggests a potential link between redox regulation and the enhanced uptake observed with 6′-SL, further work using ROS scavengers or NOX inhibition would be required to directly establish causality. Overall, these findings demonstrate that 6'-SL influences both oxidative stress and macrophage function, increasing basal ROS production while mitigating ROS accumulation under prolonged inflammation.

Conversely, the suppression of ROS production following prolonged 24 hour LPS stimulation in HMO-treated BMDMs suggests that HMOs interfere with pro-inflammatory amplification, possibly by inhibiting mitochondrial ROS production or enhancing antioxidant responses post-activation. Since LPS-induced TLR signaling activates NF-κB and drives ROS production through NOX and mitochondrial pathways, the data shown suggest that HMOs may dampen this response. This could occur through direct interference with TLR signaling or by altering cellular metabolism to shift macrophages away from an inflammatory state. Given that NF-κB can be both activated and repressed by ROS depending on the dose and duration of exposure, it's plausible that HMOs shape NF-κB signalling indirectly by modulating cellular redox state. This would be consistent with the current cytokine data, where LPS-induced IL-1β and TNF-α are suppressed by HMOs, two classic NF-κB-dependent genes.

Current data also indicates that 6'-SL significantly enhances phagocytosis in both primary and immortalised BMDMs. These findings align with previous studies showing that sialylated HMOs can enhance innate immune functions, including bacterial clearance. As discussed in Chapter 3, Jepsen et al. (2024) reported that 6'-SL enhances phagocytosis in

human macrophages in response to *Staphylococcus aureus*[254]. Feng et al. (2025) found that co-supplementation of 2'-FL and 6'-SL in healthy mice significantly increased macrophage phagocytosis (measured via carbon clearance), compared to 2′-FL alone[285], strengthening the idea that these HMOs can enhance innate microbial-clearance functions *in vivo.* TLR activation in macrophages is well known to enhance phagocytosis through a multistep innate immune signalling cascade: LPS binding to TLR4 along with co-receptors MD-2 and CD14 activate both Myeloid differentiation primary response 88 (MyD88)-dependent and TIR-domain-containing adapter-inducing interferon-β (TRIF)-dependent pathways[286]. The MyD88 pathway recruits interleukin-1 receptor-associated kinase (IRAK)4/1 and TNF receptor-associated factor (TRAF)6, leading to mitogen-activated protein kinase (MAPK) (including p38, JNK, ERK) and NF-κB activation, while the TRIF pathway activates Interferon regulatory factor 3 (IRF3) alongside NF-κB, supporting type-I interferon and pro-inflammatory gene expression. Together, these cascades promote cytoskeletal rearrangements via Rho GTPases (Rac1, Cdc42)[287,288], upregulate phagocytic receptors such as FcγRs, CR3, and scavenger receptors, and increase opsonin production, thereby boosting microbial uptake[289].

Jepsen et al. also showed 6'-SL increased pro-inflammatory cytokine production, indicating a pronounced activation of macrophage inflammatory pathways. In contrast, while we observed an increase in phagocytic activity in BMDMs treated with 6'-SL, the cytokine response in this murine model was more nuanced. Specifically, under 24 hour LPS stimulation, we noted a suppression of key inflammatory markers such as IL-1β and TNF-α. This divergence suggests that the immunomodulatory effects of 6'-SL may vary based on species-specific differences[245] between human and murine macrophages or the distinct immune responses elicited by bacterial pathogens versus LPS stimuli. These findings highlight the importance of considering both the cellular context and the nature of the immune challenge when evaluating HMO effects. The ability of 6'-SL to enhance phagocytosis suggests that it may serve as an immune-priming molecule, equipping macrophages with a heightened capacity for pathogen clearance without driving excessive inflammation. Together, the ROS and phagocytosis data suggest that HMOs orchestrate a finely tuned antimicrobial program, amplifying innate functions while preventing overactivation.

Comparing studies on the effects of HMOs on cytokine production is challenging due to significant differences in HMO structure, concentrations used, cell types, and experimental conditions. Concentrations used *in vitro* often vary widely, with some studies using physiologically relevant levels while others employ supraphysiological doses, potentially leading to inconsistent findings. Additionally, differences in macrophage models, such as primary macrophages, monocyte-derived macrophages, or immortalised cell lines can influence cytokine responses due to variations in receptor expression and metabolic states. The presence of inflammatory stimuli, treatment duration, and methods used to measure cytokine levels further complicate comparisons. These methodological discrepancies highlight the need for broader experimental approaches to better understand how HMOs regulate cytokine production in specific conditions.

The investigation into the effects of HMOs on macrophage cytokine production revealed significant immunomodulatory properties, particularly under prolonged inflammatory conditions. Specifically, these findings indicate that HMO-treated BMDMs exhibit a marked reduction in TNF-α secretion with a combination of 24 hours LPS stimulation compared to non-HMO treated controls. This suggests that HMOs may exert anti-inflammatory effects during sustained inflammation. Treatment with 6'-SL in combination with LPS for 4 hours resulted in increased IL-1β production. Mechanistically, this likely reflects the two-step regulation of IL-1β: LPS provides the priming signal that induces transcription of pro-IL-1β, while the ROS elevation observed with 6'-SL treatment serves as an additional activation signal that promotes inflammasome assembly and cleavage of pro-IL-1β into its mature, secreted form. Notably, 6'-SL alone did not induce IL-1β production, indicating that it is not inherently pro-inflammatory but can modulate the response to additional stimuli. Furthermore, the data indicates that HMO treatments significantly reduced IL-1β levels at both 6 hour and 24 hour time points following LPS and ATP stimulation, suggesting that HMOs may attenuate inflammasome activation or IL-1β release under sustained inflammatory conditions. Overall, these findings demonstrate that HMOs exert distinct immunomodulatory effects on macrophage cytokine production. HMOs, particularly 6'-SL, suppress TNF-α and IL-1β secretion in response to prolonged inflammatory stimuli, while also modulating IL-10 levels in M1 macrophages. These results suggest a potential role for HMOs in regulating macrophage-driven inflammation, particularly under conditions of chronic immune activation.

These observations align with existing literature highlighting the anti-inflammatory potential of HMOs. For instance, current findings are consistent with that of Jin et al. (2023) who showed 3'-SL and 6'-SL suppressed mRNA expression of TNF-α, and IL-1β in LPS-induced RAW 264.7 cells. Pessentheiner et al. (2024) demonstrated that 3'-SL reduces low-grade inflammation and atherosclerosis in mice by attenuating pro-inflammatory cytokine expression in macrophages[280]. Sotgiu et al. (2006) showed mononuclear cells (MNCs) isolated from multiple sclerosis patients and healthy controls, when stimulated with LPS *ex vivo* and treated with 2'-FL, exhibited reduced TNF-α production compared to LPS-treated controls[290]. This aligns with the findings that 2'-FL similarly decreases inflammatory cytokine production in macrophages following prolonged LPS exposure. The consistency between these results suggests that 2'-FL exerts a broader immunomodulatory effect across different immune cell types and disease contexts, reinforcing its potential as an anti-inflammatory agent. Zhang et al. (2019) demonstrated that a fraction of HMOs induced expression of a number of cytokines (IL-1β, IL-6, IL-10, TNF-α) in RAW264.7 macrophages[269]. These increases occur, without the presence of LPS. Although this study does not show an increase in cytokine production with HMO treatments in the absence of LPS, this may be explained due to discrepancies in cell line and the use of a general fraction of breast milk rather than individual HMOs. Elucidating that other HMOs present in the fraction could be responsible for this increase in inflammatory cytokines.

This study observed that 6'-SL treatment significantly reduced IL-10 secretion in M1 macrophages following 24 hour LPS exposure, suggesting a role in modulating the resolution phase of inflammation in classically activated macrophages. Conversely, no significant changes in IL-10 production were observed in M2 macrophages following HMO treatment, although 6'-SL showed a trending non-significant increase in IL-10 production. This indicates that alternative macrophage activation remains unaffected by HMOs. Study by Jepsen et al. (2024) showed no difference in IL-10 production in M1 macrophages treated with different HMOs[254], Sotgiu et al. (2006) claims 2'-FL decreases IL-10 production in LPS treated macrophages, although the results are not significant[290]. These studies, along with current data, indicate that the effects of HMOs on IL-10 production may be context-dependent, influenced by macrophage polarisation state, specific HMO structure, and inflammatory conditions.

These findings, supported by current literature, highlight the potential of HMOs to modulate macrophage-mediated immune responses under inflammatory conditions. The observed reduction in pro-inflammatory cytokines such as TNF-α and IL-1β, along with the selective modulation of IL-10 in M1 macrophages, highlights the nuanced role of HMOs in regulating immune responses. These insights contribute to a growing body of evidence supporting the therapeutic potential of HMOs in managing inflammation and promoting immune homeostasis.

In conclusion, this research provides novel insights into the immunomodulatory roles of HMOs in macrophages, demonstrating their ability to regulate oxidative stress, cytokine production, and phagocytosis (summary **Figure 4.15**). By investigating how HMOs influence macrophage function, this work contributes to a growing body of evidence supporting the role of dietary glycans in immune regulation. These results provide further evidence supporting the role of HMOs in shaping immune responses and also have potential implications for the development of functional food components and synthetic HMOs as immunomodulatory agents in both early life and adult health with potential implications for therapeutic interventions targeting immune dysregulation and inflammatory diseases.

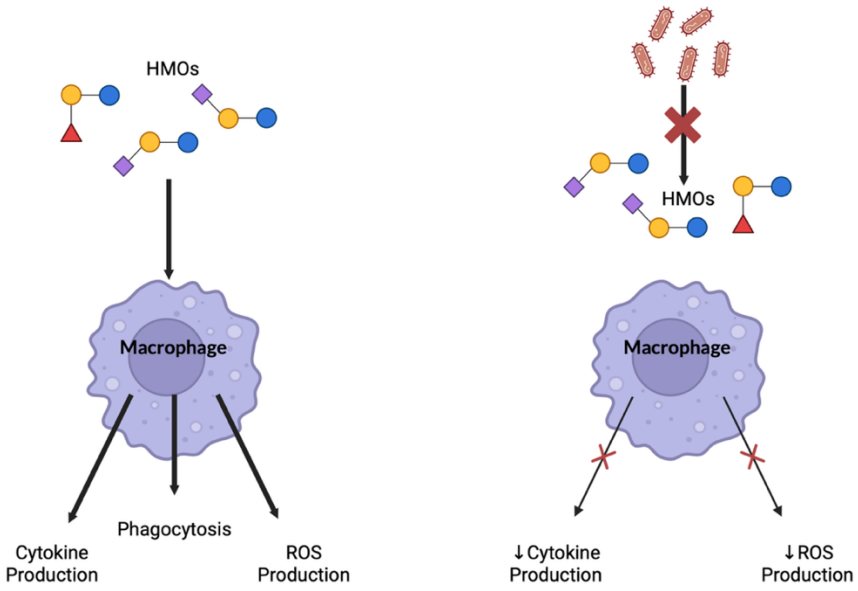

Figure 4. 15: **Schematic Overview of HMOs Effect on Macrophage in Resting and Inflammatory States**

Chapter 5

Metabolic and Functional Effects of Human Milk Oligosaccharides on Dendritic Cells and T-Cells

5.1. Introduction

DCs and T-cells play pivotal roles in orchestrating immune responses, bridging innate and adaptive immunity. DCs are professional APCs responsible for capturing, processing, and presenting antigens to naïve T-cells, thereby initiating and directing T-cell responses. The functional state of a DC, ranging from tolerogenic to immunogenic, is tightly regulated by environmental cues and cellular metabolism. Recent advances have highlighted how metabolic pathways such as oxidative phosphorylation, glycolysis, and fatty acid metabolism influence DC differentiation, cytokine production, and antigen presentation capacity[291]. Immunogenic DCs, often stimulated by PAMPs such as LPS, exhibit increased glycolysis and decreased mitochondrial respiration to support the rapid energy demands of activation[292]. In contrast, tolerogenic DCs rely more on oxidative phosphorylation and fatty acid oxidation, which supports a regulatory phenotype capable of inducing T-cell tolerance[227]. Likewise, metabolic cues profoundly shape T-cell function. Naïve T-cells predominantly utilise oxidative phosphorylation, whereas upon activation, effector T-cells; including Th1, Th17, and cytotoxic $CD8^+$ T-cells, undergo metabolic reprogramming characterised by elevated glycolysis to meet biosynthetic and energy demands[293]. Conversely, Tregs and memory T-cells maintain metabolic profiles reliant on mitochondrial respiration and lipid oxidation, promoting longevity and suppressive function[294].

Given the centrality of metabolism in defining DC and T-cell fate and function, there is increasing interest in how bioactive compounds may modulate immune metabolism to fine-tune immune responses. DCs can acquire a tolerogenic phenotype under certain microenvironmental cues, characterised by low expression of co-stimulatory molecules, reduced pro-inflammatory cytokine secretion, and enhanced production of regulatory mediators such as IL-10 and TGF-β[295,296]. These tolerogenic DCs play a crucial role in maintaining peripheral tolerance by promoting the differentiation and expansion of Tregs and suppressing pathogenic effector T-cell responses[297]. Several studies have reported that HMOs can modulate DC maturation and cytokine secretion, promoting anti-inflammatory profiles and supporting the development of Tregs[298]. Specific HMOs induce a semi-mature, tolerogenic phenotype in human monocyte-derived DCs[299] promoting the differentiation of naïve $CD4^+$ T-cells into Tregs, suggesting a role for HMOs in fostering immune tolerance during early life. Further mechanistic insights examined the influence of acidic HMOs on

DC-mediated T-cell polarisation[298,300]. These HMOs were shown to enhance Th1 and Th17 cytokine responses while dampening Th2-associated cytokine production[301]. Importantly, it has also been demonstrated that treatment of DCs with HMOs altered their capacity to modulate T-cell responses, pointing to a direct immunoregulatory role of HMOs at the DC-T-cell interface[300]. This immunomodulatory capacity extends to tissue-resident DCs as well. 3′-SL has been shown to activate intestinal $CD11c^+$ DCs, inducing a cytokine milieu that promotes Th1 and Th17 cell responses[302]. These findings were further supported by *in vitro* co-culture models, where DCs exposed to HMOs primed T-cells toward pro-inflammatory or tolerogenic phenotypes depending on the HMO structure and environmental context. Beyond DCs, effects of HMOs on T-cells have also been described. Other studies reported that acidic HMOs can increase IFN-γ and IL-13 production in both $CD4^+$ and $CD8^+$ T-cells derived from cord blood, implying an intrinsic ability to modulate T-cell cytokine output[298]. Together, these studies provide a compelling framework for understanding how HMOs shape immune function during early life. By modulating DC phenotype and function, and influencing T-cell polarisation, HMOs contribute to the development of immune tolerance and protection against pathogenic inflammation.

However, key questions remain regarding the structural specificity of HMO interactions, the tissue context in which these effects occur, and how these mechanisms might be leveraged therapeutically beyond infancy. This chapter addresses this critical gap by investigating the metabolic and immunological effects of HMOs on bone marrow-derived DCs and $CD8^+$ T-cells. Given that immune cell function is intrinsically linked to their metabolic state, understanding how HMOs impact energy pathways such as glycolysis and oxidative phosphorylation provides valuable insight into how these glycans may condition responses. Furthermore, as T-cell activation and polarisation are metabolically demanding processes, identifying how HMOs influence the metabolic profile of T-cells could clarify their role in skewing immune responses toward tolerance or inflammation. The rationale for this study lies in the recognition that while HMOs can modulate cytokine production and cell surface markers, the metabolic basis of these effects remains under-investigated. By elucidating how individual HMOs alter metabolic programming in DCs and T-cells, this chapter aims to uncover novel mechanisms by which maternal milk components shape the immune system during early life, and potentially beyond. Such insights expand our

understanding of maternal-infant immune interactions and highlight the therapeutic potential of HMOs in immune-mediated diseases.

Aims of This Chapter:

- Characterise the impact of individual HMOs on the metabolic profile of BMDCs, focusing on glycolysis and oxidative phosphorylation.
- Evaluate whether direct treatment of T-cells with specific HMOs alters their intrinsic metabolic programming, independent of DC interaction, thereby identifying potential mechanisms by which HMOs shape T-cell fate and function.
- Determine how individual HMOs influence DC and T-Cell effector functions, including cytokine production, ROS generation, under both basal and inflammatory conditions.

5.2. Methods

BMDCs were generated by culturing bone marrow progenitors in GM-CSF for 8 days, yielding loosely adherent immature DCs. Cells were stimulated with LPS under the same concentration and timing conditions used for BMDMs. HMOs were administered as a single-dose treatment, either alone or in combination with LPS, depending on the experimental setup.

T-cells were isolated from spleens and activated using anti-CD3. Cells were subsequently polarised with IL-2 to generate effector-like cells or with IL-15 to induce a memory-like phenotype. Once polarisation was established, HMOs were added as a single treatment without further replenishment.

Cell Viability

- **Alamar Blue**

Cells were seeded in 96-well flat-bottom plates at 400,000 cells/mL (in 200 µL) for DCs and 500,000 cells/mL for effector and memory T-cells. Wells were pre-coated with poly-D-lysine for T-cells. Cells were rested for ≥3 hours at 37 °C before treatment with HMOs: 4mM, 2 mM and 1 mM 2′-FL, 2 mM, 1 mM and 0.5 mM 3′-SL, or 6′-sialyllactose 6′-SL, for 24 hours ±100 ng/mL LPS (DCs only). Following treatment, cells were spun down in plate, 20 µL of supernatant was discarded and replaced with 20 µL Alamar Blue reagent, incubated for 4 hours. Untreated live control and a dead control were included. Absorbance was measured at 570 nm and 600 nm.

- **Flow Cytometry Live/Dead**

Cells were seeded in 6-well plates with same cell density as above (in 1 mL) and treated with HMOs: 2 mM 2′-FL, 1 mM 3′-SL, or 6′-sialyllactose 6′-SL for 24 hours ±100 ng/mL LPS (DCs only). Cells were detached with 10 mM EDTA in PBS, transferred to FACS tubes, washed with 2mL PBS, centrifuged, and resuspended in PBS containing fixable viability stain BV510. Samples were incubated 15 minutes at room temperature in the dark, washed again, resuspended in 200 µL FACS buffer, and immediately analysed on a FACSCanto (BV510 channel).

Seahorse Metabolic Flux Analysis

General seahorse protocol can be found in Chapter 2.

- **Mito Stress Test**

Cells were seeded in Seahorse XF96 plates at the same densities and rested as above, then treated overnight (16-18 hours) with HMOs ±4 hours LPS (100 ng/mL, DCs only). Prior to assay, cells were washed twice with Seahorse assay medium and incubated for 1 hour in a non-CO_2 incubator. Baseline OCR/ECAR was recorded (3 measurements), followed by sequential injection of oligomycin, FCCP, and rotenone/antimycin A with 3 measurements after each.

- **Timecourse Assay**

As above, but after baseline measurements, either media (vehicle control), LPS (for DCs only), or no treatment was injected. OCR or ECAR was recorded every 6 minutes for 6 hours.

Metabolic Gene PCR

Cells were seeded in 96 well plates at the same densities and rested as above, then treated overnight (16-18 hours) with HMOs ± 4 hours LPS (100 ng/mL, DCs only). RNA was extracted, cDNA synthesised, and qPCR performed using SYBR Green Master Mix with 2 µL cDNA and 0.5 µM primers (listed in **Table 2.4**). Cycling is described in chapter 2. Gene expression was normalised to housekeeping gene (*hprt*) and analysed via ΔΔCt method.

Extracellular Lactate Production

Following overnight HMO ± 4 hour LPS treatment (for DCs), cells were centrifuged in-plate and 50 µL supernatant was mixed with 50 µL Lactate-Glo reagent in a white 96-well plate. After 1 hour room temperature incubation, luminescence was read.

ROS Production

Cells were seeded, treated, and collected as for Live/Dead. After washing, cells were resuspended in PBS containing 5 µM MitoSOX and incubated 30 minutes room temperature in the dark. Cells were washed, resuspended in 200 µL FACS buffer, and analysed immediately on a FACSCanto (PE channel).

ELISA

Following treatment described above, 50 µL supernatant was transferred to pre-coated ELISA plates coated with primary antibody and blocked with BSA. Samples were diluted 1:5 (TNF-α), 1:10 (IL-10), or 1:20 (IL-1β). Assay was completed per manufacturer protocol (see Chapter 2). Absorbance was read at 450 nm.

5.3. HMOs Cytotoxic Effect in DCs and T-Cells

To confirm that the metabolic effects observed in DCs and T-cells were not attributable to cytotoxicity, cell viability was assessed following treatment with increasing concentrations of 2′-FL, 3′-SL, or 6′-SL for 24 hours.

Alamar Blue assays demonstrated no significant decrease in viability in BMDCs treated with HMOs, either alone or in combination with LPS stimulation. Absorbance measurements at 570/600 nm remained comparable to the untreated controls across all HMO conditions (**Figure 5.1 A-C**). Flow cytometry analysis using BV510 live/dead staining corroborated these findings, with the proportion of live BMDCs unaffected by HMO exposure. Quantification of live-cell frequencies as fold change relative to untreated controls confirmed the HMOs were not cytotoxic under all conditions tested (**Figure 5.1 D-H**).

Similarly, viability assays in effector and memory T-cells revealed no evidence of cytotoxicity following HMO treatment. Alamar Blue absorbance measurements showed stable cell viability across 2′-FL, 3′-SL, and 6′-SL treatment groups (**Figure 5.2 A-C**). Flow cytometry analysis confirmed that the proportion of viable cells was consistent with media-treated controls, with no reduction in live-cell frequency attributable to HMO treatment (**Figure 5.2 D-H**).

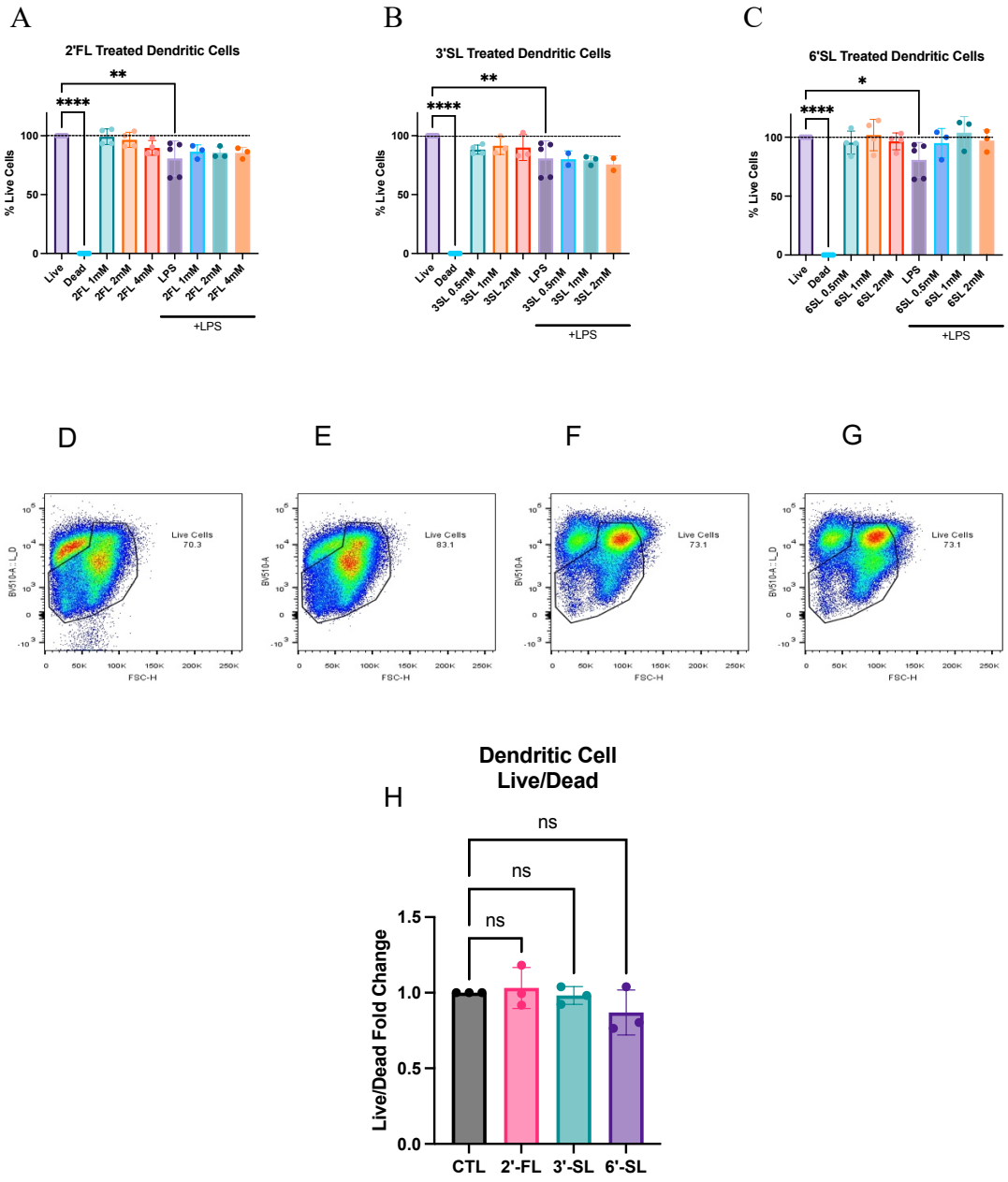

Figure 5. 1: **Viability Assessment of DCs Following HMO Treatment**

BMDCs treated with increasing concentrations of HMOs ± 100 ng/mL LPS for 24 hours. (A) 2'-FL (B) 3'-SL and (C) 6'-SL analysed for cell viability using Alamar blue. Live cells treated with (D) media control (E) 2'-FL (F) 3'-SL and (G) 6'-SL were stained using BV510 and analysed by flow cytometry. (H) live treated cells compared as a fold change of their control. Data shown is from at least 3 independent experiments (n=3). Data is presented as the mean ± SEM. Two-way ANOVA was used to calculate statistical significance with a P-value of < 0.05 deemed statistically significant. ns indicates $p>0.05$, * $p<0.05$, ** $p<0.01$, **** $p<0.0001$

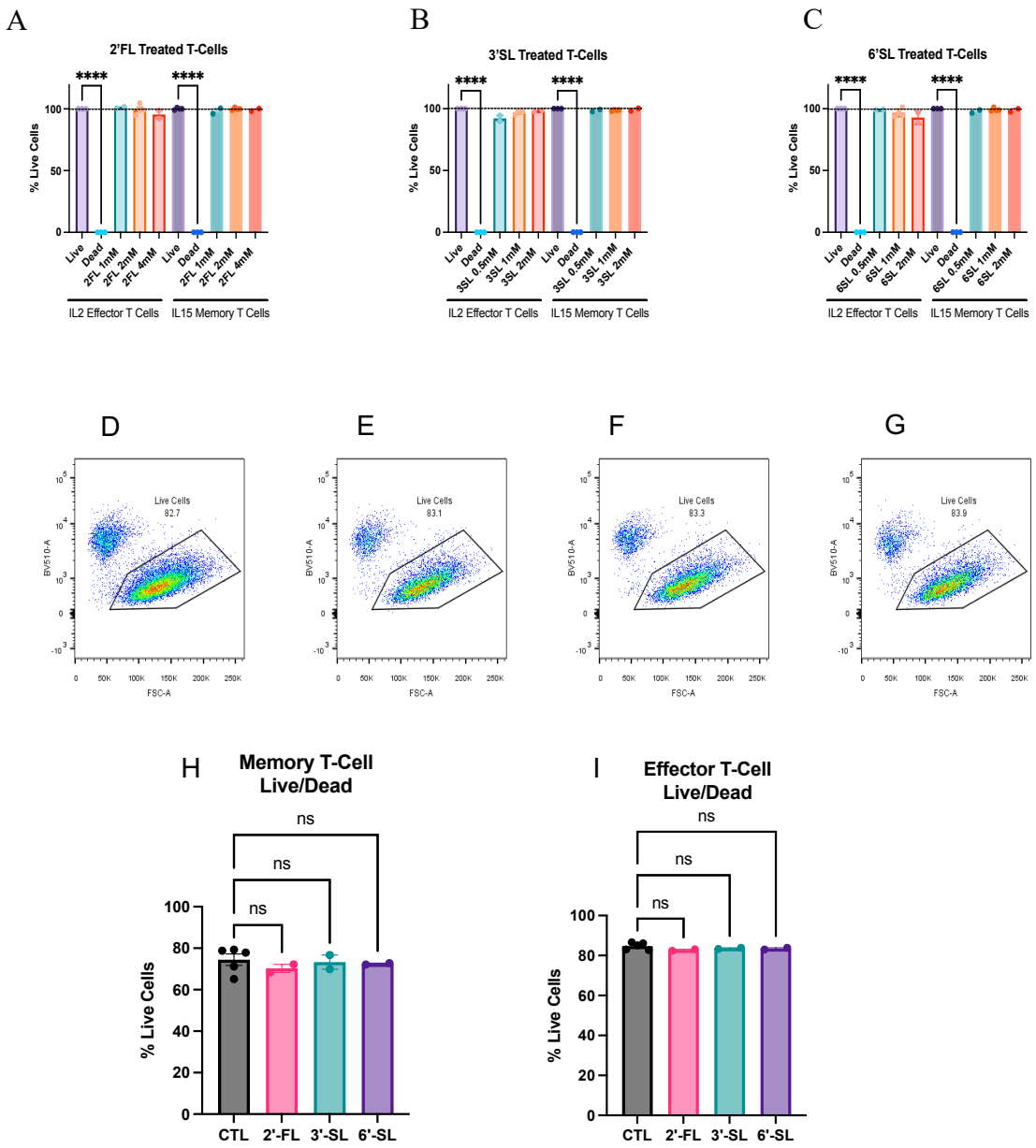

Figure 5. 2: **Viability Assessment of T-Cells Following HMO Treatment**

T-cells treated with increasing concentrations of HMOs ± IL-2/IL-15 for 24 hours. (A) 2'-FL (B) 3'-SL and (C) 6'-SL, analysed for cell viability using Alamar blue. Live cells treated with (D) media control (E) 2'-FL (F) 3'-SL and (G) 6'-SL were stained using BV510 and analysed by flow cytometry. (H) live treated cells compared as a fold change of their control. Data shown is from at least 3 independent experiments (n=3). Data is presented as the mean ± SEM. Two-way ANOVA was used to calculate statistical significance with a P-value of < 0.05 deemed statistically significant. ns indicates p>0.05, **** p<0.0001

5.4. Metabolic Profiling of DC Subsets by OCR and ECAR

To investigate the metabolic programming of DCs under different activation states, OCR and ECAR were measured as indicators of mitochondrial respiration and glycolytic activity, respectively. Three DC populations were profiled: unactivated DCs, immunogenic DCs stimulated with LPS for 4 hours, and prolonged DC stimulation with LPS for 24 hours (**Figure 5.3 and Figure 5.4**). Unactivated DCs exhibited relatively similar, slightly decreased OCR and ECAR values compared to 4 hour LPS activated DCs. In contrast, DCs subjected to prolonged 24 hour LPS stimulation displayed a significant reduction in OCR compared to both unactivated and 4 hour stimulated DCs.

To investigate the metabolic reprogramming of DCs upon activation, we performed quantitative PCR analysis on BMDCs stimulated with LPS for 4 hours to induce an activated phenotype. The expression of genes involved in oxidative phosphorylation and glycolysis was compared between resting and activated DCs. As shown in **Figure 5.5 A**, activated DCs exhibited a marked downregulation in the expression of key oxidative phosphorylation genes, including *ndufb6, sdha, uqcrc1, cox6c, and atp5f1*, relative to unactivated controls. This suggests a suppression of mitochondrial respiratory activity upon LPS stimulation. Conversely, glycolytic gene expression was upregulated in activated DCs, as illustrated in **Figure 5.5 B**. These findings are consistent with a metabolic switch from oxidative phosphorylation to glycolysis during pro-inflammatory DC activation.

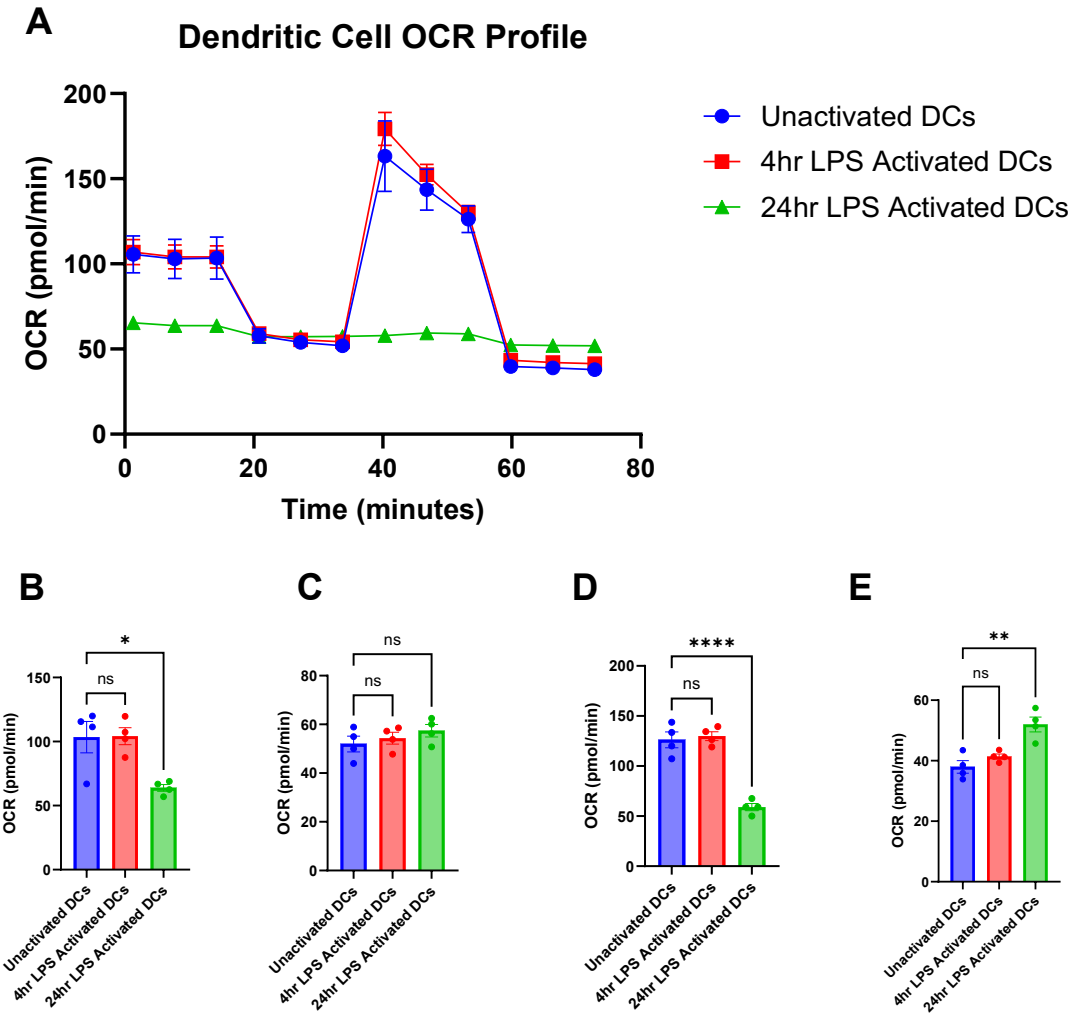

Figure 5. 3: **Metabolic Profiling of DC Subsets using OCR Measurements**

(A) DC OCR Profile. OCR (pmol/min) which was measured to assess mitochondrial respiration in unactivated DCs (blue), DCs activated with 100 ng/mL LPS for 4 hours (red), and DCs activated with LPS for 24 hours (green) (B) basal OCR rate (C) oligomycin induced OCR rate (D) FCCP induced OCR rate (E) Rotenone/Antimycin A induced OCR rate. Data shown is from 4 independent experiments (n=4). One-way ANOVA was used to calculate statistical significance with a P-value of < 0.05 deemed statistically significant. ns indicates $p>0.05$, * $p<0.05$, ** $p<0.01$ **** $p<0.0001$

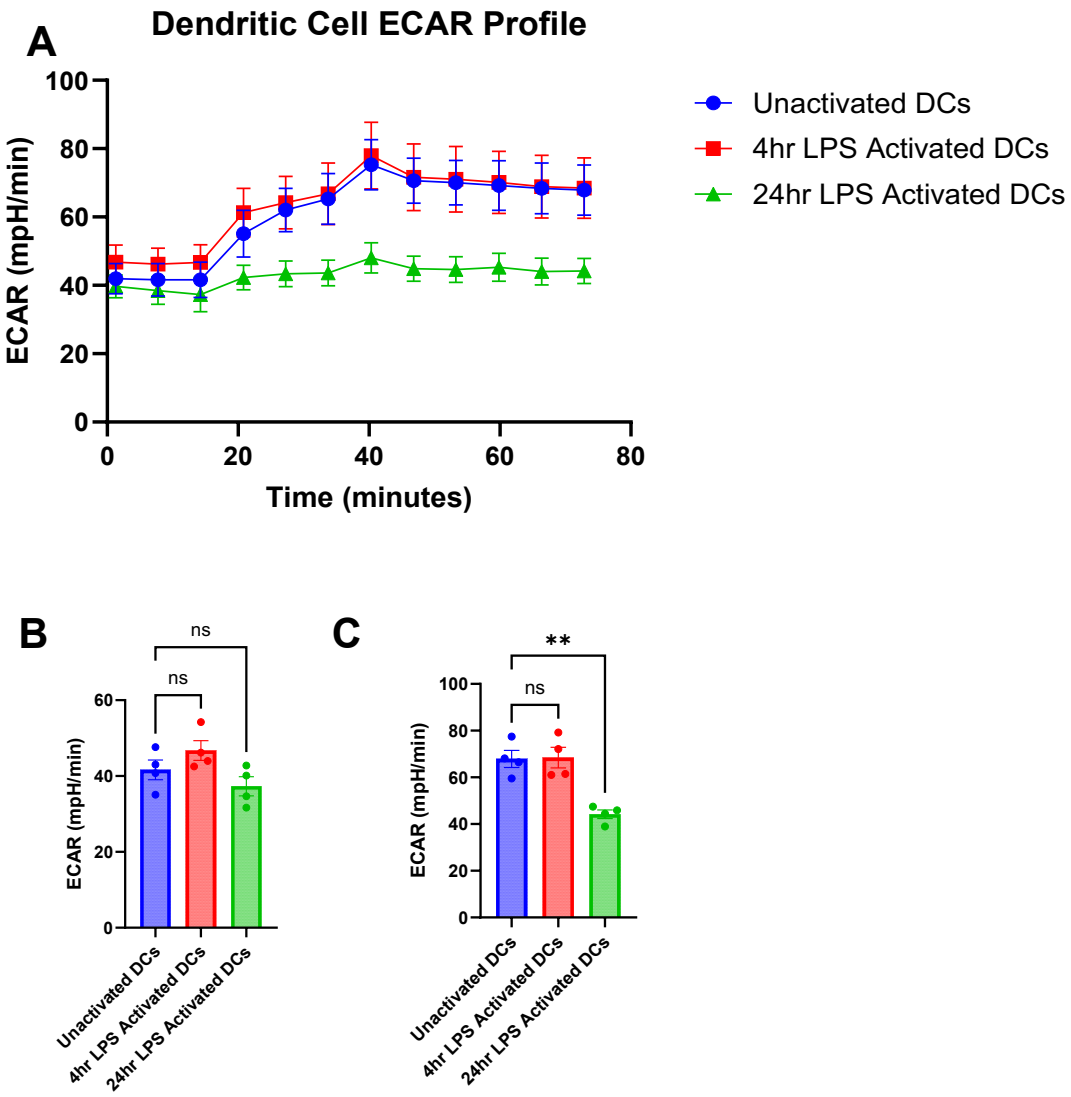

Figure 5. 4: **Metabolic Profiling of DC Subsets using ECAR Measurements**

(A) DC OCR Profile. ECAR (mpH/min) which was measured to assess glycolytic activity in unactivated DCs (blue), DCs activated with 100 ng/mL LPS for 4 hours (red), and DCs activated with LPS for 24 hours (green). (B) basal ECAR rate (C) oligomycin induced ECAR rate Data shown is from at least 3 independent experiments (n=3). Data is presented as the mean ± SEM. One-way ANOVA was used to calculate statistical significance with a P-value of < 0.05 deemed statistically significant. ns indicates $p>0.05$, ** $p<0.01$.

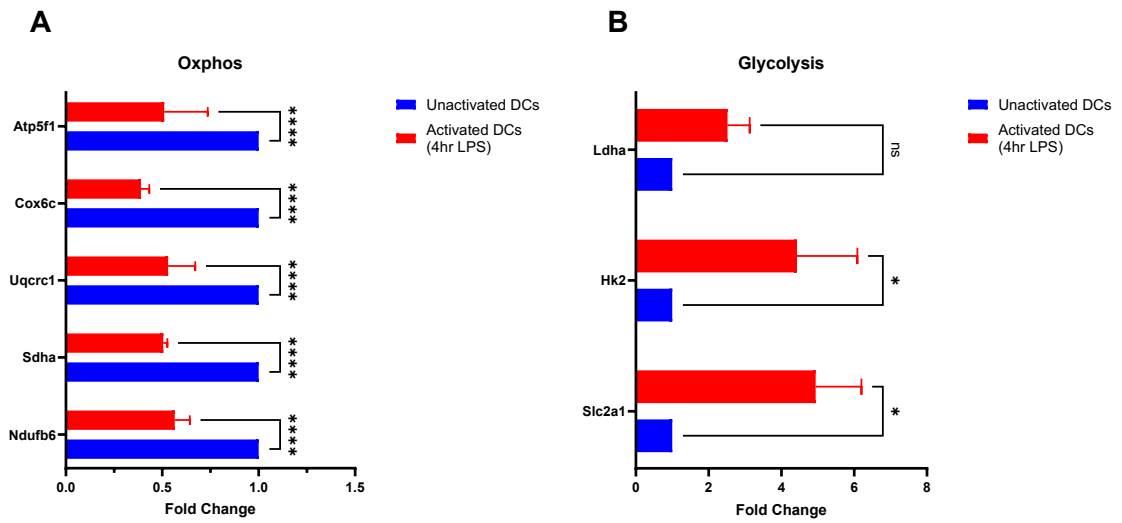

Figure 5. 5: **Gene Expression Analysis of Oxidative Phosphorylation and Glycolysis in DC Subsets**

Quantitative PCR (qPCR) analysis of key metabolic genes involved in oxidative phosphorylation and glycolysis in bone marrow-derived DCs (BMDCs). (A) Expression levels of oxidative phosphorylation-related genes *Ndufb6, Sdha, Uqcrc1, Cox6c, and Atp5f1* in untreated DCs (blue bars) and LPS-stimulated DCs after 4 hours (red bars). (B) Expression levels of glycolytic genes *Slc2a1, Hk2, and Ldha* in untreated (blue bars) and 4 hour LPS treated (red bars) DCs. Data are presented as fold change relative to a control. Data shown is from 4 independent experiments (n=4). Data *is* presented as mean ± SEM. ns indicates $p>0.05$, * $p<0.05$, **** $p<0.0001$

5.5. HMOs Effect on Metabolic Phenotype in DCs

To determine whether HMOs influence resting, untreated DC metabolism, immature BMDCs were treated with 2′-FL, 3′-SL, or 6′-SL and subjected to extracellular flux analysis to assess mitochondrial respiration and glycolytic activity.

Treatment of BMDCs with 2'-FL and 3'-SL showed no change in OCR values. Treatment with 6′-SL however, induced a pronounced suppression of mitochondrial respiration relative to both untreated controls and other HMO-treated groups (**Figure 5.6A**). Quantification of respiratory parameters confirmed this trend: basal OCR, oligomycin inhibited OCR, FCCP stimulated maximal OCR, and rotenone/antimycin A inhibited OCR were all significantly reduced in 6′-SL treated cells compared with untreated, 2′-FL, or 3′-SL treated BMDCs (**Figure 5.6 B-E**). Neither 2′-FL nor 3′-SL significantly altered basal OCR relative to their control, however 3'-SL was shown to slightly increase the FCCP rate.

Parallel assessment of cellular glycolysis revealed a similar suppressive effect upon exposure to 6′-SL. Basal ECAR and oligomycin-induced ECAR were significantly lower in 6′-SL treated BMDCs relative to untreated groups (**Figure 5.7 A-C**). No significant changes were observed in cells treated with 2′-FL or 3′-SL compared with the controls at basal ECAR.

To confirm results observed in seahorse ECAR was as a result of glycolysis, lactate was measured as a byproduct of glycolysis. Lactate release into the culture supernatants in any HMO treated DCs did not show significant differences compared with untreated controls (**Figure 5.8**).

To investigate transcriptional correlates of the metabolic suppression induced by 6′-SL, quantitative PCR was performed on a panel of oxidative phosphorylation related genes (*ndufb6, sdha, uqcrc1, cox6c*, and *atp5f1*). Heat map analysis revealed a broad downregulation of expression of these genes in BMDCs treated with 6′-SL compared with untreated, 2′-FL, or 3′-SL treated cells (**Figure 5.9**). 2′-FL did not elicit any changes across this gene set. 3'-SL however was shown to slightly increase oxidative phosphorylation gene expression. Expression of key glycolytic genes *(slc2a1, hk2*, and *ldha*) was also examined. Consistent with the ECAR and lactate data, no HMO treatment led to alteration in transcript levels of *ldha*. 6'-SL was shown to have a slight decrease in slc2a1 expression whereas 2′-FL and 3′-SL treatments showed minimal deviation from controls (**Figure 5.10**).

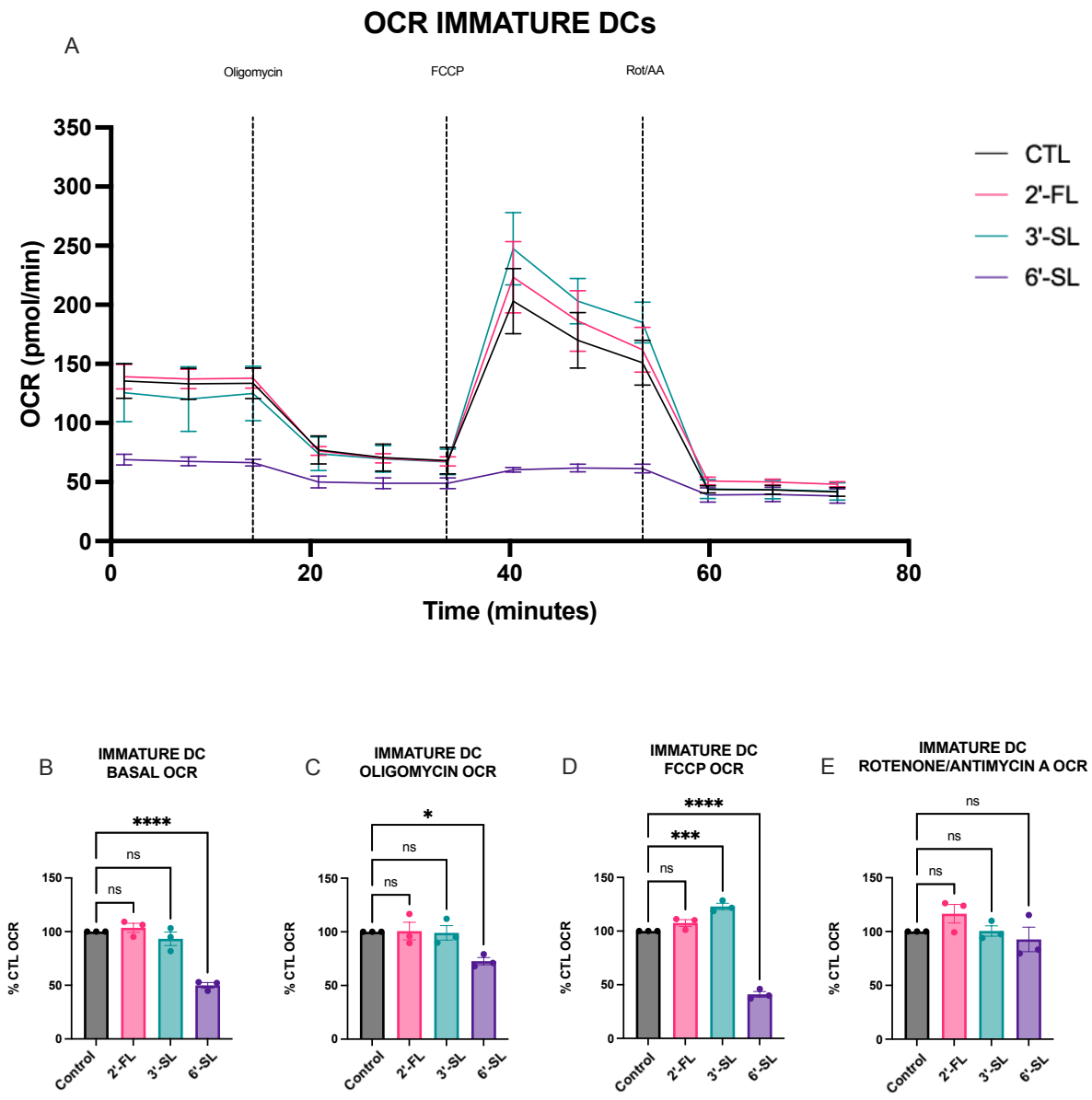

Figure 5. 6: **Mito Stress Test OCR Measurement in Immature DCs Treated with HMOs**

BMDCs were treated with HMOs; 2'-FL (2 mM), 3'-SL (1 mM), or 6'-SL (1 mM) overnight. (A) representative time-course graph of OCR. (B) basal OCR rate (C) oligomycin induced OCR rate (D) FCCP induced OCR rate (E) Rotenone/Antimycin A induced OCR rate. Data shown is from 3 independent experiments (n=3). Data is presented as the mean ± SEM. One-way ANOVA was used to calculate statistical significance with a P-value of < 0.05 deemed statistically significant. ns indicates $p>0.05$, * $p<0.05$, *** $p<0.001$, **** $p<0.0001$

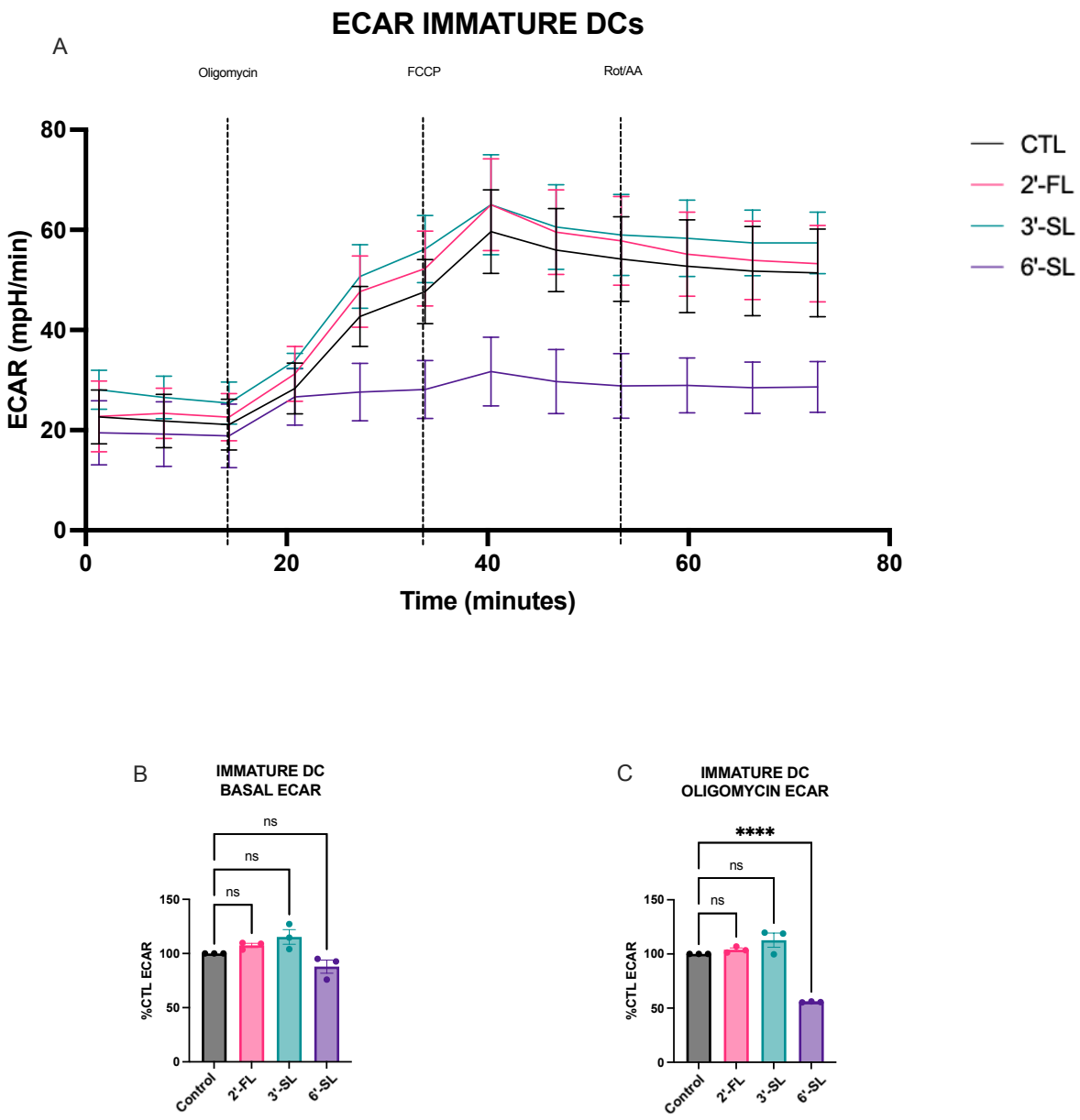

Figure 5. 7: **Mito Stress Test ECAR Measurement in Immature DCs Treated with HMOs**

BMDCs were treated with HMOs; 2'-FL (2 mM), 3'-SL (1 mM), or 6'-SL (1 mM) overnight. (A) representative time-course graph of ECAR. (B) basal ECAR rate (C) oligomycin induced ECAR rate Data shown is from at least 3 independent experiments (n=3). Data is presented as the mean ± SEM. One-way ANOVA was used to calculate statistical significance with a P-value of < 0.05 deemed statistically significant. ns indicates $p>0.05$, **** $p<0.0001$

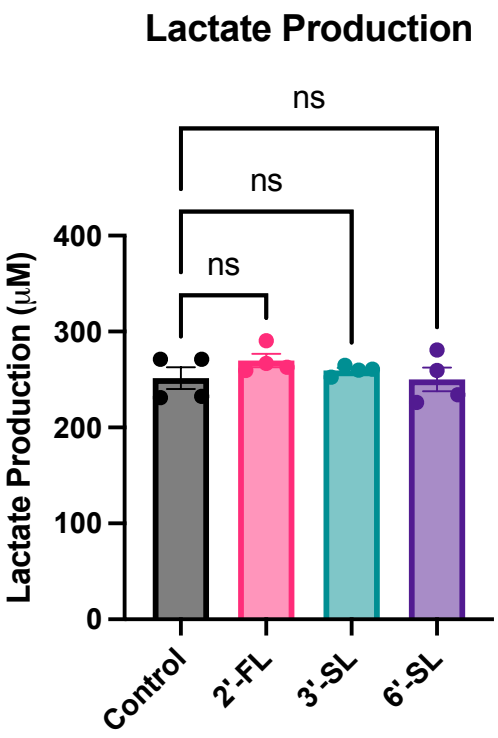

Figure 5. 8: **Extracellular Lactate Production in Immature DCs Following HMO Treatment**

BMDCs were treated with HMOs overnight. Lactate production was measured via lactate quantification assay via luminescence (RLU). Data shown is from 4 independent experiments (n=4). Data is presented as the mean ± SEM. One-way ANOVA was used to calculate statistical significance with a P-value of < 0.05 deemed statistically significant. ns indicates $p>0.05$,

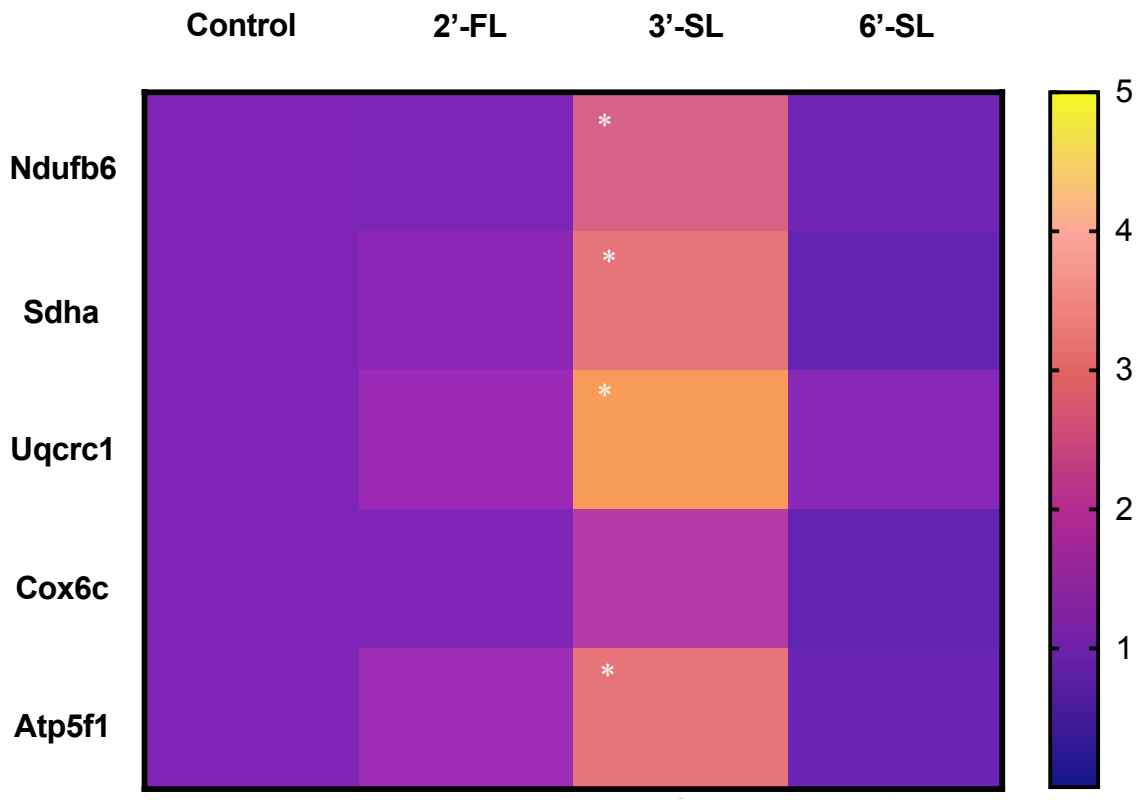

Figure 5. 9: **Expression of Oxidative Phosphorylation Genes in Immature DCs Treated with HMOs**

Quantitative PCR analysis was performed to assess the mRNA expression of key genes involved in oxidative phosphorylation (*ndufb6, sdha, uqcrc1, cox6c*, and *atp5f1*) in BMDCs following treatment with HMOs; 2'-FL (2 mM), 3'-SL (1 mM), or 6'-SL (1 mM). The heat map shows relative expression levels, with each column representing a treatment condition and each row representing a specific gene. Expression values are log2-transformed and normalised to housekeeping genes. Data shown is from 3 independent experiments (n=3). * indicates $p<0.05$

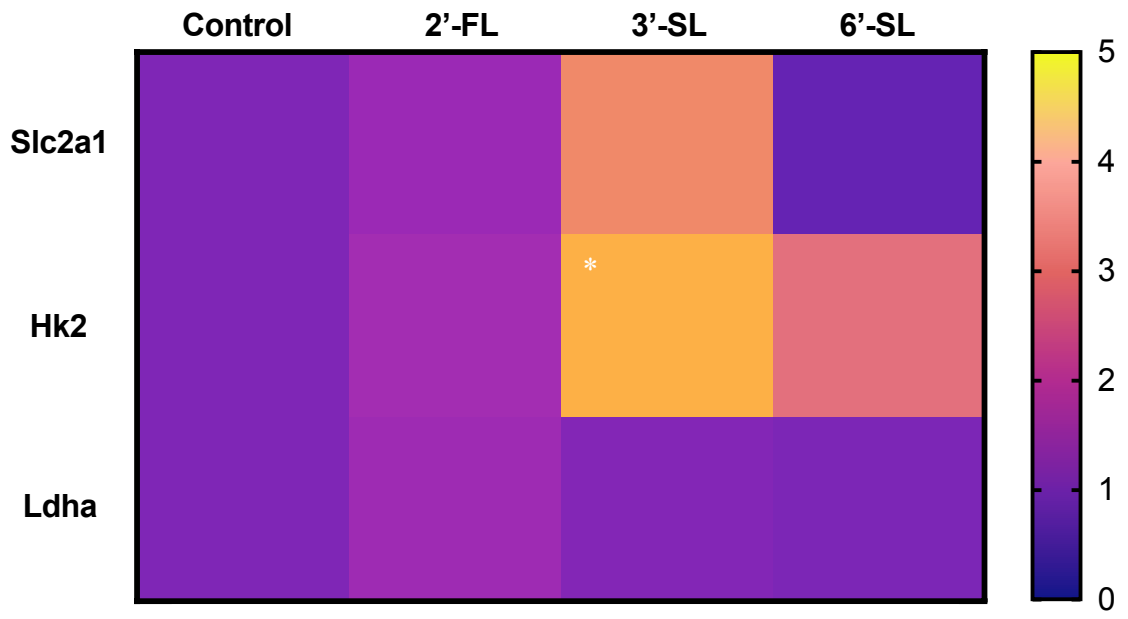

Figure 5. 10*:* **Expression of Glycolysis Genes in immature DCs Treated with HMOs**

BMDCs were treated with HMOs; 2'-FL (2 mM), 3'-SL (1 mM), or 6'-SL (1 mM) and the expression of key glycolytic genes (*slc2a1, hk2, ldha*) was analysed by quantitative PCR. The heat map presents normalised, log2-transformed expression values, with each row representing an individual gene and each column corresponding to a specific HMOs; 2'-FL (2 mM), 3'-SL (1 mM), or 6'-SL (1 mM). Data shown is from 3 independent experiments (n=3). * indicates $p<0.05$

5.6. HMOs Effect on Metabolic Phenotype in LPS Activated DCs

To determine whether the effects of HMOs on DC metabolism were altered following activation with LPS, BMDCs were treated with 2′-FL, 3′-SL, or 6′-SL in combination with LPS stimulation for 4 hours and subjected to extracellular flux analysis, lactate quantification, and transcriptional profiling of metabolic genes.

In LPS-activated BMDCs, 6′-SL significantly decreased mitochondrial respiration relative to untreated, 3'-SL and 2′-FL treated controls. Suppression was evident across multiple respiratory parameters, including basal OCR, oligomycin inhibited OCR, FCCP-stimulated OCR, and rotenone/antimycin A inhibited OCR (**Figure 5.11 A-E**). Neither 2′-FL nor 3′-SL induced consistent changes in OCR compared with LPS alone.

Unlike immature BMDCs, basal ECAR in activated BMDCs was significantly altered by 6'-SL and also selectively prevented the oligomycin induced rise in ECAR that was evident in the control, 2′-FL, and 3′-SL treated cells (**Figure 5.12 A-C**). These findings suggest that 6′-SL restricts the capacity of activated BMDCs to enhance glycolytic flux in response to mitochondrial inhibition.

Consistent with the ECAR data, lactate secretion was significantly reduced in BMDCs treated with 6′-SL in the presence of LPS stimulation compared with controls. 3'-SL also was shown to decrease lactate production although not having displayed a difference in ECAR. By contrast, 2′-FL treatment did not alter lactate levels (**Figure 5.13**).

To determine whether transcriptional reprogramming paralleled metabolic phenotypes, qPCR analysis was performed on oxidative phosphorylation related genes. Heat map visualisation revealed that 6′-SL markedly downregulated the expression of *ndufb6, sdha, uqcrc1, cox6c,* and *atp5f1* compared with controls and other HMO treatments, which had minimal effect (**Figure 5.14**). Transcriptional analysis of *slc2a1, hk2,* and *ldha* demonstrated significant reductions in gene expression following 6′-SL treatment, with 2'-FL and 3′-SL resulting in partial upregulation of *ldha* (**Figure 5.15**).

Both immature and activated BMDCs treated with HMOs were evaluated for spare respiratory capacity. 6′-SL significantly reduced spare respiratory capacity in both states compared with the untreated controls. 3′-SL was shown to increase spare respiratory capacity in both immature and activated DCs (although not significant in activated DCs), while 2′-FL showed no significant effect on spare respiratory capacity (**Figure 5.16**). Assessment of glycolytic reserve revealed a parallel trend. In both immature and activated

BMDCs, 6′-SL significantly suppressed glycolytic reserve, while 3′-SL induced moderate non-significant reduction in activated cells. Again, 2′-FL treatment did not significantly alter glycolytic reserve compared with controls (**Figure 5.17**).

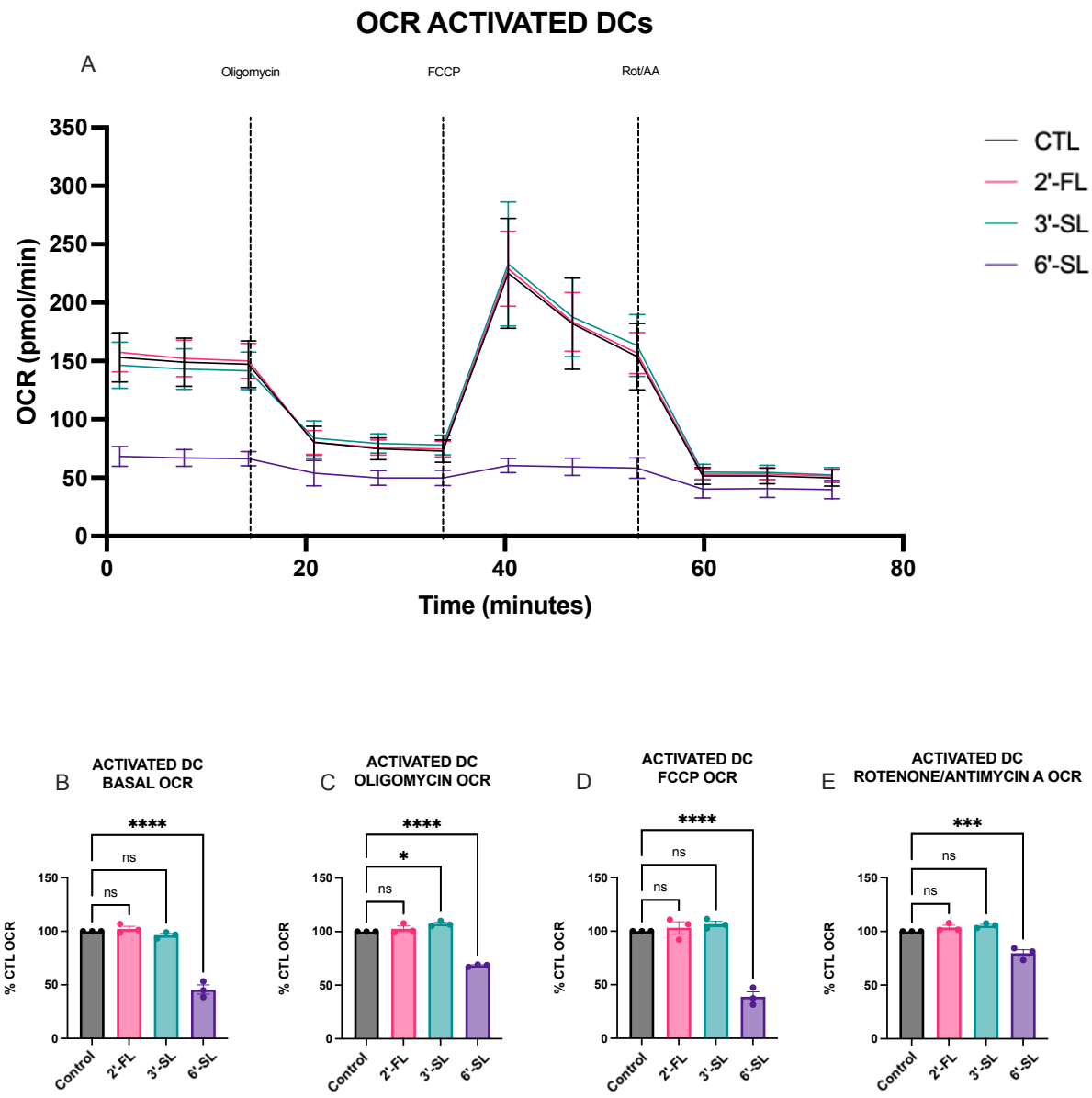

Figure 5. 11: **Mito Stress Test OCR Measurement in Activated DCs Treated with HMOs**

BMDCs were treated with HMOs; 2'-FL (2 mM), 3'-SL (1 mM), or 6'-SL (1 mM) + LPS (100 ng/mL) for 4 hours. (A) representative time-course graph of OCR. (B) basal OCR rate (C) oligomycin induced OCR rate (D) FCCP induced OCR rate (E) Rotenone/Antimycin A induced OCR rate. Data shown is from 3 independent experiments (n=3). Data is presented as the mean ± SEM. One-way ANOVA was used to calculate statistical significance with a P-value of < 0.05 deemed statistically significant. ns indicates $p>0.05$, * $p<0.05$, *** $p<0.001$, **** $p<0.0001$

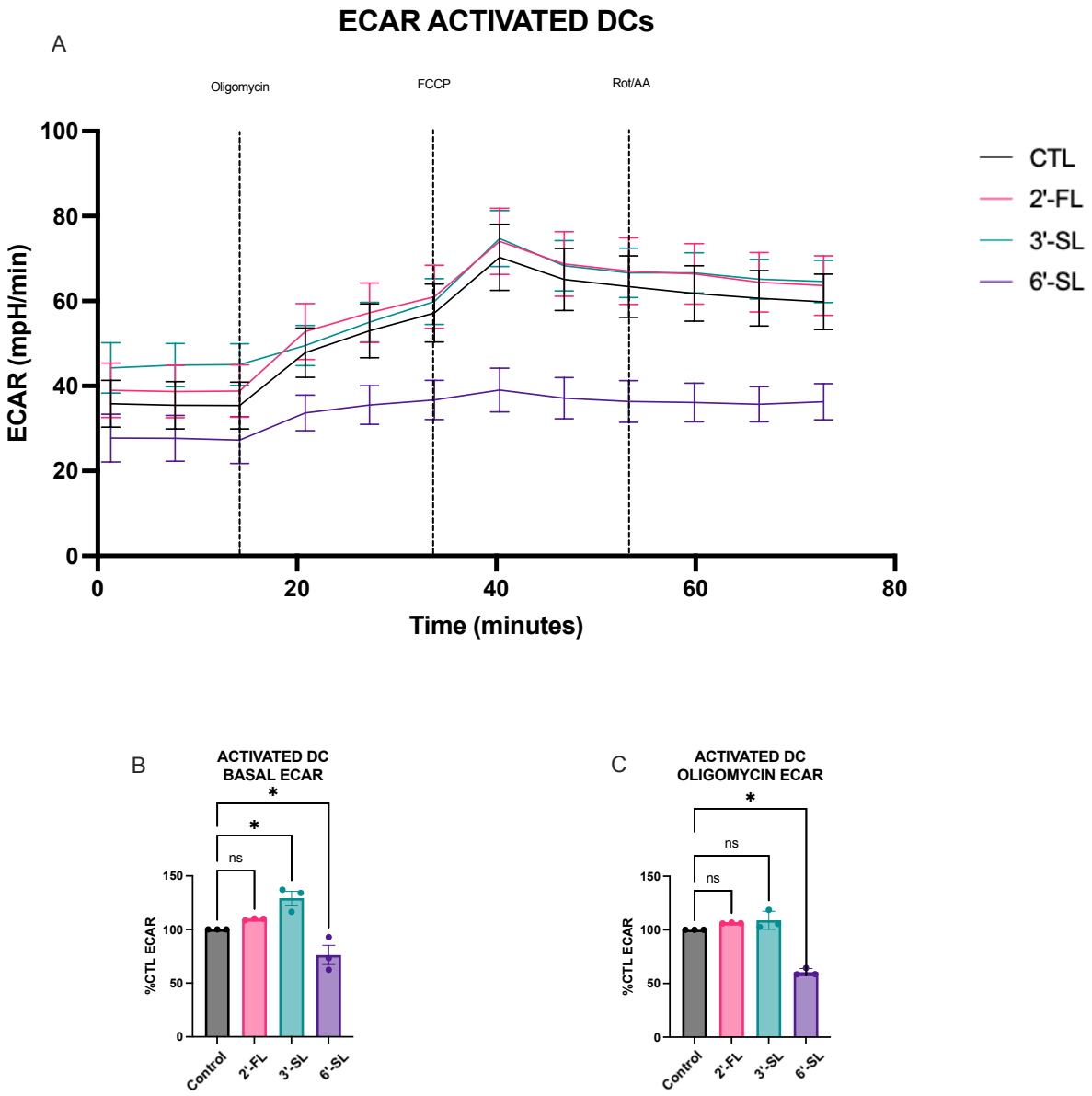

Figure 5. 12: **Mito Stress Test ECAR Measurement in Activated DCs Treated with HMOs**

BMDCs were treated with HMOs; 2'-FL (2 mM), 3'-SL (1 mM), or 6'-SL (1 mM) + LPS (100 ng/mL) for 4 hours. (A) representative time-course graph of ECAR. (B) basal ECAR rate (C) oligomycin induced ECAR. Data shown is from 3 independent experiments (n=3). Data is presented as the mean ± SEM. One-way ANOVA was used to calculate statistical significance with a P-value of < 0.05 deemed statistically significant. ns indicates p>0.05, * p<0.05

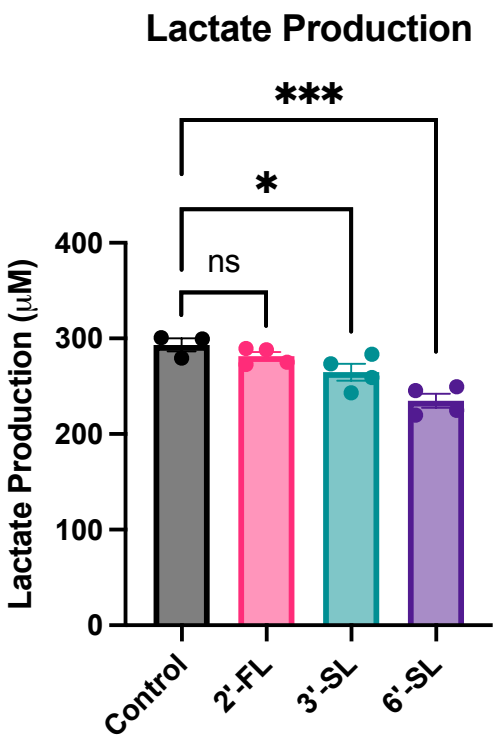

Figure 5. 13: **Extracellular Lactate Production in Activated DCs Following HMO Treatment**

BMDCs were treated with HMOs overnight and then treated with LPS for 4 hours. Lactate production was measured via lactate quantification assay via luminescence (RLU). Data shown is from 4 independent experiments (n=4). Data is presented as the mean ± SEM. One-way ANOVA was used to calculate statistical significance with a P-value of < 0.05 deemed statistically significant. ns indicates $p>0.05$, * $p<0.05$, *** $p<0.001$

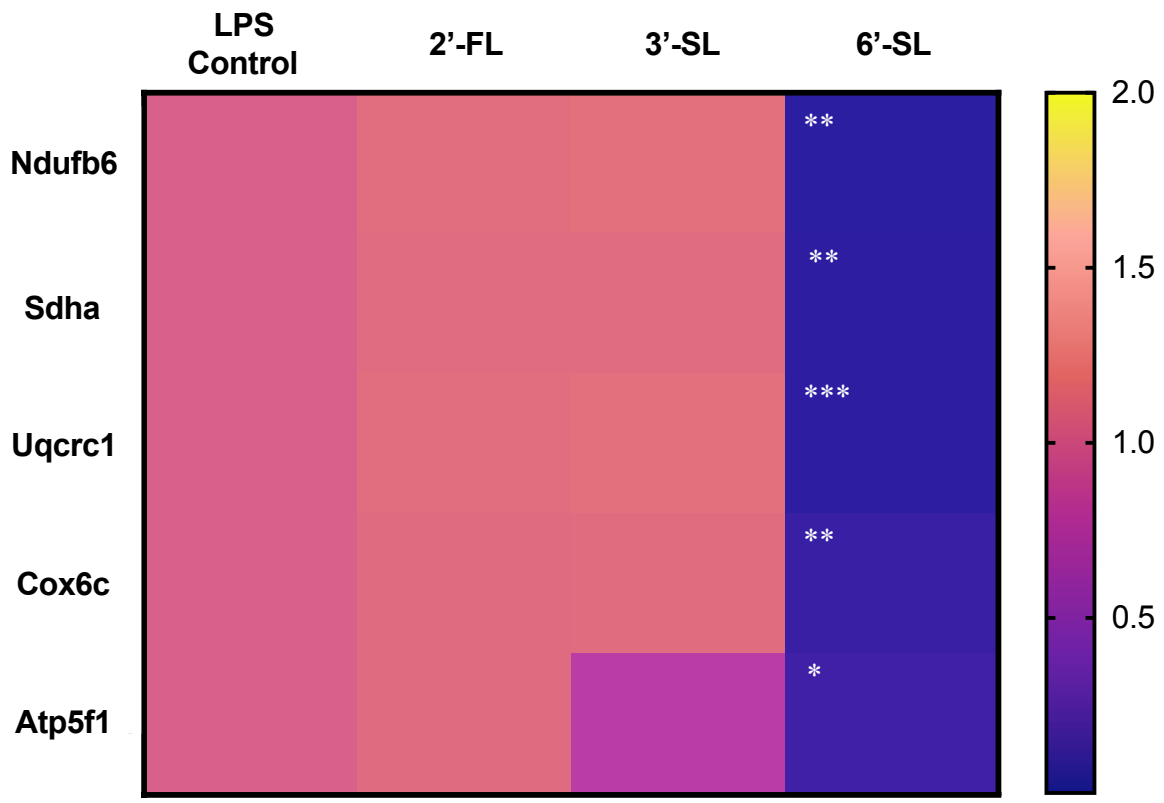

Figure 5. 14: **Expression of Oxidative Phosphorylation Genes in Activated DCs Treated with HMOs**

Quantitative PCR analysis was performed to assess the mRNA expression of key genes involved in oxidative phosphorylation (*ndufb6, sdha, uqcrc1, cox6c*, and *atp5f1*) in BMDCs following treatment with HMOs; 2'-FL (2 mM), 3'-SL (1 mM), or 6'-SL (1 mM) + 100 ng/mL LPS for 4 hours. The heat map shows relative expression levels, with each column representing a treatment condition and each row representing a specific gene. Expression values are log2-transformed and normalised to housekeeping genes. Data shown is from 3 independent experiments (n=3). * indicates $p<0.05$, ** $p<0.01$, *** $p<0.001$

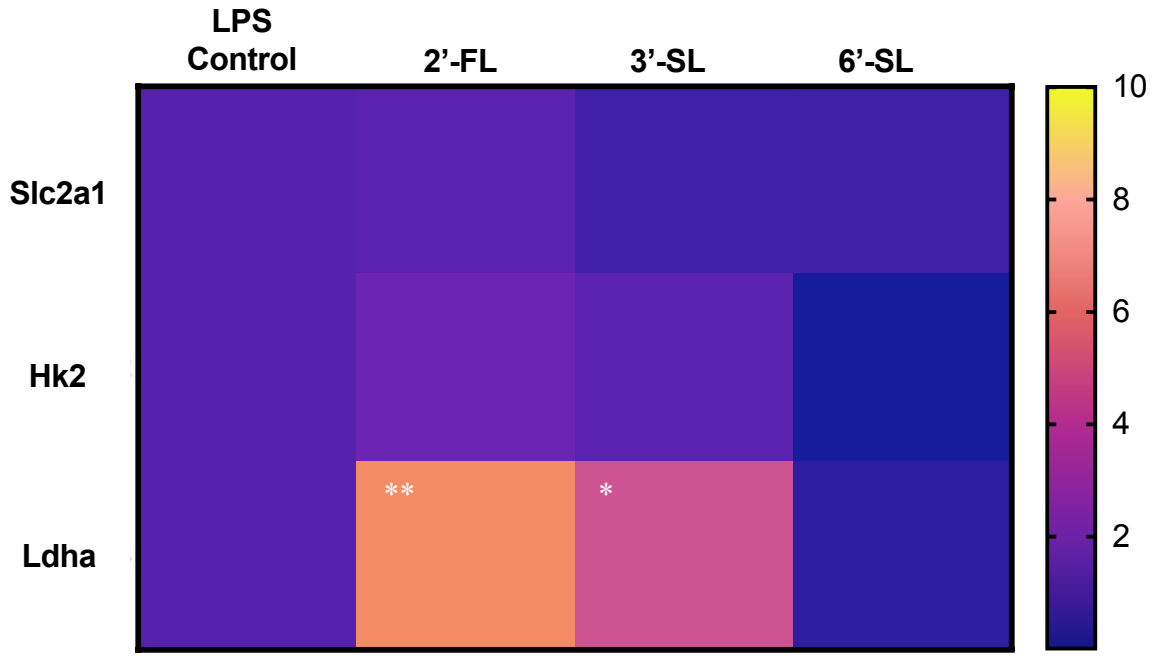

Figure 5. 15: **Expression of Glycolysis Genes in Activated DCs Treated with HMOs**

BMDCs were treated with HMOs; 2'-FL (2 mM), 3'-SL (1 mM), or 6'-SL (1 mM) + 100 ng/mL LPS for 4 hours and the expression of key glycolytic genes (*slc2a1, hk2, ldha*) was analysed by quantitative PCR. The heat map presents normalised, log2-transformed expression values, with each row representing an individual gene and each column corresponding to a specific HMOs; 2'-FL (2 mM), 3'-SL (1 mM), or 6'-SL (1 mM). Data shown is from 3 independent experiments (n=3). * indicates $p<0.05$, ** $p<0.01$

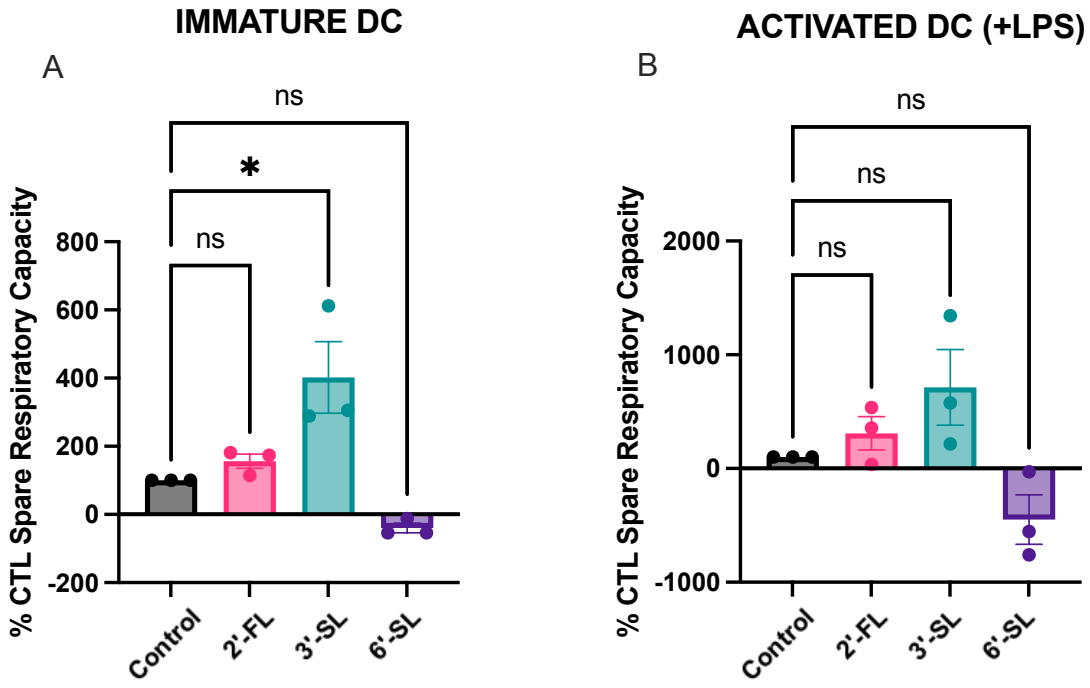

Figure 5. 16: **Spare Respiratory Capacity in Immature and Activated DCs Following HMO Treatment**

BMDCs were polarised into immature (naïve) or activated (stimulated with 100 ng/mL LPS) states and treated with control, 2'-FL, 3'-SL, or 6'-SL. Spare Respiratory Capacity was measured and normalised to control values (expressed as % CTL). Data are shown as mean ± SEM (n=3 per group). One-way ANOVA was used to calculate statistical significance with a P-value of < 0.05 deemed statistically significant. ns indicates $p>0.05$, * $p<0.05$.

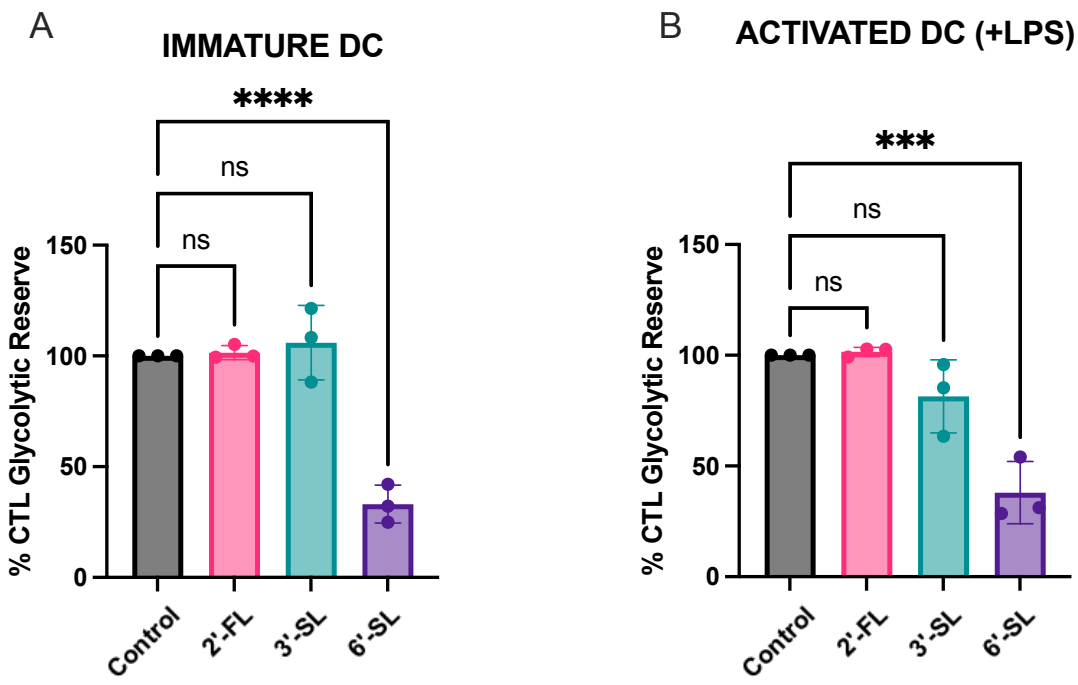

Figure 5. 17: **Glycolytic Reserve in Immature and Activated DCs Following HMO Treatment**

BMDCs were polarised into immature (naïve) or activated (stimulated with 100 ng/mL LPS) states and treated with control, 2'-FL, 3'-SL, or 6'-SL. Glycolytic reserve was measured and normalised to control values (expressed as % CTL). Data are shown as mean ± SEM (n=3 per group). One-way ANOVA was used to calculate statistical significance with a P-value of < 0.05 deemed statistically significant. ns indicates $p>0.05$, *** $p<0.001$, **** $p<0.0001$

5.7. HMOs Temporal Effect on DCs

To assess whether the metabolic effects of HMOs on DCs were sustained over time, OCR and ECAR were measured in immature and LPS-activated BMDCs treated with 2′-FL, 3′-SL, or 6′-SL for up to 6 hours.

In relation to immature BMDCs, 6′-SL treatment led to a persistent reduction in mitochondrial respiration across the 6 hour time course (**Figure 5.18 A**). Quantification revealed significantly lower basal OCR, with suppression maintained through to 6 hours (**Figure 5.18 B-C**). By contrast, 2′-FL and 3′-SL did not significantly alter OCR relative to the untreated controls. Parallel analysis of glycolysis revealed that BMDCs treated with HMOs did not display any variation from control and maintained this metabolic phenotype through to 6 hours (**Figure 5.19 A-C**).

When BMDCs were stimulated with LPS, the suppressive effect of 6′-SL on mitochondrial respiration was evident at early time points but was no longer significant at 6 hours (**Figure 5.20 A-C**). OCR values in 6′-SL treated, LPS-activated DCs converged with those of the untreated controls over the course of the experiment. In contrast to OCR, glycolytic activity in LPS-activated BMDCs was sensitive to 6′-SL treatment. ECAR for all treatments were similar to that of control, prior to injection of LPS. Upon LPS addition, control, 2'-FL and 3'-SL treated cells observed in increase in glycolysis, however 6'-SL stunted this LPS induced glycolytic increase. ECAR remained significantly decreased in 6′-SL treated cells compared with controls after 6 hours of LPS stimulation (**Figure 5.21 A-C**). This effect was not observed with 2′-FL or 3′-SL.

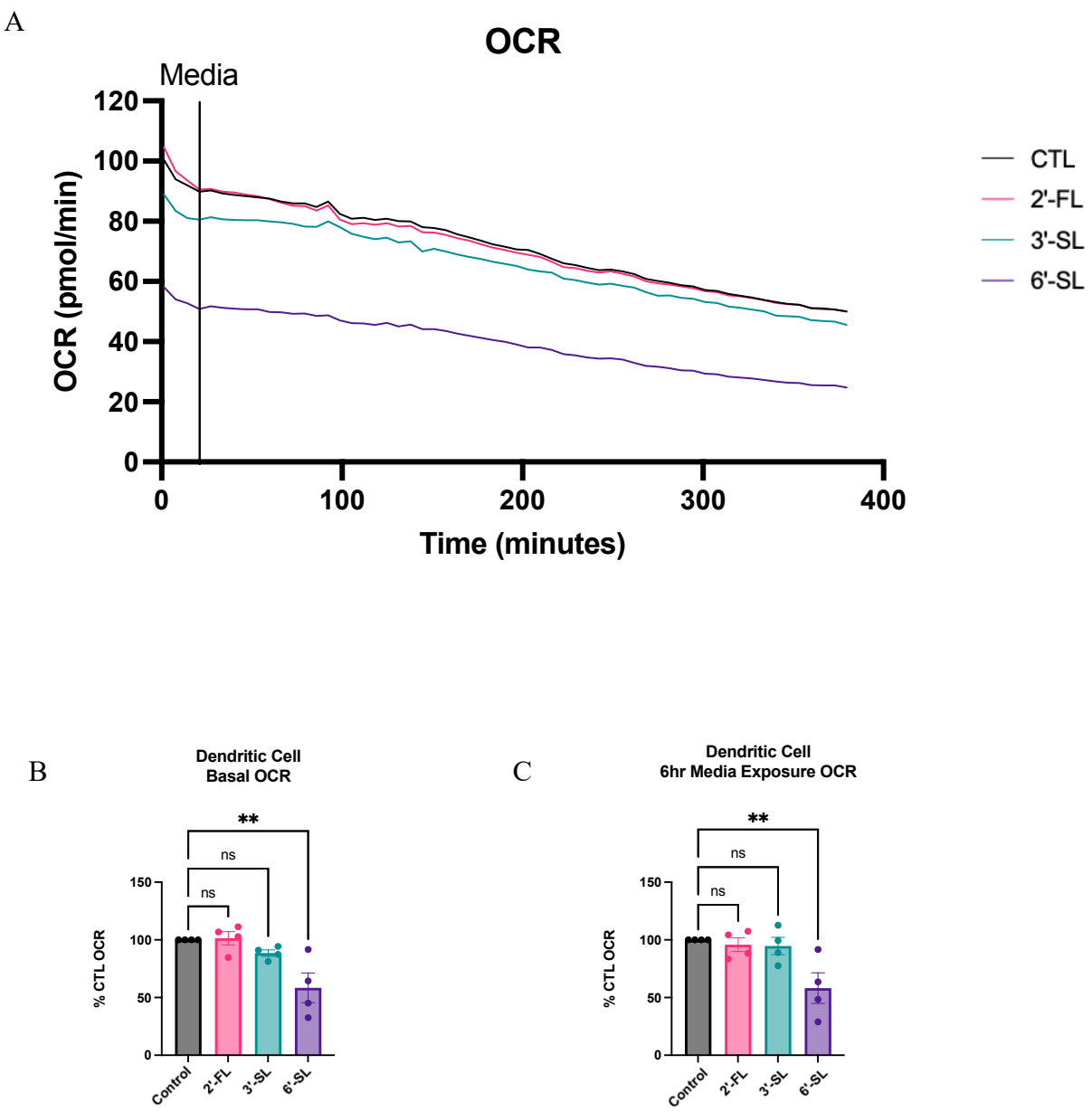

Figure 5. 18: **Time-Course of OCR in Immature DCs Over 6 Hours Following HMO Pre-Treatment**

BMDCs were treated with HMOs (2 mM 2'-FL and 1 mM 3'-SL and 6'-SL) overnight. OCR was measured using a SeahorseXFe96 analyser over 6 hours. (A) representative time-course graphs for OCR. (B) basal OCR (C) OCR after 6 hour from 4 independent experiments (n=4). Data is presented as the mean ± SEM. One-way ANOVA was used to calculate statistical significance with a P-value of < 0.05 deemed statistically significant. ns indicates $p>0.05$, ** $p<0.01$.

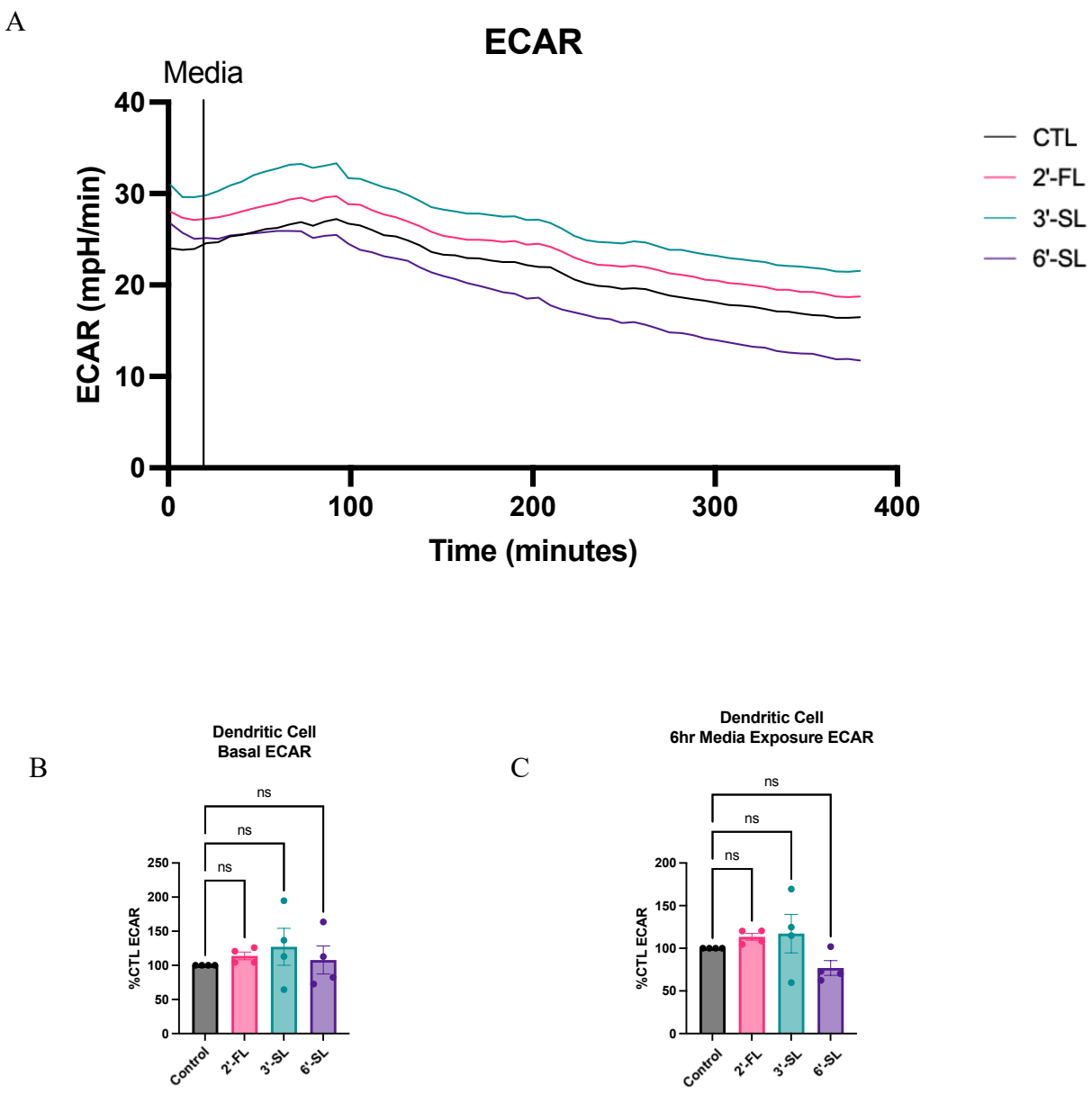

Figure 5. 19: **Time-Course of ECAR in Immature DCs Over 6 Hours Following HMO Pre-Treatment**

BMDCs were treated with HMOs (2 mM 2'-FL and 1 mM 3'-SL and 6'-SL) overnight. ECAR was measured using a SeahorseXFe96 analyser over 6 hours. (A) representative time-course graphs for ECAR. (B) basal ECAR (C) ECAR after 6 hour from 4 independent experiments (n=4). Data is presented as the mean ± SEM. One-way ANOVA was used to calculate statistical significance with a P-value of < 0.05 deemed statistically significant. ns indicates $p>0.05$.

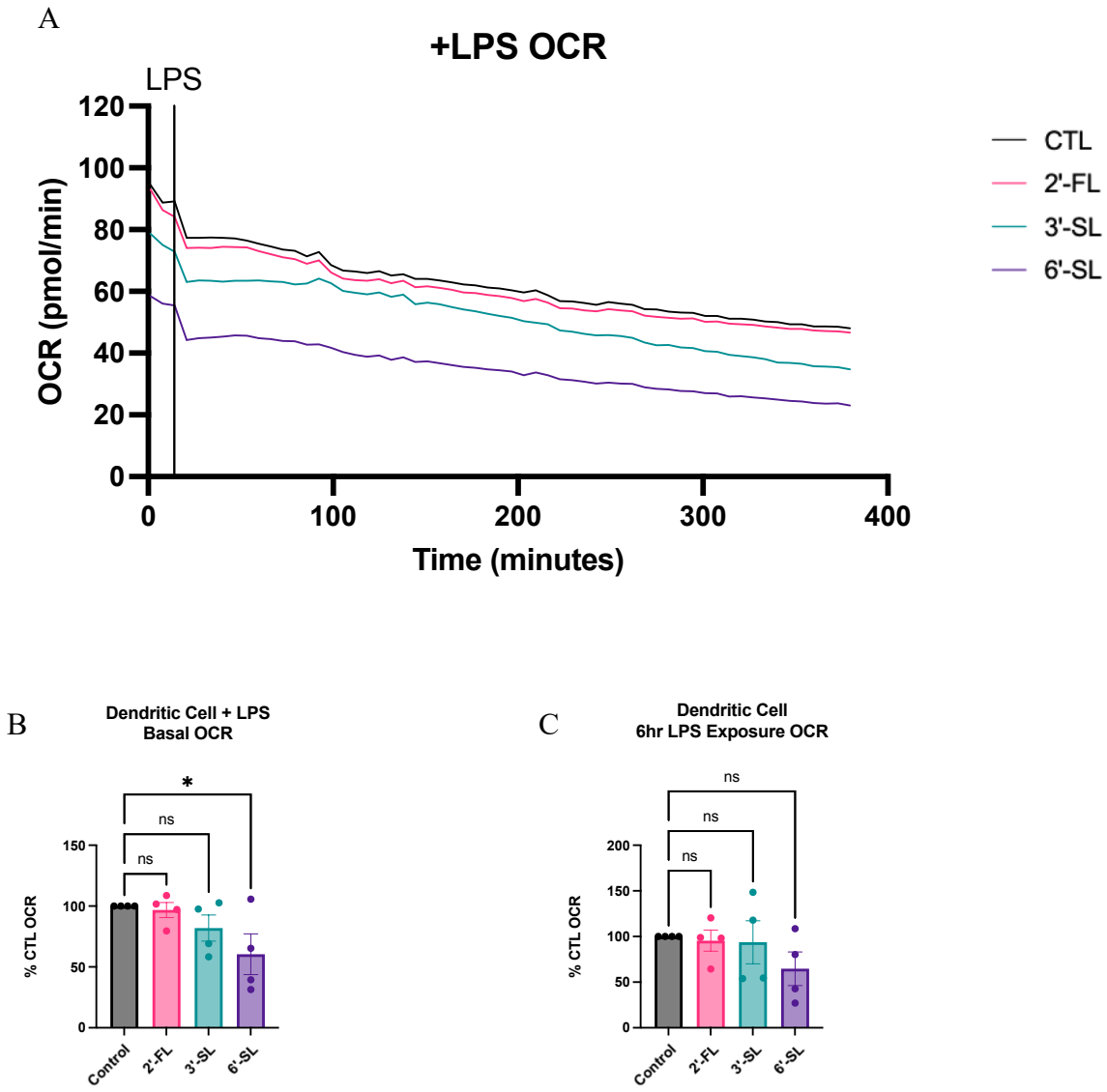

Figure 5. 20: **Time-Course of OCR in DCs Over 6 Hours After 6 hour LPS Stimulation Following Overnight HMO Pre-Treatment**

BMDCs were treated with HMOs (2 mM 2'-FL and 1 mM 3'-SL and 6'-SL) overnight. OCR was measured using a SeahorseXFe96 analyser in the presence of LPS over 6 hours. (A) representative time-course graphs for OCR. (B) basal OCR (C) OCR after 6 hour LPS treatment from 4 independent experiments (n=4). Data is presented as the mean ± SEM. One-way ANOVA was used to calculate statistical significance with a P-value of < 0.05 deemed statistically significant. ns indicates $p>0.05$, * $p<0.05$.

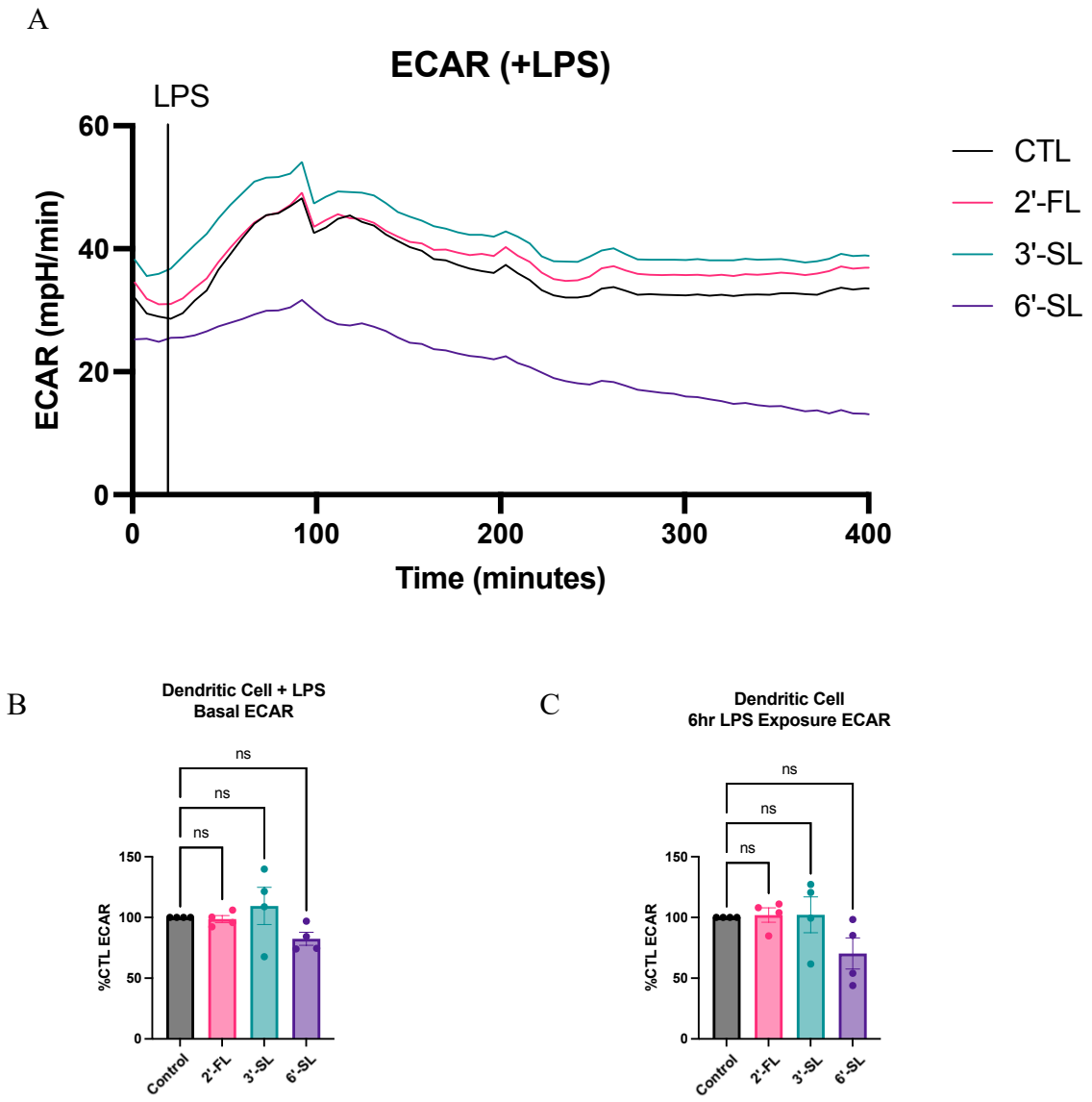

Figure 5. 21: **Time-Course of ECAR in DCs Over 6 Hours After 6 hour LPS Stimulation Following Overnight HMO Pre-Treatment**

BMDCs were treated with HMOs (2 mM 2'-FL and 1 mM 3'-SL and 6'-SL) overnight. ECAR was measured using a SeahorseXFe96 analyser in the presence of LPS over 6 hours. (A) representative time-course graphs for ECAR. (B) basal ECAR (C) ECAR after 6 hour LPS treatment from 4 independent experiments (n=4). Data is presented as the mean ± SEM. One-way ANOVA was used to calculate statistical significance with a P-value of < 0.05 deemed statistically significant. ns indicates p>0.05.

5.8. Metabolic Profiling of Effector and Memory T-Cells

To evaluate the metabolic activity of effector (cultured in IL-2) and memory T-cells (cultured in IL-15), ECAR and OCR **(Figure 5.22 and Figure 5.23)** were measured as indicators of mitochondrial respiration and glycolytic activity, respectively. Effector T-cells exhibit significantly higher basal OCR and spare respiratory capacity compared to memory T-cells, which demonstrate markedly lower basal OCR. Similarly, effector T-cells displayed elevated basal ECAR and glycolytic reserve relative to their memory T-cell counterparts. Effector T-cells displayed elevated OCR, consistent with increased mitochondrial activity required to support rapid proliferation and effector functions. In contrast, memory T-cells exhibited consistently lower basal OCR compared with effector populations indicative of their inactive state, not requiring energy like its effector counterpart (**Figure 5.22).** Effector T-cells displayed markedly higher ECAR when compared to memory T-cells consistent with a metabolic program skewed toward aerobic glycolysis (Warburg-like metabolism) to meet the bioenergetic and biosynthetic demands of effector differentiation Memory T-cells, by comparison, maintained relatively low ECAR values, suggesting reduced dependence on glycolysis (**Figure 5.23**).

To investigate the metabolic differences between effector and memory T-cells, we performed quantitative PCR analysis on IL-2 treated (effector) and IL-15 treated (memory). The expression of genes involved in oxidative phosphorylation and glycolysis was compared between the two T-cell phenotypes. As shown in **Figure 5.24 A**, stimulation of murine splenic T-cells with anti-CD3 in the presence of IL-15 induced a transcriptional profile consistent with a memory-like metabolic state, characterised by increased *slc2a1*, decreased *hk*2 and *ldha,* downregulation of complex I, IV, and ATP synthase subunits (*ndufb6, cox6c, atp5f1*), but upregulation of complex II/III subunits (*sdha, uqcrc1*). (**Figure 5.24 B**)

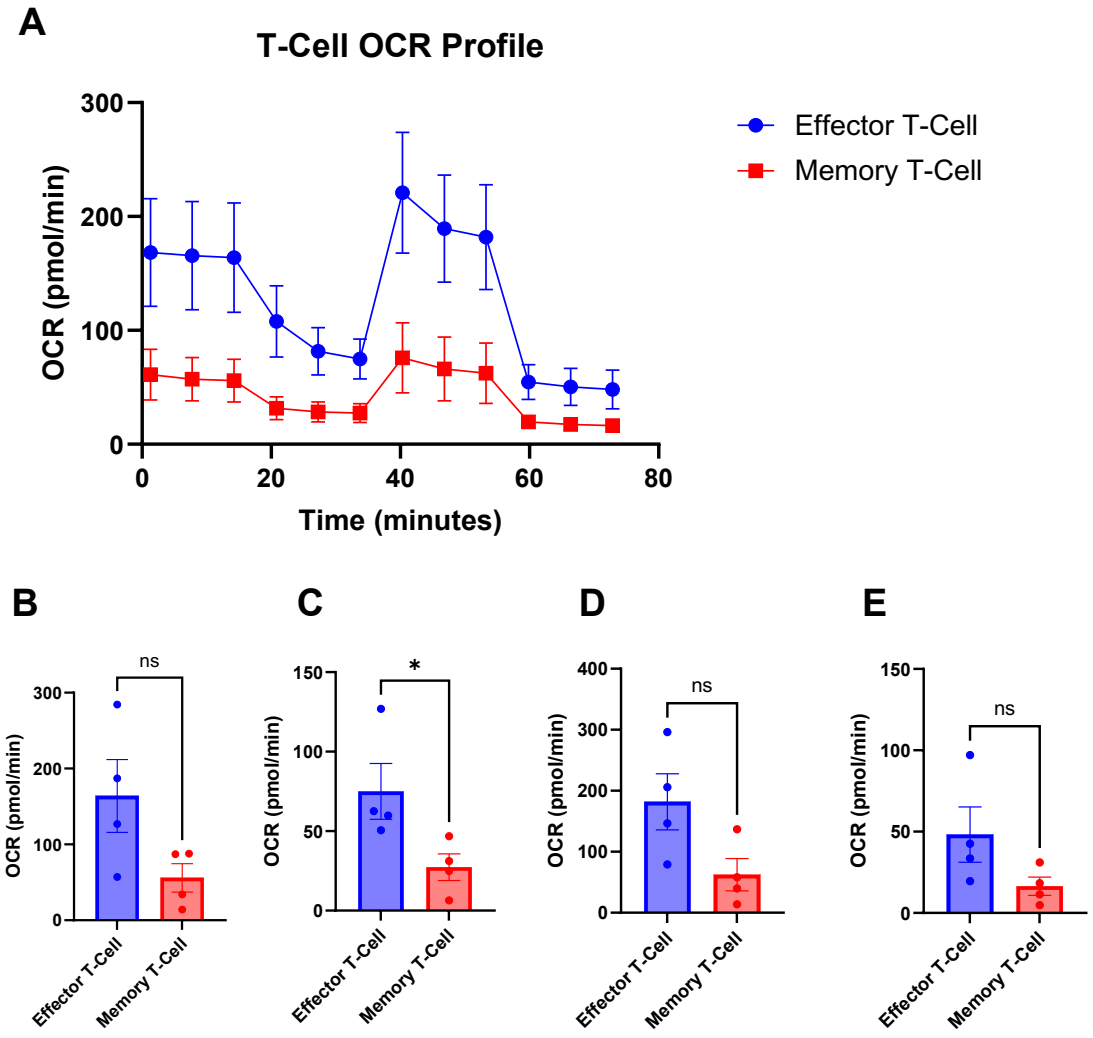

Figure 5. 22: **Metabolic Profiling of Effector and Memory T-cells Using OCR and ECAR Measurements**

(A)T-Cell OCR Profile. OCR (pmol/min) was measured to assess mitochondrial respiration in effector T-cells (blue) and memory T-cells (red) at multiple time points. (B) basal OCR rate (C) oligomycin induced OCR rate (D) FCCP induced OCR rate (E) Rotenone/Antimycin A induced OCR rate. Data shown is from 4 independent experiments (n=4). Data is presented as the mean ± SEM. One-way ANOVA was used to calculate statistical significance with a P-value of < 0.05 deemed statistically significant. ns indicates $p>0.05$, * $p<0.05$.

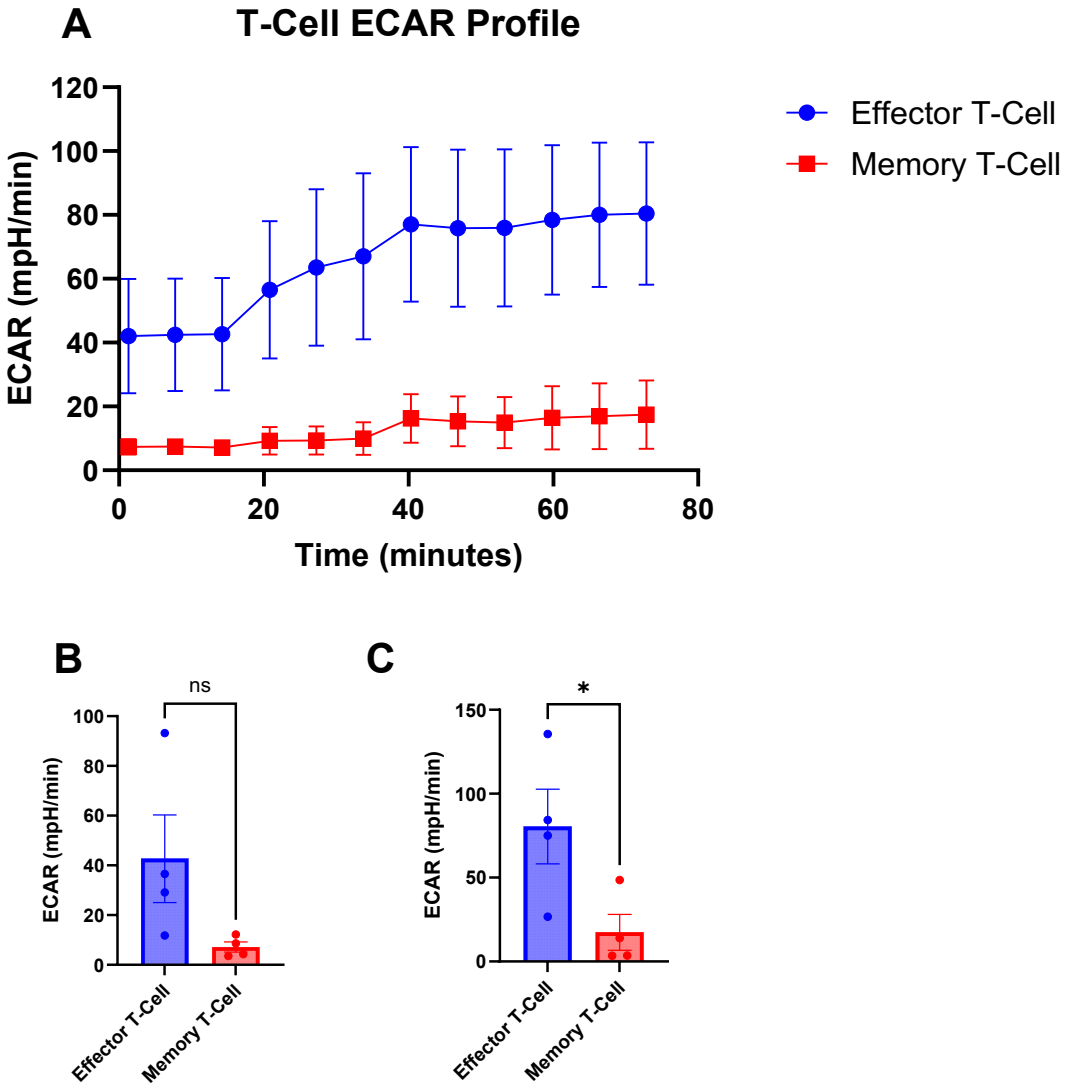

Figure 5. 23: **Metabolic Profiling of Effector and Memory T-cells Using OCR and ECAR Measurements**

(A) T-Cell ECAR Profile. ECAR (mpH/min) was measured to evaluate glycolytic activity in effector T-cell (blue) and memory T-cell (red) populations. (B) basal ECAR rate (C) oligomycin induced ECAR rate. Data shown is from 4 independent experiments (n=4). Data is presented as the mean ± SEM. One-way ANOVA was used to calculate statistical significance with a P-value of < 0.05 deemed statistically significant. ns indicates $p>0.05$, * $p<0.05$.

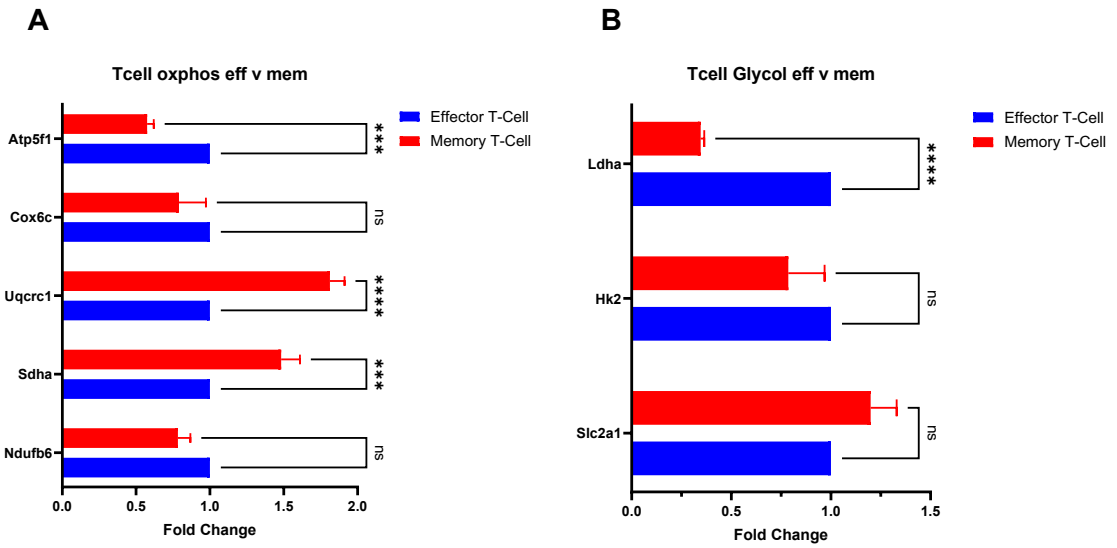

Figure 5. 24: **Gene Expression Analysis of Oxidative Phosphorylation and Glycolysis in T-Cell Subsets**

Quantitative PCR (qPCR) analysis of key metabolic genes involved in oxidative phosphorylation and glycolysis in effector and memory T-cells. (A) Expression levels of oxidative phosphorylation-related genes *ndufb6, sdha, uqcrc1, cox6c,* and *atp5f1* in effector T-cells (blue bars) and memory T-cells (red bars). (B) Expression levels of glycolytic genes *slc2a1, hk2,* and *ldha* in effector T-cells (blue bars) and memory T-cells (red bars). Data are presented as fold change relative to a control. Data shown is from 4 independent experiments (n=4). Data *is* presented as mean ± SEM. ns indicates $p>0.05$, *** $p<0.001$ ****<0.0001

5.9. HMOs Effect on Effector T-Cell Metabolism

To determine whether HMOs alter metabolic programming in effector T-cells, OCR and ECAR were assessed alongside lactate production and gene expression of metabolic regulators.

No significant changes were observed in basal OCR in effector T-cells, oligomycin induced OCR (reflecting ATP-linked respiration), FCCP induced OCR (maximal respiration), or rotenone/antimycin-A inhibited OCR (non-mitochondrial respiration) following treatment with any of the three HMOs (**Figure 5.25**). Similarly, ECAR remained unaffected in these cells across basal and oligomycin stimulated conditions (**Figure 5.26**). Despite the absence of changes in OCR or ECAR, lactate assays revealed increased lactate release in HMO-treated effector T-cells (**Figure 5.27**).

Gene expression analysis of the panel of oxidative phosphorylation and glycolysis-associated genes supported these findings, indicating no major transcriptional changes upon HMO exposure (**Figures 5.28 and 5.29**).

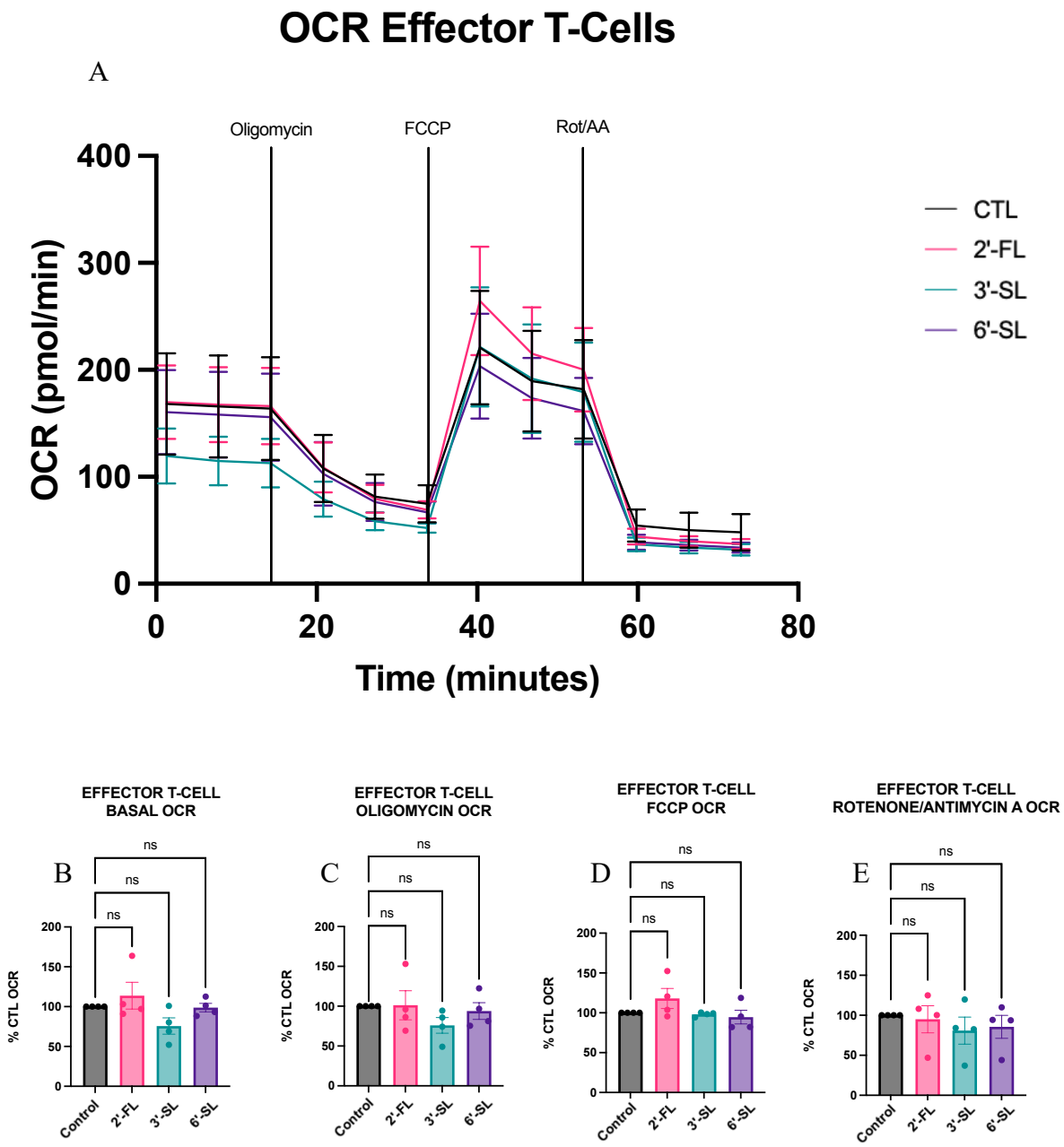

Figure 5. 25: **Mito Stress Test OCR Measurement in Effector T-Cells Treated with HMOs**

Effector T-Cells were treated with HMOs; 2'-FL (2 mM), 3'-SL (1 mM), or 6'-SL (1 mM). (A) representative time-course graph of OCR. (B) basal OCR rate (C) oligomycin induced OCR rate (D) FCCP induced OCR rate (E) Rotenone/Antimycin A induced OCR rate. Data shown is from 4 independent experiments (n=4). Data is presented as the mean ± SEM. One-way ANOVA was used to calculate statistical significance with a P-value of < 0.05 deemed statistically significant. ns indicates $p>0.05$.

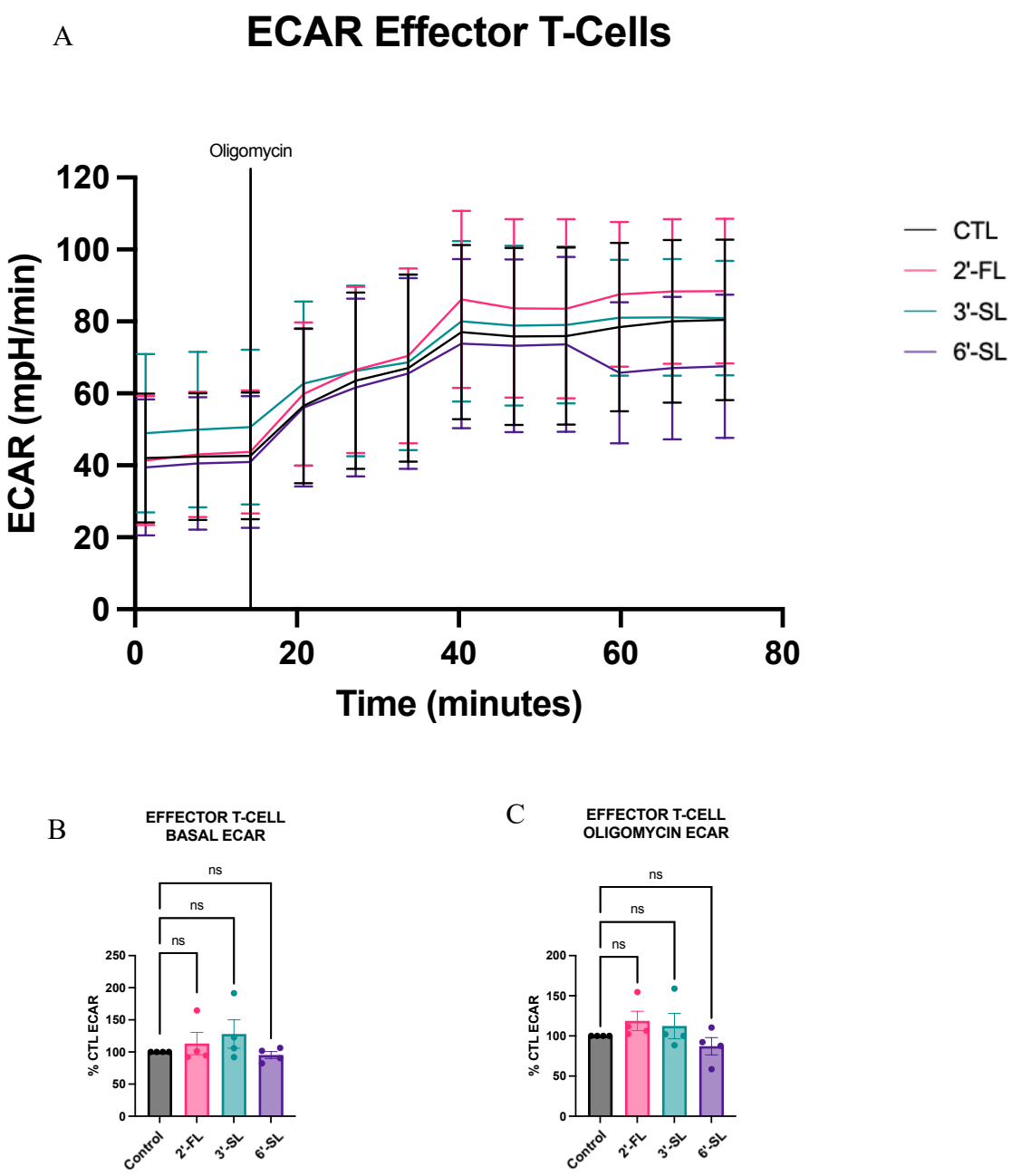

Figure 5. 26: **Mito Stress Test ECAR Measurement in Effector T-Cells Treated with HMOs**

Effector T-Cells were treated with HMOs; 2'-FL (2 mM), 3'-SL (1 mM), or 6'-SL (1 mM). (A) representative time-course graph of ECAR. (B) basal ECAR rate (C) oligomycin induced ECAR rate Data shown is from 4 independent experiments (n=4). Data is presented as the mean ± SEM. One-way ANOVA was used to calculate statistical significance with a P-value of < 0.05 deemed statistically significant. ns indicates $p>0.05$.

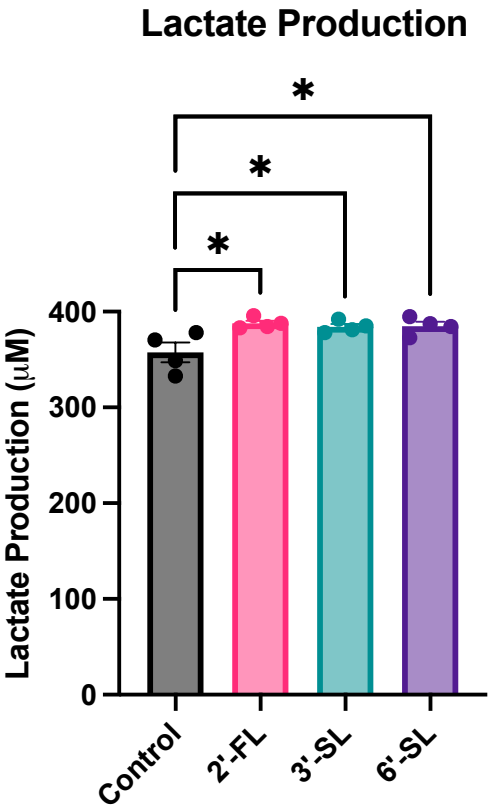

Figure 5. 27: **Extracellular Lactate Production in Effector T-Cells Following HMO Treatment**

Effector T-Cells were treated with HMOs overnight. Lactate production was measured via lactate quantification assay via luminescence (RLU). Data shown is from 4 independent experiments (n=4). Data is presented as the mean ± SEM. One-way ANOVA was used to calculate statistical significance with a P-value of < 0.05 deemed statistically significant. * Indicates $p<0.05$

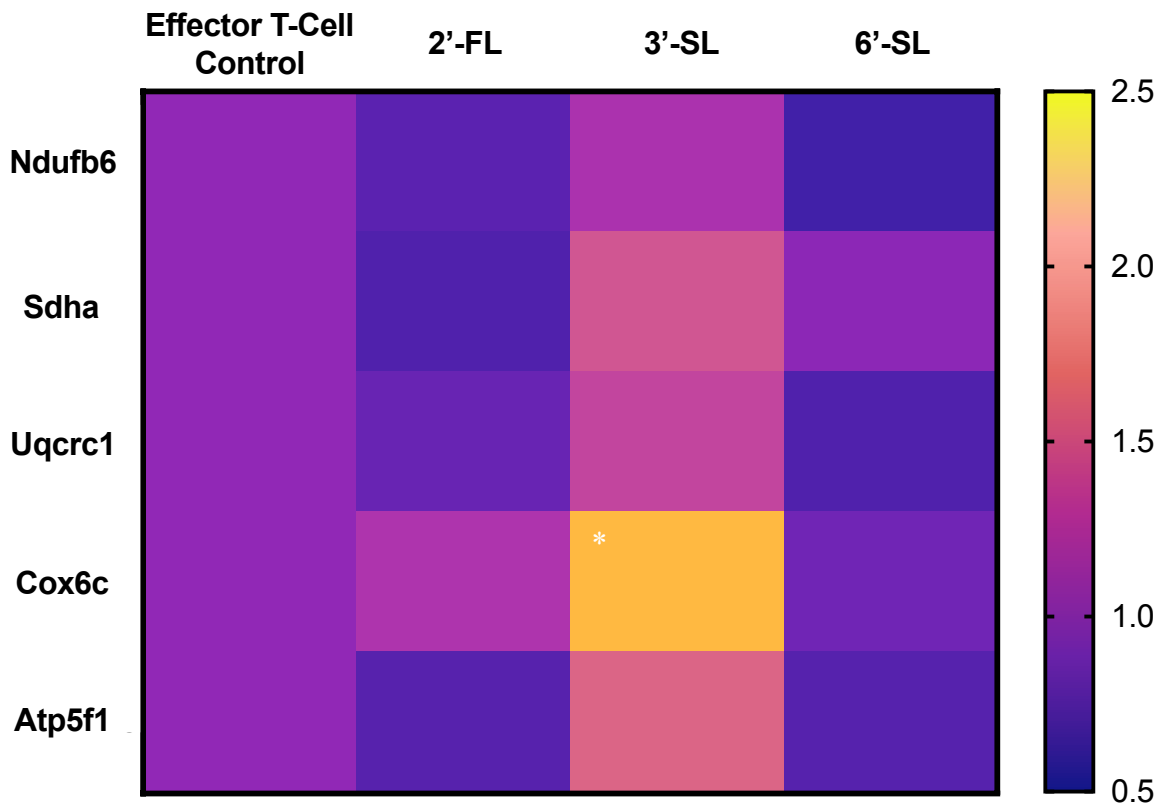

Figure 5. 28: **Expression of Oxidative Phosphorylation Genes in Effector T-Cells Treated with HMOs**

Quantitative PCR analysis was performed to assess the mRNA expression of key genes involved in oxidative phosphorylation (*ndufb6, sdha, uqcrc1, cox6c*, and *atp5f1*) in Effector T-Cells following treatment with HMOs; 2'-FL (2 mM), 3'-SL (1 mM), or 6'-SL (1 mM). The heat map shows relative expression levels, with each column representing a treatment condition and each row representing a specific gene. Expression values are log2-transformed and normalised to housekeeping genes. Data shown is from 3 independent experiments (n=3). * indicates $p<0.05$

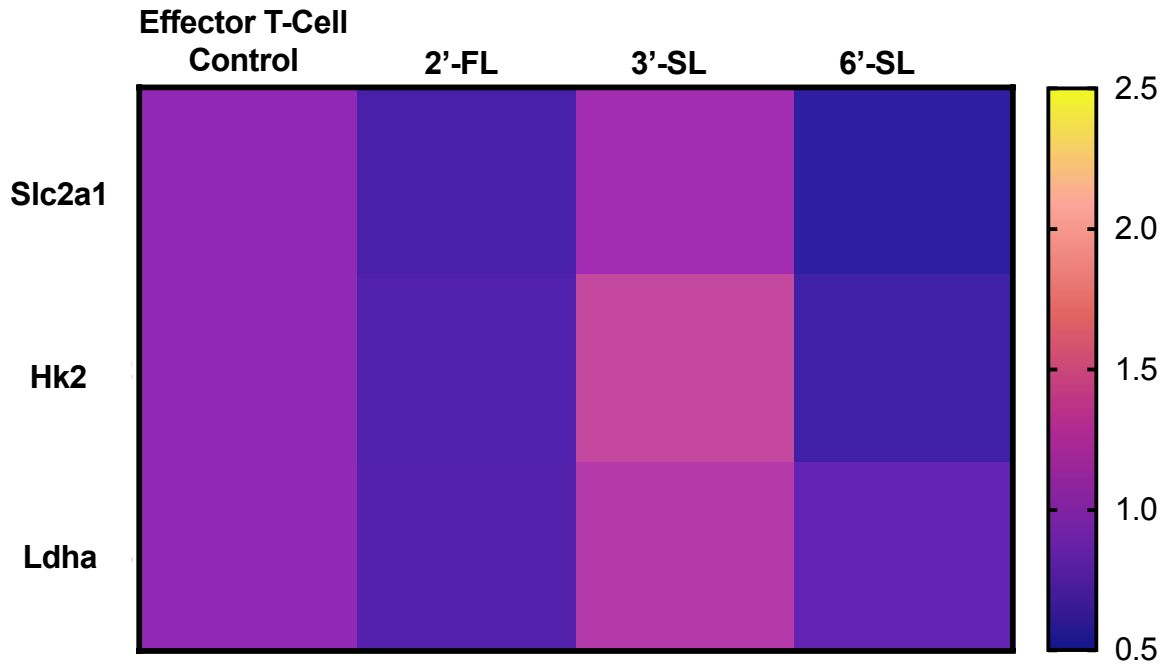

Figure 5. 29*:* **Expression of Glycolysis Genes in Effector T-Cells Treated with HMOs**

Effector T-Cells were treated with HMOs; 2'-FL (2 mM), 3'-SL (1 mM), or 6'-SL (1 mM) + 100 ng/mL LPS for 4 hours and the expression of key glycolytic genes (*slc2a1, hk2, ldha*) was analysed by quantitative PCR. The heat map presents normalised, log2-transformed expression values, with each row representing an individual gene and each column corresponding to a specific HMOs; 2'-FL (2 mM), 3'-SL (1 mM), or 6'-SL (1 mM). Data shown is from 3 independent experiments (n=3).

5.10. HMOs Effect on Memory T-Cell Metabolism

To determine whether HMOs alter metabolic programming in memory T-cells, OCR and ECAR were assessed alongside lactate production and gene expression of metabolic regulators.

Treatment with 2′-FL, 3′-SL, or 6′-SL did not significantly affect mitochondrial respiration in memory T-cells. Basal OCR remained comparable to untreated controls across all HMO treatments, and no differences were observed in oligomycin, FCCP, or rotenone/antimycin A sensitive respiration (**Figure 5.30 A-E**). These data suggest that HMOs do not alter oxidative phosphorylation capacity in memory T-cells. Similarly, basal glycolytic activity was unaffected by HMO treatment. Both basal and oligomycin-induced ECAR values were unchanged compared with control groups (**Figure 5.31 A-C**).

Despite the absence of changes in OCR or ECAR, lactate assays revealed decreased lactate release in HMO-treated memory T-cells (**Figure 5.32)**. With 6′-SL resulting in significantly decreased extracellular lactate compared to controls, while 2′-FL and 3'-SL exerted a more modest non-significant effect.

Transcriptomic analysis of key oxidative phosphorylation genes (*ndufb6, sdha, uqcrc1, cox6c*, and *atp5f1*) revealed minimal effects associated with the HMOs (**Figure 5.33**). Expression levels remained largely stable across treatments, with only subtle variation between 3′-SL and 6′-SL treated groups. Similarly, glycolytic gene expression was also insensitive to HMO treatment (**Figure 5.34**).

Measurement of mitochondrial stress responses revealed no significant changes in spare respiratory capacity in either effector or memory T-cells following HMO treatment (**Figure 5.35**). Likewise, HMO exposure did not alter glycolytic reserve in either effector or memory subsets (**Figure 5.36**).

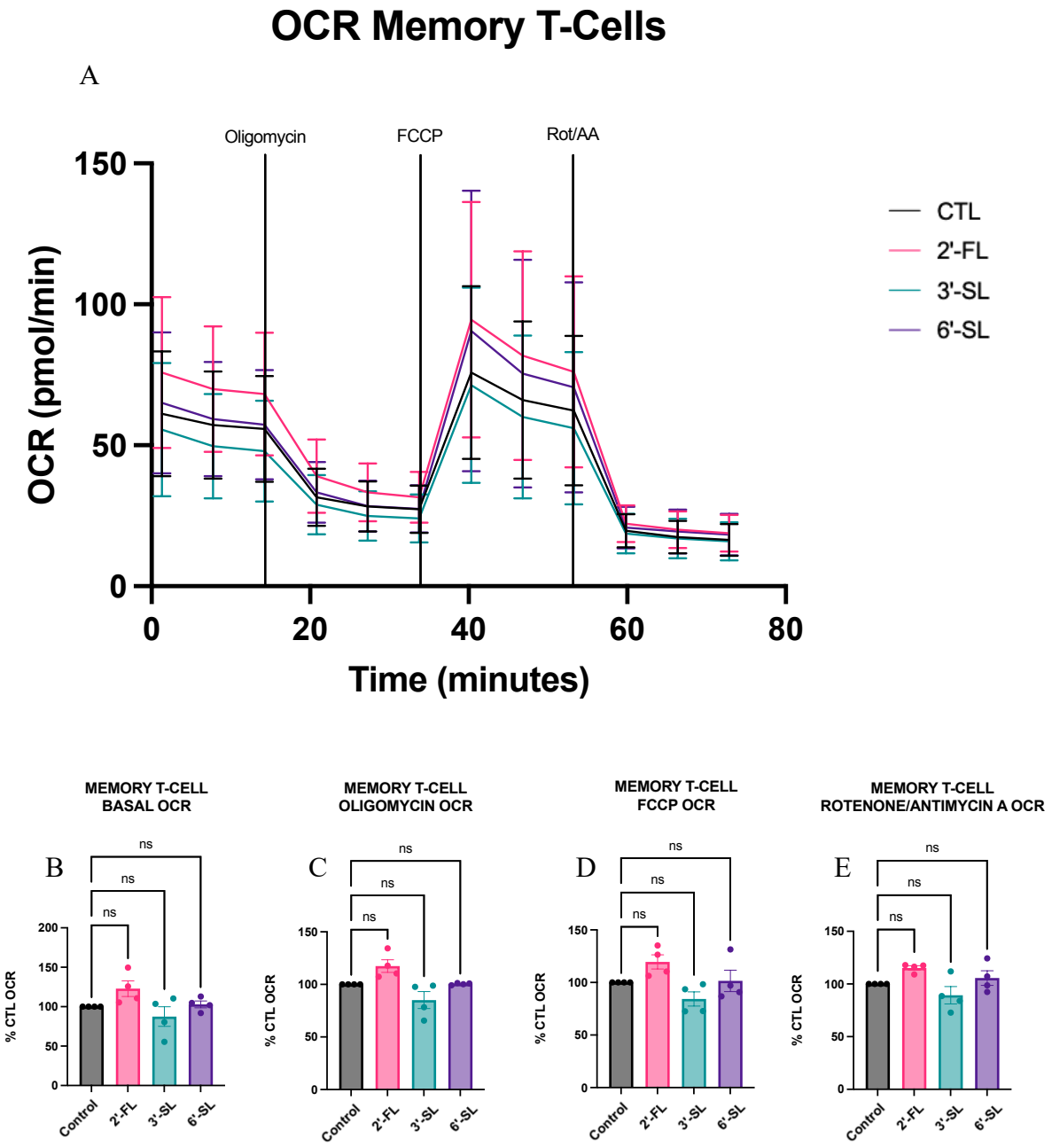

Figure 5. 30: **Mito Stress Test OCR Measurement in Memory T-Cells Treated with HMOs**

Memory T-Cells were treated with HMOs; 2'-FL (2 mM), 3'-SL (1 mM), or 6'-SL (1 mM). (A) representative time-course graph of OCR. (B) basal OCR rate (C) oligomycin induced OCR rate (D) FCCP induced OCR rate (E) Rotenone/Antimycin A induced OCR rate. Data shown is from 4 independent experiments (n=4). Data is presented as the mean ± SEM. One-way ANOVA was used to calculate statistical significance with a P-value of < 0.05 deemed statistically significant. ns indicates $p>0.05$.

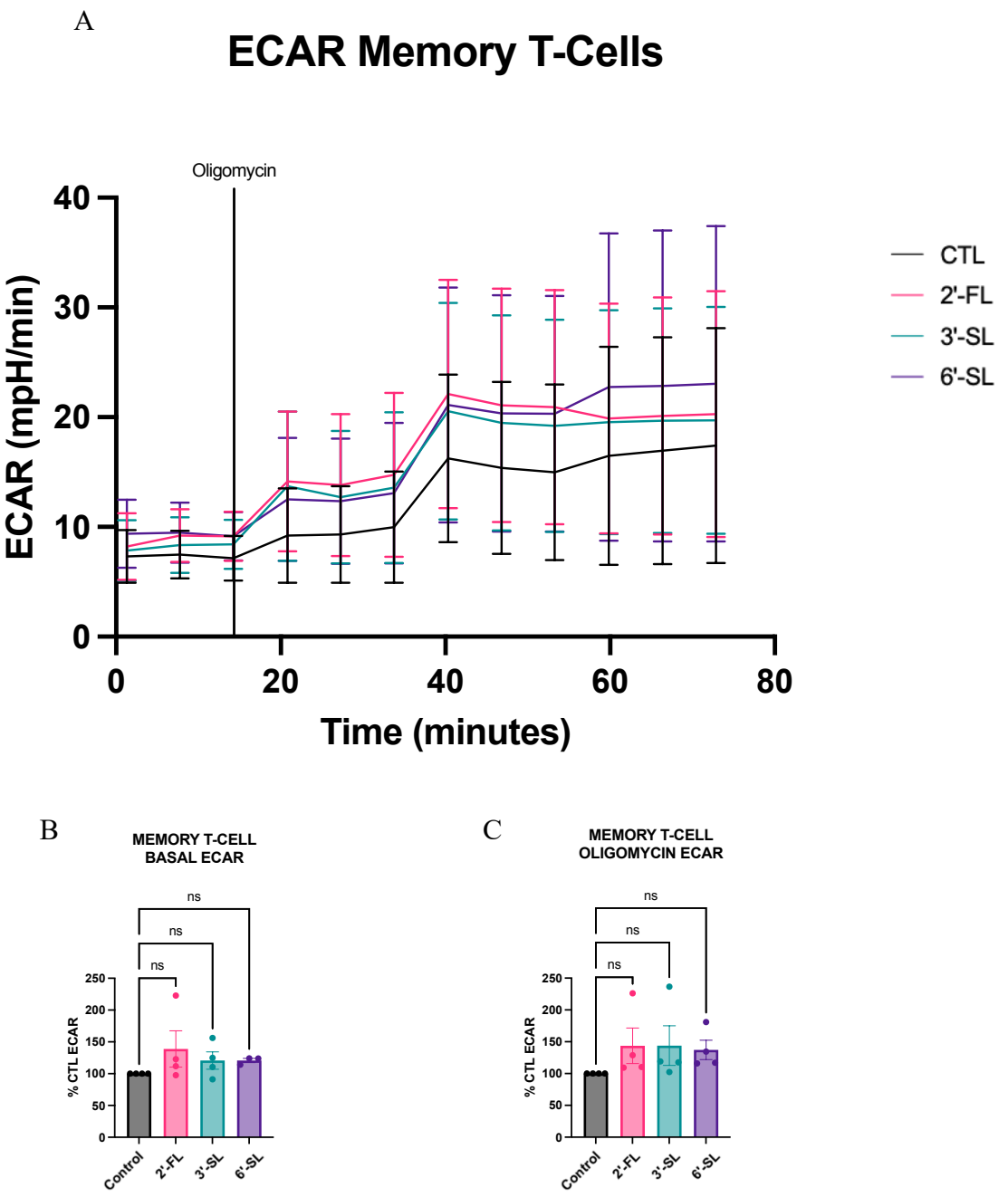

Figure 5. 31: **Mito Stress Test ECAR Measurement in Memory T-Cells Treated with HMOs**

Memory T-Cells were treated with HMOs; 2'-FL (2 mM), 3'-SL (1 mM), or 6'-SL (1 mM). (A) representative time-course graph of ECAR. (B) basal ECAR rate (C) oligomycin induced ECAR rate Data shown is from 4 independent experiments (n=4). Data is presented as the mean ± SEM. One-way ANOVA was used to calculate statistical significance with a P-value of < 0.05 deemed statistically significant. ns indicates $p>0.05$.

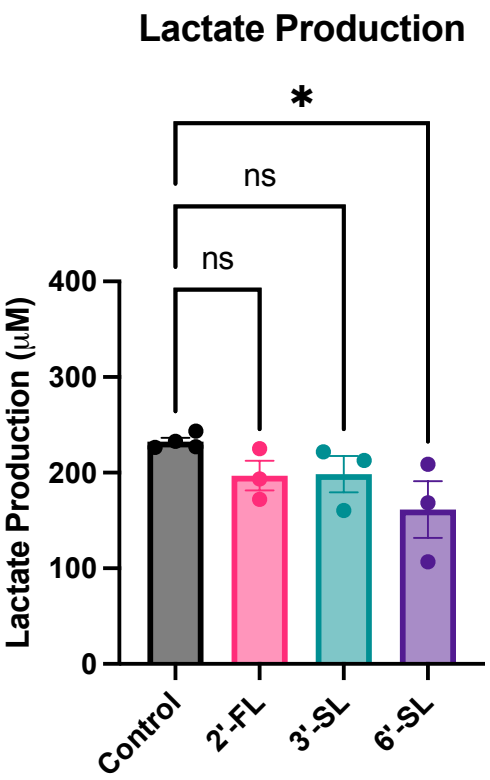

Figure 5. 32: **Extracellular Lactate Production in Memory T-Cells Following HMO Treatment**

Memory T-Cells were treated with HMOs overnight. Lactate production was measured via lactate quantification assay via luminescence (RLU). Data shown is from 3 independent experiments (n=3). Data is presented as the mean ± SEM. One-way ANOVA was used to calculate statistical significance with a P-value of < 0.05 deemed statistically significant. ns indicates $p>0.05$,* $p<0.05$.

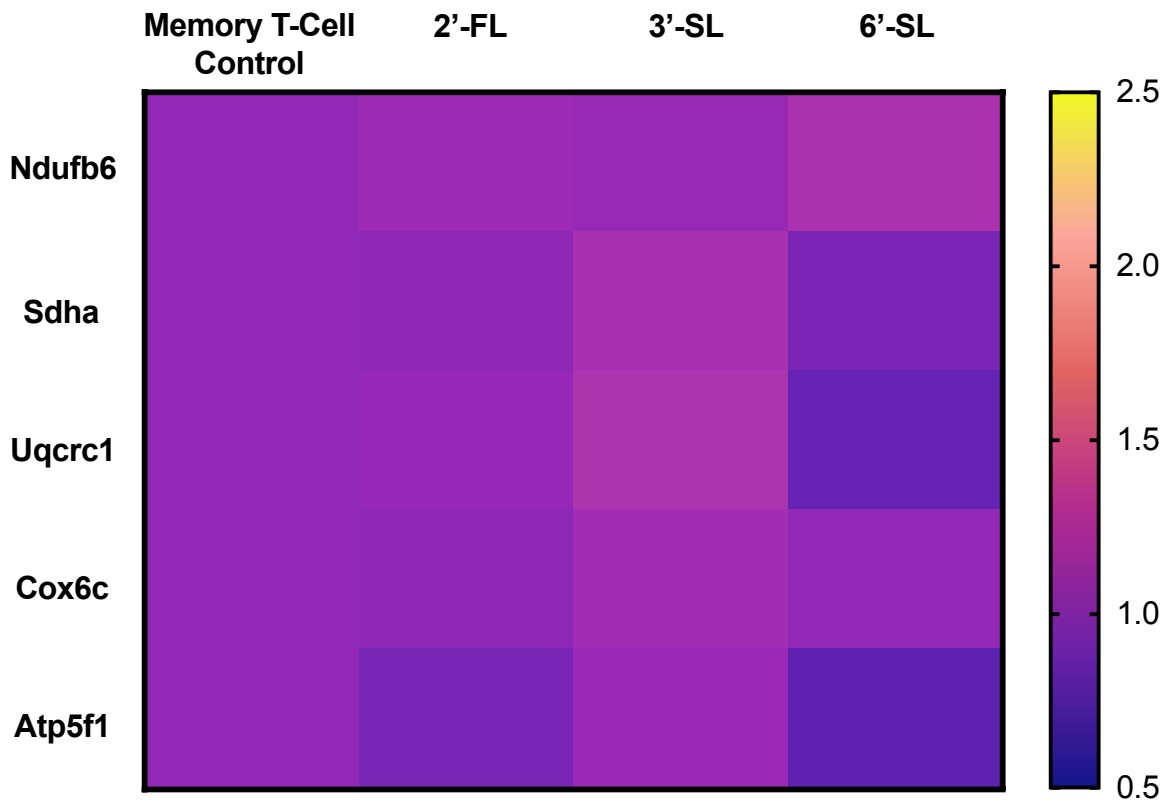

Figure 5. 33: **Expression of Oxidative Phosphorylation Genes in Memory T-Cells Treated with HMOs**

Quantitative PCR analysis was performed to assess the mRNA expression of key genes involved in oxidative phosphorylation (*ndufb6, sdha, uqcrc1, cox6c*, and *atp5f1*) in Memory T-Cells following treatment with HMOs; 2'-FL (2 mM), 3'-SL (1 mM), or 6'-SL (1 mM). The heat map shows relative expression levels, with each column representing a treatment condition and each row representing a specific gene. Expression values are log2-transformed and normalised to housekeeping genes. Data shown is from 3 independent experiments (n=3).

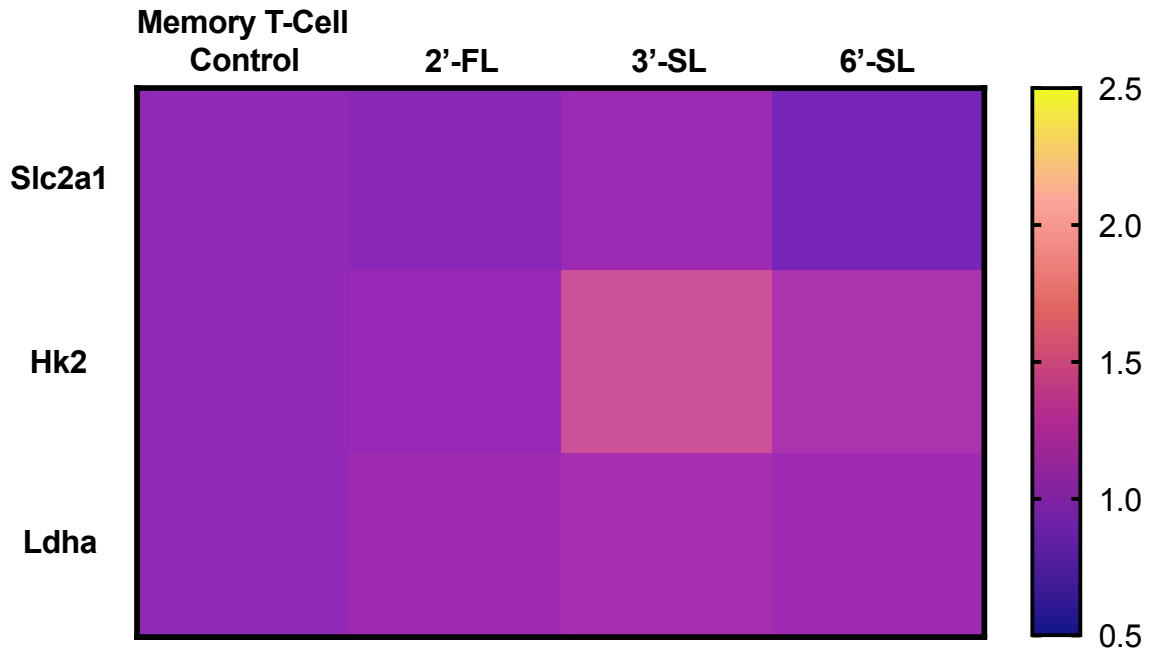

Figure 5. 34: **Expression of Glycolysis Genes in Memory T-Cells Treated with HMOs**

Memory T-Cells were treated with HMOs; 2'-FL (2 mM), 3'-SL (1 mM), or 6'-SL (1 mM) and the expression of key glycolytic genes (*slc2a1, hk2, ldha*) was analysed by quantitative PCR. The heat map presents normalised, log2-transformed expression values, with each row representing an individual gene and each column corresponding to a specific HMOs; 2'-FL (2 mM), 3'-SL (1 mM), or 6'-SL (1 mM). Data shown is from 3 independent experiments (n=3).

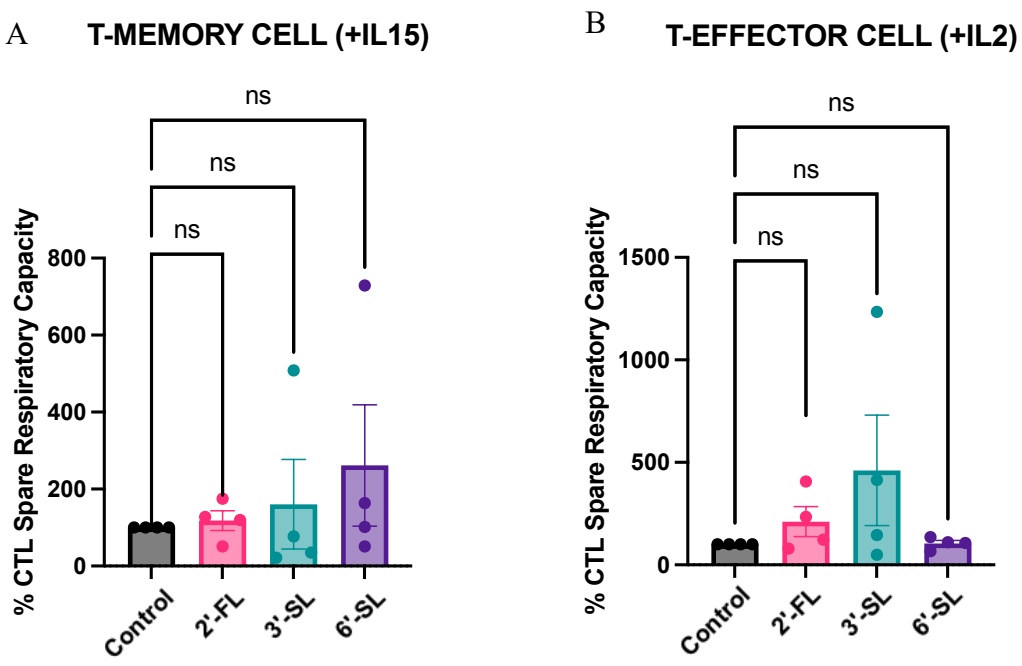

Figure 5. 35: **Spare Respiratory Capacity in Effector and Memory T-Cells Treated with HMOs**

T-Cells were polarised into (A) Memory (stimulated with 100 ng/mL IL-15), or (B) Effector (cultured with 40 ng/mL IL-2) states and treated with media, 2'-FL, 3'-SL, or 6'-SL. Spare Respiratory Capacity was measured and normalised to control values (expressed as % CTL). Data are shown as mean ± SEM (n=4 per group). One-way ANOVA was used to calculate statistical significance with a P-value of < 0.05 deemed statistically significant. ns indicates $p>0.05$.

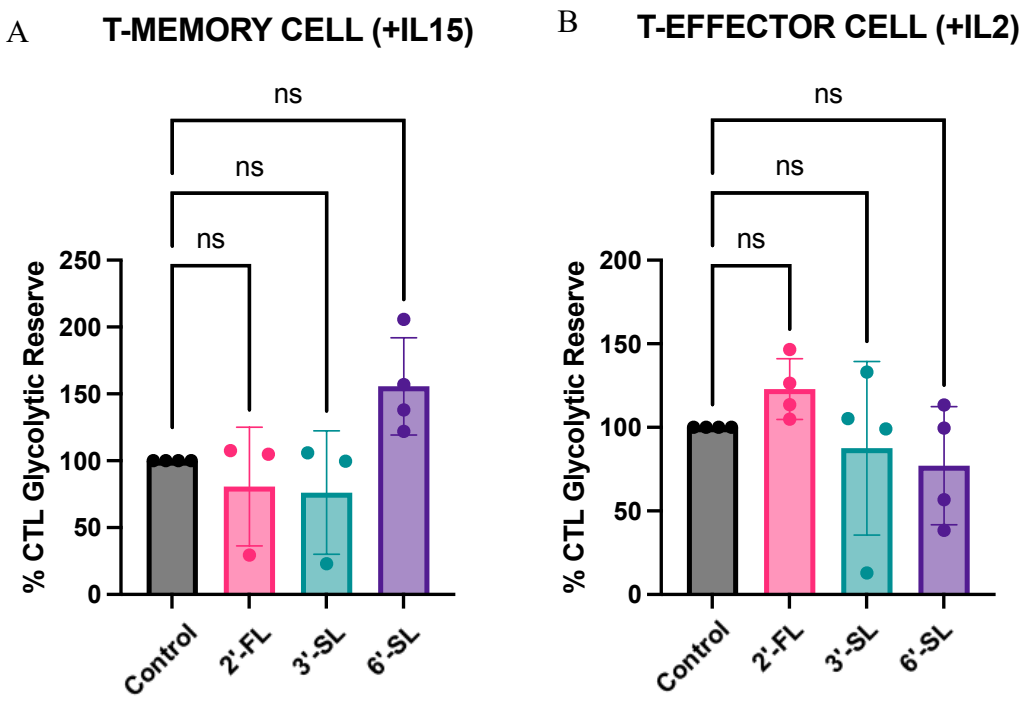

Figure 5. 36: **Glycolytic Reserve in Effector and Memory T-Cells Treated with HMOs**

T-Cells were polarised into (A) Memory (stimulated with 100 ng/mL IL-15), or (B) Effector (cultured with 40 ng/mL IL-2) states and treated with media, 2'-FL, 3'-SL, or 6'-SL. Glycolytic reserve was measured and normalised to control values (expressed as % CTL). Data are shown as mean ± SEM (n=4 per group). One-way ANOVA was used to calculate statistical significance with a P-value of < 0.05 deemed statistically significant. ns indicates $p>0.05$.

5.11. HMOs Temporal Effects on T-Cells

To assess whether HMOs exert delayed metabolic effects on T-cells beyond acute measurements, effector and memory T-cells were treated with 2′-FL, 3′-SL, or 6′-SL and monitored for OCR and ECAR changes over a 6 hour period.

OCR measurements showed no significant effect of HMO treatment on basal mitochondrial respiration in effector T-cells across the 6 hour assay. Both basal OCR and terminal OCR values after 6 hours remained unchanged between the HMO-treated groups and the untreated controls (**Figure 5.37 A-C**). Likewise, ECAR profiling revealed no significant alterations in glycolytic activity in effector T-cells treated with any of the HMOs examined. Both basal and 6 hour ECAR values were comparable across all conditions (**Figure 5.38 A-C**).

Similar to effector T-cells, memory T-cells demonstrated no significant differences in OCR following HMO treatment. Neither basal nor 6 hour OCR levels were affected by exposure to 2′-FL, 3′-SL, or 6′-SL (**Figure 5.39 A-C**). ECAR analysis of memory T-cells also revealed no effect of HMOs on glycolytic activity. Both basal ECAR and values recorded at 6 hours were consistent across all treatment groups (**Figure 5.40 A-C**).

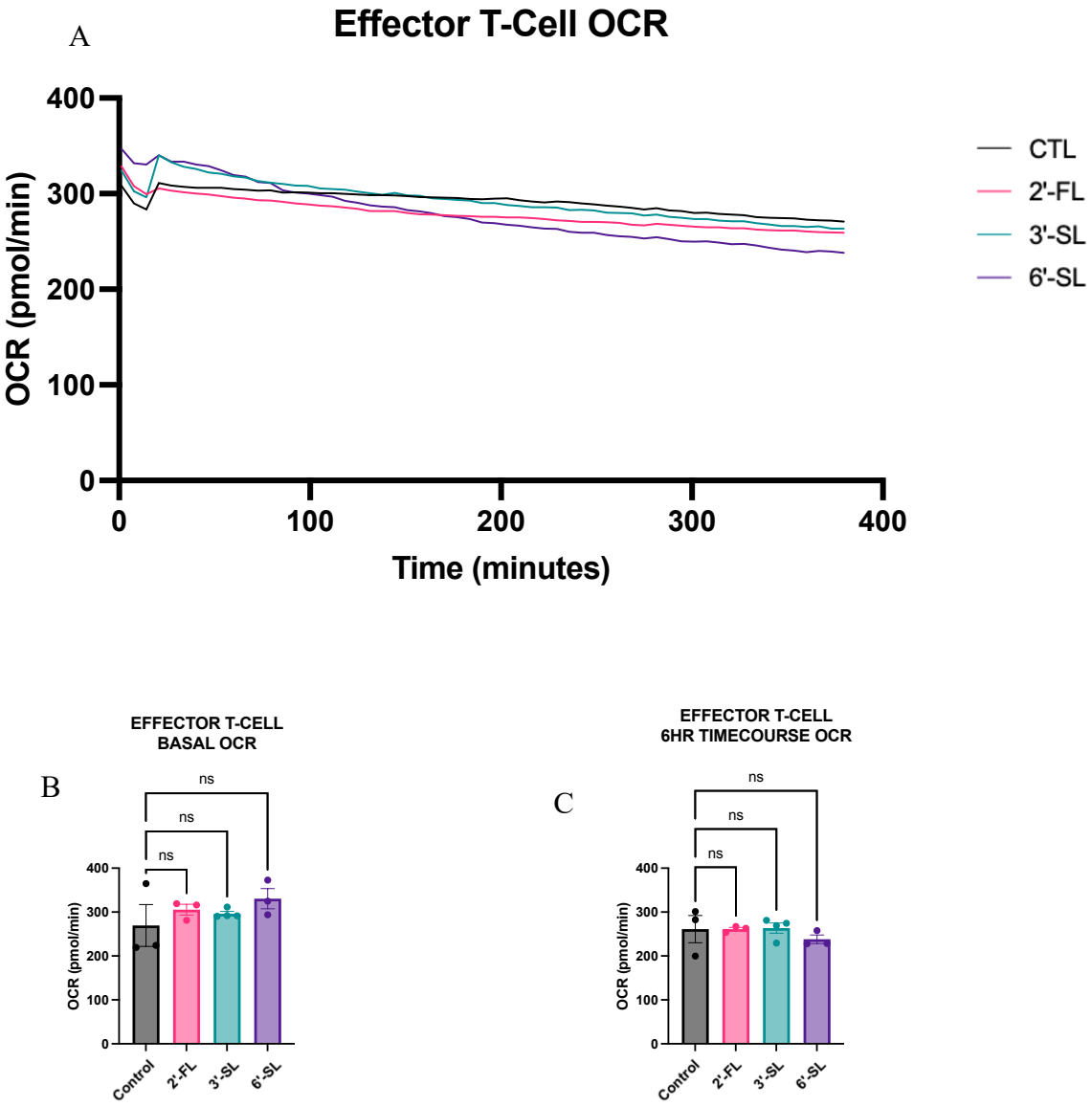

Figure 5. 37: **Time-Course of OCR in Effector T-Cells Over 6 Hours Following Overnight HMO Pre-Treatment**

Effector T-Cells were treated with HMOs (2 mM 2'-FL and 1 mM 3'-SL and 6'-SL). OCR was measured using a SeahorseXFe96 analyser over 6 hours. (A) representative time-course graphs for OCR. (B) basal OCR (C) OCR after 6 hour from 3 independent experiments (n=3). Data is presented as the mean ± SEM. One-way ANOVA was used to calculate statistical significance with a P-value of < 0.05 deemed statistically significant. ns indicates $p>0.05$.

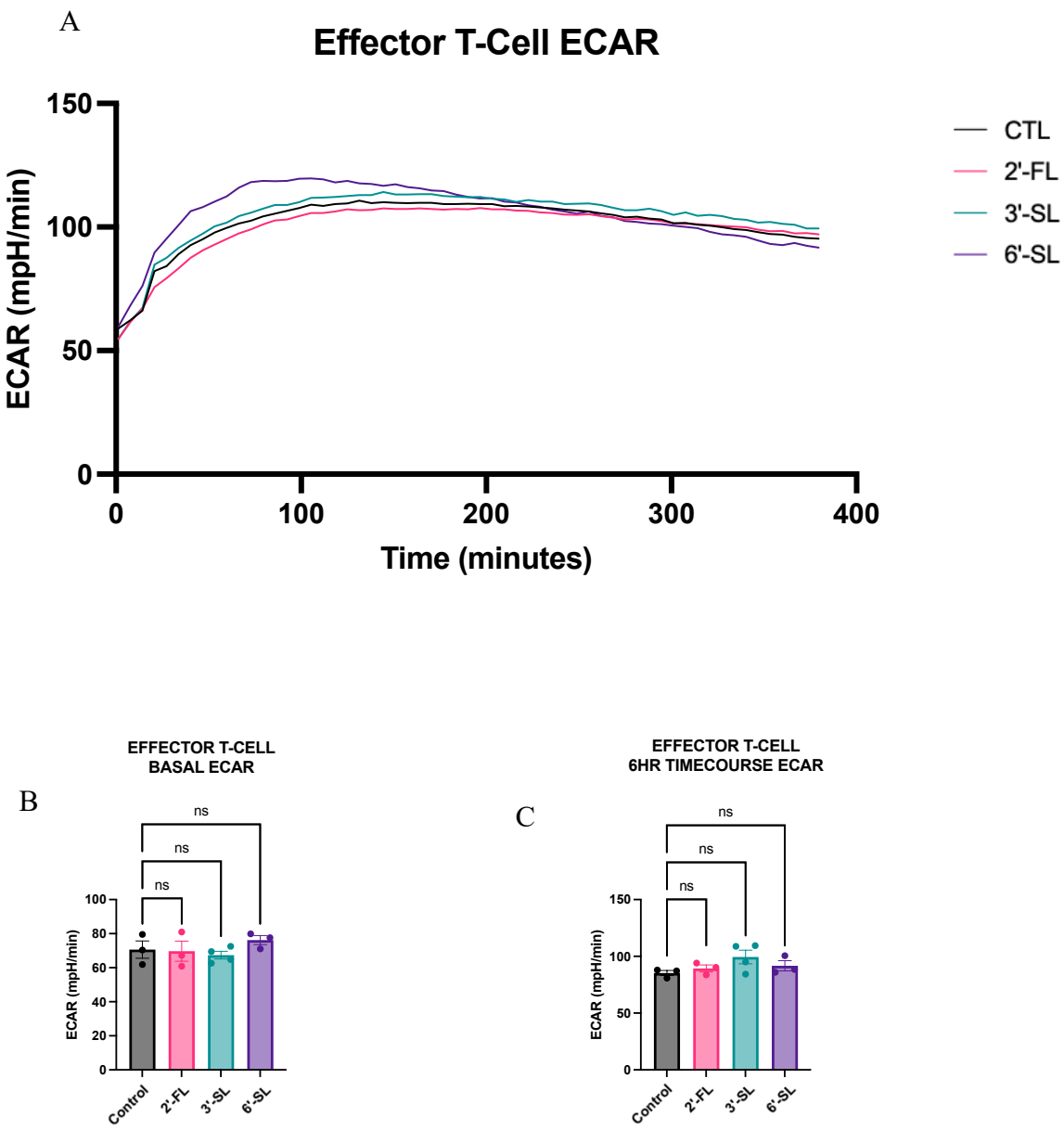

Figure 5. 38: **Time-Course of ECAR in Effector T-Cells Over 6 Hours Following Overnight HMO Pre-Treatment**

Effector T-Cells were treated with HMOs (2 mM 2'-FL and 1 mM 3'-SL and 6'-SL). ECAR was measured using a SeahorseXFe96 analyser over 6 hours. (A) representative time-course graphs for ECAR. (B) basal ECAR (C) ECAR after 6 hour from 3 independent experiments (n=3). Data is presented as the mean ± SEM. One-way ANOVA was used to calculate statistical significance with a P-value of < 0.05 deemed statistically significant. ns indicates $p>0.05$.

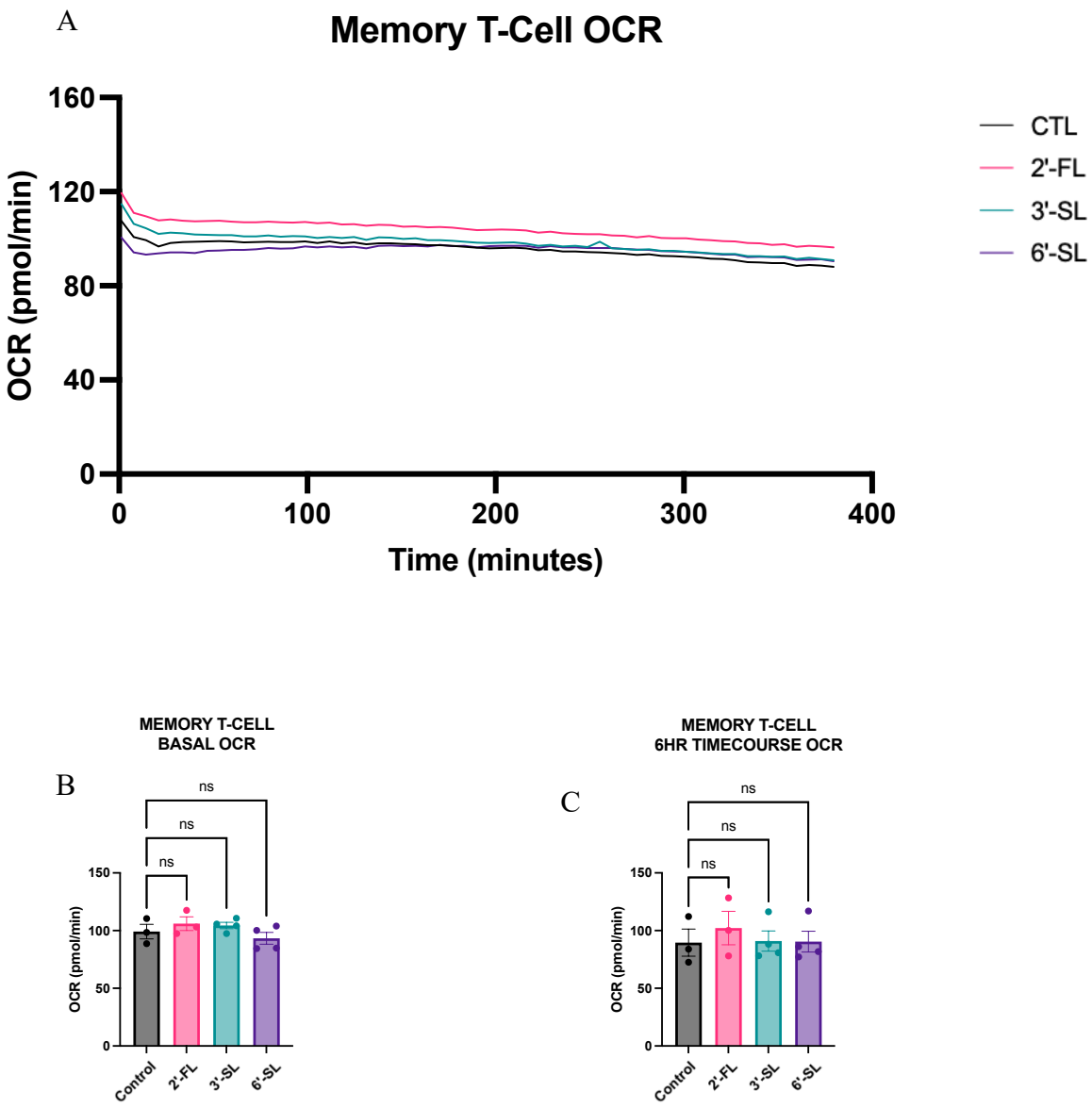

Figure 5. 39: **Time-Course of OCR in Memory T-Cells Over 6 Hours Following Overnight HMO Pre-Treatment**

Memory T-Cells were treated with HMOs (2 mM 2'-FL and 1 mM 3'-SL and 6'-SL). OCR was measured using a SeahorseXFe96 analyser over 6 hours. (A) representative time-course graphs for OCR. (B) basal OCR (C) OCR after 6 hour from 3 independent experiments (n=3). Data is presented as the mean ± SEM. One-way ANOVA was used to calculate statistical significance with a P-value of < 0.05 deemed statistically significant. ns indicates $p>0.05$.

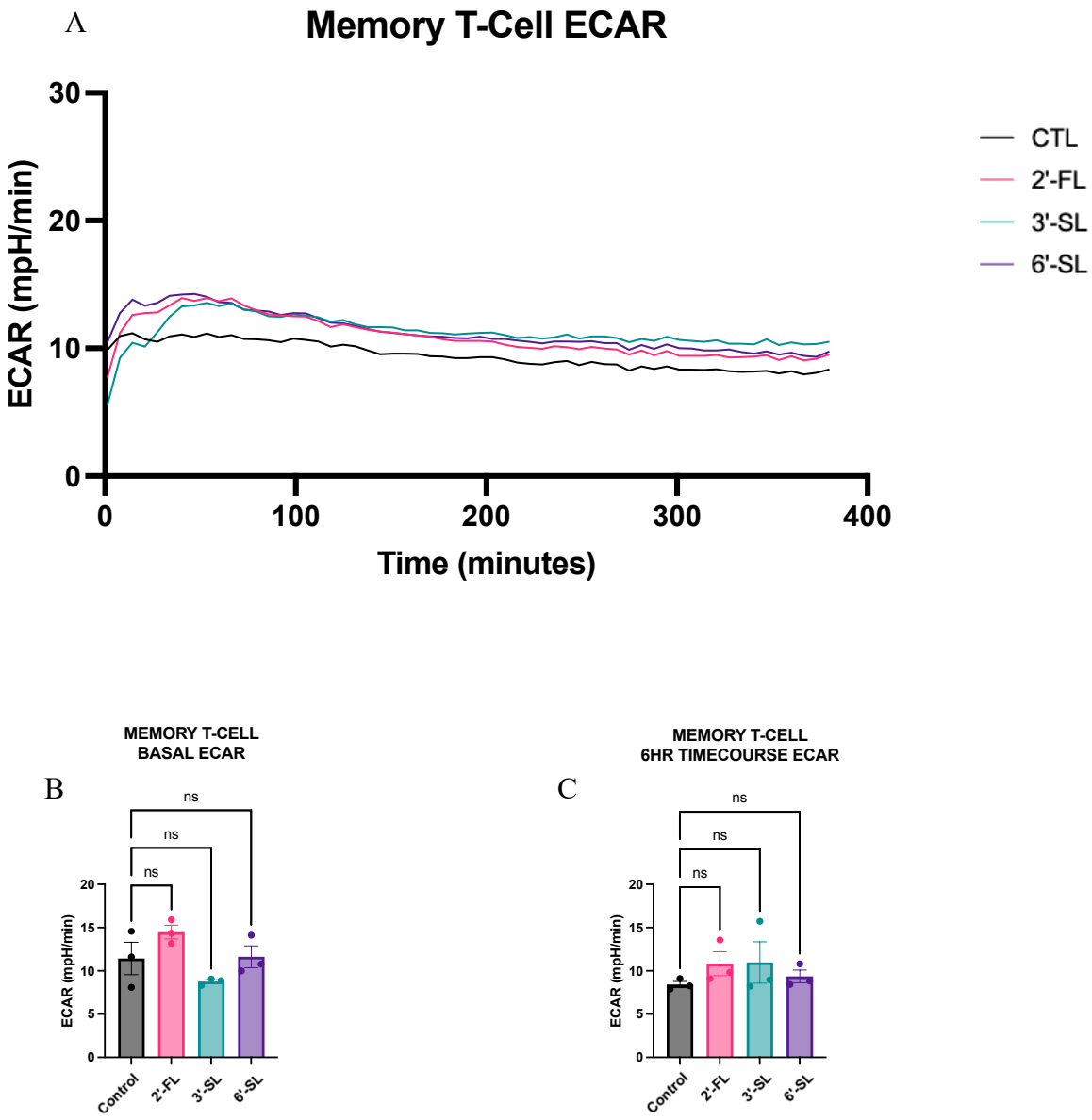

Figure 5. 40: **Time-Course of ECAR in Memory T-Cells Over 6 Hours Following Overnight HMO Pre-Treatment**

Memory T-Cells were plated at $8x10^4$ cells per well in a 96-well seahorse plate and incubated at 37°C overnight treated with HMOs (2 mM 2'-FL and 1 mM 3'-SL and 6'-SL). Data in Fig 3.6 (A) representative time-course graphs for ECAR. (B) basal ECAR (C) ECAR after 6 hour from 3 independent experiments (n=3). Data is presented as the mean ± SEM. One-way ANOVA was used to calculate statistical significance with a P-value of < 0.05 deemed statistically significant. ns indicates $p>0.05$.

5.12. Immunomodulatory Effects of HMOs on DCs and T-Cells

To assess the impact of HMOs on mitochondrial ROS in DCs, BMDCs were treated with 2′-FL, 3′-SL, or 6′-SL and analysed by flow cytometry following MitoSOX™ staining. Treatment with 6′-SL significantly decreased basal ROS levels relative to untreated controls (**Figure 5.41 B-C**). In addition, all HMOs trend to reduced ROS production in BMDCs stimulated with LPS for 4 hours compared to the LPS control, however none of these were significant (**Figure 5.41 D-E**).

The effect of HMOs on TNF-α production in BMDCs was next examined. Overnight treatment with 6′-SL alone significantly increased TNF-α production compared to untreated controls (**Figure 5.42 A**). When BMDCs were stimulated with LPS for 4 hours, HMO treatment did not enhance TNF-α production relative to the LPS control (**Figure 5.42 B**).

IL-1β production was then evaluated under conditions requiring inflammasome activation. No detectable IL-1β was observed in untreated or HMO-treated BMDCs, nor in cells exposed to LPS alone (**Figure 5.43 A-B**). Robust IL-1β secretion was only detected following combined stimulation with LPS for 4 hours and ATP for 30 minutes. Under these conditions, all HMO treatments significantly reduced IL-1β production compared to the LPS+ATP control (**Figure 5.43 C**).

To determine whether HMOs altered IL-10 production in DCs, BMDCs were treated overnight with 2′-FL, 3′-SL, or 6′-SL in the presence or absence of LPS. HMOs did not induce IL-10 above baseline levels in unstimulated BMDCs (**Figure 5.44 A**). In contrast, 6′-SL significantly increased IL-10 production following 4 hour LPS stimulation compared to the LPS control, (**Figure 5.44 B**).

Finally, the effect of HMOs on T-cell cytokine production was evaluated. Effector and memory T-cells treated overnight with 2′-FL, 3′-SL, or 6′-SL in the absence of LPS did not display increased TNF-α production compared to media-treated controls (**Figure 5.45 A-B**).

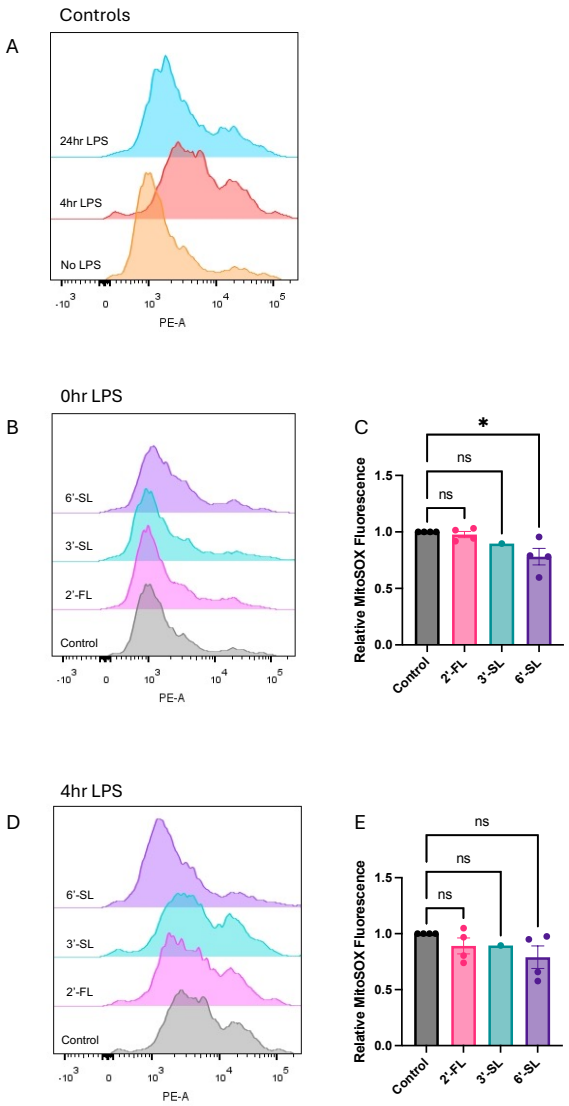

Figure 5. 41**: ROS Levels in Immature and Mature DCs Following HMO Production**

Representative flow cytometry histograms and quantification of ROS levels in BMDCs treated with HMOs. BMDCs were stained with MitoSOX™ and analysed by flow cytometry to assess mitochondrial ROS production. (A) Controls (B) DCs Treated with HMOs, No LPS (C) Quantification of median fluorescence intensity (MFI) normalised and compared to untreated control. (D) DCs Treated with HMOs + 4 hour LPS (E) Quantification of median fluorescence intensity (MFI) normalised and compared to 4 hour LPS control. Data shown is from at least 4 independent experiments (n=4). Data is presented as the mean ± SEM. One-way ANOVA was used to calculate statistical significance with a P-value of < 0.05 deemed statistically significant. ns indicates $p>0.05$, * $p<0.05$.

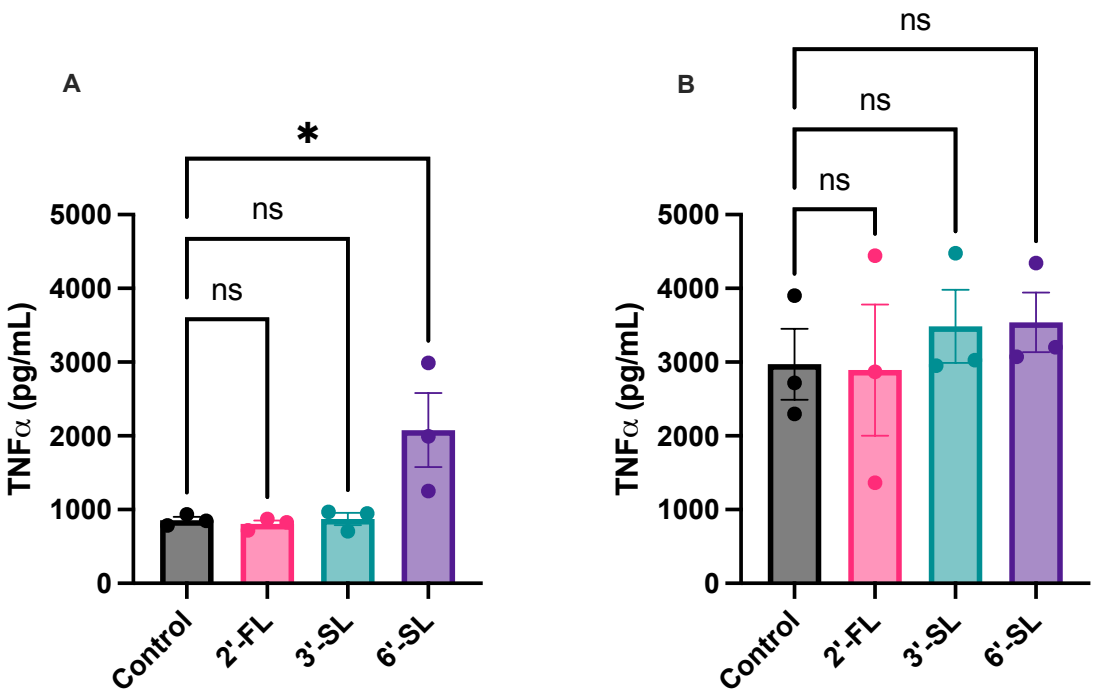

Figure 5. 42: **TNFα Production in DCs Treated with HMOs**

BMDCs were treated overnight with HMOs (*2 mM* 2'-FL, *1 mM* 3'-SL and 6'-SL) ± LPS (100 ng/mL) for 0hour (CTL), *4 hour*. (A) show HMOs treated alone, No LPS (B) HMO treated + 4 *hour* LPS. Data shown is from at least 3 independent experiments (n=3). Data is presented as the mean ± SEM. One-way ANOVA was used to calculate statistical significance with a P-value of < 0.05 deemed statistically significant. ns indicates $p>0.05$, * $p<0.05$.

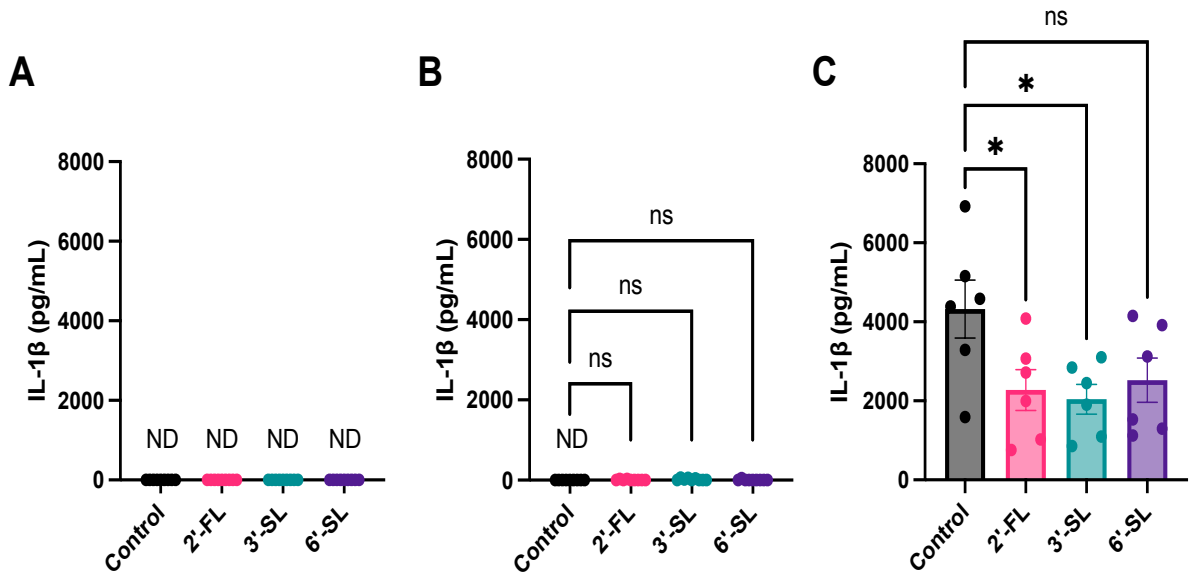

Figure 5. 43: **IL-1β Production in DCs Treated with HMOs**

BMDCs were treated overnight with HMOs (2 mM 2'-FL, 1 mM 3'-SL and 6'-SL) ± LPS (100 ng/mL) for 0hour (CTL), 4 hour with the last half hour treated ± ATP (5 mM). (A) show HMOs treated alone, No LPS (B) HMO treated + 4 hour LPS (C) HMO treated + 4 hour LPS + 30 minutes ATP. Data shown is from at least 3 independent experiments (n=3). Data is presented as the mean ± SEM. ND = Not Detected. One-way ANOVA was used to calculate statistical significance with a P-value of < 0.05 deemed statistically significant. ns indicates $p>0.05$, * $p<0.05$.

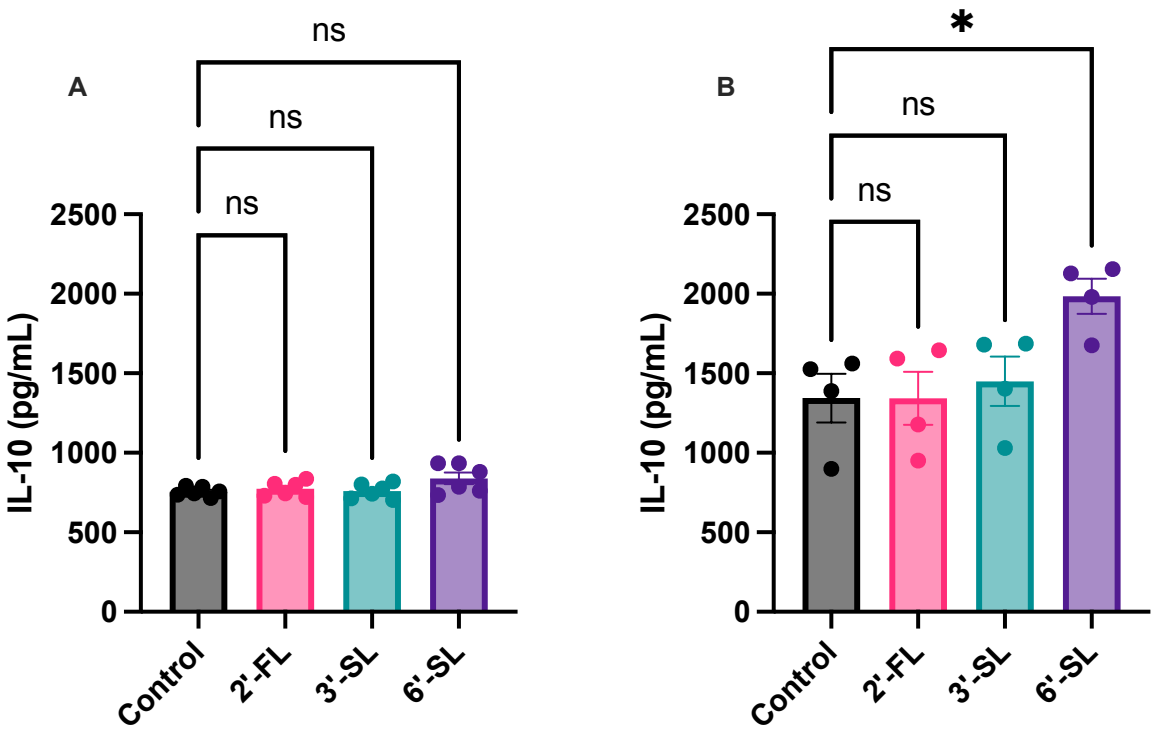

Figure 5. 44: **IL-10 Production in DCs Treated with HMOs**

BMDCs were treated overnight with HMOs (2 mM 2'-FL, 1 mM 3'-SL and 6'-SL) ± LPS (100 ng/mL) for 0hour (CTL), 4 hour. (A) show HMOs treated alone, No LPS (B) HMO treated + 4 hour LPS. Data shown is from 2 (A) and 4 (B) independent experiments. Data is presented as the mean ± SEM. ND = Not Detected. One-way ANOVA was used to calculate statistical significance with a P-value of < 0.05 deemed statistically significant. ns indicates $p>0.05$, * $p<0.05$.

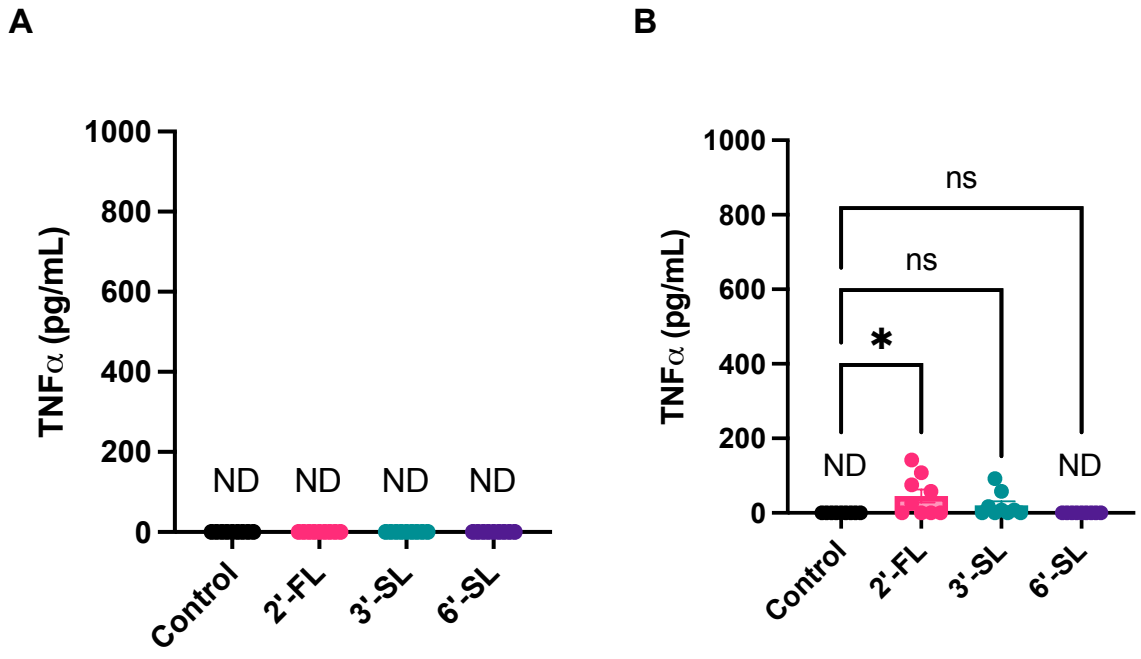

Figure 5. 45 **TNF-α Production in T-Cells Treated with HMOs**

T-cells were treated overnight with HMOs (2 mM 2'-FL, 1 mM 3'-SL and 6'-SL). (A) Memory T-Cells treated with HMOs treated alone, (B) Effector T-Cells with HMOs treated alone. Data shown is from at least 3 independent experiments (n=3). Data is presented as the mean ± SEM. ND = Not Detected. One-way ANOVA was used to calculate statistical significance with a P-value of < 0.05 deemed statistically significant. ns indicates $p>0.05$, * $p<0.05$.

5.13. Discussion

This chapter investigates the influence of HMOs on DCs and T-cell metabolism and function. Extracellular flux analysis was used to profile OCR and ECAR to assess how 2'-FL, 3'-SL, and 6'-SL alter oxidative phosphorylation, glycolysis, and metabolic flexibility across immature and activated DCs as well as effector and memory T-cell subsets. These results were complemented with assays of lactate production, spare respiratory capacity, and glycolytic reserve to provide further insight into HMO-mediated metabolic rewiring. Gene expression analysis of oxidative phosphorylation and glycolysis pathways was performed to link functional metabolic outcomes to transcriptional regulation. In parallel, cell viability and cytokine production was also evaluated to confirm that HMO exposure did not compromise immune cell health or their immunological outputs. Together, these studies provide a comprehensive view of how HMOs impact metabolic programming and effector functions in DCs and T-cells, offering insights into their broader role in shaping adaptive immune responses.

The current findings demonstrate that HMO treatment pose differing effects on BMDCs, with 6'-SL, significantly reducing both OCR and ECAR in BMDCs, indicating a suppression of both mitochondrial respiration and glycolysis. This suggests that 6'-SL exerts immunometabolic effect on DCs, potentially inducing a metabolically quiescent or suppressed state. Such a profile is distinct from the classical metabolic rewiring associated with immunogenic activation and may reflect a tolerogenic or regulatory DC phenotype. DCs are critical regulators of adaptive immunity, and their function is also tightly coupled to metabolism. Immunogenic DCs activated for short periods with LPS show glycolytic induction, while prolonged stimulation induces a tolerogenic phenotype associated with oxidative suppression[227,292]. Our baseline metabolic profiling confirmed these established patterns, validating our system. Importantly, when DCs were exposed to HMOs, particularly 6′-SL, we observed suppression of both OCR and ECAR, accompanied by reduced lactate production and downregulation of oxidative phosphorylation and glycolytic genes. This profile resembled that of tolerogenic DCs, which are well-recognised inducers of Tregs[296], and our findings provide a plausible mechanistic bridge between HMO exposure and the tolerogenic immune environment described in breastfed infants. In 3’-SL treated DCs, upregulation of oxidative phosphorylation genes together with increased spare respiratory capacity without unchanged basal respiration was observed. This may indicate

enhanced mitochondrial readiness and resilience; a metabolic signature priming DC states capable of rapid response without promoting immunogenic activation. 2'-FL did not have any discernible effect on metabolic or gene signature or lactate output of DCs.

These observations align with emerging literature suggesting that specific HMOs can promote anti-inflammatory immune environments by modulating innate immune cell function[299,303]. In the context of DCs, metabolic suppression may correspond with reduced co-stimulatory capacity, diminished cytokine secretion, and impaired T-cell priming which are all hallmarks of tolerogenic DCs[296]. Further, prior studies have shown that the sialylated HMO 6'-SL can engage siglecs, including siglec-5 and siglec-10, which are expressed on DCs and are associated with inhibitory signalling pathways that suppress inflammatory responses[304,305]. It has already been established that HMO 3'-SL is not acting through siglec-E, the murine homologue for siglec-5/7 present on immune cells in macrophages and therefore may be acting in an alternative manner. Interestingly, while most immunogenic stimuli such as TLR ligands drive glycolysis to support DC activation, certain regulatory signals can restrain this metabolic shift and maintain DCs in an immature or regulatory state. For example, vitamin D and retinoic acid are known to alter glycolysis and mitochondrial respiration in DCs, promoting a tolerogenic phenotype[306,307]. Our results suggest that HMOs may act in a similar manner. Further mechanistic studies are warranted to delineate the precise receptors and signalling events involved. The observed suppression of both OCR and ECAR that was observed suggests more than just a shift in activation state, it may reflect a state of metabolic dormancy or immune exhaustion, depending on context. In the neonatal setting, this could be a beneficial mechanism to avoid overactivation during the initial stages of microbial colonisation. Alternatively, in pathological settings, such immunometabolic suppression might impair protective immunity. Understanding how the local tissue microenvironment modulates the outcome of HMO-DC interactions will be essential for determining the therapeutic potential of HMOs in immunoregulation.

Collectively, these data add to a growing body of evidence suggesting that HMOs, do not function solely as prebiotics but act as immunoregulatory molecules capable of directly modulating innate immune cell metabolism and function. By dampening both

mitochondrial and glycolytic activity in DCs, 6'-SL may play a pivotal role in shaping immune tolerance and controlling inflammatory responses in early life. This suppression of energy metabolism suggests that 6'-SL drives DCs into a low-energy, potentially semi-mature or tolerogenic state. The decrease in oxidative phosphorylation could be due to 6'-SL interfering with mitochondrial activity, potentially through downregulation of key enzymes within the electron transport chain. At the same time, the reduction in glycolysis indicates that 6'-SL likely inhibits key glycolytic enzymes or transporters, thereby decreasing glucose uptake and metabolism, which is also implied due to the downregulation of *slc2a1*. The timecourse assay revealed that DCs that are injected with LPS undergo an immediate increase in glycolysis, similar to macrophages, in order to facilitate the biosynthetic demands of immune activation. However, 6'-SL stunted this inherent increase in glycolysis, which was corroborated by the lactate production assay where 6'-SL was associated with less extracellular lactate production compared to the control and other HMO treated DCs.

A further insight comes from the balance of metabolic suppression and viability. One concern with reduced OCR and ECAR is that it may simply reflect cytotoxicity of the HMOs. However, viability assays confirmed that DCs and T-cells remained intact under all HMO conditions, consistent with prior reports of HMO safety at physiological concentrations[4]. This strengthens the interpretation that HMOs act as immunometabolic modulators, not as toxic inhibitors. The observation that ROS production was suppressed without signs of oxidative stress further supports this interpretation, suggesting that 6′-SL stabilises mitochondrial function rather than damaging it. Such fine-tuned modulation could be therapeutically advantageous, allowing immune responses to be dampened without compromising cell survival.

Prior studies have reported conflicting effects of HMOs on DCs, largely depending on receptor context, and experimental conditions. Our cytokine analyses show in resting DCs, 6′-SL enhanced TNF-α production, suggesting a mild activation effect under basal conditions, with 2'-FL and 3'-SL having no effect. This is consistent with reports that some HMOs can engage TLRs, leading to NF-κB activation[308]. However, during LPS stimulation, the same treatment does not affect TNF-α production but markedly reduces

IL-1β production while enhancing IL-10 output. This duality points to context-dependent modulation; in the absence of inflammatory cues, 6′-SL may act as a weak agonist, while under strong pathogen-associated stimulation it functions as a brake, limiting excessive inflammation. Mechanistically, the reduction in IL-1β likely reflects interference with inflammasome activation, as IL-1β release requires a secondary signal to LPS for activation, and HMOs significantly reduced this output. Given that mitochondrial ROS are known triggers of NLRP3 inflammasome activation, the observed suppression of mitochondrial ROS by 6′-SL provides a plausible link between metabolic regulation, oxidative stress, and cytokine output. Thus, 6′-SL appears to orchestrate a coordinated program of dampened ROS generation, restrained inflammasome activity, and skewing toward IL-10 production, altogether shifting DCs toward a regulatory phenotype. The simultaneous suppression of glycolysis and oxidative phosphorylation may also limit the energy available for DCs to mount a full inflammatory response, further reducing cytokine production. Prior studies have revealed that specific HMOs can modulate immune responses in DCs by influencing cytokine production, thereby contributing to the maintenance of immune homeostasis[114,300]. Cells cultured with specific HMOs and subsequently treated with LPS for 48 hours showed a trending increase in IL-12p70 and TNF-α in 2'-FL and 6'-SL cultured cells. This study also showed that HMOs did not affect expression of key DC surface markers in human monocyte derived DCs including CD14, HLA-DR, CD80, CD86 and PD-L1. Xiao et al. (2019) demonstrated that pooled HMOs can drive human monocyte derived DCs toward a regulatory phenotype[299], promoting IL-10, IL-6 and IL-27 secretion but not IL-12p70 and TNF-α on their own. When treated with LPS, the HMO treated DCs maintained their IL-10 and IL-27 secretion and reduced LPS-induced production of IL-12p70, IL-6 and TNF-α. The same group Xiao et al. (2018) further showed that 2′-FL conditioned DCs can enhance antiviral T-cell priming *in vivo*[110]. These data highlight that DC responses may depend on HMO structure and combinatorial presentation. Analysing a receptor-specific view, Noll et al. (2016) and Mukherjee et al. (2022) showed direct binding of specific HMOs to DC-SIGN[71,76], while Akkerman et al. (2022) reported that fermentation-dependent metabolites from 2′-FL/GOS mixtures alter DC cytokine output via AhR[309], suggesting that 2'-FL alone may not drive DC immunomodulation but rather the metabolites produced during fermentation by bacteria present in the gut and also in combination with other oligosaccharides. In the context of the current data, these studies collectively support a model in which HMOs do not universally

activate DCs but instead tune their responsiveness, with effects emerging primarily in the presence of additional inflammatory or microbial signals.

Overall, the combined suppression of both metabolic pathways, decreased inflammatory cytokine output, and ROS levels suggest HMOs can alter DCs into a tolerogenic state. In this state, DCs are less likely to fully activate T-cells and initiate a robust immune response, thereby contributing to immune tolerance. This tolerogenic state may be particularly beneficial in preventing excessive immune activation in conditions such as chronic inflammation or autoimmunity, or in maintaining immune tolerance at mucosal surfaces such as the gut.

The biological rationale for this effect may lie in the evolutionary role of HMOs in early life. Breastfed infants receive HMOs in high concentrations during the neonatal period, a critical window of immune development and microbial colonisation. DCs play a vital role in establishing immune tolerance to commensal microbes and dietary antigens during this phase[297]. Tolerogenic DC phenotypes are known to induce T-cell anergy or the generation of regulatory T-cells rather than effector T-cell activation[296]. Such a phenotype would be consistent with the function of HMOs in early life: establishing a tolerogenic environment that allows for the safe colonisation of commensal microbiota, the development of oral tolerance, and the prevention of hyperinflammatory responses to environmental antigens[310]. This indirect mechanism whereby HMOs condition innate immune cells to adopt anti-inflammatory or tolerogenic phenotypes, offers a compelling model for how maternal milk components shape the neonatal immune system. Macrophages and DCs, upon exposure to HMOs, may reduce pro-inflammatory cytokine secretion, dampen metabolic activity, and limit their capacity to prime T-cells. In doing so, they act as a molecular relay through which HMOs influence T-cell outcomes, helping to prevent inappropriate activation in the immunologically sensitive neonatal gut.

Additionally, the effects of HMOs on the metabolic activity of differentiated effector and memory $CD8^+$ T-cells were also investigated. Effector and memory T-cells are metabolically distinct; effector cells mainly rely on glycolysis, while memory cells favour oxidative phosphorylation and spare respiratory capacity[311]. Our profiling confirmed these

established differences, providing a strong baseline for examining whether HMOs carry out direct effects on these cells. Despite prior evidence indicating strong immunomodulatory effects of HMOs on innate immune cells such as macrophages and DCs, we found no significant alterations in OCR, ECAR, spare respiratory capacity, or glycolytic reserve in T-cells exposed to 2'-FL, 3'-SL, or 6'-SL. Interestingly, while HMOs did not substantially alter OCR or ECAR in either effector or memory T-cells, they did increase lactate output in effector T-cells and decrease lactate production in memory cells. This suggests a subtle shift in metabolic balance without overt reprogramming. Although the mechanism remains unclear, it raises the possibility that HMOs tune metabolic intermediates such as lactate to regulate T-cell differentiation or recall responses. This is interesting as lactate has been shown to promote Treg recruitment[312]. Lactate is a metabolic by-product but also a signalling molecule that promotes Treg differentiation and suppresses effector T-cell function[313], therefore these findings suggest that HMOs may restrain inflammatory T-cell metabolism while favouring pathways that bias towards immune regulation.

The lack of direct metabolic impact may reflect the primary biological role of HMOs in shaping the neonatal immune system, which is predominantly reliant on the innate immune arm during early life. HMOs are among the first bioactive components encountered by the infant immune system through breastfeeding, and their functions appear to be evolutionarily optimised to promote immediate, nonspecific host protection, the establishment of mucosal homeostasis, and microbiota colonisation[4,314,315]. The innate immune system, composed of rapidly responsive cells such as macrophages and DCs, is the first line of defence in neonates, and is therefore a logical primary target for modulation by HMOs. As previously mentioned, prior studies have demonstrated that HMOs can alter the phenotype and function of innate immune cells by modulating cytokine production, surface receptor expression, and cellular metabolism[298,299,303]. In contrast, T-cells, particularly memory and effector subsets are antigen-experienced, highly specialised lymphocytes that rely on specific signals for activation, including antigen presentation, co-stimulation, and cytokine priming. Our findings suggest that HMOs alone do not alter the metabolic or functional state of these cells. This aligns with the current understanding that adaptive immunity in neonates is relatively immature[316], with T-cell responses developing over time in response to antigenic exposure and microbial colonisation[317]. It is plausible

that HMOs influence adaptive immune outcomes indirectly by modulating the function of antigen-presenting cells, such as DCs and macrophages, which then guide T-cell differentiation and activation[318,319].

The receptor profile of T-cells may contribute to this unresponsiveness. Many of the known HMO-binding receptors, including DC-SIGN, siglec-5/-7, and certain TLRs, are either absent or expressed at low levels on mature T-cells, whereas they are abundantly expressed on macrophages, DCs and epithelial cells[320]. Instead, T-cell activation and function are primarily mediated by antigen recognition through the TCR and costimulatory signals provided by APCs, such as DCs[321]. This receptor distribution likely further restricts the capacity of HMOs to act directly on T-cells. Importantly, our experimental model used already polarised T-cells, meaning their metabolism was largely established. Metabolic reprogramming is most dynamic during early T-cell activation, where naïve T-cells undergo a shift toward aerobic glycolysis to support proliferation and effector functions[322,323]. Thus, while HMOs may not impact terminally differentiated T-cells, future studies could explore whether these sugars influence T-cell priming indirectly, such as by skewing DC cytokine production or antigen processing in a way that biases T-cell polarisation toward regulatory or Th2 phenotypes, as has been suggested in both *in vitro* and *in vivo* models. HMOs are complex glycans that require specific glycosidases for breakdown, and their uptake has been primarily observed in epithelial cells and phagocytic innate immune cells[4,324]. Without appropriate receptors or metabolic pathways, T-cells are unlikely to directly respond to HMOs in a manner that influences their metabolic or functional state.

Consistent with the observation made here that HMOs exert minimal direct effects on differentiated T-cells, most functional impacts reported *in vivo* appear to be APC-mediated rather than T-cell intrinsic. Xiao et al. (2018) demonstrated that 2′-FL enhances antigen-specific $CD4^+$ and $CD8^+$ responses following influenza vaccination[325], but this effect was attributed to improved DC priming rather than direct T-cell stimulation. Similarly, Xiao et al. (2019) demonstrated that pooled HMOs promote $FoxP3^+$ Treg differentiation only when DCs are present[299], not in isolated T-cell cultures. In a complementary study using human PBMCs, T-cells were activated via anti-CD3/CD28 stimulation in the presence of

individual HMOs for 24 hours. The different HMO structures induced distinct cytokine signatures, with some favouring Th1-type responses and others enhancing regulatory profiles. Although the model does not isolate DCs specifically, it supports the concept that HMOs can directly influence T-cell differentiation, reinforcing their role as structure-specific modulators of adaptive immunity[43]. Kang et al. (2020) reported that orally administered 3′-SL attenuated T-cell mediated pathology in atopic dermatitis by increasing Tregs and suppressing Th1/Th2/Th17 cytokines[326], again suggesting indirect metabolic or cytokine cues. Brosseau et al. (2025) further confirmed that gestational or dietary HMO exposure reshapes T-cell cytokine profiles *ex vivo*[327,328], but only within intact immune networks. Taken together, these studies reinforce the concept that while T-cell outcomes can be strongly influenced by HMOs *in vivo* and *ex vivo*, such effects likely arise from HMO-conditioned DCs or macrophages, supporting the conclusion that T-cells are responders rather than direct targets of HMO action.

This data suggests that HMOs do not directly modulate the metabolic activity of effector or memory $CD8^+$ T-cells. Rather, their immunological functions likely focus on shaping the innate immune population in early life, thereby fostering a protective mucosal environment and indirectly influencing adaptive immunity. These findings highlight the cell-type specificity of HMO action and the importance of studying immune networks both as integrated systems and in isolation. Evidence from existing studies on HMOs suggest that their immunological effects are more pronounced during the initial stages of immune activation[4], where macrophages and DCs play a dominant role in sensing and responding to environmental cues[329]. T-cells, as part of the adaptive immune system, are downstream effectors that rely on the activation of innate immune cells[330]. Therefore, the immunomodulatory capacity of HMOs may be mediated indirectly through APC-driven T-cell priming rather than direct interactions with T-cells. Therefore, the absence of PRRs, limited metabolic capacity, and the downstream role of T-cells in immune responses support the notion that HMOs are unlikely to exert direct effects on T-cells. Future studies focusing on the crosstalk between APCs and T-cells in response to HMO treatment will be essential to further elucidate the indirect pathways through which HMOs may modulate adaptive immune responses.

Taken together, our findings build a cohesive picture; HMOs can act as modulators of DC metabolism and function, reducing ROS, restraining inflammasome-driven IL-1β release, and enhancing IL-10 secretion. These effects collectively bias DCs toward a more anti-inflammatory phenotype, likely shaping downstream T-cell responses through altered antigen presentation and cytokine signalling. By contrast, T-cells themselves are insensitive to direct HMO modulation (Summary shown in **Figure 5.46**). The results support a model in which HMOs act primarily on the innate immune system, particularly APCs, to sculpt the downstream immunological effects of the infant. Rather than driving T-cell responses directly, HMOs appear to modulate the upstream cellular and metabolic context that determines how, and to what extent T-cells are engaged. This mode of action reflects an evolutionarily refined mechanism to balance immune protection and tolerance during a critical developmental window and suggests potential applications of HMOs or their analogues in immune modulation therapies targeting autoimmune, allergic, or inflammatory disorders.

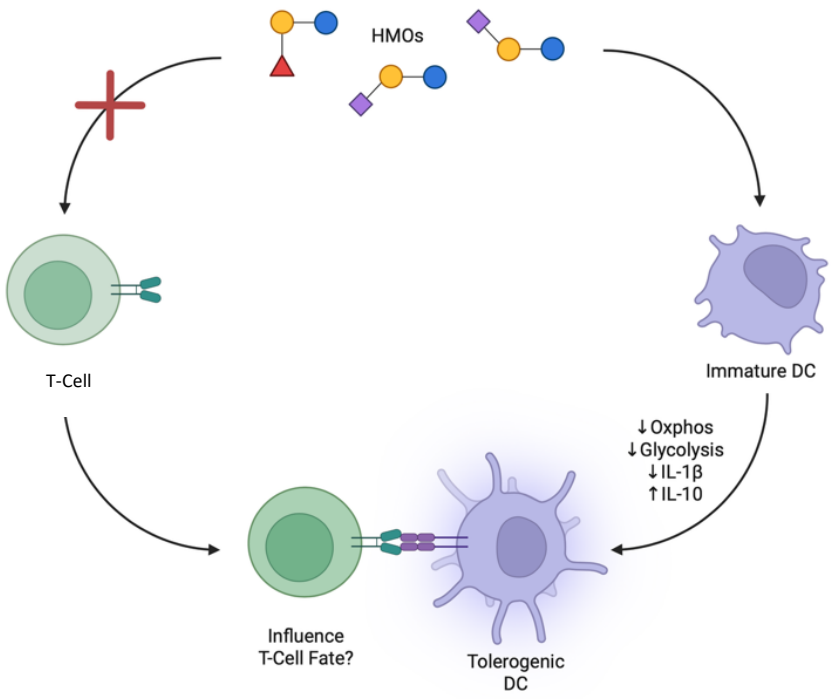

Figure 5. 46: **Overview of HMO-Mediated Metabolic Regulation in DCs and T-Cells**

Chapter 6

Heterologous Expression and Functional Evaluation of Glycosyltransferases for Human Milk Oligosaccharides Synthesis

6.1. Introduction

HMOs are highly diverse oligosaccharides that play crucial roles in infant nutrition, shaping gut microbiota composition and modulating immune system development[4]. While previous chapters of this thesis focused on the immunomodulatory effects of individual HMOs on macrophages, DCs, and T-cells, understanding these effects in a controlled experimental setting requires access to well-defined HMO structures. Naturally occurring HMOs are produced in the mammary gland through the sequential action of glycosyltransferases, a family of enzymes responsible for catalysing the transfer of monosaccharide units to specific acceptor molecules, thereby generating linear, branched, and terminally modified oligosaccharides. Glycosyltransferases are classified based on the type of linkage they catalyse and their donor/acceptor specificity. In HMO biosynthesis, β1,3- and β1,4-galactosyltransferases (B3GALT, B4GALT) extend the lactose core; β1,3-*N*-acetylglucosaminyltransferases (B3GNT) introduce GlcNAc residues that enable branching; fucosyltransferases (FUT) add fucose in α1,2-, α1,3-, or α1,4-linkages; and sialyltransferases (ST3GAL, ST6GAL, ST6GALNAC) terminate glycans with α2,3- or α2,6-linked sialic acids. The combinatorial activity of these enzymes gives rise to the remarkable structural diversity of HMOs. While more than 200 unique HMOs have been identified in human milk[331], the coordinated reconstitution of these pathways *in vitro* remains a significant technical challenge. Natural extraction is inefficient and chemical synthesis remains cost-prohibitive, necessitating the development of recombinant biosynthetic platforms for scalable HMO production.

The production of HMOs has most commonly been pursued through three primary strategies; chemical synthesis, enzymatic synthesis, and microbial fermentation. While each method has advanced the field, significant challenges remain in achieving scalable, cost-effective, and structurally diverse HMO biosynthesis resemblant of that in human milk. Chemical synthesis offers full control over structure but requires complex multi-step reactions, expensive starting materials, and yields that are often too low for commercial viability[332]. Enzymatic synthesis, using purified glycosyltransferases *in vitro*, has been used to generate select HMOs such as 2′-FL and 6′-SL[179]. While it can offer regio- and stereoselectivity, enzymatic production still relies on costly nucleotide-sugar donors (e.g., UDP-Gal, CMP-Sia) and lacks the scalability and efficiency of living systems. Microbial fermentation, particularly in engineered *E. coli* and *S. cerevisiae*, represents the most

widely adopted industrial approach[185]. These systems have been optimised to alter metabolic pathways and overexpress glycosyltransferases, enabling commercial-scale production of several HMOs. However, microbial systems often struggle with the generation of complex glycan structures, particularly those requiring precise human-like sialylation patterns.

Unlike microbial or enzymatic systems, mammalian cells naturally support human glycosylation pathways, including intracellular trafficking and post-translational modification machinery required for proper enzyme activity. By introducing multiple glycosyltransferases, this system questions whether expression of these enzymes enables cellular self-assembly of sialylated HMOs from lactose and supplemented UDP-sugars in a mammalian expression system. This strategy establishes a platform for producing defined HMOs *in vitro*, bridging the gap between enzymatic pathway knowledge and practical access to specific oligosaccharide structures. The generation of these molecules provides the foundation for future studies exploring HMO-mediated modulation of immune cell function, as detailed in previous chapters, and contributes to the broader goal of developing scalable, mammalian-based systems for HMO production. Some recent work has begun to push mammalian glycoengineering forward. For example, Jaroentomeechai et al. demonstrated that mammalian cells can be engineered to assemble glycans, glycopeptides, and glycomodules[333], providing a proof of concept for *in vitro* glycosylation pathway reconstruction. In non-HMO systems, co-expression of human sialyltransferases has enhanced glycosylation fidelity in recombinant proteins[334]. However, to date, no mammalian cell platform has been shown to autonomously synthesise defined sialylated HMOs from lactose and supplemented precursors, integrating extension, branching, and terminal modification.

This chapter addresses the construction of a mammalian cell-based platform for the production of HMOs through the coordinated expression of multiple glycosyltransferases. An initial pool of 15 candidate enzymes were screened for their predicted involvement in HMO branching, extension, and terminal sialylation. Through pathway mapping and literature-guided selection, a final panel of three key enzymes was chosen for plasmid-based expression. Attempts were made to subclone these enzymes into a single expression

plasmid and transfected into HEK293 cells to test whether the cells can self-assemble target HMOs from lactose and supplemented nucleotide sugars. In the native mammary epithelial Golgi apparatus, glycosyltransferases involved in HMO biosynthesis are spatially organised within a confined luminal environment, enabling sequential and cooperative enzymatic activity. This proximity facilitates efficient handover of intermediate glycan structures between enzymes, promoting elongation, branching, and terminal sialylation. By co-expressing multiple glycosyltransferases from a single construct, this work aimed to partially emulate such spatial and temporal coordination in a heterologous system, thereby increasing the likelihood of sequential glycosylation events leading to longer and more complex sialylated HMO structures, as predicted by the computational models. The outcome of these experiments establishes whether mammalian self-assembly of sialylated HMOs is feasible and lays groundwork for scalable, defined HMO production.

Aims of This Chapter:

- Identify and shortlist key glycosyltransferase enzymes based on their predicted role in HMO biosynthesis, focusing on enzymes required for lactose elongation and terminal sialylation, with the goal of synthesising sialylated HMOs and extended structures
- Clone and assemble the selected genes into a single expression plasmid, using restriction digest and Gibson Assembly techniques to generate a functional construct.
- Validate plasmid integrity and expression in mammalian cells, using HEK293 cells transfected with the construct and GFP as a reporter to assess transfection efficiency and expression levels.
- Establish a platform for cell-based HMO biosynthesis by preparing transfected cells for treatment with exogenous lactose and nucleotide sugar donors, enabling the synthesis of structurally related HMOs.

6.2. Methods

Plasmids

All original single glycosyltransferase expressing plasmids used were obtained from DNASU Plasmid Repository (Arizona State University). Samples were acquired as glycerol stocks in T1/T5 phage resistant DH5-α bacteria. The glycosyltransferases were expressed in the mammalian expression vector pGEn2-DEST with a CMV promoter and N-terminal 8xHis, AviTag, and Super GFP tags; ampicillin resistance in bacteria was used.

Bacterial Culture and Plasmid Preparation

Plasmid constructs were maintained in *E. coli* DH5α and streaked onto LB agar plates containing ampicillin at 100 μg/mL. Plates were incubated overnight at 37°C. A single colony was inoculated into 4 mL of LB broth containing ampicillin at 100ug/mL and cultured for 8-12 hours at 37 °C. Plasmid DNA was isolated from the bacterial culture using the Qiagen Spin Maxiprep Kit according to the manufacturer's instructions. DNA concentration and purity were assessed by Nanodrop spectrophotometry at 260/280 nm and 260/230 nm. Purified plasmids were either submitted to Eurofins Genomics for Whole Plasmid Sequencing (WPS) or used for downstream applications described below.

Transfection of HEK293 Cells

HEK293 cells were seeded in 24-well plates at 500,000 cells/well and allowed to rest overnight. The following day, for each well, 0.5 μg plasmid DNA was diluted in 50 μL Opti-MEM. Separately, 2 μL Lipofectamine 2000 was diluted in 50 μL Opti-MEM and incubated for 5 minutes at room temperature. DNA and Lipofectamine solutions were combined and incubated for 20 minutes to allow complex formation before being added dropwise to cells in 600 μL antibiotic-free DMEM. Cells were cultured for 36-48 hours before analysis.

For transfection efficiency assessment, plates of HEK293 cells transfected with plasmid were transferred to the Incucyte live-cell imaging system, and phase-contrast and fluorescence images were acquired every 2-4 hours for 48 hours for GFP quantification

Restriction Digest

Plasmid DNA (5 μg) was digested using FastDigest restriction enzymes (see **Table 2.6**) in 50 μL reactions containing 10x buffer and nuclease-free water. Reactions were incubated at 37 °C for 5-15 minutes as specified by supplier, followed by enzyme inactivation (65-80

°C for 5-10 minutes). Digestion products were quantified by Nanodrop and analysed by agarose gel electrophoresis.

Agarose Gel Electrophoresis and Gel Extraction

Unless otherwise stated, a 1 % agarose gel was prepared in 125 mL 1x TAE buffer with SYBR Safe (1:10 000). DNA samples mixed with 6x loading dye were loaded alongside a DNA ladder and run at 75V for 60-90 minutes. Gels were visualised under UV illumination. Bands of interest were excised and purified using the QIAquick Gel Extraction Kit (Qiagen), with DNA eluted in 30 µL Buffer EB and quantified by Nanodrop.

PCR Amplification of Inserts

PCR reactions were prepared using Q5 High-Fidelity 2x Master Mix (NEB) with 10 ng plasmid DNA, 0.5 µM primers, and nuclease-free water to 20 µL. No-template controls were included. Cycling conditions were as outlined in Chapter 2 Table 2.7. Products were verified by agarose gel electrophoresis described above and purified using the GeneJET PCR Purification Kit and QIAquick Gel Extraction Kit as per manufacturer's instructions.

Gibson Assembly

Vector backbone and inserts were combined at a 2:1 molar ratio in Gibson Master Mix (20 µL total reaction volume; 0.02–0.1 pmol DNA). Reactions were incubated at 50 °C for 60 minutes and stored on ice prior to transformation.

Transformation of *E. coli* DH5α

Chemically competent *E. coli* DH5α were thawed on ice, and 2 µL of Gibson reaction from above was added to 50 µL cells. After 30 minutes on ice, cells were heat-shocked at 42 °C for 30 seconds, returned to ice for 2 minutes, and rescued with 950 µL SOC medium for 60 minutes at 37 °C at 180rpm. 100uL was then plated on LB agar with 100 µg/mL ampicillin and incubated overnight. Colonies were picked into 5 mL LB + Ampicillin and grown for ~16 h before plasmid miniprep using Qiagen Miniprep kit. Gibson Assembly success was determined by performing a BamHI-EcoRI double digest as described above and being run on a 1% agarose gel also described above.

Cell-Based HMO Production

Following 36 hours of transfection, HEK293 cells expressing glycosyltransferase constructs were washed twice with pre-warmed PBS to remove residual FBS-derived lactose. Cells were then incubated in serum-free DMEM supplemented with 10 mM lactose

as an exogenous acceptor substrate. Control wells included non-transfected HEK293 cells treated with lactose and transfected cells without lactose. Cells were maintained for an additional 12 hours at 37°C, 5% CO_2. Conditioned media was analysed for HMO production by HPAEC-PAD

Glycosyltransferase Isolation

HEK293 cells transfected as above for 36-48 hours were harvested on ice by washing twice with PBS and scraping cells in 500uL of PBS. The cells were transferred to a 15mL falcon and pelleted at 5000×g for 5 minutes at 4°C. Pellets were resuspended in digitonin-based lysis buffer (described in Chapter 2) and incubated for 10 minutes. This cell lysis mix was transferred to a homogeniser where cells were homogenised 15-20 times. Lysates were transferred back into an eppendorf and clarified at 2000×g for 5 minutes, followed by 20 000×g for 30 minutes at 4°C. The supernatant was collected. Protein concentration was determined by Bradford assay. Heat-inactivated lysate (95°C, 10 minutes) or cells processed with no transfection served as negative control.

Glycosyltransferase Enzyme Assay

Reactions (100 µL) contained 50 mM HEPES pH 7.5 or 50 mM MES pH 6.5 or 5.5, 10 mM $MnCl_2$, 150 mM NaCl, 10% glycerol, 0.1% BSA, 1 mM DTT, 1 mM CMP-Neu5Ac, 1 mM UDP-Galactose and UDP-GlcNAc and 10 mM lactose. Cell supernatant (50µg) was added last. Controls lacking enzyme, donor, or acceptor were included. The reaction was left for 6 hours at 37°C and then processed for analysis via HPAEC-PAD

HPAEC-PAD Analysis

Oligosaccharides were analysed using a Thermo Dionex ICS-6000 (full method described in Chapter 2). Samples were clarified by centrifugation (8000×g, 5 minutes), filtered through 0.22 µM PVDF, diluted 1 in 100 in ultrapure water, and 5 µL injected. Oligosaccharides were quantified by peak area comparison to standards.

6.3. Validation of Glycosyltransferase Constructs for Heterologous Expression

An initial panel of 15 candidate glycosyltransferase genes, representing key enzymatic activities in glycan branching, elongation, and terminal sialylation, was assembled based on literature reports and biosynthetic pathway mapping. These included isoforms from the beta-1,3- and beta-1,4-galactosyltransferases (B3GALT, B4GALT), beta-1,3-*N*-acetylglucosaminyltransferases (B3GNT), beta-1,6-*N*-acetylglucosaminyltransferases (GCNT), fucosyltransferases (FUT), and alpha-2,3-, alpha-2,6-, and alpha-2,6-*N*-acetylgalactosaminide sialyltransferases (ST3GAL, ST6GAL, ST6GALNAC). To confirm the integrity and correct sequence of the glycosyltransferase constructs used in this study, WPS was performed on each plasmid. The resulting WPS maps verified the presence of the expected gene inserts, orientation, and sequence fidelity relative to reference sequences. Plasmid map for one of each family is shown (**Figure 6.1-6.8**). Each glycosyltransferase gene is present in a pGEN2-Dest vector which is a mammalian expression plasmid that supports multisite recombination, enabling insertion of several genes in a defined order under separate or shared promoters; it includes a strong CMV promoter for high expression, a selectable antibiotic resistance marker (ampicillin) for stable cell line generation, and 8xHistidine tag, Avi tag, GFP, and TEV cleavage site, making it suitable for coordinated co-expression of multiple glycosyltransferases in a single construct.

Sequencing of the plasmid containing B3GALT4 **(Figure 6.1**) demonstrated successful incorporation of the full-length coding sequence without mutations or truncations. Similarly, the plasmid containing B3GALT5 (**Figure not shown**) showed complete alignment with the reference sequence, confirming the correct construct assembly. The construct carrying B3GNT2 (**Figure 6.2**) was validated, with the sequencing results confirming accurate integration and no observed deviations from the expected sequence. Verification of B4GALT1 (**Figure not shown**) was validated against reference sequence. B4GALT3 presented as a double plasmid, with two vector backbones in one whole plasmid (**Figure not shown**). B4GALT4 (**Figure 6.3**) plasmid showed complete fidelity, confirming these galactosyltransferase genes were correctly cloned into their respective plasmid backbones.

The fucosyltransferase constructs were also validated. WPS results confirmed the correct sequence of the FUT2 (**Figure 6.4**), FUT3 (**Figure not shown**), and FUT4 (**Figure not shown**) plasmids, each showing no sequence alterations, deletions, or frameshifts.

The plasmid encoding GCNT3 (**Figure 6.5**) was verified, showing identical sequence identity to the expected gene and ensuring suitability for downstream functional studies.

Among the sialyltransferase family, sequencing confirmed the accuracy of constructs for ST3GAL1 **(Figure 6.6**), ST3GAL3 (**Figure not shown**), and ST6GAL1 (**Figure 6.7**), with each plasmid containing the full-length open reading frame in correct orientation. Validation was also achieved for ST6GALNAC3 (**Figure 6.8**) and ST6GALNAC6 (**Figure not shown**), confirming successful cloning and absence of mutations.

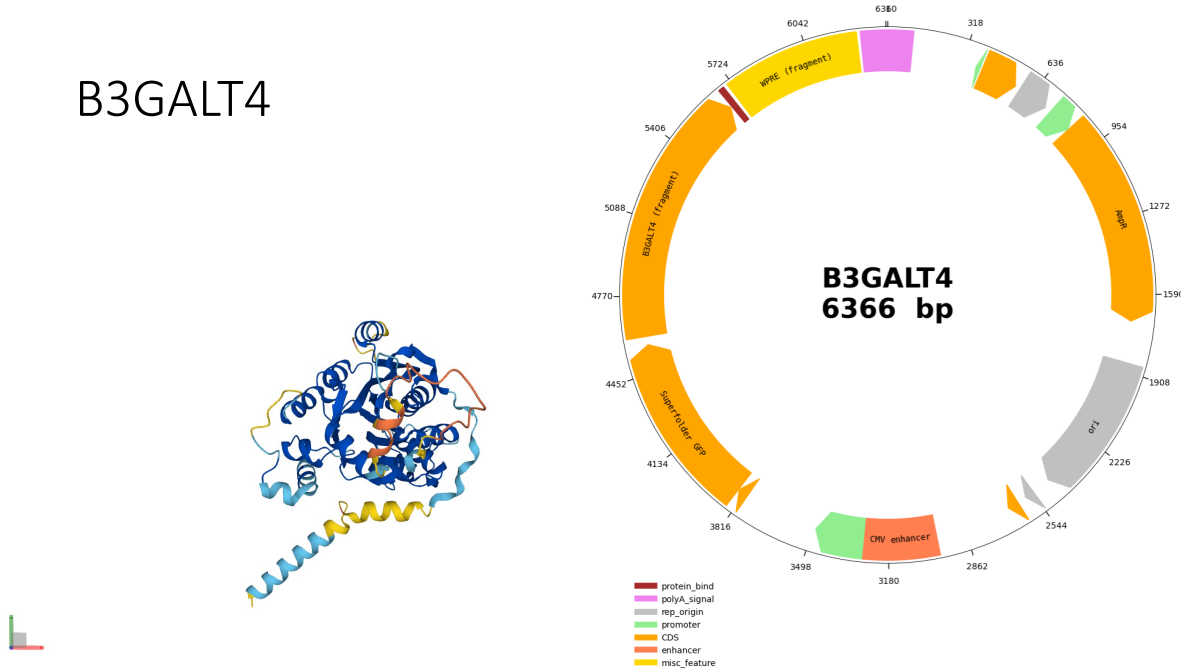

Figure 6. 1: **Plasmid Map Containing B3GALT4 gene**

The plasmid map depicts all annotated features, including the B3GALT4 gene (1059 bp), GFP reporter, AMP resistance gene, CMV promoter and enhancer, WPRE element, and other standard plasmid features. The total plasmid length is 6366 base pairs. The corresponding protein structure of B3GALT4 is shown, obtained from the Protein Data Bank (PDB).

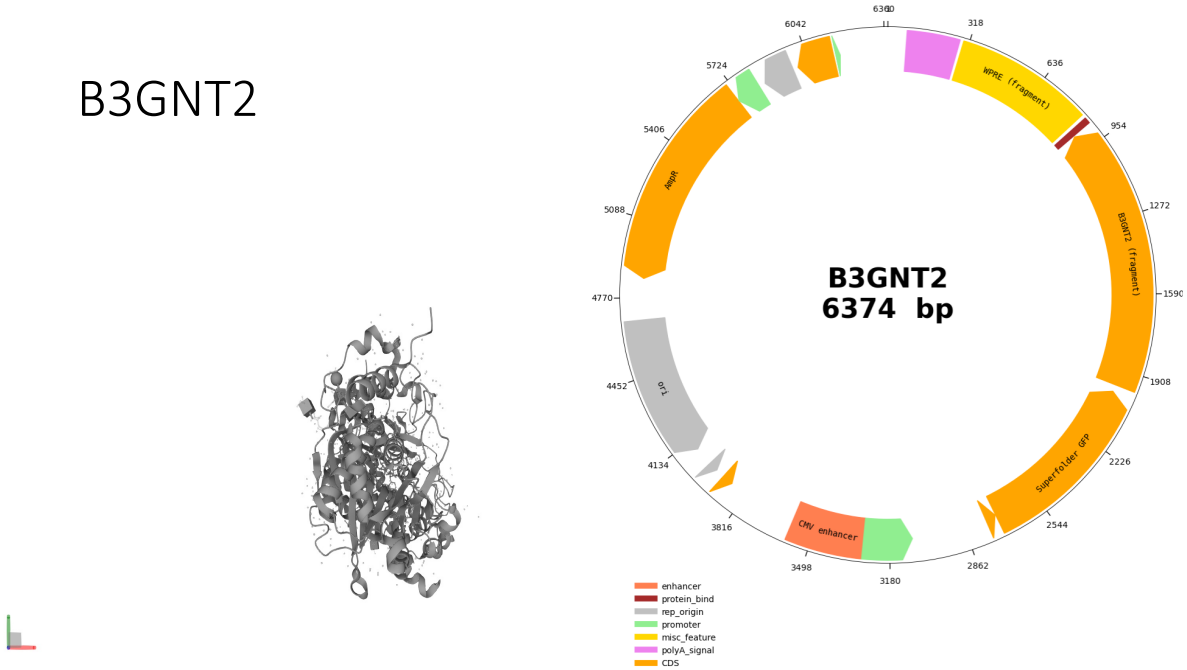

Figure 6. 2: **Plasmid Map Containing B3GNT2 gene**

The plasmid map depicts all annotated features, including the B3GNT2 gene (1089 bp), GFP reporter, AMP resistance gene, CMV promoter and enhancer, WPRE element, and other standard plasmid features. The total plasmid length is 6374 base pairs. The corresponding protein structure of B3GNT2 is shown, obtained from the PDB.

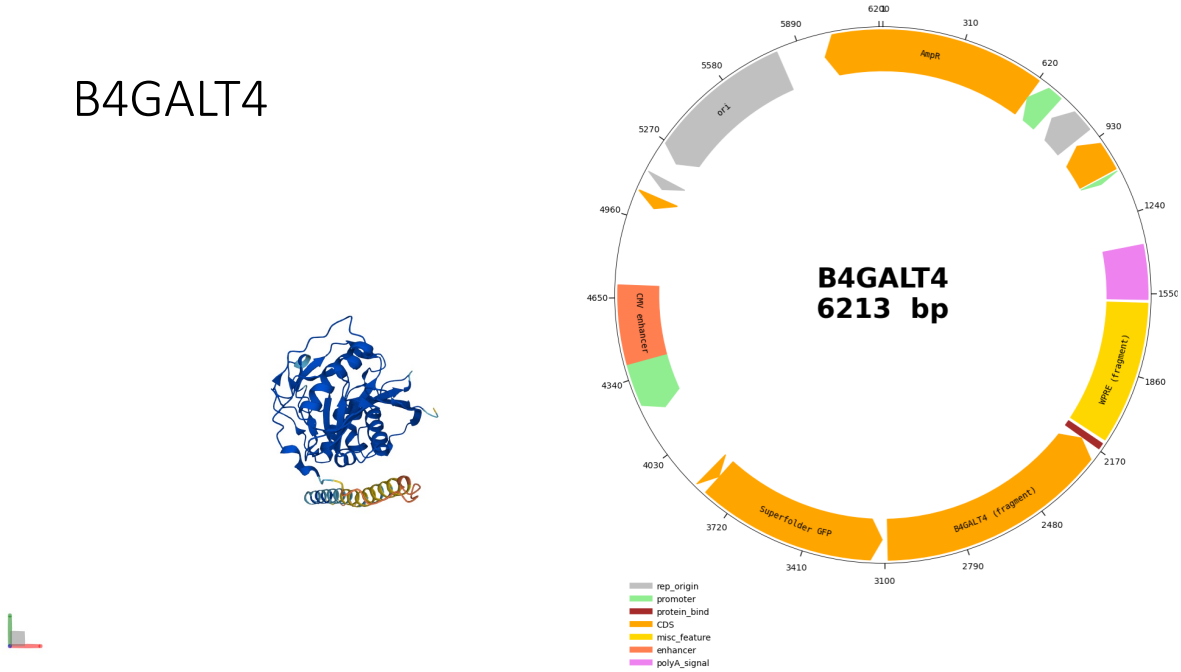

Figure 6. 3: **Plasmid Map Containing B4GALT4 gene**

The plasmid map depicts all annotated features, including the B4GALT4 gene (909 bp), GFP reporter, AMP resistance gene, CMV promoter and enhancer, WPRE element, and other standard plasmid features. The total plasmid length is 6213 base pairs. The corresponding protein structure of B4GALT4 is shown, obtained from the PDB.

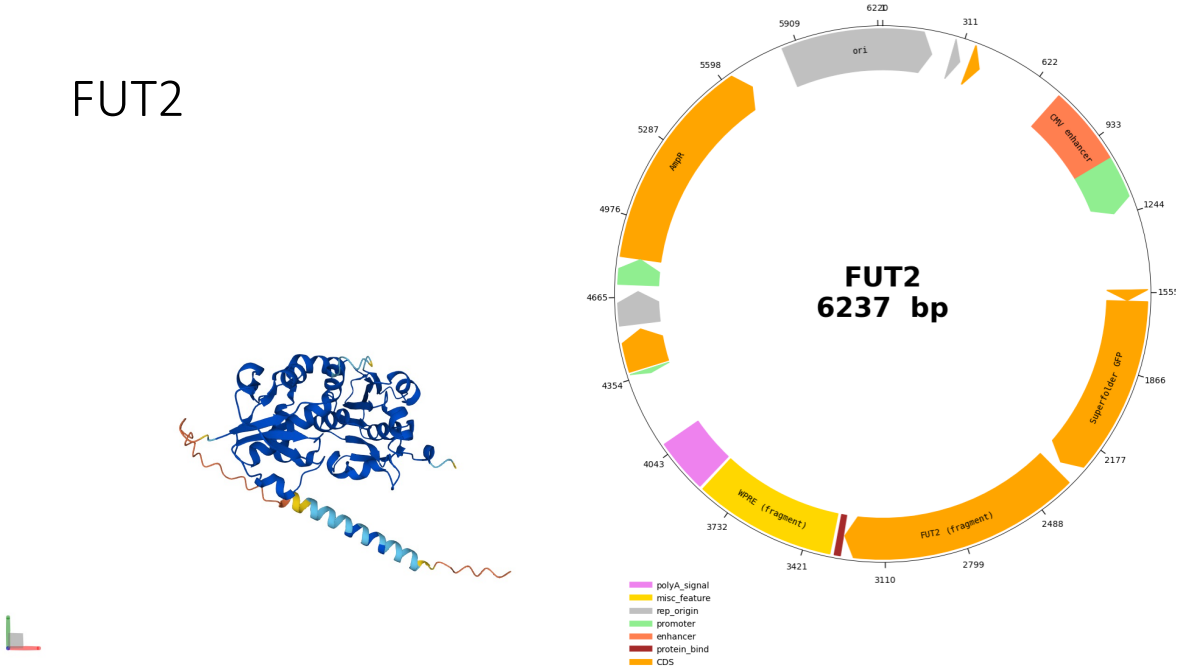

Figure 6. 4: **Plasmid Map Containing FUT2 gene**

The plasmid map depicts all annotated features, including the FUT2 gene (930 bp), GFP reporter, AMP resistance gene, CMV promoter and enhancer, WPRE element, and other standard plasmid features. The total plasmid length is 6237 base pairs. The corresponding protein structure of FUT2 is shown, obtained from the PDB.

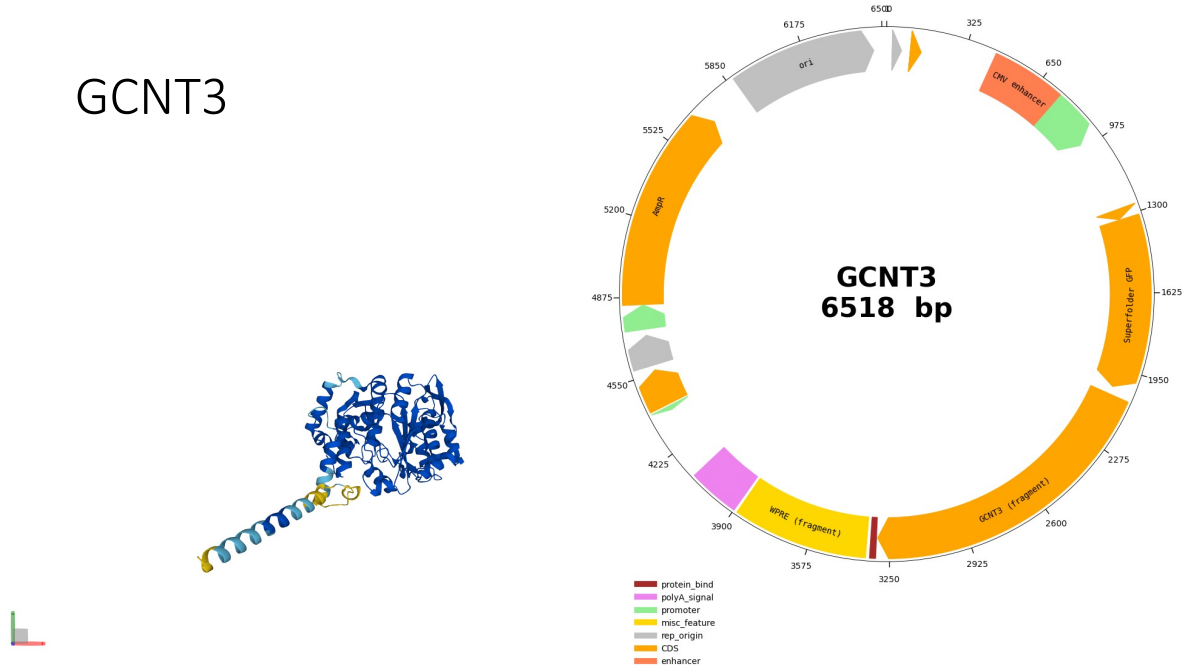

Figure 6. 5: **Plasmid Map Containing GCNT3 gene**

The plasmid map depicts all annotated features, including the GCNT3 gene (1233 bp), GFP reporter, AMP resistance gene, CMV promoter and enhancer, WPRE element, and other standard plasmid features. The total plasmid length is 6518 base pairs. The corresponding protein structure of GCNT3 is shown, obtained from the PDB.

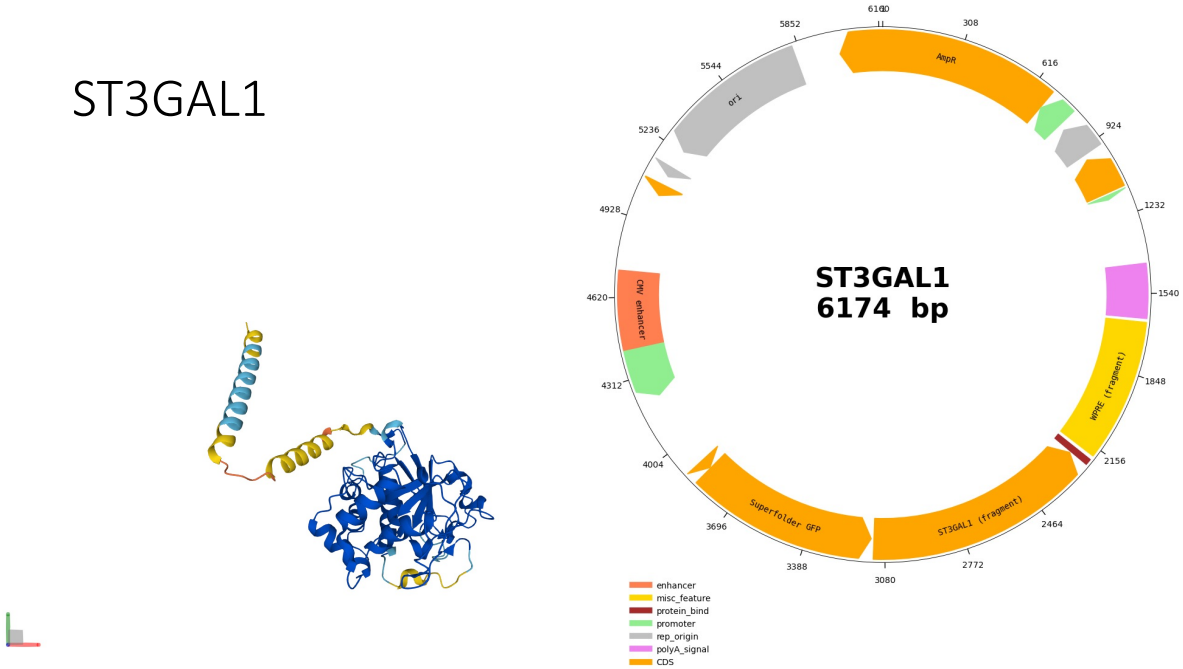

Figure 6. 6: **Plasmid Map Containing ST3GAL1 gene**

The plasmid map depicts all annotated features, including the ST3GAL1 gene (870 bp), GFP reporter, AMP resistance gene, CMV promoter and enhancer, WPRE element, and other standard plasmid features. The total plasmid length is 6174 base pairs. The corresponding protein structure of ST3GAL1 is shown, obtained from the PDB.

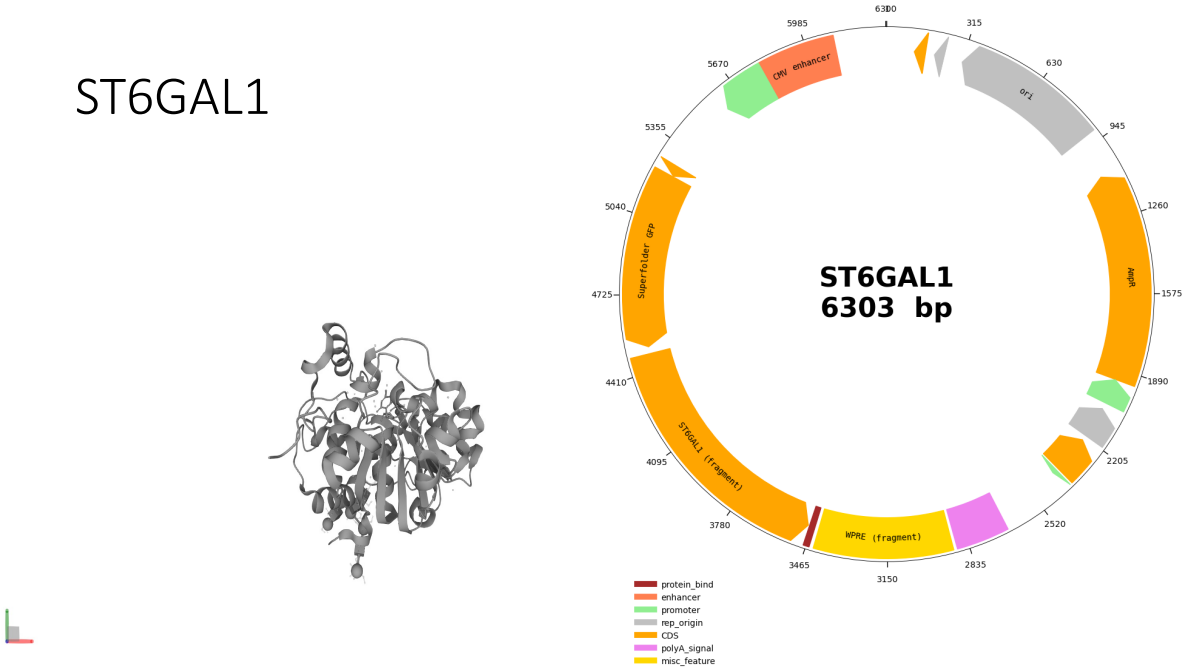

Figure 6. 7: **Plasmid Map Containing ST6GAL1 gene**

The plasmid map depicts all annotated features, including the ST6GAL1 gene (999 bp), GFP reporter, AMP resistance gene, CMV promoter and enhancer, WPRE element, and other standard plasmid features. The total plasmid length is 6303 base pairs. The corresponding protein structure of ST6GAL1 is shown, obtained from the PDB.

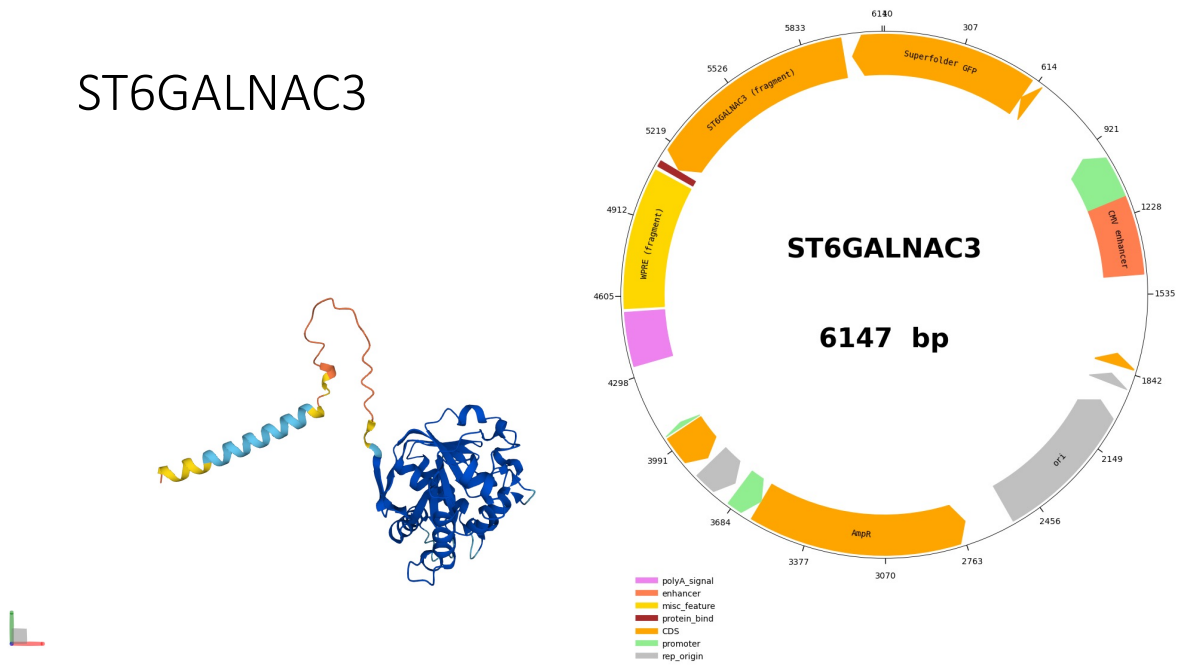

Figure 6. 8: **Plasmid Map Containing ST6GALNAC3 gene**

The plasmid map depicts all annotated features, including the ST6GALNAC3 gene (843 bp), GFP reporter, AMP resistance gene, CMV promoter and enhancer, WPRE element, and other standard plasmid features. The total plasmid length is 6147 base pairs. The corresponding protein structure of ST6GALNAC3 is shown, obtained from the PDB.

Table 6. 1: **Summary of WPS Data From Plasmids Expressing Human Glycosyltransferases**

Name	Base Pairs	GT Insert (base pairs)	Protein Length (amino acids)
B3GALT4	6366	1059	353
B3GALT5	6237	933	311
B3GNT2	6374	1089	363
B4GALT1	6315	1020	340
B4GALT3	DP	*	*
B4GALT4	6213	909	303
FUT2	6237	930	310
FUT3	6251	969	323
FUT4	6360	1056	352
GCNT3	6518	1233	411
ST3GAL1	6174	870	290
ST3GAL3	6216	912	304
ST6GAL1	6303	999	333
ST6GALNAC3	6147	843	281
ST6GALNAC6	6210	909	303

*Sequenced Plasmid B4GALT3 revealed plasmid contained two vector backbones - therefore could not decipher correct size of plasmid

6.4. Evaluation of Glycosyltransferase Expression in Heterologous Mammalian Systems

Given that HMOs are synthesised by MECs in vivo, initial transfection experiments were performed using a mammary epithelial cell line to provide a biologically relevant expression system. The MCF7 cell line was selected for this purpose; however, its use proved impractical for systematic optimisation due to low and inconsistent transfection efficiency. In addition, the requirement for extensive media supplementation and the characteristically slow growth rate of MCF7 cells rendered this system costly and time-inefficient for iterative transfection and expression analyses. As a result, subsequent optimisation focused on more permissive mammalian cell lines (HeLas and HEK293s) with established high transfection efficiency.

Following sequence validation of the glycosyltransferase plasmids, optimisation of transfection efficiency was performed using GFP-tagged constructs as reporters. Transfection efficiency was first tested in HeLa cells using the FUT2 plasmid as a GFP-reporter construct. While some GFP signal was detectable (**Figure 6.9**), overall expression was low and inconsistent across the cell population. This indicated that HeLa cells were suboptimal for our experimental requirements, prompting a switch to HEK293 cells, which are widely used for high-efficiency plasmid expression (**Figure 6.10**). To refine conditions for downstream experiments, a timecourse optimisation was carried out in HEK293 cells using the FUT2 plasmid. GFP expression was monitored over a 48 hour period (**Figures 6.11-6.15**). Cells imaged immediately after transfection (0 hours) showed no detectable GFP signal (**Figure 6.11**). By 12 hours post-transfection, GFP expression was observed (**Figure 6.12**). Fluorescence intensity increased markedly, reaching high expression at 24 hours (**Figure 6.13**), with a peak signal at 36 hours (**Figure 6.14**). By 48 hours post-transfection, GFP levels declined, suggesting transient expression consistent with plasmid-based transfection (**Figure 6.15**). These results confirmed that the plasmids could be introduced into mammalian cells and that GFP provided a reliable readout of transfection efficiency. In addition to this, comparative analysis of different constructs revealed variability in transfection efficiency, with GFP-positive cells ranging across plasmids (**Figure 6.16**). To confirm these observations quantitatively, flow cytometry was performed on HEK293 cells transfected with GFP-tagged constructs. The results validated that a substantial proportion of the cell population expressed GFP, consistent with

successful plasmid delivery (**Figure 6.17**). GFP fluorescence detected by flow cytometry in transfected cells confirmed successful intracellular expression of the GFP-fusion protein.

Together, these findings established HEK293 cells as a suitable model for plasmid expression studies. The timecourse analysis provided an optimal window, between 24 and 36 hours post-transfection, for assessing transgene expression before plasmid-driven GFP expression began to decline. This optimisation was critical for ensuring reproducibility in subsequent assays involving glycosyltransferase expression.

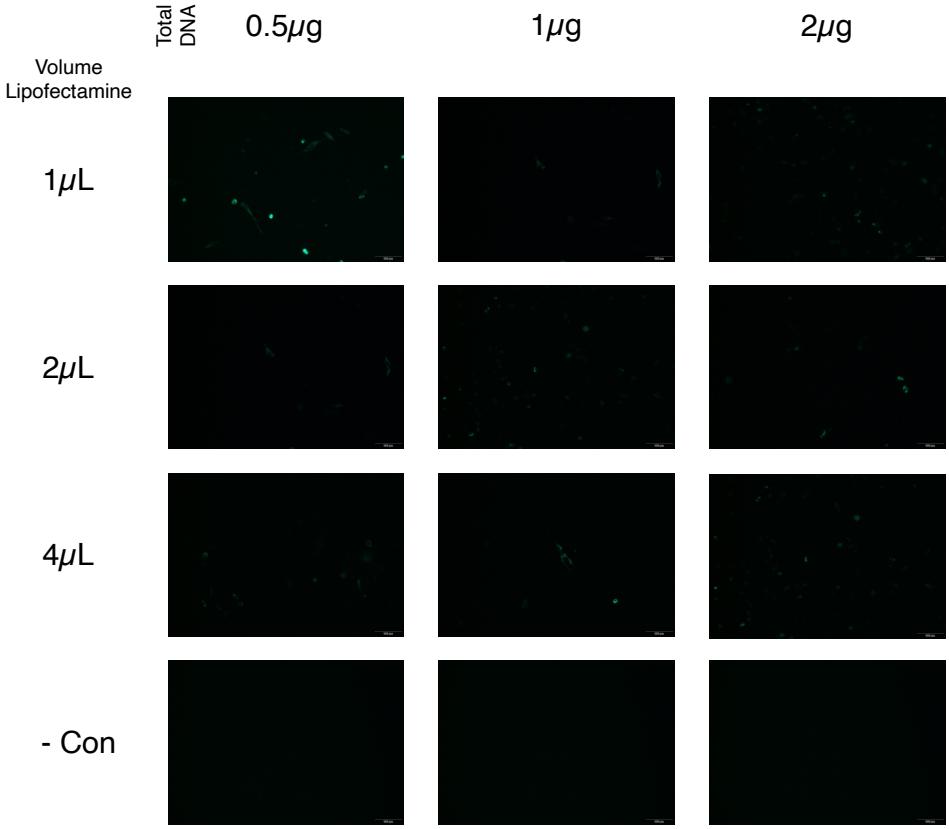

Figure 6. 9: **GFP-Based Transfection Optimisation in HeLa Cells using FUT2 Plasmid**

HeLa cells were transfected with 0.5, 1, or 2 µg of FUT2 plasmid DNA using 1, 2, or 4 µL of Lipofectamine 2000, respectively. Following transfection, plates were transferred to the Sartorius IncuCyte live-cell imaging system, and green channel fluorescence was monitored for 12 hours to assess GFP expression.

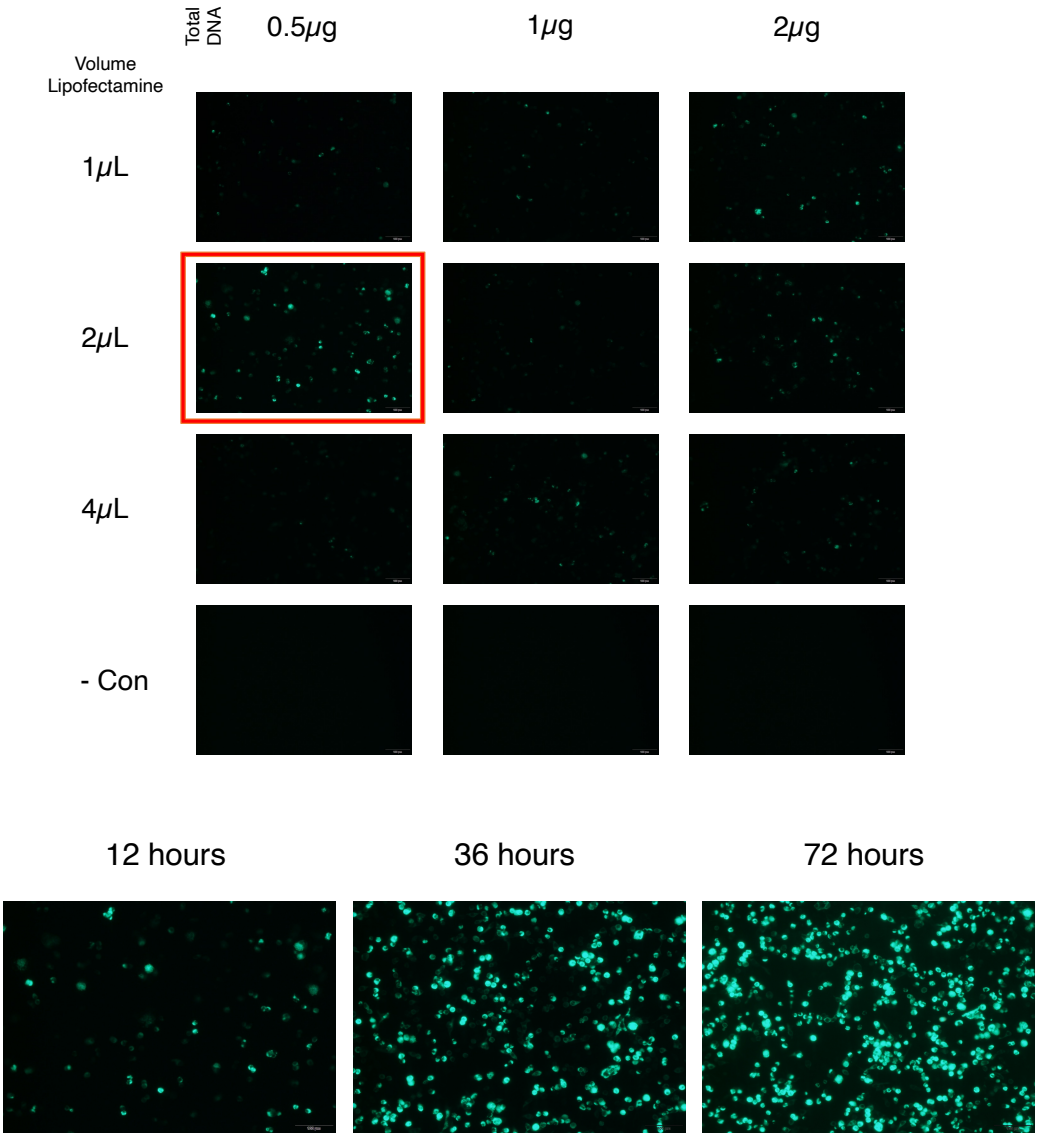

Figure 6. 10**: Timecourse and GFP-Based Transfection Optimisation in HEK293 Cells using FUT2 Plasmid**

HEK293 cells were transfected with 0.5, 1, or 2 µg of FUT2 plasmid DNA using 1, 2, or 4 µL of Lipofectamine 2000, respectively. Following transfection, plates were transferred to the Sartorius IncuCyte live-cell imaging system, and green channel fluorescence was monitored for 12 hours to assess GFP expression. For further imaging, the condition of 0.5 µg DNA with 2 µL Lipofectamine 2000 was selected, with GFP monitored for 36 and 72 hours post-transfection.

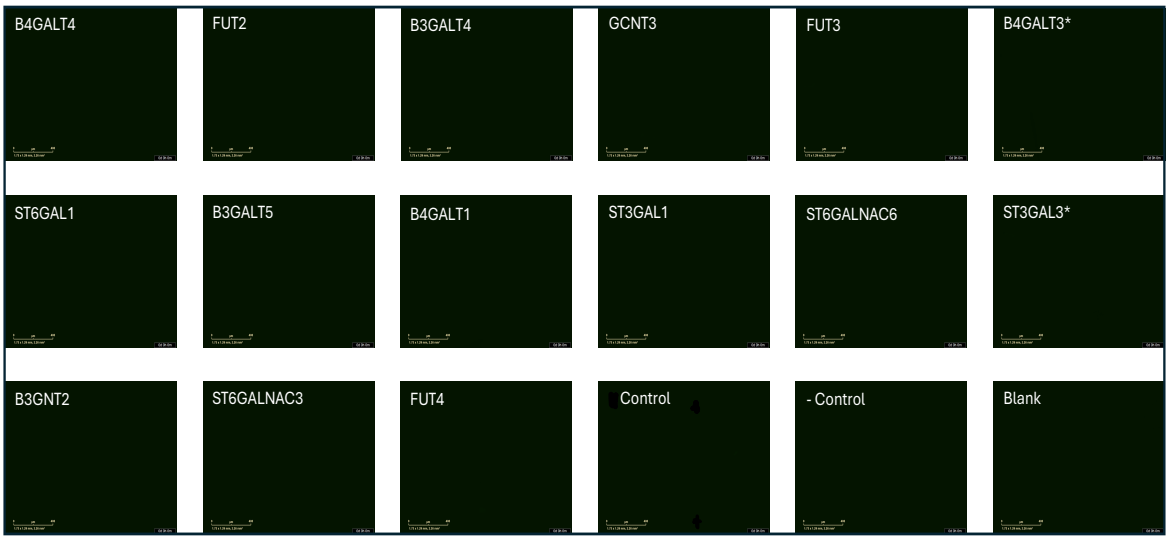

Figure 6. 11: **HEK293 cells imaged at 0 hours post-transfection with glycosyltransferase expressing plasmid**

HEK293 cells were transfected with 0.5 µg of each separate plasmid DNA and 2 µL Lipofectamine 2000. Following transfection, plates were transferred to the Sartorius IncuCyte live-cell imaging system, and green channel fluorescence was measured immediately (0 hours, 0 minutes) to establish the baseline signal.

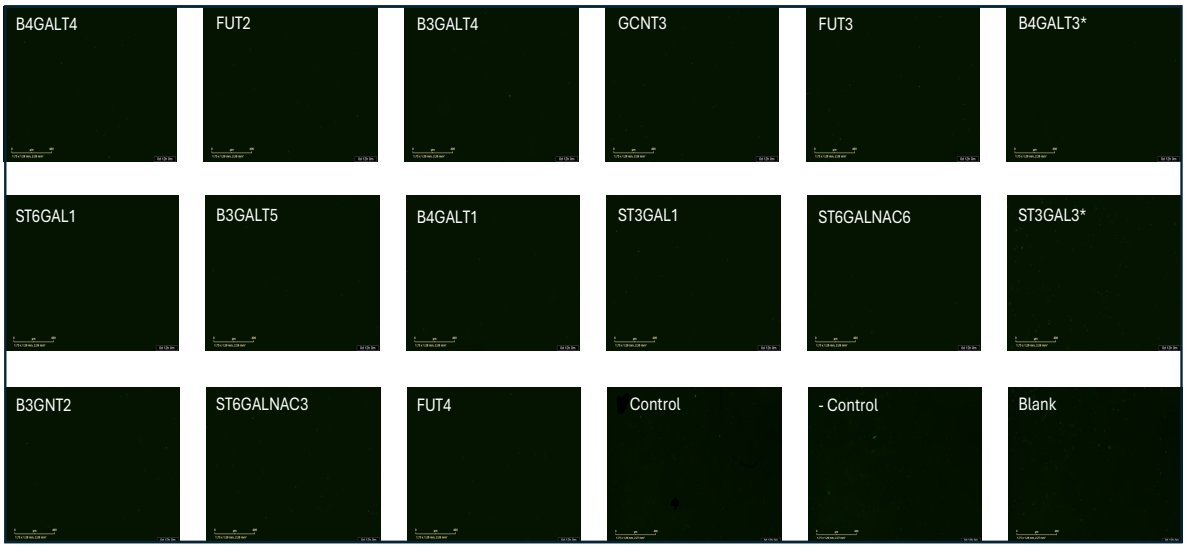

Figure 6. 12: **HEK293 cells imaged at 12 hours post-transfection with glycosyltransferase expressing plasmid**

HEK293 cells were transfected with 0.5 µg of each separate plasmid DNA and 2 µL Lipofectamine 2000. Following transfection, plates were transferred to the Sartorius IncuCyte live-cell imaging system, and green channel fluorescence was measured after 12 hours to analyse GFP expression.

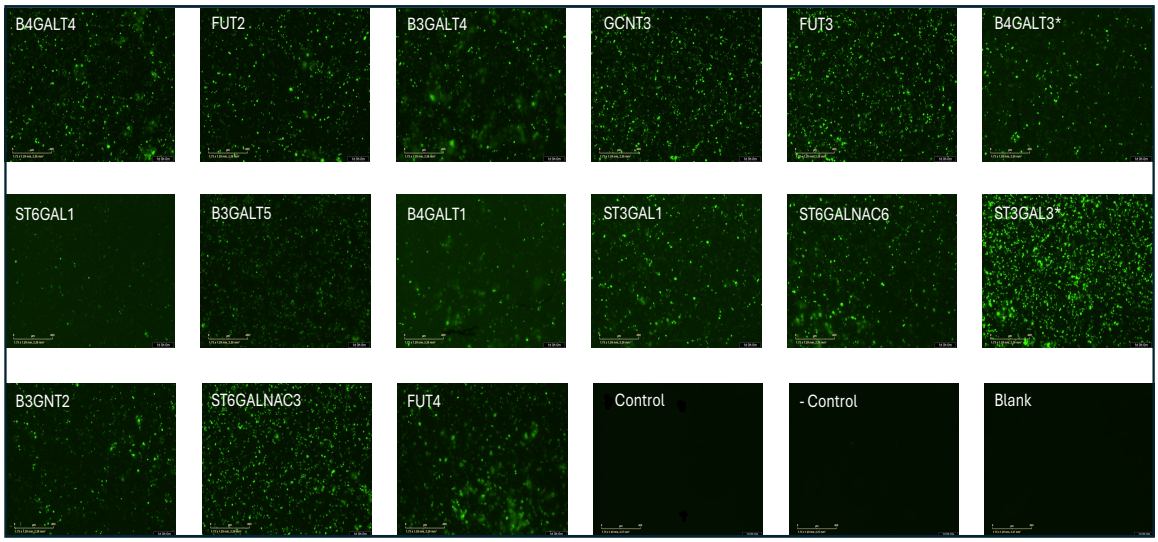

Figure 6. 13: **HEK293 cells imaged at 24 hours post-transfection with glycosyltransferase expressing plasmid**

HEK293 cells were transfected with 0.5 µg of each separate plasmid DNA and 2 µL Lipofectamine 2000. Following transfection, plates were transferred to the Sartorius IncuCyte live-cell imaging system, and green channel fluorescence was measured after 24 hours to analyse GFP expression.

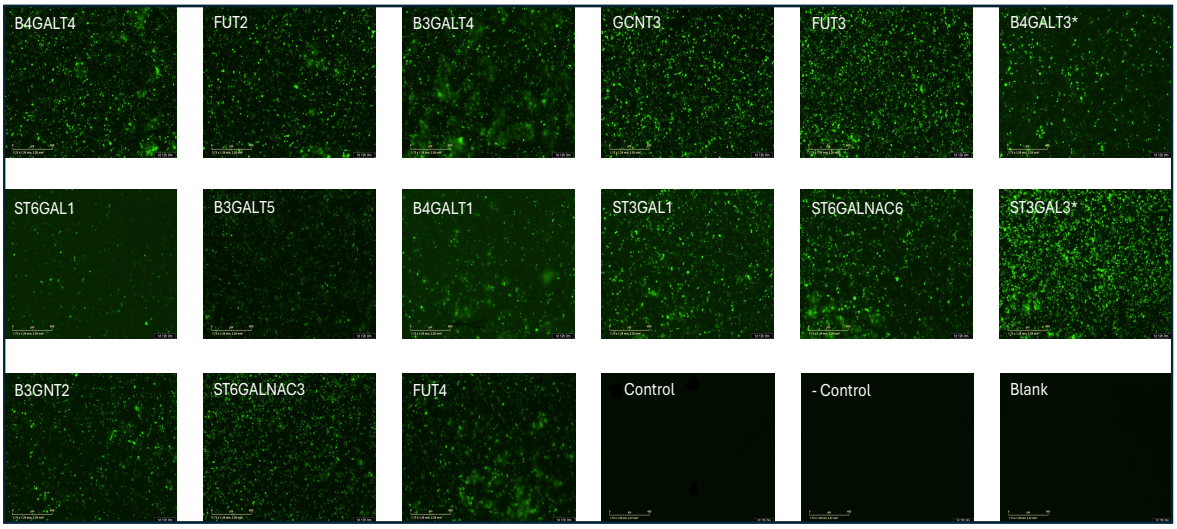

Figure 6. 14: **HEK293 cells imaged at 36 hours post-transfection with glycosyltransferase expressing plasmid**

HEK293 cells were transfected with 0.5 µg of each separate plasmid DNA and 2 µL Lipofectamine 2000. Following transfection, plates were transferred to the Sartorius IncuCyte live-cell imaging system, and green channel fluorescence was measured after 36 hours to analyse GFP expression.

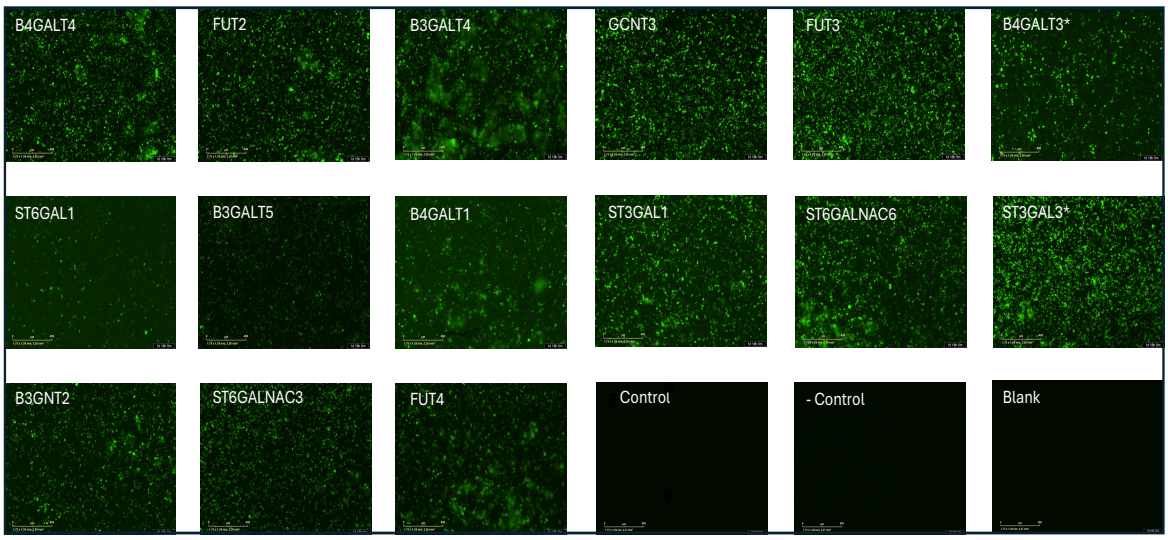

Figure 6. 15: **HEK293 cells imaged at 48 hours post-transfection with glycosyltransferase expressing plasmid**

HEK293 cells were transfected with 0.5 µg of each separate plasmid DNA and 2 µL Lipofectamine 2000. Following transfection, plates were transferred to the Sartorius IncuCyte live-cell imaging system, and green channel fluorescence was measured after 48 hours to analyse GFP expression.

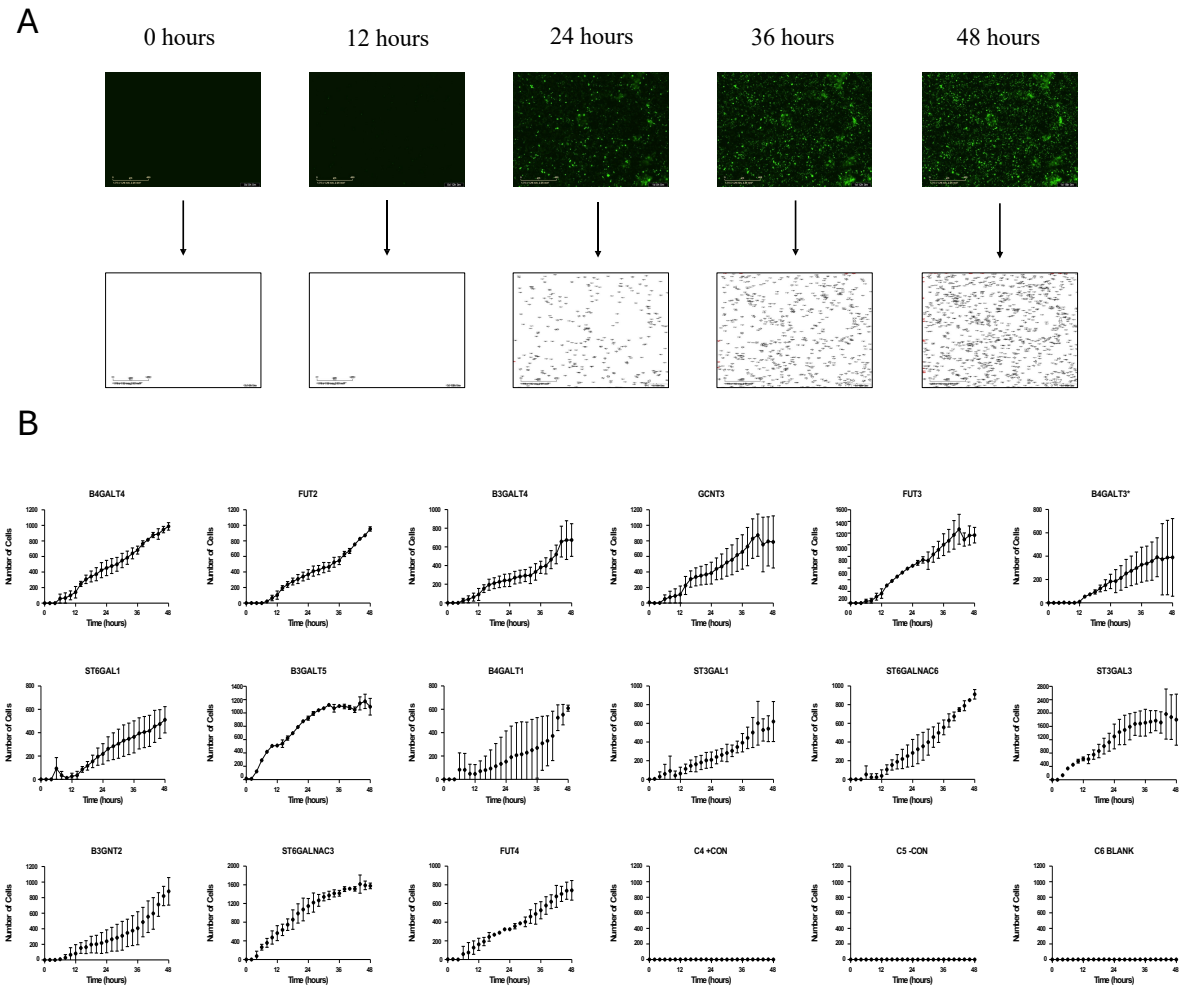

Figure 6. 16: **Quantification of GFP-Positive HEK293 Cells Across Constructs**

All imaging data from IncuCyte live-cell monitoring of GFP expression were exported to ImageJ for analysis. (A) B4GALT4 example timecourse to show how cell size parameter was defined to enable automated counting of GFP-positive cells in each field of view. (B) The number of GFP-expressing cells per plasmid construct was quantified at each hourly timepoint, and values were plotted to generate expression profiles over time.

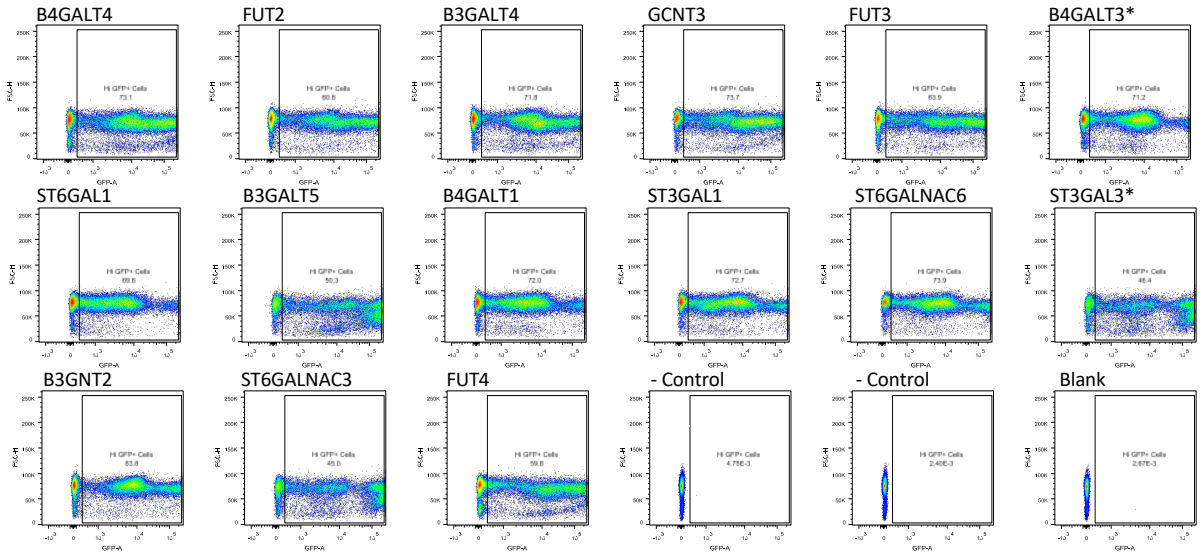

Figure 6. 17: **Flow Cytometry Analysis Confirming GFP Expression in Transfected HEK293 Cells**

HEK293 cells transiently transfected with plasmids encoding individual glycosyltransferases fused to GFP 48 hours post-transfection analysed by flow cytometry to assess GFP expression. Histograms show the distribution of GFP-positive cells for each glycosyltransferase, confirming successful transfection and expression across the panel.

6.5. Preparation of Glycosyltransferase Gene Fragments for Construct Assembly

To enable subcloning of validated glycosyltransferase genes, restriction enzyme digests were determined for each plasmid to isolate both the gene insert and its corresponding backbone. The restriction enzyme pairs selected for each construct are listed in **Table 6.2**. Most constructs employed an EcoRI-BamHI double digest, while others required alternative combinations such as EcoRI-Van91I (FUT2, GCNT3), EcoRI-PfoI (FUT3), or Bpu1102I-BamHI (B4GALT3, ST3GAL3). These tailored restriction strategies were chosen based on the unique multiple cloning site configurations of each vector.

Following digestion, agarose gel electrophoresis was performed to assess successful separation of plasmid backbones from gene inserts. Clear band patterns consistent with the predicted sizes were observed for the majority of constructs (**Figure 6.18**). The intensity and resolution of the bands indicated efficient digestion and liberation of the intended inserts.

To further validate the isolated inserts, the insert bands were excised from the gel and subjected to gel extraction, ensuring clean isolation of the glycosyltransferase inserts from the backbone fragments. These excised fragments were re-run on agarose gels for confirmation (**Figure 6.19**). Distinct bands at the expected molecular weights for each glycosyltransferase insert were detected, confirming the accuracy of the restriction digest and gel extraction strategy. These results verified that all constructs could be processed to yield clean inserts suitable for downstream cloning and expression experiments.

Table 6. 2: **Restriction Enzyme Pairs Used for Insert and Backbone Isolation**

No.	Plasmid Gene Insert	1st Restriction	2nd Restriction
1	B4GALT4	EcoRI	BamHI
2	FUT2	EcoRI	Van91I
3	B3GALT4	EcoRI	BamHI
4	GCNT3	EcoRI	Van91I
5	FUT3	EcoRI	PfoI
6	B4GALT3	Bpu1102I	BamHI
7	ST6GAL1	EcoRI	BamHI
8	B3GALT5	Bpu10I	BamHI
9	B4GALT1	EcoRI	BamHI
10	ST3GAL1	EcoRI	BamHI
11	ST6GALNAC6	EcoRI	BamHI
12	ST3GAL3	Bpu1102I	BamHI
13	B3GNT2	EcoRI	BamHI
14	ST6GALNAC3	EcoRI	BamHI
15	FUT4	EcoRI	BamHI

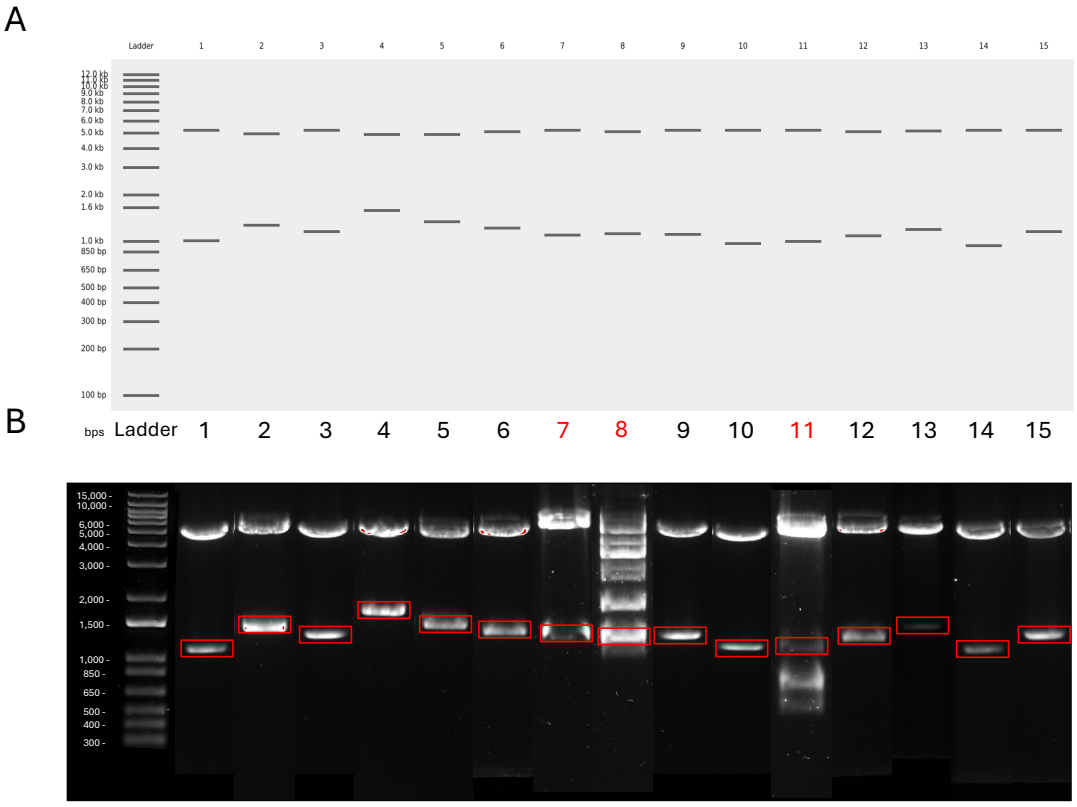

Figure 6. 18: ***In Silico*** **and Actual Agarose Gel of Double-Digested Plasmids Showing Insert and Backbone Separation**

(A) *In silico* prediction of restriction digest products showing separation of gene inserts from plasmid backbones. (B) 1% agarose gel electrophoresis of double-digested plasmids (100 µg DNA loaded per well) using restriction enzyme pairs listed in **Table 6.2**. with the correctly sized glycosyltransferase gene inserts highlighted in red boxes for each of the 15 plasmids

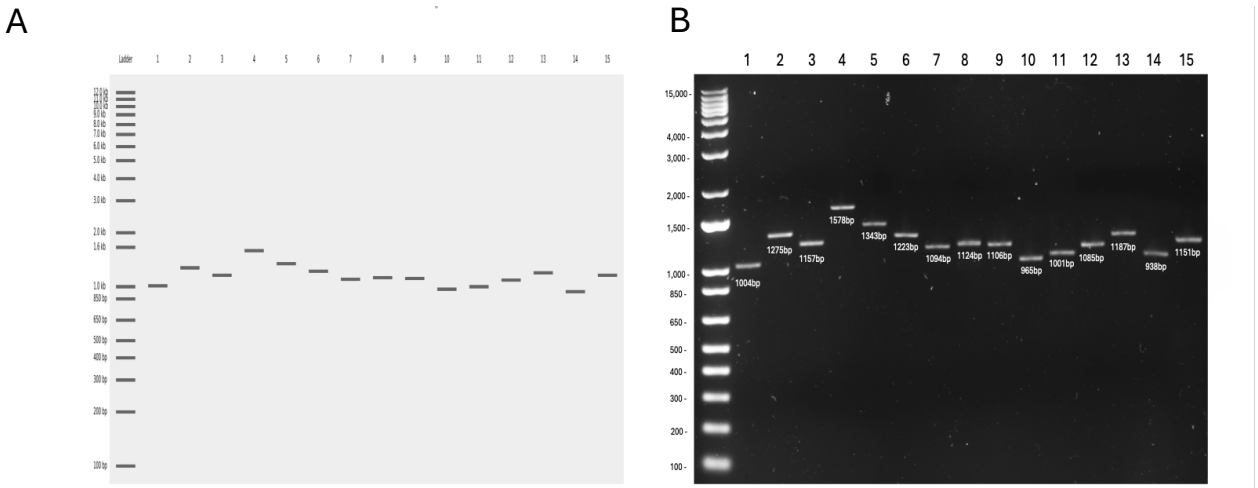

Figure 6. 19: ***In Silico*** **prediction and Confirmation of Extracted Glycosyltransferase Inserts via Agarose Gel Electrophoresis**

Inserts were excised and purified by gel extraction. Products were run on a 2% agarose gel to verify correct size and isolation. (A) *In silico* prediction of expected fragment sizes. (B) Experimental gel image of purified inserts. Lanes 1-15 represent glycosyltransferase inserts undergone restriction digest (as per **Table 6.2**) and gel purification.

6.6. *In Silico* Modelling of HMO Biosynthesis

To complement the cloning and restriction validation of glycosyltransferase constructs, O-Glycologue modelling was used to predict the potential HMO structures generated by selected enzyme combinations using lactose as the starting acceptor molecule.

When B4GALT4, B3GNT2, and ST3GAL1 were modelled together, the predicted pathways generated extended lacto-series oligosaccharides with additional galactosyl and *N*-acetylglucosaminyl residues, alongside sialylated derivatives (**Figure 6.20 A**). These results aligned with the known enzymatic functions of B4GALT4 (β1,4-galactosylation), B3GNT2 (β1,3-*N*-acetylglucosaminylation), and ST3GAL1 (α2,3-sialylation), confirming that their coordinated activity could yield complex, branched HMOs. A separate simulation with B4GALT4, B3GNT2, and ST6GAL1 produced an alternative panel of structures (**Figure 6.20 B**). In this case, the incorporation of ST6GAL1 shifted the pathway toward α2,6-linked sialylated species, generating distinct HMO variants compared to the ST3GAL1-containing set.

The combined modelling outputs were visualised as predicted biosynthetic pathways (**Figure 6.21**). These pathway maps illustrated how different glycosyltransferase pairings drive specific structural outcomes, highlighting the importance of enzyme selection in tailoring HMO synthesis.

Figure 6. 20: **O-Glycologue predictions of HMO structures generated by B4GALT4, B3GNT2, and ST3GAL1 or ST6GAL1 using lactose as a starter molecule**

HMO structures were simulated i*n silico* using the O-Glycologue enzyme simulator with lactose as the starting substrate. (A) Enzyme activities for B4GALT4, B3GNT2, and ST3GAL1 were selected. (B) Enzyme activities for B4GALT4, B3GNT2, and ST6GAL1 were selected. The simulator iteratively generated product structures over multiple reaction cycles, following the parameters set within the O-Glycologue platform. Resulting structures represent predicted HMOs formed under the defined enzyme set.

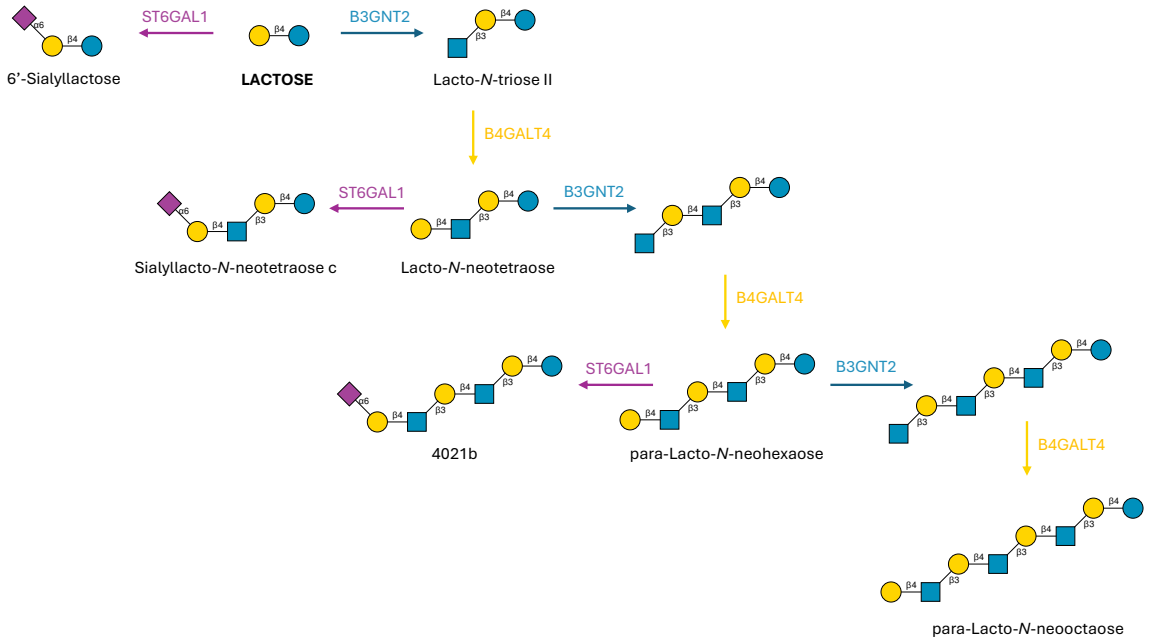

Figure 6. 21: **HMO structures produced by B4GALT4, B3GNT2 and ST6GAL1 using Lactose as starting molecule**

Diagram illustrating sequential actions of B4GALT4, B3GNT2, and ST6GAL1 on lactose as the starting molecule. Each enzyme is shown acting on the growing glycan chain to generate specific intermediates, which in turn serve as substrates for subsequent glycosyltransferase activities. Pathway arrows indicate the order of enzymatic reactions predicted by the O-Glycologue model.

6.7. Assembly of Multigene Glycosyltransferase Constructs

To generate a plasmid containing ST6GAL1, B3GNT2, and B4GALT4, gene fragments were amplified with primers specifically designed to include overlapping sequences for Gibson Assembly. Each primer incorporated 20-25 bp overhangs complementary to adjacent fragments, allowing precise ligation. Additionally, the primers included Glycine-Serine (G4S) linker sequences to provide flexible peptide linkers between the genes, ensuring proper folding and functional independence of the expressed proteins.

Initial attempts to amplify ST6GAL1, B3GNT2, and B4GALT4 directly from intact plasmid templates using Gibson-compatible primers were unsuccessful, with no specific amplification observed despite optimisation of PCR conditions. This was likely due to plasmid size, secondary structure, or primer accessibility constraints. Consequently, a restriction digestion and gel excision strategy was adopted to isolate individual gene fragments, which were then used as templates for reliable PCR amplification.

PCR products were first validated by comparison with *in silico* predictions. The ST6GAL1 plasmid was linearised using EcoRI (**Figure 6.22**), while B4GALT4 and B3GNT2 were excised as individual inserts following double digestion with EcoRI and BamHI (**Figures 6.23 and 6.24**). These isolated fragments were subsequently used as templates for PCR amplification, employing primers designed to introduce overhangs complementary to adjacent fragments. The predicted and observed fragment sizes were consistent across all three genes (**Figure 6.25**). Primer sequences and expected product lengths are summarised in Table 6.3 and **Figure 6.26**. The corresponding plasmids were linearised or digested to isolate gene fragments for assembly. Amplification of B4GALT4 (961 bp) and B3GNT2 (1139 bp) was optimised using temperature gradient PCR (**Figures 6.27 and 6.28**).

A Gibson Assembly strategy was then employed to join the three fragments via their designed overhangs and G4S linkers (summarised in **Figure 6.29**). Following assembly, the recombinant plasmid was transformed into DH5α *E. coli*. Since the plasmid contains an ampicillin resistance (AmpR) gene, transformed cells were first streaked on LB agar containing ampicillin to select for colonies containing intact plasmid (summarised in **Figure 6.30**). The final plasmid map predicted integration of ST6GAL1, B3GNT2, and B4GALT4 in the expected configuration (**Figure 6.31**). Colonies were subsequently screened for the presence of the construct. Plasmid minipreps were performed from individual colonies, and the results revealed that the final product did not

contain ST6GAL1-B3GNT2-B4GALT4 in a single vector and only ST6GAL1-B3GNT2 was transformed into the vector. This result was visualised on gel to confirm insert integrity (**Figure 6.32**) and sent for sequencing confirmation (**Figure 6.33**).

Transfection of HEK293 cells with plasmids encoding dual glycosyltransferase inserts resulted in detectable expression of the fluorescent reporter, confirming successful plasmid uptake (**Figure 6.34**). Fluorescence microscopy revealed clear GFP signal in transfected cells, whereas no fluorescence was observed in non-transfected controls. To quantify transfection efficiency, GFP-positive cells were measured by flow cytometry and gated relative to the non-transfected population. A distinct GFP^+ population was observed in transfected samples, indicating effective plasmid delivery and reporter expression.

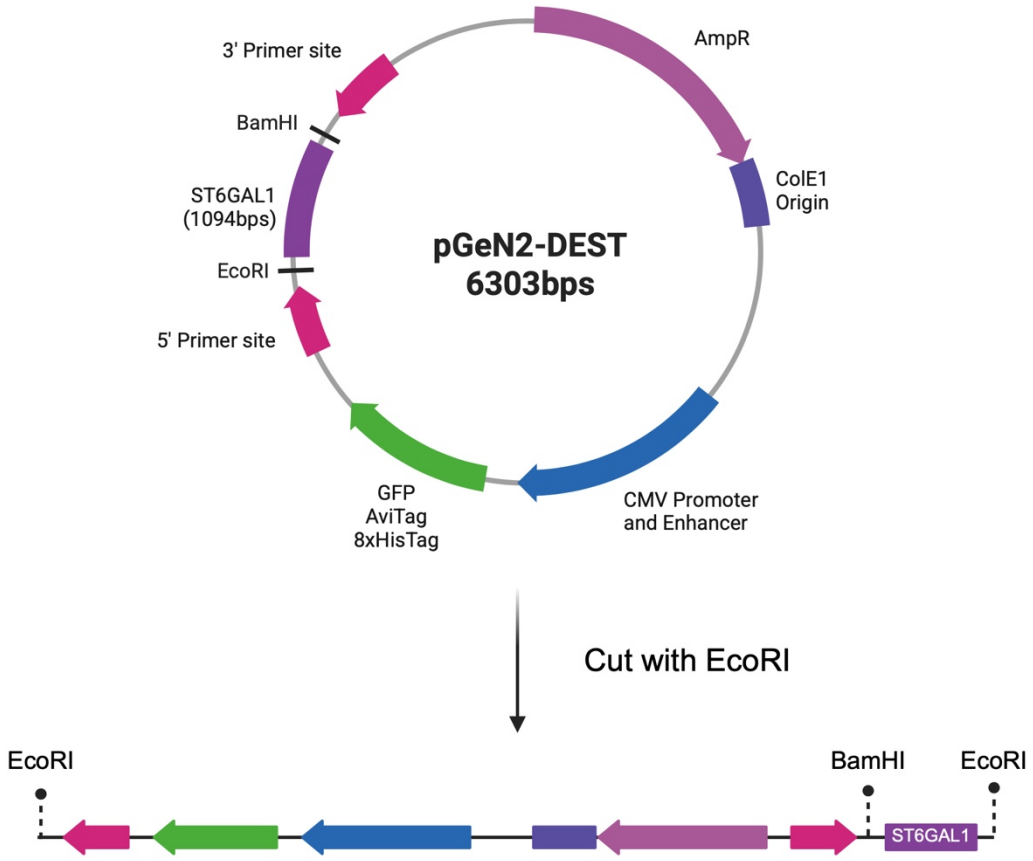

Figure 6. 22: **ST6GAL1 Plasmid Map visualisation and Linearisation by EcoRI Digestion**

Schematic representation of the plasmid construct containing the ST6GAL1 gene, with annotated restriction sites and relevant genetic elements including the promoter, antibiotic resistance marker, and multiple cloning site. The plasmid was linearised by EcoRI digestion to confirm the presence and correct orientation of the insert.

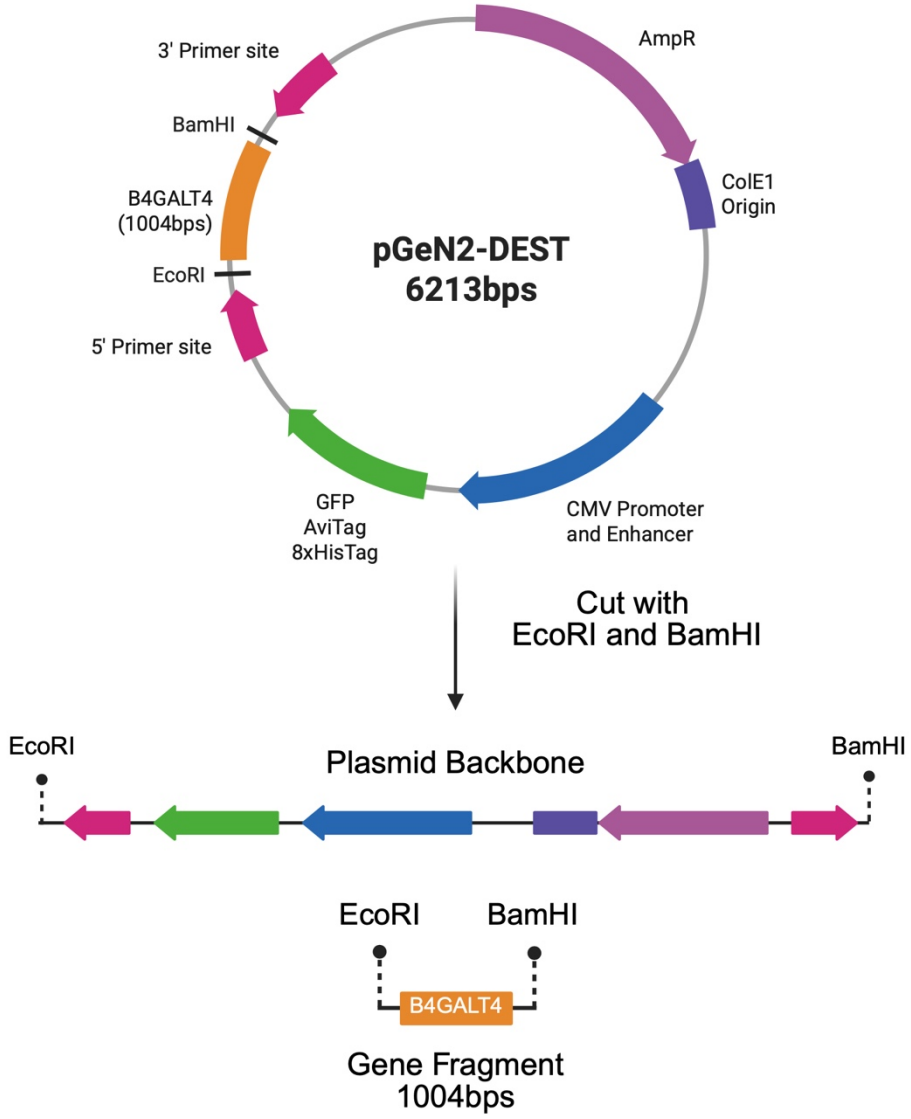

Figure 6. 23: **B4GALT4 Plasmid Map visualisation and Gene Fragment Isolation by EcoRI and BamHI**

Schematic representation of the plasmid construct containing the B4GALT4 gene, with annotated restriction sites and relevant genetic elements including the promoter, antibiotic resistance marker, and multiple cloning site. The bottom panel shows the expected linear DNA fragments following EcoRI and BamHI digestion used for gene fragment isolation.

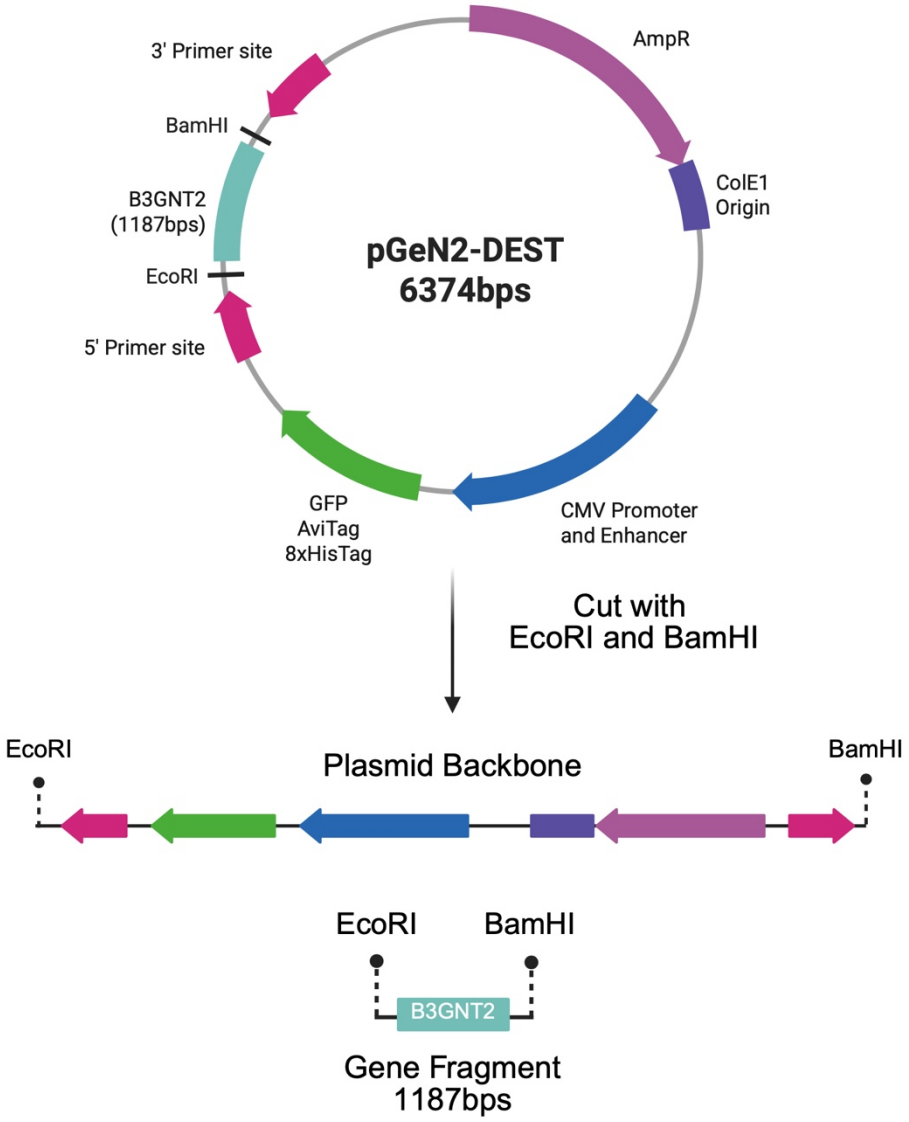

Figure 6. 24: **B3GNT2 Plasmid Map visualisation and Gene Fragment Isolation by EcoRI and BamHI**

Schematic representation of the plasmid construct containing the B3GNT2 gene, with annotated restriction sites and relevant genetic elements including the promoter, antibiotic resistance marker, and multiple cloning site. The bottom panel shows the expected linear DNA fragments following EcoRI and BamHI digestion used for gene fragment isolation.

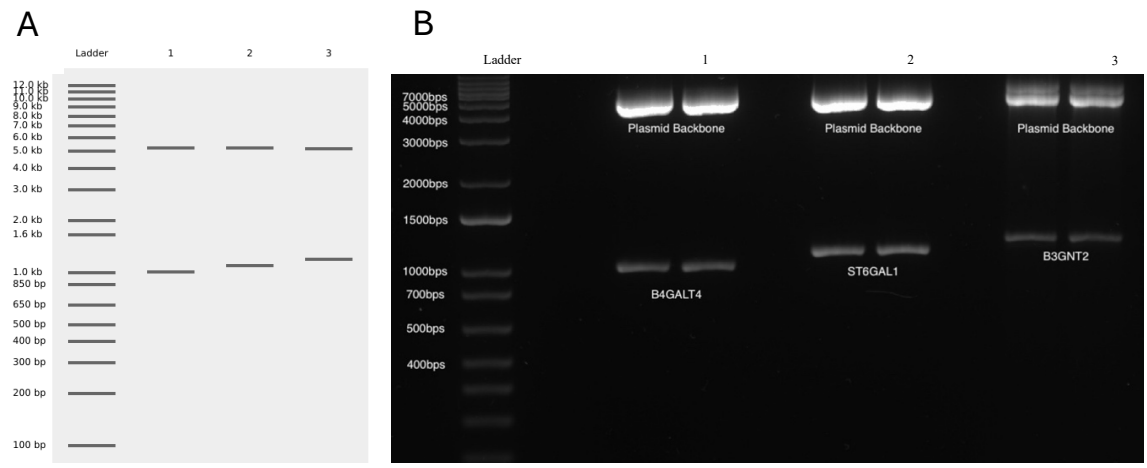

Figure 6. 25: ***In Silico*** **gel prediction vs Confirmation Gel of Final Gene Inserts for Gibson Assembly**

(A) Simulated agarose gel showing predicted fragment sizes following EcoRI/BamHI double digestion of B4GALT4 (lane 1), ST6GAL1 (lane 2), and B3GNT2 (lane 3) plasmids. (B) Experimental 1% agarose gel loaded with 100µg of DNA per lane, displaying the actual banding pattern obtained after double digestion with EcoRI and BamHI.

A

B

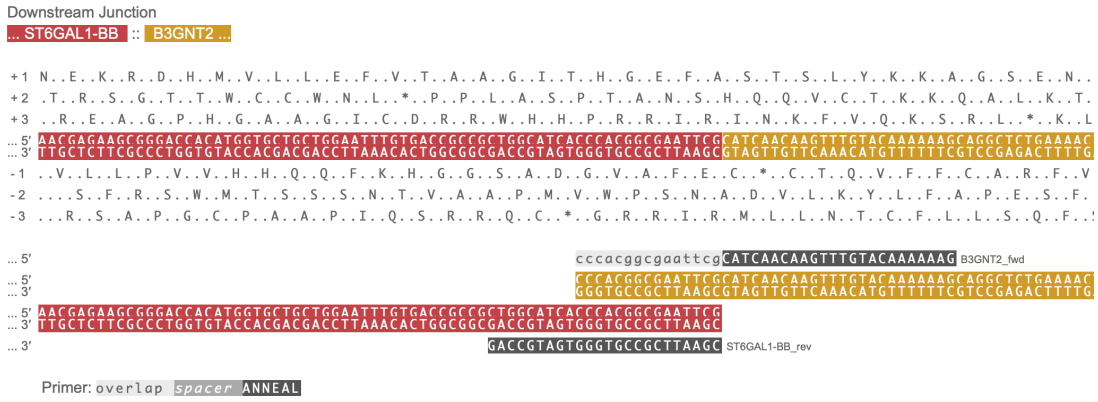

C

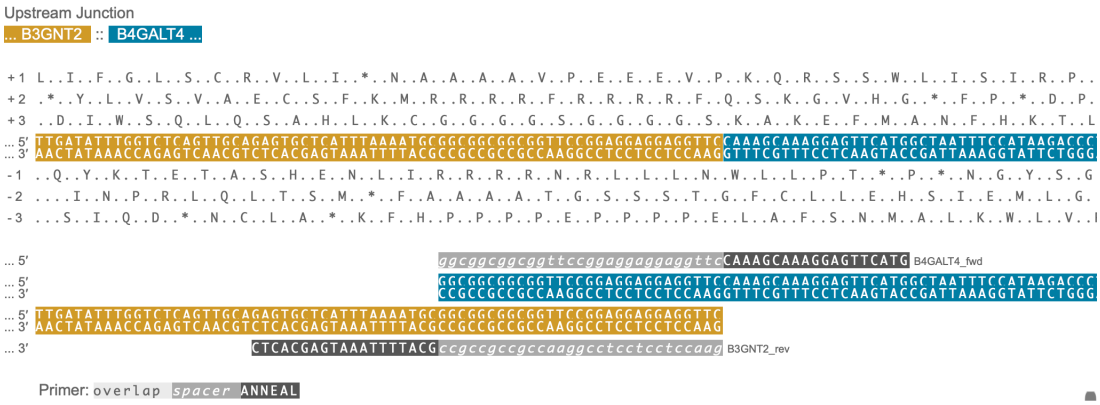

Figure 6. 26: ***In Silico*** **visualisation of overlapping sequences compatible for GAC**

Schematic representation of the overlapping DNA sequences designed for Gibson Assembly Cloning (GAC). (A) Junction between B4GALT4 and ST6GAL1BB, (B) junction between ST6GAL1BB and B3GNT2, (C) junction between B3GNT2 and B4GALT4. Each overlap region is shown to demonstrate sequence compatibility for seamless assembly.

Table 6. 3: **Forward and Reverse Primer Sequence for Extension of Inserts for Gibson Assembly Cloning compatible overhangs**

Primer	Sequence 5'-3'	Product Length
ST6GAL1-fwd	gtttggtgca*ggaggaggaggctcc*GAATTCGCATCAACAAGTTTGTACAAAAAAGCAG	6328bps
ST6GAL1-rev	GCCGTGGGTGATGCCAGC	
B3GNT2-fwd	ccgctggcatcacccacggcAAAAATGGAAAAGGGGAAG	1139bps
B3GNT2-rev	*ggaaccaccaccaccggaaccaccaccacc*GCATTTTAAATGAGCACTC	
B4GALT4-fwd	*ggtggtggtggttccggtggtggtggttcc*AAAGCAAAGGAGTTCATG	961bps
B4GALT4-rev	atgcgaattc*ggagcctcctcctcc*TGCACCAAACCAGAAATC	

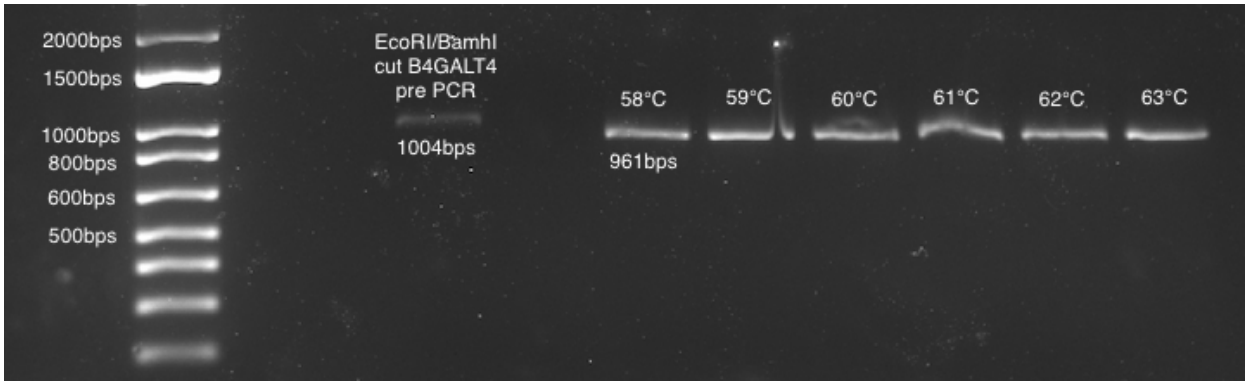

Figure 6. 27: **Temperature Gradient PCR Optimisation for B4GALT4 Amplification with Overhangs**

Image of a 1% agarose gel showing PCR products generated under a temperature gradient to optimise annealing conditions for B4GALT4 amplification with Gibson Assembly-compatible overhangs. The gel displays bands corresponding to the expected amplicon size, allowing identification of the optimal annealing temperature for specific and efficient amplification.

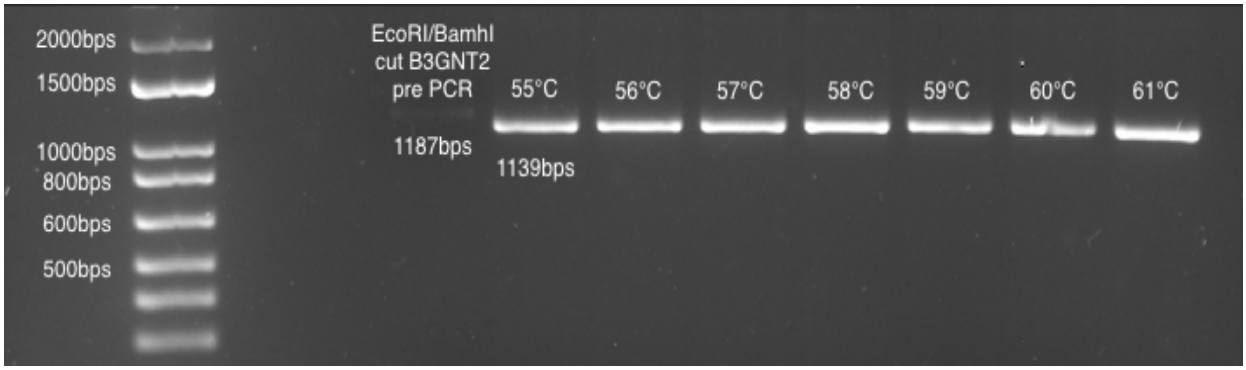

Figure 6. 28: **Temperature Gradient PCR Optimisation for B3GNT2 Amplification with Overhangs**

Image of a 1% agarose gel showing PCR products generated under a temperature gradient to optimise annealing conditions for B3GNT2 amplification with Gibson Assembly-compatible overhangs. The gel displays bands corresponding to the expected amplicon size, allowing identification of the optimal annealing temperature for specific and efficient amplification.

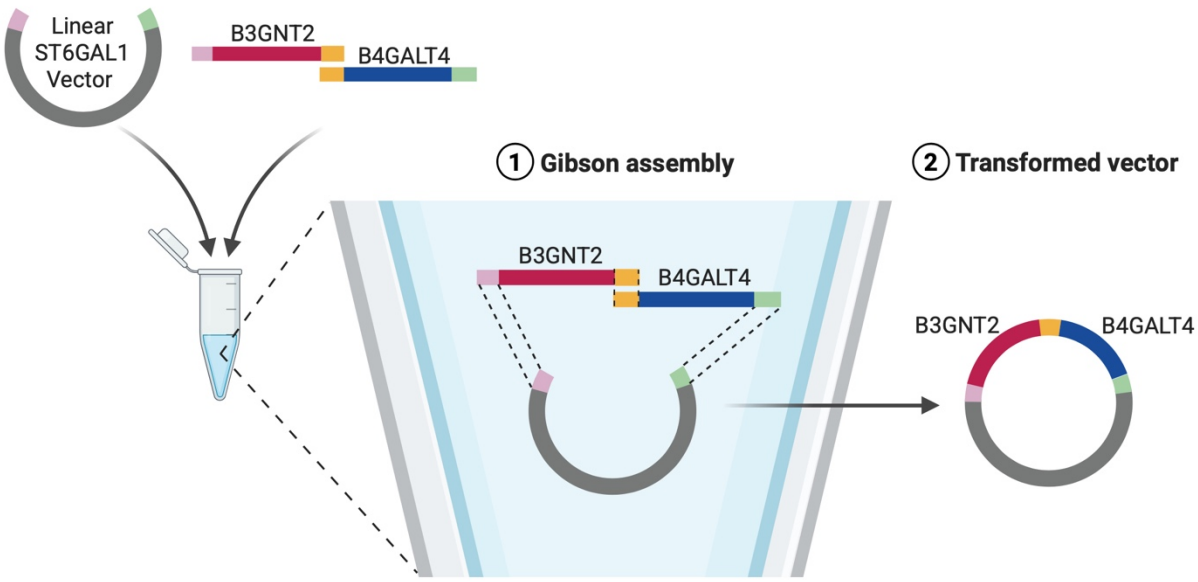

Figure 6. 29: **Overview of Gibson Assembly Protocol for Triple-Gene Construct with B3GNT2, B4GALT4 and ST6GAL1**

Diagram showing the Gibson Assembly reaction setup, where the linearised ST6GAL1 vector (present at 2x molar excess) and amplified B3GNT2 and B4GALT4 inserts with complementary overlapping ends were combined in a single reaction tube on ice. The Gibson Assembly process facilitates the seamless joining of fragments into a complete plasmid.

A

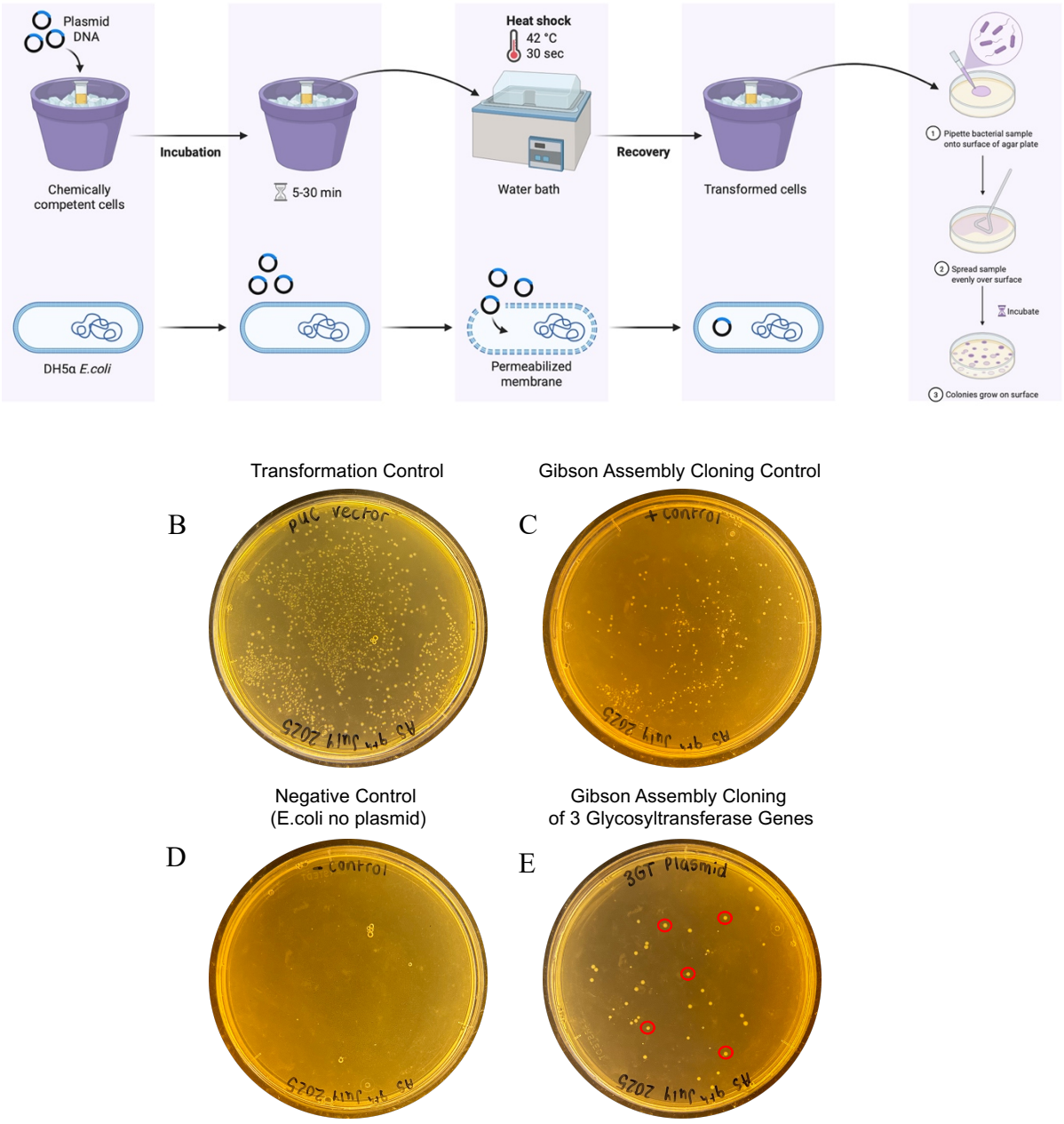

Figure 6. 30: **Transformation of DH5α *E. coli* with Plasmid**

(A) Schematic of the transformation protocol. Chemically competent *E. coli* was incubated on ice with plasmid DNA for 30 minutes, subjected to heat shock at 42 °C for 30 seconds, returned to ice for 2 minutes, then mixed with SOC medium and plated onto LB agar containing 100 µg/mL ampicillin. Plates were incubated overnight to allow colony formation. (B-E) Representative images of plates showing colonies for (B) transformation control, (C) Gibson assembly cloning control, (D) negative control with no plasmid, and (E) experimental plate with DH5α transformed with the Gibson Assembly Cloning product plasmid.

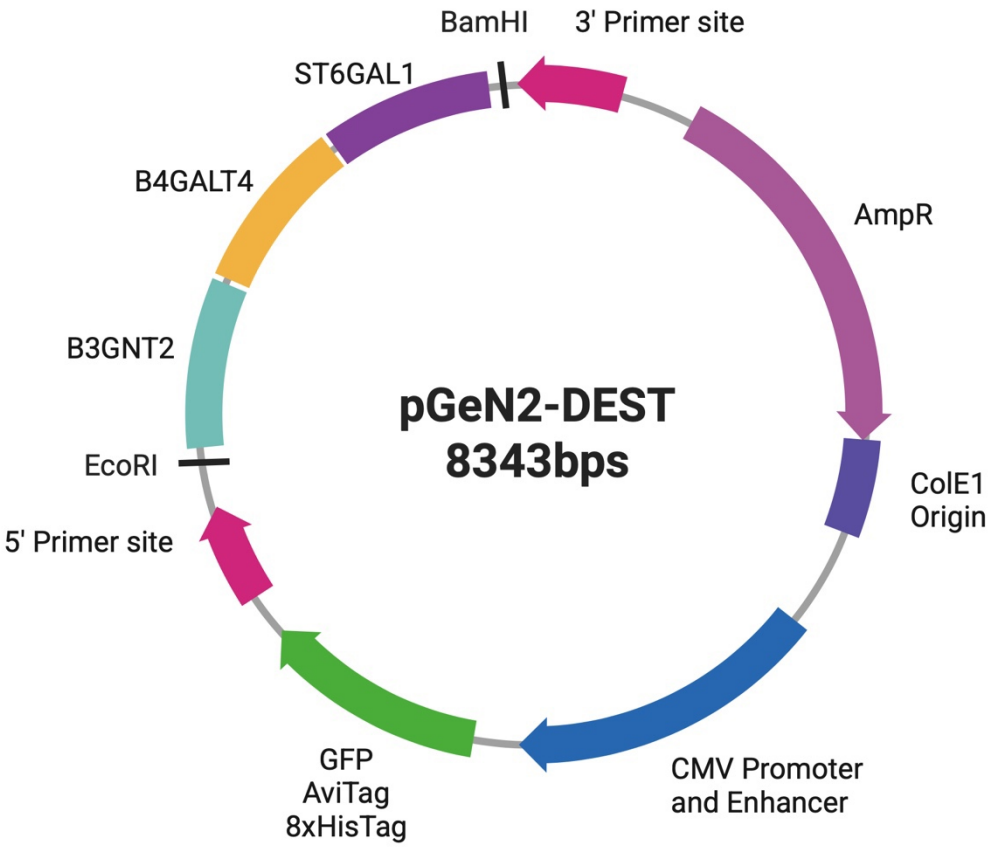

Figure 6. 31: **Predicted Final Plasmid Product Containing All Three Glycosyltransferase Genes**

Schematic representation of the predicted plasmid construct, containing the three glycosyltransferase genes B4GALT4, ST6GAL1, and B3GNT2 assembled in sequence. The map illustrates gene arrangement, vector backbone features, and relevant restriction sites, representing the expected final construct following successful Gibson Assembly.

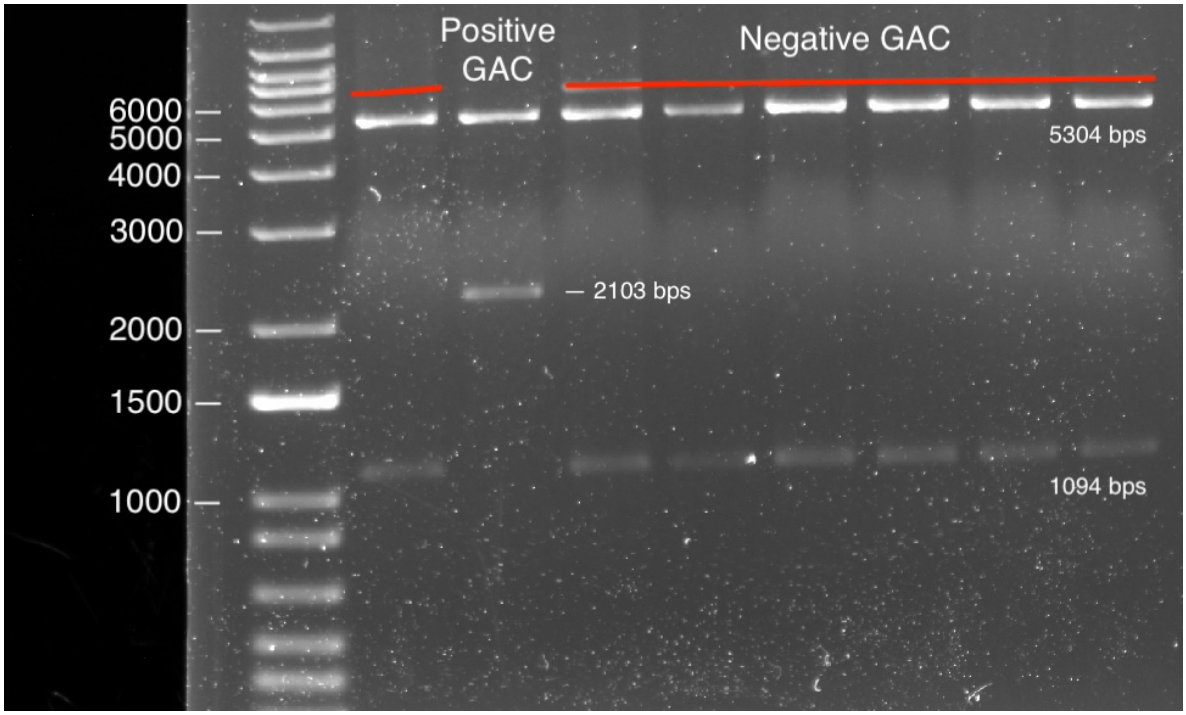

Figure 6. 32: **Restriction Digest screening of Gibson Assembly Cloning products**

Restriction digest screening of plasmids isolated from single colonies following Gibson Assembly Cloning (GAC). Colonies were grown on LB agar plates containing ampicillin, and plasmids were purified by miniprep from *E. coli* DH5α. Each plasmid was digested with BamHI and EcoRI to verify correct assembly. Lane 1 contains the DNA ladder; lanes 2-9 contain restriction digest products from individual GAC colonies.

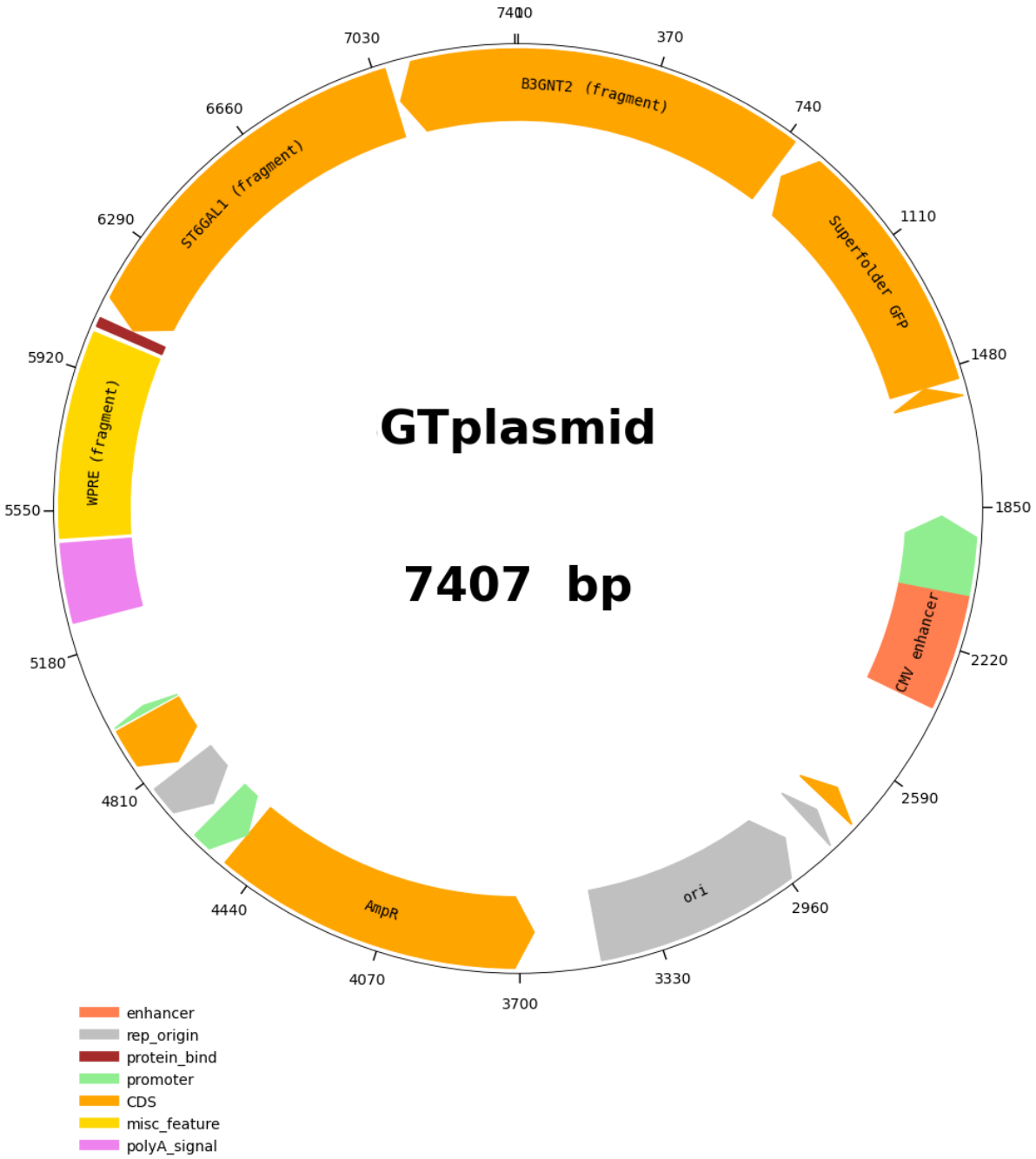

Figure 6. 33: **Plasmid Map of Two Glycosyltransferases Successfully Transformed into pGeN2-DEST Vector**

Plasmid map generated from sequencing data provided by Eurofins, showing successful incorporation of the B3GNT2 and ST6GAL1 genes into the pGeN2-DEST vector. The map illustrates the gene arrangement, orientation, and key vector features including the promoter, antibiotic resistance marker, and restriction sites, confirming correct dual-gene insertion within the construct.

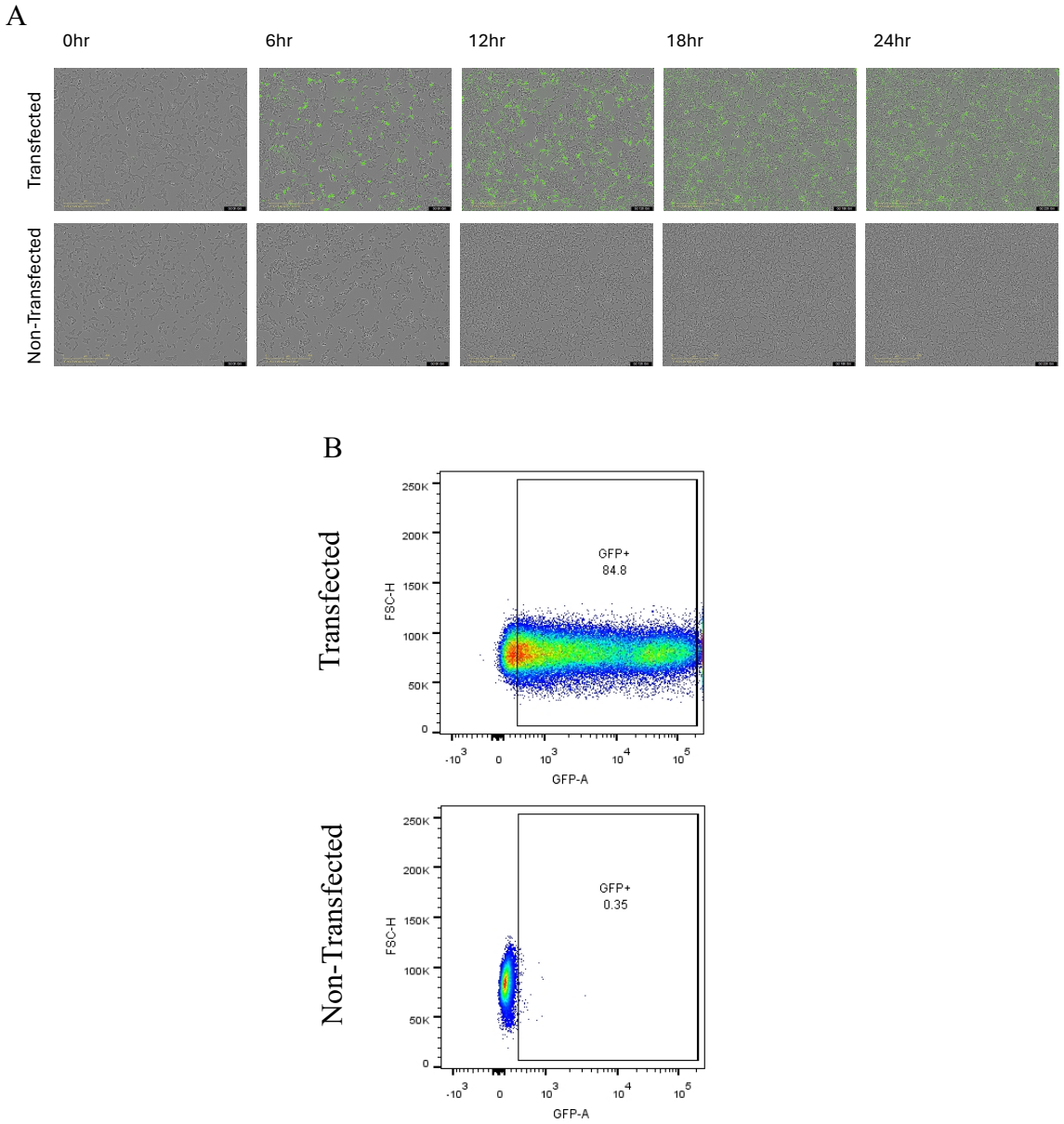

Figure 6. 34: **Transfection Efficiency of Plasmid Transformed with Two Glycosyltransferases**

(A) Representative images of HEK293 cells following transfection with plasmids containing two glycosyltransferase inserts. Transfection efficiency was assessed by fluorescent reporter expression. (B) Flow cytometry-based quantification of GFP expression in transfected and non-transfected HEK293 cells. GFP-positive cells were gated based on fluorescence intensity relative to the non-transfected control. The percentage of GFP^+ cells indicate transfection efficiency.

6.8. Assessment of Heterologous Glycosyltransferase Expression for HMO Production

To assess whether HEK293 cells could be engineered to produce HMOs, two different glycosyltransferase expression strategies were tested. In one condition, cells were transfected with a plasmid encoding ST6GAL1 alone. A second condition involved a G4S-linked bicistronic construct expressing ST6GAL1 and B3GNT2 (linked ST6GAL1-B3GNT2 plasmid) which was co-transfected with a separate plasmid encoding B4GALT4. Lactose was added to the culture media following transfection to provide the relevant acceptor and donor substrates. Conditioned media were centrifuged, filtered, and analysed for secreted oligosaccharides by high-performance anion-exchange chromatography with pulsed amperometric detection (HPAEC-PAD).

To establish reference retention times for downstream analysis, individual HMO standards including 3'-SL, 6'-SL and LNnT were resolved by HPLC under the same conditions used for cell culture supernatants. Unexpectedly, DMEM alone produced a distinct peak at the expected retention time of Lacto-*N*-neotetraose (LNnT) (**Figure 6.35 A**), indicating potential co-elution with a media-derived component. As a result, LNnT cannot be reliably confirmed in subsequent culture samples using this method due to possible signal masking. In contrast, 6′-SL and 3′-SL standards generated discrete, non-overlapping peaks when analysed alongside DMEM controls (**Figure 6.35 B**), and no corresponding peaks were detected in the DMEM-only samples. Furthermore, DMEM spiked with 6′-SL or 3′-SL displayed clear peaks at the expected retention times, confirming that their detection would not be obscured in culture media.

Due to significant baseline noise of DMEM and peak distortion observed during initial chromatographic runs, all samples were diluted 1 in 100 prior to injection. This was necessary to prevent column overloading and peak shifting caused by matrix-associated interference, but it also reduced overall detection sensitivity for low-abundance HMOs.

In cells expressing ST6GAL1 alone, 6′-SL was detectable but present only at very low levels, close to the system's lower limit of quantification (**Figure 6.36**). When ST6GAL1 was co-expressed with B3GNT2 using the linked construct, 6′-SL levels were reduced (**Figure 6.37**), indicating that B3GNT2 expression may have interfered with ST6GAL1-mediated synthesis No alternative sialylated lactose structures or relevant intermediates were detectable in any of the conditions tested.

We also investigated whether LNnT could be detected as an intermediate or end product in the co-transfection model, as it could theoretically arise from the combined activity of B3GNT2 and B4GALT4. However, reliable detection by HPLC was not possible due to two confounding factors; first, LNnT and lactose exhibited nearly identical retention times under the chromatographic conditions used, preventing clear separation; and second, DMEM alone produced a peak at the same retention time, indicating a co-eluting media-derived component unrelated to LNnT. Consequently, any LNnT that may have been synthesised could be masked by both lactose interference and non-specific background signal from the culture medium. Therefore, confirmation of LNnT production will require more specific structural analysis, such as mass spectrometry.

A

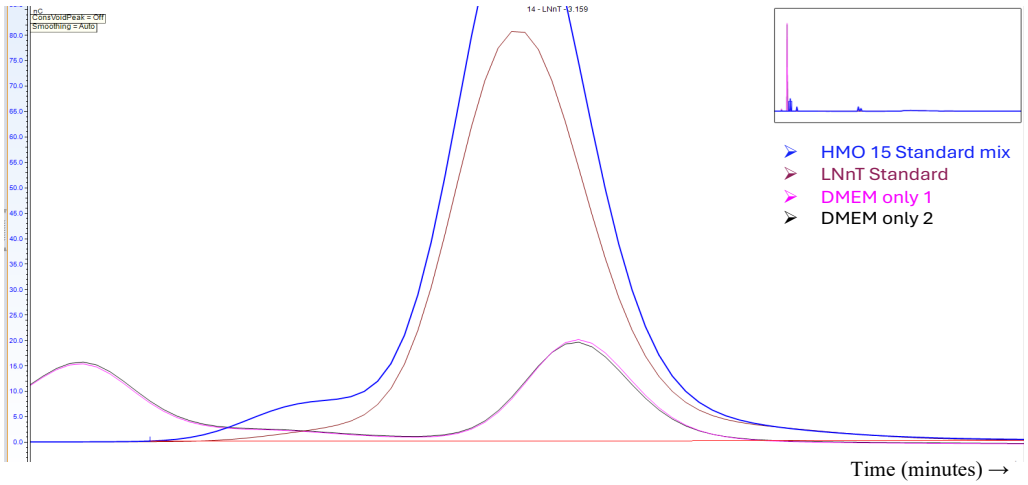

B

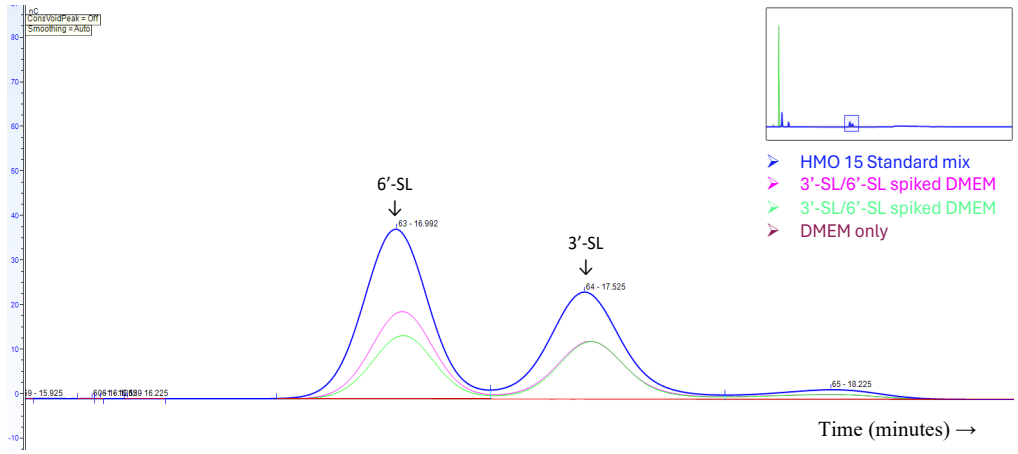

Figure 6. 35: **HPLC chromatograms of a 15-component HMO standard mix for reference peak identification in DMEM**

(A) Chromatogram of the isolated LNnT standard. (B) Chromatogram of the isolated individual 6′-SL and 3′-SL standards run alongside DMEM controls to confirm absence of overlapping background peaks.

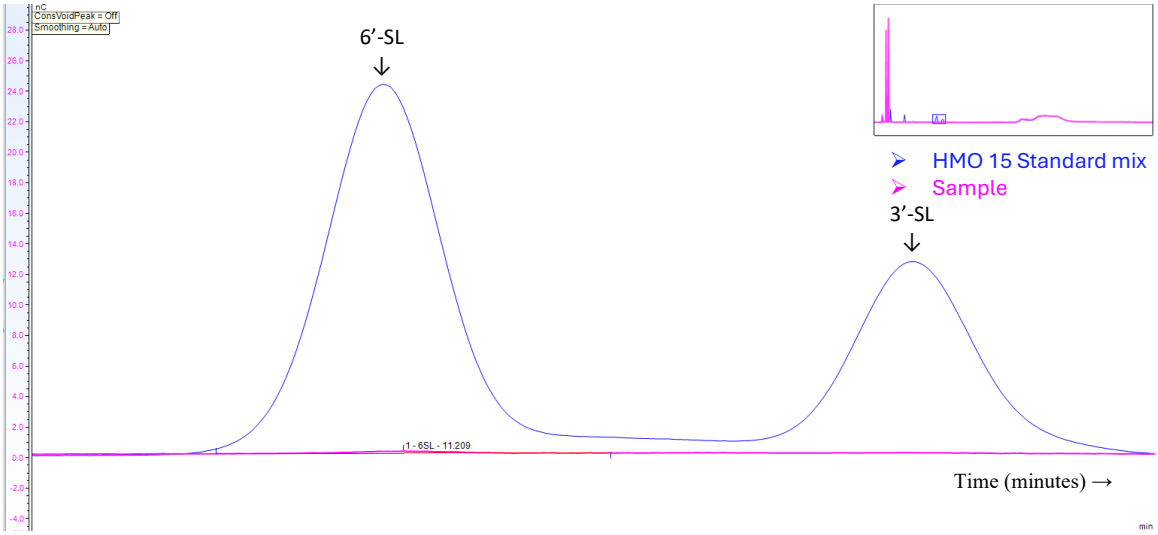

Figure 6. 36: **HPLC chromatograms of secreted oligosaccharides from ST6GAL1 glycosyltransferase-transfected HEK293 cells**

Chromatogram of the media from HEK293 cells transfected with ST6GAL1 and supplemented with lactose was analysed by HPLC. The sample chromatogram is shown alongside 6′-SL and 3′-SL standards for comparison of retention times. Standards are shown in blue, and the sample run is shown in pink.

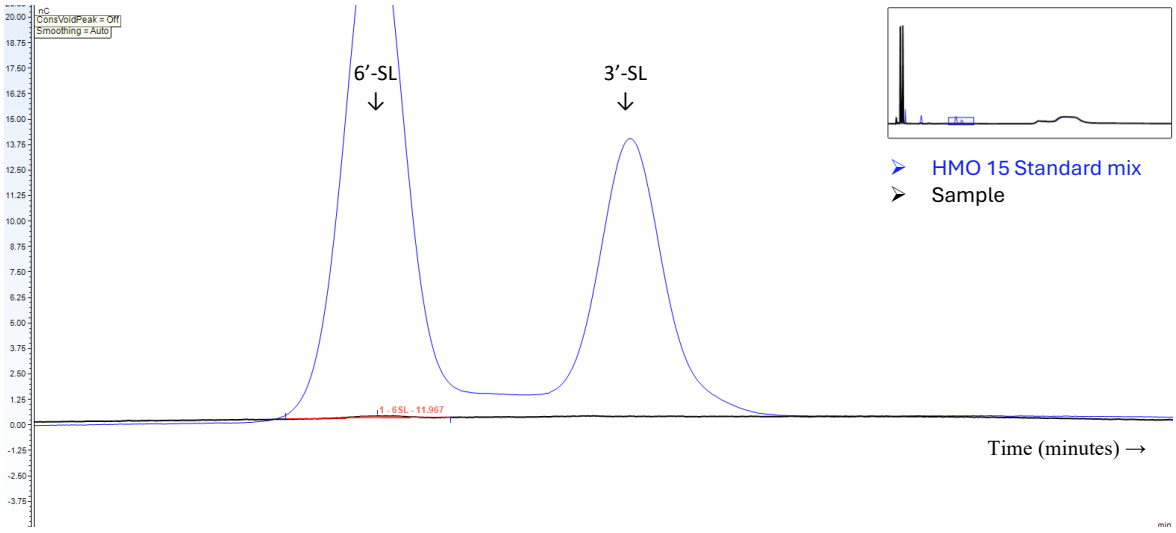

Figure 6. 37: **HPLC chromatograms of secreted oligosaccharides from ST6GAL1-B3GNT2 glycosyltransferase-transfected HEK293 cells**

Chromatogram of the media from HEK293 cells transfected with the dual ST6GAL1-B3GNT2 plasmid and treated with lactose was analysed by HPLC. The resulting chromatogram is shown with 6′-SL and 3′-SL standards to allow comparison of peak retention. Standards are shown in blue, and the sample run is shown in black.

Table 6. 4: **Transfection Conditions, Substrate Supplementation, and HPLC Detection of 6′-SL in Glycosyltransferase-Transfected Cells**

Transfection Condition	Supplementation	6'-SL Detected by HPLC	µg/mL	Figure
ST6GAL1	Lactose	Yes	4.5785	6.36
B3GNT2-ST6GAL1	Lactose	Yes	3.0764	6.37
No Transfection	Lactose	No	-	Not Shown

6.9. *In Vitro* Characterisation of Glycosyltransferase Activity Across pH Conditions for HMO Production

To assess whether enzymatic conditions contributed to the low levels of 6′-SL observed in whole-cell assays, glycosyltransferase activity was examined under controlled *in vitro* conditions following crude isolation of the expressed enzymes. Enzyme preparations derived from transfected HEK293 cells were incubated with lactose and CMP-Neu5Ac, UDP-Galactose, UDP-GlcNAc in buffered reactions, and activity was assessed across three pH values (5.5, 6.5, and 7.5). HEPES and MES buffers were used to maintain pH stability within the tested range.

HPLC analysis was first optimised to determine whether buffer composition or pH interfered with peak identification. A 15-component HMO standard mix was analysed in parallel with MES-based enzyme buffer, HEPES-based enzyme buffer, and lysis buffer (**Figure 6.38**) and also lactose (**Figure 6.39**). No peaks corresponding to 3′-SL or 6′-SL were detected in any buffer alone, confirming that neither buffer system contributed interfering signals at the expected retention times of the sialyllactose standards. Similarly, LNnT did not overlap with any buffer-derived peaks, indicating that buffer background would not interfere with its detection in principle. However, lactose remained a confounding factor for LNnT analysis due to its co-elution under the chromatographic conditions used.

Crude ST6GAL1 enzyme preparations were incubated with lactose and CMP-Neu5Ac at pH 6.5 in MES buffer (**Figure 6.40)**. Following 1:100 dilution to minimise peak shifting and baseline distortion, a clear peak corresponding to 6′-SL was observed when compared to standards, indicating successful enzymatic sialylation. When both ST6GAL1 and ST3GAL1 were combined under the same conditions (**Figure 6.41**), both 6′-SL and 3′-SL peaks were detected, confirming dual sialyltransferase activity in the crude extract.

To test for sequential elongation towards LNnT formation, B3GNT2 and B4GALT4 were included alongside ST6GAL1 and ST3GAL1 and assessed at different pH conditions. At pH 7.5 in HEPES buffer (**Figure 6.42**), distinct 3′-SL and 6′-SL peaks were detected; however, no additional peak could be confidently assigned to LNnT due to co-elution with lactose. When the same enzyme combination was tested at pH 6.5 (**Figure 6.43 A**), both sialyllactose species were again detected. Comparison against the LNnT standard (**Figure 6.43 B**) suggested a possible increase in signal around the LNnT retention region, but this

could not be distinguished from lactose interference. At pH 5.5 in MES buffer (**Figure 6.44**), sialylation activity was retained but no evidence of further elongation was detected.

Finally, to assess whether the pre-linked B3GNT2-ST6GAL1 fusion retained enzymatic activity when combined with B4GALT4 and ST3GAL1, the fusion construct was tested at pH 7.5 (**Figure 6.45**) and pH 6.5 (**Figure 6.46**). In both conditions, 3′-SL and 6′-SL were clearly detected, indicating that both enzymes within the fusion remained functional. No unambiguous LNnT peak could be resolved due to persistent lactose co-elution, consistent with observations from the non-fusion enzyme combinations.

Collectively, these data demonstrate that crude enzyme preparations were catalytically active and capable of producing both 3′-SL and 6′-SL across multiple buffer systems and pH conditions (summarised in table 6.5). However, LNnT detection remained inconclusive due to chromatographic overlap with lactose, despite minimal interference from buffer components. Therefore, confirmation of LNnT synthesis will require alternative analytical strategies such as mass spectrometry-based structural assignment.

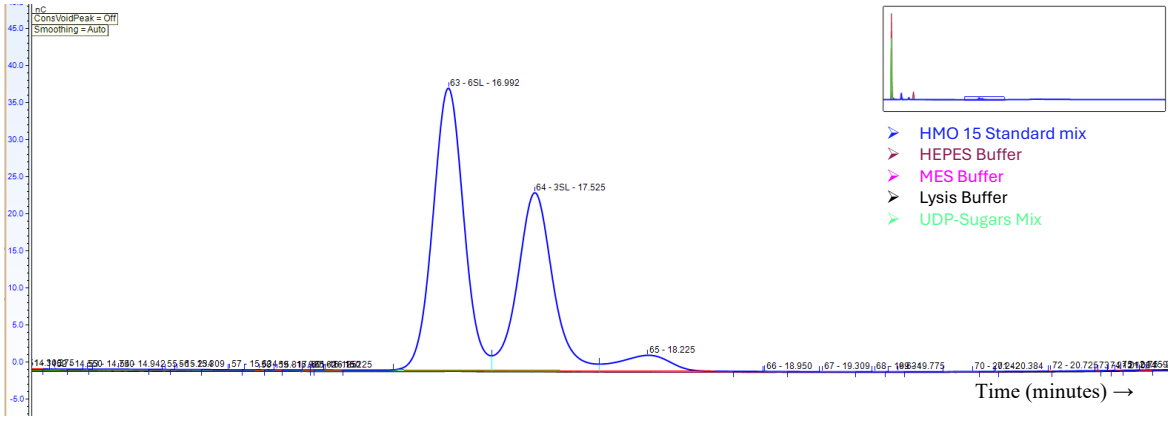

Figure 6. 38: **HPLC chromatograms of a 15-component HMO standard mix for reference peak identification in MES/HEPES**

The resulting chromatogram is shown with 6′-SL and 3′-SL standards to allow comparison of peak retention. Chromatograms of the 15 HMO standard mix (blue) compared to MES based enzyme buffer (pink), HEPES based enzyme buffer (brown) and lysis buffer (black) were run to establish reference retention times for subsequent enzymatic assays.

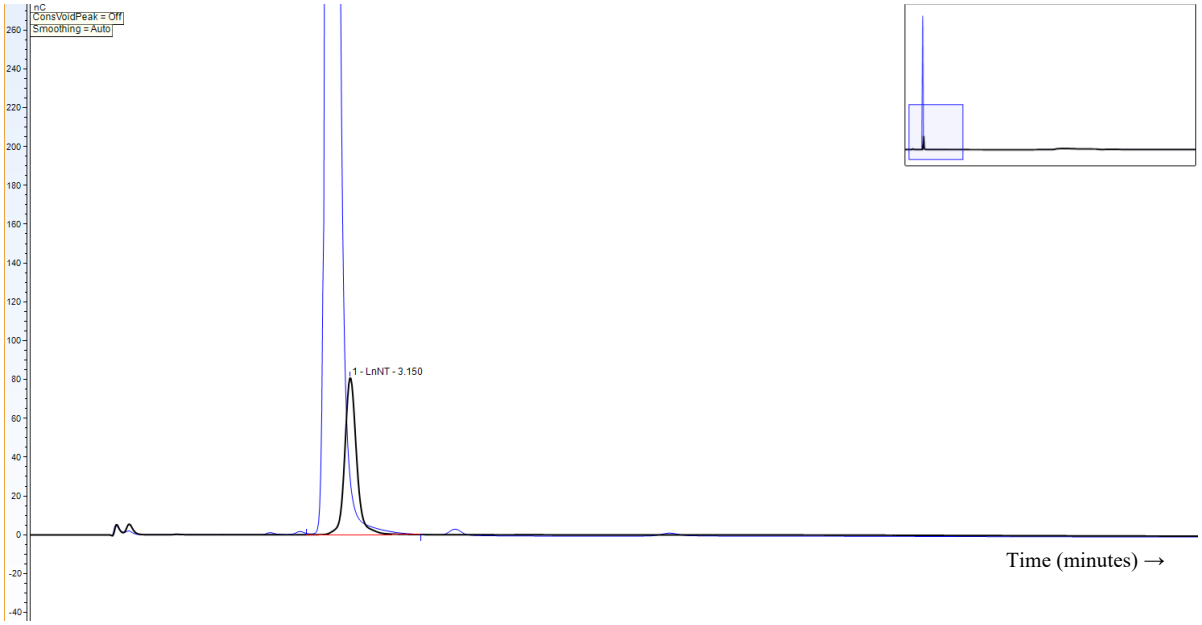

Figure 6. 39: **HPLC chromatograms of the LNnT standard for reference peak against Lactose**

The resulting chromatogram is shown with LNnT standards to allow comparison of peak retention. Chromatograms of the LNnT standard (black) compared to Lactose standard (blue) were run to establish reference retention times for subsequent enzymatic assays.

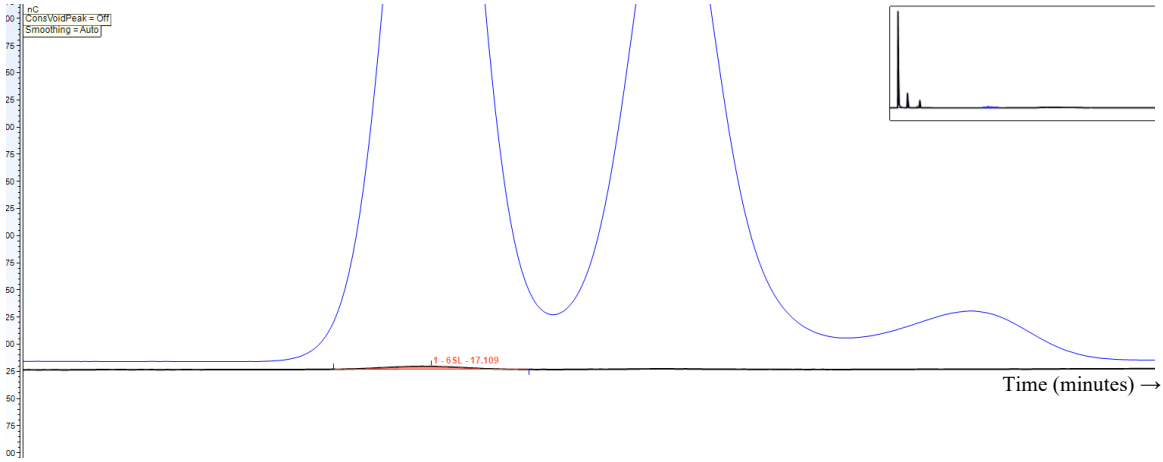

Figure 6. 40: **HPLC chromatograms of secreted oligosaccharides from extracted ST6GAL1 treated with lactose and UDP sugars, reaction pH 6.5**

HPLC trace of the ST6GAL1 enzyme preparation reacted with lactose and CMP-Neu5Ac in MES buffer (pH 6.5). Peaks were compared with HMO standards for identification. Standards are shown in blue, and the sample run is shown in black.

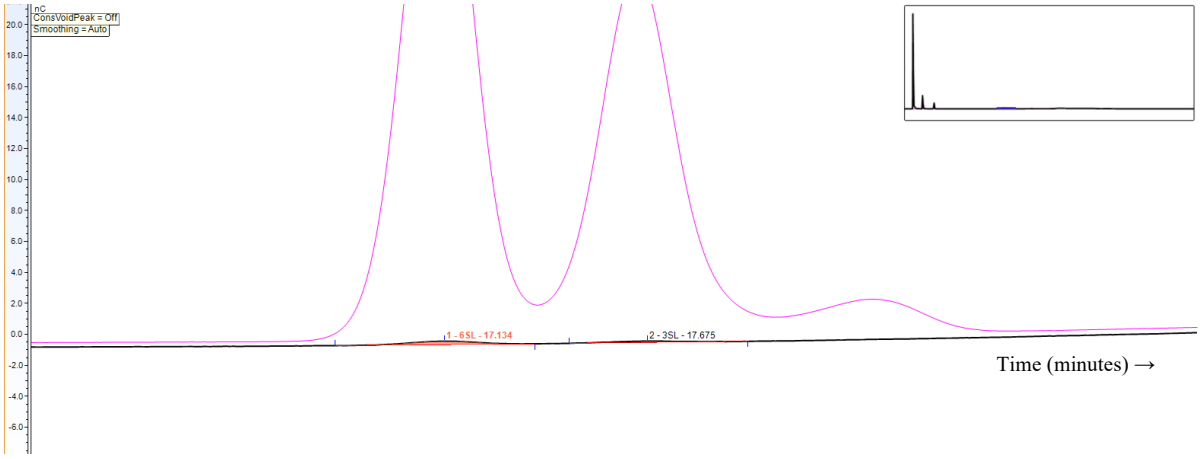

Figure 6. 41: **HPLC chromatograms of secreted oligosaccharides from extracted ST6GAL1 and ST3GAL1 treated with lactose and UDP sugars, reaction pH 6.5**

HPLC trace of the ST6GAL1 and ST3GAL1 enzymes preparation reacted with lactose and CMP-Neu5Ac in MES buffer (pH 6.5). Peaks were compared with HMO standards for identification. Standards are shown in pink, and the sample run is shown in black.

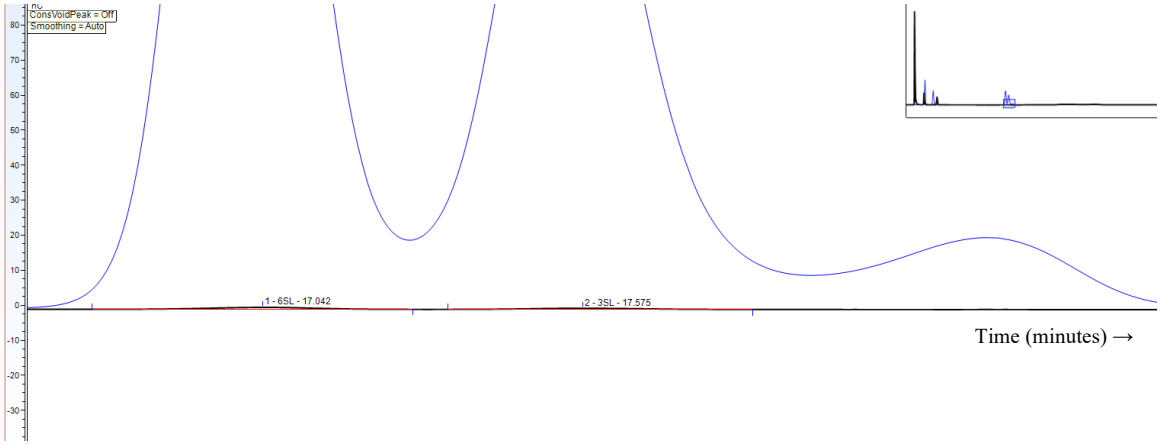

Figure 6. 42: **HPLC chromatograms of secreted oligosaccharides from extracted B3GNT2, B4GALT4, ST6GAL1 and ST3GAL1 treated with lactose and UDP sugars, reaction pH 7.5**

HPLC trace of the ST6GAL1, B3GNT2, B4GALT4 and ST3GAL1 enzyme preparation reacted with lactose and CMP-Neu5Ac in HEPES buffer (pH 7.5). Peaks were compared with HMO standards for identification. Standards are shown in blue, and the sample run is shown in black.

A

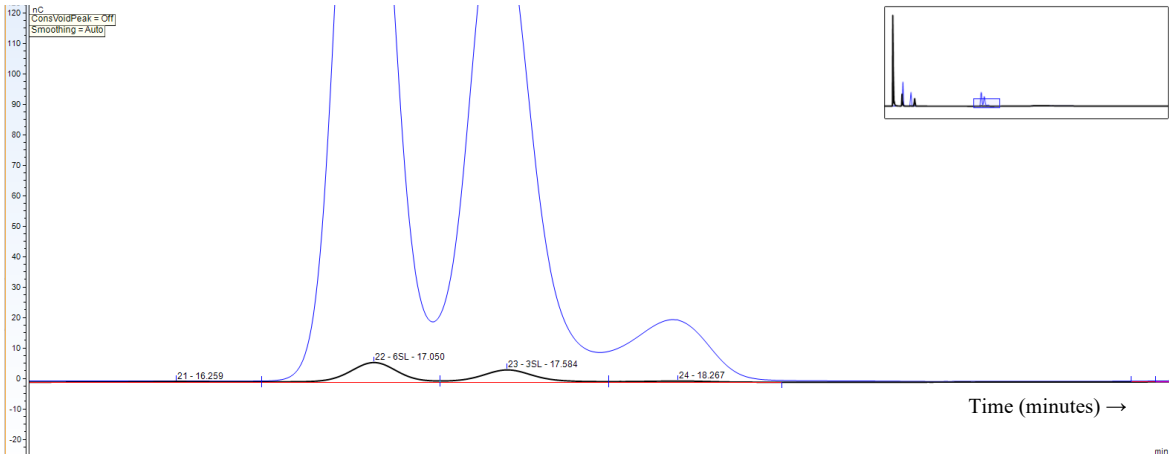

B

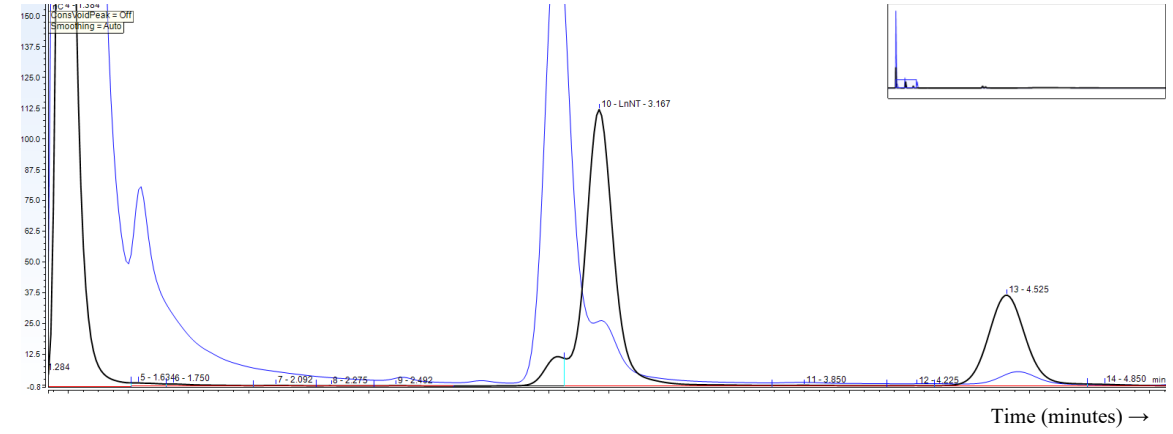

Figure 6. 43: **HPLC chromatograms of secreted oligosaccharides from extracted B3GNT2, B4GALT4, ST6GAL1 and ST3GAL1 treated with lactose and UDP sugars, reaction pH 6.5**

HPLC trace of the ST6GAL1, B3GNT2, B4GALT4 and ST3GAL1 enzyme preparation reacted with lactose and CMP-Neu5Ac in MES buffer (pH 6.5). Peaks were compared with HMO standards for identification. (A) Sample against 3'-SL and 6'-SL standards. Standards are shown in blue, and the sample run is shown in black. (B) Sample against LNnT standard. Standards are shown in black, and the sample run is shown in blue.

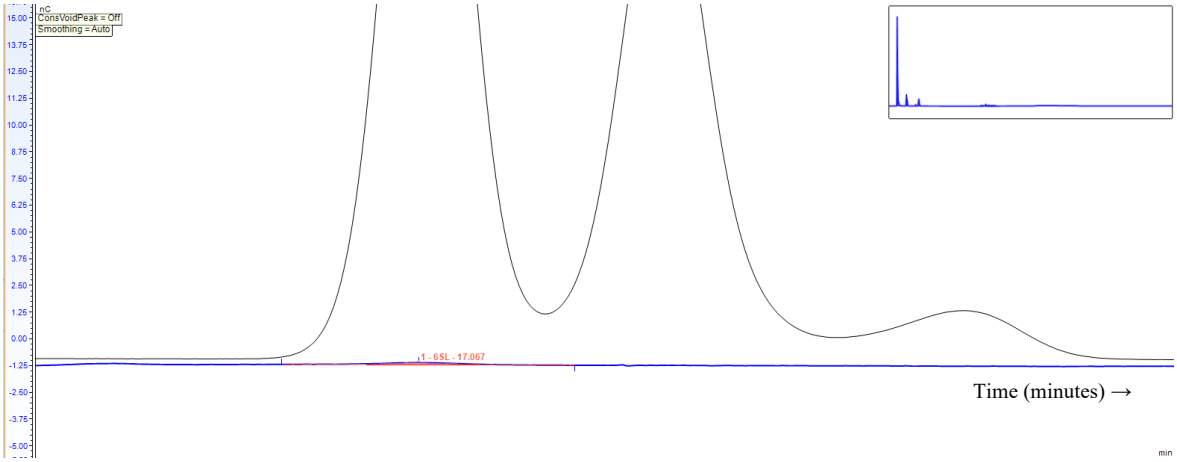

Figure 6. 44: **HPLC chromatograms of secreted oligosaccharides from extracted B3GNT2, B4GALT4, ST6GAL1 and ST3GAL1 treated with lactose and UDP sugars, reaction pH 5.5**

HPLC trace of the ST6GAL1, B3GNT2, B4GALT4 and ST3GAL1 enzyme preparation reacted with lactose and CMP-Neu5Ac in MES buffer (pH 5.5). Peaks were compared with HMO standards for identification. Standards are shown in black, and the sample run is shown in blue.

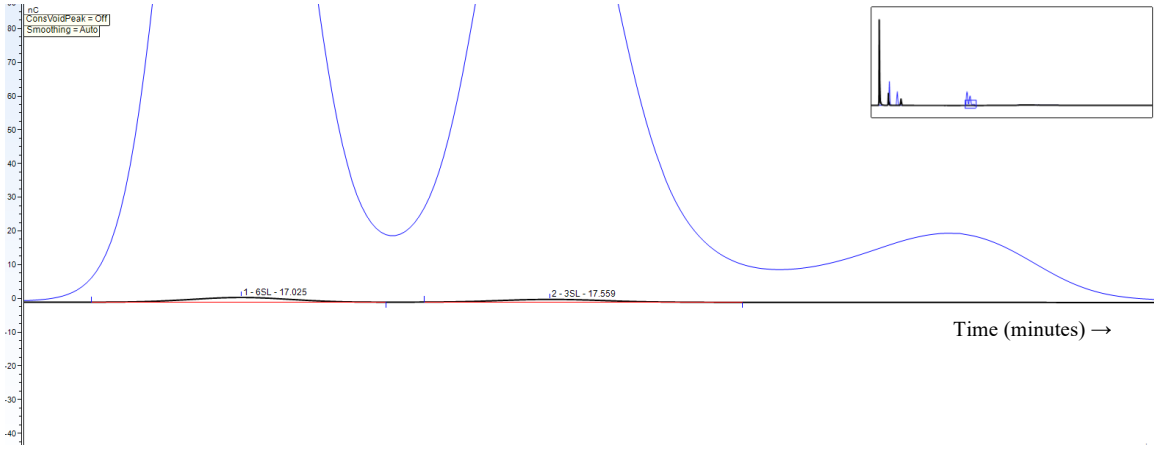

Figure 6. 45: **HPLC chromatograms of secreted oligosaccharides from extracted B3GNT2-ST6GAL1, B4GALT4 and ST3GAL1 treated with lactose and UDP sugars, reaction pH 7.5**

HPLC trace of the ST6GAL1-B3GNT2, B4GALT4 and ST3GAL1 enzyme preparation reacted with lactose and CMP-Neu5Ac in HEPES buffer (pH 7.5). Peaks were compared with HMO standards for identification. Standards are shown in blue, and the sample run is shown in black.

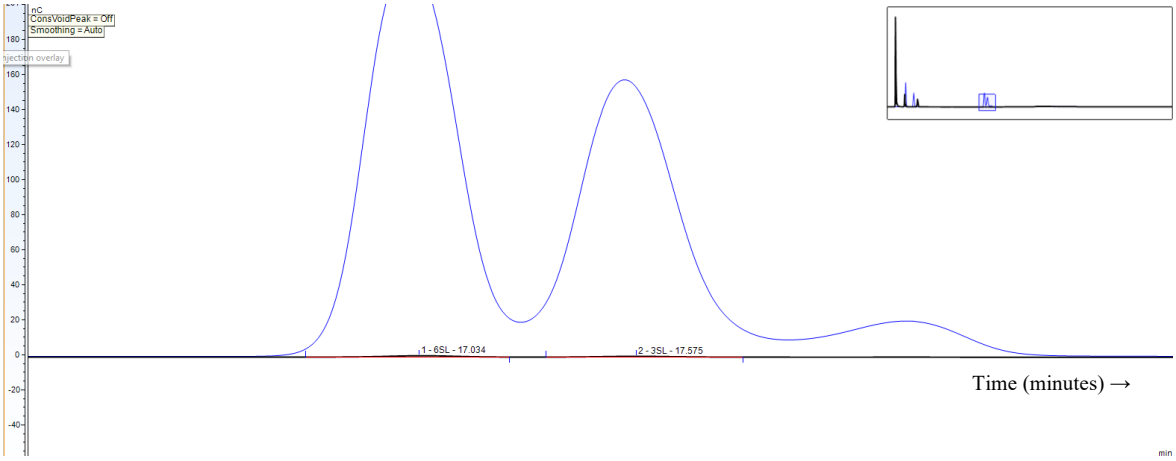

Figure 6. 46: **HPLC chromatograms of secreted oligosaccharides from extracted B3GNT2-ST6GAL1, B4GALT4 and ST3GAL1 treated with lactose and UDP sugars, reaction pH 6.5**

HPLC trace of the ST6GAL1-B3GNT2, B4GALT4 and ST3GAL1 enzyme preparation reacted with lactose and CMP-Neu5Ac in MES buffer (pH 6.5). Peaks were compared with HMO standards for identification. Standards are shown in blue, and the sample run is shown in black.

Table 6. 5: **Summary of HPAEC-PAD results from Eznymatic Reaction**

Enzymes Present	Temperature	pH	HMO Detection by HPLC	µg/mL	Figure
ST6GAL1	37	6.5	6'-SL	3.0865	6.40
ST6GAL1 **ST3GAL1**	37	6.5	3'-SL 6'-SL	5.582 3.1648	6.41
B3GNT2 **B4GALT4** **ST6GAL1** **ST3GAL1**	37	7.5	3'-SL 6'-SL	11.94 13.57	6.42
B3GNT2 **B4GALT4** **ST6GAL1** **ST3GAL1**	37	6.5	3'-SL 6'-SL LNnT	170 175 UQ	6.43
B3GNT2 **B4GALT4** **ST6GAL1** **ST3GAL1**	37	5.5	6'-SL	2.8540	6.44
B3GNT2- ST6GAL1 **B4GALT4** **ST3GAL1**	37	7.5	3'-SL 6'-SL	16.60 18.66	6.45
B3GNT2- ST6GAL1 **B4GALT4** **ST3GAL1**	37	6.5	3'-SL 6'-SL	29.97 34.04	6.46
B3GNT2- ST6GAL1 **B4GALT4** **ST3GAL1**	37	5.5	N/D	-	Not Shown

UQ = unquantifiable N/D = not detected

6.10. Discussion

This chapter aimed to address a central challenge in HMO biology; the scalable, efficient production of structurally defined HMOs for experimental and therapeutic use. Although significant advances have been made in both chemical and enzymatic synthesis, these approaches remain resource-intensive and often inefficient, particularly for sialylated HMOs, which are difficult to generate due to the instability of sialic acid donors and the strict linkage specificity required for their immunological activity[4]. The approach pursued here was to design a plasmid system expressing multiple glycosyltransferases, with the goal of recapitulating fragments of the human glycosylation machinery in a tractable host. By combining enzymes such as B3GNT2, B4GALT4, and ST6GAL1 in linked configurations, this system was intended to enable the biosynthesis of sialylated HMOs or possibly even elongated HMOs, but specifically 6′-SL, which was shown in the first part of this thesis to exert dominant immunomodulatory effects on immune cells. The rationale behind this strategy was guided by prior mapping of HMO biosynthetic pathways and computational modelling of glycan structures, allowing us to narrow down from an initial pool of fifteen candidate enzymes to a minimal set sufficient to extend lactose through GlcNAc priming, galactosylation, and sialylation, providing a proof-of-concept for the creation of a flexible platform for mammalian HMO biosynthesis.

The goal of producing HMOs in mammalian cell culture is to mimic, as faithfully as possible, the native glycan biosynthesis that occurs in the human mammary gland. Mammalian cells contain the endogenous glycosylation machinery (glycosyltransferases, glycosidases, transporters, architecture) to execute many of these modifications with high fidelity. Genetic glycoengineering in mammalian systems has been used to adjust and refine glycosylation patterns, showing that engineered mammalian cells can faithfully produce glycans according to the designed biosynthetic capacities[333]. Additionally, mammalian glycosylation control is already a well-studied quality attribute in biopharmaceuticals, illustrating that mammalian cells are robust platforms for precise glycoforms[335]. In contrast, microbial systems (bacteria, yeast) inherently lack many of the specific glycosyltransferases and metabolic pathways of mammalian glycosylation[334]. Many glycosyltransferases used in microbial HMO production are derived from pathogenic bacteria, raising concerns about endotoxin contamination, while yeast-based systems are inherently limited by their inability to synthesise sialic acid and tend instead to produce

mannose-rich glycan structures. Additionally, reconstruction of human-like glycosylation in microbes demands extensive pathway engineering, and the results often include unwanted side products or structural heterogeneity[336]. Mammalian cells are metabolically competent to synthesise nucleotide sugar donors (e.g. UDP-galactose, UDP-*N*-acetylglucosamine, CMP-sialic acid) via their endogenous pathways. These activated sugar donors are essential substrates for glycosyltransferases in HMO biosynthesis. In microbial systems, one often must introduce and optimise pathways for nucleotide sugar synthesis and regeneration, which can become metabolic bottlenecks. Given that mammalian cells inherently combine correct enzyme localisation, compartmentalisation, substrate availability, and protein processing pathways, they provide a coherent and physiologically aligned system for HMO synthesis with fewer off target glycoforms and lower purification burdens.

We evaluated whether truncated glycosyltransferases expressed in HEK293 cells could catalyse the synthesis of sialylated human milk oligosaccharides under controlled *in vitro* conditions. These experiments were motivated by the need to assess the intrinsic catalytic potential of mammalian enzymes in a simplified environment before committing to more complex cell-based production systems. While mammalian expression systems offer native folding, post-translational modifications, and access to CMP-Neu5Ac, the cellular context also imposes constraints related to localisation, substrate availability, and donor pool compartmentalisation. The truncated enzymes examined here were intentionally designed to exclude their trans-Golgi membrane-anchoring domain, producing soluble catalytic fragments. This design simplifies recovery if required and only attaches catalytic domains but eliminates the structural orientation and microenvironment that may be required for high glycosylation efficiency. The *in vitro* characterisation of glycosyltransferases derived from HEK293 cells provides insight into both the retained catalytic specificity of these enzymes and the mechanistic constraints imposed by their cytosolic localisation. Unlike their native counterparts, which are embedded in the Golgi apparatus via transmembrane domains, the engineered constructs lack these anchoring sequences and are therefore soluble, as evidenced by measurable activity in the cleared supernatant after centrifugation while negligible activity is detected in the cell pellet fraction. This relocalisation affects enzymatic efficiency. In the Golgi, spatial organisation ensures optimal substrate specificity, localised donor pools, and stable microenvironmental conditions, all of which

enhance collision frequency between enzyme and acceptor substrates and facilitate sequential glycosylation. The absence of such compartmentalisation may impose diffusion-limited constraints, reducing the probability of productive enzyme-substrate interactions and potentially explains the resulting low yields of 3′-SL and 6′-SL observed, despite the enzymes retaining intrinsic catalytic potential and linkage specificity.

The results confirmed that measurable enzymatic activity could be detected from the soluble preparations, with minimal formation of sialyllactose observed across a narrow pH window. These findings indicate that the catalytic domains of ST6GAL1 and related enzymes retain functionality independent of membrane anchoring. However, the low HMO production suggests that truncation may limit reaction efficiency, more so based on pH, that the Golgi provides. ST6GAL1 is naturally present on the trans-golgi[337]. Loss of this orientation, coupled with the absence of Golgi-like ionic and lipid environments, would likely explain the reduced turnover. The observation that activity was confined to the soluble fraction of the lysate, with no detectable activity in the pellet, supports the conclusion that the truncated enzymes were released into the cytosol and subsequently recovered in the supernatant. This localisation eliminates access to Golgi-resident substrates which may impact outputs of HMOs. The experiments demonstrate that activity is detectable predominantly under mildly acidic pH conditions (pH 6.5), consistent with the luminal pH of the Golgi[338], which optimises protein folding, donor binding, and transition-state stabilisation. The increased detection of 6′- and 3′-SL at this pH suggests that partial restoration of the native protonation state of catalytic residues improves donor binding. At higher or lower pH values, the soluble enzymes display substantially diminished activity, likely due to conformational destabilisation and reduced affinity for CMP-Neu5Ac donors or lactose acceptors. In contrast, the cytosolic pH of HEK293 cells is maintained near neutrality (approximately pH 7.2–7.4), which deviates substantially from the optimal pH identified in the cell-free assays. Expression of truncated glycosyltransferases within this neutral cytosolic environment is therefore likely to reduce catalytic efficiency prior to cell lysis, due to suboptimal protonation of active-site residues required for donor binding and catalysis. This pH mismatch provides a mechanistic explanation for the low yields observed in HEK293-based expression systems, despite retention of intrinsic enzymatic activity when reactions are conducted at pH 6.5 *in vitro*. These observations highlight that truncation and localisation do not abolish catalytic function but exacerbate environmental

sensitivity and revealing the delicate balance of factors that govern glycosyltransferase activity *in vivo*. Moreover, the cytosolic context lacks the CMP-Neu5Ac transporter and nucleotide sugar recycling systems that replenish donor substrates in the Golgi, so reactions quickly reach equilibrium. These factors together rationalise the trace product formation observed.

Temperature variation between 30 °C and 37 °C did not produce a marked difference, which is typical for mammalian enzymes already evolved for physiological temperature ranges as observed in other studies utilising glycosyltransferase GCNT2[339]. Together, these findings demonstrate that even in crude extracts, truncated glycosyltransferases can maintain correct folding and donor specificity, yet their catalytic efficiency may be limited by loss of membrane context and potentially inefficient substrate channelling.

Co-incubation of multiple enzymes did not enhance overall yield. This likely reflects the absence of spatial coordination normally conferred by the Golgi architecture. In native systems, glycosyltransferases are arranged sequentially along cisternal sub-compartments[340], enabling efficient hand-off of intermediate products. Without this organisation, soluble enzymes may compete rather than cooperate, and intermediates diffuse randomly in solution. This lack of compartmentalisation may also disrupt the stoichiometric balance of donor and acceptor substrates required for efficient chain extension. Modelling studies of glycan biosynthesis predict that such loss of enzyme proximity drastically reduces flux through sequential pathways[341,342], which may explain the failure of simple co-expression to generate significant product increases in this work. A recent mechanistic study demonstrated that B4GALT1 and ST6GAL1 do not act independently within the Golgi but instead form transient homo- and heteromeric assemblies that are essential for full catalytic function[343]. Using molecular docking, mutagenesis, and FRET-based interaction assays, the authors showed that B4GALT1 and ST6GAL1 engage via noncatalytic electrostatic surfaces while leaving their active sites exposed, thereby enabling sequential glycan elongation without steric interference. Notably, disruption of this spatial proximity correlates with impaired glycosylation, highlighting that enzyme co-localisation and physical interaction are rate-limiting features of pathway flux. These findings strongly support the rationale behind engineered enzyme

fusions in HMO synthesis strategies, including the attempts in this study to pre-link glycosyltransferases such as B3GNT2-ST6GAL1. By artificially enforcing proximity, such constructs may compensate for the absence of native Golgi organisation in expression systems such as HEK293 cells, although their cytosolic mis-localisation may still limit activity.

The gene selection process was informed by literature-based functional mapping and reinforced by computational modelling of glycan structures. WPS sequencing confirmed the integrity of all candidate constructs, allowing us to make informed decisions based not only on expression quality but also on the specificity of enzyme-substrate interactions. Among the galactosyltransferases screened, B4GALT4 emerged as the optimal candidate for β1,4-galactose addition to GlcNAc, supported by both structural predictions and its expression efficiency in mammalian systems. Similarly, B3GNT2 was selected as the only β1,3-*N*-acetylglucosaminyltransferase in the panel that could effectively extend lactose into a GlcNAc-primed intermediate, a necessary precursor for further elaboration. ST6GAL1 was the only sialyltransferase with α2,6 specificity toward terminal galactose, making it essential for the final capping step required to form 6′-SL and ST3GAL1 was the sialyltransferase with α2,3 specificity toward terminal galactose, required to form 3′-SL.

HEK293 cells provide a tractable platform for glycoengineering, but their endogenous glycosylation capacity is limited compared to the full human glycome. Narimatsu et al. systematically mapped human glycosyltransferases and applied targeted CRISPR-based knock-out and knock-in approaches in HEK293 to generate sublibraries of isogenic cell lines with defined glycan features[344]. The analysis demonstrated that while HEK293 cells contain the core machinery required for *N*- and *O*-glycosylation, they lack several glycosyltransferases necessary for the synthesis of more specialised structures, including certain fucosylated and sialylated motifs. As a result, the HEK293 glycome is relatively restricted, upon which defined glycan pathways can be reconstructed. Importantly, the study showed that the introduction of specific human glycosyltransferases is sufficient to expand the glycan repertoire of HEK293 cells to display otherwise absent human motifs. These findings highlight both the limitations of HEK293 as a model of natural human

glycosylation and its utility as a chassis for controlled glycan engineering, making it a promising host for the production of defined oligosaccharides such as HMOs.

One major strength of this approach lies in its biological relevance. Unlike microbial fermentation systems, which often struggle to replicate human-like glycosylation, HEK293 cells provide the correct post-translational context to support native enzymatic activity. This strategy builds upon the broader field of synthetic glycobiology, where efforts have been directed toward microbial and mammalian cell platforms for HMO production[345,346] Engineered strains of *E.coli* have already reached industrial production levels for fucosylated HMOs such as 2′-FL[347], which is now incorporated into commercial infant formulas[348]. However, the production of sialylated HMOs in bacteria has been less efficient, primarily because establishing functional CMP-sialic acid biosynthetic pathways and ensuring effective sialyltransferase activity remain major obstacles[349]. This is especially valuable for producing sialylated HMOs like 3'-SL and 6′-SL, which require precise linkage specificity and coordinated transport of nucleotide sugar donors such as CMP-sialic acid. Mammalian cell lines offer a more favourable environment for sialylation due to their endogenous sialic acid metabolism. The plasmid design pursued here represents a hybrid solution, aiming to combine the metabolic competency of mammalian hosts with the modular control provided by synthetic expression systems.

The selection of a G4S (Glycine$_4$-Serine or GGGGS) linker for the fusion of glycosyltransferases in this study was driven by its well-documented advantages in recombinant protein engineering[350-353]. Glycine and serine residues confer flexibility and hydrophilicity to the linker, reducing steric hindrance and enhancing solubility, which is crucial for maintaining the functional integrity of the fused enzymes[354]. Additionally, the G4S linker has been shown to support the independent folding of adjacent protein domains, thereby preserving their catalytic activities in multidomain constructs[355]. These properties make the G4S linker an optimal choice for constructing fusion proteins aimed at efficient and functional glycosylation in mammalian expression systems.

Methodologically, the detection of both 3′- and 6′-SL by HPAEC-PAD supports the specificity of the enzymatic reaction but also exposes the analytical limitations of the

technique. HPAEC-PAD provides excellent sensitivity for charged oligosaccharides and allows clear differentiation of 3′- and 6′-isomers based on retention time shifts arising from differences in linkage configuration and overall interaction with the stationary phase, even though they share molecular weight. The approach proved less robust for neutral structures such as LNnT. In this case, co-eluting components from the culture medium (DMEM), combined with overlapping retention profiles from residual lactose, generated substantial background interference that obscured LNnT-specific peaks. To mitigate this, samples were diluted up to 1:100, yet this reduced sensitivity and caused peak shifting due to altered matrix composition. Further to this, PAD detection alone cannot confirm linkage without orthogonal validation such as LC-MS/MS fragmentation or exoglycosidase digestion. Future analyses should therefore integrate complementary mass spectrometry approaches to confirm structural assignments and quantify yields with greater confidence.

Nevertheless, several limitations must be acknowledged. First, while plasmid construction and expression validation were successful, further optimisation is required. Additionally, while this system was designed to minimise enzyme number, it is possible that co-expression of additional accessory enzymes, such as CMP-sialic acid transporters or nucleotide sugar regenerating enzymes or lactose transporters could improve HMO yield.

Choice of glycosyltransferase must be carefully considered: while ST6GAL1 is critical for α-2,6 linkages, other sialyltransferases such as ST6GAL2 may be more suitable in microbial cell contexts due to differences in folding and donor substrate specificity[356]. The current findings highlight both the promise and the complexity of such systems. Conceptually, the construction of multi-enzyme plasmids demonstrates the feasibility of rebuilding glycosylation pathways in synthetic hosts. The choice of enzymes was guided by their roles in HMO biosynthesis: B3GNT2 catalyses the addition of β-1,3 *N*-acetylglucosamine, B4GALT4 carries out β-1,4 galactosylation, and ST6GAL1 provides the critical α-2,6-sialylation step[356]. The selection of isotypes in this model may not necessarily be the best for optimal HMO production. Importantly, the arrangement of these enzymes may influence yield, consistent with the principle of metabolic channelling, where co-localisation of sequential enzymes enhances flux and reduces intermediate loss[357]. Additionally, balancing pathway flux remains the central challenge. Merely co-expressing enzymes is probably insufficient; their activity must be orchestrated through synthetic circuits that dynamically adjust expression based on metabolic demand. Advances in

synthetic biology, including CRISPR-based regulation and synthetic scaffolding proteins, could prove invaluable here[358]. Also, the choice of host system will ultimately determine feasibility. While mammalian expression ensures correct folding and localisation, microbial hosts retain advantages in scalability and cost.

Several design strategies emerge from this analysis. Expressing full-length enzymes with their native transmembrane domain would restore Golgi localisation and allow access to endogenous CMP-Neu5Ac transport systems, likely improving reaction efficiency. Co-expression of CMP-Neu5Ac synthetase and transporter proteins may further enhance donor supply.

In comparing these findings with existing HMO production strategies, it is clear that microbial or cell-free systems currently achieve superior yields. Engineered *E. coli* and *B. subtilis* strains expressing bacterial sialyltransferases, together with CMP-Neu5Ac regeneration pathways, can produce high mg/L to low g/L concentrations of 6′-SL *in vitro*[359,360]. These systems benefit from high enzyme expression levels and reduced metabolic burden from native glycosylation. While mammalian cells such as HEK293 provide human-like glycosylation machinery, they are metabolically complex and tightly regulate nucleotide-sugar pools. The advantage of HEK293 systems lies in their ability to generate correctly folded, post-translationally modified enzymes. The challenge is therefore to retain this folding benefit while restoring the spatial organisation and donor availability that drive high productivity.

For future work, these findings provide several avenues for enhancing *in vitro* human milk oligosaccharide synthesis. Restoration of spatial organisation could increase the effective concentration of donor and acceptor substrates and improve sequential glycosylation efficiency. Optimisation of reaction parameters, including pH, temperature, and donor-to-acceptor ratios, is also essential, as minor deviations can disproportionately affect the activity of cytosolic, truncated enzymes. Parallel efforts should explore co-expression of nucleotide sugar transporters (e.g., SLC35A1 for CMP-sialic acid import) or sugar nucleotide regeneration enzymes, as donor pool insufficiency from the cells own metabolism may be an additional bottleneck in cytosolic systems. Future iterations of the

construct may include internal ribosome entry sites (IRES) or 2A peptide sequences, inducing ribosomal skipping to facilitate polycistronic expression under a single promoter, simplifying transfection and improving stoichiometric balance between enzymes. Furthermore, the combination of HPAEC-PAD with complementary analytical approaches, such as mass spectrometry or NMR, would enable rigorous structural confirmation and quantification of low-abundance products, ensuring that enzymatic specificity is maintained despite artificial localisation. Collectively, the data demonstrate that while truncation facilitates solubility and simplifies handling, it introduces fundamental limitations that must be addressed to achieve productive biosynthesis of sialylated human milk oligosaccharides. These insights advance our understanding of the interplay between enzyme structure, localisation, and reaction conditions and establish a mechanistic framework for future engineering of efficient *in vitro* HMO production platforms.

Collectively, these findings demonstrate that glycosyltransferases expressed in HEK293 cells can catalyse specific HMO linkages but at extremely low efficiency potentially due to disrupted localisation, limited donor access, and absence of compartmentalisation. The work establishes a foundation for mechanistic exploration of enzyme function outside the Golgi and identifies key variables; membrane tethering, pH, donor regeneration, and enzyme proximity, that all must be addressed to advance mammalian HMO biosynthesis. Improving these factors will be central to translating the intrinsic catalytic potential observed here into a functional production platform capable of synthesising human milk oligosaccharides at useful yields.

These observations have significant translational implications. Industrially, demand for sialylated HMOs is increasing, as their inclusion in infant nutrition is expected to more closely replicate the functional benefits of human milk. While 2′-FL and LNnT are already mass-produced[188], commercial supply of 3′-SL and 6′-SL remains limited. This work suggests that multi-enzyme plasmid systems could provide a pathway to scalable production, though considerable optimisation will be needed to achieve more viable yields. Current availability of these molecules is a limiting factor in the field, constraining *in vivo* validation and receptor mapping studies. A robust synthetic system for their production would open the door to systematic investigations of dose-response relationships, analysis

with other milk components, and functional testing in infection, allergy, and autoimmunity models[299]. Moreover, sufficient supply would enable structural studies, such as crystallography or NMR-based receptor binding analyses, to clarify which glycan motifs drive specific immunometabolic outcomes.

In conclusion, this chapter demonstrates the feasibility of engineering plasmid systems for sialylated HMO biosynthesis while highlighting the biological and technical barriers that remain. The capacity to produce 3′-SL and 6′-SL at scale is not merely an industrial goal but a must for advancing immunological research into their mechanisms of action. The future of HMO biology lies in integrating immunological insights with synthetic glycobiology, an intersection that will allow us to move from descriptive studies of maternal milk to rational exploitation of its components as therapeutic immunomodulators.

Chapter 7

General Discussion

The work presented in this thesis aims to advance our understanding of HMOs as direct modulators of immune cell metabolism and function. The outputs extend their significance beyond the well-established role as prebiotic substrates for the infant gut microbiota. HMOs have been detected in circulation, indicating potential interactions with systemic immune cells[241]. Previous studies have reported broad effects of HMOs on inflammation or epithelial responses, yet few have dissected their direct actions on individual immune cell types using metabolism focused approaches. To date, much of the research that has been conducted on HMOs and immune cells has either investigated pooled HMOs from breast milk or studied the situation *in vivo*, which makes it difficult to ascertain the direct effects of individual HMO on individual cell types. Chapters 3-5 address that gap by examining the effects of three predominant HMOs (2′-FL, 3′-SL, 6′-SL) individually on macrophages, DCs and T-cells. Metabolic flux analysis, gene expression profiling and complex assays were employed to analyse the cells individual metabolism. Additionally, ROS and cytokine measurements, phagocytosis, and receptor signalling readouts were used to interrogate their functional outputs.

Chapter 3 demonstrated that HMOs reprogram macrophage metabolism in a structure and activation dependent manner. Sialylated HMOs (3′-SL and 6′-SL) broadly suppress mitochondrial respiration while enhancing glycolysis in a basal state but subvert overactive glycolytic response in an inflammatory context. This result suggests an innate immune cell priming effect reminiscent of trained immunity. Conversely, 2′-FL supported oxidative phosphorylation and maintained a metabolic profile more resemblant of M2 macrophages. These effects were also validated at the transcriptional level, indicating durable metabolic reprogramming rather than just transient substrate use. Overall, the findings of this chapter suggest that different HMO structures engage different metabolic pathways that balances immune priming, influencing basal capacity while preventing a full inflammatory cascade.

Chapter 4 revealed that the HMOs not only influenced metabolic changes but also modulated immunomodulatory outcomes. 6′-Sialylactose was found to enhance phagocytic activity and elevate basal ROS production, indicative of heightened antimicrobial response. However, under prolonged inflammatory stress, all three HMOs prevented excessive ROS production and diminished cytokine release. These findings reflect a controlled activation

model where certain HMOs may induce early innate immune defence while preventing an exacerbated or hyper inflammatory response. Rather than functioning purely as inflammatory enhancers or suppressors, HMOs appear to alter innate responses according to specific inflammatory conditions.

Chapter 5 expanded immunometabolism analysis to DCs and also adaptive immunity, via T-cell analysis. DCs were found to be modulated by 6′-SL in particular, driving them towards a metabolically quiescent state, while also subverting LPS induced glycolytic increase. Effector and memory T-cells were found to be unresponsive to direct metabolic modulation. This finding aligns with the concept that HMOs shape adaptive immunity indirectly by acting on antigen-presenting cells rather than directly on T-cells themselves. The results suggest that T-cells are secondary responders and not primary targets of HMOs.

Chapters 3-5 provide further insight into HMOs role as nuanced immunometabolic signalling molecules. The results position HMOs as more than prebiotic, inert nutrients. Highlighting their capacity to alter innate immune cell energetics and immunological output in a structure and cell state dependent manner. This could suggest an evolutionary role for HMOs in sculpting neonatal immune development at a multi-cell level. The present work demonstrates specific, cell-intrinsic immunometabolic effects that cannot be explained by microbiota mediation alone. In doing so, it reinforces the broader concept of immunometabolism, whereby metabolic pathways are integral to immune function[130]. HMOs expand the current immunometabolism framework by representing exogenous dietary molecules capable of altering immune cell metabolism. The implications of this research suggest that HMOs may represent a class of maternally derived immunomodulators with potential therapeutic relevance in both neonatal and adult contexts.

These findings also raise intriguing questions about the evolutionary timing of HMO production. Integrated transcriptomic analyses of human lactocytes have shown that expression of ST6GAL1, the key glycosyltransferase responsible for 6′-SL biosynthesis, is maximal immediately postpartum, coinciding with the period when the infant immune system is most immature[361]. Certain FUTs such as FUT2, 6 and 8 are expressed in the

earlier weeks postpartum, with FUT10 and 11 being expressed later. Longitudinal profiling of human milk confirms that 6′-SL concentrations are highest in colostrum and early milk, then decline steadily over subsequent months[362]. In contrast, 2'-FL concentrations while higher in colostrum, remain higher for longer postpartum, before eventually waning. This timing overlaps with a developmental window in which innate immunity grows to be the primary line of defence, as adaptive immunity takes months to mature[363]. HMOs are metabolically costly for the mother to produce, requiring significant investment in activated nucleotide sugars and enzymatic activity, also redirecting the calories in the form of lactose away from the infant into an alternate form they cannot digest[364]. Their persistence across human populations and their dominance in early lactation suggest strong evolutionary pressure to maintain these structures despite their cost. This implies disproportionate benefit, most likely in the form of enhanced neonatal survival through reduced infection risk. Given the findings presented in this thesis, it is plausible that HMOs provides targeted support to neonatal innate immunity. By boosting pathogen clearance yet tempering excessive inflammation, HMOs may help infants mount effective early responses while avoiding excessive inflammatory outcomes. This hypothesis aligns with epidemiological evidence that shows breastfed infants experience fewer respiratory and gastrointestinal infections when compared to formula fed infants[365]. While causality cannot yet be established, the temporal alignment between early postpartum and high HMO concentrations, the dominance of innate immunity, and reduced infection rates suggest that evolutionary selection may have shaped HMO secretion to optimise early-life immune defence. From a translational perspective, this reinforces the priority of developing scalable production systems for HMOs particularly those that are sialylated. If nature has heavily invested in these molecules, then reproducing them for formula or as therapeutic agents may yield equal benefits.

The broader implications of these findings are significant. First, they highlight HMOs as potential therapeutic agents for modulating immune metabolism in contexts such as autoimmunity and chronic inflammation. The research opens translational avenues in adult medicine as well as neonatal, as synthetic HMOs could be harnessed to modulate immune responses in diseases where metabolic rewiring is central, such as sepsis, or inflammatory bowel disease. Second, HMOs could provide a mechanistic basis for epidemiological observations further linking breastfeeding to reduced risk of allergies, asthma, and

autoimmune disease[365]. If maternal HMOs condition infant immune cells toward tolerance and restrained inflammation, this could contribute directly to protective effects that have been observed previously, independent of microbiota composition.

While this thesis provides new insights into how specific HMOs modulate macrophage, DC and T-cell function, several limitations must be acknowledged. First, all experiments were performed using murine immune cells, which, while well-established as a model system, may not fully capture the complexity of human immune responses. Differences including receptor expression and signaling thresholds between murine and human cells may limit the direct translational relevance of these findings. To fully validate translational potential, it will be necessary to extend these studies to human monocyte-derived macrophages and DCs, ideally complemented by tissue-resident immune cells, organoid systems and *in-vivo* models that more accurately capture physiological microenvironments to determine whether the modulatory effects of 2′-FL, 3′-SL, and 6′-SL extend beyond the murine system. Extending analyses to human primary cells will enhance clinical relevance. While *in vitro* metabolic profiling provides mechanistic insight, it cannot capture the layered complexity of an organism where microbiota-derived metabolites, tissue microenvironments, and systemic feedback loops converge. Most assays were conducted under highly controlled *in vitro* conditions, with stimuli such as LPS or anti-CD3 used to model inflammatory or activation states. These reductionist systems were critical for delineating mechanism and direct effects but may not replicate the environments of tissues such as the gut and circulatory immune system, where HMOs naturally interact with immune cells alongside microbiota, epithelial barriers, additional dietary components and other factors. Testing the effects of HMO in *in vivo* models of infection, allergy, autoimmunity, and chronic inflammation will be essential to establish whether the effects described here translate into meaningful functional outcomes at the organismal level.

A second limitation lies in the structural reductionism of this work focusing on three specific HMOs (2′-FL, 3′-SL, and 6′-SL) provides mechanistic clarity but inevitably sacrifices physiological complexity. Human milk contains over 200 oligosaccharide structures[366], and synergistic or antagonistic interactions between these components almost certainly shape natural outcomes observed. For example, other studies revealed that

different combinations and concentrations of HMOs together, altered cytokine output in a Caco-2 model[243]. It is therefore plausible that the effects observed for individual HMOs in isolation may be modulated or even reconfigured when presented in the full maternal milk matrix or even simple combinations such as 2'-FL and 3'-SL. Future studies that compare mixtures to single sugars will be essential to bridge insight of specific effects with physiological reality. Additionally, integrating HMO-driven immune modulation with microbiota-derived signals such as SCFAs may reveal synergistic mechanisms that more fully explain how maternal milk shapes neonatal immunity.

In addition, the scope of this thesis was limited to select immune cell subsets. While macrophages, DCs, and T-cells represent critical effectors of innate and adaptive immunity, the immune system operates as an interconnected network. It remains unknown how HMO-induced changes in one cell population influence others through cytokine or metabolic crosstalk. While this study provides detailed insight into the effects of HMOs on macrophages, DC and T-Cell metabolism and function individually, an important next step would be to explore how HMOs influence the APCs in the context of adaptive immunity. In particular, performing co-culture experiments using HMO-treated DCs and T-cells to assess whether the effects observed here translate into downstream adaptive immune alteration. Such research would build upon the findings presented in this thesis and extend the relevance of HMOs in adaptive immune modulation. This may uncover novel mechanisms and assess whether dietary glycans influence host immunity beyond infancy by targeting long-term adaptive immunity in this indirect manner. The indirect mechanism of how HMOs impact T-cells is currently supported by previous studies showing HMOs skew macrophages and DCs toward anti-inflammatory phenotypes, suppress pro-inflammatory cytokines, and promote regulatory T-cell induction *in vitro* and *in vivo*[298,300]. Such an approach would bridge the innate and adaptive findings, clarifying whether metabolic reprogramming in DCs translate into functional long-term shifts in T-cell fate and function. Also, expanding this work to include other circulatory immune cells such as regulatory T-cells, NK cells, neutrophils, eosinophils or B cells could reveal broader immunological consequences of HMO exposure.

The final chapter addressed a practical barrier; most structurally defined HMOs remain inaccessible at scale, including branched and sialylated structures. Reconstruction of HMO biosynthesis pathways using truncated glycosyltransferases in HEK293 cells demonstrated retained catalytic specificity of enzymes such as ST6GAL1. Additionally, when ST6GAL1 was linked to B3GNT2 (B3GNT2-ST6GAL1), specific sialylated HMO, 6'-SL was still detected at marginal levels. Co-incubation of crude enzyme extract of multiple enzymes involved in the synthesis of multiple HMOs showed marginal production of three HMOs at pH 6.5, mirroring computational predictions and physiological requirements of the enzymes.

Efforts to synthesise HMOs have historically centred around microbial fermentation systems, where engineered *E. coli* or *Saccharomyces* strains are designed to express glycosyltransferases to reconstruct segments of the HMO biosynthetic pathway. While these approaches have succeeded in producing fucosylated HMOs such as 2′-FL at commercial scale, more complex or sialylated HMOs remain largely absent from infant formulas, this may be in part due to challenges in achieving scalable production. This limitation is rarely acknowledged explicitly in the literature but is implicitly reflected in market availability; the HMOs remain either prohibitively expensive or functionally inaccessible. The prevailing assumption has been that microbial hosts require additional enzymes, metabolic redirection or donor supplementation to close this gap. However, the work presented in Chapter 6 challenges mammalian cell systems to exploit their native metabolism and ability to express human glycosyltransferases and other relevant cell machinery.

The implications of these findings extend directly back to the immunological findings in earlier chapters. If the most potent immunomodulatory HMOs cannot be produced reliably, then their therapeutic exploitation will remain speculative, regardless of how compelling their biological effects are shown to be. Chapter 6 thus acts as the necessary translational bridge highlighting that the bottleneck in HMO therapeutics is not discovery, but production. HMOs cannot become immunoregulatory interventions until scalable, structure-specific synthesis is achieved. The failure of current microbial systems to possess

proper enzyme function further suggests that mammalian platforms, long dismissed as inefficient, may in fact be better suited to high-fidelity glycan production.

Chapter 6 provides a valuable insight into the challenges of reconstructing HMO biosynthesis in mammalian systems. Also, several limitations must be acknowledged in interpreting the current outcomes. First, the use of truncated glycosyltransferases, while necessary to facilitate secretion and detect soluble catalytic activity, inherently removed their transmembrane domain, preventing assessment of whether full-length, correctly localised enzymes might have yielded more productive synthesis. As a result, it is difficult to determine whether the glycan yield observed was attributed to enzyme catalytic inefficiency, impaired access to donor substrates, or mis-localisation of the enzyme within the cell. Perhaps the next phase of this study should involve re-establishing Golgi-like enzyme ordering, either through full-length glycosyltransferase constructs or through synthetic systems that enforce enzyme proximity. Membrane-anchored fusion proteins arranged in sequential order could provide a controlled platform to test whether spatial hierarchy is sufficient to restore productive glycan assembly. Rather than fusion proteins of glycosyltransferases on freely diffusing enzymes in suspension or cytosolic expression as examined here. Second, the intracellular availability and utilisation of nucleotide-sugar donors such as CMP-sialic acid were never actually directly quantified, meaning that limited donor access could have contributed to low reaction efficiency without being experimentally verified. Third, the analytical methods used to detect product formation were endpoint-based, which potentially may overlook transient intermediates or low-abundance products that might have revealed partial pathway activity. Finally, all experiments were carried out in HEK293 cells, which possesses a glycosylation profile that may not accurately replicate the Golgi architecture or donor dynamics of more physiologically relevant epithelial cell types. Expanding beyond HEK293 cells to maybe even mammary epithelial lines, may further increase pathway fidelity and HMO production.

A further avenue for future research lies in expanding beyond linear mono-sialylated or fucosylated structures toward branched and higher-order HMOs, which remain almost entirely unexplored both biologically and synthetically. At present, the vast majority of

functional studies (including those in this thesis) rely on commercially accessible single-branch HMOs such as 2′-FL, 3′-SL, and 6′-SL, not only because these represent the dominant structures in human milk, but also because they are the only ones that can be reliably produced. In reality, a significant proportion of native HMOs are internally branched, multi-sialylated, or combine both fucosylation and sialylation within the same scaffold, yet virtually nothing is known about whether these multi-antennary structures engage the gut, the microbiota or even immune cells differently. The increased size and branching of these more complex HMO may allow for other unknown effects on gut-microbiota or even immune cells. However, without synthetic access to these glycans, their function remains speculative. Therefore, future engineering efforts should aim not only to reconstruct linear pathways but to enable controlled branching. Once even small quantities of defined branched HMOs become available, they can be directly compared to their linear counterparts in already established cell assays to determine whether branching confers distinct signalling capacity or other effects. In this sense, the synthesis of complex HMOs is not merely a technical query, but the key to understanding whether modulation by HMOs is governed by chemical identity or by architectural sophistication.

Final Conclusion

In conclusion, this thesis demonstrates that HMOs, long considered primarily as microbiota substrates, are direct immunometabolic modulators. By reprogramming macrophage and DC metabolism and function, HMOs establish a cell-intrinsic layer of innate immune regulation. These findings broaden the conceptual framework of HMO biology, linking maternal glycans to infant immune development through direct metabolic mechanisms. The synthetic glycobiology work undertaken in this thesis represents a step toward overcoming the bottleneck of HMO availability. While yields were low and technical challenges remain, these experiments highlight the principle that synthetic biology and immunology are complementary rather than parallel fields. Immunological studies can identify molecules of interest, while synthetic biology provide the means to generate them in sufficient quantities for translational application. While further work is required to validate and extend these insights, the data presented here highlights the evolutionary sophistication of maternal-infant molecular communication and open new perspectives in both basic immunology and synthetic biology.

Bibliography

1 Lönnerdal, B. in *Protein in Neonatal and Infant Nutrition: Recent Updates: 86th Nestlé Nutrition Institute Workshop, Beijing, May 2015* Vol. 86 (eds J. Bhatia, R. Shamir, & Y. Vandenplas) 0 (S.Karger AG, 2016).

2 Zivkovic, A. M., German, J. B., Lebrilla, C. B. & Mills, D. A. Human milk glycobiome and its impact on the infant gastrointestinal microbiota. *Proc Natl Acad Sci U S A* **108 Suppl 1**, 4653-4658 (2011). https://doi.org/10.1073/pnas.1000083107

3 Wiciński, M., Sawicka, E., Gębalski, J., Kubiak, K. & Malinowski, B. Human Milk Oligosaccharides: Health Benefits, Potential Applications in Infant Formulas, and Pharmacology. *Nutrients* **12** (2020). https://doi.org/10.3390/nu12010266

4 Bode, L. Human milk oligosaccharides: every baby needs a sugar mama. *Glycobiology* **22**, 1147-1162 (2012). https://doi.org/10.1093/glycob/cws074

5 Adeline Gauhe *et al.* Bifidus Factor IV. Preparations Obtained from. Human Milk. (1953).

6 Zhang, S. *et al.* Gold standard for nutrition: a review of human milk oligosaccharide and its effects on infant gut microbiota. *Microb Cell Fact* **20**, 108 (2021). https://doi.org/10.1186/s12934-021-01599-y

7 Mulinge, M. M. *et al.* The Role of Maternal Secretor Status and Human Milk Oligosaccharides on Early Childhood Development: A Systematic Review and Meta-Analysis. *Breastfeed Med* **19**, 409-424 (2024). https://doi.org/10.1089/bfm.2023.0274

8 Blank, D., Dotz, V., Geyer, R. & Kunz, C. Human milk oligosaccharides and Lewis blood group: individual high-throughput sample profiling to enhance conclusions from functional studies. *Adv Nutr* **3**, 440s-449s (2012). https://doi.org/10.3945/an.111.001446

9 Wu, S., Tao, N., German, J. B., Grimm, R. & Lebrilla, C. B. Development of an annotated library of neutral human milk oligosaccharides. *J Proteome Res* **9**, 4138-4151 (2010). https://doi.org/10.1021/pr100362f

10 Wu, S., Grimm, R., German, J. B. & Lebrilla, C. B. Annotation and structural analysis of sialylated human milk oligosaccharides. *J Proteome Res* **10**, 856-868 (2011). https://doi.org/10.1021/pr101006u

11 Orczyk-Pawiłowicz, M. & Lis-Kuberka, J. The Impact of Dietary Fucosylated Oligosaccharides and Glycoproteins of Human Milk on Infant Well-Being. *Nutrients* **12** (2020). https://doi.org/10.3390/nu12041105

12 Chen, X. Human Milk Oligosaccharides (HMOS): Structure, Function, and Enzyme-Catalyzed Synthesis. *Adv Carbohydr Chem Biochem* **72**, 113-190 (2015). https://doi.org/10.1016/bs.accb.2015.08.002

13 McDonald, A. G., Mariethoz, J., Davey, G. P. & Lisacek, F. In silico analysis of the human milk oligosaccharide glycome reveals key enzymes of their biosynthesis. *Scientific Reports* **12**, 10846 (2022). https://doi.org/10.1038/s41598-022-14260-4

14 Lane, J. A., O'Callaghan, J., Carrington, S. D. & Hickey, R. M. Transcriptional response of HT-29 intestinal epithelial cells to human and bovine milk oligosaccharides. *Br J Nutr* **110**, 2127-2137 (2013). https://doi.org/10.1017/S0007114513001591

15 Bakker-Zierikzee, A. M. *et al.* Faecal SIgA secretion in infants fed on pre- or probiotic infant formula. *Pediatr Allergy Immunol* **17**, 134-140 (2006). https://doi.org/10.1111/j.1399-3038.2005.00370.x

16 Maryam Kebbe, Kartik Shankar, Leanne M Redman & Andres, A. Human Milk Components and the Infant Gut Microbiome at 6 Months: Understanding the

Interconnected Relationship,. *The Journal of Nutrition* (2024). https://doi.org/10.1016/j.tjnut.2024.02.029.

17 Krajmalnik-Brown, R., Ilhan, Z. E., Kang, D. W. & DiBaise, J. K. Effects of gut microbes on nutrient absorption and energy regulation. *Nutr Clin Pract* **27**, 201-214 (2012). https://doi.org/10.1177/0884533611436116

18 Pickard, J. M., Zeng, M. Y., Caruso, R. & Nunez, G. Gut microbiota: Role in pathogen colonization, immune responses, and inflammatory disease. *Immunol Rev* **279**, 70-89 (2017). https://doi.org/10.1111/imr.12567

19 Yao, Q. *et al.* The Milk Active Ingredient, 2'-Fucosyllactose, Inhibits Inflammation and Promotes MUC2 Secretion in LS174T Goblet Cells In Vitro. *Foods* **12** (2023). https://doi.org/10.3390/foods12010186

20 Wu, R. Y. *et al.* Human Milk Oligosaccharides Increase Mucin Expression in Experimental Necrotizing Enterocolitis. *Molecular Nutrition & Food Research* **63**, 1800658 (2019). https://doi.org/10.1002/mnfr.201800658

21 Li, M. *et al.* An In Vitro Colonic Fermentation Study of the Effects of Human Milk Oligosaccharides on Gut Microbiota and Short-Chain Fatty Acid Production in Infants Aged 0-6 Months. *Foods* **13** (2024). https://doi.org/10.3390/foods13060921

22 Kuntz, S. *et al.* Influence of microbially fermented 2 -fucosyllactose on neuronal-like cell activity in an in vitro co-culture system. *Front Nutr* **11**, 1351433 (2024). https://doi.org/10.3389/fnut.2024.1351433

23 Yahagi, K. Fucosylated human milk oligosaccharide-utilizing bifidobacteria regulate the gut organic acid profile of infants. *Biosci Microbiota Food Health* **43**, 92-99 (2024). https://doi.org/10.12938/bmfh.2023-069

24 Koh, A., De Vadder, F., Kovatcheva-Datchary, P. & Backhed, F. From Dietary Fiber to Host Physiology: Short-Chain Fatty Acids as Key Bacterial Metabolites. *Cell* **165**, 1332-1345 (2016). https://doi.org/10.1016/j.cell.2016.05.041

25 Schwab, C. & Ganzle, M. Lactic acid bacteria fermentation of human milk oligosaccharide components, human milk oligosaccharides and galactooligosaccharides. *FEMS Microbiol Lett* **315**, 141-148 (2011). https://doi.org/10.1111/j.1574-6968.2010.02185.x

26 Schwab, C. *et al.* Trophic Interactions of Infant Bifidobacteria and Eubacterium hallii during L-Fucose and Fucosyllactose Degradation. *Front Microbiol* **8**, 95 (2017). https://doi.org/10.3389/fmicb.2017.00095

27 Walsh, C., Lane, J. A., van Sinderen, D. & Hickey, R. M. Human milk oligosaccharide-sharing by a consortium of infant derived Bifidobacterium species. *Sci Rep* **12**, 4143 (2022). https://doi.org/10.1038/s41598-022-07904-y

28 Fukuda, S. *et al.* Bifidobacteria can protect from enteropathogenic infection through production of acetate. *Nature* **469**, 543-547 (2011). https://doi.org/10.1038/nature09646

29 Bolognini, D., Tobin, A. B., Milligan, G. & Moss, C. E. The Pharmacology and Function of Receptors for Short-Chain Fatty Acids. *Molecular Pharmacology* **89**, 388-398 (2016). https://doi.org/10.1124/mol.115.102301

30 Parada Venegas, D. *et al.* Short Chain Fatty Acids (SCFAs)-Mediated Gut Epithelial and Immune Regulation and Its Relevance for Inflammatory Bowel Diseases. *Front Immunol* **10**, 277 (2019). https://doi.org/10.3389/fimmu.2019.00277

31 Canfora, E. E., Jocken, J. W. & Blaak, E. E. Short-chain fatty acids in control of body weight and insulin sensitivity. *Nat Rev Endocrinol* **11**, 577-591 (2015). https://doi.org/10.1038/nrendo.2015.128

32 Davie, J. R. Inhibition of histone deacetylase activity by butyrate. *J Nutr* **133**, 2485S-2493S (2003). https://doi.org/10.1093/jn/133.7.2485S
33 Jing, X., Lyu, J. & Xiong, J. Acetate regulates GAPDH acetylation and T helper 1 cell differentiation. *Mol Biol Cell* **34**, br10 (2023). https://doi.org/10.1091/mbc.E23-02-0070
34 Smith, P. M. *et al.* The microbial metabolites, short-chain fatty acids, regulate colonic Treg cell homeostasis. *Science* **341**, 569-573 (2013). https://doi.org/10.1126/science.1241165
35 Furusawa, Y. *et al.* Commensal microbe-derived butyrate induces the differentiation of colonic regulatory T cells. *Nature* **504**, 446-450 (2013). https://doi.org/10.1038/nature12721
36 Arpaia, N. *et al.* Metabolites produced by commensal bacteria promote peripheral regulatory T-cell generation. *Nature* **504**, 451-455 (2013). https://doi.org/10.1038/nature12726
37 Ackerman, D. L. *et al.* Antimicrobial and Antibiofilm Activity of Human Milk Oligosaccharides against Streptococcus agalactiae, Staphylococcus aureus, and Acinetobacter baumannii. *ACS Infect Dis* **4**, 315-324 (2018). https://doi.org/10.1021/acsinfecdis.7b00183
38 Craft, K. M., Gaddy, J. A. & Townsend, S. D. Human Milk Oligosaccharides (HMOs) Sensitize Group B Streptococcus to Clindamycin, Erythromycin, Gentamicin, and Minocycline on a Strain Specific Basis. *ACS Chemical Biology* **13**, 2020-2026 (2018). https://doi.org/10.1021/acschembio.8b00661
39 Chambers, S. A. *et al.* A Solution to Antifolate Resistance in Group B Streptococcus: Untargeted Metabolomics Identifies Human Milk Oligosaccharide-Induced Perturbations That Result in Potentiation of Trimethoprim. *mBio* **11** (2020). https://doi.org/10.1128/mBio.00076-20
40 Duska-McEwen, G., Senft, A. P., Ruetschilling, T. L., Barrett, E. G. & Buck, R. H. Human Milk Oligosaccharides Enhance Innate Immunity to Respiratory Syncytial Virus and Influenza <i>in Vitro</i&gt. *Food and Nutrition Sciences* **05**, 1387-1398 (2014). https://doi.org/10.4236/fns.2014.514151
41 Sato, Y., Kanayama, M., Nakajima, S., Hishida, Y. & Watanabe, Y. Sialyllactose Enhances the Short-Chain Fatty Acid Production and Barrier Function of Gut Epithelial Cells via Nonbifidogenic Modification of the Fecal Microbiome in Human Adults. *Microorganisms* **12** (2024). https://doi.org/10.3390/microorganisms12020252
42 Boll, E. J. *et al.* Human milk oligosaccharides differentially support gut barrier integrity and enhance Th1 and Th17 cell effector responses in vitro. *Front Immunol* **15**, 1359499 (2024). https://doi.org/10.3389/fimmu.2024.1359499
43 Suligoj, T. *et al.* Effects of Human Milk Oligosaccharides on the Adult Gut Microbiota and Barrier Function. *Nutrients* **12** (2020). https://doi.org/10.3390/nu12092808
44 Jarzynka, S. *et al.* Human Milk Oligosaccharides Exhibit Biofilm Eradication Activity Against Matured Biofilms Formed by Different Pathogen Species. *Front Microbiol* **12**, 794441 (2021). https://doi.org/10.3389/fmicb.2021.794441
45 Moore, R. E. *et al.* Anti-biofilm Activity of Human Milk Oligosaccharides in Clinical Strains of Streptococcus agalactiae with Diverse Capsular and Sequence Types. *Chembiochem* **24**, e202200643 (2023). https://doi.org/10.1002/cbic.202200643
46 Piotrowski, M., Wultanska, D. & Pituch, H. The prebiotic effect of human milk oligosaccharides 3'- and 6'-sialyllactose on adhesion and biofilm formation by

Clostridioides difficile - pilot study. *Microbes Infect* **24**, 104929 (2022). https://doi.org/10.1016/j.micinf.2021.104929

47 Pantaleon, V. *et al.* The Clostridium difficile Protease Cwp84 Modulates both Biofilm Formation and Cell-Surface Properties. *PLoS One* **10**, e0124971 (2015). https://doi.org/10.1371/journal.pone.0124971

48 Craft, K. M., Thomas, H. C. & Townsend, S. D. Interrogation of Human Milk Oligosaccharide Fucosylation Patterns for Antimicrobial and Antibiofilm Trends in Group B Streptococcus. *ACS Infect Dis* **4**, 1755-1765 (2018). https://doi.org/10.1021/acsinfecdis.8b00234

49 Bhowmik, A. *et al.* Human Milk Oligosaccharides as Potential Antibiofilm Agents: A Review. *Nutrients* **14** (2022). https://doi.org/10.3390/nu14235112

50 Manthey, C. F., Autran, C. A., Eckmann, L. & Bode, L. Human milk oligosaccharides protect against enteropathogenic Escherichia coli attachment in vitro and EPEC colonization in suckling mice. *J Pediatr Gastroenterol Nutr* **58**, 165-168 (2014). https://doi.org/10.1097/MPG.0000000000000172

51 Coppa, G. V. *et al.* Human milk oligosaccharides inhibit the adhesion to Caco-2 cells of diarrheal pathogens: Escherichia coli, Vibrio cholerae, and Salmonella fyris. *Pediatr Res* **59**, 377-382 (2006). https://doi.org/10.1203/01.pdr.0000200805.45593.17

52 Morrow, A. L. *et al.* Human milk oligosaccharides are associated with protection against diarrhea in breast-fed infants. *J Pediatr* **145**, 297-303 (2004). https://doi.org/10.1016/j.jpeds.2004.04.054

53 Gustafsson, A. *et al.* Carbohydrate-dependent inhibition of Helicobacter pylori colonization using porcine milk. *Glycobiology* **16**, 1-10 (2006). https://doi.org/10.1093/glycob/cwj031

54 P. M. Simon, P. L. Goode, A. Mobasseri & Zopf, D. Inhibition of Helicobacter pylori Binding to Gastrointestinal Epithelial Cells by Sialic Acid-Containing Oligosaccharides. *Infect Immun* **65**, 750-757 (1997). https://doi.org/10.1128/iai.65.2.750-757.1997

55 Bengt Andersson, Oscar Porras, Lars A. Hanson, Teresa Lagergard & Svanborg-Eden, C. Inhibition of Attachment of Streptococcus pneumoniae and Haemophilus influenzae by Human Milk Oligosaccharides. *The Journal of Infectious Diseases* **153** (1986).

56 Laucirica, D. R., Triantis, V., Schoemaker, R., Estes, M. K. & Ramani, S. Milk Oligosaccharides Inhibit Human Rotavirus Infectivity in MA104 Cells. *J Nutr* **147**, 1709-1714 (2017). https://doi.org/10.3945/jn.116.246090

57 Yuan, P. *et al.* Structural studies of the parainfluenza virus 5 hemagglutinin-neuraminidase tetramer in complex with its receptor, sialyllactose. *Structure* **13**, 803-815 (2005). https://doi.org/10.1016/j.str.2005.02.019

58 Imberty, A. & Varrot, A. Microbial recognition of human cell surface glycoconjugates. *Curr Opin Struct Biol* **18**, 567-576 (2008). https://doi.org/10.1016/j.sbi.2008.08.001

59 Koromyslova, A., Tripathi, S., Morozov, V., Schroten, H. & Hansman, G. S. Human norovirus inhibition by a human milk oligosaccharide. *Virology* **508**, 81-89 (2017). https://doi.org/10.1016/j.virol.2017.04.032

60 Yu, W. *et al.* Evaluation and Mechanistic Investigation of Human Milk Oligosaccharide against SARS-CoV-2. *J Agric Food Chem* **71**, 16102-16113 (2023). https://doi.org/10.1021/acs.jafc.3c04275

61 Liu, F. T. & Stowell, S. R. The role of galectins in immunity and infection. *Nat Rev Immunol* **23**, 479-494 (2023). https://doi.org/10.1038/s41577-022-00829-7

62 El-Hawiet, A. *et al.* High-Throughput Label- and Immobilization-Free Screening of Human Milk Oligosaccharides Against Lectins. *Anal Chem* **89**, 8713-8722 (2017). https://doi.org/10.1021/acs.analchem.7b00542
63 El-Hawiet, A. *et al.* Screening natural libraries of human milk oligosaccharides against lectins using CaR-ESI-MS. *Analyst* **143**, 536-548 (2018). https://doi.org/10.1039/c7an01397c
64 J. Hirabayashi *et al.* Oligosaccharide specificity of galectins: a search by frontal affinity chromatography. *Biochimica et Biophysica Acta (BBA) - Reviews on Biomembranes,* **1572**, 232-254 (2002). https://doi.org/10.1016/S0304-4165(02)00311-2
65 al., P. C. e. Siglecs: a family of sialic-acid binding lectins. **8**, v (1998). https://doi.org/10.1093/oxfordjournals.glycob.a018832
66 von Gunten, S. & Bochner, B. S. Basic and clinical immunology of Siglecs. *Ann N Y Acad Sci* **1143**, 61-82 (2008). https://doi.org/10.1196/annals.1443.011
67 Koliwer-Brandl, H. *et al.* Lectin inhibition assays for the analysis of bioactive milk sialoglycoconjugates. *International Dairy Journal* **21**, 413-420 (2011). https://doi.org/10.1016/j.idairyj.2011.01.005
68 Bhunia, A. *et al.* Saturation transfer difference NMR and computational modeling of a sialoadhesin-sialyl lactose complex. *Carbohydr Res* **339**, 259-267 (2004). https://doi.org/10.1016/j.carres.2003.09.021
69 Li, N. *et al.* Cloning and characterization of Siglec-10, a novel sialic acid binding member of the Ig superfamily, from human dendritic cells. *J Biol Chem* **276**, 28106-28112 (2001). https://doi.org/10.1074/jbc.M100467200
70 Alphey, M. S., Attrill, H., Crocker, P. R. & van Aalten, D. M. High resolution crystal structures of Siglec-7. Insights into ligand specificity in the Siglec family. *J Biol Chem* **278**, 3372-3377 (2003). https://doi.org/10.1074/jbc.M210602200
71 Noll, A. J. *et al.* Human DC-SIGN binds specific human milk glycans. *Biochem J* **473**, 1343-1353 (2016). https://doi.org/10.1042/bcj20160046
72 Geijtenbeek, T. B. & Gringhuis, S. I. Signalling through C-type lectin receptors: shaping immune responses. *Nat Rev Immunol* **9**, 465-479 (2009). https://doi.org/10.1038/nri2569
73 Ley, K. Functions of Selectins. *Results Probl Cell Differ* **33**, 177-200 (2001). https://doi.org/10.1007/978-3-540-46410-5_10
74 S. Rudloff, C. Stefan, G. Pohlentz & Kunz, C. Detection of ligands for selectins in the oligosaccharide fraction of human milk. *EurJNut* **41**, 85-92 (2002). https://doi.org/10.1007/s003940200012
75 L. Bode *et al.* Inhibition of monocyte, lymphocyte, and neutrophil adhesion to endothelial cells by human milk oligosaccharides. *Thromb Haemost* **92**, 1402-1410 (2004). https://doi.org/10.1160/TH04-01-0055
76 Mukherjee, R. *et al.* Human Milk Oligosaccharide 2'-Fucosyllactose Inhibits Ligand Binding to C-Type Lectin DC-SIGN but Not to Langerin. *Int J Mol Sci* **23** (2022). https://doi.org/10.3390/ijms232314745
77 Molteni, M., Gemma, S. & Rossetti, C. The Role of Toll-Like Receptor 4 in Infectious and Noninfectious Inflammation. *Mediators Inflamm* **2016**, 6978936 (2016). https://doi.org/10.1155/2016/6978936
78 He, Y., Lawlor, N. T. & Newburg, D. S. Human Milk Components Modulate Toll-Like Receptor-Mediated Inflammation. *Adv Nutr* **7**, 102-111 (2016). https://doi.org/10.3945/an.115.010090
79 Kurakevich, E., Hennet, T., Hausmann, M., Rogler, G. & Borsig, L. Milk oligosaccharide sialyl(alpha2,3)lactose activates intestinal CD11c+ cells through

TLR4. *Proc Natl Acad Sci U S A* **110**, 17444-17449 (2013). https://doi.org/10.1073/pnas.1306322110

80 Thomas, P. G. *et al.* Maturation of dendritic cell 2 phenotype by a helminth glycan uses a Toll-like receptor 4-dependent mechanism. *J Immunol* **171**, 5837-5841 (2003). https://doi.org/10.4049/jimmunol.171.11.5837

81 Thomas, P. G., Carter, M. R., Da'dara, A. A., DeSimone, T. M. & Harn, D. A. A helminth glycan induces APC maturation via alternative NF-kappa B activation independent of I kappa B alpha degradation. *J Immunol* **175**, 2082-2090 (2005). https://doi.org/10.4049/jimmunol.175.4.2082

82 Cheng, L., Kiewiet, M. B. G., Groeneveld, A., Nauta, A. & de Vos, P. Human milk oligosaccharides and its acid hydrolysate LNT2 show immunomodulatory effects via TLRs in a dose and structure-dependent way. *Journal of Functional Foods* **59**, 174-184 (2019). https://doi.org/https://doi.org/10.1016/j.jff.2019.05.023

83 Oliveira-Nascimento, L., Massari, P. & Wetzler, L. M. The Role of TLR2 in Infection and Immunity. *Front Immunol* **3**, 79 (2012). https://doi.org/10.3389/fimmu.2012.00079

84 Chen, Y., Lin, J., Zhao, Y., Ma, X. & Yi, H. Toll-like receptor 3 (TLR3) regulation mechanisms and roles in antiviral innate immune responses. *J Zhejiang Univ Sci B* **22**, 609-632 (2021). https://doi.org/10.1631/jzus.B2000808

85 Yang, J. & Yan, H. TLR5: beyond the recognition of flagellin. *Cell Mol Immunol* **14**, 1017-1019 (2017). https://doi.org/10.1038/cmi.2017.122

86 S. Bauer *et al.* Human TLR9 Confers Responsiveness to Bacterial DNA via Species-Specific CpG Motif Recognition. *Proceedings of the National Academy of Sciences* **98**, 9237-9242 (2001). https://doi.org/10.1073/pnas

87 Goehring, K. C., Kennedy, A. D., Prieto, P. A. & Buck, R. H. Direct evidence for the presence of human milk oligosaccharides in the circulation of breastfed infants. *PLoS One* **9**, e101692 (2014). https://doi.org/10.1371/journal.pone.0101692

88 Dotz, V. *et al.* 13C-labeled oligosaccharides in breastfed infants' urine: individual-, structure- and time-dependent differences in the excretion. *Glycobiology* **24**, 185-194 (2014). https://doi.org/10.1093/glycob/cwt099

89 Ruhaak, L. R., Stroble, C., Underwood, M. A. & Lebrilla, C. B. Detection of milk oligosaccharides in plasma of infants. *Anal Bioanal Chem* **406**, 5775-5784 (2014). https://doi.org/10.1007/s00216-014-8025-z

90 Dotz, V., Rudloff, S., Meyer, C., Lochnit, G. & Kunz, C. Metabolic fate of neutral human milk oligosaccharides in exclusively breast-fed infants. *Mol Nutr Food Res* **59**, 355-364 (2015). https://doi.org/10.1002/mnfr.201400160

91 Zhang, W. *et al.* In vitro immunomodulatory effects of human milk oligosaccharides on murine macrophage RAW264.7 cells. *Carbohydr Polym* **207**, 230-238 (2019). https://doi.org/10.1016/j.carbpol.2018.11.039

92 Xiao, L. *et al.* Human milk oligosaccharides promote immune tolerance via direct interactions with human dendritic cells. *Eur J Immunol* **49**, 1001-1014 (2019). https://doi.org/10.1002/eji.201847971

93 Eiwegger, T. *et al.* Human milk--derived oligosaccharides and plant-derived oligosaccharides stimulate cytokine production of cord blood T-cells in vitro. *Pediatr Res* **56**, 536-540 (2004). https://doi.org/10.1203/01.PDR.0000139411.35619.B4

94 Kenneth M. Murphy, Casey Weaver & Berg, L. J. *Janeway's Immunobiology*. 10th Edition edn, 960 (Norton & Company, 2022).

95 Pak, M. E. *et al.* Anti-Neuroinflammatory Effects of the Human Milk Oligosaccharide, 2'-Fucosyllactose, Exerted via Modulation of M2 Microglial

Activation in a Mouse Model of Ischemia-Reperfusion Injury. *Antioxidants (Basel)* **12** (2023). https://doi.org/10.3390/antiox12061281

96 Atochina, O. & Harn, D. LNFPIII/LeX-stimulated macrophages activate natural killer cells via CD40-CD40L interaction. *Clin Diagn Lab Immunol* **12**, 1041-1049 (2005). https://doi.org/10.1128/CDLI.12.9.1041-1049.2005

97 Terrazas, L. I., Walsh, K. L., Piskorska, D., McGuire, E. & Harn, D. A., Jr. The schistosome oligosaccharide lacto-N-neotetraose expands Gr1(+) cells that secrete anti-inflammatory cytokines and inhibit proliferation of naive CD4(+) cells: a potential mechanism for immune polarization in helminth infections. *J Immunol* **167**, 5294-5303 (2001). https://doi.org/10.4049/jimmunol.167.9.5294

98 Bi, C., Fu, Y., Zhang, Z. & Li, B. Prostaglandin E2 confers protection against diabetic coronary atherosclerosis by stimulating M2 macrophage polarization via the activation of the CREB/BDNF/TrkB signaling pathway. *FASEB J* **34**, 7360-7371 (2020). https://doi.org/10.1096/fj.201902055R

99 Kim, J., Kim, Y. J. & Kim, J. W. Bacterial Clearance Is Enhanced by alpha2,3- and alpha2,6-Sialyllactose via Receptor-Mediated Endocytosis and Phagocytosis. *Infect Immun* **87** (2019). https://doi.org/10.1128/IAI.00694-18

100 Xie, Q. *et al.* Supplementing maternal diet with milk oligosaccharides and probiotics helps develop the immune system and intestinal flora of offsprings. *Food Sci Nutr* **11**, 6868-6877 (2023). https://doi.org/10.1002/fsn3.3579

101 Abou Assale, T. *et al.* 6'-sialyllactose ameliorates the ototoxic effects of the aminoglycoside antibiotic neomycin in susceptible mice. *Front Immunol* **14**, 1264060 (2023). https://doi.org/10.3389/fimmu.2023.1264060

102 Jin, Y., Jeon, H., Le Lam Nguyen, T., Kim, L. & Heo, K. S. Human milk oligosaccharides 3'-sialyllactose and 6'-sialyllactose attenuate LPS-induced lung injury by inhibiting STAT1 and NF-kappaB signaling pathways. *Arch Pharm Res* **46**, 897-906 (2023). https://doi.org/10.1007/s12272-023-01470-1

103 Rosa, F. *et al.* Human Milk Oligosaccharides Impact Cellular and Inflammatory Gene Expression and Immune Response. *Front Immunol* **13**, 907529 (2022). https://doi.org/10.3389/fimmu.2022.907529

104 S. Sotgiu *et al.* Immunomodulation of Fucosyl-Lactose and Lacto-N-Fucopentaose on Mononuclear Cells from Multiple Sclerosis and Healthy Subjects. *InternatIonal journal of BIomedIcal scIence* **2**, 114-120 (2006). https://doi.org/10.59566/IJBS.2006.2114

105 Comstock, S. S. *et al.* Dietary Human Milk Oligosaccharides but Not Prebiotic Oligosaccharides Increase Circulating Natural Killer Cell and Mesenteric Lymph Node Memory T Cell Populations in Noninfected and Rotavirus-Infected Neonatal Piglets. *J Nutr* **147**, 1041-1047 (2017). https://doi.org/10.3945/jn.116.243774

106 Zuurveld, M. *et al.* Ovalbumin-Induced Epithelial Activation Directs Monocyte-Derived Dendritic Cells to Instruct Type 2 Inflammation in T Cells Which Is Differentially Modulated by 2'-Fucosyllactose and 3-Fucosyllactose. *J Innate Immun* **15**, 222-239 (2023). https://doi.org/10.1159/000526528

107 Ayechu-Muruzabal, V. *et al.* Human Milk Oligosaccharide 2'-Fucosyllactose Modulates Local Viral Immune Defense by Supporting the Regulatory Functions of Intestinal Epithelial and Immune Cells. *Int J Mol Sci* **23** (2022). https://doi.org/10.3390/ijms231810958

108 Zuurveld, M. *et al.* Butyrate interacts with the effects of 2'FL and 3FL to modulate in vitro ovalbumin-induced immune activation, and 2'FL lowers mucosal mast cell activation in a preclinical model for hen's egg allergy. *Front Nutr* **10**, 1305833 (2023). https://doi.org/10.3389/fnut.2023.1305833

109 Ayechu-Muruzabal, V. *et al.* Exposure of Intestinal Epithelial Cells to 2'-Fucosyllactose and CpG Enhances Galectin Release and Instructs Dendritic Cells to Drive Th1 and Regulatory-Type Immune Development. *Biomolecules* **10** (2020). https://doi.org/10.3390/biom10050784

110 Xiao, L. *et al.* Human Milk Oligosaccharide 2'-Fucosyllactose Improves Innate and Adaptive Immunity in an Influenza-Specific Murine Vaccination Model. *Front Immunol* **9**, 452 (2018). https://doi.org/10.3389/fimmu.2018.00452

111 Croft, M., So, T., Duan, W. & Soroosh, P. The significance of OX40 and OX40L to T-cell biology and immune disease. *Immunol Rev* **229**, 173-191 (2009). https://doi.org/10.1111/j.1600-065X.2009.00766.x

112 Diskin, B. *et al.* PD-L1 engagement on T cells promotes self-tolerance and suppression of neighboring macrophages and effector T cells in cancer. *Nature Immunology* **21**, 442-454 (2020). https://doi.org/10.1038/s41590-020-0620-x

113 Xiao, L. *et al.* Human milk oligosaccharides protect against the development of autoimmune diabetes in NOD-mice. *Sci Rep* **8**, 3829 (2018). https://doi.org/10.1038/s41598-018-22052-y

114 Perdijk, O., van Neerven, R. J. J., Meijer, B., Savelkoul, H. F. J. & Brugman, S. Induction of human tolerogenic dendritic cells by 3'-sialyllactose via TLR4 is explained by LPS contamination. *Glycobiology* **28**, 126-130 (2018). https://doi.org/10.1093/glycob/cwx106

115 Eiwegger, T. *et al.* Prebiotic oligosaccharides: in vitro evidence for gastrointestinal epithelial transfer and immunomodulatory properties. *Pediatr Allergy Immunol* **21**, 1179-1188 (2010). https://doi.org/10.1111/j.1399-3038.2010.01062.x

116 Lin, K., Chen, S. & Chen, G. Role of Memory T Cells and Perspectives for Intervention in Organ Transplantation. *Front Immunol* **6**, 473 (2015). https://doi.org/10.3389/fimmu.2015.00473

117 Ivetic, A., Hoskins Green, H. L. & Hart, S. J. L-selectin: A Major Regulator of Leukocyte Adhesion, Migration and Signaling. *Frontiers in Immunology* **10** (2019). https://doi.org/10.3389/fimmu.2019.01068

118 Azagra-Boronat, I. *et al.* Immunomodulatory and Prebiotic Effects of 2'-Fucosyllactose in Suckling Rats. *Front Immunol* **10**, 1773 (2019). https://doi.org/10.3389/fimmu.2019.01773

119 Comstock, S. S., Wang, M., Hester, S. N., Li, M. & Donovan, S. M. Select human milk oligosaccharides directly modulate peripheral blood mononuclear cells isolated from 10-d-old pigs. *Br J Nutr* **111**, 819-828 (2014). https://doi.org/10.1017/S0007114513003267

120 Monaco, M. H. *et al.* Formula supplementation with human and bovine milk oligosaccharides modulates blood IgG and T-helper cell populations, and ex vivo LPS-stimulated cytokine production in a neonatal preclinical model. *Front Immunol* **14**, 1327853 (2023). https://doi.org/10.3389/fimmu.2023.1327853

121 Lei, K. *et al.* 2'-fucosyllactose inhibits imiquimod-induced psoriasis in mice by regulating Th17 cell response via the STAT3 signaling pathway. *Int Immunopharmacol* **85**, 106659 (2020). https://doi.org/10.1016/j.intimp.2020.106659

122 Li, X. *et al.* Alterations of milk oligosaccharides in mothers with gestational diabetes mellitus impede colonization of beneficial bacteria and development of RORgammat(+) Treg cell-mediated immune tolerance in neonates. *Gut Microbes* **15**, 2256749 (2023). https://doi.org/10.1080/19490976.2023.2256749

123 Yang, B. H. *et al.* Foxp3(+) T cells expressing RORgammat represent a stable regulatory T-cell effector lineage with enhanced suppressive capacity during

intestinal inflammation. *Mucosal Immunol* **9**, 444-457 (2016). https://doi.org/10.1038/mi.2015.74

124 Vos AP *et al.* Dietary supplementation of neutral and acidic oligosaccharides enhances Th1-dependent vaccination responses in mice. *Pediatr Allergy Immunol* **18**, 304–312 (2007). https://doi.org/10.1111/j.1399-3038.2006.00515.x

125 Toutounchi, N. S. *et al.* Human Milk Oligosaccharide 3'-GL Improves Influenza-Specific Vaccination Responsiveness and Immunity after Deoxynivalenol Exposure in Preclinical Models. *Nutrients* **13** (2021). https://doi.org/10.3390/nu13093190

126 Xiao, L. *et al.* The Combination of 2'-Fucosyllactose with Short-Chain Galacto-Oligosaccharides and Long-Chain Fructo-Oligosaccharides that Enhance Influenza Vaccine Responses Is Associated with Mucosal Immune Regulation in Mice. *J Nutr* **149**, 856-869 (2019). https://doi.org/10.1093/jn/nxz006

127 Schijf, M. A. *et al.* Specific dietary oligosaccharides increase Th1 responses in a mouse respiratory syncytial virus infection model. *J Virol* **86**, 11472-11482 (2012). https://doi.org/10.1128/JVI.06708-11

128 Brown, A. F. *et al.* Memory Th1 Cells Are Protective in Invasive Staphylococcus aureus Infection. *PLoS Pathog* **11**, e1005226 (2015). https://doi.org/10.1371/journal.ppat.1005226

129 O'Neill, L. A., Kishton, R. J. & Rathmell, J. A guide to immunometabolism for immunologists. *Nat Rev Immunol* **16**, 553-565 (2016). https://doi.org/10.1038/nri.2016.70

130 O'Neill, L. A. & Pearce, E. J. Immunometabolism governs dendritic cell and macrophage function. *J Exp Med* **213**, 15-23 (2016). https://doi.org/10.1084/jem.20151570

131 Kelly, B. & O'Neill, L. A. Metabolic reprogramming in macrophages and dendritic cells in innate immunity. *Cell Res* **25**, 771-784 (2015). https://doi.org/10.1038/cr.2015.68

132 Hu, T. *et al.* Metabolic regulation of the immune system in health and diseases: mechanisms and interventions. *Signal Transduction and Targeted Therapy* **9**, 268 (2024). https://doi.org/10.1038/s41392-024-01954-6

133 Viola, A., Munari, F., Sánchez-Rodríguez, R., Scolaro, T. & Castegna, A. The Metabolic Signature of Macrophage Responses. *Front Immunol* **10**, 1462 (2019). https://doi.org/10.3389/fimmu.2019.01462

134 Wu, L. *et al.* Metabolic regulation of dendritic cell activation and immune function during inflammation. *Front Immunol* **14**, 1140749 (2023). https://doi.org/10.3389/fimmu.2023.1140749

135 Shi, Y., Zhang, H. & Miao, C. Metabolic reprogram and T cell differentiation in inflammation: current evidence and future perspectives. *Cell Death Discov* **11**, 123 (2025). https://doi.org/10.1038/s41420-025-02403-1

136 Duan, H., Wang, L., Huangfu, M. & Li, H. The impact of microbiota-derived short-chain fatty acids on macrophage activities in disease: Mechanisms and therapeutic potentials. *Biomedicine & Pharmacotherapy* **165**, 115276 (2023). https://doi.org/https://doi.org/10.1016/j.biopha.2023.115276

137 Heine, R. G. & Tang, M. L. K. Dietary approaches to the prevention of food allergy. *Curr Opin Clin Nutr Metab Care* **11**, 320-328 (2008). https://doi.org/10.1097/MCO.0B013E3282FBF589

138 Vandenplas, Y. *et al.* The role of milk feeds and other dietary supplementary interventions in preventing allergic disease in infants: Fact or fiction? *Clin Nutr* **40**, 358-371 (2021). https://doi.org/10.1016/j.clnu.2020.10.025

139 Sekerel, B. E. *et al.* An Expert Panel Statement on the Beneficial Effects of Human Milk Oligosaccharides (HMOs) in Early Life and Potential Utility of HMO-Supplemented Infant Formula in Cow's Milk Protein Allergy. *J Asthma Allergy* **14**, 1147-1164 (2021). https://doi.org/10.2147/JAA.S323734

140 Zuurveld, M. *et al.* Immunomodulation by Human Milk Oligosaccharides: The Potential Role in Prevention of Allergic Diseases. *Front Immunol* **11**, 801 (2020). https://doi.org/10.3389/fimmu.2020.00801

141 Cukrowska, B., Bierla, J. B., Zakrzewska, M., Klukowski, M. & Maciorkowska, E. The Relationship between the Infant Gut Microbiota and Allergy. The Role of Bifidobacterium breve and Prebiotic Oligosaccharides in the Activation of Anti-Allergic Mechanisms in Early Life. *Nutrients* **12** (2020). https://doi.org/10.3390/nu12040946

142 Jennings, S. & Prescott, S. L. Early dietary exposures and feeding practices: role in pathogenesis and prevention of allergic disease? *Postgrad Med J* **86**, 94-99 (2010). https://doi.org/10.1136/pgmj.2009.086892

143 Han, S. M., Binia, A., Godfrey, K. M., El-Heis, S. & Cutfield, W. S. Do Human Milk Oligosaccharides Protect Against Infant Atopic Disorders and Food Allergy? *Nutrients* **12** (2020). https://doi.org/10.3390/nu12103212

144 Kang, L. J. *et al.* 3'-Sialyllactose as an inhibitor of p65 phosphorylation ameliorates the progression of experimental rheumatoid arthritis. *Br J Pharmacol* **175**, 4295-4309 (2018). https://doi.org/10.1111/bph.14486

145 Labourel, A. *et al.* O-Mucin-degrading carbohydrate-active enzymes and their possible implication in inflammatory bowel diseases. *Essays Biochem* **67**, 331-344 (2023). https://doi.org/10.1042/EBC20220153

146 Kennedy, J. M., De Silva, A., Walton, G. E., Poveda, C. & Gibson, G. R. Comparison of prebiotic candidates in ulcerative colitis using an in vitro fermentation model. *J Appl Microbiol* **135** (2024). https://doi.org/10.1093/jambio/lxae034

147 Fu, C., Sun, W., Wang, X. & Zhu, X. Human breast milk: A promising treatment for necrotizing enterocolitis. *Early Hum Dev* **184**, 105833 (2023). https://doi.org/10.1016/j.earlhumdev.2023.105833

148 Bode, L. Human Milk Oligosaccharides in the Prevention of Necrotizing Enterocolitis: A Journey From in vitro and in vivo Models to Mother-Infant Cohort Studies. *Front Pediatr* **6**, 385 (2018). https://doi.org/10.3389/fped.2018.00385

149 Abbas, S. *et al.* Tailoring Human Milk Oligosaccharides to Prevent Necrotising Enterocolitis Among Preterm Infants. *Front Nutr* **8**, 702888 (2021). https://doi.org/10.3389/fnut.2021.702888

150 Zhao, M. *et al.* An Overview of Sugar Nucleotide-Dependent Glycosyltransferases for Human Milk Oligosaccharide Synthesis. *J Agric Food Chem* **71**, 12390-12402 (2023). https://doi.org/10.1021/acs.jafc.3c02895

151 Urashima, T., Hirabayashi, J., Sato, S. & Kobata, A. Human Milk Oligosaccharides as Essential Tools for Basic and Application Studies on Galectins. *Trends in Glycoscience and Glycotechnology* **30**, SE51-SE65 (2018). https://doi.org/10.4052/tigg.1734.1SE

152 Brew, K., Vanaman, T. C. & Hill, R. L. The role of alpha-lactalbumin and the A protein in lactose synthetase: a unique mechanism for the control of a biological reaction. *Proc Natl Acad Sci U S A* **59**, 491-497 (1968). https://doi.org/10.1073/pnas.59.2.491

153 Hennet, T. *et al.* Genomic cloning and expression of three murine UDP-galactose: beta-N-acetylglucosamine beta1,3-galactosyltransferase genes. *J Biol Chem* **273**, 58-65 (1998). https://doi.org/10.1074/jbc.273.1.58
154 Powell, J. T. & Brew, K. On the interaction of alpha-lactalbumin and galactosyltransferase during lactose synthesis. *J Biol Chem* **250**, 6337-6343 (1975).
155 Hennet, T. The galactosyltransferase family. *Cell Mol Life Sci* **59**, 1081-1095 (2002). https://doi.org/10.1007/s00018-002-8489-4
156 He, Z. & Liu, F. Two Novel α 1,2-Fucosyltransferase Alleles in an H-Deficient Phenotype Individual. *Transfus Med Hemother* **41**, 375-379 (2014). https://doi.org/10.1159/000366235
157 Martin, S. L., Edbrooke, M. R., Hodgman, T. C., van den Eijnden, D. H. & Bird, M. I. Lewis X biosynthesis in Helicobacter pylori. Molecular cloning of an alpha(1,3)-fucosyltransferase gene. *J Biol Chem* **272**, 21349-21356 (1997). https://doi.org/10.1074/jbc.272.34.21349
158 Daniels, G. in *Human Blood Groups* 11-95 (2013).
159 Pei, C. *et al.* Characterization and application of active human α2,6-sialyltransferases ST6GalNAc V and ST6GalNAc VI recombined in Escherichia coli. *Enzyme Microb Technol* **177**, 110426 (2024). https://doi.org/10.1016/j.enzmictec.2024.110426
160 Kono, M. *et al.* Mouse beta-galactoside alpha 2,3-sialyltransferases: comparison of in vitro substrate specificities and tissue specific expression. *Glycobiology* **7**, 469-479 (1997). https://doi.org/10.1093/glycob/7.4.469
161 Fassio, F., Facioni, M. S. & Guagnini, F. Lactose Maldigestion, Malabsorption, and Intolerance: A Comprehensive Review with a Focus on Current Management and Future Perspectives. *Nutrients* **10** (2018). https://doi.org/10.3390/nu10111599
162 Shan, M., Yang, D., Dou, H. & Zhang, L. Fucosylation in cancer biology and its clinical applications. *Prog Mol Biol Transl Sci* **162**, 93-119 (2019). https://doi.org/10.1016/bs.pmbts.2019.01.002
163 Schneider, M., Al-Shareffi, E. & Haltiwanger, R. S. Biological functions of fucose in mammals. *Glycobiology* **27**, 601-618 (2017). https://doi.org/10.1093/glycob/cwx034
164 Chen, X. & Varki, A. Advances in the biology and chemistry of sialic acids. *ACS Chem Biol* **5**, 163-176 (2010). https://doi.org/10.1021/cb900266r
165 Li, Y. & Chen, X. Sialic acid metabolism and sialyltransferases: natural functions and applications. *Appl Microbiol Biotechnol* **94**, 887-905 (2012). https://doi.org/10.1007/s00253-012-4040-1
166 Petit, D. *et al.* Integrative view of α2,3-sialyltransferases (ST3Gal) molecular and functional evolution in deuterostomes: significance of lineage-specific losses. *Mol Biol Evol* **32**, 906-927 (2015). https://doi.org/10.1093/molbev/msu395
167 Janetzko, J. & Walker, S. The making of a sweet modification: structure and function of O-GlcNAc transferase. *J Biol Chem* **289**, 34424-34432 (2014). https://doi.org/10.1074/jbc.R114.604405
168 Qasba, P. K., Ramakrishnan, B. & Boeggeman, E. Structure and function of beta -1,4-galactosyltransferase. *Curr Drug Targets* **9**, 292-309 (2008). https://doi.org/10.2174/138945008783954943
169 Pérez-Escalante, E. *et al.* Human milk oligosaccharides as bioactive compounds in infant formula: recent advances and trends in synthetic methods. *Crit Rev Food Sci Nutr* **62**, 181-214 (2022). https://doi.org/10.1080/10408398.2020.1813683
170 Zhu, L. *et al.* Human Milk Oligosaccharides: A Critical Review on Structure, Preparation, Their Potential as a Food Bioactive Component, and Future

Perspectives. *J Agric Food Chem* **71**, 15908-15925 (2023). https://doi.org/10.1021/acs.jafc.3c04412

171 Gan, J., Cao, C., Stahl, B., Zhao, X. & Yan, J. Advances and challenges for obtaining human milk oligosaccharides: Extraction from natural sources and synthesis by intentional design. *Trends in Food Science & Technology* **141**, 104203 (2023). https://doi.org/https://doi.org/10.1016/j.tifs.2023.104203

172 Xu, L. L. & Townsend, S. D. Synthesis as an Expanding Resource in Human Milk Science. *J Am Chem Soc* **143**, 11277-11290 (2021). https://doi.org/10.1021/jacs.1c05599

173 Kellman, B. P. *et al.* Elucidating Human Milk Oligosaccharide biosynthetic genes through network-based multi-omics integration. *Nature Communications* **13**, 2455 (2022). https://doi.org/10.1038/s41467-022-29867-4

174 Nemeth, B. A., Tsang, S. W. Y., Geske, R. S. & Haney, P. M. Golgi Targeting of the GLUT1 Glucose Transporter in Lactating Mouse Mammary Gland. *Pediatric Research* **47**, 444-450 (2000). https://doi.org/10.1203/00006450-200004000-00006

175 Liu, H. *et al.* High-Throughput Screening and Directed Evolution of β-1,3-N-Acetylglucosaminyltransferase for Enhanced LNnT Production in Engineered Saccharomyces cerevisiae. *J Agric Food Chem* **73**, 7966-7974 (2025). https://doi.org/10.1021/acs.jafc.5c01311

176 Zeuner, B., Teze, D., Muschiol, J. & Meyer, A. S. Synthesis of Human Milk Oligosaccharides: Protein Engineering Strategies for Improved Enzymatic Transglycosylation. *Molecules* **24** (2019). https://doi.org/10.3390/molecules24112033

177 Ohtsuka, E., Ikehara, M. & Söll, D. Recent developments in the chemical synthesis of polynucleotides. *Nucleic Acids Res* **10**, 6553-6570 (1982). https://doi.org/10.1093/nar/10.21.6553

178 Lv, Z., Liu, H., Hao, H., Rahman, F. U. & Zhang, Y. Chemical synthesis of oligosaccharides and their application in new drug research. *Eur J Med Chem* **249**, 115164 (2023). https://doi.org/10.1016/j.ejmech.2023.115164

179 Tseng, H.-W. *et al.* Controllable Enzymatic Synthesis of Natural Asymmetric Human Milk Oligosaccharides. *JACS Au* **4**, 4496-4506 (2024). https://doi.org/10.1021/jacsau.4c00830

180 Zheng, J., Xu, H., Fang, J. & Zhang, X. Enzymatic and chemoenzymatic synthesis of human milk oligosaccharides and derivatives. *Carbohydr Polym* **291**, 119564 (2022). https://doi.org/10.1016/j.carbpol.2022.119564

181 Endo, T., Koizumi, S., Tabata, K. & Ozaki, A. Large-scale production of CMP-NeuAc and sialylated oligosaccharides through bacterial coupling. *Appl Microbiol Biotechnol* **53**, 257-261 (2000). https://doi.org/10.1007/s002530050017

182 Drouillard, S., Mine, T., Kajiwara, H., Yamamoto, T. & Samain, E. Efficient synthesis of 6'-sialyllactose, 6,6'-disialyllactose, and 6'-KDO-lactose by metabolically engineered E. coli expressing a multifunctional sialyltransferase from the Photobacterium sp. JT-ISH-224. *Carbohydr Res* **345**, 1394-1399 (2010). https://doi.org/10.1016/j.carres.2010.02.018

183 Liu, J. J. *et al.* Biosynthesis of a Functional Human Milk Oligosaccharide, 2'-Fucosyllactose, and l-Fucose Using Engineered Saccharomyces cerevisiae. *ACS Synth Biol* **7**, 2529-2536 (2018). https://doi.org/10.1021/acssynbio.8b00134

184 Bode, L. *et al.* Overcoming the limited availability of human milk oligosaccharides: challenges and opportunities for research and application. *Nutr Rev* **74**, 635-644 (2016). https://doi.org/10.1093/nutrit/nuw025

185 Palur, D. S. K., Pressley, S. R. & Atsumi, S. Microbial Production of Human Milk Oligosaccharides. *Molecules* **28** (2023). https://doi.org/10.3390/molecules28031491
186 Xu, M., Meng, X., Zhang, W., Shen, Y. & Liu, W. Improved production of 2'-fucosyllactose in engineered Saccharomyces cerevisiae expressing a putative α-1, 2-fucosyltransferase from Bacillus cereus. *Microb Cell Fact* **20**, 165 (2021). https://doi.org/10.1186/s12934-021-01657-5
187 EFSA Panel on Dietetic Products, N. & Allergies. Safety of 2′-O-fucosyllactose as a novel food ingredient pursuant to Regulation (EC) No 258/97. *EFSA Journal* **13**, 4184 (2015). https://doi.org/https://doi.org/10.2903/j.efsa.2015.4184
188 Vandenplas, Y. *et al.* Human Milk Oligosaccharides: 2'-Fucosyllactose (2'-FL) and Lacto-N-Neotetraose (LNnT) in Infant Formula. *Nutrients* **10** (2018). https://doi.org/10.3390/nu10091161
189 Estorninos, E. *et al.* Term infant formula supplemented with milk-derived oligosaccharides shifts the gut microbiota closer to that of human milk-fed infants and improves intestinal immune defense: a randomized controlled trial. *Am J Clin Nutr* **115**, 142-153 (2022). https://doi.org/10.1093/ajcn/nqab336
190 Bosheva, M. *et al.* Infant Formula With a Specific Blend of Five Human Milk Oligosaccharides Drives the Gut Microbiota Development and Improves Gut Maturation Markers: A Randomized Controlled Trial. *Front Nutr* **9**, 920362 (2022). https://doi.org/10.3389/fnut.2022.920362
191 Puccio, G. *et al.* Effects of Infant Formula With Human Milk Oligosaccharides on Growth and Morbidity: A Randomized Multicenter Trial. *J Pediatr Gastroenterol Nutr* **64**, 624-631 (2017). https://doi.org/10.1097/mpg.0000000000001520
192 EFSA Panel on Nutrition, N. F. *et al.* Safety of the extension of use of 2′-fucosyllactose (2′-FL) as a novel food pursuant to Regulation (EU) 2015/2283. *EFSA Journal* **21**, e08334 (2023). https://doi.org/https://doi.org/10.2903/j.efsa.2023.8334
193 EFSA Panel on Nutrition, N. F. *et al.* Safety of 3-fucosyllactose (3-FL) produced by a derivative strain of Escherichia coli K-12 DH1 as a novel food pursuant to Regulation (EU) 2015/2283. *EFSA Journal* **21**, e08026 (2023). https://doi.org/https://doi.org/10.2903/j.efsa.2023.8026
194 EFSA Panel on Nutrition, N. F. *et al.* Safety of lacto-N-tetraose (LNT) as a novel food pursuant to Regulation (EU) 2015/2283. *EFSA Journal* **17**, e05907 (2019). https://doi.org/https://doi.org/10.2903/j.efsa.2019.5907
195 EFSA Panel on Dietetic Products, N. & Allergies. Safety of lacto-N-neotetraose as a novel food ingredient pursuant to Regulation (EC) No 258/97. *EFSA Journal* **13**, 4183 (2015). https://doi.org/https://doi.org/10.2903/j.efsa.2015.4183
196 EFSA Panel on Nutrition, N. F. *et al.* Safety of 3'-sialyllactose (3'-SL) sodium salt produced by derivative strains of Escherichia coli BL21 (DE3) as a Novel Food pursuant to Regulation (EU) 2015/2283. *EFSA Journal* **20**, e07331 (2022). https://doi.org/https://doi.org/10.2903/j.efsa.2022.7331
197 EFSA Panel on Nutrition, N. F. *et al.* Safety of 6′-sialyllactose (6′-SL) sodium salt produced by a derivative strain (Escherichia coli NEO6) of E. coli W (ATCC 9637) as a Novel Food pursuant to Regulation (EU) 2015/2283. *EFSA Journal* **21**, e08025 (2023). https://doi.org/https://doi.org/10.2903/j.efsa.2023.8025
198 EFSA Panel on Nutrition, N. F. *et al.* Safety of 2'-fucosyllactose/difucosyllactose mixture as a novel food pursuant to Regulation (EU) 2015/2283. *EFSA Journal* **17**, e05717 (2019). https://doi.org/https://doi.org/10.2903/j.efsa.2019.5717

199 EFSA Panel on Nutrition, N. F. *et al.* Safety of lacto-N-fucopentaose I/2'-fucosyllactose (LNFP-I/2'-FL) mixture as a novel food pursuant to Regulation (EU) 2015/2283. *EFSA Journal* **21**, e8412 (2023). https://doi.org/https://doi.org/10.2903/j.efsa.2023.8412
200 Artemenko, N. V., McDonald, A. G., Davey, G. P. & Rudd, P. M. Databases and tools in glycobiology. *Methods Mol Biol* **899**, 325-350 (2012). https://doi.org/10.1007/978-1-61779-921-1_21
201 McDonald, A. G., Tipton, K. F. & Davey, G. P. A Knowledge-Based System for Display and Prediction of O-Glycosylation Network Behaviour in Response to Enzyme Knockouts. *PLoS Comput Biol* **12**, e1004844 (2016). https://doi.org/10.1371/journal.pcbi.1004844
202 Leman, J. K. *et al.* Macromolecular modeling and design in Rosetta: recent methods and frameworks. *Nat Methods* **17**, 665-680 (2020). https://doi.org/10.1038/s41592-020-0848-2
203 Jumper, J. *et al.* Highly accurate protein structure prediction with AlphaFold. *Nature* **596**, 583-589 (2021). https://doi.org/10.1038/s41586-021-03819-2
204 McDonald, A. G. & Davey, G. P. O-Glycologue: A Formal-Language-Based Generator of O-Glycosylation Networks. *Methods Mol Biol* **2370**, 223-236 (2022). https://doi.org/10.1007/978-1-0716-1685-7_11
205 McDonald, A. G., Tipton, K. F., Stroop, C. J. & Davey, G. P. GlycoForm and Glycologue: two software applications for the rapid construction and display of N-glycans from mammalian sources. *BMC Res Notes* **3**, 173 (2010). https://doi.org/10.1186/1756-0500-3-173
206 Yang, M. *et al.* Functional and informatics analysis enables glycosyltransferase activity prediction. *Nature Chemical Biology* **14**, 1109-1117 (2018). https://doi.org/10.1038/s41589-018-0154-9
207 Taujale, R. *et al.* Mapping the glycosyltransferase fold landscape using interpretable deep learning. *Nature Communications* **12**, 5656 (2021). https://doi.org/10.1038/s41467-021-25975-9
208 Go, S.-R., Lee, S.-J., Ahn, W.-C., Park, K.-H. & Woo, E.-J. Enhancing the thermostability and activity of glycosyltransferase UGT76G1 via computational design. *Communications Chemistry* **6**, 265 (2023). https://doi.org/10.1038/s42004-023-01070-6
209 Yang, Y. *et al.* Optimizing Trilobatin Production via Screening and Modification of Glycosyltransferases. *Molecules* **29** (2024). https://doi.org/10.3390/molecules29030643
210 Kitagawa, H. *et al.* Novel Oligosaccharides with the Sialyl-Lea Structure in Human Milk1. *The Journal of Biochemistry* **114**, 504-508 (1993). https://doi.org/10.1093/oxfordjournals.jbchem.a124207
211 McGuire, M. K. *et al.* What's normal? Oligosaccharide concentrations and profiles in milk produced by healthy women vary geographically. *Am J Clin Nutr* **105**, 1086-1100 (2017). https://doi.org/10.3945/ajcn.116.139980
212 van Leeuwen, S. S. *et al.* Rapid milk group classification by 1H NMR analysis of Le and H epitopes in human milk oligosaccharide donor samples. *Glycobiology* **24**, 728-739 (2014). https://doi.org/10.1093/glycob/cwu036
213 De Leoz, M. L. *et al.* A quantitative and comprehensive method to analyze human milk oligosaccharide structures in the urine and feces of infants. *Anal Bioanal Chem* **405**, 4089-4105 (2013). https://doi.org/10.1007/s00216-013-6817-1
214 Tonon, K. M., Miranda, A., Abrão, A., de Morais, M. B. & Morais, T. B. Validation and application of a method for the simultaneous absolute quantification of 16

neutral and acidic human milk oligosaccharides by graphitized carbon liquid chromatography - electrospray ionization - mass spectrometry. *Food Chem* **274**, 691-697 (2019). https://doi.org/10.1016/j.foodchem.2018.09.036

215 Galeotti, F. *et al.* Capillary electrophoresis separation of human milk neutral and acidic oligosaccharides derivatized with 2-aminoacridone. *Electrophoresis* **35**, 811-818 (2014). https://doi.org/10.1002/elps.201300490

216 Martín-Sosa, S., Martín, M. J., García-Pardo, L. A. & Hueso, P. Sialyloligosaccharides in human and bovine milk and in infant formulas: variations with the progression of lactation. *J Dairy Sci* **86**, 52-59 (2003). https://doi.org/10.3168/jds.S0022-0302(03)73583-8

217 Christensen, A. S., Skov, S. H., Lendal, S. E. & Hornshøj, B. H. Quantifying the human milk oligosaccharides 2'-fucosyllactose and 3-fucosyllactose in different food applications by high-performance liquid chromatography with refractive index detection. *J Food Sci* **85**, 332-339 (2020). https://doi.org/10.1111/1750-3841.15005

218 Amézqueta, S., Subirats, X., Fuguet, E., Ràfols, C. & Rosés, M. in *Handbook of Analytical Separations* Vol. 8 (ed Klára l Valkó) 633-666 (Elsevier Science B.V., 2020).

219 van Leeuwen, S. S. Challenges and Pitfalls in Human Milk Oligosaccharide Analysis. *Nutrients* **11** (2019). https://doi.org/10.3390/nu11112684

220 Wu, L. D., Ruhaak, L. R. & Lebrilla, C. B. Analysis of Milk Oligosaccharides by Mass Spectrometry. *Methods Mol Biol* **1503**, 121-129 (2017). https://doi.org/10.1007/978-1-4939-6493-2_10

221 Porfirio, S. *et al.* New strategies for profiling and characterization of human milk oligosaccharides. *Glycobiology* **30**, 774-786 (2020). https://doi.org/10.1093/glycob/cwaa028

222 Kaliva, M. & Vamvakaki, M. in *Polymer Science and Nanotechnology* (ed Ravin Narain) 401-433 (Elsevier, 2020).

223 Kortesniemi, M., Jafari, T., Zhang, Y. & Yang, B. (1)H NMR Metabolomics of Chinese Human Milk at Different Stages of Lactation among Secretors and Non-Secretors. *Molecules* **27** (2022). https://doi.org/10.3390/molecules27175526

224 Bharti, S. K. & Roy, R. Quantitative 1H NMR spectroscopy. *TrAC Trends in Analytical Chemistry* **35**, 5-26 (2012). https://doi.org/https://doi.org/10.1016/j.trac.2012.02.007

225 Orecchioni, M., Ghosheh, Y., Pramod, A. B. & Ley, K. Macrophage Polarization: Different Gene Signatures in M1(LPS+) vs. Classically and M2(LPS–) vs. Alternatively Activated Macrophages. *Frontiers in Immunology* **Volume 10 - 2019** (2019). https://doi.org/10.3389/fimmu.2019.01084

226 Viola, A., Munari, F., Sánchez-Rodríguez, R., Scolaro, T. & Castegna, A. The Metabolic Signature of Macrophage Responses. *Frontiers in Immunology* **Volume 10 - 2019** (2019). https://doi.org/10.3389/fimmu.2019.01462

227 Krawczyk, C. M. *et al.* Toll-like receptor-induced changes in glycolytic metabolism regulate dendritic cell activation. *Blood* **115**, 4742-4749 (2010). https://doi.org/10.1182/blood-2009-10-249540

228 Yunna, C., Mengru, H., Lei, W. & Weidong, C. Macrophage M1/M2 polarization. *European Journal of Pharmacology* **877**, 173090 (2020). https://doi.org/https://doi.org/10.1016/j.ejphar.2020.173090

229 Li, M., Hou, Q., Zhong, L., Zhao, Y. & Fu, X. Macrophage Related Chronic Inflammation in Non-Healing Wounds. *Front Immunol* **12**, 681710 (2021). https://doi.org/10.3389/fimmu.2021.681710

230 Yang, S., Zhao, M. & Jia, S. Macrophage: Key player in the pathogenesis of autoimmune diseases. *Front Immunol* **14**, 1080310 (2023). https://doi.org/10.3389/fimmu.2023.1080310
231 Wculek, S. K., Dunphy, G., Heras-Murillo, I., Mastrangelo, A. & Sancho, D. Metabolism of tissue macrophages in homeostasis and pathology. *Cellular & Molecular Immunology* **19**, 384-408 (2022). https://doi.org/10.1038/s41423-021-00791-9
232 Dousdampanis, P., Aggeletopoulou, I. & Mouzaki, A. The role of M1/M2 macrophage polarization in the pathogenesis of obesity-related kidney disease and related pathologies. *Frontiers in Immunology* **Volume 15 - 2024** (2025). https://doi.org/10.3389/fimmu.2024.1534823
233 Lun, H., Li, P., Li, J. & Liu, F. The effect of intestinal flora metabolites on macrophage polarization. *Heliyon* **10**, e35755 (2024). https://doi.org/https://doi.org/10.1016/j.heliyon.2024.e35755
234 Ney, L.-M. *et al.* Short chain fatty acids: key regulators of the local and systemic immune response in inflammatory diseases and infections. *Open Biology* **13**, 230014 (2023). https://doi.org/doi:10.1098/rsob.230014
235 Horneck Johnston, C. J. H. *et al.* Recognition of yeast β-glucan particles triggers immunometabolic signaling required for trained immunity. *iScience* **27**, 109030 (2024). https://doi.org/10.1016/j.isci.2024.109030
236 Hussain, T. *et al.* Oxidative Stress and Inflammation: What Polyphenols Can Do for Us? *Oxidative Medicine and Cellular Longevity* **2016**, 7432797 (2016). https://doi.org/https://doi.org/10.1155/2016/7432797
237 Grabarczyk, M. *et al.* Role of Plant Phytochemicals: Resveratrol, Curcumin, Luteolin and Quercetin in Demyelination, Neurodegeneration, and Epilepsy. *Antioxidants (Basel)* **13** (2024). https://doi.org/10.3390/antiox13111364
238 Videla, L. A., Valenzuela, R., Del Campo, A. & Zúñiga-Hernández, J. Omega-3 Lipid Mediators: Modulation of the M1/M2 Macrophage Phenotype and Its Protective Role in Chronic Liver Diseases. *International Journal of Molecular Sciences* **24**, 15528 (2023).
239 Chang, W.-H., Ting, H.-C., Chen, W.-W., Chan, J.-F. & Hsu, Y.-H. H. Omega-3 and omega-6 fatty acid differentially impact cardiolipin remodeling in activated macrophage. *Lipids in Health and Disease* **17**, 201 (2018). https://doi.org/10.1186/s12944-018-0845-y
240 Singh, R. P., Niharika, J., Kondepudi, K. K., Bishnoi, M. & Tingirikari, J. M. R. Recent understanding of human milk oligosaccharides in establishing infant gut microbiome and roles in immune system. *Food Research International* **151**, 110884 (2022). https://doi.org/https://doi.org/10.1016/j.foodres.2021.110884
241 Ruhaak, L. R., Stroble, C., Underwood, M. A. & Lebrilla, C. B. Detection of milk oligosaccharides in plasma of infants. *Analytical and Bioanalytical Chemistry* **406**, 5775-5784 (2014). https://doi.org/10.1007/s00216-014-8025-z
242 Slater, A. S., Hickey, R. M. & Davey, G. P. Interactions of human milk oligosaccharides with the immune system. *Frontiers in Immunology* **Volume 15 - 2024** (2025). https://doi.org/10.3389/fimmu.2024.1523829
243 Walsh, C., Lane, J. A., van Sinderen, D. & Hickey, R. M. Tailored Combinations of Human Milk Oligosaccharides Modulate the Immune Response in an In Vitro Model of Intestinal Inflammation. *Biomolecules* **14**, 1481 (2024).
244 Hickey, R. & Urashima, T. (2021).

245 Domínguez-Andrés, J., Joosten, L. A. & Netea, M. G. Induction of innate immune memory: the role of cellular metabolism. *Curr Opin Immunol* **56**, 10-16 (2019). https://doi.org/10.1016/j.coi.2018.09.001
246 Ip, W. K. E., Hoshi, N., Shouval, D. S., Snapper, S. & Medzhitov, R. Anti-inflammatory effect of IL-10 mediated by metabolic reprogramming of macrophages. *Science* **356**, 513-519 (2017). https://doi.org/10.1126/science.aal3535
247 Arts, R. J. *et al.* Glutaminolysis and Fumarate Accumulation Integrate Immunometabolic and Epigenetic Programs in Trained Immunity. *Cell Metab* **24**, 807-819 (2016). https://doi.org/10.1016/j.cmet.2016.10.008
248 Mills, E. L., Kelly, B. & O'Neill, L. A. J. Mitochondria are the powerhouses of immunity. *Nat Immunol* **18**, 488-498 (2017). https://doi.org/10.1038/ni.3704
249 He, Y. *et al.* The human milk oligosaccharide 2'-fucosyllactose modulates CD14 expression in human enterocytes, thereby attenuating LPS-induced inflammation. *Gut* **65**, 33-46 (2016). https://doi.org/10.1136/gutjnl-2014-307544
250 Ji, J. *et al.* Microbial metabolite butyrate facilitates M2 macrophage polarization and function. *Scientific Reports* **6**, 24838 (2016). https://doi.org/10.1038/srep24838
251 Ji, J., Hu, S.-L., Cui, Z.-W. & Li, W.-F. Probiotic Bacillus amyloliquefaciens mediate M1 macrophage polarization in mouse bone marrow-derived macrophages. *Archives of Microbiology* **195**, 349-356 (2013). https://doi.org/10.1007/s00203-013-0877-7
252 Christoffersen, T. E. *et al.* In Vitro Comparison of the Effects of Probiotic, Commensal and Pathogenic Strains on Macrophage Polarization. *Probiotics and Antimicrobial Proteins* **6**, 1-10 (2014). https://doi.org/10.1007/s12602-013-9152-0
253 Van den Bossche, J., O'Neill, L. A. & Menon, D. Macrophage Immunometabolism: Where Are We (Going)? *Trends Immunol* **38**, 395-406 (2017). https://doi.org/10.1016/j.it.2017.03.001
254 Jepsen, S. D. *et al.* Human milk oligosaccharides regulate human macrophage polarization and activation in response to Staphylococcus aureus. *Front Immunol* **15**, 1379042 (2024). https://doi.org/10.3389/fimmu.2024.1379042
255 Mills, E. L. *et al.* Succinate Dehydrogenase Supports Metabolic Repurposing of Mitochondria to Drive Inflammatory Macrophages. *Cell* **167**, 457-470.e413 (2016). https://doi.org/10.1016/j.cell.2016.08.064
256 Galván-Peña, S. & O'Neill, L. A. Metabolic reprograming in macrophage polarization. *Front Immunol* **5**, 420 (2014). https://doi.org/10.3389/fimmu.2014.00420
257 Van den Bossche, J. *et al.* Mitochondrial Dysfunction Prevents Repolarization of Inflammatory Macrophages. *Cell Rep* **17**, 684-696 (2016). https://doi.org/10.1016/j.celrep.2016.09.008
258 Tannahill, G. M. *et al.* Succinate is an inflammatory signal that induces IL-1β through HIF-1α. *Nature* **496**, 238-242 (2013). https://doi.org/10.1038/nature11986
259 Wang, B. *et al.* Lactobacillus rhamnosus GG promotes M1 polarization in murine bone marrow-derived macrophages by activating TLR2/MyD88/MAPK signaling pathway. *Anim Sci J* **91**, e13439 (2020). https://doi.org/10.1111/asj.13439
260 Peña, J. A. & Versalovic, J. Lactobacillus rhamnosus GG decreases TNF-alpha production in lipopolysaccharide-activated murine macrophages by a contact-independent mechanism. *Cell Microbiol* **5**, 277-285 (2003). https://doi.org/10.1046/j.1462-5822.2003.t01-1-00275.x
261 Chang, P. V., Hao, L., Offermanns, S. & Medzhitov, R. The microbial metabolite butyrate regulates intestinal macrophage function via histone deacetylase

inhibition. *Proc Natl Acad Sci U S A* **111**, 2247-2252 (2014). https://doi.org/10.1073/pnas.1322269111

262 Wang, Z. *et al.* Inulin alleviates inflammation of alcoholic liver disease via SCFAs-inducing suppression of M1 and facilitation of M2 macrophages in mice. *International Immunopharmacology* **78**, 106062 (2020). https://doi.org/https://doi.org/10.1016/j.intimp.2019.106062

263 Foata, F., Sprenger, N., Rochat, F. & Damak, S. Activation of the G-protein coupled receptor GPR35 by human milk oligosaccharides through different pathways. *Scientific Reports* **10**, 16117 (2020). https://doi.org/10.1038/s41598-020-73008-0

264 Pagano, E. *et al.* Activation of the GPR35 pathway drives angiogenesis in the tumour microenvironment. *Gut* **71**, 509-520 (2022). https://doi.org/10.1136/gutjnl-2020-323363

265 Contreras, R. G., Torres-Carrillo, A., Flores-Maldonado, C., Shoshani, L. & Ponce, A. Na+/K+-ATPase: More than an Electrogenic Pump. *International Journal of Molecular Sciences* **25**, 6122 (2024).

266 Barnett, D. J. M. *et al.* Human milk oligosaccharides, antimicrobial drugs, and the gut microbiota of term neonates: observations from the KOALA birth cohort study. *Gut Microbes* **15**, 2164152 (2023). https://doi.org/10.1080/19490976.2022.2164152

267 Watanabe, S., Alexander, M., Misharin, A. V. & Budinger, G. R. S. The role of macrophages in the resolution of inflammation. *J Clin Invest* **129**, 2619-2628 (2019). https://doi.org/10.1172/jci124615

268 Wang, N., Liang, H. & Zen, K. Molecular Mechanisms That Influence the Macrophage M1–M2 Polarization Balance. *Frontiers in Immunology* **5** (2014). https://doi.org/10.3389/fimmu.2014.00614

269 Zhang, W. *et al.* In vitro immunomodulatory effects of human milk oligosaccharides on murine macrophage RAW264.7 cells. *Carbohydrate Polymers* **207**, 230-238 (2019). https://doi.org/https://doi.org/10.1016/j.carbpol.2018.11.039

270 Kuntz, S., Rudloff, S. & Kunz, C. Oligosaccharides from human milk influence growth-related characteristics of intestinally transformed and non-transformed intestinal cells. *British Journal of Nutrition* **99**, 462-471 (2008). https://doi.org/10.1017/S0007114507824068

271 Hester, S. N. & Donovan, S. M. Individual and Combined Effects of Nucleotides and Human Milk Oligosaccharides on Proliferation, Apoptosis and Necrosis in a Human Fetal Intestinal Cell Line. *Food and Nutrition Sciences* **03**, 1567-1576 (2012).

272 EFSA Panel on Nutrition, N. F. *et al.* Safety of 6′-Sialyllactose (6′-SL) sodium salt as a novel food pursuant to Regulation (EU) 2015/2283. *EFSA Journal* **18**, e06097 (2020). https://doi.org/https://doi.org/10.2903/j.efsa.2020.6097

273 Sodhi, C. P. *et al.* The human milk oligosaccharides 2'-fucosyllactose and 6'-sialyllactose protect against the development of necrotizing enterocolitis by inhibiting toll-like receptor 4 signaling. *Pediatr Res* **89**, 91-101 (2021). https://doi.org/10.1038/s41390-020-0852-3

274 Zhang, W., He-Yang, J., Tu, W. & Zhou, X. Sialylated human milk oligosaccharides prevent intestinal inflammation by inhibiting toll like receptor 4/NLRP3 inflammasome pathway in necrotizing enterocolitis rats. *Nutr Metab (Lond)* **18**, 5 (2021). https://doi.org/10.1186/s12986-020-00534-z

275 Sodhi, C. P. *et al.* Necrotizing enterocolitis: specific human milk oligosaccharides prevent enteric glia loss and hypomotility. *Pediatric Research* (2025). https://doi.org/10.1038/s41390-025-04077-y

276 Yu, H., Jin, Y., Jeon, H., Kim, L. & Heo, K. S. Protective effect of 6'-Sialyllactose on LPS-induced macrophage inflammation via regulating Nrf2-mediated oxidative stress and inflammatory signaling pathways. *Korean J Physiol Pharmacol* **28**, 503-513 (2024). https://doi.org/10.4196/kjpp.2024.28.6.503

277 Asakuma, S. *et al.* Effect of Human Milk Oligosaccharides on Messenger Ribonucleic Acid Expression of Toll-like Receptor 2 and 4, and of MD2 in the Intestinal Cell Line HT-29. *Journal of Applied Glycoscience* **57**, 177-183 (2010). https://doi.org/10.5458/jag.57.177

278 Craft, K. M. & Townsend, S. D. Mother Knows Best: Deciphering the Antibacterial Properties of Human Milk Oligosaccharides. *Accounts of Chemical Research* **52**, 760-768 (2019). https://doi.org/10.1021/acs.accounts.8b00630

279 Craft, K. M., Thomas, H. C. & Townsend, S. D. Sialylated variants of lacto-N-tetraose exhibit antimicrobial activity against Group B Streptococcus11Electronic supplementary information (ESI) available. See DOI: 10.1039/c8ob02080a. *Organic & Biomolecular Chemistry* **17**, 1893-1900 (2019). https://doi.org/https://doi.org/10.1039/c8ob02080a

280 Pessentheiner, A. R. *et al.* The human milk oligosaccharide 3′sialyllactose reduces low-grade inflammation and atherosclerosis development in mice. *JCI Insight* **9** (2024). https://doi.org/10.1172/jci.insight.181329

281 Ganeshan, K. & Chawla, A. Metabolic regulation of immune responses. *Annu Rev Immunol* **32**, 609-634 (2014). https://doi.org/10.1146/annurev-immunol-032713-120236

282 Nguyen, D. V., Jin, Y., Nguyen, T. L. L., Kim, L. & Heo, K. S. 3'-Sialyllactose protects against LPS-induced endothelial dysfunction by inhibiting superoxide-mediated ERK1/2/STAT1 activation and HMGB1/RAGE axis. *Life Sci* **338**, 122410 (2024). https://doi.org/10.1016/j.lfs.2023.122410

283 Nogueira, V. & Hay, N. Molecular pathways: reactive oxygen species homeostasis in cancer cells and implications for cancer therapy. *Clin Cancer Res* **19**, 4309-4314 (2013). https://doi.org/10.1158/1078-0432.Ccr-12-1424

284 Agarwal, M., Biswas, P., Bhattacharya, A. & Sinha, D. K. Reactive oxygen species-mediated cytoplasmic stiffening impairs the phagocytic ability of the macrophage. *Journal of Cell Science* **133** (2020). https://doi.org/10.1242/jcs.236471

285 Feng, K. *et al.* The combined effects of 2′-fucosyllactose and 6′-sialyllactose on immune function and gut microbiota in healthy mice. *Food Bioscience* **71**, 107366 (2025). https://doi.org/https://doi.org/10.1016/j.fbio.2025.107366

286 Akira, S. & Takeda, K. Toll-like receptor signalling. *Nat Rev Immunol* **4**, 499-511 (2004). https://doi.org/10.1038/nri1391

287 Blander, J. M. & Medzhitov, R. Regulation of Phagosome Maturation by Signals from Toll-Like Receptors. *Science* **304**, 1014-1018 (2004). https://doi.org/doi:10.1126/science.1096158

288 Kong, L. & Ge, B.-X. MyD88-independent activation of a novel actin-Cdc42/Rac pathway is required for Toll-like receptor-stimulated phagocytosis. *Cell Research* **18**, 745-755 (2008). https://doi.org/10.1038/cr.2008.65

289 Underhill, D. M. & Goodridge, H. S. Information processing during phagocytosis. *Nature Reviews Immunology* **12**, 492-502 (2012). https://doi.org/10.1038/nri3244

290 Sotgiu, S. *et al.* Immunomodulation of fucosyl-lactose and lacto-N-fucopentaose on mononuclear cells from multiple sclerosis and healthy subjects. *Int J Biomed Sci* **2**, 114-120 (2006).

291 Pearce, E. L. & Pearce, E. J. Metabolic pathways in immune cell activation and quiescence. *Immunity* **38**, 633-643 (2013). https://doi.org/10.1016/j.immuni.2013.04.005
292 Everts, B. *et al.* TLR-driven early glycolytic reprogramming via the kinases TBK1-IKKε supports the anabolic demands of dendritic cell activation. *Nat Immunol* **15**, 323-332 (2014). https://doi.org/10.1038/ni.2833
293 Chang, C. H. *et al.* Posttranscriptional control of T cell effector function by aerobic glycolysis. *Cell* **153**, 1239-1251 (2013). https://doi.org/10.1016/j.cell.2013.05.016
294 Michalek, R. D. *et al.* Cutting edge: distinct glycolytic and lipid oxidative metabolic programs are essential for effector and regulatory CD4+ T cell subsets. *J Immunol* **186**, 3299-3303 (2011). https://doi.org/10.4049/jimmunol.1003613
295 Steinman, R. M., Hawiger, D. & Nussenzweig, M. C. Tolerogenic dendritic cells. *Annu Rev Immunol* **21**, 685-711 (2003). https://doi.org/10.1146/annurev.immunol.21.120601.141040
296 Maldonado, R. A. & von Andrian, U. H. How tolerogenic dendritic cells induce regulatory T cells. *Adv Immunol* **108**, 111-165 (2010). https://doi.org/10.1016/b978-0-12-380995-7.00004-5
297 Manicassamy, S. & Pulendran, B. Dendritic cell control of tolerogenic responses. *Immunol Rev* **241**, 206-227 (2011). https://doi.org/10.1111/j.1600-065X.2011.01015.x
298 Eiwegger, T. *et al.* Human milk--derived oligosaccharides and plant-derived oligosaccharides stimulate cytokine production of cord blood T-cells in vitro. *Pediatr Res* **56**, 536-540 (2004). https://doi.org/10.1203/01.Pdr.0000139411.35619.B4
299 Xiao, L. *et al.* Human milk oligosaccharides promote immune tolerance via direct interactions with human dendritic cells. *European Journal of Immunology* **49**, 1001-1014 (2019). https://doi.org/https://doi.org/10.1002/eji.201847971
300 Perdijk, O., van Neerven, R. J. J., van den Brink, E., Savelkoul, H. F. J. & Brugman, S. The oligosaccharides 6'-sialyllactose, 2'-fucosyllactose or galactooligosaccharides do not directly modulate human dendritic cell differentiation or maturation. *PLOS ONE* **13**, e0200356 (2018). https://doi.org/10.1371/journal.pone.0200356
301 Boll, E. J. *et al.* Human milk oligosaccharides differentially support gut barrier integrity and enhance Th1 and Th17 cell effector responses in vitro. *Frontiers in Immunology* **Volume 15 - 2024** (2024). https://doi.org/10.3389/fimmu.2024.1359499
302 Kurakevich, E., Hennet, T., Hausmann, M., Rogler, G. & Borsig, L. Milk oligosaccharide sialyl(α2,3)lactose activates intestinal CD11c⁺ cells through TLR4. *Proceedings of the National Academy of Sciences* **110**, 17444-17449 (2013). https://doi.org/doi:10.1073/pnas.1306322110
303 He, Y., Liu, S., Leone, S. & Newburg, D. S. Human colostrum oligosaccharides modulate major immunologic pathways of immature human intestine. *Mucosal Immunology* **7**, 1326-1339 (2014). https://doi.org/https://doi.org/10.1038/mi.2014.20
304 Chen, G. Y., Tang, J., Zheng, P. & Liu, Y. CD24 and Siglec-10 selectively repress tissue damage-induced immune responses. *Science* **323**, 1722-1725 (2009). https://doi.org/10.1126/science.1168988

305 Macauley, M. S., Crocker, P. R. & Paulson, J. C. Siglec-mediated regulation of immune cell function in disease. *Nat Rev Immunol* **14**, 653-666 (2014). https://doi.org/10.1038/nri3737
306 Sun, C. M. *et al.* Small intestine lamina propria dendritic cells promote de novo generation of Foxp3 T reg cells via retinoic acid. *J Exp Med* **204**, 1775-1785 (2007). https://doi.org/10.1084/jem.20070602
307 Ferreira, G. B. *et al.* Vitamin D3 Induces Tolerance in Human Dendritic Cells by Activation of Intracellular Metabolic Pathways. *Cell Rep* **10**, 711-725 (2015). https://doi.org/10.1016/j.celrep.2015.01.013
308 He, Y., Lawlor, N. T. & Newburg, D. S. Human Milk Components Modulate Toll-Like Receptor–Mediated Inflammation. *Advances in Nutrition* **7**, 102-111 (2016). https://doi.org/https://doi.org/10.3945/an.115.010090
309 Akkerman, R. *et al.* Combining galacto-oligosaccharides and 2′-fucosyllactose alters their fermentation kinetics by infant fecal microbiota and influences AhR-receptor dependent cytokine responses in immature dendritic cells. *Food & Function* **13**, 6510-6521 (2022). https://doi.org/10.1039/D2FO00550F
310 Gopalakrishna, K. P. & Hand, T. W. Influence of Maternal Milk on the Neonatal Intestinal Microbiome. *Nutrients* **12** (2020). https://doi.org/10.3390/nu12030823
311 van der Windt, G. J. *et al.* CD8 memory T cells have a bioenergetic advantage that underlies their rapid recall ability. *Proc Natl Acad Sci U S A* **110**, 14336-14341 (2013). https://doi.org/10.1073/pnas.1221740110
312 Gu, X.-Y. *et al.* Impact of lactate on immune cell function in the tumor microenvironment: mechanisms and therapeutic perspectives. *Frontiers in Immunology* **Volume 16 - 2025** (2025). https://doi.org/10.3389/fimmu.2025.1563303
313 Angelin, A. *et al.* Foxp3 Reprograms T Cell Metabolism to Function in Low-Glucose, High-Lactate Environments. *Cell Metab* **25**, 1282-1293.e1287 (2017). https://doi.org/10.1016/j.cmet.2016.12.018
314 Triantis, V., Bode, L. & van Neerven, R. J. J. Immunological Effects of Human Milk Oligosaccharides. *Front Pediatr* **6**, 190 (2018). https://doi.org/10.3389/fped.2018.00190
315 Walker, W. A. Role of nutrients and bacterial colonization in the development of intestinal host defense. *J Pediatr Gastroenterol Nutr* **30 Suppl 2**, S2-7 (2000).
316 Pieren, D. K. J., Boer, M. C. & de Wit, J. The adaptive immune system in early life: The shift makes it count. *Front Immunol* **13**, 1031924 (2022). https://doi.org/10.3389/fimmu.2022.1031924
317 Simon, A. K., Hollander, G. A. & McMichael, A. Evolution of the immune system in humans from infancy to old age. *Proc Biol Sci* **282**, 20143085 (2015). https://doi.org/10.1098/rspb.2014.3085
318 Kuntz, S., Rudloff, S. & Kunz, C. Oligosaccharides from human milk influence growth-related characteristics of intestinally transformed and non-transformed intestinal cells. *Br J Nutr* **99**, 462-471 (2008). https://doi.org/10.1017/s0007114507824068
319 Ghosh, S. *et al.* Colonic microbiota alters host susceptibility to infectious colitis by modulating inflammation, redox status, and ion transporter gene expression. *Am J Physiol Gastrointest Liver Physiol* **301**, G39-49 (2011). https://doi.org/10.1152/ajpgi.00509.2010
320 Le Pendu, J., Ruvoën-Clouet, N., Kindberg, E. & Svensson, L. Mendelian resistance to human norovirus infections. *Semin Immunol* **18**, 375-386 (2006). https://doi.org/10.1016/j.smim.2006.07.009

321 Janeway, C. A., Jr. How the immune system protects the host from infection. *Microbes Infect* **3**, 1167-1171 (2001). https://doi.org/10.1016/s1286-4579(01)01477-0
322 Buck, M. D., O'Sullivan, D. & Pearce, E. L. T cell metabolism drives immunity. *J Exp Med* **212**, 1345-1360 (2015). https://doi.org/10.1084/jem.20151159
323 Pearce, E. L., Poffenberger, M. C., Chang, C. H. & Jones, R. G. Fueling immunity: insights into metabolism and lymphocyte function. *Science* **342**, 1242454 (2013). https://doi.org/10.1126/science.1242454
324 Craft, K. M. & Townsend, S. D. The Human Milk Glycome as a Defense Against Infectious Diseases: Rationale, Challenges, and Opportunities. *ACS Infect Dis* **4**, 77-83 (2018). https://doi.org/10.1021/acsinfecdis.7b00209
325 Xiao, L. *et al.* Human Milk Oligosaccharide 2′-Fucosyllactose Improves Innate and Adaptive Immunity in an Influenza-Specific Murine Vaccination Model. *Frontiers in Immunology* **Volume 9 - 2018** (2018). https://doi.org/10.3389/fimmu.2018.00452
326 Kang, L.-J. *et al.* 3′-Sialyllactose prebiotics prevents skin inflammation via regulatory T cell differentiation in atopic dermatitis mouse models. *Scientific Reports* **10**, 5603 (2020). https://doi.org/10.1038/s41598-020-62527-5
327 Zuurveld, M. *et al.* Specific Human Milk Oligosaccharides Differentially Promote Th1 and Regulatory Responses in a CpG-Activated Epithelial/Immune Cell Coculture. *Biomolecules* **13** (2023). https://doi.org/10.3390/biom13020263
328 Brosseau, C. *et al.* "Microbial and immune modulation by 2'-fucosyllactose supplementation during gestation: a strategy to prevent food allergies". *Gut Microbes* **17**, 2523813 (2025). https://doi.org/10.1080/19490976.2025.2523813
329 Lee, M., Du, H., Winer, D. A., Clemente-Casares, X. & Tsai, S. Mechanosensing in macrophages and dendritic cells in steady-state and disease. *Front Cell Dev Biol* **10**, 1044729 (2022). https://doi.org/10.3389/fcell.2022.1044729
330 Iwasaki, A. & Medzhitov, R. Control of adaptive immunity by the innate immune system. *Nat Immunol* **16**, 343-353 (2015). https://doi.org/10.1038/ni.3123
331 Cheng, Y. J. & Yeung, C. Y. Recent advance in infant nutrition: Human milk oligosaccharides. *Pediatr Neonatol* **62**, 347-353 (2021). https://doi.org/10.1016/j.pedneo.2020.12.013
332 Bandara, M. D., Stine, K. J. & Demchenko, A. V. Chemical Synthesis of Human Milk Oligosaccharides: Lacto-N-hexaose Galβ1→3GlcNAcβ1→3 [Galβ1→4GlcNAcβ1→6] Galβ1→4Glc. *J Org Chem* **84**, 16192-16198 (2019). https://doi.org/10.1021/acs.joc.9b02701
333 Jaroentomeechai, T. *et al.* Mammalian cell-based production of glycans, glycopeptides and glycomodules. *Nature Communications* **15**, 9668 (2024). https://doi.org/10.1038/s41467-024-53738-9
334 Senra, R. L. *et al.* Co-expression of human sialyltransferase improves N-glycosylation in Leishmania tarentolae and optimizes the production of humanized therapeutic glycoprotein IFN-beta. *Journal of Biotechnology* **394**, 24-33 (2024). https://doi.org/https://doi.org/10.1016/j.jbiotec.2024.08.002
335 O'Flaherty, R. *et al.* Mammalian cell culture for production of recombinant proteins: A review of the critical steps in their biomanufacturing. *Biotechnology Advances* **43**, 107552 (2020). https://doi.org/https://doi.org/10.1016/j.biotechadv.2020.107552
336 Li, Z. *et al.* Advances in bacterial glycoprotein engineering: A critical review of current technologies, emerging challenges, and future directions. *Biotechnology*

Advances **79**, 108514 (2025). https://doi.org/https://doi.org/10.1016/j.biotechadv.2024.108514

337 GC, S., Bellis, S. L. & Hjelmeland, A. B. ST6Gal1: Oncogenic signaling pathways and targets. *Frontiers in Molecular Biosciences* **Volume 9 - 2022** (2022). https://doi.org/10.3389/fmolb.2022.962908

338 Kellokumpu, S. Golgi pH, Ion and Redox Homeostasis: How Much Do They Really Matter? *Front Cell Dev Biol* **7**, 93 (2019). https://doi.org/10.3389/fcell.2019.00093

339 Li, Y. *et al.* Enzymatic modular synthesis of asymmetrically branched human milk oligosaccharides. *Carbohydrate Polymers* **333**, 121908 (2024). https://doi.org/https://doi.org/10.1016/j.carbpol.2024.121908

340 Tu, L. & Banfield, D. Localization of Golgi-resident glycosyltransferases. *Cellular and molecular life sciences : CMLS* **67**, 29-41 (2009). https://doi.org/10.1007/s00018-009-0126-z

341 Fisher, P., Spencer, H., Thomas-Oates, J., Wood, A. J. & Ungar, D. Modeling Glycan Processing Reveals Golgi-Enzyme Homeostasis upon Trafficking Defects and Cellular Differentiation. *Cell Rep* **27**, 1231-1243.e1236 (2019). https://doi.org/10.1016/j.celrep.2019.03.107

342 Yadav, A., Vagne, Q., Sens, P., Iyengar, G. & Rao, M. Glycan processing in the Golgi as optimal information coding that constrains cisternal number and enzyme specificity. *Elife* **11** (2022). https://doi.org/10.7554/eLife.76757

343 Khoder-Agha, F. *et al.* Assembly of B4GALT1/ST6GAL1 heteromers in the Golgi membranes involves lateral interactions via highly charged surface domains. *J Biol Chem* **294**, 14383-14393 (2019). https://doi.org/10.1074/jbc.RA119.009539

344 Narimatsu, Y. *et al.* An Atlas of Human Glycosylation Pathways Enables Display of the Human Glycome by Gene Engineered Cells. *Mol Cell* **75**, 394-407.e395 (2019). https://doi.org/10.1016/j.molcel.2019.05.017

345 Walsh, C., Lane, J. A., van Sinderen, D. & Hickey, R. M. From lab bench to formulated ingredient: Characterization, production, and commercialization of human milk oligosaccharides. *Journal of Functional Foods* **72**, 104052 (2020). https://doi.org/https://doi.org/10.1016/j.jff.2020.104052

346 Pressley, S. R., McGill, A. S., Luu, B. & Atsumi, S. Recent advances in the microbial production of human milk oligosaccharides. *Current Opinion in Food Science* **57**, 101154 (2024). https://doi.org/https://doi.org/10.1016/j.cofs.2024.101154

347 Priem, B., Gilbert, M., Wakarchuk, W. W., Heyraud, A. & Samain, E. A new fermentation process allows large-scale production of human milk oligosaccharides by metabolically engineered bacteria. *Glycobiology* **12**, 235-240 (2002). https://doi.org/10.1093/glycob/12.4.235

348 Alliet, P. *et al.* Safety and efficacy of a probiotic-containing infant formula supplemented with 2'-fucosyllactose: a double-blind randomized controlled trial. *Nutr J* **21**, 11 (2022). https://doi.org/10.1186/s12937-022-00764-2

349 Zhang, X. *et al.* Microbial production of sialic acid and sialylated human milk oligosaccharides: Advances and perspectives. *Biotechnology Advances* **37**, 787-800 (2019). https://doi.org/https://doi.org/10.1016/j.biotechadv.2019.04.011

350 Hu, W. *et al.* A flexible peptide linker enhances the immunoreactivity of two copies HBsAg preS1 (21-47) fusion protein. *J Biotechnol* **107**, 83-90 (2004). https://doi.org/10.1016/j.jbiotec.2003.09.009

351 Bai, Y. & Shen, W. C. Improving the oral efficacy of recombinant granulocyte colony-stimulating factor and transferrin fusion protein by spacer optimization. *Pharm Res* **23**, 2116-2121 (2006). https://doi.org/10.1007/s11095-006-9059-5

352 Huston, J. S. *et al.* Protein engineering of antibody binding sites: recovery of specific activity in an anti-digoxin single-chain Fv analogue produced in Escherichia coli. *Proceedings of the National Academy of Sciences* **85**, 5879-5883 (1988). https://doi.org/doi:10.1073/pnas.85.16.5879
353 Bergeron, L. M., Gomez, L., Whitehead, T. A. & Clark, D. S. Self-renaturing enzymes: Design of an enzyme-chaperone chimera as a new approach to enzyme stabilization. *Biotechnology and Bioengineering* **102**, 1316-1322 (2009). https://doi.org/https://doi.org/10.1002/bit.22254
354 Chen, X., Zaro, J. L. & Shen, W. C. Fusion protein linkers: property, design and functionality. *Adv Drug Deliv Rev* **65**, 1357-1369 (2013). https://doi.org/10.1016/j.addr.2012.09.039
355 van Rosmalen, M., Krom, M. & Merkx, M. Tuning the Flexibility of Glycine-Serine Linkers To Allow Rational Design of Multidomain Proteins. *Biochemistry* **56**, 6565-6574 (2017). https://doi.org/10.1021/acs.biochem.7b00902
356 Harduin-Lepers, A., Mollicone, R., Delannoy, P. & Oriol, R. The animal sialyltransferases and sialyltransferase-related genes: a phylogenetic approach. *Glycobiology* **15**, 805-817 (2005). https://doi.org/10.1093/glycob/cwi063
357 Abernathy, M. H., He, L. & Tang, Y. J. Channeling in native microbial pathways: Implications and challenges for metabolic engineering. *Biotechnol Adv* **35**, 805-814 (2017). https://doi.org/10.1016/j.biotechadv.2017.06.004
358 Dueber, J. E. *et al.* Synthetic protein scaffolds provide modular control over metabolic flux. *Nature Biotechnology* **27**, 753-759 (2009). https://doi.org/10.1038/nbt.1557
359 Drouillard, S., Mine, T., Kajiwara, H., Yamamoto, T. & Samain, E. Efficient synthesis of 6′-sialyllactose, 6,6′-disialyllactose, and 6′-KDO-lactose by metabolically engineered E. coli expressing a multifunctional sialyltransferase from the Photobacterium sp. JT-ISH-224. *Carbohydrate Research* **345**, 1394-1399 (2010). https://doi.org/https://doi.org/10.1016/j.carres.2010.02.018
360 Chen, Q. *et al.* Metabolic engineering of Bacillus subtilis for de novo synthesis of 6′-sialyllactose. *Systems Microbiology and Biomanufacturing* **5** (2024). https://doi.org/10.1007/s43393-024-00279-3
361 Nyquist, S. K. *et al.* Integrated 'omics analysis reveals human milk oligosaccharide biosynthesis programs in human lactocytes. *bioRxiv* (2025). https://doi.org/10.1101/2025.03.17.643803
362 Plows, J. F. *et al.* Longitudinal Changes in Human Milk Oligosaccharides (HMOs) Over the Course of 24 Months of Lactation. *J Nutr* **151**, 876-882 (2021). https://doi.org/10.1093/jn/nxaa427
363 Govers, C., Calder, P. C., Savelkoul, H. F. J., Albers, R. & van Neerven, R. J. J. Ingestion, Immunity, and Infection: Nutrition and Viral Respiratory Tract Infections. *Front Immunol* **13**, 841532 (2022). https://doi.org/10.3389/fimmu.2022.841532
364 Urashima, T., Fukuda, K. & Messer, M. Evolution of milk oligosaccharides and lactose: a hypothesis. *Animal* **6**, 369-374 (2012). https://doi.org/10.1017/s1751731111001248
365 Victora, C. G. *et al.* Breastfeeding in the 21st century: epidemiology, mechanisms, and lifelong effect. *The Lancet* **387**, 475-490 (2016). https://doi.org/10.1016/S0140-6736(15)01024-7
366 Thurl, S. *et al.* Variation of human milk oligosaccharides in relation to milk groups and lactational periods. *Br J Nutr* **104**, 1261-1271 (2010). https://doi.org/10.1017/s0007114510002072